CRANFIELD UNIVERSITY

G C CARVALHO

AN ADAPTIVE CONTROL SYSTEM FOR OFF-LINE PROGRAMMING IN ROBOTIC GAS METAL ARC WELDING

SCHOOL OF INDUSTRIAL AND MANUFACTURING SCIENCE

PhD THESIS

CRANFIELD UNIVERSITY

SCHOOL OF INDUSTRIAL AND MANUFACTURING SCIENCE

PhD Thesis

Academic Year 1996-97

G C CARVALHO

An adaptive control system for off-line programming in robotic gas metal arc welding

Supervisor: Dr. R McMaster

October 1997

This thesis is submitted in fulfilment of the requirement for the degree of PhD

ABSTRACT

The aim of this work was to develop an integration concept for using off-line programming in robotic gas metal arc welding of thin sheet steel. Off-line welding parameter optimization and on-line monitoring and adaptive control of process stability and torch-to-workpiece relative distance were used to ensure weld consistency.

The concept developed included four main aspects: a) the use of a CAD system to design the workpiece; b) the use of a welding off-line programming system to design the welds, generate the welding parameters and to extract geometrical information from the CAD models to generate a robot program; c) the use of a graphical simulation system to simulate the robot movements; and d) the use of monitoring and adaptive control for ensuring that the required weld quality is delivered.

The CAD system was chosen to be the basis for the development of the welding off-line programming system. The generation of optimized welding parameters was based on empirical welding models and the robot program generation was based on on-line programming experience.

A PC based monitoring and control system was developed to provide on-line position and process control. The position control was carried out by pre-weld adjusting the initial position of the workpiece using a wire touch sensor and on-line adjusting the torch-to-workpiece distance by moving the workpiece based on the information provided by a through-the-arc sensor. The process control was carried out by automatically trimming the welding voltage such that the most stable process could be obtained. The stability of the process was estimated by using previously established monitoring indices. It was assumed that the off-line welding parameter optimization would provide the deposition rate necessary to produce the required weld quality.

Successful welding control trials were performed showing the effectiveness of the adaptive control strategy.

An off-line programming system has been developed and the programs generated have been tested by simulation. This showed that simulated positioning errors, produced by deliberate wrong path data, were successfully compensated for by the control system developed in this work.

ACKNOWLEDGEMENTS

I would like to express my thanks to my supervisor Robert McMaster for his continuing guidance and encouragement. I am also very greatful to Babatunde Ogunbiyi, Robert Apps, John Norrish, John Nixon and John Savill for their very supportive technical assistance during this project.

I acknowledge the financial support of the National Research Council (CNPq) of the Brazilian Ministry for Science and Technology, without which this project would not have been possible.

I would also like to thank Sadek Alfaro for his support and encouragement. Finally, I am greatful and indebted to all members of my immediate and extended family for their support, especially my mother Cremilda and my wife Giovana.

I dedicate this work to the memory of my late father

Aristides Alves de Carvalho Pires

(1927-1996)

and my late grandfather

Beltrando Caribé

(1907-1996)

I praise God for their life and achievements

"Quem não vive para servir não serve para viver"

(Those who do not live to serve do not serve to live)

Beltrando Caribé

CONTENTS

FIGURES

TABLES

APPENDICES

[1] Data structure used in AutoLISP

NOTATION

A_e	Electrode sectional area	[mm^2]
$\alpha, \beta, \delta, \gamma$	Regression constants	
Conf_Bad_Ign	Output from the confidence of bad ignition model	
DCI	Dip Consistency Index	
DipR	Dip resistance	[Ω]
$DipR_i$	Dip resistance calculated for a sample of welding voltage and current	[Ω]
$DipR_{mean}$	The arithmetic average of the $DipR_i$ calculated in a fixed time period	[Ω]
$DipR_{SD}$	Standard deviation of the dip resistances measured within a fixed time period	[Ω]
ΔSO	Variation in stand-off	[mm]
ΔV	Variation in welding voltage	[V]
ε	Prediction percentage error	[%]
ϕ	Proportionality constant between variation in stand-off and resulting variation in welding current	[mm/A]
ϕ_{calc}	Calculated value of ϕ	[mm/A]
ϕ_{meas}	Measured value of ϕ	[mm/A]
f(.)	Function	
G, GAP	Gap size	[mm]
I_{mean} , Imean	Mean welding current: arithmetic average of the welding current transient samples acquired in a fixed time pediod	[A]
Imax_320	Maximum welding current produced by the Migatronic BDH320 welding power source in dip mode of metal transfer	[A]
Imax_550	Maximum welding current produced by the Migatronic BDH550 welding power source in dip mode of metal transfer	[A]
Imean_320	Mean welding current produced by the Migatronic BDH320 welding power source	[A]
Imean_550	Mean welding current produced by the Migatronic BDH550 welding power source	[A]
I_{bk}	Background welding current: the arithmetic average of all the current transient samples less than or equal to I_{mean}	[A]
I_{max}	Maximum welding current: the maximum value in the welding current transient samples	[A]
I_{min}	Minimum welding current: the minimum value in the welding current transient samples	[A]
I_{pk}	Peak welding current: the arithmetic average of all the current samples greater than I_{mean}	[A]
I_{pred}	Expected welding current predicted by an empirical model	[A]
It_{bk}	Background current time: the arithmetic average of the time duration of the background periods in the welding current transient samples	[ms]

It_{pk}	Peak current time: the arithmetic average of the time duration of the peaks in the welding current transient samples	[ms]
j	Current density	[A/m^2]
K_1 , K_2, ...	Regression constants	
λ_1 , λ_2, ...	Constants	
L_a	Arc length	[mm]
L_e	Electrode stickout	[mm]
Leg	Leg length	[mm]
Leg_{av}	Average leg length	[mm]
Leg_b	Bottom leg length (horizontal-vertical fillet joint)	[mm]
Leg_{pred}	Expected average leg length predicted by the welding parameters generator	[mm]
Leg_{req}	Minimum required leg length	[mm]
Leg_s	Side leg length (horizontal-vertical fillet joint)	[mm]
Leg_1	Leg length at the web side in a flat position fillet weld	[mm]
Leg_2	Leg length at the flange side in a flat position fillet weld	[mm]
η	Resistivity	[Ω.m]
N_b	Number of transient samples with values equal or smaller than the samples average	
N_{Dip}	Number of welding voltage transient samples complying with $V \leq V_{bk}$	
N_p	Number of transient samples with values greater than the samples average	
N_{Tb}	Number of periods in which the data samples are consecutively smaller than the samples average	
N_{Tp}	Number of periods in which the data samples are consecutively greater than the samples average	
N_W	Number of transient data samples acquired in a fixed time period (window)	
P_d	Pressure exerted by the arc on the weld pool	[Pa]
Pen	Weld penetration (depth of fusion)	[mm]
Pen_1	Weld penetration in the web plate in a flat position fillet weld	[mm]
Pen_2	Weld penetration in the flange plate in a flat position fillet weld	[mm]
Pen_{av}	Average weld penetration	[mm]
Pen_b	Bottom weld penetration (horizontal-vertical fillet joint)	[mm]
Pen_{pred}	Expected average weld penetration predicted by the welding parameters generator	[mm]
Pen_s	Side weld penetration (horizontal-vertical fillet joint)	[mm]
POS	Binary operator which indicates if a weld is non-positional (0) or positional (1)	
PR	Power Ratio	
Pr(arc)	Possibility measure of bad arc ignition	

Pr(*ign*)	Possibility measure of process being unstable	
Pr(*und*)	Possibility measure of undercut	
P_v	Maximum pressure exerted on the base of the weld pool by the column of molten metal	[Pa]
$P_{zh.s}$	Pressure of the layer of molten metal in the crater of the weld pool	[Pa]
θ	Temperature	[°C]
θ_{av}	Average temperature	[°C]
R	Electrical resistance	[Ω]
R^2	Coefficient of determination of a regression model	
σ	Temperature coefficient of resistance	[$°C^{-1}$]
SE	Standard error of a regression model	
SO	Contact tip-to-workpiece distance (stand-off)	[mm]
SO_{act} , *SOact*	Actual stand-off	[mm]
SO_{est}	Estimated stand-off	[mm]
SO_f , SO_{end}	Stand-off value at the end of a welding torch slope path	[mm]
$SO_{filtered}$	Filtered stand-off estimation	[mm]
SO_{ref}	Reference stand-off	[mm]
SO_{req} , SOreq	Required stand-off	[mm]
SO_{start}	Stand-off value at the start of a welding torch slope path	[mm]
S_W	Welding travel speed	[m/min]
T, T_{mn}	Plate thickness, minimum plate thickness	
T_C	The component tolerance	[mm]
T_J	The welding wire-to-joint positioning tolerance	[mm]
T_T	The torch guidance tolerance	[mm]
$\sqrt{TI}$	Tranfer Index	
$\sqrt{TSI}$	Transfer Stability Index	
V	Electrical potential, welding voltage	[V]
$\sqrt{V_{bk}}$	The arithmetic average of all the voltage transient samples less than or equal to V_{mean}.	[V]
$\sqrt{V_{mean}}$, Vmean	arithmetic average of the welding voltage transient samples acquired in a fixed time period	[V]
$\sqrt{V_{min}}$	The minimum value in the welding voltage transient samples	[V]
$\sqrt{V_{max}}$	The maximum value in the welding voltage transient samples	[V]
$\sqrt{V_{pk}}$	The arithmetic average of all the current samples greater than V_{mean}	[V]
V_{req}	Required welding voltage	[V]
V_{set} , *Vset*	Power source set-up voltage	[V]
$\sqrt{Vt_{pk}}$	Peak voltage time: the arithmetic average of the time duration of the peaks in the welding voltage transient samples	[ms]

Vt_{bk}	Background voltage time: the arithmetic average of the time duration of the background periods in the welding voltage transient samples	[ms]
WFS	Wire feed speed	[m/min]
WFS_{ign}	The ideal wire feed speed required to give good arc ignition	[m/min]
WFS_{set}	Power source set-up wire feed speed	[m/min]
w_m	Wire melting rate	[m/min]
$y=f(x)$	y is a function of x	

Vectorial notation:

p, n	Small letter(s) in bold style: 3x1 vectors
p_x^{Ref}	p vector component in the X direction of the reference co-ordinates frame
p_y^{Ref}	p vector component in the Y direction of the reference co-ordinates frame
p_z^{Ref}	p vector component in the Z direction of the reference co-ordinates frame
^{T}	Superscript *"T"* : indicates transposed of a vector or matrix
ap	Weld approach vector
wdr	Weld withdrawing vector
M	Bold capital letter : 4x4 transformation matrix
m_{ij}	Matrix component: ith row, jth column
$\mathbf{M}_{Ref1}^{Ref2}$	Transformation matrix which defines the *Ref2* co-ordinates frame in terms of the *Ref1* co-ordinates
$\|\mathbf{p}\|$	Norm of vector **p**

1. Introduction

Welding is the third largest fabrication process used in the metal working industry, after assembly and machining. It is a special process that requires skilled operators to achieve good weld quality. However, the high cost of skilled welders and the demand for higher productivity and consistent weld quality have led to an increasing use of robots in welding operations.

Before a robot can execute a task it needs programming. In the case of robotic arc welding, most of the operations are programmed on-line, via a teach pendant. This results in a downtime, since the production line must be stopped during the programming phase. For an established product design with high volume production, this downtime might not be critical. However, the programming time could represent a considerable amount of the total costs in cases such as small batch production and short life products. To reduce this downtime, off-line programming can be used.

With off-line programming (OLP), the robot is programmed remotely without interrupting the production machine, by using a computer work station or a personal computer (PC), and suitable software. The robot movements can be programmed, simulated (and corrected, if necessary) on the computer and finally downloaded to the robot controller for prompt execution. Hence, off-line programming should solve one of the outstanding robot application problems, which is the downtime cost due to on-line programming. Another benefit of OLP is that the component design data available in CAD drawings could be used to define the welds during the programming task.

However, OLP has not been widely adopted by the industry for demanding applications such as resistance and arc welding, because the current systems require lengthy calibration sessions after the programming phase and this may consume most of the time saved by using the off-line technique. This is due to the inaccuracy of the geometrical models used to represent the robot, the welding cell and the workpiece, plus other factors such as robot absolute accuracy, calibration of the workcell, fixturing and workpiece positioning, and dimensional tolerances.

It should be noted that the time for programming can be chosen to best fit in with the manufacturing cycle. Also, in the event of positional errors due to errors in tool offset (for example, due to accidental collision between the tool and the workpiece), a previously calibrated robot need not be totally reprogrammed. These make off-line programming an obvious choice for robot programming if the need for post-programming calibration can be reduced or eliminated.

It is generally accepted that for quality welds to be produced, consistent and precise positioning of the wire tip relative to the joint line and consistent joint fit-up must be ensured. Inaccuracy in OLP could, therefore, influence weld quality by causing joint-to-wire tip positioning errors, resulting in bead misplacement. This could also cause variation in the contact tip-to-workpiece distance (stand-off) which could result in arc instability and inadequate penetration. It should be noted that these problems become more pronounced when welding thin sheets, since the weld sizes are generally small, requiring tighter positioning tolerances. Therefore, for this work an adaptive workpiece positioning system was proposed and a stand-off monitoring and control strategy developed.

Also, optimised welding parameters must be selected in order to produce good quality welds. Most of the off-line programming systems available do not incorporate welding knowledge or expertise; generally skilled welders are needed since the task of setting the welding parameters is left to the user. Therefore, in this work welding knowledge was integrated with the off-line programming technique; the welding parameters were obtained automatically by using empirical models of the welding process and a numerical optimisation method. Also on-line voltage tuning was implemented to ensure process stability.

1.1 Objectives

The main objective of this project was to develop an integrated fabrication concept covering welded component design, welding procedure generation, process monitoring and adaptive control and, based on this concept, to implement a self-compensating positional and process control system for welding, which avoids the requirement for lengthy calibration sessions after off-line programming and ensures that a stable process is always achieved.

Specifically, the following goals were set:

- to identify the sources of error and propose corrective measures;
- to incorporate welding models into a CAD system, that is, integrating the weld design and the welding procedure generation;
- to generate positional data for off-line programming based on the CAD model of the part and on the geometry of the welding cell;
- to design and build the hardware necessary for on-line monitoring and control;
- to develop a sensor for pre-weld position adjustment;
- to develop monitoring algorithms for metal transfer, process stability and stand-off;
- to develop a robot independent part positioning system giving precise stand-off control.

1.2 Thesis organisation

This thesis contains nine chapters and eleven appendices. The figures are placed at the end of each chapter and the tables are included within the text.

Chapter 1 presents the need for improved control in robotic arc welding and introduces the aim of the project with an overview of the proposed off-line programming and control strategy and objectives.

Chapter 2 presents a literature review of robotic gas metal arc welding with emphasis on the welding process characteristics and stability assessment, off-line programming, process monitoring and adaptive control of the welding process and the position of the welding torch.

Chapter 3 identifies the sources of error and describes the proposed strategy for off-line programming and control of arc welding operations, giving emphasis to the off-line programming aspects.

Chapter 4 describes the on-line positional and process control strategies.

Chapter 5 presents the experimental materials and equipment used.

Chapter 6 describes the modelling work and the integration of the control system proposed in Chapter 4, showing the results of the welding trials carried out during its commissioning.

Chapter 7 shows the results obtained with the control system developed.

Chapter 8 discusses the proposed system, the results obtained and possible industrial exploitation.

Chapter 9 concludes and suggests further work that could be carried out to enhance the work done.

Appendices A to **K** show details about the off-line programming module developed, description of electronic circuits built, description of the monitoring and control software developed and welding data collected during this research work.

2. Literature Review

Robotic welding is the most predominant application of industrial robots in the world [ref. 1]. Among the welding processes resistance spot welding and gas metal arc welding (GMAW) are the most common applications. This chapter presents a brief overview of robotic gas metal arc welding, focusing on the aspects relevant to the programming and control of an integrated robotic welding cell.

2.1 GMAW process

2.1.1 Process description [refs. 2 and 3]

GMAW is a process that uses the heat generated by an electric arc, produced between the end of a continuously fed welding electrode and the weld pool, to fuse the joint (see Figure 2.1). The entire weld area, including the arc, molten pool and electrode, is shielded by an externally supplied shielding gas. The shielding may be an inert gas, such as argon or helium, or a mixture of an inert gas with oxygen (O_2) and/or carbon dioxide (CO_2).

It should be noted that the composition of the shielding gas affects the way the metal is transferred from the electrode and the stability of the process. A mixture of argon with up to 20% CO_2 and 5% O_2 is normally used to ensure a robust process performance [refs. **2, 3, 4**]. (see Figure 2.2)

2.1.2 Modes of metal transfer

The way in which the metal is transferred from the consumable electrode tip to the molten weld pool affects arc stability, spatter level, fume generation rate, bead appearance and the positional capabilities of the process [ref. 3].

The modes of metal transfer are divided into two, namely: *Free flight* and *Dip* [refs. 3, 5, 6].

In *free-flight*, the metal is transferred from the filler wire to the workpiece in discrete droplets through a continuously maintained arc (see Figure 2.3). *Globular*, *spray* and *pulse* transfer are all sub-classifications of free-flight metal transfer [refs. **3**, 7].

Globular transfer is characterised by low and irregular transfer rate of large metal droplets. The transfer of metal droplets from the electrode to the molten pool is dominated by gravitational forces, therefore limiting its applicability to the flat position [refs. **2, 5**]. Another limitation of the globular transfer mode is the excessive spatter generation due to either the splashing of liquid metal from the weld pool when the large droplet is transferred or the overheating and explosive disintegration of the large droplet when short circuited with the weld pool in a short arc (low voltage) situation.

Spray transfer is characterised by small droplets (with equal or smaller diameter to that of the filler wire) which are projected axially through the arc and transferred to the molten pool in a high frequency stream.

In *pulse transfer*, the welding current and voltage are pulsed in such a manner that a controlled spray transfer is obtained with a mean current below the normal transition level for spray transfer. Two levels of current are used: a low *background current*, which is applied to maintain the arc, and a high *pulse-current* in which level drop growth, necking of wire tip and detachment occur [refs. **3, 5, 9, 10, 11**].

Dip transfer is characterised by a periodic short circuiting of the arc gap. The short circuiting is intentionally induced by feeding the wire towards the workpiece at a speed which exceeds the rate at which the wire is melted by the arc (burn-off rate) [ref. **3**]. Ideally, metal is expected to be transferred from the electrode to the workpiece only during a period when the electrode is in contact with the weld pool and no metal is transferred across the arc (see Figure 2.4)[ref. **2**]. The metal transfer occurs due to the high short-circuit current, which causes the molten metal bridge between the the wire tip and the molten pool to pinch off and rupture. A portion of the molten electrode tip is transferred to the weld pool and the arc is re-established. After the rupture, the arc gap increases somewhat due to a rapid fusion of the electrode[1], and to a weld pool retraction[2]. The volume of the drop of molten metal on the end of the electrode increases and the burn-off rate decreases until it is smaller than the feed speed, hence starting another cycle. [refs. **2, 3, 5, 12**].

Dip transfer produces a small, fast freezing weld pool that is generally suited for joining thin sections, for positional welding and for bridging large root openings (joint gap).

2.1.3 Welding arc electrical characteristics

Conventional GMAW power sources are normally designed with constant-voltage (CV) characteristics in order to provide self-adjustment and stabilisation of the welding arc [ref. **3**]. The voltage across the arc is directly related to the type of plasma gas used and to its length. If the arc length increases the voltage across the arc will also increase. The self-adjustment of the arc provided by a constant voltage power source will be discussed later in this chapter.

The voltage developed between the end of the contact tip and the workpiece in the GMAW process is the sum of the voltage drop in the wire extension, due to resistive effects, plus the voltage fall across the arc [ref. **3**]. It is commonly assumed that the total arc voltage is made up of three separate and distinct parts, the cathode (negative electrode) potential drop, the drop in the arc column and the anode (positive electrode) drop. The cathode potential drop has a magnitude of the order of the excitation potential of the electrode vapour (around 10V) and the anode voltage fall generally lies between 1 volt and 12 volts and depends on the nature of the plasma. The cathode and the anode falls occur in a very short distance from the respective electrodes (*cathode region* and *anode region*) and present very high voltage gradients (electric fields). The arc column, however, presents a relatively low voltage gradient and the voltage fall can be approximated by a linear function of its length [ref. **6**]. It is

---

[1] The electrode burn-off rate, which corresponds to the peak short circuiting current, is greater than its feed speed.

[2] The weld pool retraction results from an electrical explosion that forms during the rupture of the bridge between the molten electrode and the weld pool [ref. **12**]

generally accepted that far from the electrodes the plasma in the arc column is in equilibrium, small gradients of temperature, concentration and potential do not disturb the local thermodynamic equilibrium significantly [refs. **6** and **14**]. Because of its extremely small size, the cathode region is rather autonomous: any changes in arc geometry, or current redistribution in the column or near the anode do not affect the cathode region significantly. In contrast, the anode region presents a negative voltage-current density characteristic or, in other words, the voltage drop across the region decreases when current density increases [ref. **14**]. A typical voltage distribution across the arc can be viewed in Figure 2.5.

The type of the plasma gas will play an important role on how the anode region negative voltage-current density characteristic (V-J curve) will affect the arc. According to Nemchinsky [ref. **14**], the Lorentz force[3], which is the major force that detaches the molten metal droplet from the electrode-anode at high currents, depends very much on the current distribution inside the pendant droplet. This, in turn, will depend on the level of current constriction at the anode tip (near anode plasma)[4]: the more pronounced is the current constriction the less effective will be the Lorentz force in detaching the droplet. The author [ref. **14**] also states that some gas characteristics such as high electron-to-atom (molecule) mass ratio, high gas thermal conductivity and high electron-atom (molecule) collision cross section make the V-J curve fall more steeply, increasing the current constriction in the near anode plasma and, therefore, decreasing the effective Lorentz force. This was in concordance with the results obtained by Rhee and Kannatey-Asibu [ref. **15**] on the variation of the *spray transition current*[5] for different shielding gases (see Figure 2.6). It should be noted that the above mentioned explanation was proposed by Nemchisky [ref. **14**] as an attempt to explain how the different gases affect the behaviour of the welding arc. It should also be noted that the same author used a rather confusing notation by using the voltage-current (V-I) terminology to denote voltage-current density (V-J), giving rise to dubious interpretation.

2.1.4 Weld pool behaviour

The weld pool physical behaviour affects the final quality of the weld bead. According to Paton et al. [ref. **16**], the molten metal in a weld pool must be in a dynamic equilibrium for a weld free of defects to form. The defects that could occur normally take the form of undercut, lack of fusion and inconsistent bead cross section. The weld pool dynamic equilibrium can be expressed by the equation: [ref. **16**]

---

[3] Lorentz force is an electromagnetic force which results from the interaction between the current density J passing through a conductor and the magnetic field B, induced by the same current density: $F = J \times B$, force per unit

[4] When the current flows in a compound body consisting of two differently conducting media, the distribution of the current inside the body is determined by the conduction conditions in the worst conducting part of this body. Since plasma conductivity is much smaller than metal conductivity, the current distribution inside the droplet adjusts itself to the current distribution in the plasma [ref. **14**].

[5] *Spray Transition Current* is defined as the welding current level at which the transition from globular to spray transfer mode occurs (see Figure 2.6). Its value depends on the filler material size and composition, and also, on the composition of the shielding gas [ref. **3**].

$$P_d = P_v - P_{zhs} \tag{2.1}$$

where P_d is the pressure exerted by the arc on the weld pool; P_v, is the maximum pressure exerted on the base of the weld pool by the column of molten metal; and $P_{zh.s}$ is the pressure of layer of molten metal in the crater region of the weld pool. Figure 2.7 shows the pressure distribution across the pool. The same authors [ref. **16**] state that the condition necessary for the weld pool dynamic equilibrium to be maintained is attained when $P_v > P_d$. However, P_v decreases with increasing welding speed until it gets to a point at which the equilibrium condition does not hold any more, leading to the formation of defects. If the welding current is increased, both P_v and P_d increase, with P_d growing more rapidly than P_v. At a particular critical value of the welding current for each welding speed, P_d becomes equal to P_v, and above this current level, $P_d > P_v$ again leading to defects.

It should be noted that the pool behaviour described above dealt with the case of partially penetrated welds. In the case of fully penetrated welds, the shape of the pool is governed basically by forces of surface tension [ref. **17**]. The weight of the weld pool and the arc pressure are of secondary importance [ref. **17**]. The stability of the pool depends on the correct balance between the weld pool's length and width, if the balance is incorrect, the pool will collapse and burn-through will occur. However, Stolbov and Masakov [ref. **18**] stated that one of the main reasons for the destruction of the weld pool is the high pressure in the centre of the arc which causes local thinning and rupture of a liquid bridge. Another important factor for weld pool collapse is the presence of gap in the joint [ref. **18**].

2.1.5 Process stability

The definition of stability in GMAW is very subjective. Process stability has normally been referred to as *arc stability* in most published works. This nomenclature is adequate when assessing free-flight metal transfer mode. However, when the stability of a short circuiting welding process is considered it cannot be treated as arc stability, since in this case the arc is extinguished regularly, being essentially unstable. The cyclic repetition of this unstable system is what makes the process viable, the regularity of this behaviour being an indication of process stability [refs. **19, 20**]. It should be noted that good arc stability does not imply that the weld pool is going to be in dynamic equilibrium. For example, when welding with high welding currents and high travel speeds, the resulting weld pool dynamic behaviour might lead to undercut despite the arc being stable (see section 2.1.4). Therefore, the present author will adopt *process stability* instead of *arc stability*, since it is a more generic term and it does not imply any special mode of metal transfer. Hence, *process stability* will be defined in the present work as a set of process behavioural characteristics that are necessary for producing a good bead quality and a satisfactory welding performance.

This definition is in line with Philpott's definition [ref. **21**]. Philpott defined stability in GMA welding as the process ability to provide a regular metal transfer without spatter, a uniform heat input along the weld (i.e. maintaining constant welding current and voltage), smooth weld pool movements in a fixed position relative to the

electrode, and a stiff arc (i.e. flickering of the arc root around the weld pool edges does not occur).

In general, to ensure stability, two basic requirements must be satisfied: a) the mean wire melting speed has to be equal to the mean wire feeding speed [refs. **5, 22**]; b) the molten metal has to be transferred from the wire to the weld pool causing minimal process disturbances [ref. **22**].

2.1.5.1 *Wire melting behaviour in gas metal arc welding* [refs. **3, 13**]

It is generally accepted that the wire melting rate depends on the level of welding current and this behaviour can be approximated by a second order polynomial in the form of equation (2.2).

$$w_m = \alpha I + \beta L_e I^2 \qquad \textbf{(2.2)}$$

where w_m stands for the wire melting rate, I for the welding current and L_e for the wire stickout[6]. The terms α and β are constants which depend on the wire characteristics. The first term on the right side of equation (2.2) corresponds to the effect of the heat provided by the arc, while the second term accounts for the resistive heating on the wire stickout.

2.1.5.2 Instability in GMAW

The way in which instability manifests in GMAW depends upon the type of metal transfer. In dip transfer, two main forms can be identified: a) *wire stubbing in the weld pool* and b) *excessive spatter*.

Wire stubbing occurs when the short-circuit current is not high enough to provide sufficient energy for the vaporisation of the metal bridge, during the time it takes the unmelted end of the electrode to travel the approximate distance of the arc length [ref. **23**]. As a result, long duration short circuits occur and lumps of unmelted electrode wire and spatter are ejected from the weld. This is caused by either using an excessively low voltage or an excessively low rate-of-rise of short-circuit current (i.e. high inductance); both of which will also lead to arc ignition problems [refs. **19, 24**].

Spatter is generated in dip transfer as a result of the electrical explosion of the molten metal bridge that forms between the electrode and the pool during a short circuit [ref. **25**]. The level of spatter generated is directly related to the bridge explosion energy, which is dependent on the short-circuit current, on the voltage drop across the bridge and on the short-circuit time [ref. **26**]. The arc voltage exerts an indirect influence on the explosion energy, since it regulates the arc length and the droplet dimensions, and consequently the length of the bridge after short-circuiting[7]. The voltage drop across the bridge and the explosive energy depends on the length of

---

[6] Wire stickout is the length of solid wire between the contact tip and the solid/liquid interface at the wire molten end.

[7] During the arcing time, the droplet grows until it closes the arc gap. The bridge length can be approximated by the arc length. [refs. **23, 26**]

the bridge. Another factor that indirectly induces spatter is the rate-of-rise of short-circuit current [ref. 19]. An excessively high rate-of-rise induces high short-circuit currents and consequently, spatter generation.

In spray transfer, instability appears in the form of erratic movement of cathode spots when welding in low oxidising medium [ref. 22], or disruption of the plasma column caused by the growth and explosion of droplets inside the arc [refs. 27]. The latter is believed to happen due to either fast transient variation in wire feed speed, or, more likely, to local variation in wire material composition and surface condition, which affects the contact resistance at the contact tip [ref. 28]. The metal transfer disruption is often accompanied by metal ejection from the arc, or spatter. Although unstable situations have been observed in spray transfer, it generally offers a much improved level of stability compared to dip transfer.

The movement of the molten metal inside the weld pool also plays an important role on the stability of the process. In dip transfer, for example, the weld pool oscillates as a result of the pulses of pressure exerted by the repeated explosions of the metal bridges formed during the short circuits. The oscillation frequency will depend on the dimensions of the pool. It is generally agreed that the most stable situation is attained when the dip frequency becomes equal to the weld pool oscillation frequency [refs. 29, 30, 31]. In spray transfer, further to the movement induced by convection and surface tension gradients, weld pool deformation is also observed to be caused by arc pressure and by metal transferred from the electrode [ref. 32]. At higher voltages and consequently higher currents, the combination of the torch travel speed with the increased arc pressure and molten metal speeds within the weld pool may destabilise its dynamic equilibrium, causing bead malformation [ref. 16]. This may be considered as process instability.

2.1.5.3 Existing stability assessment methods

Generally spatter is used as the main visible indication of instability. A stable process generates low spatter, whereas an unstable process produces large amount of spatter which can adhere to the gas nozzle, inducing insufficient shielding which leads to porosity. Spatter can also adhere to the workpiece necessitating postweld cleaning operations such as grinding, resulting in increased manufacturing costs. [refs. 29, 33, 34].

Experienced welders normally judge the process stability by observing some process characteristics such as level and size of spatter, regularity of the arc sound, level of fume generation and arc and weld pool behaviour. The assessment is very subjective and depends on the skill of each welder.

Process stability can be objectively assessed by using descriptive statistical analysis, such as the standard deviation and coefficient of variation of the welding current and voltage waveform features. For example, in dip transfer the standard deviation of variables such as arcing voltage, short-circuiting current, arcing and short-circuiting times have been used to assess stability [ref. 3]. The smaller the standard deviation and/or coefficient of variation, the more stable the process is. It should be noted that most works carried out on the objective assessment of the stability of GMAW are mainly focused on dip transfer; globular transfer is generally considered to be unstable and spray transfer naturally stable [ref. 35].

Needham [ref. **36**] stated that in order to maintain stability in dip transfer the ratio between the arcing time and the short-circuiting time (so called "M ratio") must be kept within a specific range as constant as possible.

Mitta et al. [ref. **37**] developed an objective method for assessing process stability by correlating statistical features obtained from the current and voltage waveforms with the results from a subjective assessment of process stability performed by a skilful welder. The authors [ref. **37**] found that no single feature correlates well with process stability at all current levels. Therefore, they used multiple regression analysis to obtain an empirical model that relates the normalised standard deviation of short-circuiting time, arcing time, average short-circuiting current and average arcing current to the welder's subjective assessment of process stability.

Dilthey et al. [ref. **38**] also used a similar method to obtain rules for assessing stability. They have proposed models, based on standard deviation to mean value ratios, for assessing both short term and long term stability in short-circuiting, pulse and spray GMAW.

A different approach was adopted by Shinoda and Nishikawa [ref. **39**] for the stability assessment of dip transfer welding. They suggested that the use of current-voltage (I-V) line diagrams, instead of the commonly adopted time dependent voltage and current waveforms, would provide information on the effect of both variables as well as of their interaction on the process stability. The proposed method consisted of measuring the area in the I-V diagram corresponding to each short-circuiting cycle and calculating the standard deviation of these areas over a specified number of cycles. The authors [ref. **39**] claim that the method was successfully used for assessing the stability characteristics of different wire compositions [ref. **40**].

In contrast to the established practice of using descriptive statistical measures some authors are using ratios developed from the features of the welding current and voltage transient waveforms for stability assessment [refs. **41, 42, 43, 44, 45, 46, 47, 48, 49, 50**].

Dyurgerov [ref. **41**] found that stable metal transfer and optimum stability are attained at a certain ratio between the short circuit and the mean welding currents. This ratio was also used by Lebedev et al. [ref. **42**] to assess power source dynamics. Lipei et al. [ref. **43**] and Jennings [ref. **45**] found that the ratio relates qualitatively to the amount of spatter generated. Lipei et al. [ref. **43**] state that the ratio should be between 1.5 and 2, in order to keep the weld pool stable and prevent spatter while Lebedev and Sidoreiko [ref. **44**] found that the ideal value for the ratio is 1.75 but this can be up to 1.95. Jennings [ref. **45**] set the maximum value for the ratio at 2.35, while Lebedev [ref. **46**] set its minimum value at 1.35. Lebedev [ref. **46**] also uses the ratio of the minimum to mean current to select welding parameters for dip transfer; the minimum permissible value for this ratio is 0.29, below which poor metal transfer and arc instability were reported to occur.

Vorouin and Goloshcapov [ref. **47**] used the ratio of the short circuit time to the droplet transfer cycle time (called the time ratio) to assess process stability in dip transfer; the optimum welding condition was reported to be achieved for ratio values between 0.2 and 0.25. Popkov et al. [ref. **48**] found dip transfer conditions to be optimum if the ratio of arcing time to cycle time is between 0.6 and 0.8. Needham [ref. **49**] used the ratio of arcing time to short circuiting time (called the M ratio) to

establish the stable conditions for dip welding. Gupta et al. [ref. **50**] found the ideal value of M ratio to be between 2 and 3.

The use of indices formed from the the welding current and voltage waveforms for process assessment was further extended by Ogunbiyi [ref. **51**]. This author observed that, when moving from dip to globular and spray transfer, the variation range on the welding current and voltage waveforms reduces, or, in other words, the minimum and maximum current and voltage approach the respective welding average values. Based on this fact, three ratios, so called *Transfer Stability Index* (TSI)[8], *Transfer Index* (TI)[9], and *Dip Consistency Index* (DCI), were proposed as a means of classifying the mode of metal transfer and its stability. The first two ratios were based on features extracted from the current waveform and would give indication about mode of metal transfer and stability respectively. DCI was based on the voltage waveform and was used to predict and confirm the mode of metal transfer. Equations (2.3), (2.4) and (2.5) define the indices:

$$TI = \frac{I_{mean} - I_{min}}{I_{mean}} \tag{2.3}$$

$$TSI = \frac{I_{max}}{I_{mean}} \tag{2.4}$$

$$DCI = \frac{V_{mean} - V_{bk}}{V_{mean}} \tag{2.5}$$

where

I_{mean} is the arithmetic average of the welding current transient samples acquired in a fixed time period;

I_{min} is the minimum value in the welding current transient samples;

I_{max} is the maximum value in the welding current transient samples;

V_{mean} is the arithmetic average of the welding voltage transient samples acquired in a fixed time period;

V_{bk} is the arithmetic average of all the voltage transient samples less than or equal to V_{mean}.

The indices were combined to form monitoring rules, which were successfully applied for assessing mode of metal transfer and stability when welding with different power sources and wire and gas combinations [refs. **35, 51**].

In a further analysis, Ogunbiyi [ref. **51**] observed that the arc power oscillates during metal transfer and that the degree of the fluctuation would depend on the mode of metal transfer. As a result, a new ratio was defined and used for a quick assessment of mode of metal transfer and process stability. This ratio was called *Power Ratio* (PR):

---

[8] TSI was initially proposed by Dyurgerov [ref. 41]

[9] TI was initially developed by Lebedev [ref. 46]

$$PR = \frac{I_{bk}V_{bk}}{I_{mean}V_{mean}} \tag{2.6}$$

where

I_{bk} is the arithmetic average of all the current transient samples less than or equal to I_{mean} ; and

I_{mean} , V_{mean} and V_{bk} have the same meaning as before;

The schematic summary of how the indices in equations (2.3) to (2.6) are used to assess metal transfer stability is shown in Figure 2.8.

2.1.6 Weld quality

Quality is the totality of features and characteristics of a product or service that bear on its ability to satisfy a given need [ref. **52**]. In manufacturing, quality is defined as "compliance with certain pre-determined product characteristics over the entire manufacturing process" [ref. **38**]. Such characteristics in GMA welding will include bead size, surface appearance, mechanical properties and types and the level of defects present in the weld.

Traditionally, control of quality in welding has been performed by developing welding procedures [ref. **3**]. It is assumed that if all the process inputs remain fixed a satisfactory and repeatable weld quality will be obtained. The quality of the weld is monitored by means of final inspection and non-destructive testing.

The development of new welding procedures, however, is a costly and time-consuming process, since many trials must be performed to find a combination of welding parameters that will produce a weld without defects to the required weld size, appearance and mechanical properties.

Automatic selection of parameters has been proposed as a means of reducing the cost of procedure development. Methods such as statistical modelling and optimisation techniques [refs. **53, 54**], neural networks and fuzzy logic [ref. **55**] have been used for predicting the welding parameters given the required weld quality. To use these methods, several welding trials with different levels of welding parameters must be performed and the resulting weld bead sizes measured and assessed for presence of defects. Although good results have been reported by many researchers, these methods have a limited scope because they depend on empirical data and are specific to a particular process and consumables (i.e. wire type and size and gas).

Also, the high production rates normally attained when using robotic welding could make the final inspection of welding quality ineffective. Final inspections are usually carried out by selecting random samples from a batch of finished welds and checking their conformity with some standard quality criteria. Although the result of the final inspection is generally considered as representative of the quality of the whole batch, the problem is that during the time lag between the inspection and result of the tests, defective welds could have been fabricated.

On-line quality monitoring have been proposed as a means of reducing the reliance on final inspections [refs. **21, 51**]. The analysis of the welding current and voltage waveform transient features provide an indication of quality problems.

Philpott [ref. **21**] developed an on-line quality monitoring system which was able to detect quality problems caused by either insufficient shielding or arc instability in dip transfer gas metal arc welding. The system was based on the fact that the transient voltage and current signals and certain radio frequency (RF) components of these signals present specific signatures, that correspond to the occurrence of instability caused by inadequate voltage and by insufficient shielding. By considering that a quality problem is very likely to occur when such instabilities happen, the system was designed to label the length of weld corresponding to the block of data that was analysed, as either conform or non-conform, depending on the level of instability present. At the end of each weld, an estimate of the percentage of the total weld length corresponding to non-conform quality was calculated and compared to a specified limit, above which the weld was rejected. The indication of inadequate shielding was used to command a gas nozzle cleaning operation, before starting a new welding cycle. Although effective, this system could not prevent quality deviations from happening.

It is well established that welding process stability is intimately related to the resulting weld quality. By considering this, Norrish and Ogunbiyi [ref. **54**] proposed a strategy for monitoring and controlling GMA welding by means of off-line procedure optimisation and on-line tuning of welding parameters. The off-line optimisation would take place before the beginning of production and would select optimum welding parameters that would produce a weld to the required specification. The control strategy was anticipatory in nature and its main purpose was to detect any quality deviation trend and correct it before it could cause weld rejection, by tuning the welding parameters accordingly. The control strategy (shown in Figure 2.9) was applied successfully in a prototype control system in a production environment [ref. **56**].

2.2 Robotic arc welding

Robotic arc welding is a self-explanatory term that is normally used for characterising the application of a robot for carrying an arc welding gun through a three-dimensional pre-programmed path in order to perform an arc welding operation without operator control [ref. **58**]. A robotic welding system basically consists of a welding robot, an integrated welding power source and auxiliary equipment such as positioning table, gas nozzle cleaning station, wire cutter and torch head change systems.

This section gives an overview on the basic components found in robotic arc welding.

2.2.1 The arc welding robot

An arc welding robot is basically an industrial robot adapted to perform arc welding. According to the British Robot Association

> *An industrial robot is a reprogrammable device designed to both manipulate and transport parts, tools or specialised manufacturing*

implements through variable programmed motions for the performance of specific manufacturing tasks. [refs. **3, 57**]

In the case of robotic arc welding, the robot is primarily used for transporting the welding torch through the pre-programmed weld path, being also used for providing weld start and stop signals and for setting the welding parameters on the power source. To accomplish these input and output functions, the robot controller is normally supplied with digital inputs and outputs and analogue outputs which can be programmed to provide voltage levels corresponding to the required welding parameters.

Robots for arc welding must satisfy certain criteria which are demanded by the process itself. These include [ref. **58**]: a) the ability to move smoothly with uniform acceleration and deceleration; b) with linear motion; c) with a precise control of travel speed during welding; and d) accurately, or at least with highly repeatable motion.

The smooth acceleration is needed to ensure that the arc is not moved abruptly and thus disturbed. Linear motion is needed since the robot must follow the path of the weld joint throughout its length. Speed control is necessary for maintaining the required deposition rate. A high degree of accuracy and repeatability is required due to the low tolerance of the arc welding process to misalignment of the arc relative to the joint. [ref. **58**]

The adaptations required for an industrial robot to become an arc welding robot affect mostly its controller which, further to fulfilling the dynamic requirements cited above, must provide means of interacting with external equipments, such as welding power source, positioning table, seam trackers, etc.

2.2.2 Welding power source

The welding power source provides the electrical energy for sustaining the welding arc. Power sources for arc welding are required to produce a suitable output current and voltage characteristics for the process [ref. **3**], to give a reliable arc ignition [refs. **51, 63**], to have simple setting (for example, incorporating synergic control) and to give a reproducible stable arc [ref. **51**]. Also, in the case of robotic welding, the power source design should provide interfacing capabilities for remote control and output stabilisation [ref. **3**].

Power source designs vary from simple transformer-rectifier systems, using electromagnetic control techniques, to microprocessor-controlled electronic power regulation systems [ref. **3**]. Among the latter, the most promising designs are the ones based on inverter controllers which work at frequencies from 5 kHz to 100 kHz. In addition to resulting in lighter and smaller power sources [ref. **3**], the high frequencies attained offer [ref. **59**] smoother output, improved arc stiffness, reduced spatter generation in dip transfer, improved weld metallurgical properties and more precise control of current and voltage waveforms [refs. **3, 60**]. Figure 2.10 shows a schematic design of a typical inverter-controlled power source.

According to Yamamoto et al. [ref. **60**], the biggest advantage of inverter control in GMAW is the quick response of the controller during arc initiation, which improves arc stability. Inverter control ignites the arc instantaneously with a sharp

current peak at the moment the tip of the wire short-circuits with the base metal. Improved arc initiation contributes to the operating efficiency of GMAW robots.

2.2.2.1 Volt-ampere characteristics

Irrespective of design, it is well established that the performance of power sources depends on their static and dynamic characteristics. These are commonly referred to as *slope* and *inductance* and are normally fixed by the power source manufacturers.

The static characteristic describes the relationship between mean output current and the corresponding voltage available from the power source [ref. **51**]. A set of output-voltage *versus* output-current characteristic curves (volt-ampere curves) are used to describe the static characteristics [ref. **2**]. The slope of these curves is used to control and limit the amount of short circuit current which is attainable. The steeper the slope, the smaller is the available short circuit current [ref. **51**]. Hence, the slope can be used to reduce spatter in dip transfer mode. It must, however, be optimised since a too little magnitude might result in very high currents during short circuiting, leading to explosive transfer and spatter, whereas too much slope would lead to arc ignition problems, mainly caused by inadequate current during short circuiting [ref. **40**].

The dynamic characteristic of an arc welding power source describes its response to instantaneous variations in the load across its terminals. These transients normally occur [ref. **2**] during the striking of the arc, during rapid changes in arc length, during the transfer of metal across the arc and, in dip transfer, during arc extinction and reignition in a short-circuiting cycle. The power source design features that have an effect on the dynamic characteristics are those that provide [ref. **2**]:

1. Local transient energy storage, such as parallel capacitance circuits or dc series inductance;
2. Feedback controls in automatically regulated systems;
3. Modifications of waveform or circuit-operating frequencies.

In a conventional power source design, the dynamic characteristics are mainly determined by a dc series inductor, whose inductance can generally be adjusted by electromagnetic means [ref. **3**]. In the modern inverter-controlled power sources, the inductance effect can be achieved by electronic means [ref. **61**]. The higher the inductance is, the longer the current takes to rise to its maximum value in a short circuiting situation. This effect can be used to control spatter in dip transfer [refs. **62, 63**], since a long short-circuiting time implies that the current level necessary for breaking the molten metal bridge and, therefore, the explosion energy, will be smaller. However, an excessively high inductance may result in a short-circuiting current which is smaller than the minimum necessary for rupturing the molten bridge, leading to wire stubbing (see section 2.1.5.2). Furthermore, it may result in erratic starting and in a sluggish unstable arc [ref. **51**]. Its value must, consequently, be optimised for the different current levels [ref. **61**].

The power sources used in GMAW can be classified into two main types, namely: a) constant-voltage power source and b) constant-current power source.

Figure 2.11 shows a typical volt-ampere curve for a conventional constant-voltage (CV) power source. A true constant-voltage power source would maintain the pre-set voltage output (within its capability) at any current, although, due to internal electrical impedance in the welding circuit [ref. **2**], constant-voltage power sources present a small voltage drop with output current (negative slope). Changing that impedance will alter the slope of the volt-ampere curve.

From Figure 2.11, it can be seen that a small change in voltage produces a large change in current. When using constant wire-feed-speed, this characteristic results in a self-adjustment of the arc by which the arc length is maintained almost constant. A sudden increase in arc length caused by, for example, a rectangular step on the workpiece (see Figure 2.12) will cause a sudden increase in the arc resistance, thereby reducing the welding current and, consequently, the melting rate. Since the wire-feed-speed is constant, the arc length will reduce until a new feeding-rate to melting-rate equilibrium is achieved. Due to an increase in the stickout resistance, the new arc length will be slightly smaller than its initial value [ref. **64**].

A constant-current (CC) maintains the current almost constant over a range of voltages. The volt-ampere curves for this type of power source are normally characterised by a pronounced negative slope (see Figure 2.13), because of which a large change in voltage results in a relatively small change in current. This characteristic implies that the heating effect of the arc does not vary with small changes in stand-off and voltage. When using fixed current and wire feed speed with resistive wires an inherent self-adjustment mechanism operates, since the electrical stick-out is uniquely defined by equation (2.2) [ref. **3**]. This mechanism does not work with high conductivity materials such as aluminium. For such materials, wire feed units with variable voltage-controlled speed may be used with constant-current power sources [refs. **3, 65**].

2.3 Robot programming

The robot programming methods vary from a simple lead-through technique to high-level programming languages including graphic simulation. They can be categorised into two basic groups: *On-line programming* and *Off-line programming*.

2.3.1 On-line programming

On-line programming is a method in which it is necessary to use the actual robot. It is also called "direct programming" [ref. **66**], or "robot teaching" [ref. **67**] and can be categorised into *Manual Lead-through Programming* and *Teach Pendant Programming*. The first technique is based on moving the robot arm manually through each specific point. The second approach uses a manually operated teach pendant to achieve the same result. Both techniques utilise the point-to-point method in which the robot moves from one taught point, on the desired trajectory, to the next taught point. The mode of translation or interpolation, speed and other instructions (e.g. weld or non-weld motion) are added by the programmer.

In situations such as small batch manufacturing or short-life products, on-line programming may take a significant proportion of the total production run time, since it requires that the line must be stopped for the whole programming process and each

robot on the line must be individually programmed. Furthermore, it becomes very tedious and time consuming when hundreds of points are required to be recorded, such as in the automobile body manufacturing industry.

2.3.2 Off-line programming

Robot off-line programming is by definition the technique of generating a robot program without using a real machine. It presents several advantages over the on-line programming technique, some of which are mentioned bellow: [ref. **68**]

- reduction in robot down time due to programming;
- improvement in the work conditions for the operator by removing him from the potential hazardous environment;
- it allows the incorporation of CAD information from the workcell as well as from the workpieces into the programs.
- it permits program generation and its simulation without the use of a real robot;
- it allows the programmer to detect and correct in advance any problems;
- it facilitates the optimisation of robot programmes.

Off-line programming is classified according to the control level with which the programmer defines the tool movements. This classification has four levels [refs. **67 ,68 ,69**], which are described as follows.

a) Joint level – which requires the individual programming of each joint of the robot structure to achieve the required overall position.
b) Manipulator level – which involves specifying the robot movements in terms of world positions of the manipulator end-effector. Mathematical techniques are used to determine the individual joint values.
c) Object level – which requires the specification of the task in terms of movements and positioning of objects within the robot installation. This implies the existence of a world model of the installation, from which the information can be extracted in order to determine the necessary manipulator positions.
d) Task level – which specifies the task in the most general form, for example "*weld the first inferior joint at the inner side of the door panel*". This requires a comprehensive data base containing not only a world model, but also knowledge of the application techniques. In the case of the example, data on optimum welding parameters and methods would be necessary. Algorithms would be required to interpret the instructions and to apply them to the knowledge base to produce optimised collision free robot programs.

Most of the currently available off-line programming systems use manipulator and object levels of movement definition. Some attempts have been made to implement task level programming [refs. **70, 71**] but it is still in the early stages of development.

There is also another classification concerning the way the programs are created, namely [ref. **69**]: *language programming* and *world modelling*.

Language programming was the first off-line programming technique available. It was based in the use of textual programming languages [refs. **67, 72**]. This technique is still used but it requires the programmer to visualise objects in space, which can sometimes be very complex. It also needs a robot for the testing phase, which does not eliminate the problem of stopping the production line for some time.

In *world modelling* technique, the function data, the cycle logic and the point co-ordinate data are entered into the off-line computer and a robot independent program is generated, including all logic statements and pose co-ordinates. This program is then translated into robot specific code and afterwards, downloaded to the robot controller.

World modelling represents the "world" in which the robot is manipulating. The basis of the world modelling is the geometric model, which represents the geometry of the objects in the workspace [ref. **69**]. It provides a "virtual world" in which the programmer can "visualise" the relative positions of the several workplace components and their interrelationships. By using graphical and kinematic robot models it is also possible to graphically simulate programming tasks. A robot simulation emulates the robot motions generated by the program instructions and determines whether each movement can be executed successfully by checking if there are any collisions, if all points can be reached by the robot, in the desired orientation, and if there are any violations on the robot joints limits, either in terms of displacement or in terms of velocity.

The combined use of language programming and world modelling techniques is considered to be the best approach for off-line programming [refs. **73, 74**]. While world modelling allows interactive programming by simulating each movement as it is programmed, the textual approach permits the programmer to easily achieve the correct logic flow, which includes definition of variables and communication parameters required within the program.

Several off-line programming packages have been reported in the literature, some of which are commercially available while others were developed for research purposes or for some specific application. In the following paragraphs, a brief description of the most relevant citations will be given.

Bonney et al. [ref. **73**] described a commercially available workstation-based off-line programming package called GRASP[10], which was designed to provide both language and world modelling programming modes, and also debugging capabilities. The robot program can be run step by step and the positioning errors as well as the flow control errors can be promptly detected and corrected. The software is able to provide 3D geometric solid modelling and generalised kinematic robot modelling features, which allow users to build a world model of the robot installation on the computer. Within GRASP the robot program can be stored at object level, i.e. positions could be saved relative to the positions of objects in the workplace. This means, therefore, that the locations of these reference objects and of the robot itself in the work cell, can be changed without invalidating the program. It also includes

---

[10] BYG Systems Limited, UK.

collision detection capabilities which allow the programmer to detect and correct any potential collision that might occur during the robot operation.

Owens [ref. 75] described a MS-DOS PC[11]-based off-line programming package, Workspace[12], which was designed to be able to exchange information with CAD systems using the DXF format and to allow for the modelling of objects by using its three dimensional CAD system. This incorporates surfaces, constructive solid geometry, extruded polylines, solids and rotations. Super VGA graphics has made the simulation standard match that provided by graphics workstation-based packages. The package also includes dynamic simulation capabilities, which allow not only the evaluation of the dynamic performance of the robots but also the development of control systems for new manipulators. It also provides the programmer with textual programming allied with interactive graphical simulation and collision detection capabilities. These allow the programmer to visualise the robot movements and its interaction with the cell environment, as well as the flow control of the off-line generated programs.

Kortus et al. [ref. 74] proposed that the use of a textual based programming system allied with a PC-based graphical kinematic simulator (Workspace) may result in a cheaper alternative to the commercially available workstation based off-line programming systems.

Cook et al. [ref. 76] described a workstation-based robot simulation system (ROBOSIM), developed at NASA-USA to aid the design of robot manipulator arms by simulating their use in a variety of industrial and space-related contexts. The same authors described its use for simulating and programming robotic welding applications and emphasised that it could be used for determining the best orientation of the part relative to the robot and work table, for aiding fixture design, and for investigating different robot and positioner configurations. The system could be further developed for insertion into a complete CAD/CAM system, which would allow the welded part to be taken from its conceptual design to the production floor by computer simulation, before fabrication.

Recent developments in off-line programming have mainly focused on integrating CAD information normally available from the component design stages to the robot operation. The development of strategies for integration of manufacturing processes as well as the sensory information in the programming interface has also received significant attention. [refs. 77, 78, 79].

Chan et al. [ref. 80] described an off-line programming system which was based on a commercial CAD package (CATIA[13]) integrated with an ABB[14] IRB-2000 industrial robot. The integration was accomplished by means of a specially developed post-processor, which was responsible for translating the CAD information into the robot program (language ARLA[15]). Following the same line, Lee and El Maraghy [ref. 81] developed ROBOSIM, an off-line programming system whose graphical interface was a commercial PC-based CAD software, CADKEY. These systems were,

---

[11] Personal computer, based on the the Intel 80x86 microprocessor family
[12] Robot Simulations Ltd., UK.
[13] Computer-graphics Aided Three-dimensional Interactive Application.
[14] Asea Brown Boveri
[15] ABB Robot LAnguage.

however, developed for general robotic applications and did not include any manufacturing process specific features.

Considering the welding process, several programming systems containing some process related features have been reported in the literature. Kodaira et al. [ref. **82**], for example, described an off-line programming system with three dimensional graphics facilities, dedicated to spot welding robots. This system had an interesting feature: the ability to adapt locational data from the computer models to physical installation data of actual robots and workpieces. The authors proposed and implemented two adjustment methods, based on co-ordinate transformation, for gross adaptation and on interpolation of positioning error vectors, for local fitting. This method was claimed to give good results for the off-line programming of spot welding robots, reducing the programming time to less than one-fifth of that involved in full point teaching on an automobile production line. However, it still required some manual teaching for the implementation of the adaptive techniques. The manual intervention could be substantial for a large number of robots with just one off-line programming unit.

For the arc welding process, Quartier and Drews [ref. **83**] presented MACROWELD, an off-line programming system based on AutoCAD®. Similarly, Bréat et al. [ref. **84**] described ACT WELD, an off-line programming system tailored for robotic welding applications. Both systems presented interfaces for programming both arc welding process and robot path, with graphical simulation capabilities. The reported systems, however, would still depend on the programmer to actually set the welding parameters. In contrast, Sugitani et al. [ref. **85**] described a teaching-less CAD/CAM system which was designed to make use of CAD information allied with welding material data and design codes for automatically generating the robot program and the welding parameters, which were chosen from a pre-stored welding database. This system also included adaptive control features in terms of seam finding by means of wire-touch sensing and seam tracking by means of high speed rotating arc. In a similar manner, Cargnelli and Rogowski [ref. **86**] used a CAD package to develop an automatic robot program generator. Their system, however, allowed some interactiveness with the operator, who could modify some data after the robot program was automatically generated. It presented, though, no adaptive control facilities.

2.4 Off-line programming applied to robotic arc welding

Despite many off-line programming packages being available, this robot programming technique has not been widely adopted by the industry for demanding applications such as resistance and arc welding [ref. **87**]. The current systems require lengthy calibration sessions after the programming phase, since the "world models" used always have some dissimilarities compared to the "real world" [ref. **88**]. These dissimilarities are caused by several factors, which include [refs. **87, 88, 89**] robot accuracy, calibration of the workcell, and fixturing and workpiece tolerances. In addition, in arc welding operations, further variables appear in the form of tolerances in the component dimensions as well as joint fit up and thermal distortion, which can

cause dynamic variation in the seam position and also in the gap size. These factors may induce quality problems in the weld, which may lead to part rejection.

2.4.1 "Ideal world" *versus* "Real world"

"**Ideal world**" is adopted here to describe the idealised graphical models of the robot and its environment, as used in the simulation and off-line programming. "**Real world**" refer to the actual geometric shapes of the various components of a welding cell, including robot links, as well as their relative positions. Graphical modelling in the "ideal world" is based on the nominal values of dimensions and positions of the several components contained in a robotic cell.

There are normally inevitable differences between the computer model and the real world [refs. **73, 90**]. These differences can come from many sources. For instance, the robot may not be built or perform exactly according to the manufacturer's specifications, the torch mounting position is not exactly determined, there will be tolerances associated with tooling and parts, the layout of the cell may not be exactly as used in the simulation, some dimensional variation or even some displacement in the workpiece will occur during the manufacturing process as in the case of welding. Whatever its source, the discrepancy normally induces the off-line generated program to work improperly. There are several ways of reducing or overcoming these problems. One solution is to edit the program on-line using the robot's teach pendant [ref. **82**]. Depending on the amount of editing involved, this may or may not be a time and cost effective solution. Another method is to use the real robot to locate some keypoints within the cell and to modify the world model on the simulation system [refs. **88, 91, 92**]. The simulation system will thus contain an accurate model of the environment, as the robot "sees" it. This approach however does not compensate for dynamic movement during welding process. A third technique of compensation for these discrepancies is through the use of sensors on the real robot [ref. **73, 88**]. These may take the form of vision systems, tactile sensors, simple limit switches etc. and will depend on the particular application. The robot program should be created off-line in such a way as to make use of the information provided by these sensors to ensure that the positioning accuracy is maintained in the real cell.

2.4.2 Robot calibration

The success of an off-line programmed robot operation will depend on how close the "ideal world" matches the "real world". The robot plays an important role in matching both "worlds" since it is responsible for carrying the tool (welding torch, in the case of arc welding) through the programmed path. This is normally described in terms of world co-ordinates which are defined relative to the robot's World Co-ordinate Frame (see Figure 2.14). The robot controller uses a mathematical model of the robot structure to calculate the positions of the axes necessary to be attained for the tool to reach the command pose. If the model does not match the robot, the attained pose will be different from the command pose, resulting in inaccuracy problems.

According to the British Standards Institution [ref. **93**], *pose* is defined as the position and attitude of one co-ordinate frame with relation to another. Position includes a 3-dimensional (3D) vector of translational parameters and attitude includes a 3D-vector of angular parameters. *Command pose* is defined as the pose specified through teach programming, manual data input or explicit programming. *Attained pose* is defined as the pose achieved by the robot under automatic mode in response to the command pose.

The quantification of the deviations which occur between the command pose and the attained pose is defined as *robot pose accuracy* [ref. **93**]. The quantification of the fluctuations in the attained pose which occur for a series of repeat visits to a command pose is defined as *repeatability* [ref. **93**]. These are performance parameters that have evolved from on-line programming of industrial robots. When considering off-line programming, the *absolute accuracy* characteristics of the robot must be taken into account, since here externally generated co-ordinate data are used in much the same way as is done with CNC part programming [ref. **87**]. The *absolute accuracy* of an industrial robot is the machine's ability to achieve a specified set of co-ordinates relative to its World Co-ordinate Frame [ref. **94**]. Hence, the need for an accurate geometric model of the links and joints of the robot is essential.

In order to improve the robot accuracy, it is necessary to perform a robot calibration. Bernhardt and Albright [ref. **94**] have defined robot calibration as the term applied to the procedures used in determining actual values which describe the geometrical dimensions and mechanical characteristics of a robot structure. These are classified as kinematic and dynamic parameters. Kinematic parameters primarily describe a robot's arm lengths and relative joint-axis orientations while dynamic parameters primarily describe arm and joint masses and internal friction.

There are two main types of robot calibration [ref. **94**]: *static* and *dynamic*. Static calibration is an identification of the parameters which influence primarily the static positioning characteristics of a manipulator. It is used to identify the actual internal robot features such as joint-axis geometry, joint angle off-sets, actuator/link compliance, actuator transmission and coupling factors. All these factors may have an influence to a certain degree on the static positioning accuracy of the robot. On the other hand, dynamic calibration addresses the parameters which influence the motion characteristics. Once a robot's static parameters are identified, a dynamic calibration can take place. This type of calibration is used to determine the dynamic related characteristics of the robot structure (e.g. distribution of mass in the links, friction in actuators and joints, stiffness, etc.). Internal characteristics such as friction tend to be difficult to identify accurately, due to their coupling with other dynamic parameters [ref. **94**]

Whatever the calibration type is (static or dynamic), a similar general procedure for the identification of the unknown parameters is used. This normally starts by modelling the robot system, followed by measurement of appropriate inputs/outputs or internal reactions (e.g. position, motion, force, torque, etc.) and then ending with identification and verification of actual parameter values. The identification is performed by minimising an error function which is obtained by comparing the model computed tool positions with the measured positions. This is called *forward calibration* [ref. **91**].

Another type of robot static calibration reported in the literature is the *inverse calibration* [refs. **91, 95, 96**], in which several points in a region of the workspace are measured precisely and compared with the points reported by the robot measuring system. An empirical (or table look up) relationship is then determined. This kind of calibration does not need system modelling, which can sometimes be very difficult. Furthermore, it may be possible to obtain a better match of the system. However, it usually requires more measurements and does not provide much insight to what caused the error.

The implementation of the calibrated model can be performed in two different ways [ref. **91**]: a) *Real time inverse kinematics* and b) *Off-line inverse solution*. The first method is based on the substitution of the incorrect model by the calibrated one in the robot controller. This results in a very accurate robot movement. The second method uses the calibrated model for adjusting the command poses in such a manner that the attained poses correspond to the required world co-ordinate points. The *Real time inverse kinematics* method cannot always be implemented, since the calibrated model is normally more complex than the nominal model. The off-line inverse solution is directly applicable in off-line programming systems. However, this technique does not provide the same levels of accuracy as the *Real time inverse kinematics* method [ref. **91**]. One example of *off-line inverse solution* was described by Owens and Piatkowski [ref. **97**] when applying Workspace® and Robotrak to calibrate a waterjet-cutting robot workcell.

2.4.3 Cell calibration

The calibration issues discussed before addressed mainly the calibration of the robot arm. Another important factor in off-line programming is the calibration of the robot workcell. The relative positions of the several components of the cell must be known to the programmer for an accurate modelling of the robot environment. The measurement of the relative positions of the several cell components can be performed in several ways, the most simple being the one which uses the calibrated robot as a measuring device [refs. **87, 88, 98**].

2.4.4 Assessment of programming errors [ref. 87]

According to the definition given in section 2.2.1, a robot needs to be programmed in order to perform a specific task. Depending on the method of programming, different types of programming errors may occur.

Whatever the on-line programming method used (*manual lead-through* or *teach pendant programming*), the errors that can arise are normally due to variations in workpiece positioning and workpiece dimensional tolerances. In the case of lead through programming, additional errors due to mechanical flexing during programming may occur. The robot's relatively poor absolute accuracy is no longer an issue, since programmed points are set relative to the workpiece.

When using off-line programming, further to the errors caused by misplaced workpiece and by workpiece tolerances, faults might also happen due to perfect kinematic models being used by both the simulation and the real robot controller to drive an imperfect robot arm. Other sources of error can be found, such as geometric

and kinematic model mismatch and the use of incorrect inverse kinematic algorithms in the simulation program.

If the off-line programming method is based on language programming, in addition to the errors mentioned above, the difficulty in visualising cell components in space may result in collisions.

2.4.5 Workpiece tolerances and positioning

In an industrial environment, the components and tooling are designed in such a way that they allow small dimensional errors on their nominal values. When parts are assembled together for a subsequent welding operation, joint fit-up errors often appear in the form of joint misalignment and gap variation. These dimensional variations may increase as a result of inaccurate or worn press tools being used for shaping the parts to be welded These discrepancies are called manufacturing tolerances. The combination of parts and tooling tolerances with joint fit-up errors result in considerable variations in the joint shapes and positioning with relation to what has been designed. In addition, thermal distortion during the welding process can cause on-line joint movement. These problems are easily compensated for by a skilled manual welder. However, in robotic welding, they can cause serious quality problems, like undercut, poor weld profile, insufficient penetration and burn-through. [refs. **87, 89, 99, 100, 101**]. Hence, tighter tolerance levels are required for robotic welding.

2.5 Common production problems with robotic welding

Although robotic welding produces higher quality welds than the human welder, this is only true when conditions are right. The welding process is prone to faults not only in terms of workpiece variations, but also because of the rugged environment imposed to the equipment. Apart from inadequate welding parameters and from workpiece variations several problems can occur in robotic welding, among which the most typical are given bellow. [refs. **21, 102, 103**]

- *Wire feed slip*: Caused by dirt/grease on the feed rollers, wear on the rollers (grooves), wear in the contact tip and/or conduit, inadequate pressure on the rollers, surface contamination on the wire, dynamic effect of rapid robot motion between welds, etc.
- *Contact tip wear*: Usually caused by normal friction between the moving surfaces but consistency of wear is dependent on electrical contact characteristics and arcing within the tip.
- *Contact tip fusion*: Sudden burnback of the electrode particularly during arc ignition causes the electrode wire to fuse to the contact tip.
- *Failure to strike the arc*: caused mainly by burnback at the start of welding.
- *Wire sticking in the weld pool*: Inadequate burnback control at the end of a weld can lead to the wire sticking to the weld pool.
- *Spatter build-up around the nozzle*: Hot spatter is normally ejected during welding, sticking to most surfaces. Due to its proximity to the source of

spatter the gas nozzle is particularly affected. The accumulation of metal particles can cause turbulence on the shielding gas, which may draw some air into the shielding, inducing weld bead defects such as porosity and oxidation. This effect can be minimised by using torch cleaning stations, usually consisting of a wire brush arrangement to which the robot drives the torch periodically. A stable process also minimises the need for torch cleaning.

- *Consumables running out*: e.g. shielding gas and welding wire.
- *Torch overheating*: due to blockage in water line, or water cooling system failure.
- *Faulty lead connections*: Increased resistance due to corrosion or loose connections affects the voltage drop across the torch.
- *Robot faults*: Generally complete failure is rare but increased backlash in the gears, servo overheat and instability cause changes in travel speed and accuracy, juddering etc.

Most of these are mainly technological problems which can be dealt with by using proper maintenance procedures, carried out periodically, and by utilising some kind of fault detection system such as the ones reported in references **21, 102** and **104**.

On the other hand, faults due to workpiece variation and workpiece positioning are more difficult to deal with, since they depend on each part component. For example, if the joint is placed in a position which differs from the programmed weld path, the weld bead will be deposited in the wrong place. This may lead to bead asymmetry relative to the joint axis, which may cause lack of fusion on one side of the joint, or the robot may miss the joint completely, hence not welding the parts together. Conversely, the robot may accurately follow the seam but if a gap exists and it is wider than the allowable process tolerances, the gap will not be bridged and, consequently, burn-through will occur or the two parts will not be joined. In some applications, distortion due to heat during welding can also cause excessive gapping.

These problems can be minimised by: a) tightening the tolerance levels of the pre-welding operations such as part cutting and joint fit up [refs. **89, 105**]; b) modifying the component design approach [ref. **105**]; c) improving the weld fixture design [ref. **104**]; and/or d) using some kind of adaptiveness [refs. **87, 88**].

2.5.1 Tolerance requirements

The tolerance requirements in welding are generally related to the fulfilment of weld quality demands, which are normally set in the design stages according to standardised weld quality specifications [ref. **106**]. These usually provide the general minimum quality requirements and limitations for the various types of discontinuities commonly encountered in welds (e.g. American Welding Society Standard AWS D8.8-79 [ref. **107**]).

For weld quality assurance, it is necessary that the torch and wire electrode are guided within permissible limits relative to the centreline of the weld joint [ref. **106**]. Tolerances are determined by welding position, type and size of weld, selected process variation, welding power, etc. [refs. **106, 108**]

As a general rule, the welding process tolerances must be greater than or equal to the combined errors associated with positioning and orientation of the arc and the variability in joint fit up [ref. **105**]. The main factors which have an influence on the positioning of the wire relative to the joint centreline are [ref. **106**]: a) torch guidance; b) part positioning ; c) the straightness of the wire stickout. According to Stenke [ref. **106**], the joining tolerance, T_J , can be determined by applying equation (2.7).

$$T_J = \sqrt{T_W^2 + T_T^2 + T_C^2} \leq T_G \qquad \textbf{(2.7)}$$

where:

T_W is the wire positioning tolerance;

T_T is the torch guidance tolerance;

T_C is the component tolerance (assembly and positioning).

The resulting allowable joining tolerance must be less than the ability of the process to bridge gap tolerances (T_G).

The first two factors have already been discussed in the former sections. The third factor, the potential misalignment of the wire electrode caused by varying radii of spooling and by torch curvature, is an important element when considering robotic welding since, depending on the relation between the wire spooling plane and torch plane, the resulting wire ring diameters will differ in size. The varying radii of wire bend and variations in the contact tube-to-work distance affect the wire outlet deviations (see Figure 2.15). In order to reduce the effect of wire bend, two recommendations must be followed [ref. **106**]:

- to use wires that form the largest possible uniform rings after passing through the torch tip;
- to use the shortest possible contact tube-to-work distance with as little changes as possible.

Kuk [ref. **108**] has presented a study on the acceptable joint mislocation (see Figure 2.16) in robotic systems without adaptive control. In his study he has analysed the case of on-line programmed robots, for which case, he concluded that the largest sources of joint mislocation could be found in piece part manufacturing tolerances and in the ability of the weld fixtures to locate and hold parts accurately. It is worth mentioning that, in the situation analysed, the robot absolute accuracy did not play an important role, since the robot was taught on-line. Hence, only the effects of robot repeatability, part tolerances and part positioning accuracy were taken into account. The same author came out with a guideline table suggesting the positioning accuracy required for different weld sizes relative to the welding torch. The data from that table is repeated here for reference (see Table 2.1).

Table 2.1: Joint positioning tolerances for robotic arc welding [ref. 108]

Weld Size	*Positioning tolerance*
Up to 3.18 mm (0.125 in)	±0.38 mm (±0.015 in)
3.2 to 6.35 mm (0.126 to 0.250 in)	±0.64 mm (±0.025 in)
Above 6.35 mm (0.250 in)	±1.14 mm (±0.045 in)

Kurkin and Drikker [ref. **109**] investigated the effect of several geometrical factors on the permissible weld path deviation for 4 mm sheet steel in T joints, when using CO_2 and other gas mixtures. From the experimental results, the authors reached the following conclusions:

- the allowable joint deviation relative to the robot path (see Figure 2.16) is increased by increasing the weld leg length, as a result of reducing the welding speed;
- the positioning tolerances increase when using downhill welding;
- transverse oscillations increase positioning tolerances, but reduce the allowable gap. They may also lead to undercutting and lack of fusion defects in sheet metal welding.

Wadsworth [ref. **110**] investigated the effects of welding electrode misalignment relative to the joint centreline on the weld quality, for different transfer modes and welding speeds. The author observed that, for globular mode of metal transfer, the weld quality deteriorates with increasing welding speeds when the electrode is one wire diameter off joint centreline. The reduction in weld strength between a fillet weld made with zero wire offset and one made with the welding wire positioned one wire diameter off the joint was used to evaluate weld quality. For spray transfer, the author observed that the loss in strength was almost constant for the range of speeds studied, 305 to 610 mm/min (12 to 24 in./min)

Middle [ref. **105**] suggests that designers should design welded parts to allow the greatest possible use of flat position welding, which has larger tolerances and the highest productivity rates. The same author proposed the adoption of design procedures such that increased joint fit-up and positioning tolerances could be obtained.

2.5.2 Fixturing

In section 2.5.1, fixturing tolerances have been included in the components' tolerance group. This, however, does not imply that fixturing tolerances are less important than the other contributing factors. Consistent welds require reproducible weld placement and welding conditions. The correct placement of a weld depends on the adequate joint positioning relative to the welding torch path. Consistent joint positioning, in its turn, depends on adequate fixturing, further to joint fit up.

Widfeldt [ref. **104**] suggests that for off-line programming, the design of fixtures should be made utilising the same CAD system as used for designing the

parts, thereby making available for off-line programming correct models for all the welding cell components. The necessity of fixture design modifications due to joint accessibility problems could be easily detected and performed by using graphical simulation. The resulting CAD information should be used to manufacture the fixture.

Other possible sources of error due to fixturing are the presence of spatter or other foreign matter in the locating surfaces of the fixture, fixture wear and thermal expansion which may modify the position of the locating surfaces [ref. **111**].

2.5.3 Dynamic variation

Thermal distortion during welding is another source of variation which can affect the joint geometry during welding by modifying the weld volume (e.g. increasing gap) and also by causing deviation from the initial joint line, which may result in misplacement of the weld bead [ref. **111**]. Therefore, component and fixture design should take into account the thermal distortion in such a way as to minimise its effects [ref. **105**]. In general, the closer the fixture locating surfaces can be placed to the joint the better [ref. **108**]

2.5.4 Contact tip wear

Contact tip wear is another factor that affects the stability of the gas metal arc welding process. The contact tip (usually made of a copper alloy) is responsible for transferring the welding current to the electrode and for directing it towards the workpiece. The inner surface of the contact tip should be smooth so that the electrode slides smoothly and also makes good electrical contact [ref. **2**].

Generally, the hole in the contact tube should be 0.13 to 0.25 mm larger than the wire being used [ref. **2**]. However, due to the friction with the sliding wire and also to adhesion between wire and contact tip during welding [ref. **112**], the hole diameter increases gradually. If the electrode wears a particular area of the contact tip for long enough (as in the case of localised wear induced by wire cast - see Figure 2.17) adhesion between the wire surface and the newly exposed contact tip material will occur[16] [ref. **113**]. This introduces variations in the wire feed speed at the torch, resulting in process instability [refs. **112, 113**]. Furthermore, the worn contact tip will worsen the effect of wire cast, increasing the wire tip mislocation, relative to the joint centreline.

The rate at which the contact tube wears depends on the temperature. Therefore, any factor that might increase the contact tip temperature (e.g. higher welding currents, smaller electrode extension, less efficient external cooling, etc) will accelerate the wearing process [ref. **113**]. Harder wires also accelerate the wearing process but this can be minimised by choosing a contact tip made of a harder alloy (e.g. copper/tungsten alloy) [ref. **103**].

---

[16] The mechanism by which adhesion between wire surface and contact tip occurs is well explained in reference **113**.

In order to minimise the undesirable effects of contact tip wear, periodic contact tip replacements must be made.

2.6 Monitoring and adaptive control for robotic welding

Considering all the aspects of the gas metal arc welding process, robotics applied to arc welding and off-line programming highlighted so far, it is clear that the final quality of a weld carried out by an off-line programmed robot depends on the combination of a series of interrelated factors originated from different sources. In order to have an effective control over the weld quality the extent to which these factors affect the process must be known and controlled. The use of monitoring techniques provides the necessary process information for control actions to be taken.

Norrish and Gray [ref. **88**] suggest that, to ensure adequate performance of off-line programmed robotic arc welding operations, some degree of adaptiveness is necessary in the robot system. This could take the form of a seam tracking facility allied with some on-line monitoring and control system. The authors also suggested the implementation of statistical process control techniques for identification and correction of adverse performance trends before they cause component rejection.

In order to perform process monitoring, sensing techniques and data acquisition must be used. A brief discussion about these topics will follow.

2.6.1 Sensing

Sensing is the term used to define the measurement of qualitative or quantitative information of a process and its environment by means of sensors. A sensor for arc welding is defined as follows [ref. **114**]:

> *"A detector capable of monitoring and controlling welding operation based on its own capacity to detect external and internal situations affecting welding results and to transmit a detected value as a detection signal"*

The measured quantities are normally converted to process useful information either directly, using the measured variable itself, or indirectly, via modelling.

2.6.1.1 Sensors for robotic welding

Sensing in robotic welding can be performed through either *contact sensors* or *non-contact* sensors [ref. **51, 115**]. *Contact sensors* are those which need to have physical contact with the measured medium in order to produce a useful output. The use of thermocouples for measuring temperature, electromechanical probes for measuring torch position relative to joint path and wire touch sensor for searching for the weld joint are examples of contact sensing in welding [ref. **115**].

Non-contact sensors, on the other hand, use the arc characteristics (voltage and current), sound, electromagnetic devices and/or optics to extract information about the process and torch positioning relative to the joint [ref. **115**].

Concerning the time when the sensor is used, three techniques can be identified [ref. **51, 116**]: a) pre-weld sensing, b) real-time sensing, c) post-weld sensing.

In the literature, three main applications of sensors in robotic welding can be identified: a) joint location, b) joint tracking, c) joint recognition, d) weld recognition

2.6.1.2 Joint location

Joint location is defined as a form of adaptive control which recognizes, before welding, the position of the joint to be welded and instructs the machine to take the appropriate action [ref. **58**].

Many approaches for joint location have been reported [ref. **114**]; the most common method is the *wire touch sensing* [refs. **117, 118, 119, 120**], in which the gas metal arc welding wire is used to search for the start point. In order to accomplish this, the robot is moved to its search start point and a high voltage, ranging from 300 to 600 Vac, low current (≈30mA), signal is applied to the welding wire. The robot then moves according to a chosen search pattern, "probing" for each joint surface, in turn on up to three planes (see Figure 2.18). The surface is detected by loss of voltage as the welding wire earths on the component. Search times can be as short as three seconds per direction.

Other joint location methods make use of ultrasonics (time of flight), proximity sensors (capacitive, inductive) and optical sensors [ref. **114**]. Special attention has been given to optical sensors which are expected to give similar performance as the human eyes in the future [ref. **121**]. One such example was presented by Cheung et al. [ref. **122**] who have described a method of tracking an object by analysing its real-time laser rangefinder data. The method consisted of extracting three-dimensional lines and circles from edge points and then matching these extracted curves to the model of each object, hence obtaining their poses. The edge points were obtained from a pre-processing of each range image. Although the method presented by Cheung et al. [ref. **122**] has been devised for tracking moving objects, it could be used off-line for locating welding joints and start points, before starting welding in a robotic welding cell.

2.6.1.3 Joint tracking

Joint tracking is also defined as a form of adaptive control which monitors changes in the location of the joint to be welded and instructs the welding machine to take the appropriate corrective action. The process is based on the signals provided by suitable sensors and can take place in a preliminary (off-line) scan or in real time [ref. **58**]. Off-line joint tracking, however, does not take into account the effects of thermal distortion during welding. Therefore, it is not suitable for solving problems related to on-line joint movement.

Several joint tracking systems have been reported in the literature, the five main types of sensors being [ref. **114, 123**]:

a) Electromechanical sensors;
b) Inductive sensors;

c) Ultrasonic sensors;
d) Through-the-arc sensing;
e) Optical sensors.

2.6.1.3.1 Electromechanical sensors [refs. **114, 124**]

These sensors often appear in the form of a contact probe which outputs distance changes based on an electric signal with a tracer applied to a grove. The tracer is classified into a one or two degree-of-freedom sensor (see Figure 2.19). It can also be categorised by the output signal, which can be analog, proportional to a distance (potentiometer, LDT[17]) or digital (ON/OFF), based on the application of a limit switch. They have been widely used for a long time but they are slowly being substituted by more sophisticated methods such as through-the-arc sensing and optical sensing.

One major disadvantage of this method is that the sensor must be mounted close to the torch, which can cause problems in joints with difficult access.

2.6.1.3.2 Inductive sensors

These are non-contact sensors normally used for measuring distance from a conducting material. They are based on the principle that when a magnetic flux which interlinks a conductor is subject to change, an eddy current is generated in the conductor in order to compensate for the former change. In the case of a sensor, the magnetic field is generated by a coil, which has its impedance increased when a distance to a conductor increases [ref. **114**].

When these sensors are required to be used in a welding environment, they must have an enhanced design to protect against the generation of welding-induced disturbances due to the arc electromagnetic field and its intense heat. Such enhanced design is accomplished by using different coils for excitation and detection [refs. **114, 125**]. A common approach is to use a magnetic field generation coil and two detection coils [ref. **114**] which are designed based on the same winding number and differential connection so as to inhibit the effect induced by the other magnetic field. In a single coil type, a weak DC current is imposed on a high frequency current and the drop in the DC resistance is used to detect the temperature of the coil and compensate its effect. Practical magnetic sensors present sensitivities of 0.1mm and the scope of measurement distance is 10mm. Depending on the type of joint, different geometrical arrangement of the coils may be used [refs. **125, 127**].

Seam tracking techniques based on magnetic sensors are reported by Nomura et al. [ref. **114**] and Goldberg [ref. **127**].

2.6.1.3.3 Ultrasonic sensors [ref. **114, 126**]

An ultrasonic sensor can be used to measure the distance between the sensor and a base material by determining the time of flight of a ultrasound pulse, which is emitted by the sensor, echoed on the surface of the base material and received by a

---

[17] Linear differential transformer.

receptor. The sensors can also be built in such a way as to perform both the emission and reception of the ultrasound, resulting in very compact designs.

These kind of sensors can be used for seam tracking by either oscillating them over the joint and measuring the distances on various crossing positions, or by using two sensors mounted at 90 degrees, in the case of a fillet joint.

2.6.1.3.4 Through-the-arc sensing

Through-the-arc sensing involves the analysis of the welding current and voltage signals of processes such as gas metal arc welding (GMAW) and gas tungsten arc welding (GTAW) for joint tracking. The arc sensing method requires no additional equipment at the welding head and is applicable to a large number of welding tasks, particularly single pass fillet welds, heavy-section V butt and narrow-gap welding situations on steel. This section will only focus on the through-the-arc sensing techniques for gas metal arc welding.

Through-the-arc sensing is based on the principle that, for a constant voltage power source and constant wire feed speed, a change in the torch-to-workpiece distance[18] results in a change in the welding current, which can be measured.

According to equation (2.2), the melting rate (w_m) depends on the joule heating in the electrode stick-out and on the heat generated by the arc. The joule heating depends on the electrode resistance, which in turn depends on the electrode cross sectional area (A_e), resistivity (η) and length (L_e). Since the welding voltage and the wire feed speed are pre-set welding parameters, it is possible to calculate the distance from the contact-tip to the workpiece, *SO*.

Since the process is in steady state, it can be assumed that the melting rate (w_m) is equal to the wire feed speed (*WFS*) [refs. **128, 129**]. Hence the wire extension (L_e) could be calculated by substituting w_m for *WFS* in equation (2.2) and arranging its terms according to equation (2.8).

$$L_e = \frac{WFS - \alpha I}{\beta I^2} \tag{2.8}$$

In order to obtain the contact tip-to-workpiece distance it is also necessary to calculate the arc length. It is possible to estimate this by using an empirical formula which establishes a relationship between the arc length (L_a), the welding current (I) and the arc voltage (V_a). The empirical formula is shown in equation (2.9). It was obtained experimentally for the GTAW process but can also be applied in the case of GMAW [refs. **128, 129**].

$$V_a = K_1 L_a + K_2 + K_3 I + \frac{K_4}{I} \tag{2.9}$$

---

[18] This can be measured either by the stand-off (distance between the gas nozzle and the workpiece) or by the contact tip-to-workpiece distance. The difference between both is just a constant.

where K_1, K_2, K_3 and K_4 are constants. By arranging the terms in equation (2.9), L_a can be directly obtained as follows:

$$L_a = \frac{(V_a - K_2)I - K_3 I^2 - K_4}{K_1 I} \tag{2.10}$$

It is, however, very difficult to measure the arc voltage directly. Its value must be estimated through the calculation of the voltage drop in the wire extension (V_e). For the spray transfer mode, it is generally accepted that the electrode wire is heated according to Ohm's law as it is fed through the extension length or stick-out [ref. **128**]. There are two approaches for V_e calculation that consider the resistivity as either independent or dependent on the temperature. The second approach is more realistic and was used by Hamoy [ref. **13**] to obtain a relationship, which estimates the voltage drop in the wire extension:

$$V_e = \lambda_1 L_e j - \frac{\lambda_2 WFS}{j} \tag{2.11}$$

In equation (2.11), λ_1 is a constant equal to the effective resistivity at the end of the extension, in units of Ω.mm, λ_2 is a constant depending upon the room-temperature resistivity of the wire, $j = I/A_e$ is the current density in the wire and A_e is the wire cross-section area. Cook et al. [ref. **128**] adopted this relationship for the implementation of a through-the-arc seam tracking system.

The arc voltage can then be obtained by subtracting V_e from the welding voltage, V, as follows:

$$V_a = V - V_e \tag{2.12}$$

The value of V_a is then applied in the equation (2.10), resulting in the arc length, L_a. The addition of L_a and L_e gives the contact tip-to-workpiece distance, SO, which is the figure of interest.

$$SO = L_a + L_e \tag{2.13}$$

In the case of fillet, heavy-gauge V-groove butt and narrow gap joints, by oscillating the welding torch across the joint it is possible to generate an error signal which corresponds to the torch-to-joint deviation. This signal is fed into an adaptive control system which calculates the positioning correction necessary for the torch to track the joint [refs. **128, 129**].

Although this method has been derived for the spray transfer mode of GMAW, it can also be applied to the short-arc (dip-transfer) [ref. **128**] and pulse [ref.

129] modes of metal transfer. However, its aplication in the short-circuit transfer mode is very limited [refs. **114, 130**].

Philpott [refs.**21, 131**] observed that the sensitivity of the former method to variations in contact tip-to-workpiece distance decreased with decreasing welding current and that in dip mode of metal transfer it was not adequate for seam tracking. He therefore proposed a different method for dealing with this mode of metal transfer: only the short-circuit phase was modelled. According to the author, such an approach is beneficial for seam tracking in thin gauge plates such as the automotive pressings. His method is described in the following paragraphs.

At the short circuit, there is no arc and the electrode is in contact with the weld pool. Hence, the arc length $L_a = 0$ and, from equation (2.13), the contact tip-to-workpiece distance SO becomes:

$$SO = L_e \tag{2.14}$$

The welding circuit during the short can be considered to be a solid metal conductor. The relationship between the welding voltage and the welding current in the short circuit is given by the Ohm's law ($V=IR$), and the resistance R is proportional to the wire length and inversely proportional to its cross sectional area (A_e), as shown in equation (2.15):

$$R = \frac{\eta SO}{A_e} \tag{2.15}$$

where the η represents the resistivity.

Substituting R into Ohm's law results:

$$SO = \frac{A_e V}{\eta I} \tag{2.16}$$

The resistivity of the electrode rises with increase in the temperature and can be related by the temperature coefficient of resistance (σ):

$$\eta = \eta_0(1+\sigma\theta) \tag{2.17}$$

where η is the resistivity at temperature θ ($^{\circ}$C), and η_0 is the resistivity at temperature 0° C. Substituting equation (2.17) into equation (2.16) results:

$$L = \frac{A_e V}{\eta_0(1+\sigma\theta)I} \tag{2.18}$$

Philpott [refs. **21, 131**], based on the observations of Lesnevich [ref. **132**], considered that the average temperature of the electrode and its distribution are not affected by changes in the electrode extension. He therefore concluded that the contact tip-to-workpiece distance is directly proportional to the short circuit resistance (or dip resistance). This is represented by the equation (2.18), in which the temperature, θ, is considered as the average temperature of the electrode, θ_{av}.

Ushio et al. [ref. **130**] studied the dynamic characteristics of the arc sensor in the short circuiting mode of metal transfer in GMA welding. The authors found that characteristic features extracted from the welding current waveform, such as the welding current at the instant immediately before the short circuit and the short circuiting frequency provide a good indication of variation in contact tip-to-workpiece distance. The authors also found that the best response using these parameters occur for oscillation frequencies around 3Hz.

Another approach for modelling the torch-to-workpiece distance was proposed by Kim and Na [ref. **133**]; multiple regression analysis was used to model the welding current as a function of the welding variables (welding voltage, wire-feed speed and tip-to-workpiece distance). The regression model took into account the effect of individual factors and two factor combinations, as shown in equation (2.19):

$$I = K_1 + K_2V + K_3WFS + K_4SO + K_5V \cdot WFS + \\ + K_6WFS \cdot SO + K_7V \cdot SO \qquad (2.19)$$

where K_n , n=1..7, are regression constants, V is the welding voltage, SO is the contact tip-to-workpiece distance and WFS is the wire feed speed.

Rearranging the terms of equation (2.19), the relationship between welding current and tip-to-workpiece distance was obtained as follows:

$$I = (K_1 + K_2V + K_3WFS + K_5V \cdot WFS) + (K_4 + K_6WFS + K_7V)SO \qquad (2.20)$$

This relationship was claimed to be successfully applied for seam tracking of V-groove butt joints by oscillating the welding torch across the joint [ref. **133**].

The same technique was adopted by Ogunbiyi [ref. **51**] for monitoring and controlling the GMAW process. The model devoloped by the author [ref. **51**] is of the form:

$$I = K_1 + K_2WFS + K_3SO \cdot V + K_4SO \cdot WFS \qquad (2.21)$$

where K_n , n=1..4 , are regression constants, WFS is the wire feed speed, V is the welding voltage and SO is the contact tip-to-workpiece distance.

Considering that changes in tip-to-workpiece distance can be estimated from the deviation of the welding current from a reference value and that when the process is controlled at regular intervals a new reference value must be determined from

experimental trials, Ogunbiyi proposed the model shown in equations (2.22) and (2.23) for estimating variations in contact tip-to-workpiece distance.

$$\Delta SO_j = \phi \sum_{i=1}^{j} (I_i - I_{i-1}) \qquad (2.22)$$

$$SO_j = SO_{ref} + \Delta SO_j \qquad (2.23)$$

where ΔSO_j is the estimate of the stand-off variation at the j-th sampling interval, SO_{ref} is the reference stand-off, I_i is the average welding current at the i-th sampling interval and ϕ is a variable which depends on the welding voltage (V) and the wire feed speed (WFS), according to equation (2.24). ϕ was obtained by differentiating both sides of equation (2.21) with relation to SO while keeping the other parameters constant.

$$\phi = \frac{1}{K_3 V + K_4 WFS} \qquad (2.24)$$

where K_3= 0.1223 and K_4= -0.7396 are the regression analysis coefficients, which were obtained for 1mm (BS 2901 A18) mild steel wire and BOC Argonshield 5 (Ar + 5%CO_2 + 2%O_2).

Through-the-arc seam tracking is made possible by oscillating the torch over the joint and by calculating the torch-to-workpiece distance at the right and left oscillation extremes. The most common oscillation method is characterised by a weaving movement provided by the mechanism that holds the welding torch. Due to mechanical restrictions, the maximum movement frequency is normally about 10 Hz. This limitation results in low welding speed, which affects the process productivity. Furthermore, when welding thin sheet fillet joints the fast change of direction at the oscillation extremes may cause instability and undercut [refs. **21, 109**]. Therefore, its application to high speed welding or lap welding for thin sheets is restricted

According to Nomura et al. [ref. **134**], the sensitivity of the arc sensor is greatly affected by the oscillation frequency. The higher the oscillation frequency, the greater the available sensitivity is (for spray transfer). In order to overcome the low welding speed problem and to increase the sensor sensitivity, Nomura et al. [ref. **134**] developed the high speed rotating arc welding process, in which the rotation movement is provided by feeding the wire through a rotating electrode nozzle with an eccentric hole (resulting in an offset applied to the tip of the wire). This system can easily achieve oscillation frequencies of 100 Hz or even more, consequently increasing the sensitivity to torch-to-workpiece distance changes. Hence, this process could be applied to lap welding of thin sheets, besides fillet, V-groove and narrow-gap welding. The conventional welding process (non-rotating arc) normally produces a convex bead with penetration concentrated at the centre. On the other hand, the rotating arc produces a flat bead with smooth surface and less penetration at the

centre. This is attributed to the more uniform heat input and arc pressure distribution over the weld pool, provided by the high speed rotation. Effects on the wire burn-off were also observed in this process. The high speed rotation of the arc induces centrifugal forces to act on the droplets at the tip of the wire, affecting the droplet transfer phenomenon [ref. **135**]. Dominant forces on the droplets at the wire tip are magnetic pinch force, detachment force, rotation centrifugal force, and interfacial force. An increase in rotation speed results in increased centrifugal force, which induces the droplets to become smaller and the transfer cycle to become shorter. Correspondingly, the extent of overheating by arc heat reduces and the heat retained in the droplets (droplet temperature) decreases, resulting in an increased wire burn-off rate [refs. **134, 135**].

The principle by which the rotating arc sensor performs joint tracking is shown in the Figure 2.20 [ref. **136**]. It shows the basic patterns of arc voltage waveform in relation to the arc rotation positions (C_f , R , C_r , L) [19]. When the arc rotation axis is located at the centre of the groove ($\Delta X = 0$), the arc voltage waveform is shown as a broken line, with maximum values at C_f and C_r , and minimum at R and L. It becomes symmetrical at C_f (the front of the rotation). When the welding torch deviates, for example to the right side of the groove ($\Delta X \neq 0$), the wave form changes as shown by the solid line in Figure 2.20. The phase of the waveform advances at point C_f , where it becomes asymmetrical. By dividing the waveform at C_f into left and right, and by comparing the integrated values, S_L and S_R, the desired torch deviation can be detected. In practice, the voltage signal is likely to be distorted at the C_r side, due to the influence of the weld pool. Therefore, the phase angle of the above integration is set empirically to a value less than 90 deg.

2.6.1.3.5 Optical sensing

The optical sensing systems normally are constituted by a light source which illuminates the area of interest, an optical sensor which senses the reflected light, and a data processing system which processes the data acquired by the optical sensor and extracts the desired information, through a suitable algorithm.

In the case of welding, special requirements are imposed on these sensors, since they have to work in a very harsh environment. The intense heat, the arc light whose spectrum ranges from the ultraviolet to the visible wavelengths, fumes and spatter constitute sources of noise that must be dealt with.

Several approaches have been used so far and they can be categorised according to the kind of sensing device [ref. **137**]: (a) photoelectronic sensor; (b) linear sensor; (c) area sensor.

The simplest photoelectronic seam tracking sensors use a photoemitter and collector which are directed at a well defined joint line. Sometimes, it is necessary to use paint or to employ a tape laid parallel to the seam, to ensure that a clear signal is obtained [ref. **3**]. This kind of sensing device can also be oscillated over the joint so that it moves transversely to the seam. The quantity of light received and the sensor position (co-ordinates) at that time are placed in two dimensions. The gap and the groove position are detected and tracking is controlled [ref. **137**]. These systems are

---

[19] C_f : centre front of rotation, R : extreme right position, C_r : back position, L : extreme left position

relatively low cost but can be affected by arc glare. In order to avoid this, devices with specific wavelengths have been used in conjunction with the suitable light sources and filters, which give improved sensitivity.

The linear sensors work with the reflected light that comes from the illuminated area. They consist of a photodiode array or a line transducer and can be disposed over the joint in two different ways: (a) longitudinally or (b) transversely to the joint . In the first case, a semiconductor laser or other point light irradiates the base whereas the linear sensor captures the reflected light. Since the sensor is mounted with a defined angle relative to the base, it is possible to measure its distance from the workpiece through the reflection angle (triangulation). By oscillating the sensing system across the joint its profile can be mapped and used for seam tracking. The 3D information obtained with this kind of sensor is normally referred to as laser range data. Some examples of this kind of system have been reported by Oomen and Verbeek [ref. **138**], Björkelund [ref. **139**], Sicard and Levine [ref. **140**], Bamba [ref. **141**] and Back and Franzen [ref. **142**].

When the second approach (linear sensor transversely disposed) is used, however, the stationary sensor behaves as if it were a point sensor oscillating across the joint. It captures the reflected light and the seam profile can be obtained through the analysis of the levels of brightness of the acquired data. In this case, abrupt changes in brightness means that there is a gap or some area which does not reflect the light. Care must be taken in the analysis, however, since scratches can be misinterpreted as a joint line.

The area sensors, on the other hand, use a camera (e.g. CCD[20] cameras) to capture the image that comes from the joint. Two approaches can be used for determining the position of the joint: (a) the analysis of a structured light strip image or (b) the analysis of the direct image of the objective area.

In the first one, the camera is used to capture the image of a line of structured light which is projected over the weld seam in a transverse direction. The line image is then processed in a computer and the seam position can be calculated. With this technique, not only the joint position can be detected but the joint geometry and the gap size as well as misalignments of edges; angle of joint preparation and tack welds can also be extracted from the image. Most of the systems that use this technique sense the seam at a small distance ahead of the welding torch. Examples of these systems have been reported by Drews and Starke [ref. **143**], Davey et al. [ref. **144**], Niepold and Brümmer [ref. **145**], Nakata and Jie [ref. **146**] and Sameda [ref. **147**].

The laser stripe can be generated by optical techniques [ref. **144**] or by using a mirror to oscillate the laser across the seam [ref.**146**]. The joint profile is reproduced in the video image and this information may be digitised. The difference between the real and a reference image may be used to generate an error signal which is used by the control system to correct the lateral position of the torch. To avoid interference from the arc, a band-pass filter corresponding to the wavelength of the light source is used; in most cases this will be at the red or infrared part of the spectrum, where arc radiation levels are low. Light sources other than laser can also be used but a different

---

[20] Charge-Coupled-Device. These cameras are normally preferred for these applications due to their compact size, robustness and the susceptibility of other kinds of cameras to damage from intense light sources such as welding arcs.

technique must be employed to prevent arc light interference. For instance, Niepold and Brümmer [ref. **145**] developed a special exposure technique, in which the camera was equipped with a special shutter that could be triggered only when the arc was not obscuring the scene (during the short-circuit time of a dip-transfer welding). They have also applied four consecutive laser stripes instead of only one. According to the authors [ref. **145**], the main advantage of this approach lay in the fact that the measurement started from a section of the seam line and not from one point only. This is important, because the seam line can be disturbed locally by alterations such as tacks or spatter.

On the other hand, when structured light is not used, the direct image of the joint scene must be analysed. With a single camera it is difficult to obtain three-dimensional information concerning the joint profile but by using optical viewing systems concentric with the torch, the relative position of the joint may be determined [refs. **3, 148**]. By analysing the position of the joint line in a window of the video image, the lateral error of the torch position can be determined. Although the torch assembly is rather complex, this approach has the advantage that the arc radiation is effectively blocked by the electrode.

Suga et al. [ref. **149**] employed direct image to develop a weld line tracker for automatic TIG butt welding of thin aluminium plates. In order to decrease the effect of the arc light in the image they employed a special-purpose lighting, which illuminated the joint laterally from both sides. This reduced the effect of the arc light in the weld line recognition.

Groom et al. [ref. **150**] developed a V-groove welding seam tracking system based on the analysis of infrared images of the joint. Through an experimentally derived image processing technique, the temperature gradients surrounding the welding torch were extracted and the torch misalignment relative to the joint was determined, providing the control system with the correction signals necessary to correctly position the torch.

The optical systems have received special attention during the last years. According to Nomura et al. [ref. **114**] and Boillot et al. [ref. **121**], the optical sensors should prevail in the future. However, there are some drawbacks for these systems, namely:

1. they are still relatively expensive;
2. maintenance costs are also expensive;
3. they constitute an external equipment to be assembled on the welding torch. This can cause problems when joints with difficult access must be welded.

2.6.1.4 Joint recognition

Joint recognition is again a form of adaptive control which recognises the joint preparation to be welded, monitors the geometry of the joint ahead of the arc and takes the necessary corrective action to compensate for variations. This may be carried out in a preliminary scan or in real time [ref. **58**].

Two approaches are normally used for joint recognition: this can be performed either by a vision sensing system or via through-the-arc sensing.

The same approaches used for seam tracking are normally applied for joint recognition. Through the analysis of laser range data or a laser stripe image it is possible to determine the geometry of the joint, the presence of gap, misalignments, and to provide the control system with error signals necessary for the adaptation of the welding parameters, in order to maintain the desired weld quality.

Changes in joint geometry can be detected by analysing the variation in the welding current and voltage waveforms. With this in mind, Ogunbiyi [ref. **51**] proposed a through-the-arc model to predict gap size during welding, without weaving. Through-the-arc gap detection techniques with torch weaving have been studied by Davis [ref. **151**]. Both research works show that through-the-arc gap detection is possible. However, the proposed method was not robust enough for accurately measuring the joint gap.

2.6.1.5 Weld recognition

Weld recognition is a form of adaptive control which recognises variations in the geometry (including penetration depth) of the weld or weldpool being made and instructs the welding equipment to take the appropriate corrective action [ref. **58**].

The weld recognition techniques also make use of through-the-arc sensing and optical sensing. The arc sensor approaches are based on empirical models developed to predict the weld geometry from the welding current and voltage and travel speed [ref. **54**].

The optical systems on the other hand, can be used to view the weld pool as well as the bead profile in order to generate control actions to compensate for any occurring problems [refs. **11, 152**].

For weld recognition as well as for joint recognition, artificial intelligence such as neural networks and fuzzy logic have been utilised. These techniques have been specially applied for image processing and visual inspection [ref. **153**].

Other methods of sensing the weld include infrared backface sensing (used for penetration control), front face light sensing and voltage oscillation, which are used to detect the oscillation frequency of the pool (used for penetration control), ultrasonic penetration control, radiographic sensing, thermographic sensing and hybrid systems. All these sensing methods have been discussed by Norrish [ref. **3**].

2.6.2 Data acquisition system

VanDoren [ref. **155**] defines a data acquisition system as an electronic instrument, or group of interconnected electronic hardware items, dedicated to measurement and quantization of analog signals for digital analysis or processing.

Data acquisition systems offer specialised computer programs written to digitise, store and analyze the input data normally obtained by using appropriate sensors [refs **154, 156**].

Such systems usually consist of three main blocks [ref. **157**].

- measurement hardware, consisting mainly of sensors and signal conditioning hardware.

- digital hardware, which is basically composed of a digital computer and analog-to-digital (A/D) converters.
- signal processing component, provided by dedicated software algorithms.

2.6.3 Signal processing and interpretation

Signals in general can be classified into two groups, namely: deterministic and stochastic signals. Stochastic signals are those whose behaviour is highly unpredictable, that is, they occur randomly [ref. **155**]. On the other hand, deterministic signals are those that have known characteristics and that can be explicitly described by mathematical and physical models [refs. **155, 158**].

Stochastic signals are affected by random noise but if the noise content is negligible, the process may be regarded as deterministic. It should be noted that the welding current and voltage signals in their unsmoothed states are stochastic. [ref. **51**]

A deterministic signal can be formed from a stochastic signal provided the amplitude or time classes of the signal are formed over a sufficiently long period [ref. **158**]. Theoretically, for a precise information to be extracted from a stochastic signal an infinite record length is necessary and the information based on finite length records must always be qualified by statistical statements referring to the probability of the information being correct within a certain percentage [ref. **159**]. The period for which data is collected (i.e. sampling time) should be sufficiently long such that the mean value of a definite portion of the signal is equal to the overall average of the total signal [refs. **156, 158**] and/or the Fourier transform of data collected over a longer period should not differ significantly from the Fourier transform of the data collected over the initially chosen sampling time [ref. **159**]. This enables statistical analysis to be performed on the signal.

For monitoring gas metal arc welding, sampling times ranging from 100 milliseconds to 1 second and sampling frequencies[21] ranging from 200 Hz to 10 kHz have been reported in the literature [refs. **38, 161, 162**].

The minimum sampling frequency necessary for a sampled data to represent the continuous time signal without aliasing[22] is set theoretically by the Shannon sampling theorem as twice the maximum frequency-component of the signal [ref. **163**]. Sampling frequencies equal to or greater than 8 times the maximum signal frequency are generally used [ref. **163**].

Large amounts of data are usually collected during monitoring, most of this information is not useful for process control. The data need to be reduced to make analysis simpler, faster and to save on storage capacity [ref. **51**].

The most common data processing approach is to break the sampled transient data into its basic statistical features such as mean, minimum, maximum, standard deviation, etc. This is called feature extraction and significantly reduces the data without losing important information, filtering out irrelevant information [ref. **160**].

---

[21] Sampling frequency is the frequency at which the Analog-to-Digital converter acquire and converts the analog signal to a discrete-time signal (series of consecutively sampled data). The data is normally acquired during the sampling time at a fixed sampling frequency.

[22] Aliasing is a term used in control theory to define the distorsion that occurs in a signal when it is reconstructed from a digitized signal which was sampled with a frequency not high enough to fully represent the original analogue signal.

Chawla [ref. **161**] utilised statistical feature extraction together with a windowing technique for monitoring gas metal arc welding transient data. The windowing technique was based on acquiring data during fixed periods of time (windows) and introducing a time interval between windows, thus allowing the capture and analysis of transient welding data over a reasonable length of weld. Each window was considered as independent of the others and a feature extraction was carried out by calculating several statistical characteristics for each data window, as follows:

- Mean value, W_{mean}:

$$W_{mean} = \frac{\sum_{i=1}^{N_W} W_i}{N_W} \tag{2.25}$$

where W_i are the transient data samples and
N_W is the number of data samples acquired in a fixed time period (window).

- Standard Deviation, W_{sd}:

$$W_{sd} = \sqrt{\frac{\sum_{i=1}^{N_W} (W_i - W_{mean})^2}{N_W - 1}} \tag{2.26}$$

- Peak value, W_{pk}:

$$W_{pk} = \frac{\sum_{i=1}^{N_p} Wp_i}{N_p} \tag{2.27}$$

where Wp_i are the transient samples with values greater than W_{mean} and
N_p is the number of samples with this characteristic acquired in a window of data.

- Background value, W_{bk}:

$$W_{bk} = \frac{\sum_{i=1}^{N_b} Wb_i}{N_b} \tag{2.28}$$

where Wb_i are the transient samples with values smaller than W_{mean} and
N_b is the number of samples with this characteristic acquired in a window of data.

- Maximum value, W_{max}:

$$W_{\max} = \max(W_i); i = 1, \cdots, N_W \tag{2.29}$$

- Minimum value, W_{min}:

$$W_{\min} = \min(W_i); i = 1, \cdots, N_W \tag{2.30}$$

- Peak time, W_{Tpk}:

$$W_{Tpk} = \frac{\sum_{i=1}^{N_{Tp}} W_{Tpi}}{N_{Tp}} \tag{2.31}$$

where W_{Tpi} are the periods when the samples are greater than W_{mean} and
N_{Tp} is the number of periods in which the samples are greater than W_{mean}.

- Background time, W_{Tbk}:

$$W_{Tbk} = \frac{\sum_{i=1}^{N_{Tb}} W_{Tbi}}{N_{Tb}} \tag{2.32}$$

where W_{Tbi} are the periods when the samples are smaller than W_{mean} and
N_{Tb} is the number periods in which the samples are smaller than W_{mean}.

The statistical features calculated from equations (2.25) to (2.32) were used by Ogunbiyi [ref. **51**] to model the gas metal arc welding of thin sheet steel.

2.6.4 Process modelling

The effectiveness of a process control system is totally dependent on the models and algorithms handling the dependence between the process input and output variables [ref. **51**].

A model is the representation of a process or part of the process operation in terms of mathematical statements. The process representation can be based on observed behaviour (empirical model), it can be based on natural physical and chemical laws (theoretical model) or it may be a combination of these two approaches (semi-empirical) [refs. **164, 165**].

Empirical models are derived from the relationship between process input and output variables, normally by using regression analysis. The models are subject to the

experimental conditions and are not valid outside the range of the experiment [refs. **165, 166**]. They provide a fast approach to model building without the need for extensive and accurate knowledge of all process variables [ref. **165**]. Theoretical models are developed from first principles, based on the process scientific and physical facts. They are usually more reliable and flexible in predicting the dynamic behaviour of a process over a wide operating range. However, depending on the complexity of the process phenomena, the resulting model equations may be difficult, if not impossible, to solve [ref. **164**].

Semi-empirical models are developed with regard to established fact or knowledge of the process. They combine the advantages of theoretical and empirical models to achieve modelling accuracy. They offer a standardised process modelling strategy, even when the basic principles of the process are not understood [ref. **51**]

2.6.4.1 Experimental design

Experimental design is the process of planning experiments so that appropriate data will be collected for a representative statistical analysis to be performed, to reach valid and objective conclusions [ref. **167**]. The experimental design objectives range from process analysis to developing models for process control and establishing correlation between process inputs and outputs.

The most important part of planning an experiment, after defining the objectives of the investigation, is the identification of the inputs and outputs of the process, i.e. the factors that might affect the process behaviour, within a practical range relevant to the process, and the factors that can be used for assessing this change of behaviour [refs. **51, 167**]. Thought must be given to how the response will be measured and the probable accuracy of these measurements.

Variables in an experimental design are usually categorized into two groups, namely independent variables and dependent variables. Generally, the parameters that are directly controllable, such as machine settings, are chosen as independent variables. The responses of the process to changes in the independent variables are considered as dependent variables. In gas metal arc welding, variables such as tip-to-workpiece distance, welding speed, welding voltage, wire feed rate and gap are often treated as independent variables, whereas welding current and bead geometry are normally considered as dependent variables [refs. **51, 168**].

There are two approaches to experiment design. The planned and the intuitive sequential experiment. The planned approach is usually based on full or fractional factorial designs, while in a sequential experiment a trial and error approach is used, and various input variable combinations are selected using process knowledge [ref. **51**].

Factorial design is an experimental design technique with which, for any complete trial or replication of the experiment, all possible combinations of factor levels are investigated [ref. **167**]. It provides a systematic way of performing the least number of experiments to obtain a maximum amount of information in a multivariable environment. Factorial design is orthogonal by nature, or in other words no correlations exist between process independent variables. Consequently, experimental errors are normally distributed [refs. **51, 169**]. It is only effective, however, for a

process studied over a small range. The experiment is normally planned around a working point [ref. **170**].

Factorial design is now being used routinely in welding applications. It is mainly applied to evaluate how tolerant a procedure is to changing welding parameters [ref. **171**].

If the objective is to develop a model spanning a process operating range, factorial design might be restrictive as the physical combination of some welding parameters might lead to defects and instability. Hence, it is not always possible to use factorial experimental design. Its structure can however be used for initial experimental plan and then adapted to avoid (ie. change for better) unsatisfactory parameter combinations [ref. **51**].

2.6.4.2 Regression analysis

Regression analysis is a statistical way to derive a quantitative relationship between variables [ref. **172**]. It is frequently used to model complex multifactor processes, in which a theoretical approach is not yet fully developed. The models allow for the main quantitative relationships and can be obtained with a comparatively small amount of experimental studies [ref. **166**]. However, it cannot prove cause and effect, since these can only be inferred from physical or chemical principles or direct observation [ref. **172**].

Regression methods are frequently used to analyse data from unplanned experiments, but can also be used for designed experiments [refs. **167, 172**]. The regression models that are normally applied to fit a set of experimental points can have different mathematical structures (e.g. polinomial, multiplicative, exponential, trigonometric) [refs. **51, 167**], the most commonly applied being the polinomial ones, which can be interpreted as an expansion of the relationship investigated into a Taylor series [ref. **166**].

The modelling process consists of two stages, the development of a model structure and the estimation of the model parameters [ref. **166**]. The model structure normally presents the generallised form of equation (2.33).

$$y = f(x_1, x_2, \ldots, x_k) \qquad \textbf{(2.33)}$$

where xi (i=1, 2, ..., k) are independent or regressor variables, y is a dependent variable and f(.) is the regression equation, which can be the true functional relationship between the dependent and independent variables, if known, or an appropriate function which approximates the true functional relationship within the range of the investigated variables [ref. **167**].

The most common regression method is multiple linear regression. Linear in the sense that the response variable is linear in the unknown parameters. Multiple linear regression uses the linear model of equation (2.34) to fit a set of experimental data points [ref. **167**].

$$y = \beta_0 + \beta_1 x_1 + \beta_2 x_2 + \ldots + \beta_k x_k + \varepsilon \qquad \textbf{(2.34)}$$

where y is the dependent variable, xi (i=1, 2, ..., k) are the regressor variables, β_j (j=0, 1, 2, ..., k) are the regressor coefficients and ε, a random error with zero mean.

The regressor coefficients are estimated through using the least squares method, by which the sum of square errors is minimised. The full description of the multiple linear regression method can be found in references **167** and **173** and will not be repeated here.

The regressor variables can assume the form of non linear-functions in such a way that a non-linear curve may be fitted to the experimental points [refs. **167, 173**]. For example, a multiplicative model , as shown in equation (2.35), can be transformed to the form of equation (2.34) by applying logarithms to both sides, as shown in equation (2.36) [ref. **51**].

$$y = \alpha_0 x_1^{\alpha_1} x_2^{\alpha_2} \ldots x_k^{\alpha_k} \tag{2.35}$$

$$\log(y) = \log(\alpha_0) + \alpha_1 \log(x_1) + \alpha_2 \log(x_2) + \ldots + \alpha_k \log(x_k) \tag{2.36}$$

where αi (i=0, 1, ..., k) are constants.

When building a model, a compromise must often be made between the simplicity of the model and the accuracy of the result of the analysis. This requires making decisions about which physical variables are important and should be included in the model [ref. **51**].

In prediction oriented problems, the inclusion of variables that don't contribute to the regression model inflates the error of prediction [ref. **51**]. It is better to exclude from regression variables that are not statistically significant or that are known from previous/practical experience not to have an influence on the process output. However, deleting too many variables could lead to "underfitting" and including too many variables to "overfitting" [ref. **51**].

2.6.5 Adaptive control

To adapt means to change a behaviour to conform to new circumstances. An adaptive controller is a controller that can modify its behaviour in response to changes in the dynamics of the process and the disturbances [ref. **174**]. This implies that linear constant parameter regulators are not adaptive [ref. **174**].

In robotic welding, the term adaptive control is used in a wide sense to characterise the ability of the system to adapt to the changing environment based on the information provided by sensors (see section 2.6.1). Two main control aspects can be identified [ref. **11**]: a) the control of position and orientation of the welding torch relative to the joint (i.e. seam tracking); and b) the control of the welding process variables during welding (i.e. in process control) in such a way to adapt the process to unexpected situations such as presence of gap, variation in plate thickness, etc.

Seam tracking is based on sensing the torch-to-joint relative position and feeding it back to the robot controller in order to correct the torch path. Various sensing techniques are available and have already been discussed in section 2.6.1.3. The controller simply commands the robot movement in such a way that it can track the weld joint.

In-process welding control is a much more complicated problem, since highly coupled and non-linear dynamics are usually present [ref. **175**]. It generally involves three principal aspects: *sensing*, *modelling*, and *control*. The first two aspects have been discussed in the previous sections. The control issue entails defining control objectives and selecting suitable input and output variables to achieve these objectives [ref. **175**].

Cook et al. [ref. **175**] define the objectives of feedback control in fusion welding as to continuously sense and control in the presence of disturbances: a) the placement of the heat source relative to the joint; b) the geometry of the weld reinforcement and fusion zone; c) the mechanical properties of the completed weld; d) the microstructural evolution during solidification and cooling; e) the discontinuity formation. Most published works concentrate on controlling the first four objectives [refs. **175, 176**]. Apart from seam tracking, the geometrical characteristics of the weld bead are the most controlled features, due to their dominant influence on the mechanical properties of the joint as well as the availability of real-time optical measurement methods (e.g. for bead width) and estimation models (e.g. for bead penetration) [ref. **176**].

The variables involved in gas metal arc welding can be classified into two main groups [refs. **175, 177, 178**]: a) *indirect weld parameters* (IWP) and b) *direct weld parameters* (DWP). The indirect weld parameters are the inputs to the process and the direct weld parameters are the outputs. The indirect weld parameters include welding voltage, wire feed speed (or current), travel speed, torch-to-workpiece distance, torch angles relative to the joint, wire diameter, wire composition and shielding gas [refs. **168, 175**]. The direct weld parameters are geometry of the weld, mechanical properties, microstructure, level of discontinuities, etc. [ref. **175**]. It should be noted that some of the indirect weld parameters, such as wire diameter and composition, shielding gas and torch angle are not (or cannot be) varied on line. These do influence the process behaviour, but are normally fixed before welding [ref. **179**].

Two main types of models are normally used for control purposes: a) theoretical models, b) empirical models (see section 2.6.4). In the gas metal arc welding process, the complexity of the physical phenomena involved makes them difficult to model accurately over the entire operating range of the process. Normally, the theoretical models result in a set of non-linear differential equations which always need a numerical solution. For control purposes these models are not applicable, since they cannot be computed in real time. However, they may be useful in developing models that can be applied in design and control of multivariable weld feedback control systems [ref. **175**]. Empirical models, on the other hand, provide simple relationships that can be computed in real time for controlling the process, although, they do not provide much insight on the process phenomena.

Most work on the control of gas metal arc welding use empirical models, obtained by using some kind of process identification. This involves selecting the input and output variables and determining a mathematical relationship that fits some experimental data. This normally results in locally linearised models of the process which can be used for control purposes.

Several different control strategies have been applied to controlling the welding process. Schedule controllers, based on look-up tables, have often been used

for selecting indirect weld parameters suitable to producing the required weld quality, as a response to the bead geometry information provided by sensors [refs. **11, 178, 179, 180**]. Although these controllers are reported to provide the parameter values that most likely suit the observed seam geometry, they essentially work in open loop. Closed-loop weld process control requires the observation of parameters that describe the current state of the process [ref. **178**].

Hunter et al. [ref. **168**] used experimentally obtained steady state models to control gas metal arc welding. The authors [ref. **168**] developed the control models by fitting to equation (2.37) the experimental data obtained from a factorial experiment, in which travel speed, wire feed speed, welding voltage and contact-tip-to-workpiece distance were used as the process inputs and the geometry of a flat position fillet weld, as the output. The authors [ref. **168**] combined the resulting models in a matrix form in order to realise a multivariable controller for the gas metal arc welding process.

$$D = \alpha + \beta S_W^{\delta_1} WFS^{\delta_2} V^{\delta_3} SO^{\delta_4} + \gamma G \tag{2.37}$$

where D is a weld bead dimension (leg length, throat thickness, deposited metal height and fused metal leg length), S_W is the travel speed, WFS is the wire feed speed, V is the welding voltage, SO is the contact tip-to-workpiece distance, G is the gap size, and α, β, δ_i (i=1...4) and γ are constants.

Some authors are using identification techniques to obtain steady-state and dynamic models which are used for developing controllers for welding process. Generally the dynamic models are obtained by fitting first order [ref. **179**], second order [refs. **181, 182**] or higher order dynamics [ref. **181**] to the open loop response of the direct weld parameters to input steps in the indirect weld parameters. This normally results in locally linearised models which implies either the use of robust linear controllers, such as a robust servomechanism control framework as applied by Huisson et al. [ref. **179**], or adaptive control algorithms (e.g. a pseudogradient adaptive algorithm for automatically tuning a proportional integral controller [ref. **181**] or a multivariable one-step-ahead adaptive algorithm for adjusting model parameters in different operating ranges [ref. **182**]). Although good results have been reported, problems were encountered in dealing with gap [ref. **179**] and in implementing a true multivariable control due to the strong coupling between the direct weld parameters [ref. **182**].

More recently, intelligent control techniques have been applied in an attempt to overcome the complicated coupling between welding variables. This normally involves a substantial amount of conditions, or heuristic logic, which is developed based on previous process knowledge. One example of such control systems was presented by Sugitani et al. [refs. **183**], who used heuristic rules and process knowledge to develop an inteligent control system that simultaneously control weld bead height and back bead shape for V-groove butt joints with backing plate, in the presence of varying gap size. The proposed method used the high-current high-speed rotating arc welding process and was based on keeping the arc heat input per unit length of weld bead constant irrespective of root gap. This was accomplished by regulating only the wire feed speed and the welding voltage, such that the excess joint

volume caused by the presence of a gap would be compensated by a change in wire-feed-speed and the arc heat input, by adjusting the welding voltage. The high-current high-speed rotating arc, in this case, produces a keyhole (see Figure 2.21) whose size must be kept constant to ensure a consistent back bead shape. With the proposed strategy, the dynamic equilibrium of the molten metal in the keyhole (see Figure 2.21) was controlled, thus regulating the keyhole size The output from the high speed rotating arc sensor was compared with a reference value (which corresponds to the desired keyhole size) and an error signal was generated. The error signal was used in a proportional control scheme to adjust the values of wire feed speed and welding voltage. Three other control strategies were also tested [ref. **183**]: a) controlling only travel speed according to the gap variation; b) regulating the welding speed and current according to joint geometry; c) keeping the weld heat input per unit length and the wire feed speed constant, irrespective of joint geometry.

Also, knowledge based techniques such as fuzzy logic and neural networks are being applied to weld modelling and control [refs. **152, 184, 185, 186**]. Fuzzy logic based controllers use fuzzy sets to represent linguistic values of the input and output variables of a physical system and describe their relationships by fuzzy *if-then* rules. The idea of fuzzy control is to simulate a human expert who is able to control the system by translation of his linguistic inference rules into a control function [ref. **187**]. Artificial neural networks are highly parallel architectures consisting of simple processing elements which communicate through weighted connections. They are able to approximate functions or to solve certain tasks by learning from examples [ref. **187**]. In the learning process, input and output data are provided, weighted values assigned to the connections within the architecture, and the network (which adjusts the weights by using several criteria) is run repeatedly until the output is accurate to the required level of confidence. The resulting weights are then stored, forming the memory of the network [ref. **188**]. A full description of these techniques and their application for modelling and control can be found in the references **187** and **189**.

2.7 Analysis

This literature review has attempted to cover all aspects involved in robotic welding including the welding process, the use of robots to carry out welding operations and related production problems, off-line programming applied to welding, process monitoring, sensing, modelling and adaptive control.

The review of the literature indicates that off-line programming as applied in robotic welding cannot satisfy by itself the demands imposed by the welding process. Some kind of adaptive control is obviously needed.

There is a tendency towards the use of CAD/CAM systems in welded structures (ref. **85**), from design to the shop floor, in which the robots should behave like CNC machines. For this tendency to become widespread a need for adaptive systems (i.e. monitoring and control systems) is imperative. Although monitoring systems for welding are commonly available, very few are used integrated with off-line programming.

The aim of this work, therefore, is to develop the integration concept between an adaptive control system, off-line programming and a robotic welding system and to build and test the integrated system for robotic welding of sheet steel. The concept developed is fully described in chapter 3.

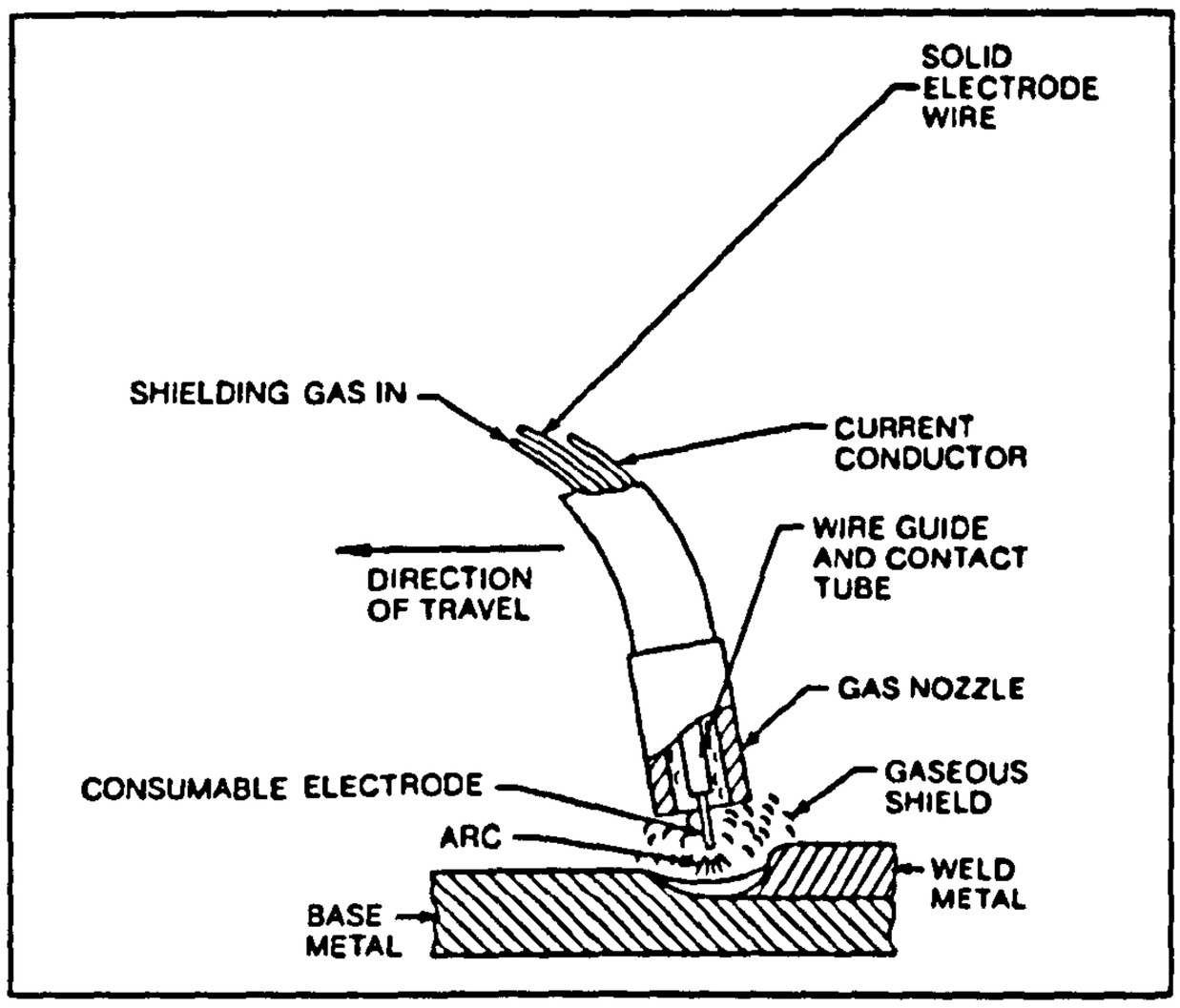

Figure 2.1 Gas Metal Arc Welding Process [ref. 2]

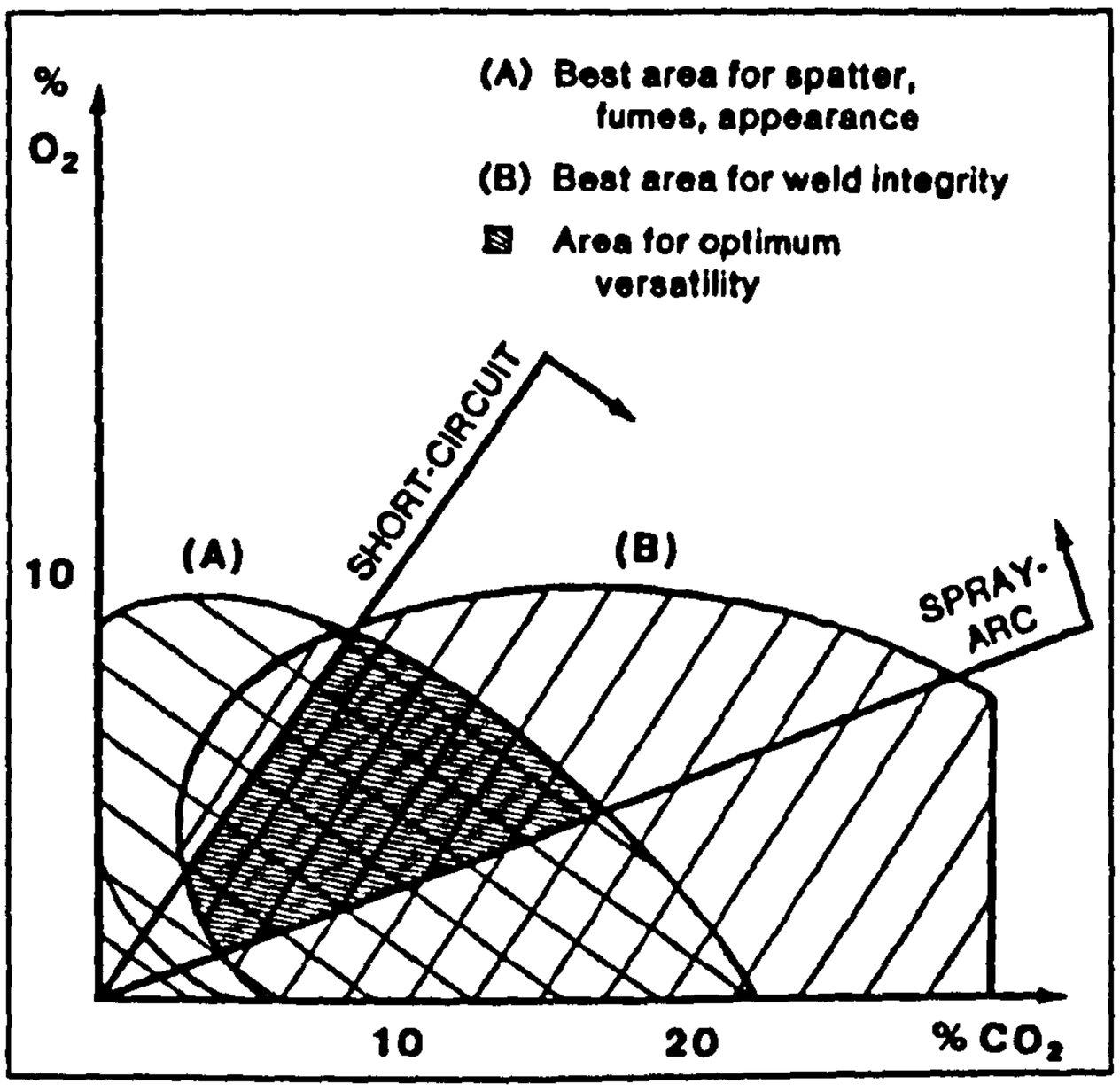

Figure 2.2 - Guide for the choice of $Ar+O_2+CO_2$ mixtures [ref. 4]

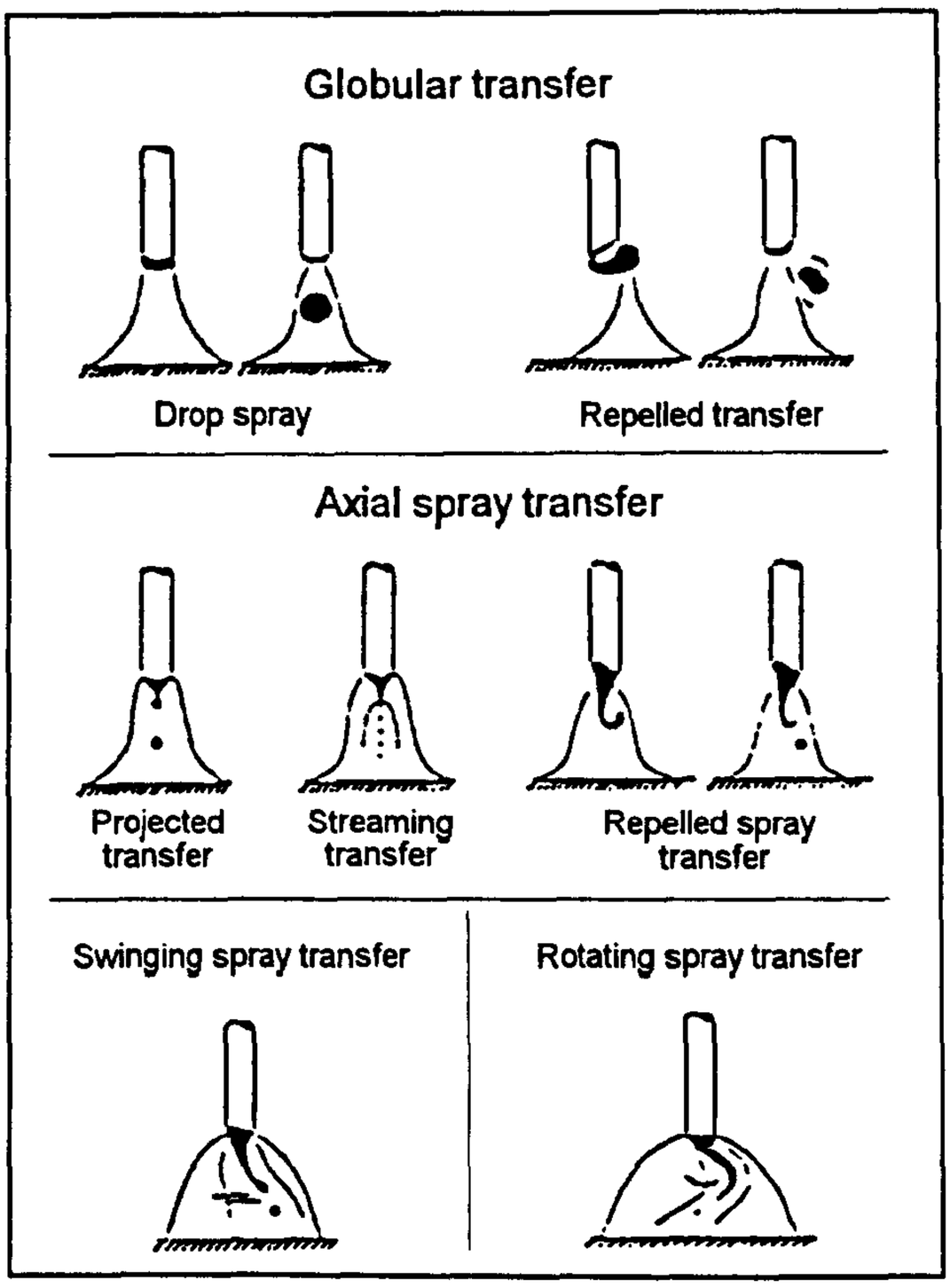

Figure 2.3 - Free-flight metal transfer [ref. 7]

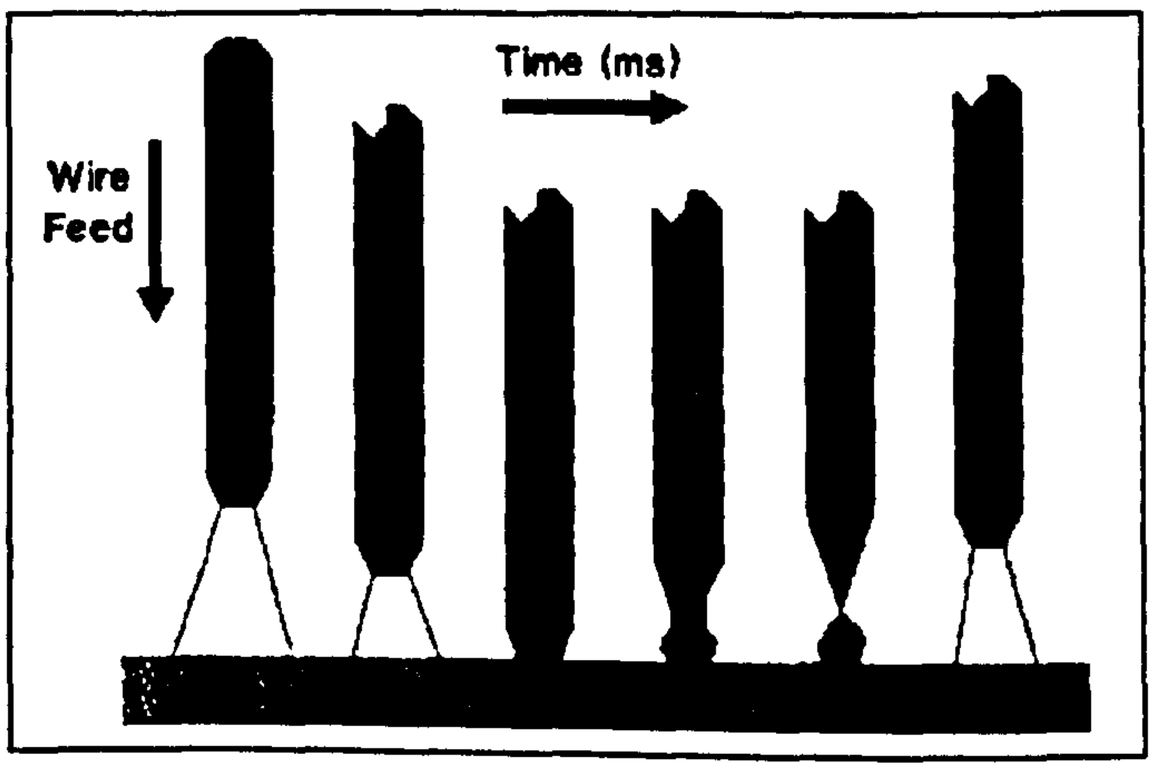

Figure 2.4 - Mechanism of dip transfer [ref. 3]

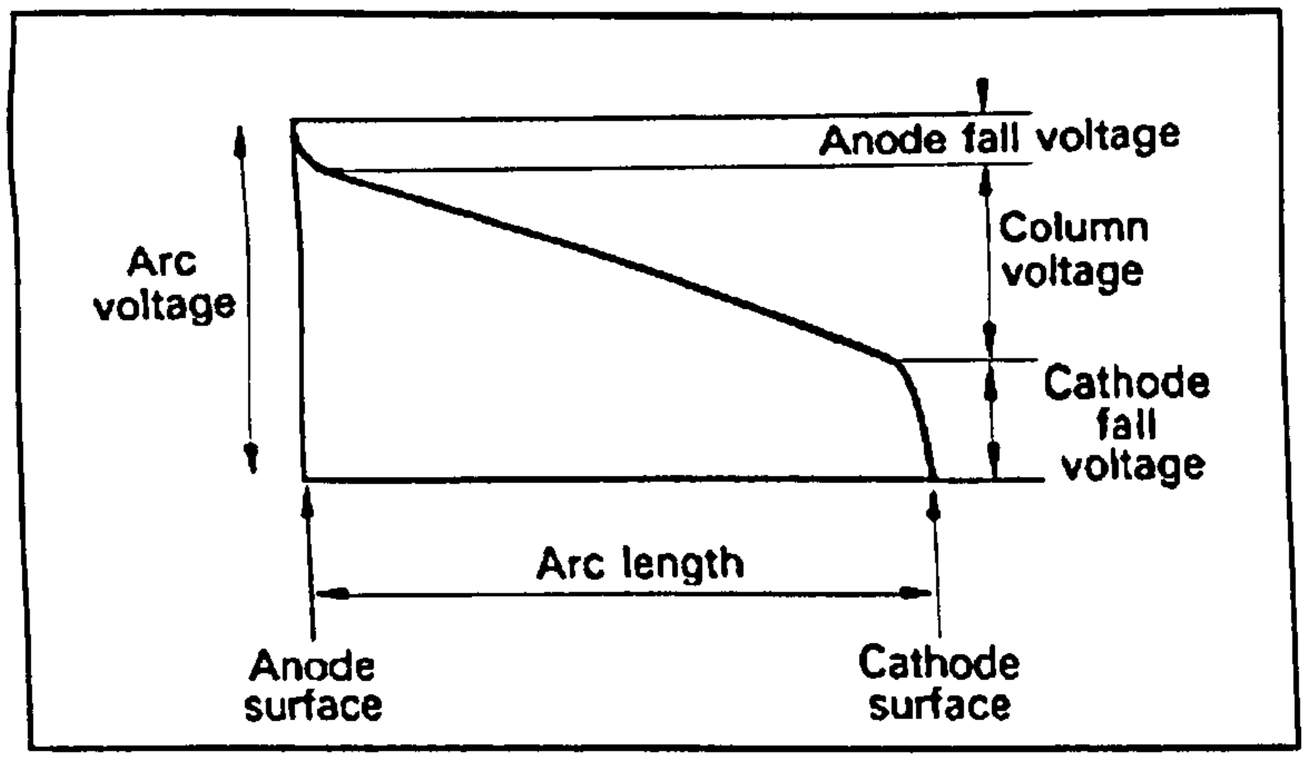

Figure 2.5 - Voltage distribution along an arc shown in diagrammatic form [ref. 6]

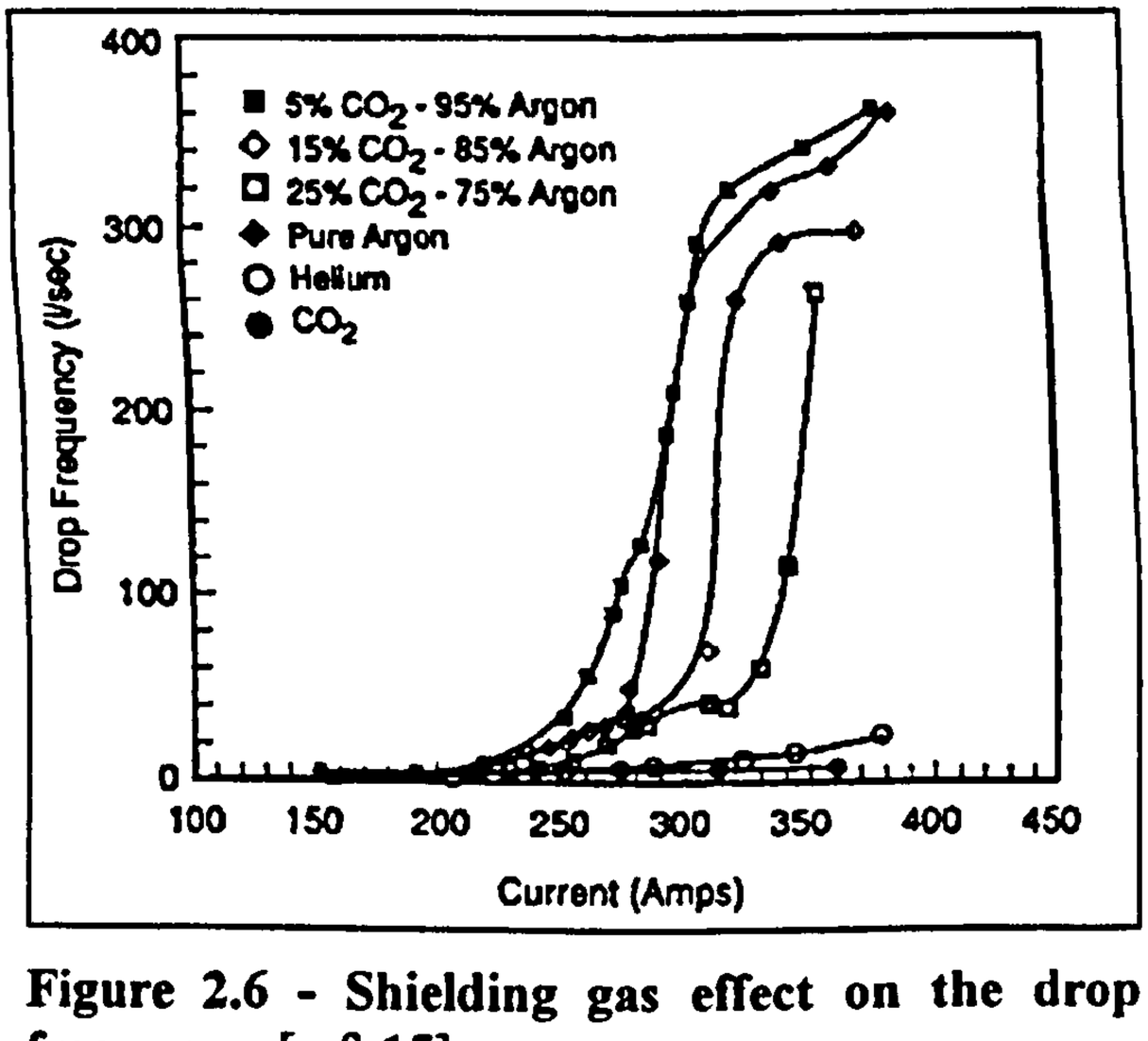

Figure 2.6 - Shielding gas effect on the drop frequency. [ref. **15**]

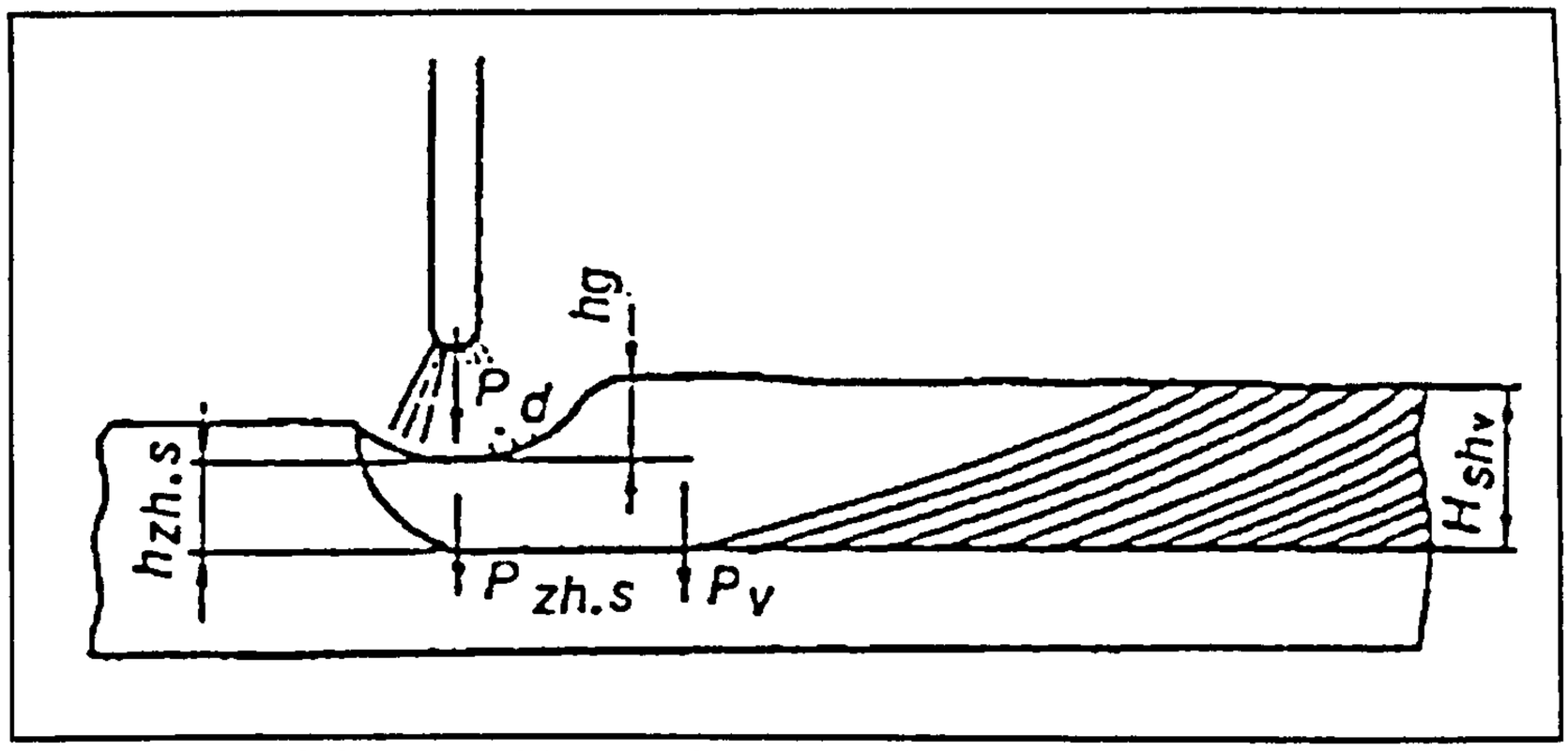

Figure 2.7 - Diagram illustrating the distribution of pressure in the weld pool [ref. 16]

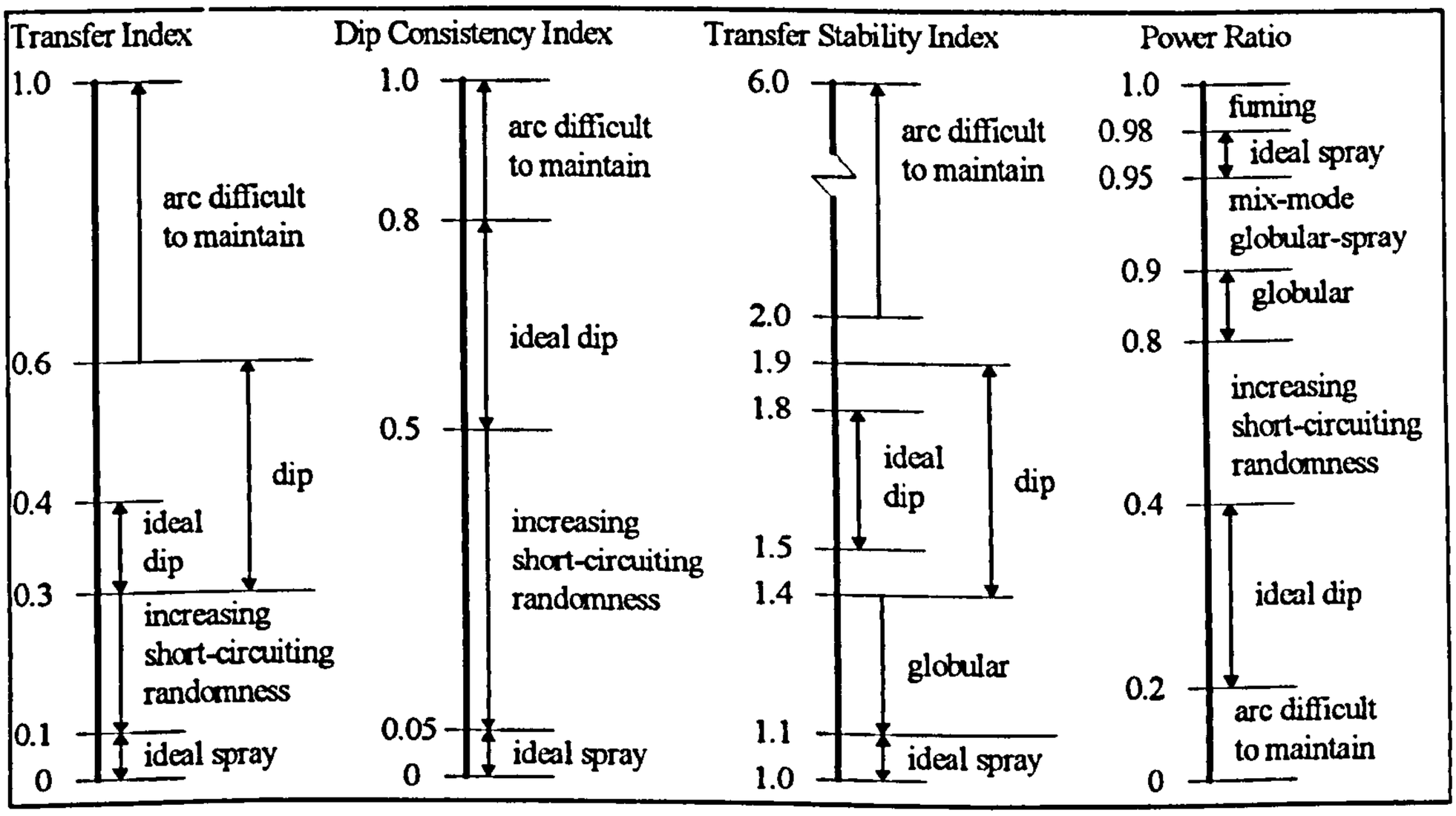

Figure 2.8 - Chart for stability assessment through Ogunbiyi's monitoring indices [ref. 51]

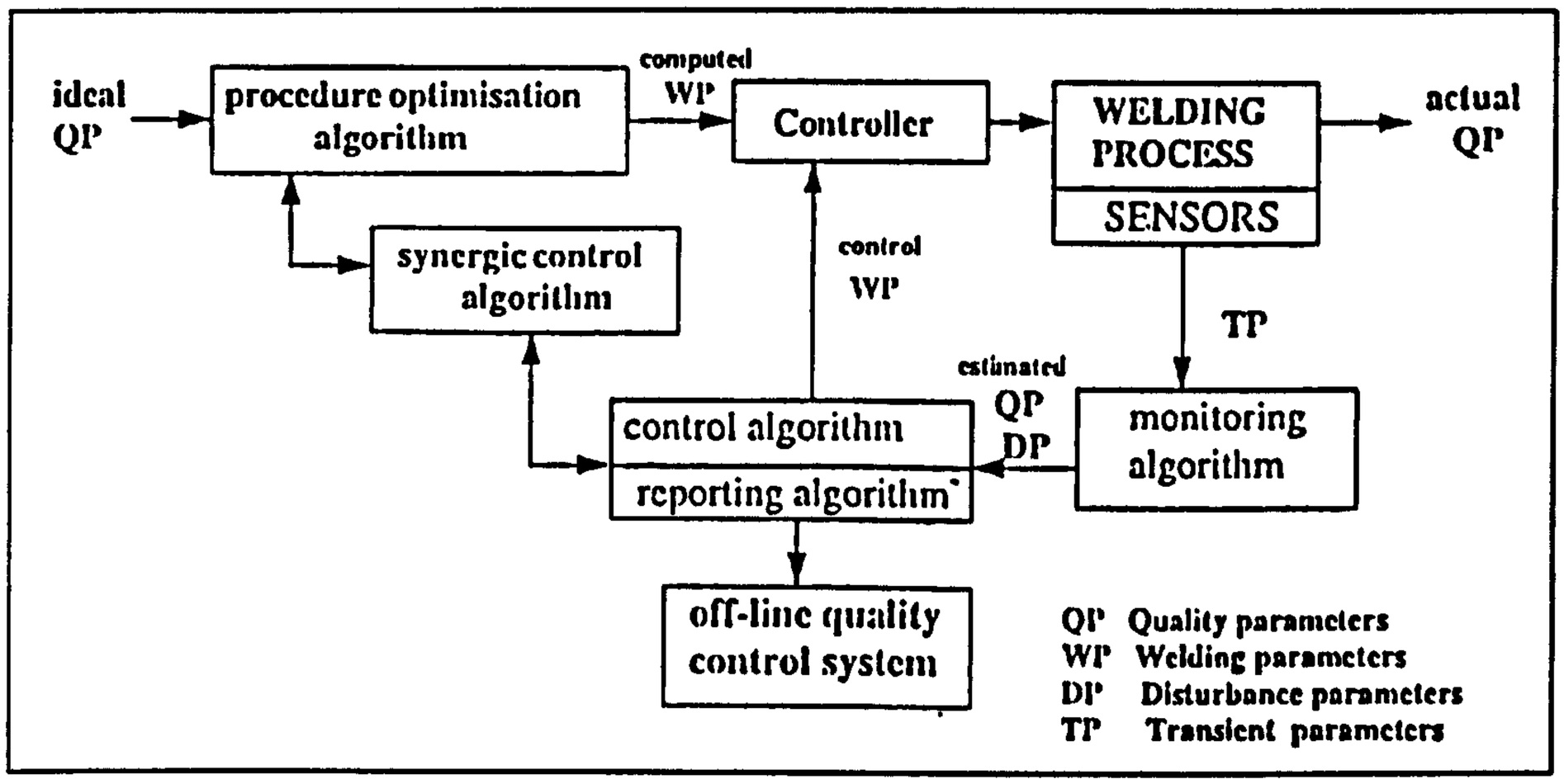

Figure 2.9 - Adaptive quality control concept proposed by Ogunbiyi [ref. 51]

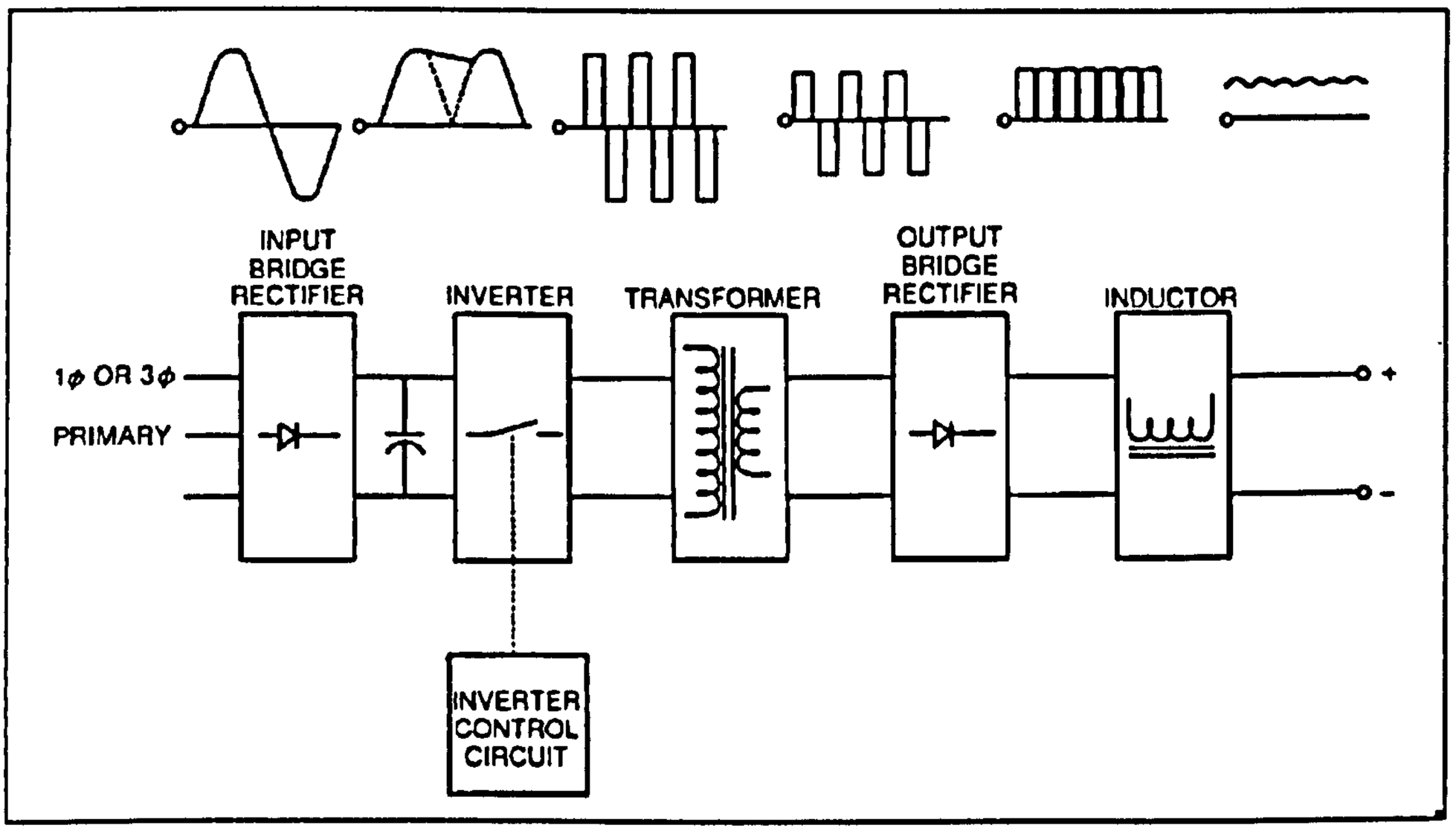

Figure 2.10 - Schematic design of a typical inverter-controlled welding power source. [ref. 2]

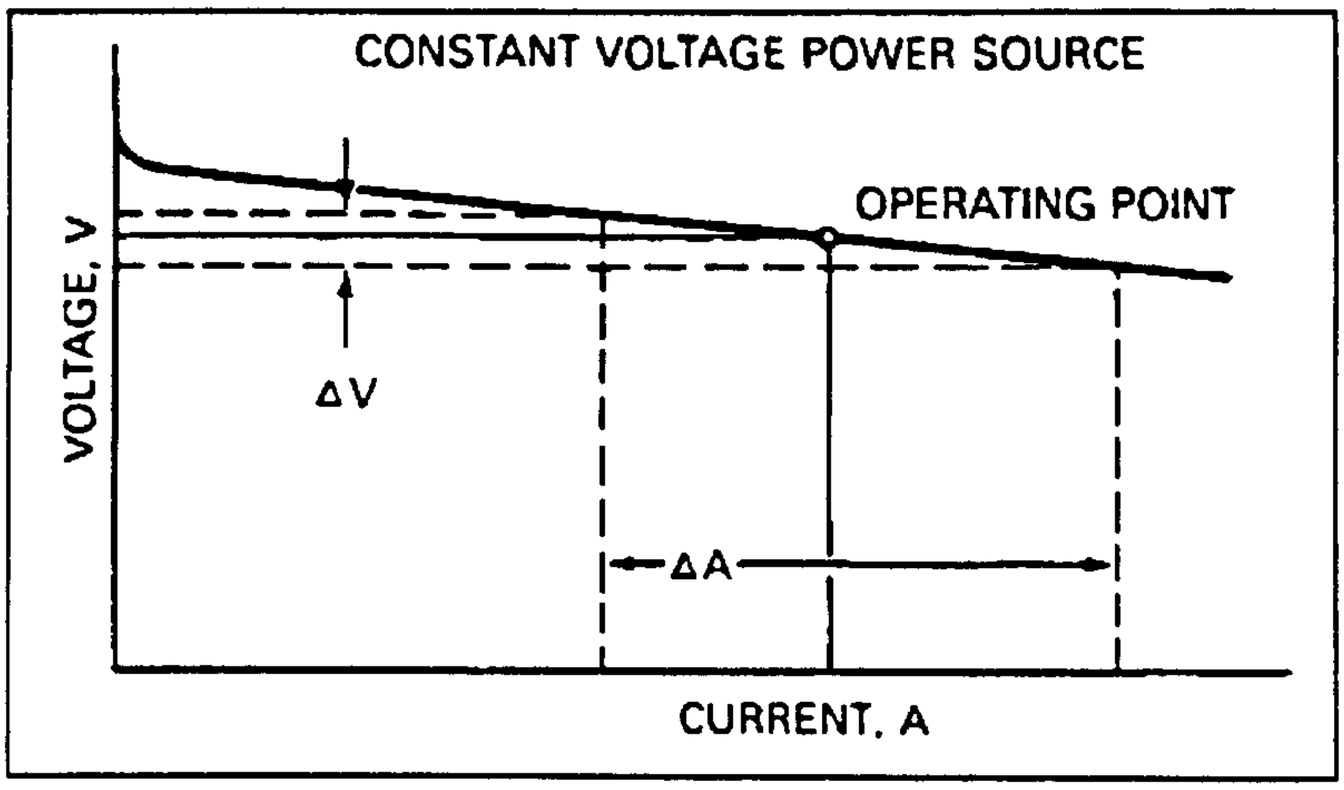

Figure 2.11 - Volt-ampere output relationship for a constant-voltage power source [ref. 2]

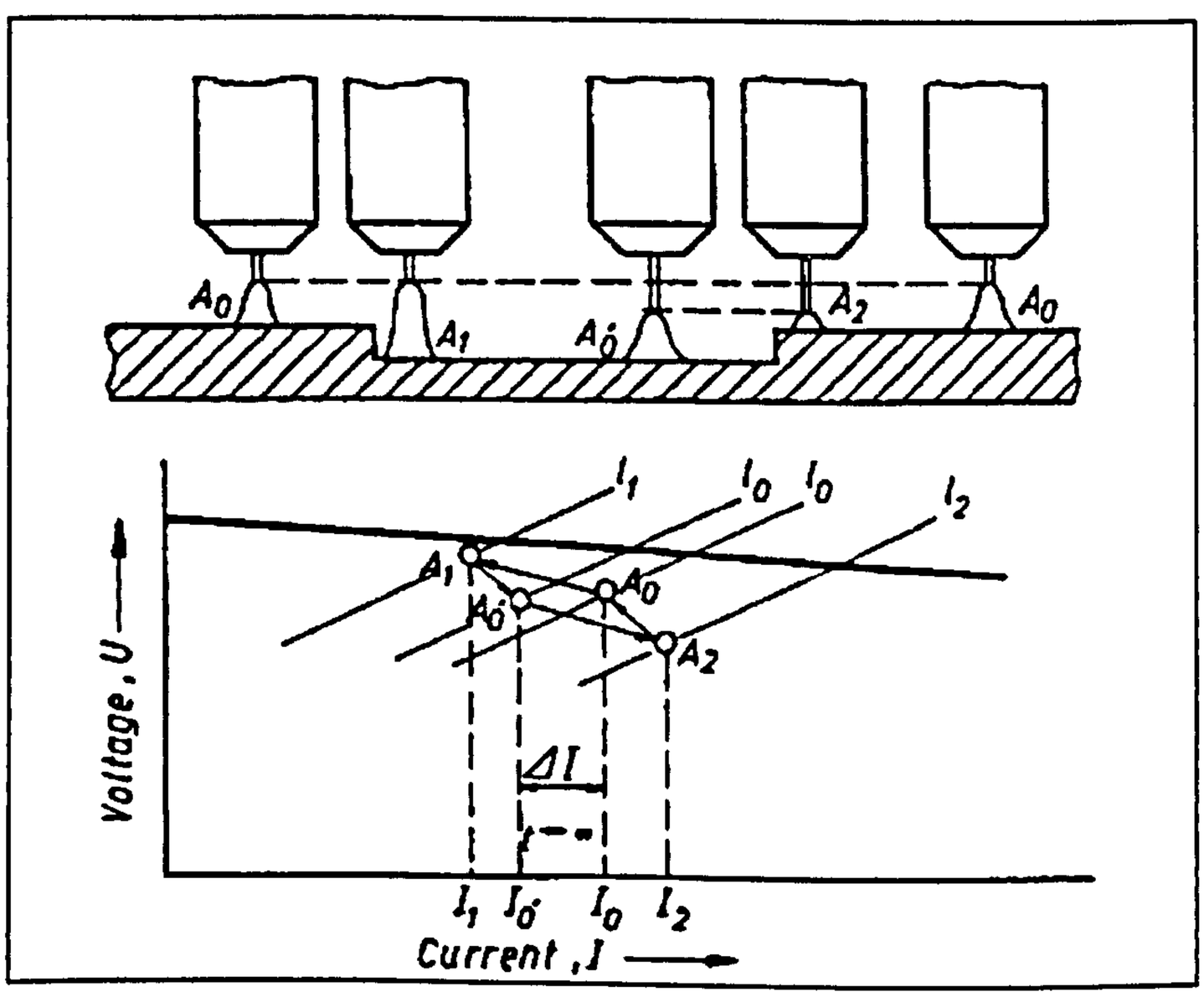

Figure 2.12 - The welding arc self-adjustment [ref. 64]

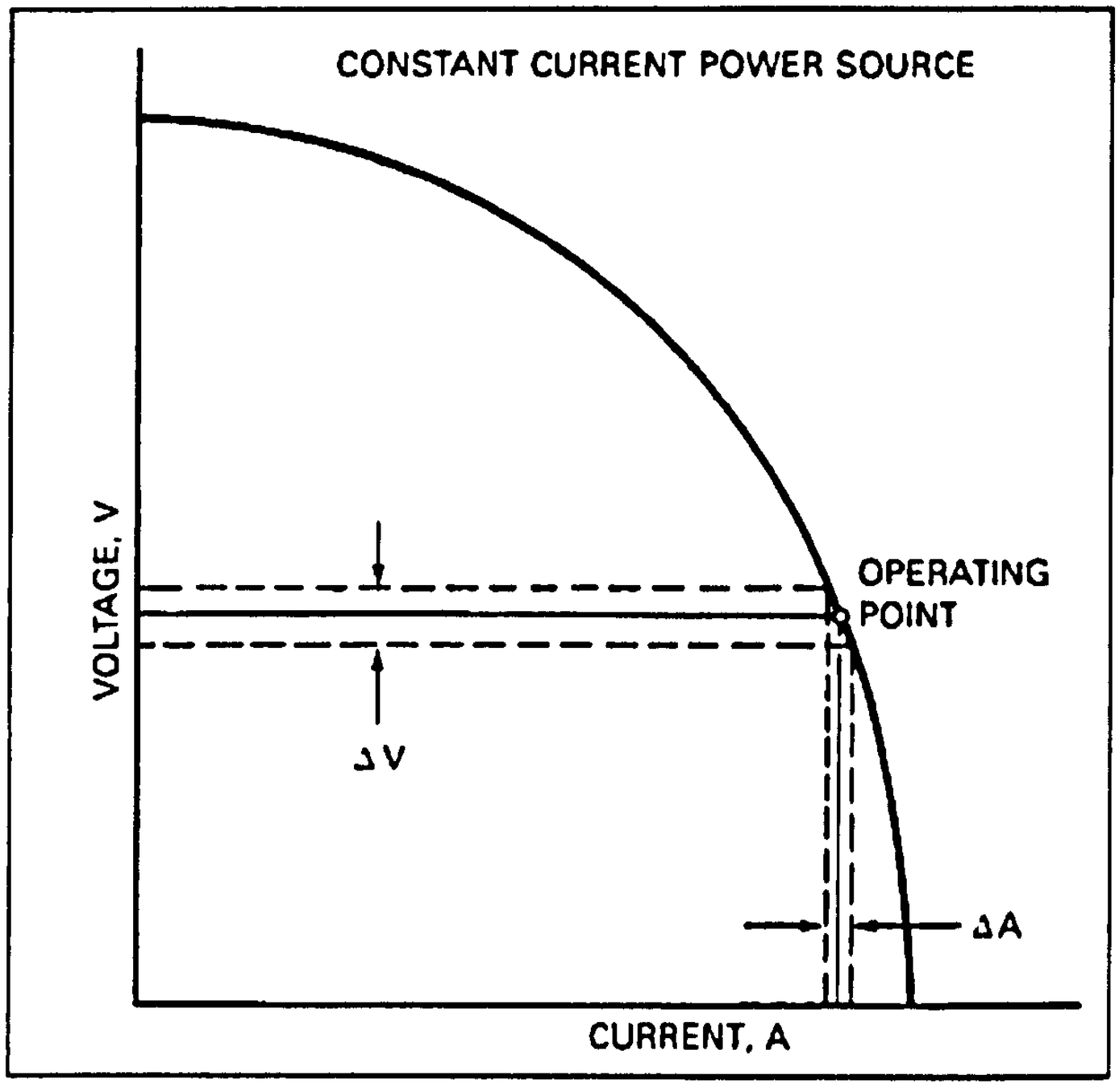

Figure 2.13 - Typical volt-ampere characteristic for a constant-current power source. [ref. 2]

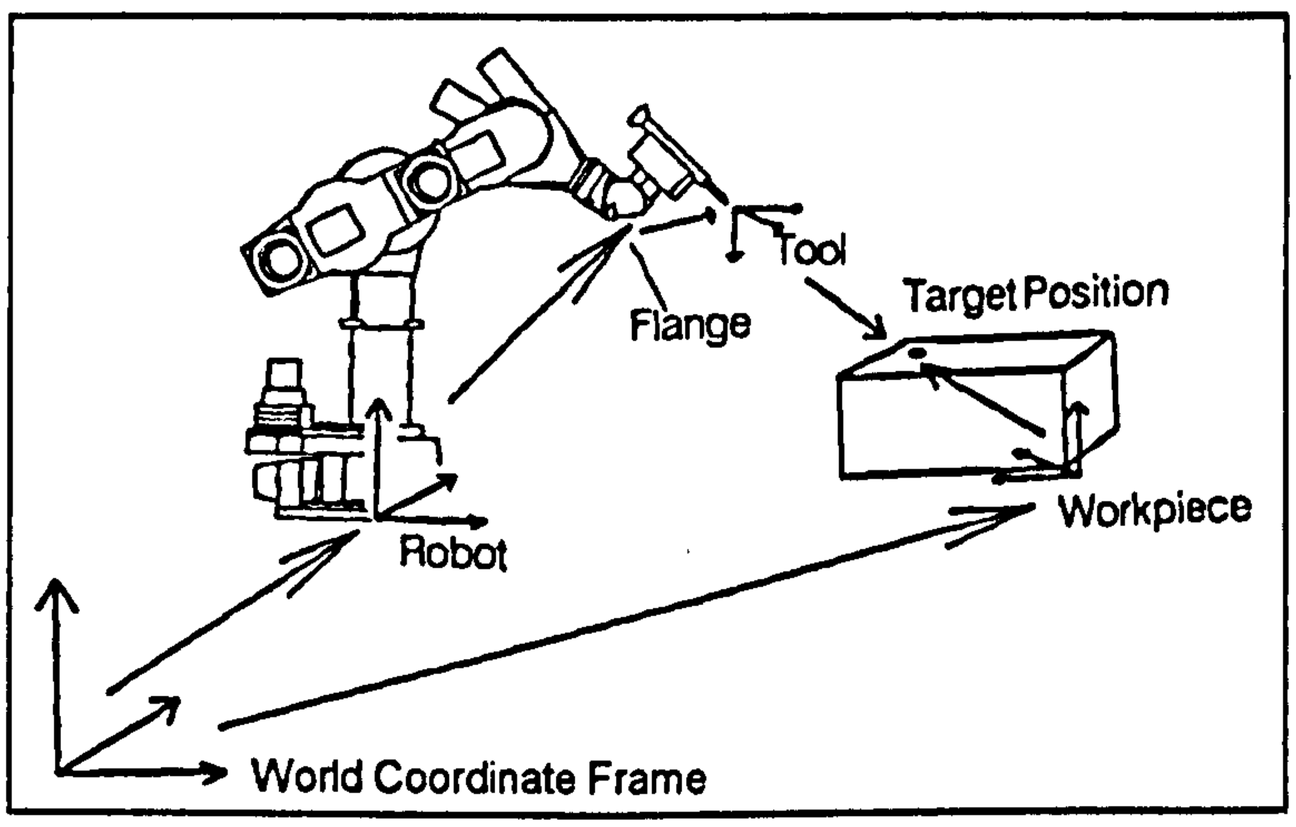

Figure 2.14 - Reference frames for relative workpiece positioning

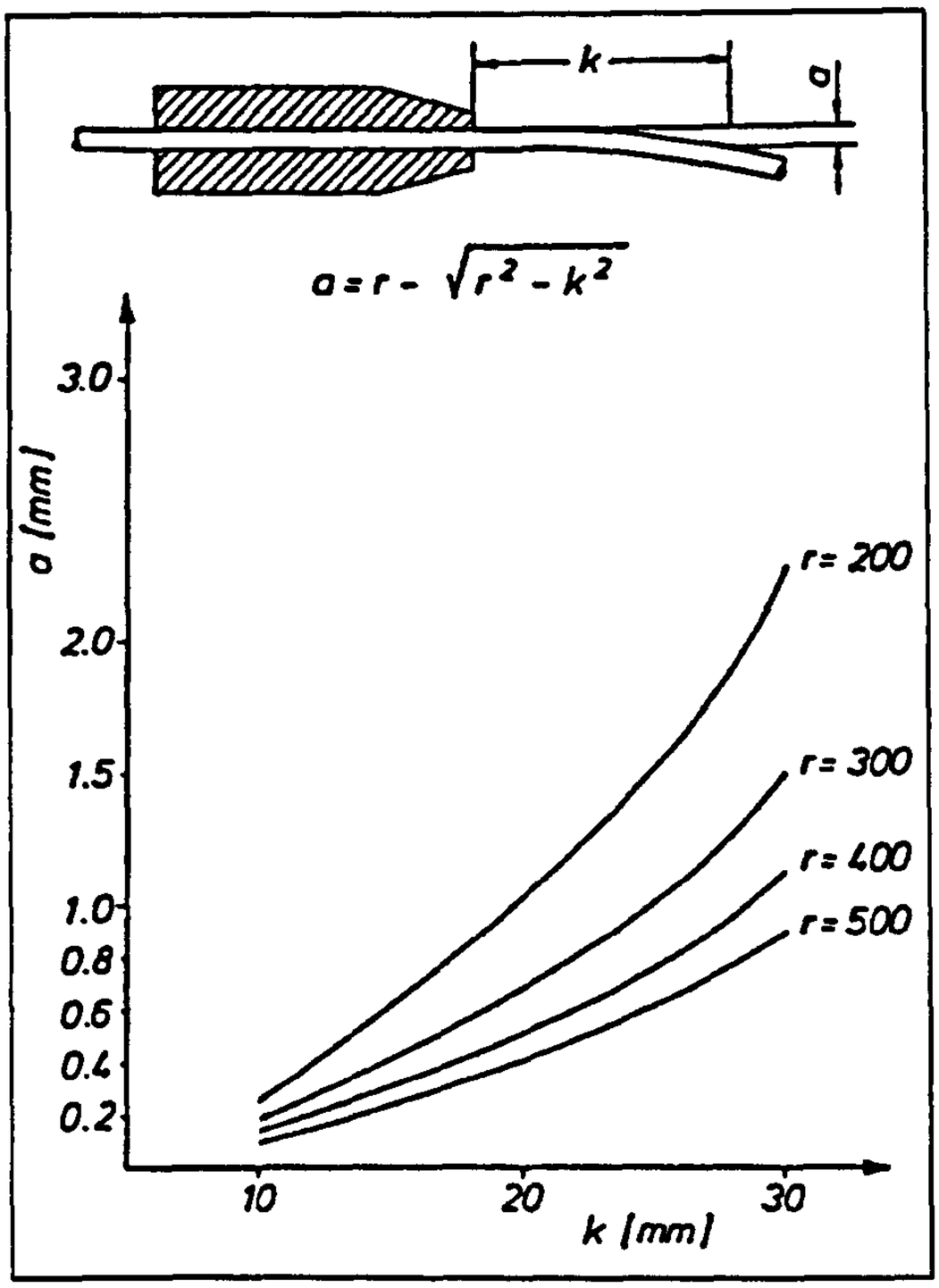

Figure 2.15 - Effect of radius of wire bend on wire outlet deviations [ref. 106]

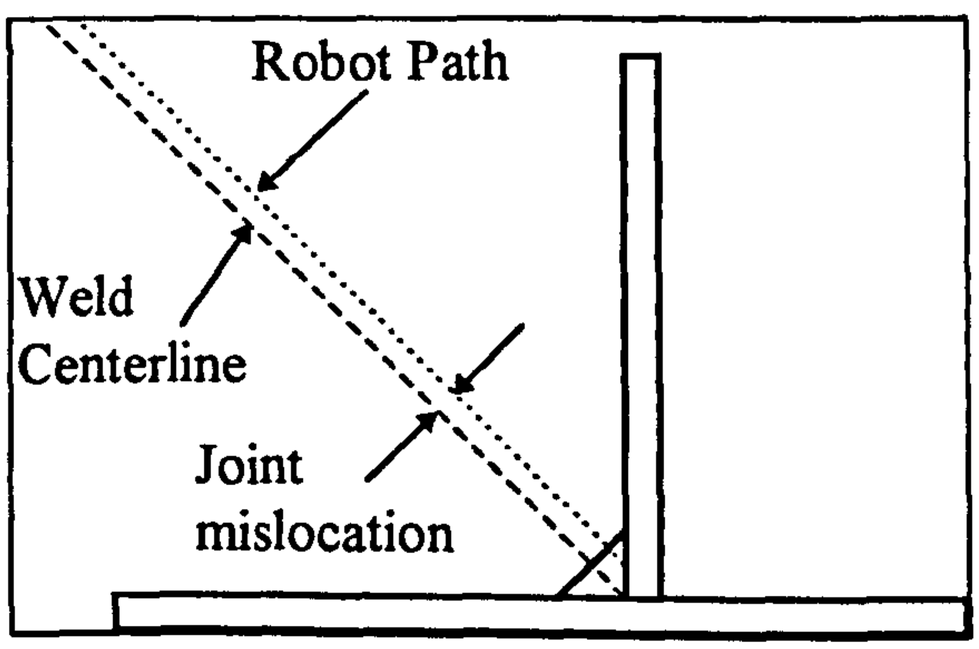

Figure 2.16 - Weld joint mislocation [ref. 108]

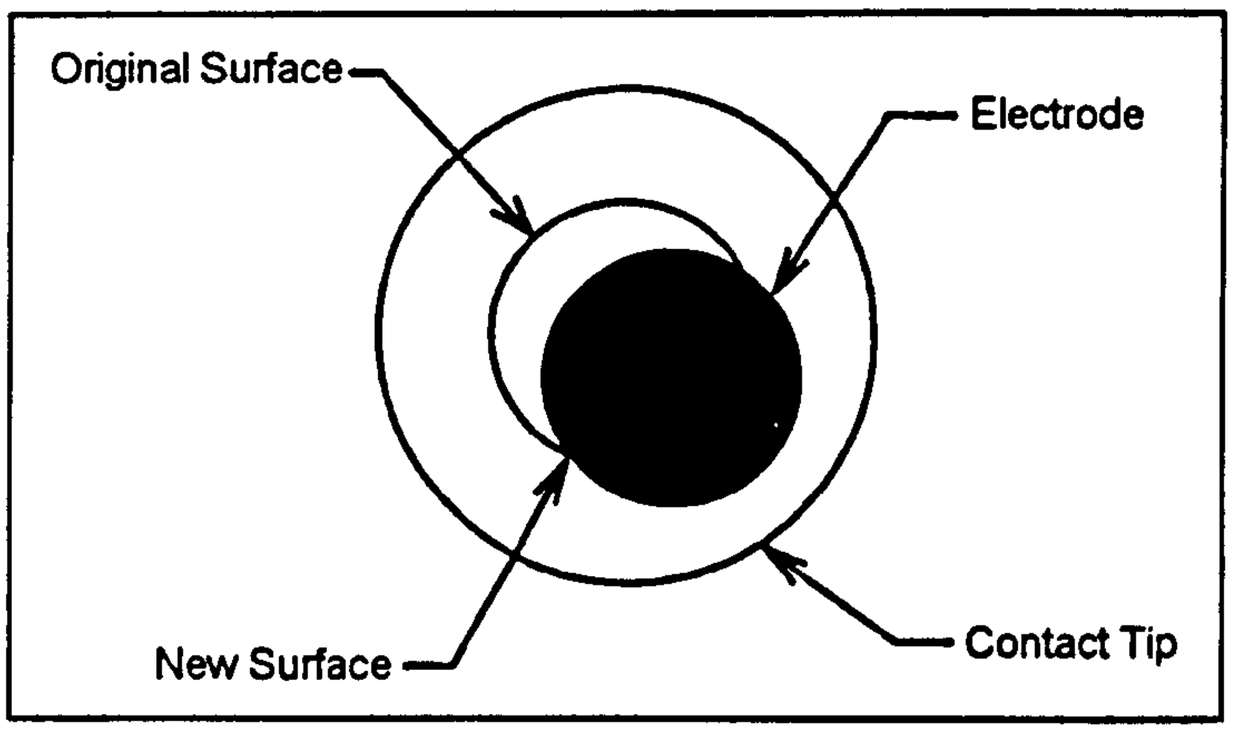

Figure 2.17 - Schematic view of contact tip outlet wear [ref. 113]

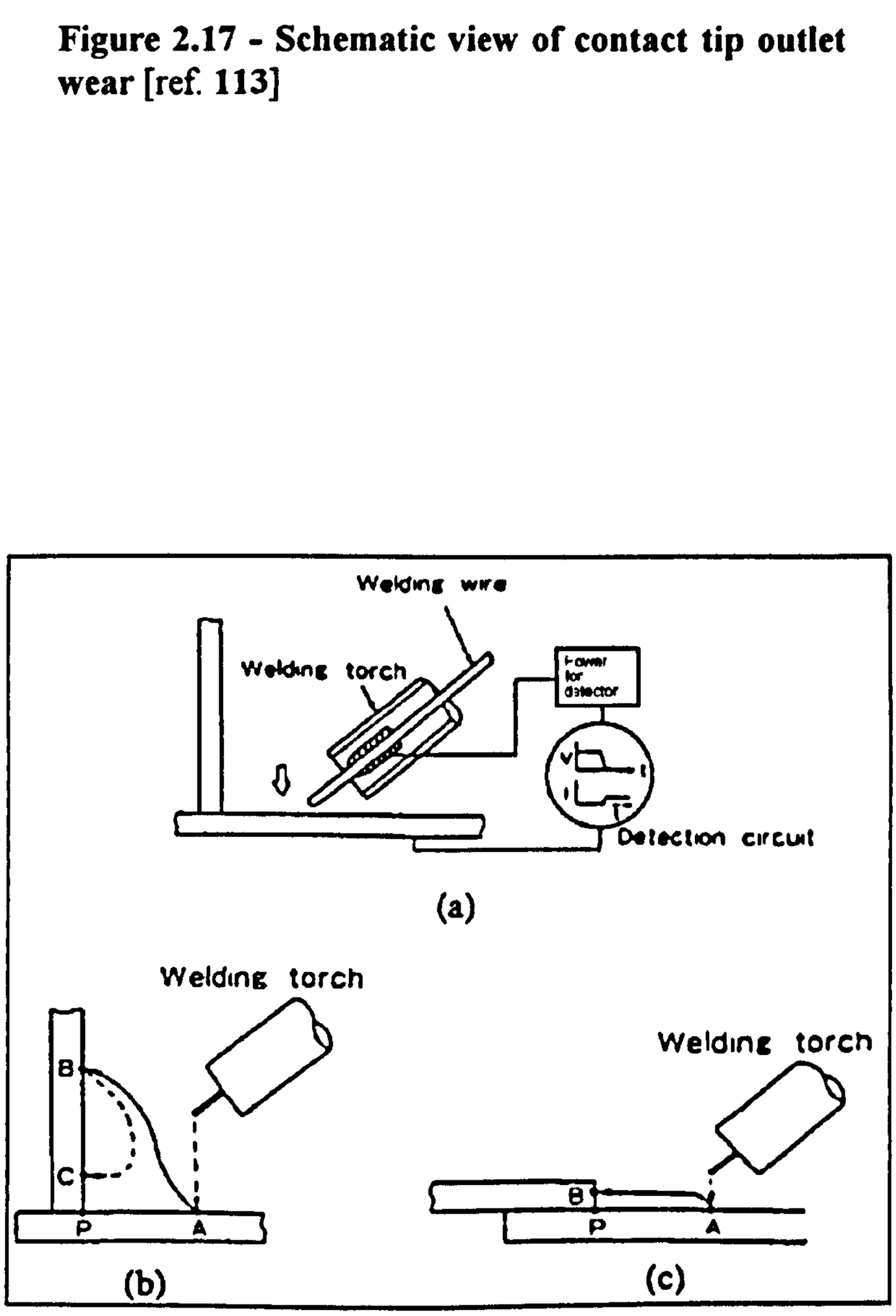

Figure 2.18 - Principle of electrode wire contact sensor (a) Principle (b) Fillet Joint (c) Lap joint [ref. 115]

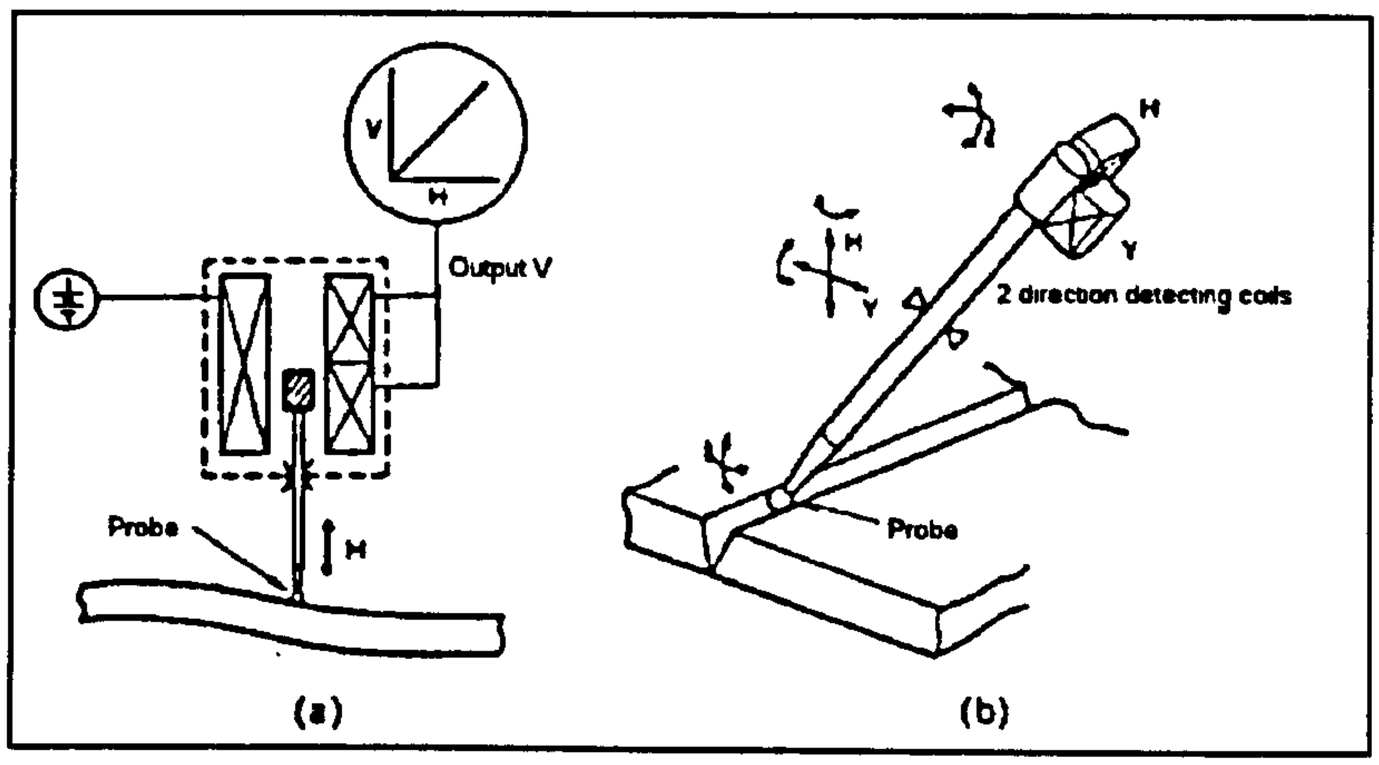

Figure 2.19 - Principle of probe contact sensor (a) One degree-of-freedom (b) Two degrees-of-freedom [ref. **115**]

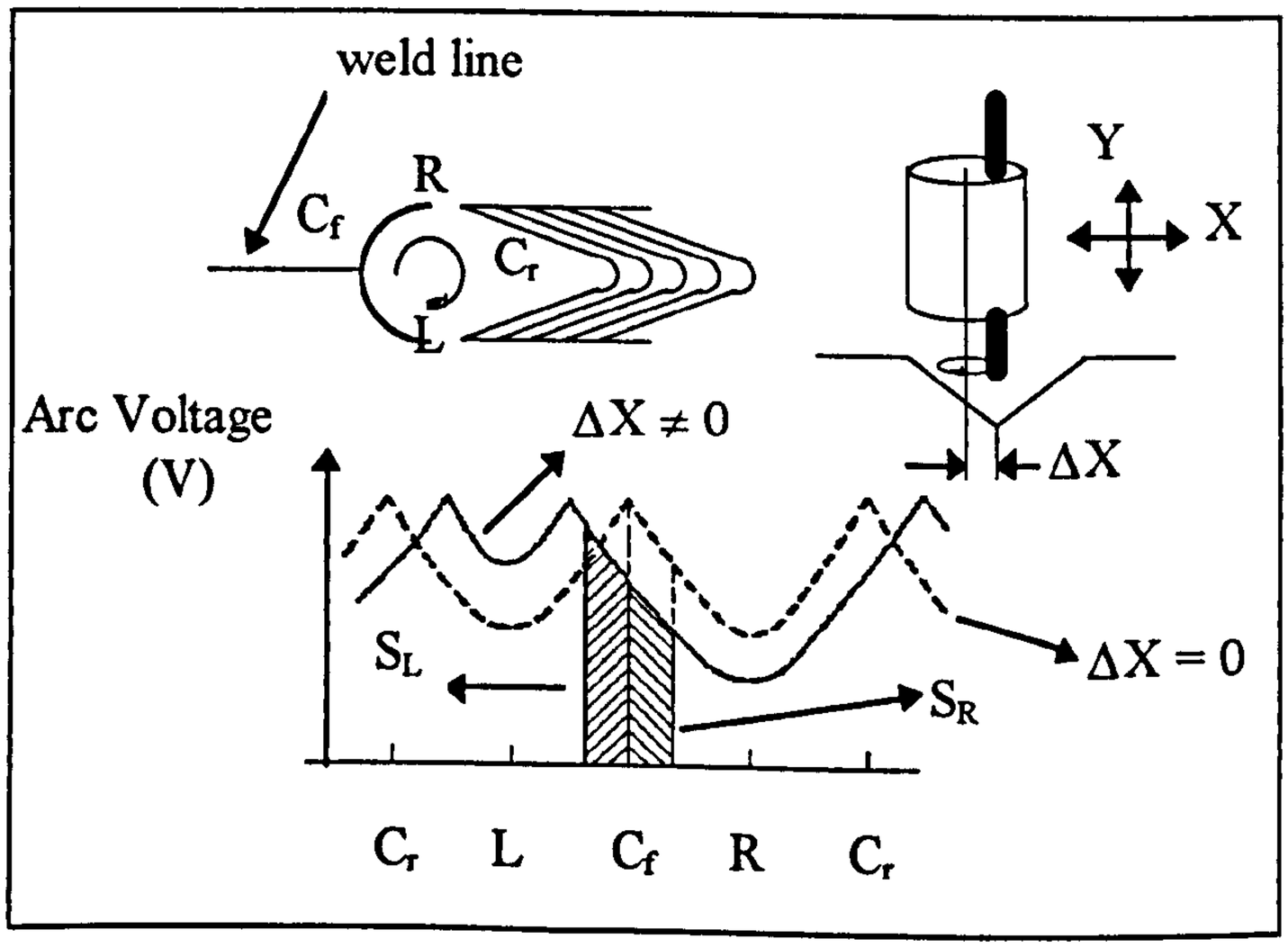

Figure 2.20 - Flow chart for the calculation of contact tip-to-workpiece distance. [ref. **136**]

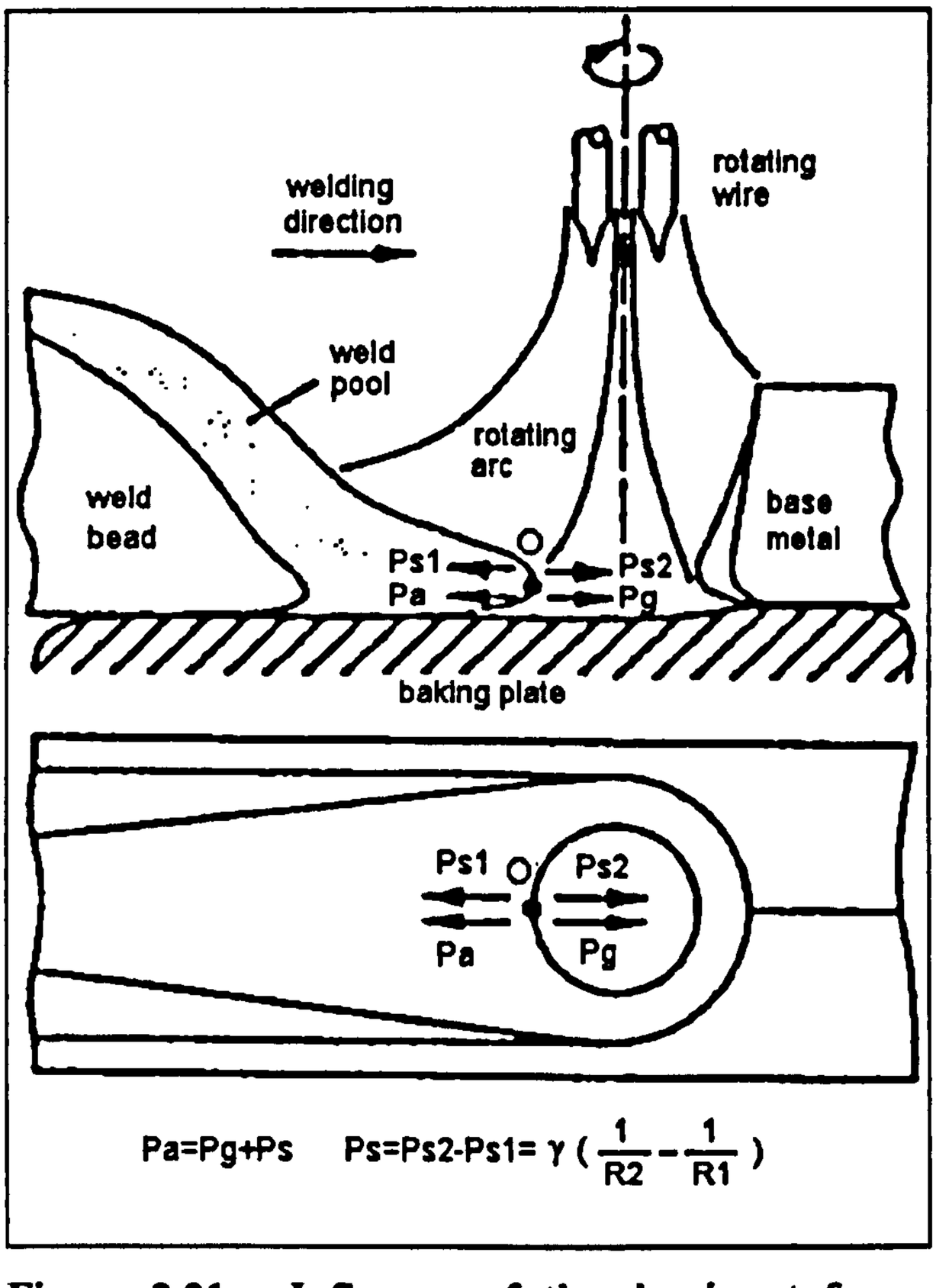

Figure 2.21 - Influence of the dominant forces acting on the front edge of the weld pool on keyhole.[ref. 183]

3. Proposed Strategy for Off-line Programming and Control of Robotic Arc Welding Operations

The primary aim of using off-line programming in robotic welding is to improve productivity by not stopping the production line during the programming of the welding tasks. However, from the literature review in the previous chapter it is clear that the application of off-line programming in robotic welding is not that straightforward. Further to the common production problems normally found in on-line programmed operations, the robot absolute accuracy appears to be an important factor.

It is generally accepted that for quality welds to be produced, two main requirements must be fulfilled:

a) the wire-tip must be positioned relative to the joint centre-line within the allowable GMAW process tolerances;
b) the welding parameters must be adequate, producing the required quality with an overall stable process.

These requirements can be achieved by off-line process optimisation and on-line monitoring and control of the welding parameters and the wire-tip position relative to the joint. Also, the off-line generated robot program should consider, in addition to the setting of adequate welding parameters, the communication issues with the external equipment normally used for implementing the monitoring and control functions.

This chapter presents the overall concept of the proposed strategy for off-line programming and control of robotic gas metal arc welding and the assumptions made to achieve this.

3.1 Identification of sources of error

For a control strategy to be effective, it is necessary that the sources of error are identified and preventive and/or corrective measures are applied. The errors that normally occur in robotic gas metal arc welding using off-line programming (see sections 2.4 and 2.5) can be classified according to their type into two main groups: a) *Positioning related errors*; b) *Process related errors*.

3.1.1 Positioning errors

The *positioning errors* are related to the torch and wire tip positioning relative to the joint centre-line. They can be further classified, according to their source, into three main groups, namely: a) *Robot errors*; b) *Programming errors*; and c) *Component errors*. This classification is proposed in order to make it easier to understand the nature of the discrepancies and deal with them separately.

3.1.1.1 Robot errors

A robot arm is a highly non-linear mechanical system which does not have a truly closed-loop position feed-back control. The position and orientation of the end-effector cannot be measured by normal sensors and it is usually estimated based on non-linear inverse kinematics which assumes that the arm is perfectly constructed according to the design specifications. In addition, the relative low stiffness of the mechanical arm, allied with gear backlash, joint compliance, etc., may cause random variation in positioning for repeated movements. This leads to errors between the *command* and *attained* poses.

When using on-line programming in welding operations, a high repeatability (see section 2.4.2) is very critical, since the robot merely plays back joint angles which were previously recorded. Here the absolute accuracy is not relevant since programmed points are set relative to the workpiece.

Tasks involving off-line programming, however, depend critically on the absolute accuracy, further to the repeatability. A robot may have high repeatability while having low absolute accuracy. Given the joint angles, the controller of a robot calculates the pose of its end-effector with respect to a co-ordinate frame attached to its base, based on a kinematic model of the manipulator structure. This model depends on several parameters such as link lengths, joint offsets, joint compliance, gear backlash, misalignment between parallel axes, link compliances, etc. Most of the time, however, not all the parameters are taken into account or are accurately defined due to manufacturing tolerances. Hence, the calculated poses will not match the required ones, resulting in positioning errors. Therefore, robot errors originate mainly from a robot's inability to achieve precisely the required co-ordinates, that is, from the lack of absolute accuracy.

3.1.1.2 Programming errors

The programming errors have already been discussed in section 2.4.4. In summary, programming errors in off-line programming result mainly from the mismatch between the *ideal world* and the *real world*, as defined in section 2.4.1. Here, perfect kinematic models are used in both the simulation and the robot controller to drive an imperfect arm. In addition, the graphical models of the workpiece and cell environment are usually based on nominal dimensions, which are subject to variations due to manufacturing tolerances.

3.1.1.3 Component errors

The component errors include: a) variation in joint shape (e.g. presence of gap and joint misalignment); b) variation in part positioning due to inadequate fixturing and/or presence of extraneous materials (e.g. spatter) on the fixture locating surfaces; and c) variation in joint shape and position due to thermal distortion. Such errors are the most difficult to deal with, since they vary from component to component within a known tolerance range.

Another source of error that will be classified under this group is the deviation of the wire tip from the torch axis due to the wire cast and contact-tip wear. This type

of error was classified into this group due to its unpredictability, a characteristic that is also found on the other component error sources.

3.1.2 Welding process errors

The process errors are related to the stability of the process (see section 2.1.5) and to the adequacy of the welding parameters to produce the required weld quality. Process errors are mainly characterised by the presence of defects such as undercut, lack of penetration, porosity and burn-through, and/or the failure to achieve some required quality specifications (such as the minimum leg length and minimum fusion penetration), as a result of inadequate choice of welding parameters for the specific requirements.

It should be noted that positioning errors may induce process errors. For example, variation in contact tip-to-workpiece distance would result in change in welding current and fusion penetration while excessive gap in the joint could lead to overpenetration and burn-through.

3.2 Error compensation and proposed corrective measures

In order to compensate for the errors more effectively, each source of error should initially be evaluated separately.

3.2.1 Robot error correction

The best way to deal with lack of positioning accuracy of a robot is to perform a kinematic calibration (see section 2.4.2). In robotic gas metal arc welding, the velocities during the process are normally low, if compared to spot welding or machine loading and unloading. Therefore, a static calibration would suffice in this case.

Considering that off-line programming is used and that it is based on a robot model, a strategy for controlling the robot errors in a robotic arc welding cell is proposed. This consists of three main actions, namely:

1. To perform an initial static forward calibration in the robot arm after the installation of the cell;
2. To calibrate the working cell: this includes workpiece positioner and can be accomplished by using the calibrated robot as a measuring tool. A new calibration of the work cell is necessary every time its layout is changed;
3. To perform periodic calibration checks in order to correct minor deviations due to drift error and to detect when a new static calibration is necessary.

Points within the cell could be equipped with measuring devices which would be responsible for detecting the drift error. These three actions should be repeated for all robots involved in the production line, thus reducing or eliminating this source of error.

3.2.2 Programming error correction

Considering that these errors are mainly caused by model mismatch, the best approach to dealing with them is to ensure that the computer models mirror exactly the robot behaviour. The robot kinematic parameters identified in the static calibration procedure could be used to correct the robot model in the computer. The workcell model can be corrected with the positions measured during the workcell calibration. In order to match the robot behaviour in both simulation and real cell, the programmer must choose the orientation representation that provides the same movements as that of the robot.

3.2.3 Component error compensation

The component errors are regarded as more complicated to accommodate than the other errors, since they depend on individual component variances.

In the literature, several different approaches have been used to deal with the component errors. Two main strategies can be identified: a) the setting of the manufacturing tolerances to the levels required by an automated welding system; and b) the use of sensors and adaptive control.

The first approach can sometimes represent a large increase in the manufacturing costs, which may be unacceptable; while the second approach provides compensation for the discrepancies, resulting in consistent welds. However, depending on the type of sensor (e.g. laser systems), the initial investment can be high.

The best approach for compensating the variation in joint positioning due to component errors is to implement pre-weld joint searching (to determine the weld start position), on-line seam tracking and on-line contact tip-to-workpiece distance control, to ensure that the weld bead is deposited in the right place and to keep the torch-to-workpiece relative distance constant. This approach was adopted in this work and will be described in detail in the next chapter.

3.2.4 Welding parameters

Setting the right combination of welding parameters is of major importance for any welding process. Particularly, in gas metal arc welding of thin sheet steel, the welding parameters must be set such that a stable and robust process is obtained and the risk of defects is minimised, yielding the required weld quality. The more stable the process is, the more robust it is to external disturbances.

Therefore, the best way to deal with process errors is to ensure that the welding parameters are adequate for the quality requirements. It is also necessary to implement on-line monitoring and control of the process, such that deterioration trends in the process stability and weld quality caused by unexpected process disturbances can be detected and corrected before they compromise the quality of the whole weld.

The control strategy proposed is based on procedural (off-line) control and on-line control methods. The procedural control is based on the off-line optimisation of welding parameters, based on previously established [ref. **51**] welding regression models, such that the welding parameters are selected from a list of predicted welding parameters which are expected to produce the required quality. The on-line control

aims at fine tuning the welding parameters such that the most stable situation is always attained.

3.3 Off-line programming and control system for robotic gas metal arc welding

Considering the positioning and process aspects mentioned in the former sections, a strategy for integrating off-line programming with robotic welding, process monitoring and adaptive control is proposed. It is assumed that the robot arm as well as the welding cell are correctly calibrated. Although it is ideal to calibrate the robot and workcell, this is not absolutely necessary since the control system provides alignment of the welding torch relative to the workpiece. This is limited, however, by the range of movement allowed, which implies that the control system can only accomodate errors within this range and hence, if the robot had large geometric errors beyond this range, then the control system would reach a limit of movement. Therefore, the proposed system addresses mainly the off-line programming aspects and the component and process errors.

The proposed concept aims to integrate the geometrical design of a component (via CAD modelling) and the welding design (via weld modelling) to generate the robot program necessary to carry out the required weld. Such a robot program would contain the necessary communication instructions and logic necessary for in-process monitoring and adaptive control to be performed, thus ensuring that the required weld quality is attained. In the present work such a system has been implemented on a personal-computer, using as its base a commercial CAD software. The idea behind this concept was to devise a system in which the welded component is dealt with from the design to the shop floor without the need for developing welding procedures and without the intervention of an operator for correcting robot path or adjusting welding parameters. The proposed system is composed of three main modules, namely: a) *CAD Module*; b) *Off-line Programming Module*; c) *Control Module*. (see Figure 3.1)

3.3.1 CAD Module

In the CAD module, the welded part is designed such that the welds are accessible from the part's exterior. A solid model of the workpiece in its final welded form should be provided in order to allow the off-line programming module to be used.

AutoCAD® (AutoDesk Inc., USA) was chosen to be the basis of the system due to its flexibility in terms of programming and modelling tools and due to the fact that it can be considered as a standard personal-computer based CAD software for the industry.

The AutoCAD programming facilities used in this work are based on AutoLISP®, a symbolic programming language whose functions are interpreted during program execution. The advantage of using this programming language is that the program becomes platform independent. It also provides modularity, i.e. new functions can be added to the program without much trouble.

3.3.2 Off-line programming module

In the off-line programming module, the welded joints are located and the quality requirements input. The module then predicts a list of welding parameters which are expected to produce the required quality and from which the user should choose the best suited set. Further to predicting the welding parameters, this module extracts geometrical information from the joint and generates the co-ordinates of the start and end of the weld as well as torch approaching and withdrawing points (positions and orientations). The geometrical and welding data are stored together with the CAD model data, as *extended entity data*[1] . Therefore, the designed welding data is kept as long as the CAD drawing exists.

The off-line programming module was developed using AutoLISP®[2] and consists of two main branches, the welding parameters generator and the robot programming branch (see Figure 3.2).

3.3.2.1 Welding parameters generator

The *welding parameters generator* (dot-dashed line in Figure 3.2) outputs optimised parameters based on the geometry required for each weld bead. The parameters are calculated based on the empirical welding models developed by Ogunbiyi [ref. **51**] for the gas metal arc welding of thin sheet steel.

Three types of prediction models are used: a) models for predicting process ideal features under stable conditions; b) models for predicting bead geometry; and c) models for predicting process stability. These models were developed by applying multiple regression and fuzzy regression analysis. The welding data used were collected for a stable process carried out with travel speeds between 0.4 m/min and 1.6 m/min, wire feed speeds between 4 m/min and 16 m/min and contact tip-to-workpiece distances (stand-off) between 12 mm and 20 mm. For each travel speed, wire feed speed and stand-off combination, the voltage was chosen to give the most stable process. The models are outlined below in equations (3.1) to (3.10).

a) Models for predicting process ideal features

Expected mean current from procedure:

$$I_{mean} = \alpha_1 + \beta_1 WFS + \delta_1 SO \cdot WFS \qquad \textbf{(3.1)}$$

Expected maximum to mean current ratio (*TSI*):

$$\frac{I_{max}}{I_{mean}} = \alpha_2 + \beta_2 I_{mean} + \delta_2 SO \qquad \textbf{(3.2)}$$

---

[1] The concept of *extended entity data* and its structure can be found in the AutoCAD Release 12 - Customization Manual

[2] A description of the AutoLISP functions and its sintax can be found in the AutoCAD Release 12 - AutoLISP Programmer's Reference

Expected mean current from transient values:

$$I_{mean} = \alpha_3 I_{max} + \beta_3 I_{\min} \tag{3.3}$$

Expected background to average voltage ratio:

$$\frac{V_{bk}}{V_{mean}} = \alpha_4 + \beta_4 I_{\min} + \delta_4 SO \tag{3.4}$$

Expected background voltage:

$$V_{bk} = \alpha_5 + \beta_5 I_{mean} + \delta_5 V_{mean} \tag{3.5}$$

where

WFS	is the wire feed speed;
SO	is the stand-off;
V	is the set-up voltage;
I_{mean}	is the average welding current;
I_{min}	is the minimum current value in a sample;
I_{max}	is the maximum current value in a sample;
V_{mean}	is the average welding voltage;
V_{bk}	is the background voltage;
$\alpha_{1...5}$, $\beta_{1...5}$, $\delta_{1...5}$	are regression coefficients.

b) Models for predicting bead geometry (see Figure 3.3)
Expected bead dimension (*BD*)

$$BD = \alpha_6 \left(\frac{WFS}{S_W} \right)^{\beta_6} \tag{3.6}$$

where

BD	is the bead dimension (Leg_s, side leg length; Leg_b, bottom leg length);
WFS	is the wire feed speed;
S_W	is the welding travel speed;
α_6 and β_6	are regression constants.

Expected weld penetration (*Pen*)

$$Pen = \alpha_7 \left(I_{mean} V_{mean} \right)^{0.5} + \beta_7 S_W \tag{3.7}$$

where

Pen is the weld penetration (side penetration, Pen_s, and bottom penetration, Pen_b);
α_7 and β_7 are regression coefficients.

Possibility measure of undercut, Pr(*und*)

$$\Pr(und) = \alpha_8 WFS + \beta_8 WFS \cdot SO + \delta_8 V \cdot S_w \tag{3.8}$$

where α_8 , β_8 and δ_8 are regression coefficients.

c) Models for predicting process stability

Possibility measure of bad arc ignition

$$\Pr(arc) = 1 - \frac{WFS_{ign}}{WFS_{set}} = 1 - \frac{V_{set} - \alpha_9}{\beta_9 WFS_{set}} \tag{3.9}$$

where
WFS_{ign} is the ideal wire feed speed required to give good arc ignition;
WFS_{set} is the set-up wire feed speed;
V_{set} is the set-up voltage;
α_9 , β_9 are regression coefficients obtained by fitting a linear relationship to V_{set}=f(WFS_{ign}).

Model for predicting power ratio (*PR*)

$$PR = \alpha_{10} + \beta_{10} I_{mean}^2 + \delta_{10} V_{mean} \tag{3.10}$$

where α_{10} , β_{10} and δ_{10} are regression constants.

The coefficients of the models are dependent on the wire type (diameter and composition), the shielding gas type and the joint type. In this work, the coefficients obtained by Ogunbiyi [ref. **51**] were utilised as a starting point (see Table 3.1). These coefficients were obtained for 1 mm mild steel welding wire[3], 1.6 mm and 3.2 mm thick mild steel sheets set in fillet joints in the horizontal vertical (2F) position and BOC Argonshield 5[4] shielding gas, using a Migatronic BDH 320 inverter power source. Although the models were obtained using 1.6 mm and 3.2 mm thick mild steel sheets, the author [ref. **51**] suggests that they can be used for prediction purposes in the range from 1.0 mm to 6.0 mm thick mild steel sheets.

[3] Oerlikon (BS 2901.A18)
[4] Ar + 5%CO_2 + 2%O_2 gas mixture

Table 3.1 - Ogunbiyi's model coefficients

		Regression Coefficients				
Variable	**Eq.No**	**α**	**β**	**δ**	**SE**	**R^2**
I_{mean}	(3.1)	61.318	24.053	-0.4611	9.98	97.22
TSI	(3.2)	2.8758	-0.002549	-0.060936	0.1237	88.12
I_{mean}	(3.3)	0.363842	0.642844	-	12.2015	99.71
V_{bk}/V_{mean}	(3.4)	-0.47318	0.002481	0.044959	0.09	92.57
V_{bk}	(3.5)	-27.3364	-0.039555	2.2558	1.441019	98.62
Leg_s	(3.6)	1.0	0.561068	-	0.0980	99.58
Leg_b	(3.6)	1.0	0.592637	-	0.129228	99.35
Pen_s	(3.7)	0.01782	-0.449818	-	0.356612	89.07
Pen_b	(3.7)	0.019058	-0.639698	-	0.415507	82.92
Pr(*und*)	(3.8)	-0.0982	0.0044	0.0265	0.3502	65.98
Pr(*arc*)	(3.9)	13.519345	0.97619	-	2.2976	48.61
PR	(3.10)	-0.9785	-7.0094E-6	0.083019	*	*

Obs: * = not available.

The algorithm used for generating welding parameters is an adaptation of the one proposed by Ogunbiyi [ref. **51**]. The algorithm searches for the combinations of welding parameters that would satisfy a series of constraints relative to bead geometry, joint position, presence of gap, weld penetration, metal transfer and stability, and arranges the predicted parameters in order of growing possibility of producing a weld with defects.

Two main types of constraints are used in the algorithm: a) *geometrical constraints* and b) *process constraints*.

The geometrical constraints refer to the weld geometry limits such as minimum allowable leg length, maximum allowable leg length, minimum allowable weld penetration, maximum allowable weld penetration and maximum allowable gap size. These constraints are normally set relative to the thinner member of the joint and can vary according to different specifications. The constraints chosen were based on the Inauxa specification [ref. **190**] (see Figure 3.3) and the AWSD8:8-79 specification [ref. **107**] (see Figure 3.4) and on the validity range of the models [ref. **51**]. The constraints are listed below.

a.1) Geometrical constraints relative to models validity range (Fillet joints)

- Minimum allowable plate thickness: 1.0 mm
- Maximum allowable plate thickness: 6.0 mm
- Minimum allowable leg length: 2.5 mm
- Maximum allowable leg length: 6.0 mm
- Minimum allowable stand-off[5]: 12 mm
- Maximum allowable stand-off: 20 mm
- Suggested stand-off: 15 mm

[5] From this point on, the contact tip-to-workpiece distance will be referred to as stand-off

a.2) Geometrical constraints from specifications:

• Depth of side wall fusion (penetration, *Pen*):	$0.1xT_{min}$[6]$<Pen\leq 0.6xT_{min}$
• Maximum leg length for lap joints:	thickness of the top plate
• Maximum gap:	min (T_{min} , 2.3 mm)

The process constraints refer to limits in the process parameters used in order to comply with the validity range of the models. In the presence of gap and/or positional welding, the mode of metal transfer is forced to dip transfer and the welding current is limited to a value in which the dip mode of metal transfer can exist.

b) Process constraints

• Minimum wire feed speed:	4.0 m/min
• Maximum wire feed speed:	16.0 m/min
• Minimum welding speed:	0.4 m/min
• Maximum welding speed:	1.6 m/min
• Maximum welding current:	340 A
• Wire diameter:	1 mm
• If there is a gap or positional welding then limit mode of metal transfer to dip and maximum welding current to:	240 A
• Maximum predicted possibility of undercut, Pr(*und*):	0.25
• Maximum possibility of bad arc ignition, Pr(*arc*):	0.40

The algorithm for searching the welding parameters is described bellow:

Step 1

Input the quality requirements (Leg length required, Leg_{req} , and its acceptable tolerance, Leg_{tol}) and the geometrical and process data (stand-off, SO, plate thickness, T_{min} , gap size, GAP, and a binary operator indicating if the weld is positional or not, POS = {0,1})

Step 2

If there is a gap or the weld is positional, then limit welding current to 240 Amps and the metal transfer mode to dip. Otherwise limit the welding current to 340 Amps.

Step 3

Set leg length search value, Leg_{spec} , to leg length required + gap size.

Step 4

Initialise wire feed speed, WFS, and the welding speed, S_W , to their minimum values, 4.0 m/min and 0.4 m/min respectively.

---

[6] Minimum plate thickness

Step 5

Given the stand-off, SO , and the wire feed speed, WFS , calculate the expected mean current, I_{mean} , using equation (3.1);

Step 6

If I_{mean} is greater than the maximum allowable value, then jump to Step 22. *Otherwise estimate the expected side leg length, Leg_{side} , and bottom leg length, Leg_{bottom} , using equation* (3.6) *and their average value, Leg_{av} .*

Step 7

If the leg length values comply with the restrictions, then calculate the expected value of the transfer stability index, TSI, from equation (3.2).

Step 8

Estimate the mode of metal transfer by comparing the TSI predicted value with the limits shown in Figure 2.8. *If the TSI predicted value is out of the range in which a stable dip transfer or a stable spray transfer is expected to occur, then force its value to one of these stable regions, using TSI = 1.25 as the threshold for switching the mode of metal transfer from dip (TSI ≥ 1.25) to spray (TSI < 1.25).*

Step 9

Estimate the value of the transfer index, TI, based on the adjusted value of TSI, using equation (3.11). *This equation results from dividing both sides of equation* (3.3) *by I_{mean} and adjusting the terms as in equation* (2.3).

$$TI = 1 - \frac{I_{min}}{I_{mean}} = 1 - \left[\frac{1}{\beta_3}\left(1 - \alpha_3 \frac{I_{max}}{I_{mean}}\right)\right] \qquad \textbf{(3.11)}$$

Step 10

Estimate the value of the dip consistency index, DCI, based on the adjusted value of TSI, on the value of TI estimated in Step 9 *and on the values of I_{mean} and SO, using equation* (3.12). *This equation was obtained by substituting I_{min} for its corresponding value, obtained from equation* (3.11), *into equation* (3.4) *and applying the latter into equation* (2.5)

$$DCI = 1 - \frac{V_{bk}}{V_{mean}} = 1 - \left\{\alpha_4 + \beta_4\left[(1 - TI) I_{mean}\right] + \delta_4 SO\right\} \qquad \textbf{(3.12)}$$

Step 11

Adjust the value of DCI to force the mode of metal transfer to either dip or spray, based on the threshold limits shown in Figure 2.8 *and on the restrictions of mode of metal transfer imposed in the case of a gap being present and/or the weld being positional:*

If I_{mean} > 240 Amps then set the mode of metal transfer to spray (DCI = 0.0)
If DCI indicates tendency to mixed globular and spray modes of metal transfer (DCI < 0.3) then make sure the transfer mode is spray (DCI = 0.0)
If DCI indicates tendency to wire stubbing in dip mode of metal transfer (DCI > 0.75), make sure that this does not occur (DCI = 0.75)
If DCI indicates tendency to globular and mixed globular and spray modes of metal transfer (DCI < 0.65) AND (there is a gap OR positional welding) then force the metal transfer to the dip mode (DCI = 0.65)

Step 12

Estimate the welding voltage, V_{mean} , using equation (3.13). *This equation was obtained by dividing both sides of equation* (3.5) *by V_{mean} , rearranging the terms and applying the definition of DCI from equation* (2.5).

$$V_{mean} = \frac{\alpha_5 + \beta_5 I_{mean}}{1 - DCI - \delta_5} \tag{3.13}$$

Step 13

Given the welding current, I_{mean} , the welding voltage, V_{mean} and the welding speed, S_W , estimate the penetration by selecting the minimum between the side penetration, Pen_s , and the bottom penetration, Pen_b , which are calculated by using equation (3.7) *with the suitable regression constants (see* Table 3.1*).*

Step 14

If the estimated minimum penetration is between 10% and 60% of the minimum plate thickness, T_{min} , then calculate the possibility measure of good arc ignition, using equation (3.9). *Otherwise jump to* Step 20.

Step 15

If a good arc ignition is expected to occur (Pr(*arc*) < 0.4 *) then estimate the possibility measure of undercut ,* Pr(*und*) . *Otherwise jump to* Step 20.

Step 16

*If undercut is likely to occur (*Pr(*und*) ≥ 0.25*) then jump to* Step 20. *Otherwise estimate the power ratio, PR, by using equation* (3.10).

Step 17

Adjust the value of PR based on the restrictions of mode of metal transfer (see Figure 2.8*). Set the PR limits as follow:*

<u>*Dip transfer:*</u>

$PR_{min1} = 0.20$

$PR_{max1} = 0.40$

<u>*Spray transfer:*</u>

$PR_{min2} = 0.95$

$PR_{max2} = 0.97$

If PR indicates an excessively low voltage ($PR < PR_{min1}$*) then make* $PR = PR_{min1}$

If PR indicates excessive voltage in dip transfer ($PR_{max1} < PR \leq 0.6$*) then make* $PR = PR_{max1}$

If PR indicates globular to spray mode of metal transfer ($0.6 < PR < PR_{min2}$*) then force spray transfer by making* $PR = PR_{min2}$

If PR indicates excessive voltage in spray transfer ($PR > PR_{max2}$*) then make* $PR = PR_{max2}$.

Step 18

Adjust the welding voltage by applying the corrected PR value to equation (3.14), *which was obtained by rearranging the terms in equation* (3.10).

$$V_{mean} = \frac{PR - \left(\alpha_{10} + \beta_{10} I_{mean}^2\right)}{\delta_{10}} \qquad \textbf{(3.14)}$$

Step 19

Store in a list the current set of predicted welding parameters.

Step 20

If welding speed, S_W , *is smaller than its maximum allowable value, then increment its value by a fixed amount (e.g. 0.1 m/min) and return to* Step 6. *Otherwise proceed to* Step 21.

Step 21

If the wire feed speed, WFS , is smaller than its maximum allowable value, then increment its value by a fixed amount (e.g. 0.5 m/min) and return to Step 5. *Otherwise proceed to* Step 22.

Step 22

Output the list of predicted sets of welding parameters in a growing order of possibility of defects being present, using as a sorting factor either Pr(*arc*), *if GAP > 0, or* Pr(*und*) *otherwise.*

This algorithm was used to generate welding parameters for the welding trials.

3.3.2.2 Robot programming

In the robot programming branch (dashed line in Figure 3.2), the weld joint positions are defined and the program extracts geometrical information about the joints. Two outputs can be obtained: a) the robot program (ASCII file), ready to be compiled, and b) a co-ordinates file, which can be used in an off-line programming software, such as Workspace to generate the robot program and to simulate it. The robot program is then translated to the specific binary code and downloaded to the robot controller for execution. The current implementation generates robot programs in ARLA (ABB Robot Language) and includes Workspace commands for simulation purposes and also commands for communicating with the control system.

The off-line programming module assumes that the plane formed by the X and Y axes of the CAD world co-ordinates frame (WCF) is parallel to the robot installation floor and that the Z-axis points to the space above the floor in a direction opposite to the gravitational force vector. The welded component should be designed in its final welded form as a continuous solid, using the solid modelling tools provided by AME (AutoCAD Modelling Extension), such that its orientation relative to the X-Y plane of the CAD WCF is as close as possible to its real orientation relative to the X-Y plane of the robot WCF (i.e. relative to the welding cell floor), since such orientation is used to extract information about the welding position and will affect the welding parameter generation. The origin of the CAD world co-ordinates frame is considered to be the origin of the workpiece co-ordinates frame in the real cell. The origin of the robot's world co-ordinates frame is assumed to coincide with the origin of the co-ordinates frame fixed at the robot basis. These considerations are easier to visualise by using graphical simulation of the robot workcell (see Figure 3.5).

The weld joint is defined by the user by either selecting the corresponding edge in the solid model or by selecting the edge adjacent surfaces (see Figure 3.6), whose intersection forms the edge that corresponds to the weld joint. By using built-in AME AutoLISP® functions[7] different types of intersection curves and related information can be obtained, depending on the types of surfaces that form the intersection. In the current implementation, only linear intersection curves were

---

[7] A description of the AME AutoLISP functions and their sintax can be found in the AutoCAD Release 12 - AME 2.1 AutoLISP and API Manual.

treated as weld joints, however other types of curves (e.g. elliptic, hyperbolic, parabolic) can also be implemented. In this case the robot welding path would be generated by subdividing the non-linear intersection curve into small linear segments, which would be treated as normal linear joints. The program checks if the chosen edge is a valid joint by verifying if it lies on the surface of the solid and if it is not an open edge (only fillet joints are currently accepted as valid). This is accomplished by extracting the normal vector to each surface forming the intersection, relative to the joint edge middle point, and defining a point in space according to equation (3.15) (see Figure 3.6 and Figure 3.7)

$$\mathbf{p} = \xi(\mathbf{n}_2 - \mathbf{n}_1) \qquad (3.15)$$

where

$\mathbf{p}$ is a vector defining a point in space

$\mathbf{n}_1$ is a unit vector normal to surface 1 at the middle point of the intersection line

$\mathbf{n}_2$ is a unit vector normal to surface 2 at the middle point of the intersection line

ξ is a small number (e.g. 0.1).

If the point defined by **p** lies inside the solid, then the joint is of the fillet type. If the point lies outside of the solid, then it is an open edge and it is not a valid joint.

The program extracts the orientation of the joint relative to the CAD world co-ordinates frame and classify the welding position based on the orientation limits suggested by Connor [ref. **191**] for fillet welds (see Figure 3.8). It then labels the joint as either non-positional (flat and horizontal) or positional (overhead and vertical). These joint positions have their most common configurations illustrated in Figure 3.9. The joint orientation is obtained from the orientation of two vectors, the vector normal to the weld surface, contained into the joint bisection plane[8], and the vector tangent to the joint longitudinal axis. This latter also indicates the welding direction. Figure 3.10 shows both directions as the approach direction line and the joint longitudinal axis.

The orientation of the welding torch relative to the joint is automatically set by the program. The torch axis will define a unit vector pointing towards the joint. This vector will be conventionally called *torch approach vector* and its orientation is given by the intersection of two planes, the joint bisection plane and the plane perpendicular to the joint longitudinal axis (see Figure 3.10). The torch approach vector is stored in the geometrical database of the line segment that corresponds to the weld joint and is calculated from two rotation angles, which are defined relative to the CAD world co-ordinates frame (see Figure 3.11): a) a positive[9] rotation of the X-axis about the Z-axis, conventionally called angle "in the XY-plane", which defines a new X'-axis; and b) a rotation of the new X'-axis about the new Y'-axis, conventionally called angle "from the XY-plane", which defines the approach direction. A negative rotation about

---

[8] Plane that contains the joint longitudinal axis and is rotated about this line by half of the joint included angle, from one of the joint's adjacent surfaces towards the other, thus bisecting the joint included angle.

[9] Using the right hand convention for defining direction of rotation.

the Y'-axis results in a positive "from the XY-plane" angle. The resulting X"-axis is multiplied by -1 to obtain the torch approach vector. Such orientation angles are defined for both weld start point and weld end point and can be changed by the user (see Figure 3.12).

Two variables called weld start and weld end offsets are also used to define the actual start and end points of the weld. Sometimes, depending on the joint design, the edge extremities extracted from the CAD model cannot be defined as weld start and end points, since it would probably result in defects at these positions. To avoid such defects the offsets are defined such that there will always be base material to receive the molten metal from the welding electrode. Different offsets can be defined for the weld start and end points and these points will be determined by moving along the joint longitudinal axis, towards its middle point, by the amount recorded in the offset variables (see Figure 3.12).

The off-line programming module permanently stores the above mentioned geometrical data in the AutoCAD drawing database as extended entity data associated with the edge that defines the joint. The welding data generated by the welding parameters generator is also stored in the same database. Appendix A shows the variables and gives the order in which they are stored in the so called "Welding extended entity data".

In order to calculate the robot teach-points[10] and to generate the robot program from the CAD geometrical data a co-ordinates transformation is necessary. In the CAD model, all geometrical data are referred to the CAD world co-ordinates frame (see Figure 3.12). The robot controller uses the robot world co-ordinates frame (see Figure 3.5) to calculate the positions and orientations of the robot end effector such that the required robot path is attained. In the off-line programming module, this co-ordinates transformation is carried out by pre-multiplying each vector defining a position or an orientation relative to the CAD world co-ordinates frame, by a 4x4 transformation matrix, according to equation (3.16). The present author will assume the readers previous knowledge about transformation matrices[11].

$$\left[(\mathbf{p}_{Robot})^T \quad 0\right]^T = \mathbf{M}_{\mathbf{Robot}}^{\mathbf{CAD}} \times \left[(\mathbf{p}_{CAD})^T \quad 0\right]^T \tag{3.16}$$

where:

$\mathbf{p}_{Robot}$ 3x1 vector which defines a position or orientation relative to the robot world co-ordinates frame;

$\mathbf{M}_{\mathbf{Robot}}^{\mathbf{CAD}}$ 4x4 matrix which defines the position and orientation of the CAD world co-ordinates frame relative to the robot world co-ordinates frame;

$\mathbf{p}_{CAD}$ 3x1 vector which defines a position or orientation relative to the CAD world co-ordinates frame;

T superscript T indicates transposed.

---

[10] Robot teach-points define poses (positions and orientations) which the robot controller uses to generate the robot path.

[11] The use of transformation matrices is a standard mathematical procedure. Good reviews about this subject can be found in references **192** and **193**.

In the off-line programming module, the referred transformation matrix is obtained by defining four points, three relative to the robot world co-ordinates frame, **p0, p1, p2** , and one relative to the table co-ordinates frame, **po** (see Figure 3.13). **p0** is used to define the origin of the table co-ordinates frame in robot world co-ordinates. **p1** is used to determine the direction of the X-axis of the table co-ordinates frame, $\mathbf{X}_t$, in robot world co-ordinates and **p2** is used to define the direction of the Y-axis of the table co-ordinates frame, $\mathbf{Y}_t$, also in robot world co-ordinates. **po** defines the origin of the workpiece (CAD) co-ordinates frame relative to the table co-ordinates frame. Equations (3.17) to (3.34) show how the transformation matrix is obtained.

$$(\mathbf{p0})^T = \left[p0_x^{Robot} \quad p0_y^{Robot} \quad p0_z^{Robot} \right] \tag{3.17}$$

$$(\mathbf{p1})^T = \left[p1_x^{Robot} \quad p1_y^{Robot} \quad p1_z^{Robot} \right] \tag{3.18}$$

$$(\mathbf{p2})^T = \left[p2_x^{Robot} \quad p2_y^{Robot} \quad p2_z^{Robot} \right] \tag{3.19}$$

$$(\mathbf{po})^T = \left[po_x^{table} \quad po_y^{table} \quad po_z^{table} \right] \tag{3.20}$$

where the subscripts *x*, *y* and *z* indicate vector components in the X, Y and Z directions. The superscript *Robot* indicates that the co-ordinates are referred to the robot world co-ordinates frame. The superscript *table* indicates that the co-ordinates are referred to the table co-ordinates frame. The superscript *T* on the vector representation means transposed.

$$\mathbf{M}_{Robot}^{table} = \begin{bmatrix} m_{11} & m_{12} & m_{13} & p0_x^{Robot} \\ m_{21} & m_{22} & m_{23} & p0_y^{Robot} \\ m_{31} & m_{32} & m_{33} & p0_z^{Robot} \\ 0 & 0 & 0 & 1 \end{bmatrix} \tag{3.21}$$

The matrix components m_{11} , m_{21} and m_{31} form a unit vector which gives the direction of the X-axis of the table co-ordinates frame relative to the robot world co-ordinates frame. Their values are obtained as follows:

$$m_{11} = \frac{p1_x^{Robot} - p0_x^{Robot}}{\|\mathbf{p1} - \mathbf{p0}\|} \tag{3.22}$$

$$m_{21} = \frac{p1_y^{Robot} - p0_y^{Robot}}{\|\mathbf{p1} - \mathbf{p0}\|} \tag{3.23}$$

$$m_{31} = \frac{p1_z^{Robot} - p0_z^{Robot}}{\|\mathbf{p1} - \mathbf{p0}\|} \tag{3.24}$$

where ||**p1** - **p0**|| is the norm of the vector that results from subtracting **p0** from **p1** and is given by

$$\|\mathbf{p1} - \mathbf{p0}\| = \sqrt{\left(p1_x^{Robot} - p0_x^{Robot}\right)^2 + \left(p1_y^{Robot} - p0_y^{Robot}\right)^2 + \left(p1_z^{Robot} - p0_z^{Robot}\right)^2} \tag{3.25}$$

The matrix components m_{12}, m_{22} and m_{32} form a unit vector which gives the direction of the Y-axis of the table co-ordinates frame relative to the robot world co-ordinates frame. Their values are obtained as follows:

$$m_{12} = \frac{p2_x^{Robot} - p0_x^{Robot}}{\|\mathbf{p2} - \mathbf{p0}\|} \tag{3.26}$$

$$m_{22} = \frac{p2_y^{Robot} - p0_y^{Robot}}{\|\mathbf{p2} - \mathbf{p0}\|} \tag{3.27}$$

$$m_{32} = \frac{p2_z^{Robot} - p0_z^{Robot}}{\|\mathbf{p2} - \mathbf{p0}\|} \tag{3.28}$$

where ||**p2** - **p0**|| is the norm of the vector that results from subtracting **p0** from **p2** and is given by

$$\|\mathbf{p2} - \mathbf{p0}\| = \sqrt{\left(p2_x^{Robot} - p0_x^{Robot}\right)^2 + \left(p2_y^{Robot} - p0_y^{Robot}\right)^2 + \left(p2_z^{Robot} - p0_z^{Robot}\right)^2} \tag{3.29}$$

The matrix components m_{13}, m_{23} and m_{33} form a unit vector which gives the direction of the Z-axis of the table co-ordinates frame relative to the robot world co-ordinates frame. Their values are obtained by calculating a vector cross product between the unit vectors that give the directions of the X-axis and the Y-axis of the table co-ordinates frame relative to the robot's world co-ordinates frame. Equations (3.30) to (3.32) give their calculated values.

$$m_{13} = m_{21}m_{32} - m_{22}m_{31} \tag{3.30}$$

$$m_{23} = m_{31}m_{12} - m_{11}m_{32} \tag{3.31}$$

$$m_{33} = m_{11}m_{22} - m_{12}m_{21} \tag{3.32}$$

It is worth noting that the CAD (workpiece) co-ordinates frame is assumed to be parallel with the table co-ordinates frame. This was assumed in order to allow different jigging systems to be used in the table. Hence, the transformation matrix that describes the CAD (workpiece) co-ordinates frame relative to the table co-ordinates frame should have the form shown in equation (3.33) which describes a parallel displacement of the table co-ordinates frame in the direction of the vector **po**.

$$\mathbf{M}_{table}^{CAD} = \begin{bmatrix} 1 & 0 & 0 & po_x^{table} \\ 0 & 1 & 0 & po_y^{table} \\ 0 & 0 & 1 & po_z^{table} \\ 0 & 0 & 0 & 1 \end{bmatrix} \tag{3.33}$$

The transformation matrix which transforms the data relative to the CAD world co-ordinates frame to the robot world co-ordinates frame is then obtained by pre-multiplying the matrix shown in equation (3.33) by the matrix shown in equation (3.21). This is shown explicitly in equation (3.34).

$$\mathbf{M}_{Robot}^{CAD} = \mathbf{M}_{Robot}^{table} \times \mathbf{M}_{table}^{CAD} \tag{3.34}$$

After applying the transformation of equation (3.34) to the geometrical data stored in the CAD database all co-ordinated data are referred to the robot world co-ordinates frame. This makes it possible to generate the poses necessary for the robot to carry out the welding operation.

Off-line programming is performed by defining a series of points in space with co-ordinate frames attached to them, thus providing the positions and orientations that the robot end tool must achieve. The robot controller calculates the movements of the robot arm such that a co-ordinates frame attached to the tool (tool co-ordinates frame) matches the co-ordinates frames defined in the off-line generated program, i.e. both origins coincide and the co-ordinate axes are parallel.

In the design stage of the weld joints approach vectors are calculated and stored in the CAD database. These vectors define the orientations with which the welding torch should approach the joint and carry out the welding operation. However, only one vector is not enough to define the attitude of the torch, since the angle of rotation about this approach vector would be undefined. Hence, a second vector must also be specified to fully define the torch attitude. In order to accomplish this, a co-ordinates frame will be attached to the welding torch thus defining the welding torch attitude relative to the robot world co-ordinates frame. This can be visualised in Figure 3.5 and more specifically, in Figure 3.14, which shows a side view

of a robot in its zero position[12] with a welding torch attached to the end of the robot arm. The torch position relative to the robot arm in its zero position is assumed to follow the configuration shown in Figure 3.14. The torch co-ordinates frame is defined such that its origin lies at the end of the electrode wire[13] with its X-axis parallel to the contact-tip longitudinal axis, pointing to the same direction as the movement of the wire when it is being fed. The Z-axis and the Y-axis are expected to follow the directions shown in Figure 3.14. In order for the robot controller to recognise the torch co-ordinates frame used for off-line programming, a Tool Centre Point[14] (TCP) must be defined accordingly. The procedures involved in defining such a TCP vary with the robot type and are normally specified in the robot's operation manual.

Considering that the approach vector (X-axis) is provided for a point in the weld, it is only necessary to define the orientation of one more axis to fix the orientation of the torch in that point. The rules used to determine the torch orientation were devised from experience in on-line programming an IRB2000 industrial robot with a curved welding torch attached to the robot end joint (see Figure 3.14). It is assumed that the robot is installed with its base fixed on the floor and the positioning table is placed in front of it, as in Figure 3.5.

In order to explain the torch orientation rules, consider the sphere shown in Figure 3.15. It is used to illustrate how the robot should behave in order to achieve different approach orientations, which are represented here as normal vectors to the sphere surface. The co-ordinates frame with origin in the centre of the sphere is parallel to the robot world co-ordinates frame, i.e. they have the same orientation. Consider that meridians are traced on the sphere surface as in Figure 3.15: each meridian together with the X-axis of the sphere co-ordinates frame will define a semi-plane that is rotated by a certain angle around the X-axis, from the XY-plane of the sphere co-ordinates frame. Now consider the semi-planes shown in Figure 3.15 and Figure 3.16. These planes are used to define regions in which different orientation rules are used. No matter what the torch approach direction is, it will always be perpendicular to the sphere surface, thus defining a plane rotated about the sphere's X-axis by a certain angle. For angles between planes 1 and 3 (rotation angle between 60 deg[15] and 120 deg from the XY-plane) the Z-axis of the torch co-ordinates frame is fixed such that it is tangent to a meridian. This implies that both X-axis and Z-axis of the torch co-ordinates frame will be contained in the plane formed by the meridian and the X-axis of the sphere co-ordinates frame. Figure 3.17 and Figure 3.18 show the resulting robot positions for approach orientations contained in planes between planes 1 and 3.

For approach orientations contained in planes 2 and 4 (rotation angles of -45 deg and 225 deg from the XY-plane, respectively) the Y-axis of the torch co-ordinates frame is fixed such that it is tangential to the corresponding meridian.

---

[12] The robot zero position is defined as the robot configuration in which all the robot joints are in their respective zero positions.

[13] Considered to have 15 mm stick-out and to be aligned with the contact tip longitudinal axis.

[14] The Tool Centre Point defines a transformation matrix between the co-ordinates frame attached to the end of the tool and the co-ordinates frame attached to the end of the robot arm. This transformation matrix vary depending on the tool configuration.

[15] "deg" in this context stands for angular degrees. 1 deg = 1/360 of a complete revolution.

Hence, the X-axis and the Y-axis of the torch co-ordinates frame will be contained in the referred planes.

For approach orientations contained in planes between planes 3 and 4, the torch co-ordinates frame will be rotated about its X-axis by an angle between 0 deg and 90 deg, proportionally to the angle of rotation of the plane which contains the approach direction, from 120 deg to 225 deg. Figure 3.19 and Figure 3.20 show the resulting robot positions for approach orientations contained in planes between planes 3 and 4.

For approach orientations contained in planes between planes 1 and 2, the torch co-ordinates frame will be rotated about its own X-axis by an angle between 0 deg and -90 deg, proportionally to the angle of rotation of the plane which contains the approach direction, from 60 deg to -45 deg. Figure 3.21 shows the resulting robot positions for approach orientations contained in planes between planes 1 and 2.

Approach orientations contained in planes between planes 2 and 4 cannot be defined. These rules were devised in order to take advantage of the mounting position of the welding torch relative to the robot's end joint.

Another important aspect of off-line programming is the definition of the robot path for approaching and withdrawing from the weld joint. In order to generate the points necessary to define such a path, it was assumed that all the welds were located on the external surface of the workpiece. The path which the torch must follow to achieve a weld start point is defined by the *weld approach points* and the path the torch must follow to withdraw from a weld end point is defined by the *weld withdrawal points*. Up to four weld approach points and up to four weld withdrawal points are defined automatically by the program for each weld, depending on the orientation of the approach vectors at the weld start and end points and on the size of the workpiece. The aim of these approach and withdrawal points is to prevent collisions between the welding torch and the workpiece. This is achieved by defining a *workpiece extension box*, which is an imaginary box whose dimensions are such that the workpiece is fully contained inside it (see Figure 3.22). This extension box is given in terms of two points[16], situated at two diagonally opposite corners of the imaginary box: a) a point with the minimum co-ordinates of the box and b) a point with the maximum co-ordinates of the box. With the minimum and maximum co-ordinates of the box, the other corners are also obtained. These points are then transformed to the robot world co-ordinates frame by using equation (3.16) and a second imaginary box is defined, the *workpiece clearance box* (see Figure 3.22), whose corners are obtained by subtracting a *clearance* value (e.g. 50 mm) from the minimum transformed co-ordinates and adding the same *clearance* value to the maximum transformed co-ordinates. The *workpiece clearance box* will define the limits outside which the welding torch can be moved without colliding with the workpiece.

Figure 3.23 shows an example of how the weld approach points are obtained. In the example of this figure, to achieve a weld start point, the robot must follow the weld approach points from **ap3** to **ap1.** The robot is always restricted to linear movements between points, thus ensuring a predictable path. Note that the torch orientation in **ap3** is such that the X-axis of the torch co-ordinates frame points downwards (-Z world co-ordinate direction) and the Z-axis of the torch co-ordinates

---

[16] Relative to the CAD world co-ordinates frame

frame points to the front of the robot (+X world co-ordinate direction). The welding torch in moved from **ap3** to **ap2** in a linear path while the torch orientation is changed to assume the orientation required for the weld start point. Keeping this orientation, the torch is moved to **ap1** and then to the weld start point (**w1**). If the point **ap2** falls under the *workpiece clearance box* (i.e. the $ap2_z$[17] = *zmin - clearance*), a further point is necessary such that the robot moves the torch in a path around the *workpiece clearance box*. Figure 3.24 illustrates this case, in which the first approach point to be achieved by the welding torch is **ap4**. These points are generated such that the first weld approach point to be achieved by the welding torch is always located at the top surface of the *workpiece clearance box*

The same rules are used for generating both weld approach points and weld withdrawal points (**wdr**).

After obtaining the welding parameters, the weld start and end points, and the approach and withdrawal points for each weld on the workpiece, the off-line programming module generates three files: a) one containing the welding parameters, which are input to the control system; b) a second file containing the robot teach-points, which describe positions in space, in terms of robot world co-ordinates, and orientations, in terms of quartenions[18], and c) a third file containing the robot program with comments explaining each command and the input and output signals necessary for communicating with the control system. Appendix C shows the user interface for the off-line programming module and some of its outputs.

3.3.2.3 Robot simulation

Having generated the robot teach points and the robot program, a simulation can be performed in order to verify if all the teach points are achievable and if any collisions are detected between the robot and the welding torch structure and also between the robot and the other components of the welding cell. If any problem is detected it can be solved by either changing the position of the workpiece (e.g. by making it further or closer to the robot and/or changing its height) or by adding more teach points in order to change the previously defined robot path. If any modifications are necessary in the workpiece positioning, the same modification must be carried out in the real cell and a new program must be generated by using the off-line programming module with a different CAD-to-Robot transformation matrix.

After correcting the detected errors, the corrected robot program can be compiled and downloaded to the robot controller for execution.

Once the system is correctly calibrated, the only possible sources of error will stem from the component error group and from process disturbances. As mentioned before, these errors should be dealt with by an on-line adaptive control system.

---

[17] Z co-ordinate of point **ap2**

[18] A quartenion (Q) is a mathematical way of representing a rotation by a certain angle about an axis by means of a scalar (s) and a vector (v): $Q = [\, s + v \,]$ (see refs. 192, 193).

3.3.3 Control module

In the control module (see Figure 3.25) the welding process and the position of the welding torch relative to the joint are monitored and controlled in order to ensure that the required weld quality is achieved. The module comprises three main parts: a) the monitoring system; b) the control of welding torch-to-workpiece relative position; c) the control of the welding process.

The monitoring system is responsible for continuously monitoring the state of the process and the relative positioning between welding torch and joint line. The welding data are acquired via suitable sensors, digitized and relayed to the main controller, where an assessment is made about the process state and control instructions are issued and transferred to the other control parts of the module.

The control of the welding torch-to-workpiece relative position is represented in Figure 3.25 by the blocks surrounded by a dashed line and comprises the main controller, the torch-to-workpiece relative position controller and the robot. In the main controller, the deviation of the required relative positioning is estimated based on the information acquired by the monitoring system. Such deviation is then transferred to the relative position controller where control instructions are generated in order to compensate for the deviations.

The control of the welding process is represented in Figure 3.25 by the blocks surrounded by a dash-dotted line and includes the main controller and the welding power source. In the main controller the changes in welding parameters that are necessary to compensate for a deviation of process behaviour are issued and transferred to the welding power source, which is responsible for ensuring that the controlled welding parameters are implemented.

Note that in Figure 3.25, the block representing the main controller is involved by the limiting boundaries of both the welding process control and the torch relative position control. Such representation was adopted to show the interdependency between torch positioning and welding process behaviour.

The control system implemented is described in detail in the next chapter.

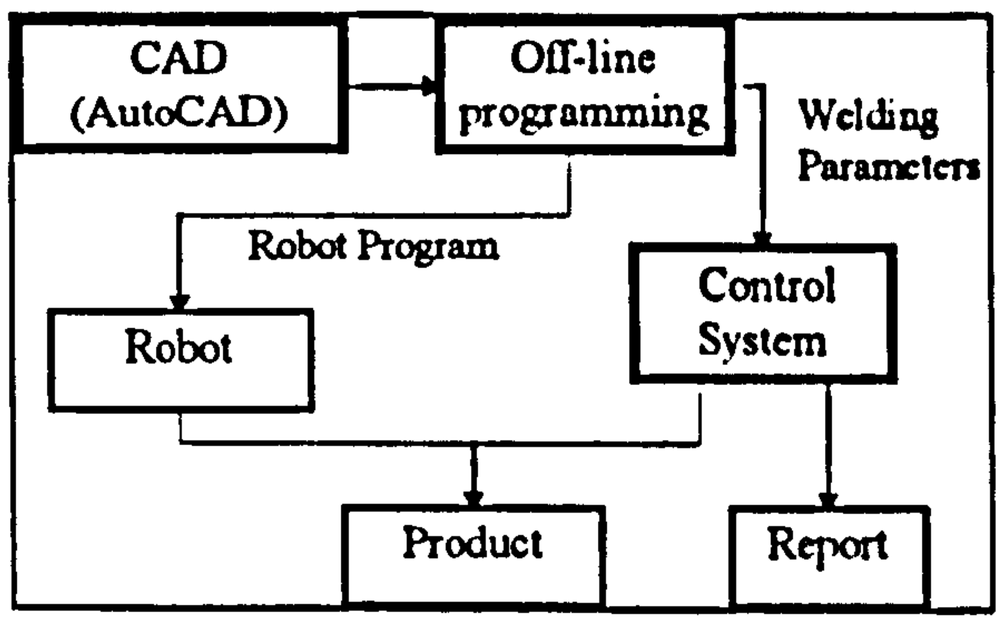

Figure 3.1 - System Overview

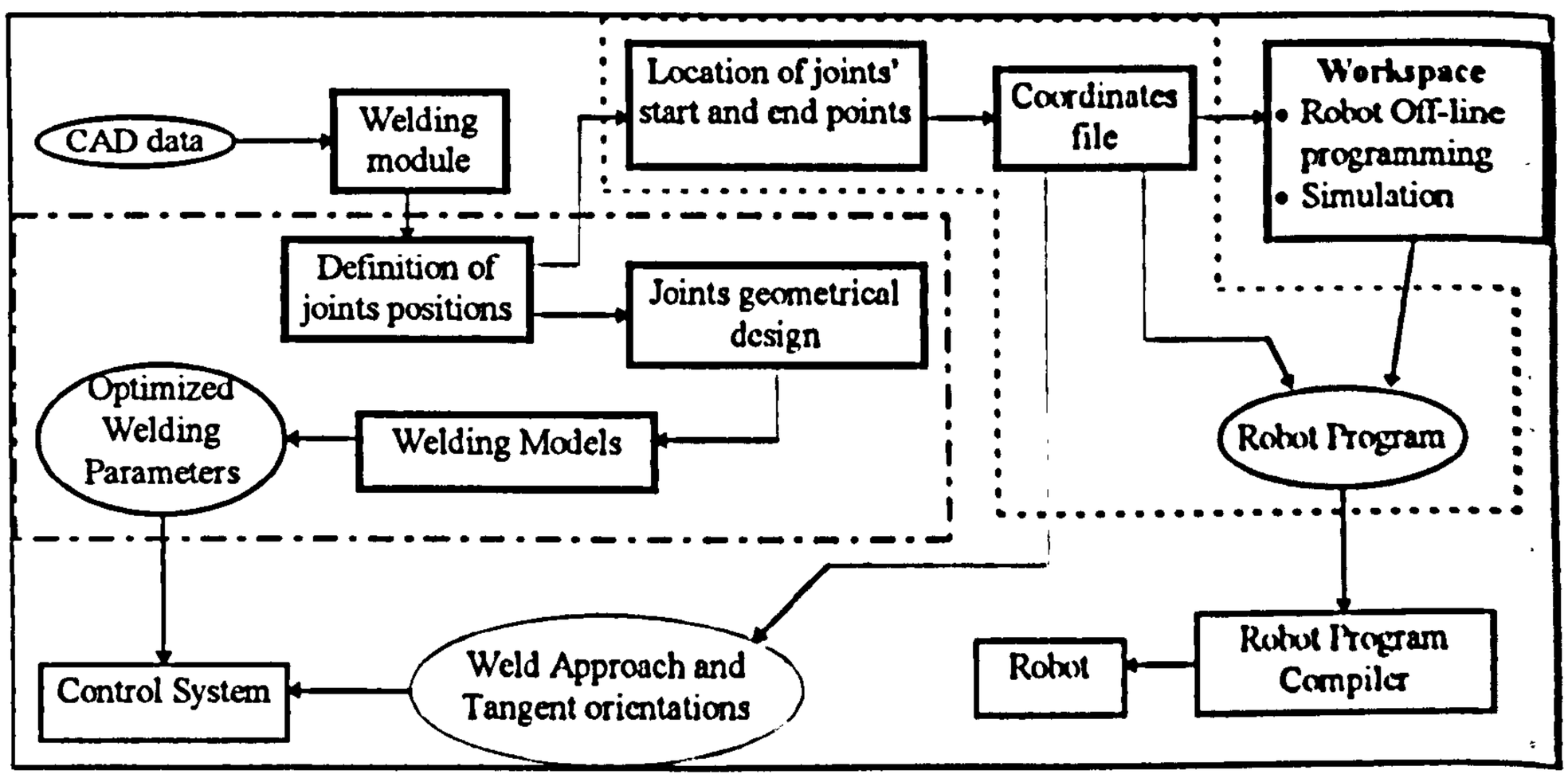

Figure 3.2 - Off-line Programming Module

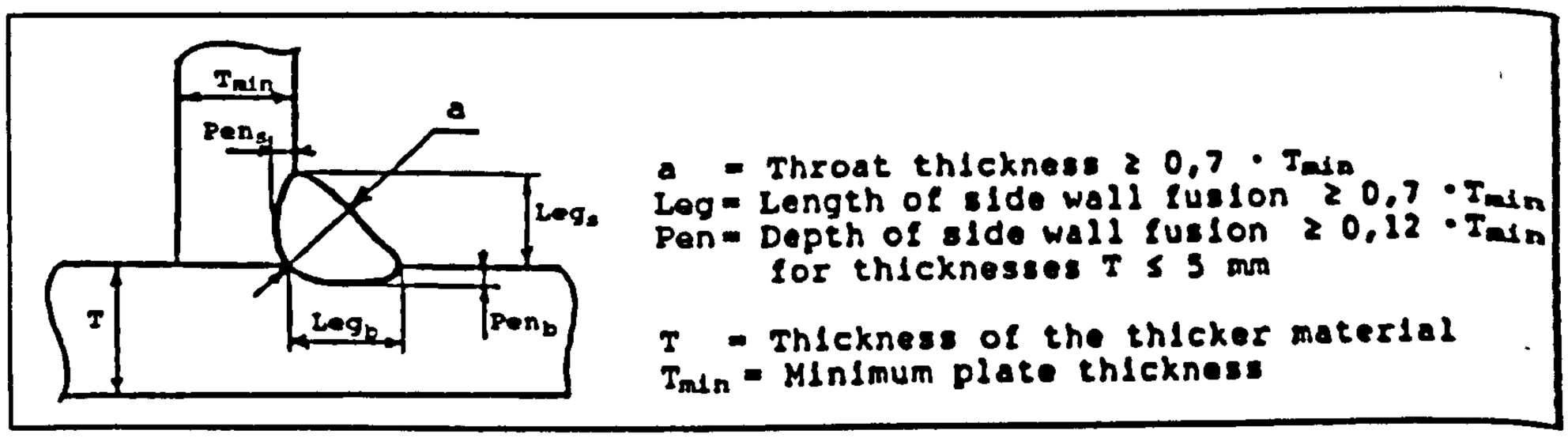

Figure 3.3 - Inauxa specifications for fillet welds [ref. 190]

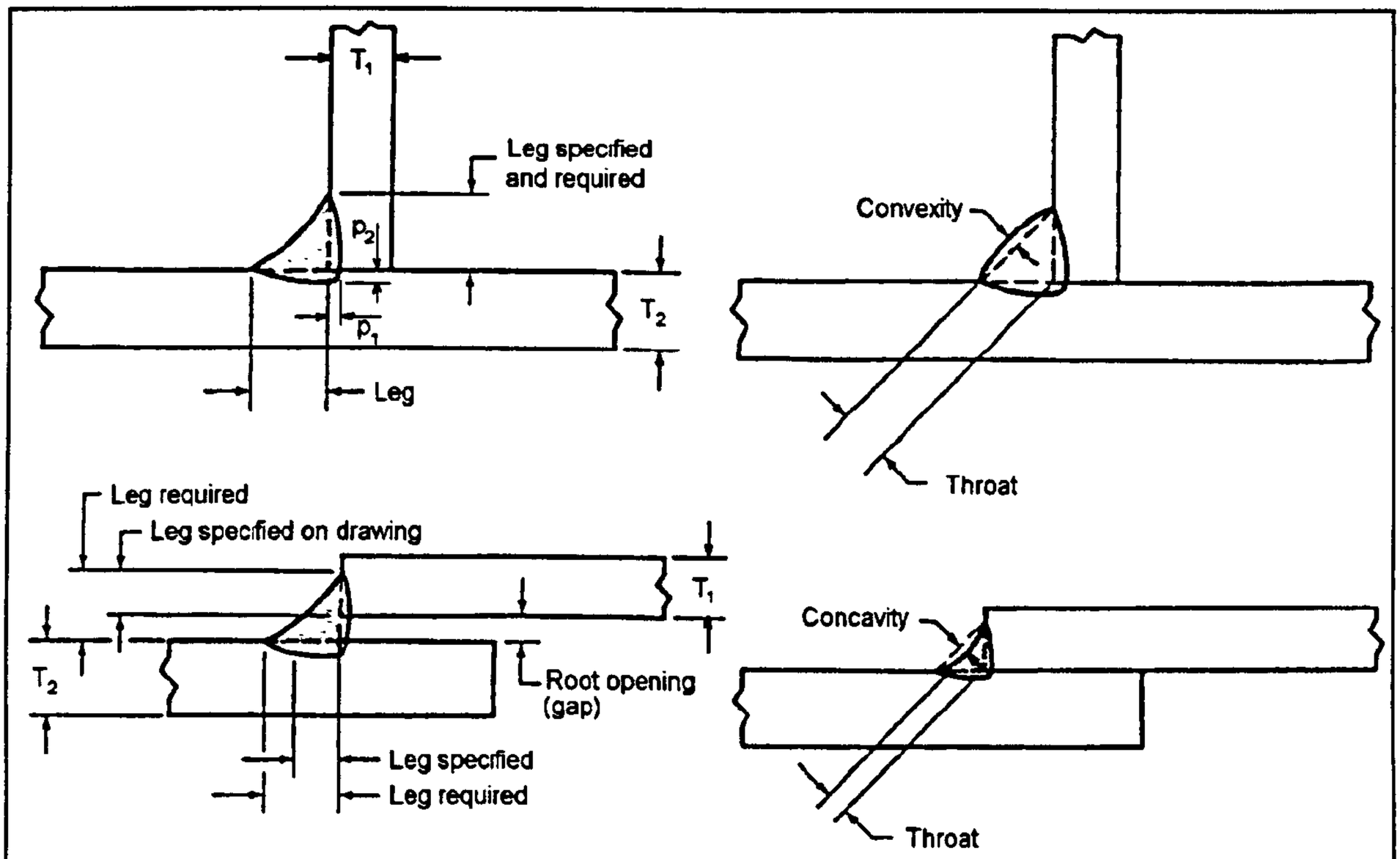

Figure 3.4 - AWS Specification for Automotive Frame Weld Quality - Fillet Weld [ref. 107]

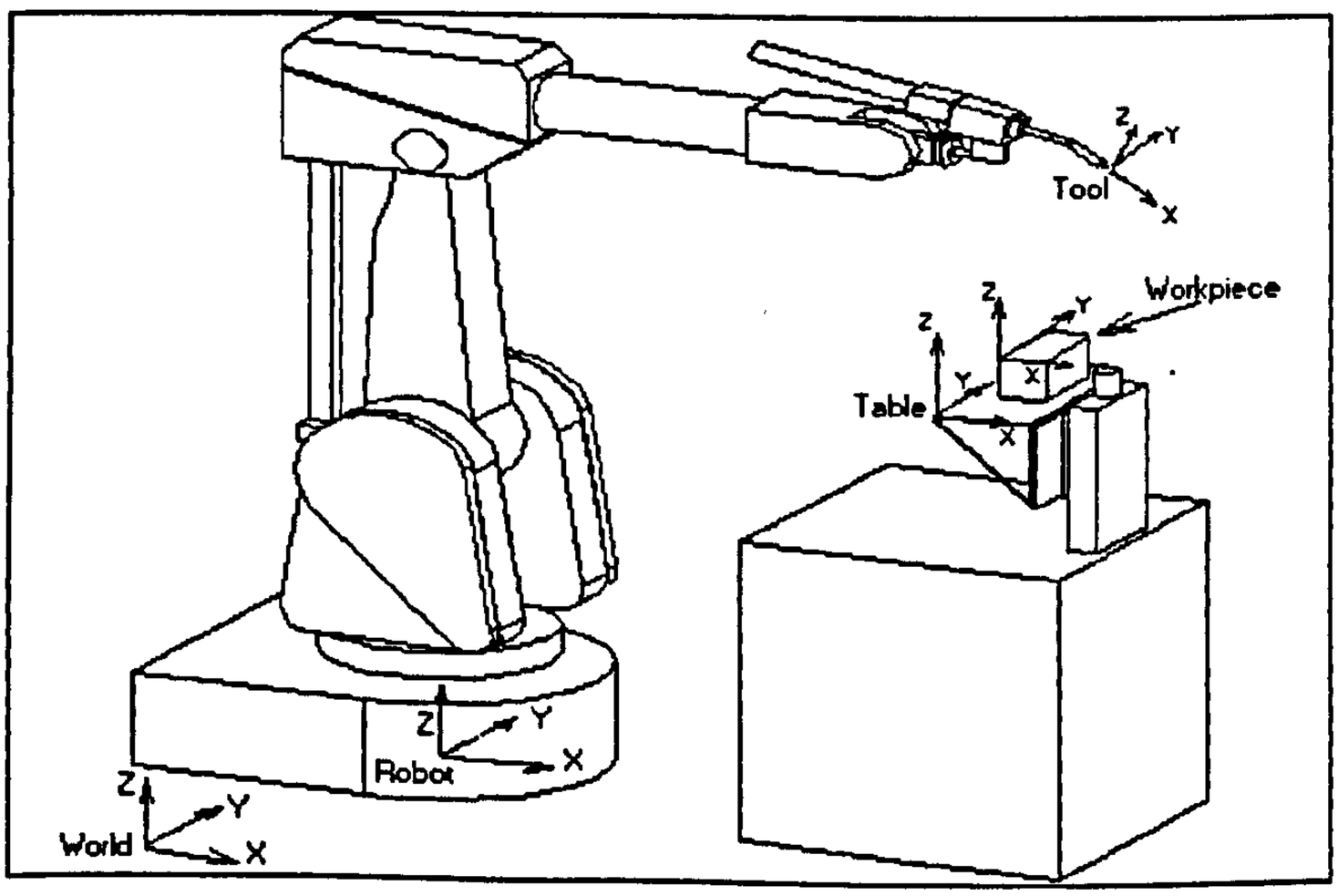

Figure 3.5 - Co-ordinate frames used for off-line programming

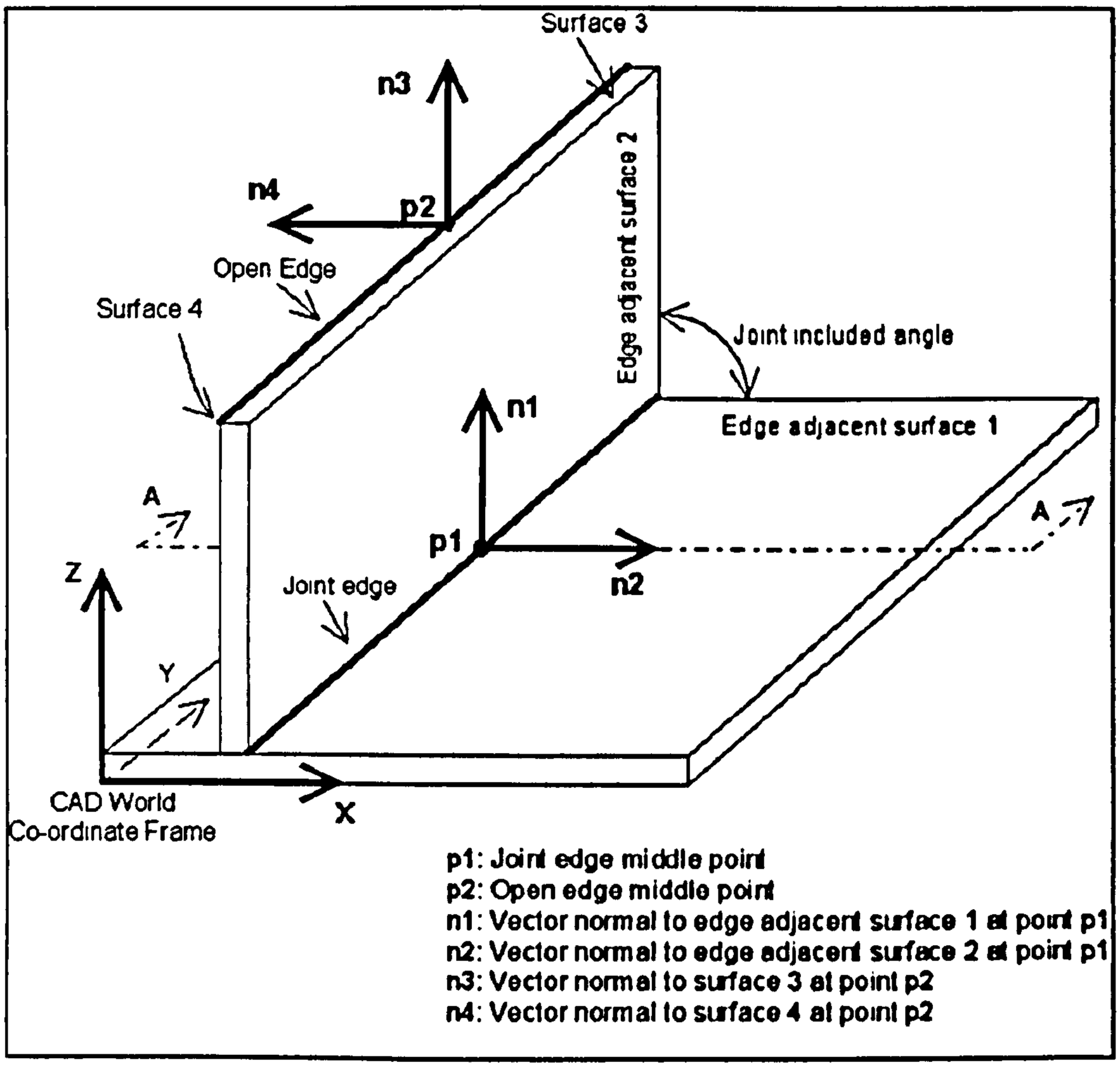

Figure 3.6 - Joint geometrical definitions

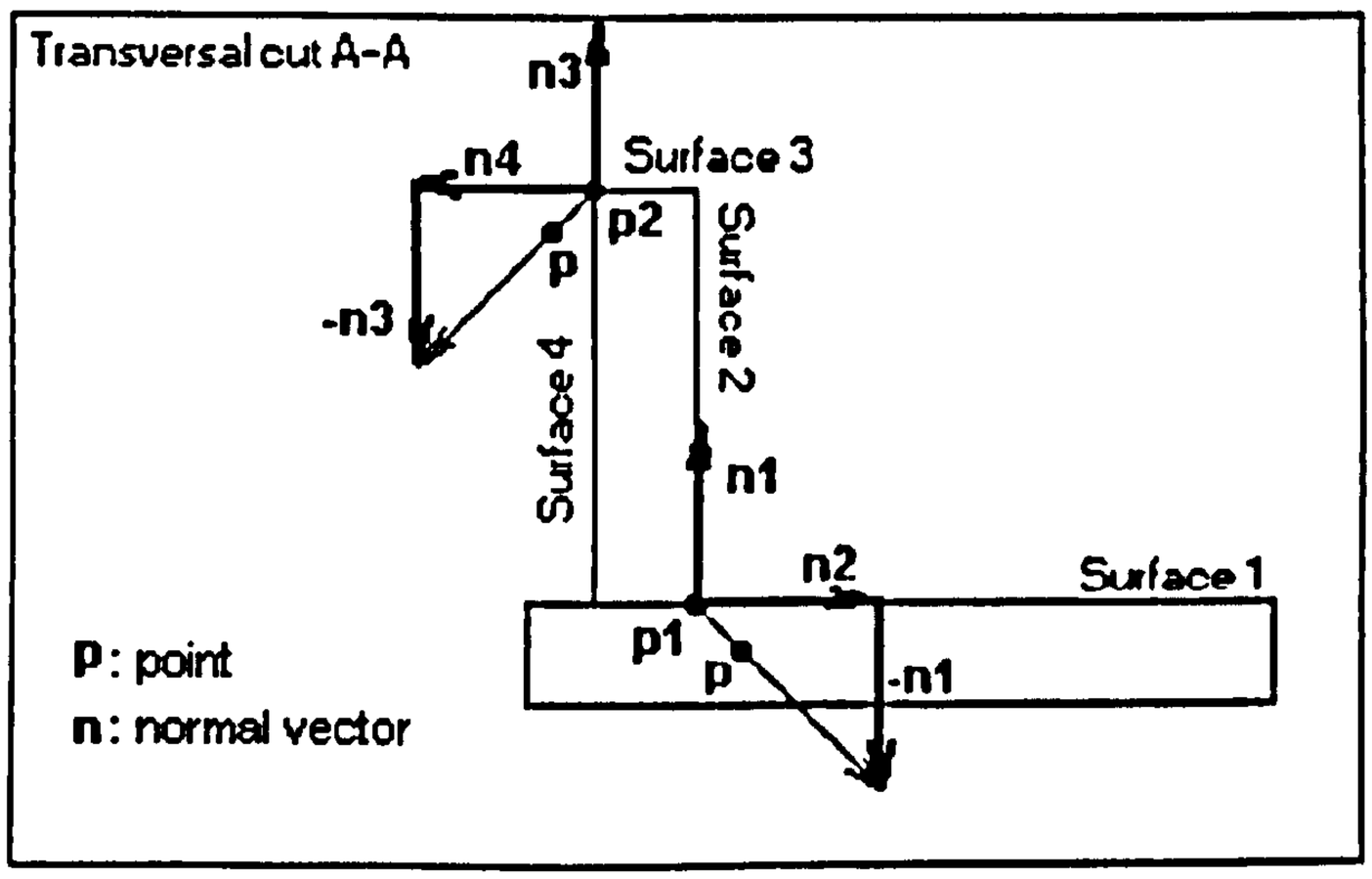

Figure 3.7 - Method for determining if surface intersection is a valid joint (Transversal cut A-A shown in Figure 3.6)

TABULATION OF POSITIONS OF FILLET WELDS			
POSITION	DIAGRAM REFERENCE	INCLINATION OF AXIS	ROTATION OF FACE
FLAT	A	0° TO 15°	150° TO 210°
HORIZONTAL	B	0° TO 15°	125° TO 150° 210° TO 235°
OVERHEAD	C	0° TO 80°	0° TO 125° 235° TO 360°
VERTICAL	D E	15° TO 80° 80° TO 90°	125° TO 235° 0° TO 360°

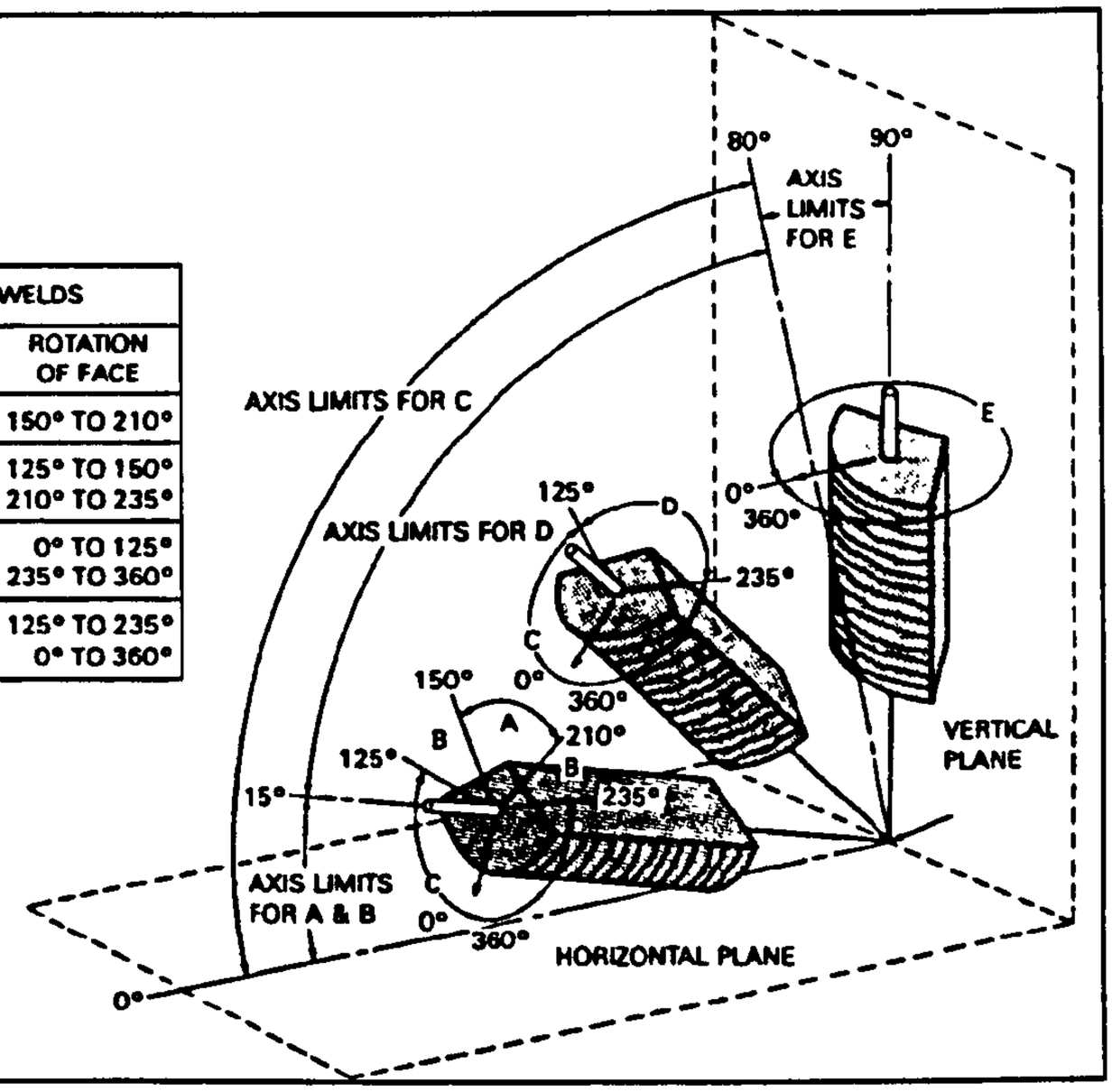

Figure 3.8 - Limiting angles for defining positions of fillet welds [ref. 191]

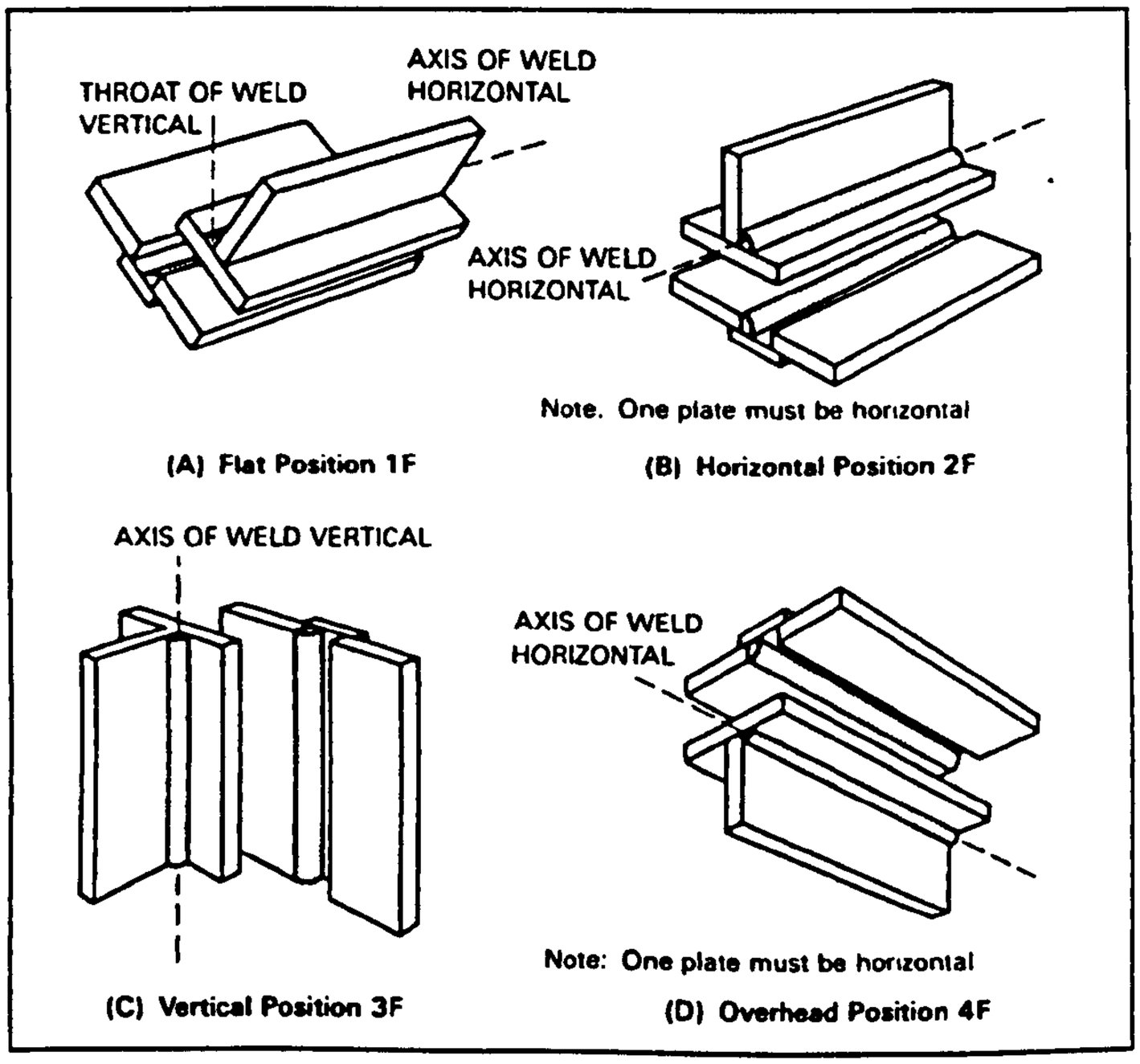

Figure 3.9 - Typical welding positions for fillet joints [ref. 191]

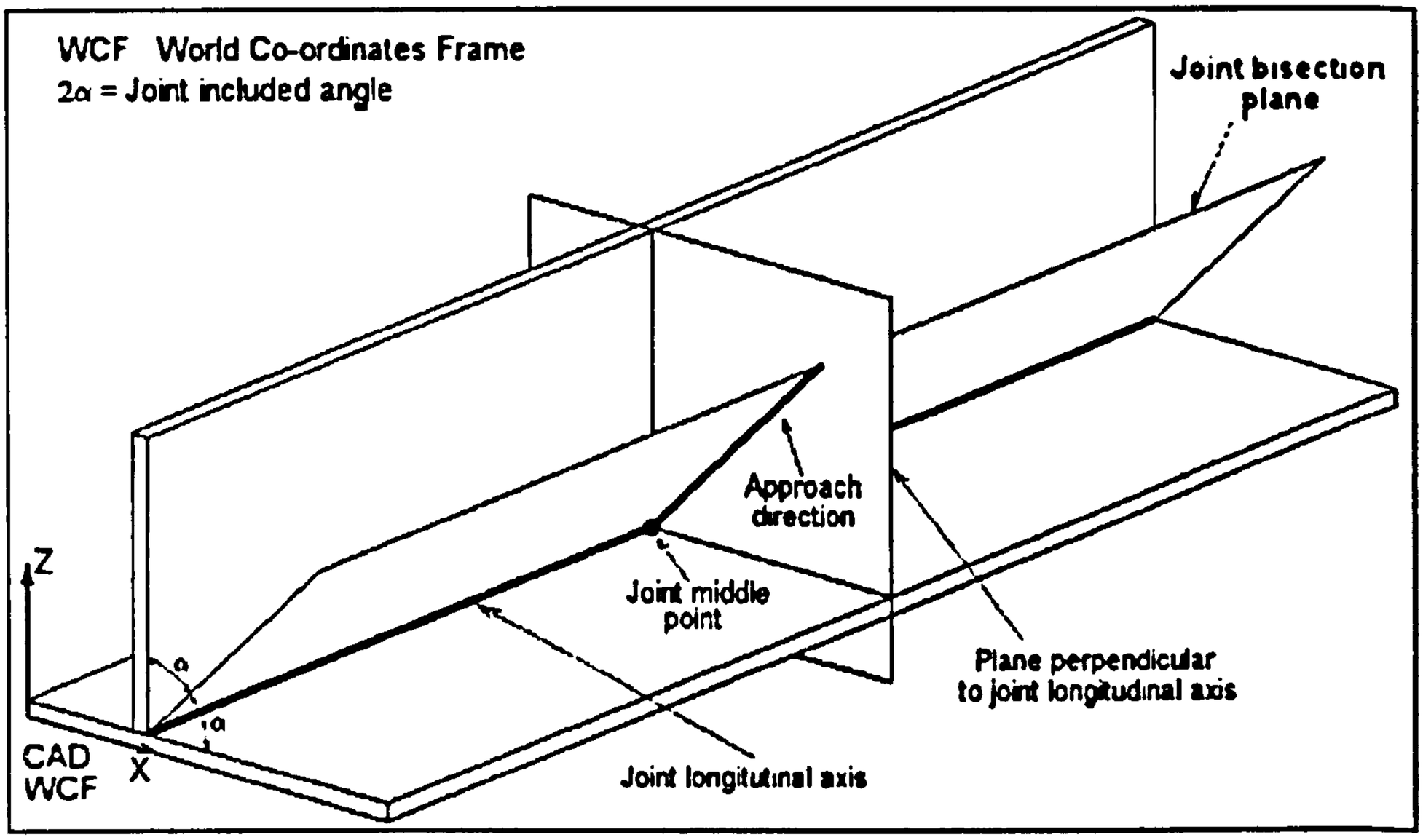

Figure 3.10 - Planes whose intersection results in a line which defines the default joint approach direction.

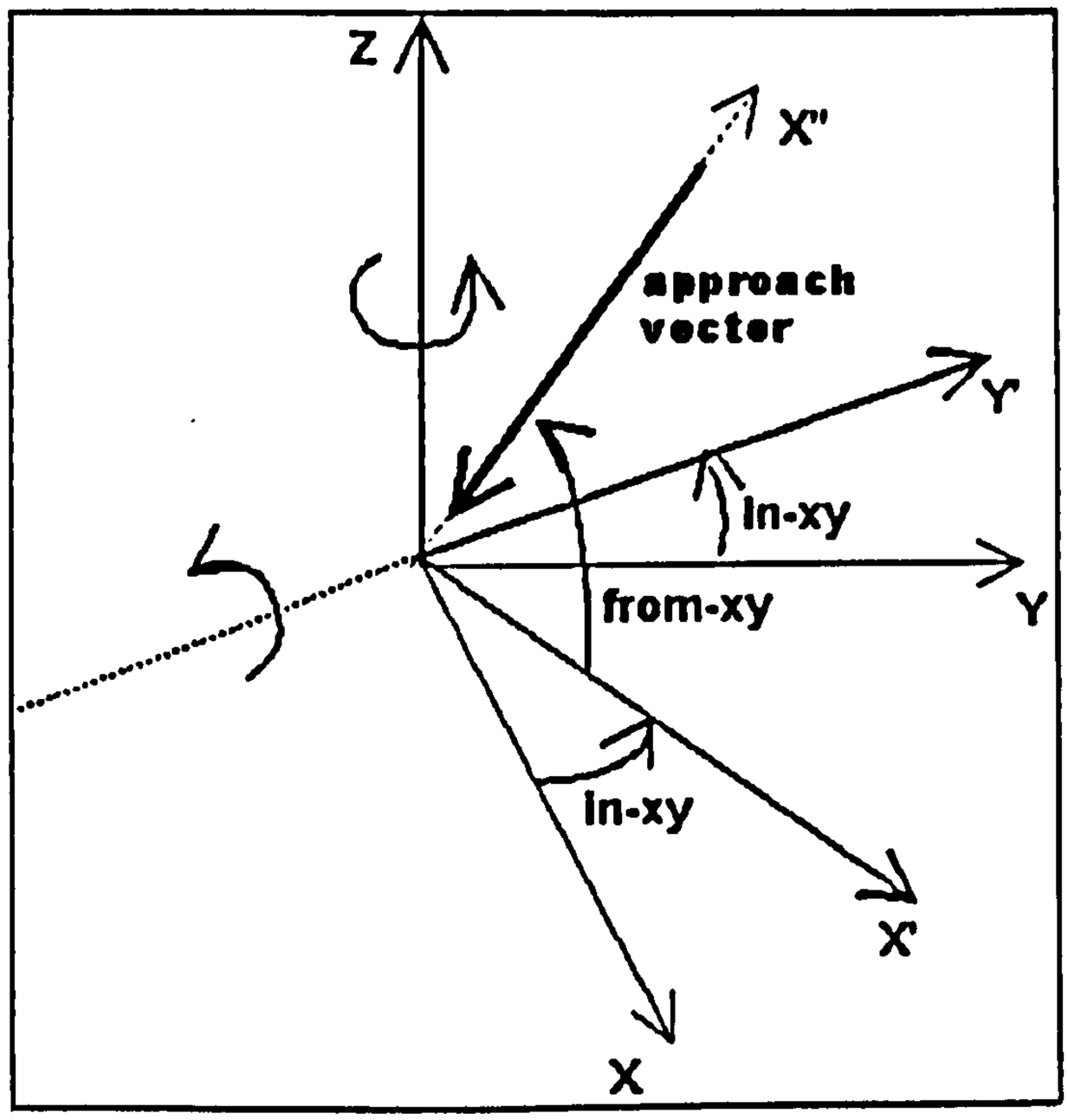

Figure 3.11 - Definition of orientation by two angles

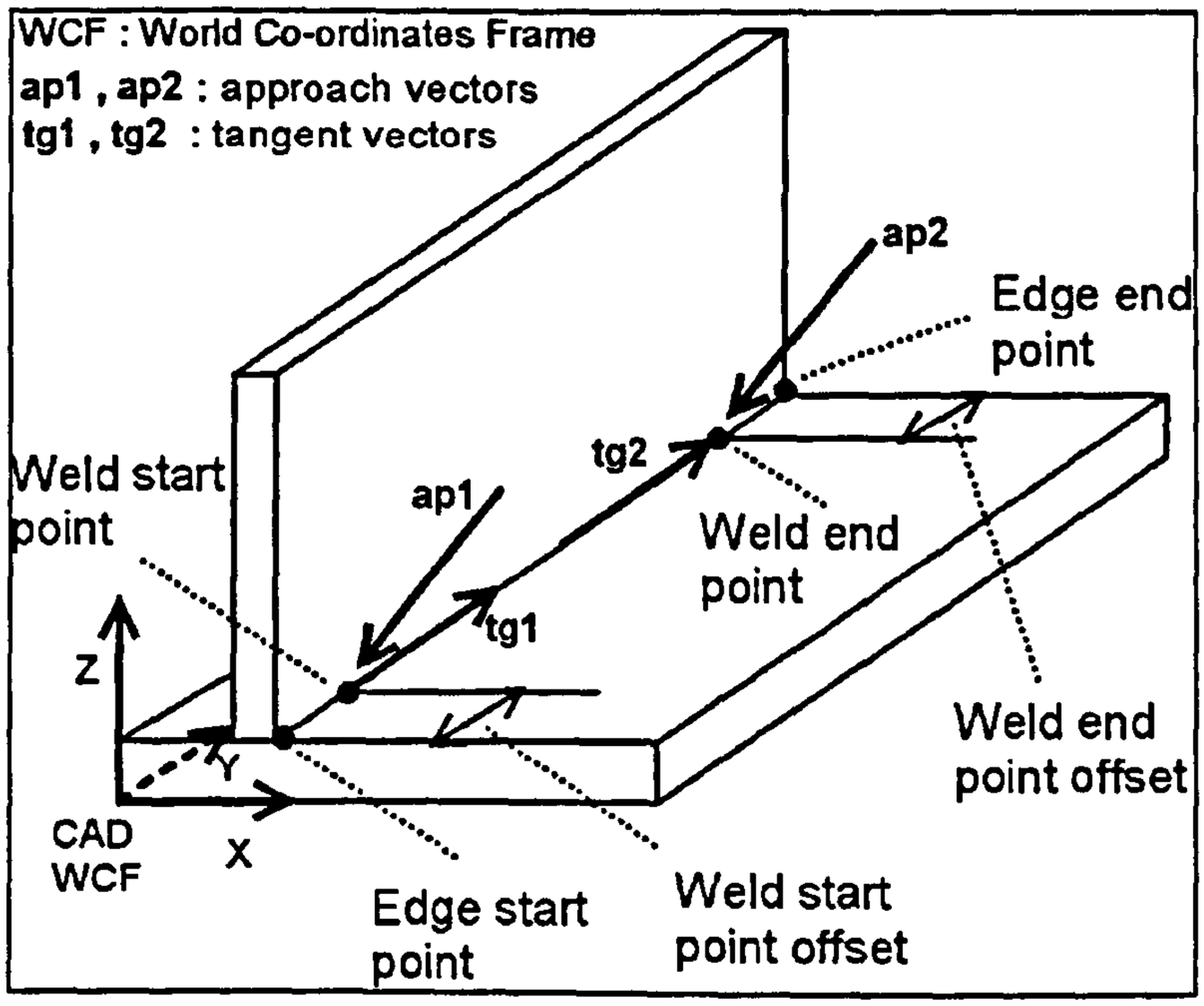

Figure 3.12 - Offsets for weld start and end points

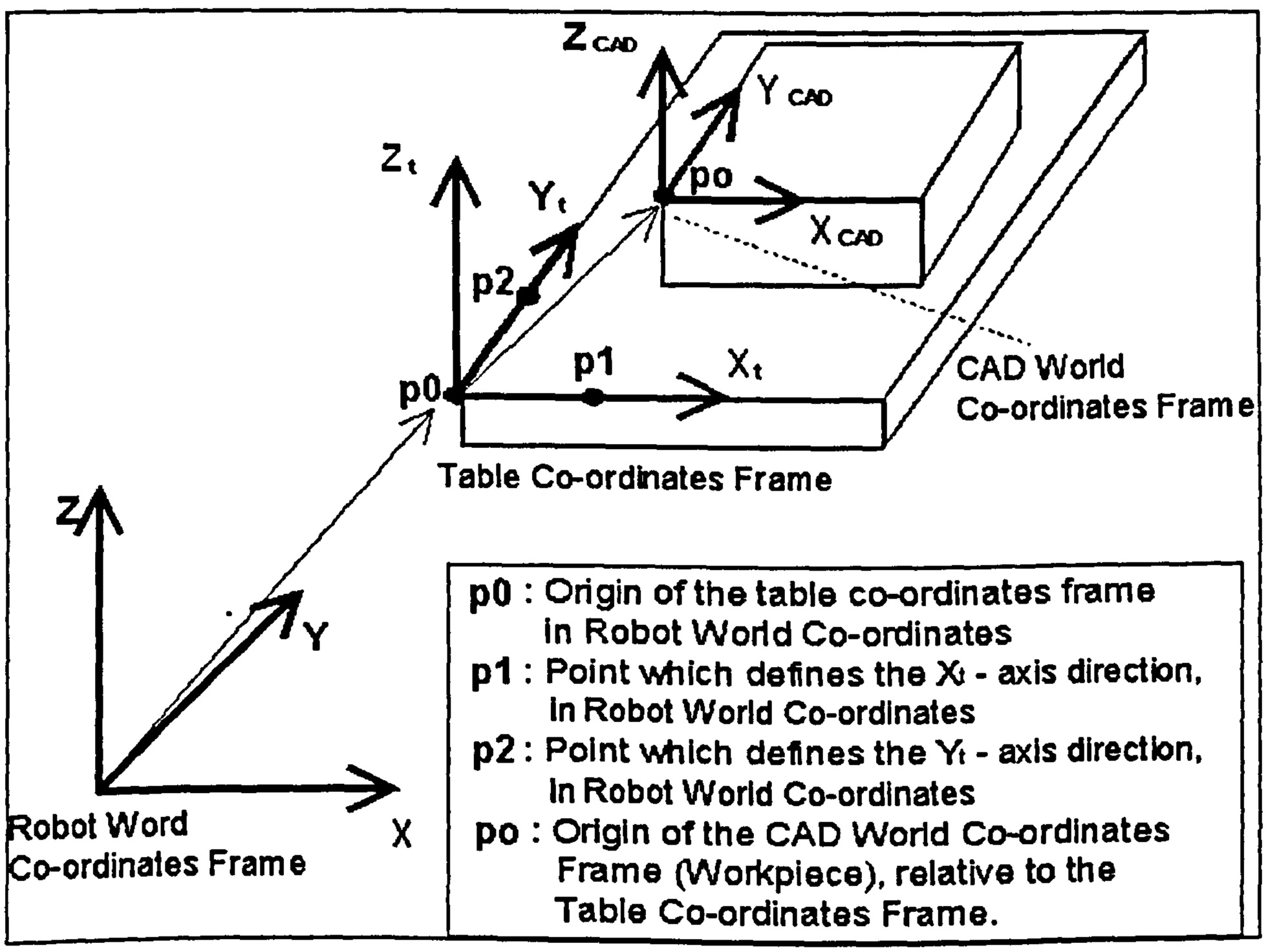

Figure 3.13 - Points used to obtain the transformation matrix between Robot World and CAD co-ordinates frames

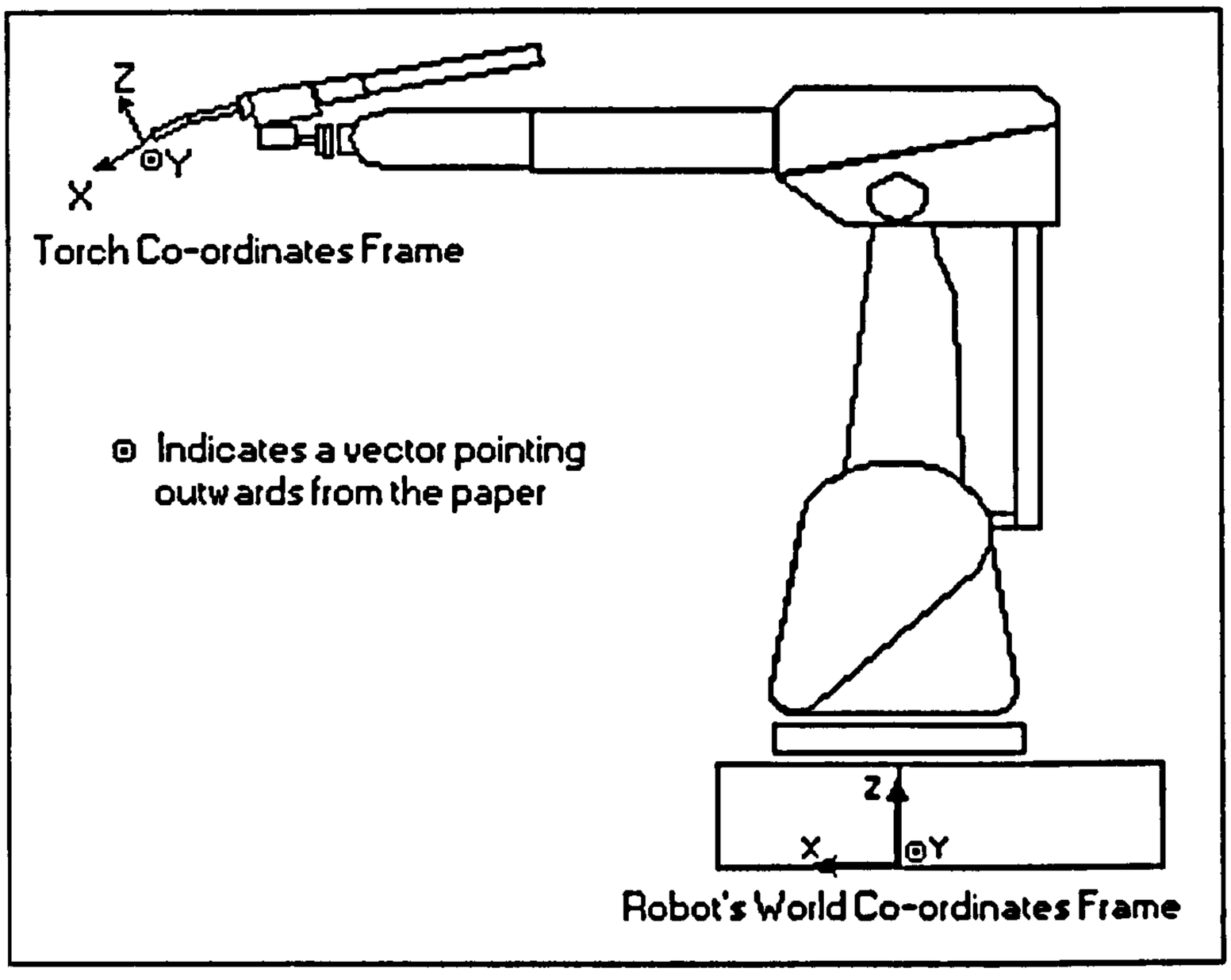

Figure 3.14 - Welding torch configuration for robot in zero position

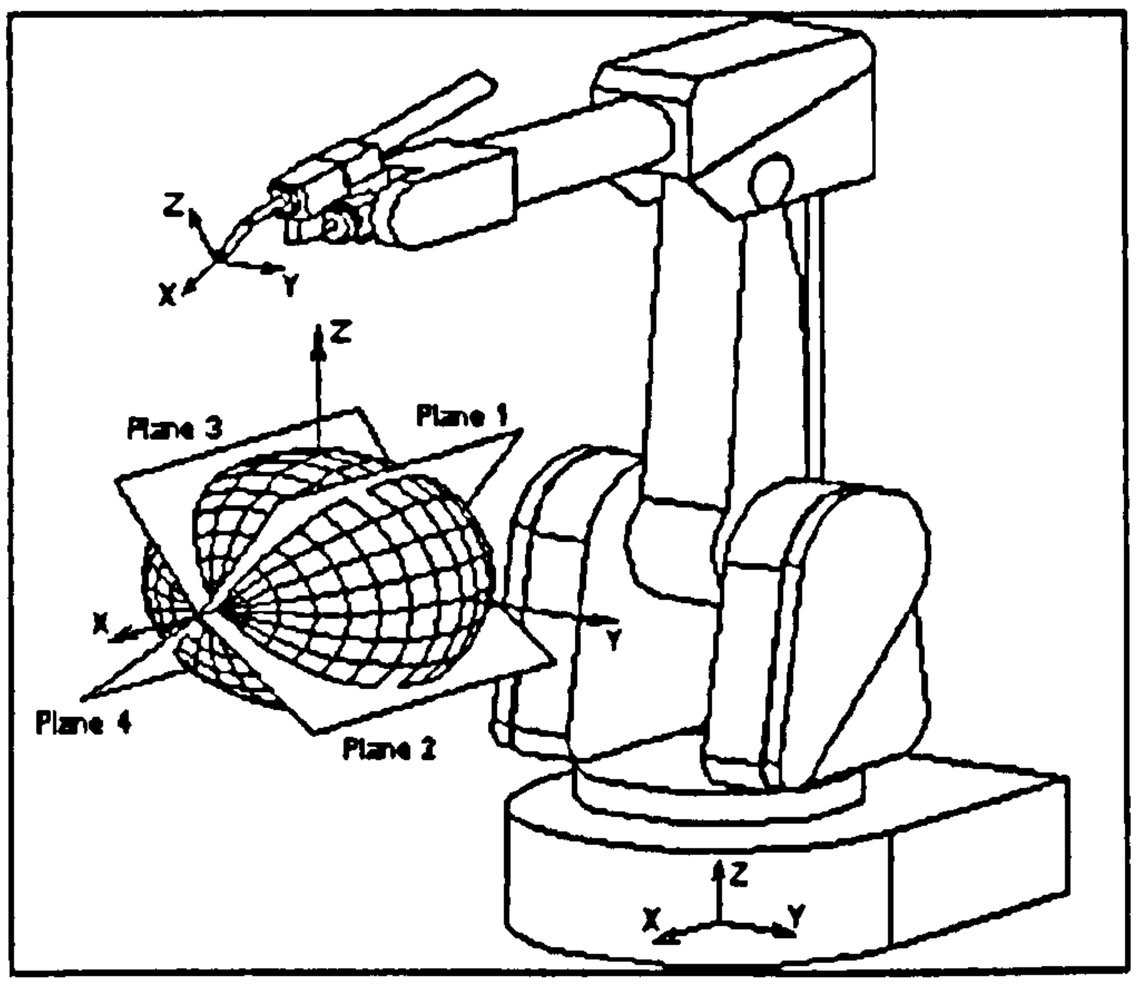

Figure 3.15 - Torch orientation sphere

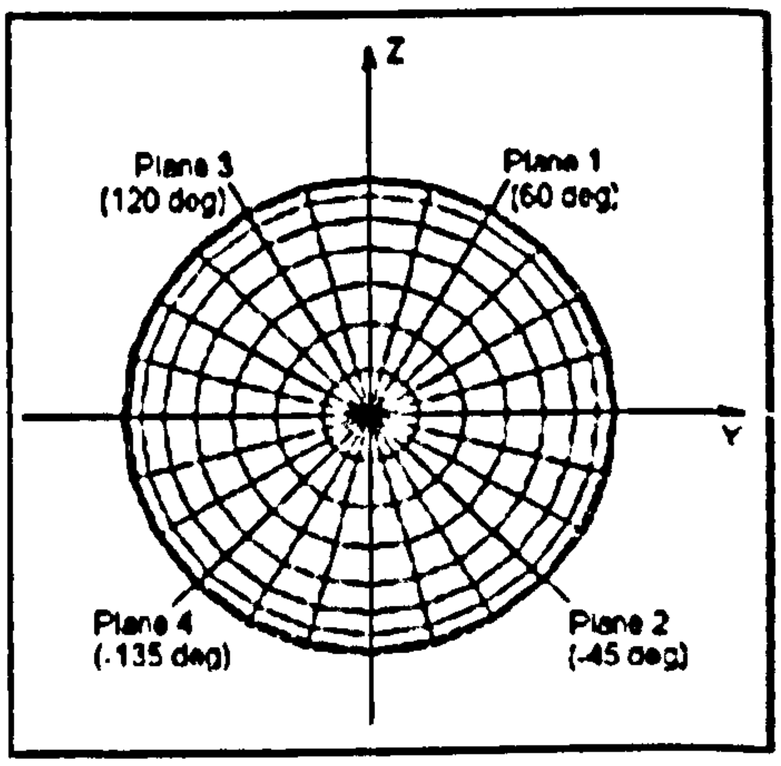

Figure 3.16 - Front view of the torch orientation sphere

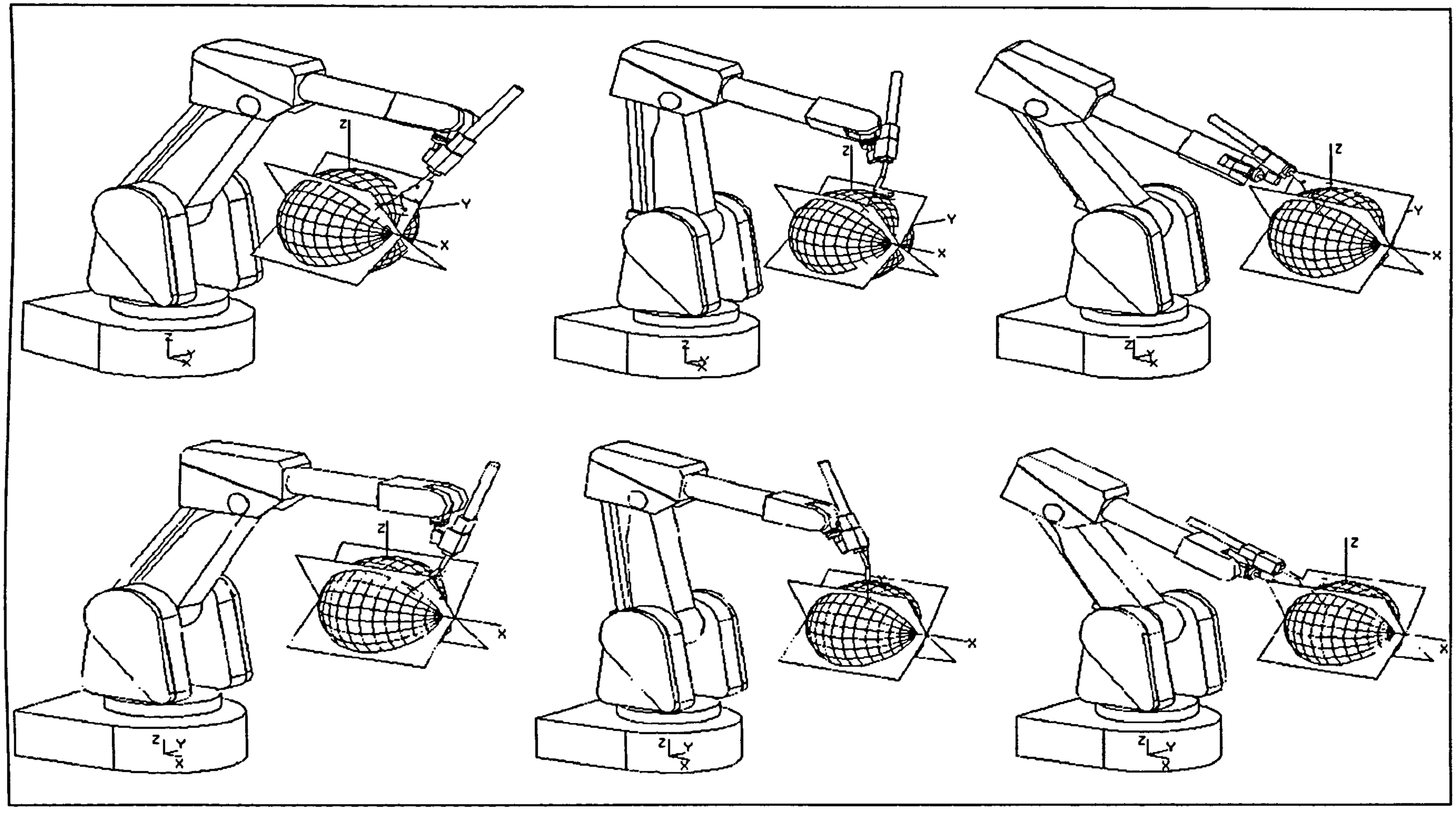

Figure 3.17 - Torch orientations for approach vector contained in planes with angles between 60 deg and 90 deg

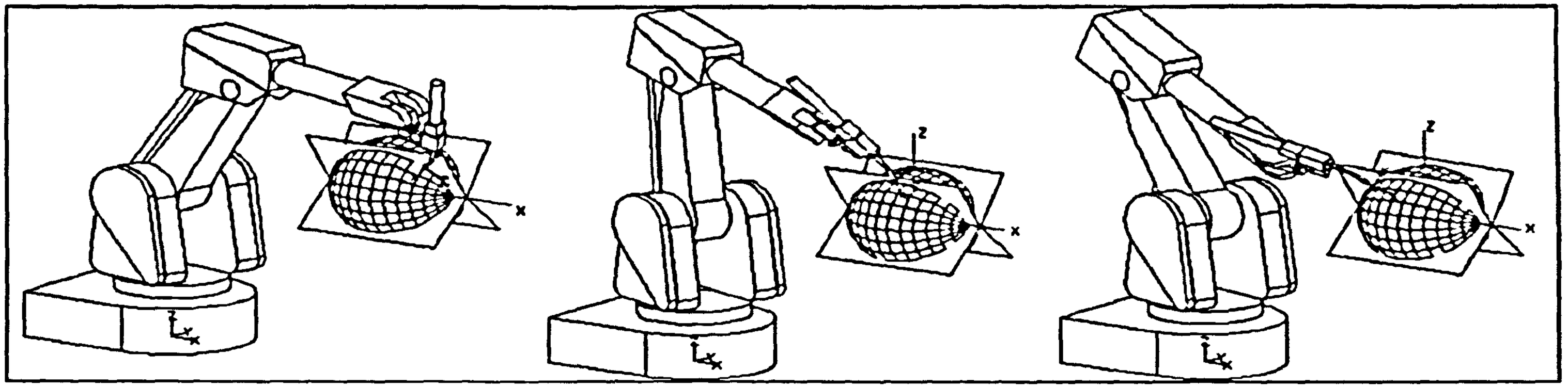

Figure 3.18 - Torch orientation for approach vector contained in plane rotated about the sphere's X-axis by 120 deg

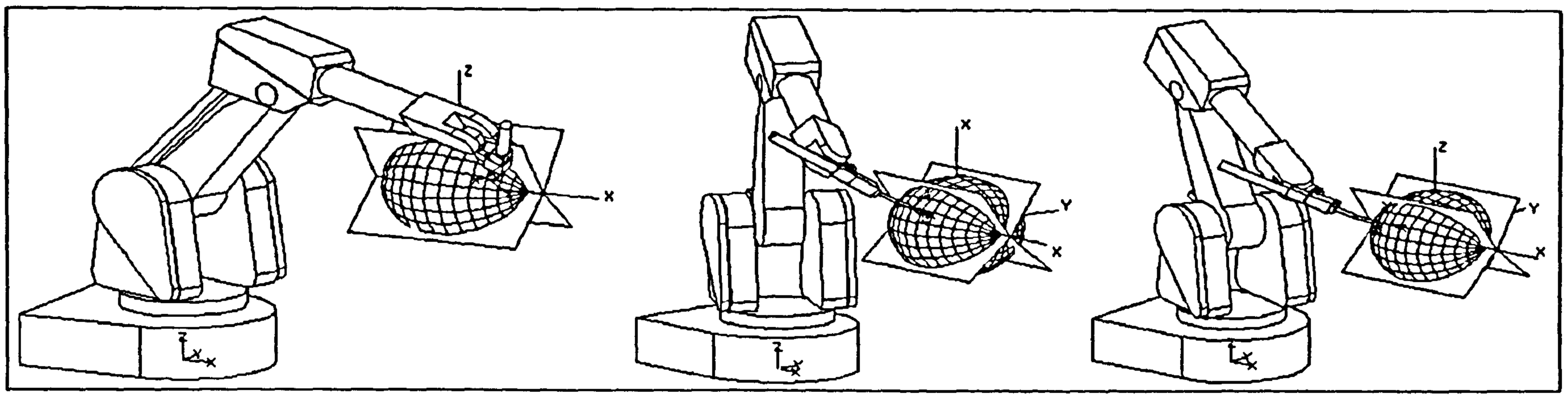

Figure 3.19 - Torch orientation for approach vector contained in plane rotated about the sphere's X-axis by 150 deg

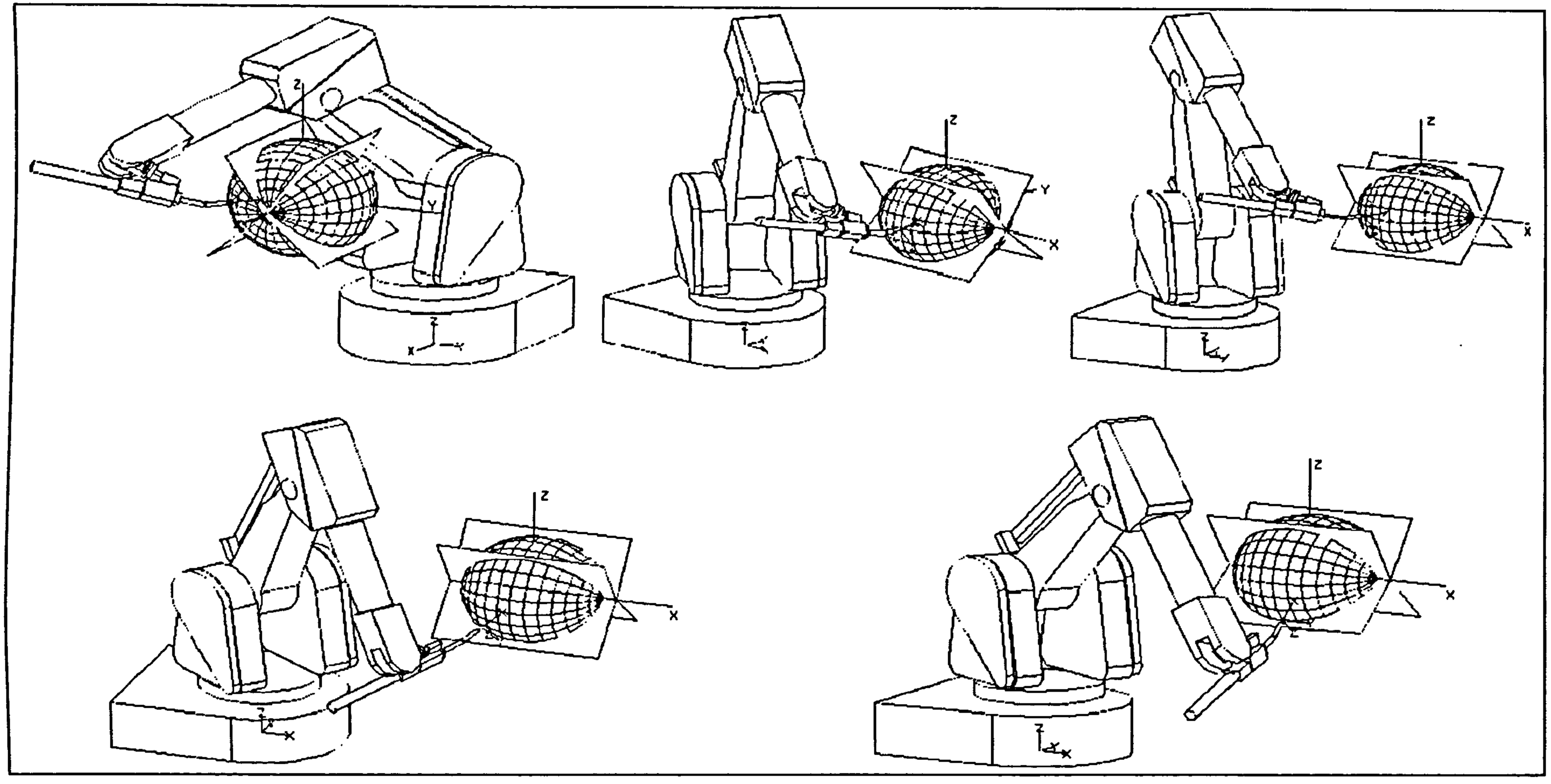

Figure 3.20 - Torch orientation for approach vector contained in plane rotated about the sphere's X-axis by angles between 180 deg and 225 deg

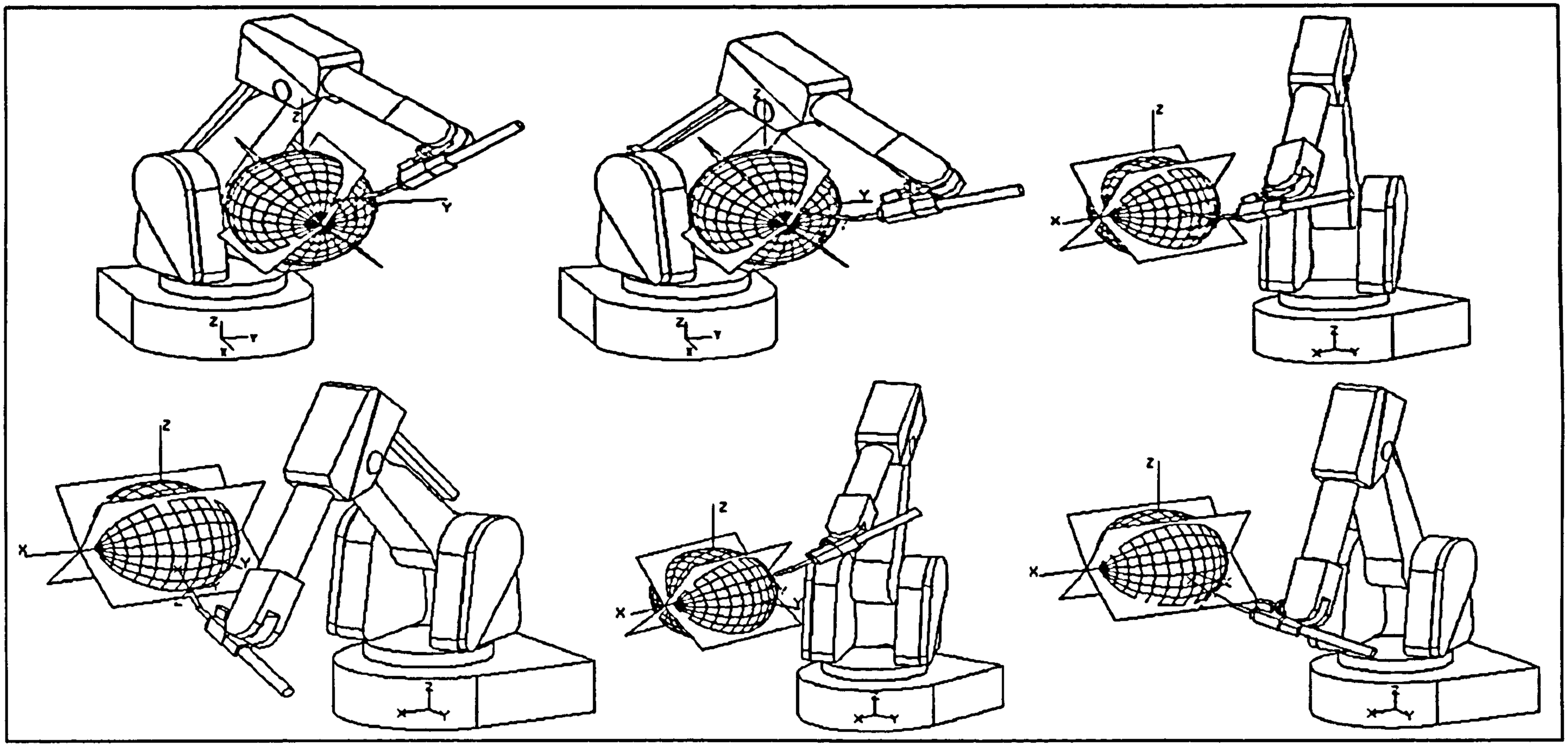

Figure 3.21 - Torch orientation for approach vector contained in plane rotated about the sphere's X-axis by angles between -45 deg and 60 deg

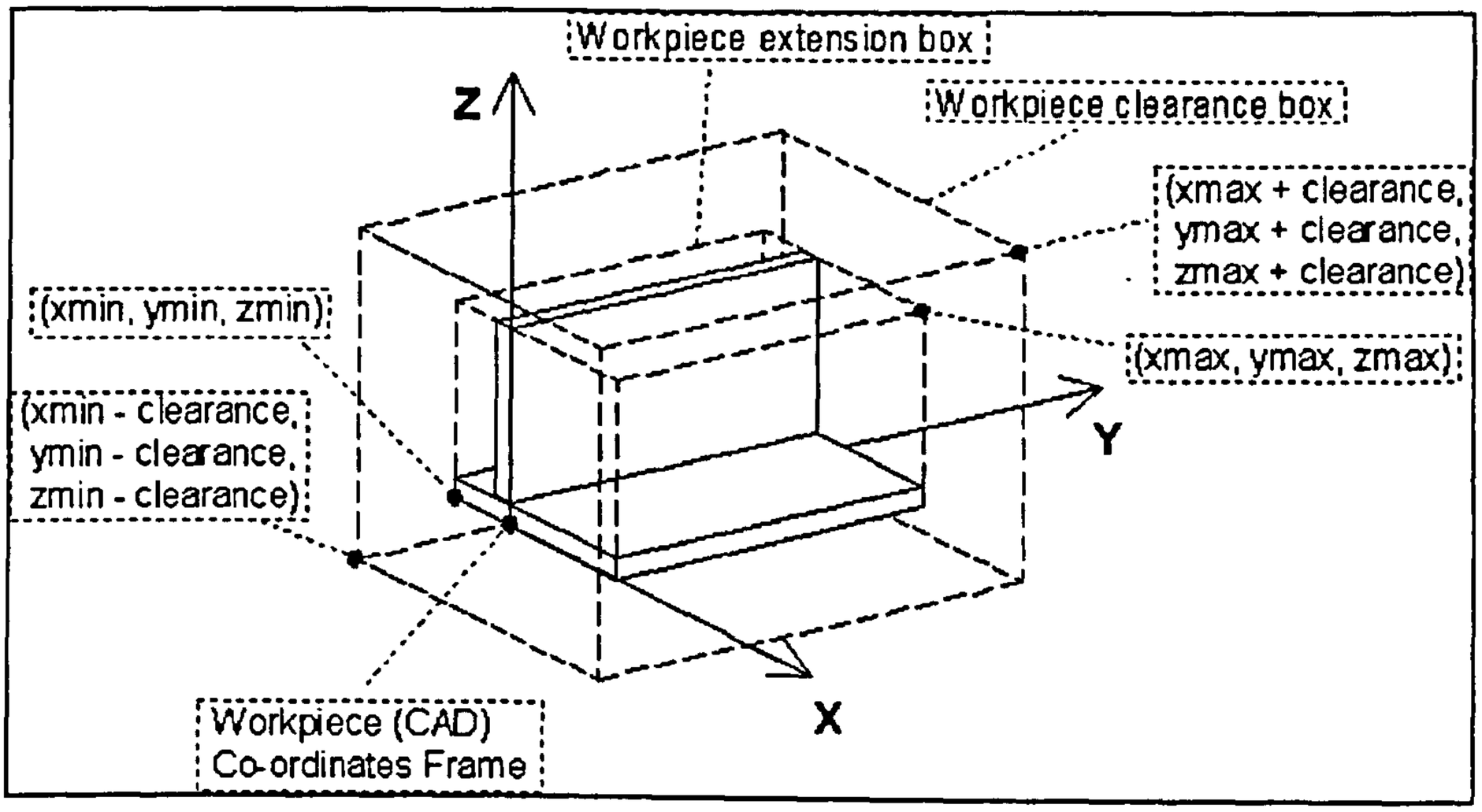

Figure 3.22 - Definition of "workpiece extension box" and "workpiece clearance box"

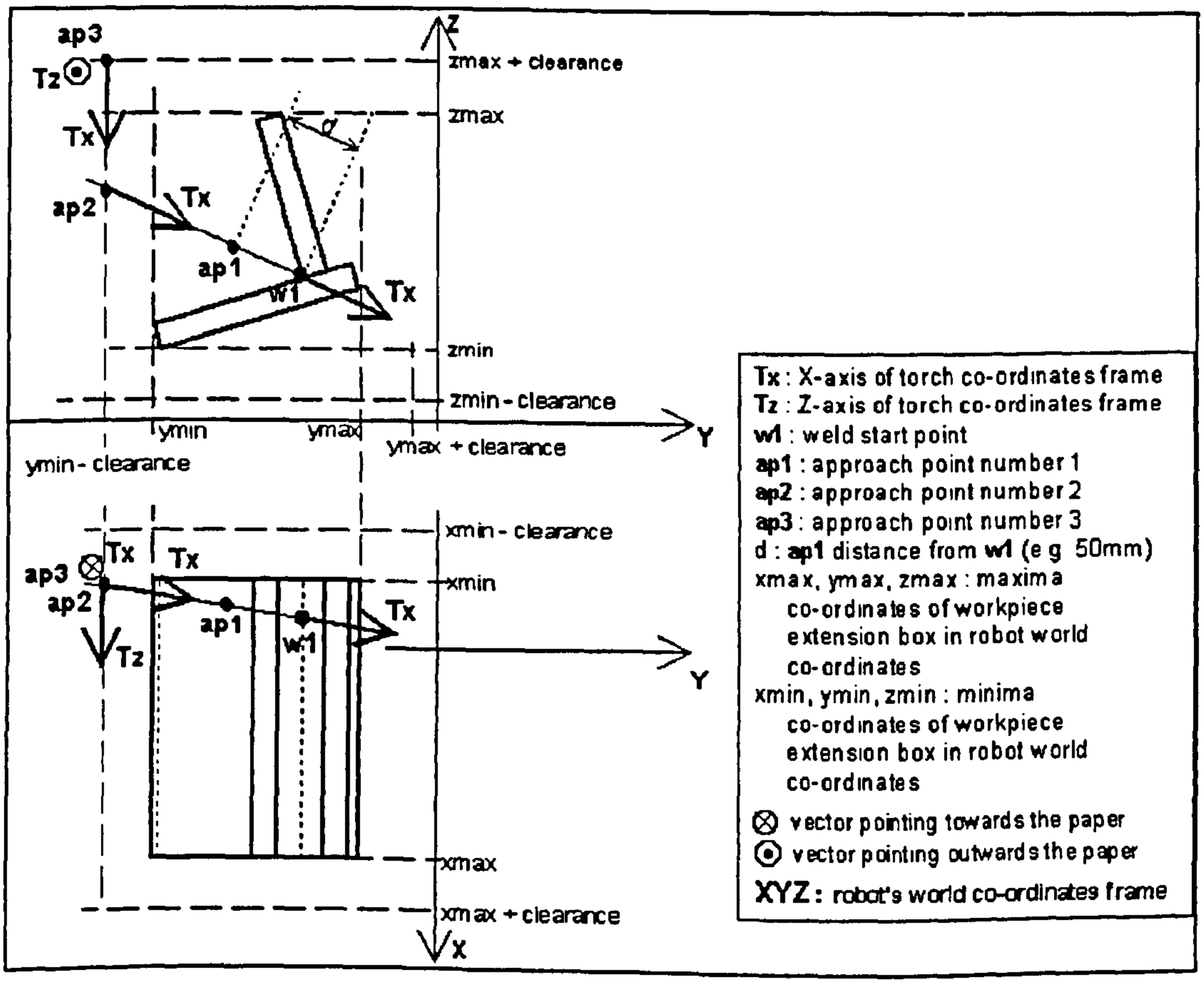

Figure 3.23 - Method used to determine the weld approach and withdrawal points

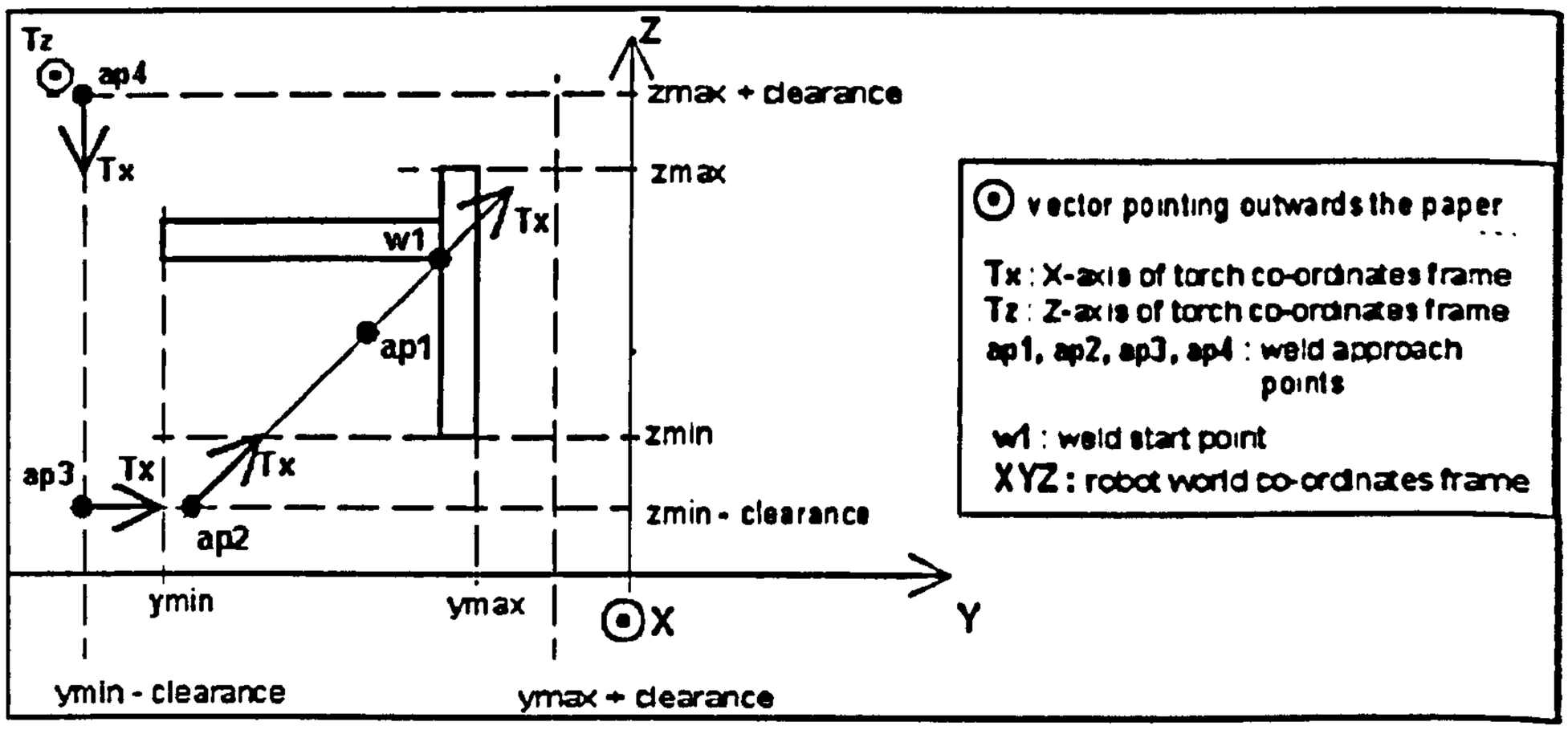

Figure 3.24 - Case when four approach points are necessary

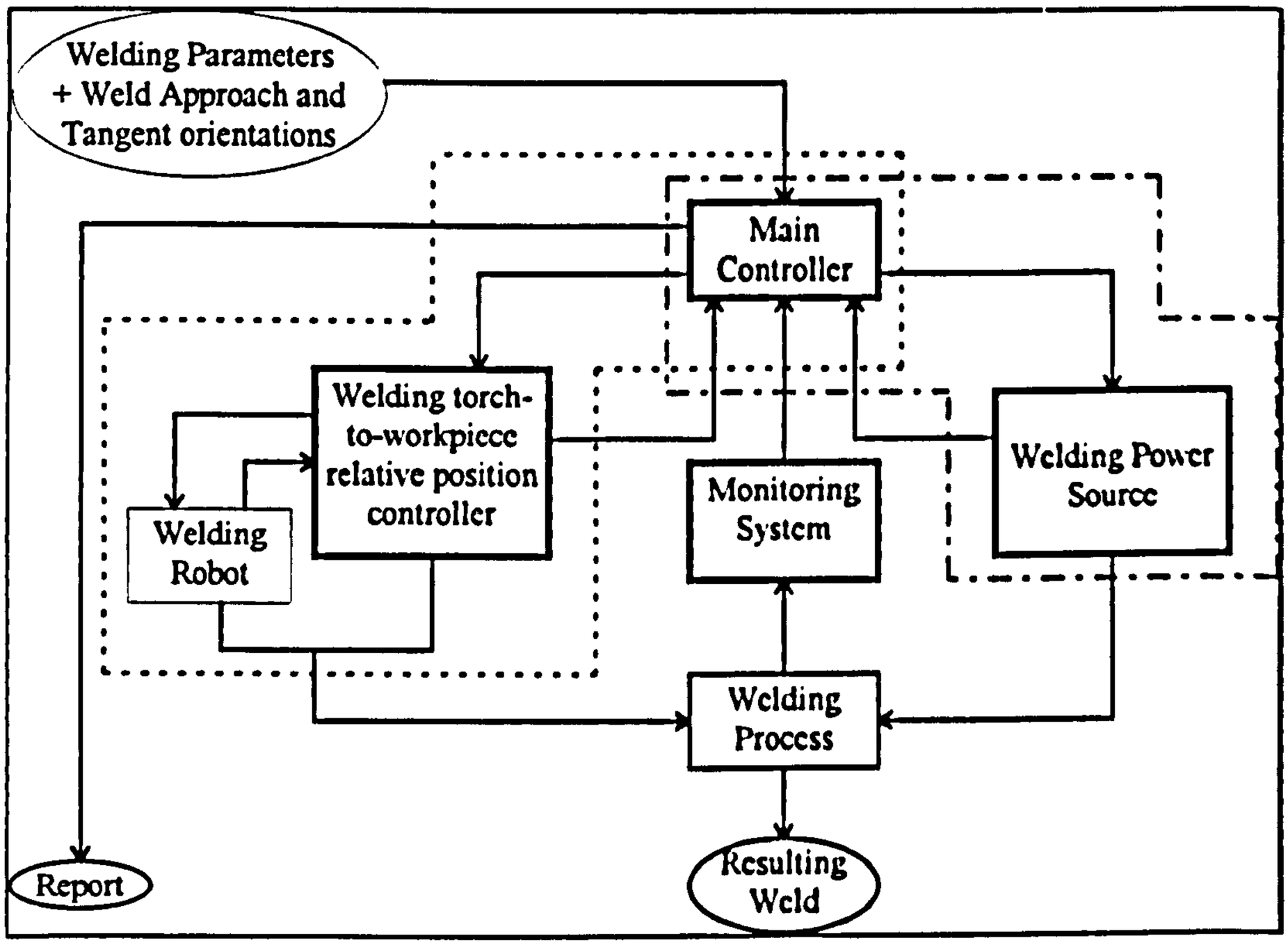

Figure 3.25 - Control system

4. On-line Control Strategy

In this chapter, a detailed explanation about the implemented control strategy will be given, along with a description of the control algorithms used and the assumptions made.

4.1 Control of relative position between welding torch and workpiece

The control of torch-to-workpiece relative position involves two main aspects: a) the control of the contact tip-to-workpiece distance (i.e. stand-off) and b) the control of the torch lateral displacement relative to the joint longitudinal axis (i.e. seam tracking).

Such control entails providing some means of adjusting the position of the torch relative to the workpiece during the welding process. To accomplish this, two approaches can be used: a) the adjustment of the robot wrist position relative to the stationary workpiece or b) the movement of the workpiece relative to the torch. The first approach is only possible if the dedicated systems designed by each robot manufacturer are allowed for, which results in limited flexibility. The second approach offers high flexibility, since the same system could be used for many different robots.

A comparison between both approaches will follow.

4.1.1 "Robot position adjustment" versus "workpiece position adjustment"

At a first look, it seems straightforward to use the robot to adjust the torch position relative to the workpiece during the welding process, since it is already moving the torch in a pre-programmed path with a pre-determined speed. However, it is not so simple to modify this pre-programmed movement during program run time. This would involve real time computationally intensive calculations, which are not always available in the robot controller or accessible by the end user. Also, the method each robot controller uses to generate reference signals for its joints in order to move its end effector to certain positions in space within a specified time frame is not standardised. Each robot manufacturer adopts different techniques and these are generally not released to end users, for safety reasons. When the robot is supplied with functions which allow modification of path during the program play-back, the extent to which the end effector position can be changed is often very limited. Therefore, unless dedicated systems are used in which adaptivity functions are allowed for, the task of adjusting the torch-position in real time becomes very difficult if not impossible.

On the other hand, if the workpiece can be moved to accommodate the differences between robot programmed path and the actual weld joint location, the task of maintaining their relative position constant as required by the process constraints can be easily achieved. This solution however would imply that the workpiece would have a limit in its dimensions. Although, considering that the differences between robot path and weld joint would be attributed only to component

errors[1], (i.e. joint positioning, joint fit-up, joint component tolerances) and that these are normally restricted in size by the allowable manufacturing tolerances, the adjustments required in workpiece positioning would be small, therefore involving low speeds and consequently, low dynamic loads.

Another advantage of using a moving table is the freedom of the user in setting the range of movement of the axes, thus allowing easy adaptation to different requirements in torch-to-workpiece relative position adjustment. One disadvantage, though, is the necessity to use a robot independent controller to control the positioning table, which might be considered as an added complication. However, the additional flexibility provided by this approach compensates for this supposedly increased complexity in the system.

4.1.2 Positioning table

Considering the aspects discussed above, it is suggested to use a three or more degrees-of-freedom positioning table, on which the workpiece would be mounted, for joint position adjustment. During the welding process only three degrees of freedom with orthogonal moving directions would be needed for adjusting the relative joint position, the remaining degrees of freedom being used for improving the orientation of the workpiece in a pre-weld operation, such that flat and horizontal welding positions could be favoured.

To implement this type of system, however, it would be necessary to use a robot independent controller to control the in-process moving axes. Such a controller would move the workpiece based on information provided by sensors. The directions of movement and the amount by which each axis should be moved could be easily calculated by using the information provided by the sensors together with the torch approach vector and the joint tangent vector. The torch approach vector provides the direction of movement necessary for adjusting the stand-off and the cross product of both vectors would give the direction of movement necessary for seam tracking. These vectors are directly obtained from the teach points file generated by the off-line programming system.

To synchronise the movements of the robot with the positioning table, digital inputs and outputs can be used. These are normally available in robot controllers.

In the present work, a table with only one degree of freedom was implemented in order to prove the effectiveness of the position control strategy. Figure 4.1 shows a sketch of the positioning table implemented.

4.1.3 Proposed control strategy

The position control strategy was based on adjusting the initial position of the weld joint in a pre-weld operation and on the in-process adjustments of position deviation compared to a pre-specified reference value.

---

[1] Assuming that the robot and its cell are correctly calibrated and that the programming errors have been eliminated

4.1.3.1 Adjustment before welding

Before the start of each new weld, the robot should be moved to a wire cutting station, where the electrode wire would be cut to a length of 11 mm. Such a length was found to be adequate for preventing collision between the welding torch gas nozzle and the side plates of a 90 degree included angle fillet weld, during the weld start point search. It would also allow the adjustment of the initial stand-off to a value between 12 mm and 20 mm, the limits set in the off-line programming module.

In the search procedure, the robot moves the welding torch to the weld approach point located at the top surface of the workpiece clearance box (**ap3** or **ap4**) (see Figures 3.22 to 3.24). It then stops and sends a signal to the table controller, which in response moves the workpiece to the table zero position. This zero position is used in the off-line programming module as the origin of the table co-ordinates frame. In reaching this zero position, the table signals the robot to move through the next approach points until it reaches **ap1**, where the robot should stop once again and signal the table to move the workpiece in the direction of the torch approach vector by a programmable amount. This amount will depend on the manufacturing tolerances of the workpiece, which will dictate the maximum difference that is likely to occur between the required joint position and actual joint position. When the table finishes the movement, it signals the robot to move the welding torch to the programmed weld start point. On reaching this point, the robot stops, switches the wire touch sensor on and signals the table controller to start the search routines. When the table finishes searching and adjusting the workpiece position, it signals back to the robot, which switches off the wire touch sensor and starts the welding sequence.

All these movements and communication issues are supervised by the main controller, which is implemented in a personal computer and connected to the table controller via a serial communications channel. The main controller is also responsible for downloading the off-line programming information to the table controller.

4.1.3.2 On-line control

The on-line position control is based on the information provided by the sensors. The position deviation is detected by the monitoring system and transferred to the table controller, which calculates the necessary movements to be performed, based on the directions of approach and tangent vectors at the point. If the approach direction at the weld start point is different from the approach direction at the weld end point, the table controller performs an interpolation to estimate the current approach orientation, based on the programmed welding travel speed and on the welding time measured until the point of interest. It then calculates the movements to be performed in each axis such that the detected position deviation is reduced.

The position control implemented in the present work is a particular case of the strategy explained above, since it addresses only the stand-off control. The implementation of the full three dimensional position control was not carried out due to the unavailability of a suitable sensor for measuring the lateral deviation of the torch relative to the joint longitudinal axis. A sensor based on the projection of an annular shaped laser light around the welding torch was proposed but its development

was considered to be outside the scope of this work. The proposed concept is described in Appendix D.

The stand-off measurement was provided by applying estimation models to the welding current and voltage waveforms. The aspects involved in this estimation are discussed in section 4.2.3.

4.2 Welding process control

The welding process control in this work was aimed at ensuring that the most stable process was always attained. The control strategy is based on the objective assessment of the process state provided by the monitoring indices developed by Ogunbiyi [ref. **51**] and on the adjustment of the welding voltage as a means to achieving process stability. It was assumed that the wire feed speed and the travel speed predicted by the off-line welding parameters generator are adequate to produce the required weld quality. Although the correction of the travel speed and/or wire feed speed might also be necessary to compensate for the excess weld volume caused by the presence of an unexpected gap, this was not implemented in the present work mainly due to the unavailability of a robust sensor for accurately measuring the joint gap. The sensor arrangement proposed in Appendix D could also be used for this purpose.

It should be noted that there is already a growing trend in equipping welding power sources with on-line automatic voltage control to ensure process stability [ref. **200**]. This is achieved by monitoring and objectively assessing the welding process stability in real time and then controlling the welding voltage based on the result of the assessment.

The development of the control rules necessary to accomplish the control objectives in this work and the implementation of these rules in a digital control system involved the consideration of several influential factors, which are discussed in the subsections below.

4.2.1 Process stability and control algorithm

It is generally accepted that the gas metal arc welding process stability depends on the mode of metal transfer. If the deposition rate is adequate and the stand-off is kept constant, then the only controllable welding parameter influencing the process stability is the welding voltage.

In order to implement the proposed control strategy, it was necessary to provide a means of objectively assessing and quantifying the process stability. The monitoring indices developed by Ogunbiyi [ref. **51**] were found to produce a good indication of the process stability state. Based on these monitoring indices and on the threshold limits shown in Figure 2.8, a set of rules were developed in order to classify the process stability into different states and to generate the welding voltage correction signals. The rules were used to develop a rule-based incremental controller [ref. **194**], which initially used only the value of the Power Ratio as the stability assessment factor and the controlled variable. The controller objective was to keep the measured value of the power ratio within the defined stable process limits for dip and spray modes of metal transfer (see Figure 2.8). The globular mode was

considered as unstable and, therefore, avoided. The control objective was achieved by increasing or decreasing the welding voltage in repeated steps until process stability was attained. The first attempted controller structure is described in Table 4.1. Table 4.2 and Table 4.3 give the linguistic representation of the variables involved.

Table 4.1 - Initial control rules based only on the Power Ratio

1	*If* PR < PRLOWDIP *then* process is unstable ΔV = +BIGTRIM
2	*If* PRLOWDIP ≤ PR < PRHIGHDIP *then* process is stable ΔV = ZEROTRIM
3	*If* PRHIGHDIP ≤ PR < PRLOWGLOBY *then* process tending to instability ΔV = -SMALLTRIM
4	*If* PRLOWGLOBY ≤ PR < PRMEDGLOBY *then* process tending to instability ΔV = -MEDTRIM
5	*If* PRMEDGLOBY ≤ PR < PRHIGHGLOBY *then* process is unstable ΔV = +BIGTRIM
6	*If* PRHIGHGLOBY ≤ PR < PRLOWSPRAY *then* process is unstable ΔV = +MEDTRIM
7	*If* PRLOWSPRAY ≤ PR < PRMEDSPRAY *then* process tending to instability ΔV = +SMALLTRIM
8	*If* PRMEDSPRAY ≤ PR < PRHIGHSPRAY *then* process is stable ΔV = ZEROTRIM
9	*If* PR ≥ PRHIGHSPRAY *then* process tending to instability ΔV = -SMALLTRIM
10	*If (* PR ≥ PRMEDGLOBY *) and (* I_{mean} < I_{spray} *) then* move to dip transfer ΔV = -BIGTRIM
11	*If (* PR ≤ PRMEDGLOBY *) and (* I_{mean} ≥ I_{spray} *) then* move to spray transfer ΔV = +BIGTRIM

where I_{spray} is the current used to switch the mode of metal transfer (I_{spray}=240 Amps)
ΔV is the voltage correction value for the control cycle.

Table 4.2 - Linguistic representation of voltage correction (ΔV)

ZEROTRIM = 0.0 volts	MEDTRIM = 0.6 volts
SMALLTRIM = 0.3 volts	BIGTRIM = 1.0 volt

Table 4.3 - Linguistic representation of PR levels

PRLOWDIP = 0.20	PRHIGHGLOBY = 0.8
PRHIGHDIP = 0.40	PRLOWSPRAY = 0.9
PRLOWGLOBY = 0.5	PRMEDSPRAY = 0.95
PRMEDGLOBY = 0.6	PRHIGHSPRAY = 0.97

These are values derived from welding trials and are based on the observation of an experienced welder

The voltage correction obtained from the rules shown in Table 4.1 was multiplied by a smoothing factor (β) and added to the currently set-up welding voltage (V_i), generating the new set-up welding voltage (V_{i+1}) which was transferred to the welding power source.

$$V_{i+1} = V_i + \beta \cdot \Delta V \tag{4.1}$$

$$\beta = \begin{cases} \left(1 - \dfrac{PR}{PRLOWDIP}\right)^{0.5} & \text{if} \quad PR < PRLOWDIP \\ 1.0 & \text{if} \quad PR \geq PRLOWDIP \end{cases} \tag{4.2}$$

The smoothing factor, β, is used in equation (4.1) to reduce the voltage correction when the value of PR is close to the stable region.

Note that the controller must wait for a certain time for the welding arc to establish before starting to generate the control signals. This time was fixed at 1 second.

When implemented, this controller did not result in an optimum behaviour across the range of wire feed speeds for dip mode of metal transfer. This was believed to occur due to the fact that the limits used for PR were suggested for monitoring purposes. In order to apply PR as a control variable, the allowable range of variation should be tightened. As a first attempt to compensate for this, two additional limits were introduced in the dip transfer range of power ratios. These limits were used to reduce the range of variation allowed initially for PR. The resulting algorithm is shown in Table 4.4 and Table 4.5.

Table 4.4 - Control rules based on Power Ratio with reduced range for dip transfer

1	*If* PR < PRLOWDIP *then* process is unstable ΔV = +BIGTRIM
2	*If* PRLOWDIP ≤ PR < minPRdip *then* process slightly tending to instability ΔV = MICROTRIM
3	*If* minPRdip ≤ PR ≤ maxPRdip *then* process stable ΔV = ZEROTRIM
4	*If* minPRdip < PR < PRHIGHDIP *then* process slightly tending to instability ΔV = -MICROTRIM
5	*If* PRHIGHDIP < PR < PRLOWGLOBY *then* process tending to instability ΔV = -SMALLTRIM
6	*If* PRLOWGLOBY < PR < PRMEDGLOBY *then* process tending to instability ΔV = -MEDTRIM
7	*If* PRMEDGLOBY < PR < PRHIGHGLOBY *then* process is unstable test rule (7.a)
7.a	*If* (I_{mean} < I_{spray}) *then* move to dip transfer ΔV = -BIGTRIM *else* move to spray transfer ΔV = BIGTRIM
8	*If* PRHIGHGLOBY < PR < PRLOWSPRAY *then* process is unstable ΔV = +MEDTRIM
9	*If* PRLOWSPRAY < PR < PRMEDSPRAY *then* process tending to instability ΔV = +SMALLTRIM
10	*If* PRMEDSPRAY < PR < PRHIGHSPRAY *then* process is stable ΔV = ZEROTRIM
11	*If* PR > PRHIGHSPRAY *then* process tending to instability ΔV = -SMALLTRIM

Table 4.5 - Linguistic representation of new limits for PR in dip transfer and of new voltage correction value

maxPRdip = 0.35	minPRdip = 0.25	MICROTRIM = 0.1

Again, the new set-up welding voltage was obtained by using equation (4.1), where the smoothing factor takes the form of equation (4.3).

$$\beta = \begin{cases} \left(1 - \dfrac{PR}{\text{minPRdip}}\right)^{0.5} & \text{if} \quad PR < \text{minPRdip} \\ 1.0 & \text{if} \quad PR \geq \text{minPRdip} \end{cases} \qquad (4.3)$$

The introduction of such a reduced range of variation (rules 2 to 4 in Table 4.4) improved the controller behaviour. However, it still resulted in excessive[2] spatter for low wire feed speeds and in a slightly oscillatory behaviour. In order to improve the controller performance further, additional rules based on the other monitoring indices[3] were introduced. The rules were developed from the observation of the behaviour of these indices during controlled trials carried out with the control rules shown in Table 4.4. It was observed that the indices would vary with different sensitivities as a response to instabilities in the process. Based on this observation, a set of interdependent rules were generated and logically organised so that the less sensitive indices would be tested before the most sensitive ones. The rules were introduced under rule number 3 in Table 4.4 and are shown in Table 4.7. Note that the amount of voltage correction used in rules 2 and 4 of Table 4.4 was increased. Table 4.6 shows the linguistic representation of the limits of DCI, TI and TSI used for fine-tuning the stability in dip transfer.

Table 4.6 - Linguistic representation of limits for DCI, TI and TSI in dip transfer

DCI-LOW = 0.4	DCI-HIGH = 0.8
TI-LOW = 0.3	TI-HIGH = 0.45
TSI-LOW = 1.6	TSI_HIGH = 1.9

Table 4.7 - Control rules based on DCI, TI and TSI

2	*If* PRLOWDIP ≤ PR < minPRdip *then* process slightly tending to instability ΔV = SMALLTRIM
3	*If* minPRdip ≤ PR ≤ maxPRdip *then* test DCI
3.a	*If* DCI < DCI-LOW *then* decrease the voltage slightly ΔV = -MICROTRIM *else* *if* DCI > DCI-HIGH *then* increase the voltage slightly ΔV = MICROTRIM *else* test TI
3.b	*If* TI > TI-HIGH *then* increase the voltage slightly ΔV = MICROTRIM *else* *if* TI < TI-LOW *then* decrease the voltage slightly ΔV = -MICROTRIM *else* test TSI
3.c	*If* TSI > TSI-HIGH *or* TSI < TSI-LOW *then* reduce the voltage slightly ΔV = -MICROTRIM *else* the process is stable ΔV = ZEROTRIM
4	*If* maxPRdip < PR < PRHIGHDIP *then* process slightly tending to instabilty ΔV = -MICROTRIM

[2] Excessive spatter in this context does not imply that the process is unstable. It just implies that a better stability state can still be achieved, generating less and finer spatter.
[3] Dip Consistency Index (DCI), Transfer Index (TI) and Transfer Stability Index (TSI)

The addition of these rules improved the controller behaviour in respect to oscillations, but the spatter generation in the low end of the wire feed speed range was still excessive. From the analysis of the optimum values of PR for different settings of wire feed speed in the dip mode of metal transfer, it was observed that an almost linear relationship existed between both variables in the range of wire feed speeds fixed for this transfer mode (from 4.0 m/min to 10.0 m/min). Taking this into account, a further reduced range of variation for PR was introduced: the lower limit of the range would be a function of the wire feed speed, according to the equation (4.4) and the higher limit would be equal to the lower limit added to the allowable range of variation, as shown in equation (4.6).

$$\text{minPRdip} = \text{PRLOWDIP} + A\left(\frac{WFS - \min WFS}{\max WFS - \min WFS}\right)^{\alpha} \qquad \textbf{(4.4)}$$

$$A = \text{PRHIGHDIP} - \text{PRLOWDIP} - \text{PRrange} \qquad \textbf{(4.5)}$$

$$\text{maxPRdip} = \text{minPRdip} + \text{PRrange} \qquad \textbf{(4.6)}$$

where

min*WFS*	is the minimum wire feed speed allowed in dip mode of metal transfer (4.0 m/min)
max*WFS*	is the maximum wire feed speed allowed in dip mode of metal transfer (10.0 m/min)
α	is a constant greater or equal to 1 (most suitable value found to be 1.05)
PRrange	is the allowable range of variation of PR between **minPRdip** and **maxPRdip**. (Value used: PRrange = 0.02)

By using the rules of Table 4.4 with rules 2 to 4 substituted by the ones from Table 4.7 and equations 4.3 to 4.6, the resulting controller was able to achieve optimum process stability for the whole range of wire feed speeds studied in the dip mode of metal transfer as well as in the spray mode. However, the speed of response of the controller was not very fast for situations in which an excessive voltage was found. In order to improve that, the negative voltage correction values in rules 4, 5, 6, 7.a, and 11 were multiplied by 1.5. The final algorithm is shown in Table 4.8 and in equations (4.1) and (4.3) to (4.6).

Table 4.8 - Final welding process control algorithm

1	*If* PR < PRLOWDIP *then* ΔV = +BIGTRIM
2	*If* PRLOWDIP ≤ PR < minPRdip *then* ΔV = SMALLTRIM
3	*If* minPRdip ≤ PR ≤ maxPRdip *then* test rule (3.a)
3.a	*If* DCI < DCI-LOW *then* ΔV = -MICROTRIM *else if* DCI > DCI-HIGH *then* ΔV = MICROTRIM *else* test rule (3.b)
3.b	*If* TI > TI-HIGH *then* ΔV = MICROTRIM *else if* TI < TI-LOW *then* ΔV = -MICROTRIM *else* test rule (3.c)
3.c	*If* TSI > TSI-HIGH *or* TSI < TSI-LOW *then* ΔV = -MICROTRIM *else* ΔV = ZEROTRIM
4	*If* minPRdip < PR < PRHIGHDIP *then* ΔV = -1.5 x MICROTRIM
5	*If* PRHIGHDIP < PR < PRLOWGLOBY *then* ΔV = -1.5 x SMALLTRIM
6	*If* PRLOWGLOBY < PR < PRMEDGLOBY *then* ΔV = -1.5 x MEDTRIM
7	*If* PRMEDGLOBY < PR < PRHIGHGLOBY *then* test rule (7.a)
7.a	*If* (I_{mean} < I_{spray}) *then* ΔV = -1.5 x BIGTRIM *else* ΔV = BIGTRIM
8	*If* PRHIGHGLOBY < PR < PRLOWSPRAY *then* ΔV = MEDTRIM
9	*If* PRLOWSPRAY < PR < PRMEDSPRAY *then* ΔV = SMALLTRIM
10	*If* PRMEDSPRAY < PR < PRHIGHSPRAY *then* ΔV = ZEROTRIM
11	*If* PR > PRHIGHSPRAY *then* ΔV = -1.5 x SMALLTRIM

Note that the controller shown above is intrinsically empirical. The stability limits for the power ratio and the other monitoring indices were also obtained empirically and the voltage correction values were suggested based on process previous knowledge and prior experience. Figure 4.2 shows the control algorithm in a schematic form with voltage trim directions. The rule based incremental controller developed above differed from the original structure presented by Luzeaux [ref. 194] in the sense that different increment sizes of the control variable were used, depending on how far the process was from the desired state. This characteristic can be considered as a fuzzyfication of the rules

An important element in the implementation of the these control algorithms is the response time of the power source to a change in the set-up parameters. This is dealt with in section 4.2.5.

The control algorithm presented above has a fast response compared to the voltage controller developed by Won and Cho [ref. 201]. The work by Won and Cho was conceptually similar to the controller developed in this work, however the stability assessment was carried out using the arc stability index developed by Mita et al. [ref. 37] (see Section 2.1.5.3) and the voltage control commands were generated by a fuzzy-logic based controller. This controller was designed to iteratively seek a

stable arc condition for dip mode metal transfer by automatically adjusting the welding voltage until stability was achieved. Overall, the technique presented by the authors [ref. **201**] was computationally time consuming; they reported that it takes about 15 cycles (90 seconds) to obtain a stable welding condition, whereas the controller developed in this work takes less than 6 seconds (see Section 7.1).

In a similar work, Mita et al. [ref. **200**] used the fuzzy logic method to automatically set the welding voltage in CO_2 gas metal arc welding. The fuzzy rules used were developed from the standard deviation of short circuiting and arcing times and were distributed into three groups, dependending on the welding current (low range: 80-200A; medium range: 210-290A; and high range: >300A). This was due to the fact that the correlation between the stability of the welding arc and the standard deviation of these parameters becomes poor as the welding current increases [ref. **37**]. In each group, different rules were used for assessing the stability of the welding arc resulting in a fast but complicated method (for example, 20 fuzzy production rules were used for the low current range and 25 rules for the medium range). Although this is a simpler approach to automatically tuning the voltage compared to the work carried out by Won and Cho [ref. **201**], Mita et al. [ref. **200**] work was found to use too many rules. The algorithm presented in this section uses only 17 rules accross the whole range of welding currents.

4.2.2 Data acquisition and processing

In order to implement the control algorithms presented in section 4.2.1, a monitoring system was developed for acquiring and digitising the welding current and voltage transient waveforms and extracting the statistical features from which the monitoring indices are calculated. The description of the hardware involved can be found in section 5.3 and the description of the software can be found in Appendix E.

Basically, the monitoring system acquires a fixed number of data points (512) at a fixed sampling rate (2.5 kHz) for both the welding current and the welding voltage. The basic statistical features of both signals are extracted using equations (2.26) to (2.33). Then the monitoring indices are calculated using equations (2.3) to (2.6) and filtered using a moving average filter, as shown in equation (4.7).

$$s_{i,filtered} = (1-\alpha)\cdot s_i + \alpha \cdot s_{i-1,filtered} \tag{4.7}$$

where

s_i	is the current calculated value of the variable
$s_{i,filtered}$	is the current filtered value of the variable
$s_{i-1,filtered}$	is the previous filtered value of the variable
α	smoothing factor (0.3)

This filter is used to reduce the effect of random variation in the monitoring indices. The filtered values are then applied to the control rules to generate the required voltage correction.

At the sampling rate used, 2.5 kHz, the acquisition boards take approximately 205 milliseconds to acquire 512 data points. This time was found sufficient to allow

the collection of welding data corresponding to a minimum of 10 short circuits in stable low[4] wire feed speed dip transfer welding [refs. **51, 161**]. Before any statistical feature extraction can start, all the points from all the analogue-to-digital converter channels must be transferred from the internal memory of the acquisition boards to the memory of the main computer. This takes approximately 15 milliseconds in the hardware used. After the transfer, the collection of a new block of data should start, while the main computer should proceed with the calculations. Considering the acquisition time, the data transfer time and the time needed for calculations and data output to the user interface and to the other controllers (table controller and welding power source), a cycle of approximately 250 milliseconds was obtained. This was conventionally called a *monitoring cycle*.

4.2.3 Stand-off estimation and control

The model proposed by Ogunbiyi [ref. **51**] and outlined in equations 2.21 to 2.24 was initially considered for in-process estimation of the stand-off. However, the model was found to be imprecise when low wire feed speeds were used. An analysis shows that the imprecision was due to the difficulty in the correct estimation of the value of the proportionality constant, ϕ , used in equation 2.22 and also in the determination of the initial welding current to be used in the same equation. However, the model was found to be useful for qualitatively indicating a change in stand-off. For control purposes an absolute quantitative measurement was necessary. In order to obtain a more reliable stand-off estimation, a new model was developed using as its input the measurement of the resistance between the contact tip and the workpiece. In dip mode metal transfer, the resistance was calculated during the short circuiting phase, when the wire could be considered as a continuous electrical conductor between the contact tip and the weld pool. In the spray mode of metal transfer, the calculated resistance was in fact the combination of the wire stick-out resistance with the arc equivalent resistance. A resistance component present in both estimations was the wire electrical contact resistance at the contact tip, which was believed to be a source of noise. The development of the models for estimating the stand-off from the calculated resistance is described in section 6.2. Equation (4.8) shows the stand-off model in a general form.

$$SO_{est} = f_1(WFS,V)\cdot R + f_2(WFS,V) \qquad \textbf{(4.8)}$$

where

SO_{est} is the estimated value for the stand-off,

R is the resistance between the points where the voltage signal is picked-up and

f_1 , f_2 are functions of the wire feed speed and welding voltage (see section 6.2).

Considering that the stand-off estimated values were obtained from the welding current and voltage waveforms and that process instabilities would influence such an estimation, the implemented controller would only estimate the stand-off if a

---

[4] Lower limit of the range used = 4 m/min.

certain level of process stability was assured, keeping the stand-off previous value otherwise. The stability level was calculated by using a model based on the Transfer Index (see equation 2.3) and on the Power Ratio (see equation 2.6). Such a model was called *Confidence of Bad Ignition* (**Conf_Bad_Ign**) and was developed to indicate the occurrence of an undesirable process instability. **Step 1** to **Step 5** below describe the proposed model.

Step 1 - *Before starting monitoring, set the stability limits for PR and TI based on the set-up welding parameters and initialise other model variables*

$\text{Conf\_Bad\_Ign}_{i-1} = 0.0$ (Assuming a good arc start)
$TI_{i,filtered} = TI_{i-1,filtered} = 1.0$
$\alpha_0 = 0.3$
$\alpha_3 = 0.5$
If mode of metal transfer = dip *then*
    $PRmin = 0.2$
    $TImax = 0.5$
    $PR_{i,filtered} = PR_{i-1,filtered} = 0.3$
    $\alpha_1 = 0.5$
else (mode of metal transfer = spray)
    $PRmin = 0.9$
    $TImax = 0.2$
    $PR_{i,filtered} = PR_{i-1,filtered} = 0.95$
    $\alpha_1 = 0.2$

Step 2 - *During monitoring, filter PR and TI using equation* (4.7) *with smoothing factor* α_0 *for filtering PR and* α_1 *for filtering TI*

$$PR_{i,filtered} = (1-\alpha_0)\cdot PR_i + \alpha_0 \cdot PR_{i-1,filtered} \quad \textbf{(4.9)}$$

$$TI_{i,filtered} = (1-\alpha_1)\cdot TI_i + \alpha_1 \cdot TI_{i-1,filtered} \quad \textbf{(4.10)}$$

Step 3 - *Test if the filtered monitoring indices indicate instability and set the possibility measure of process being unstable,* Pr(*ign*), *accordingly*

If ($PR_{i,filtered} < PRmin$) *or* ($TI_{i,filtered} > TImax$) *then*
    Pr(*ign*) = 1 : *process unstable*
else
    Pr(*ign*) = 0 : *process stable*

Step 4 - *Calculate the confidence of bad ignition by applying the moving average filter of equation* (4.7) *to the possibility measure of process being unstable,* Pr(*ign*)*, using a smoothing factor* $\alpha = 0.5$

$$\text{Conf\_Bad\_Ign}_i = (1-\alpha)\cdot \Pr(ign) + \alpha \cdot \text{Conf\_Bad\_Ign}_{i-1} \qquad \textbf{(4.11)}$$

Step 5 - *Estimate a new stand-off value* ***if and only if*** $\text{Conf\_Bad\_Ign} < 0.2$

The value **Conf_Bad_Ign = 0.2** was chosen empirically, based on prior observations of the stand-off model behaviour for different stability levels.

4.2.4 Reliability of process statistical estimates

The model used for estimating the stand-off was obtained from multiple regression analysis of average values of calculated resistance (see section 6.2). Due to the nature of the gas metal arc welding process, the welding current and voltage signals are generally corrupted with random noise which is passed over to the calculated resistance and, consequently, to the estimated stand-off. In order to reduce the oscillation in the stand-off values due to the random noise, a third order moving average filter was used. The filtered stand-off value was then transferred to the table controller, where it would be compared to the required reference stand-off and an error would be calculated. Equation (4.12) shows the filter used.

$$SO_{i,filtered} = \frac{\sum_{j=0}^{2} \alpha_j \cdot SO_{(i-j),est}}{\sum_{j=0}^{2} \alpha_j} \qquad \textbf{(4.12)}$$

where

$SO_{i,filtered}$	current filtered stand-off estimation;
$SO_{(i-j),est}$	non-filtered stand-off estimates for monitoring cycles *i*, (*i-1*) and (*i-2*);
α_j	filter weights, $\alpha_j = 1.0$ for $j=0, 1, 2$.

Although the filtered values were transferred to the table controller, the stand-off error predictions were still oscillating. In order to reduce the response of the table to random variation, threshold limits were imposed on the stand-off error signal, such that no correction would occur for errors smaller that 0.5 mm and no correction greater than 1 mm would be applied in a control cycle. A proportional control scheme with a unitary gain was adopted for adjusting the stand-off. After sending an estimated stand-off value to the table controller, the main controller would reset the stand-off filter and would only send a new estimated value after three estimation (monitoring) cycles, that is, after acquiring data for producing a filtered stand-off

from three previously estimated values. This resulted in a stand-off control cycle of approximately 750 milliseconds with maximum correction of ±1mm per cycle. This limit in the table movement was imposed to prevent any undesirable arc instability due to an excessive sudden change in stand-off. This control strategy gave a good and robust performance.

4.2.5 Communications delay

An important factor to be considered in the control loop is the delay resulting from the transfer of control instructions and their full implementation by the welding power source and the table controller. These delays were compensated for by introducing time delays between the control cycles.

In a control loop, the control instructions are the result of applying the control rules to a measured process state. If during the measurement the process state is still changing as a result of a previous control instruction, an unreliable measurement will be obtained. If the controller uses this measurement to generate new control instructions to compensate for deviations, this may result in oscillations in the control loop and in process instability. Therefore, by introducing suitable time delays in the control loop, these unstable situations can be prevented.

In the case of stand-off control, the use of a third order filter guaranteed that the table controller was given sufficient time to adjust the stand-off without incurring instability. However, since a correction signal could be issued every monitoring cycle, in the case of the welding process control a time delay should be introduced. In order to have a good estimate of this time delay, some voltage step input tests were carried out using two different ways of communicating with the welding power source[5]: a) via direct serial communication with the power source controller and b) via analogue signals, using a special interface tailored for robots. The results of the tests can be found in section 6.3. The power source was found to have a response time of approximately 50 ms for direct serial communications and 200 ms for analogue input via the robot interface. Since the serial communications protocol for the power source used was still being developed, some limitations were found in terms of available power source commands. This led the author to opt for the robot interface, thus in effect having a time delay of 200 ms. This time delay was introduced in the control cycle in such a way that the control instructions to the power source would be issued every other monitoring cycle. Consequently a voltage control cycle of approximately 500 milliseconds was obtained, that is, two control cycles would occur every second.

[5] Migatronic BDH550

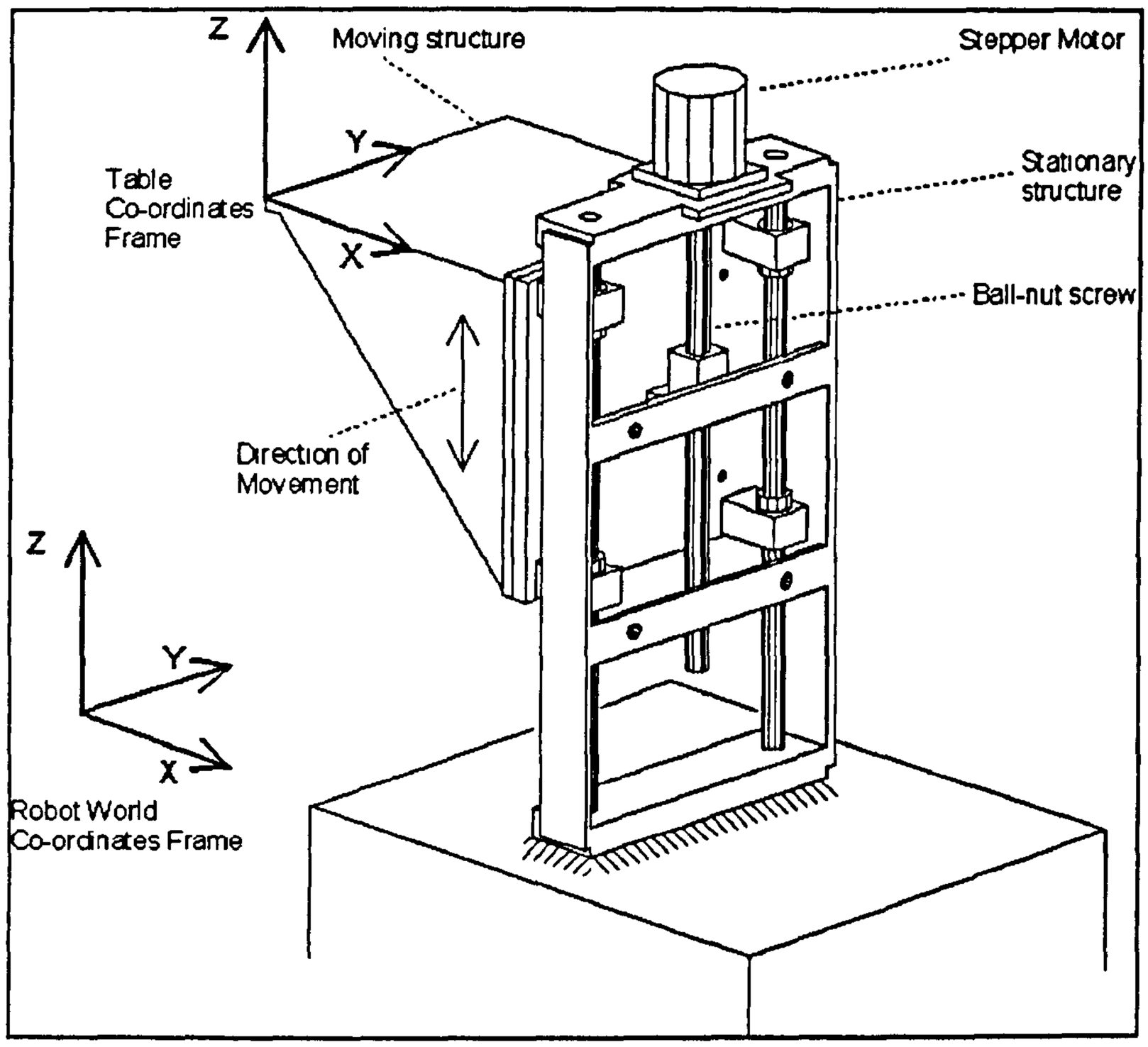

Figure 4.1 - Sketch of the moving table implemented in the control system

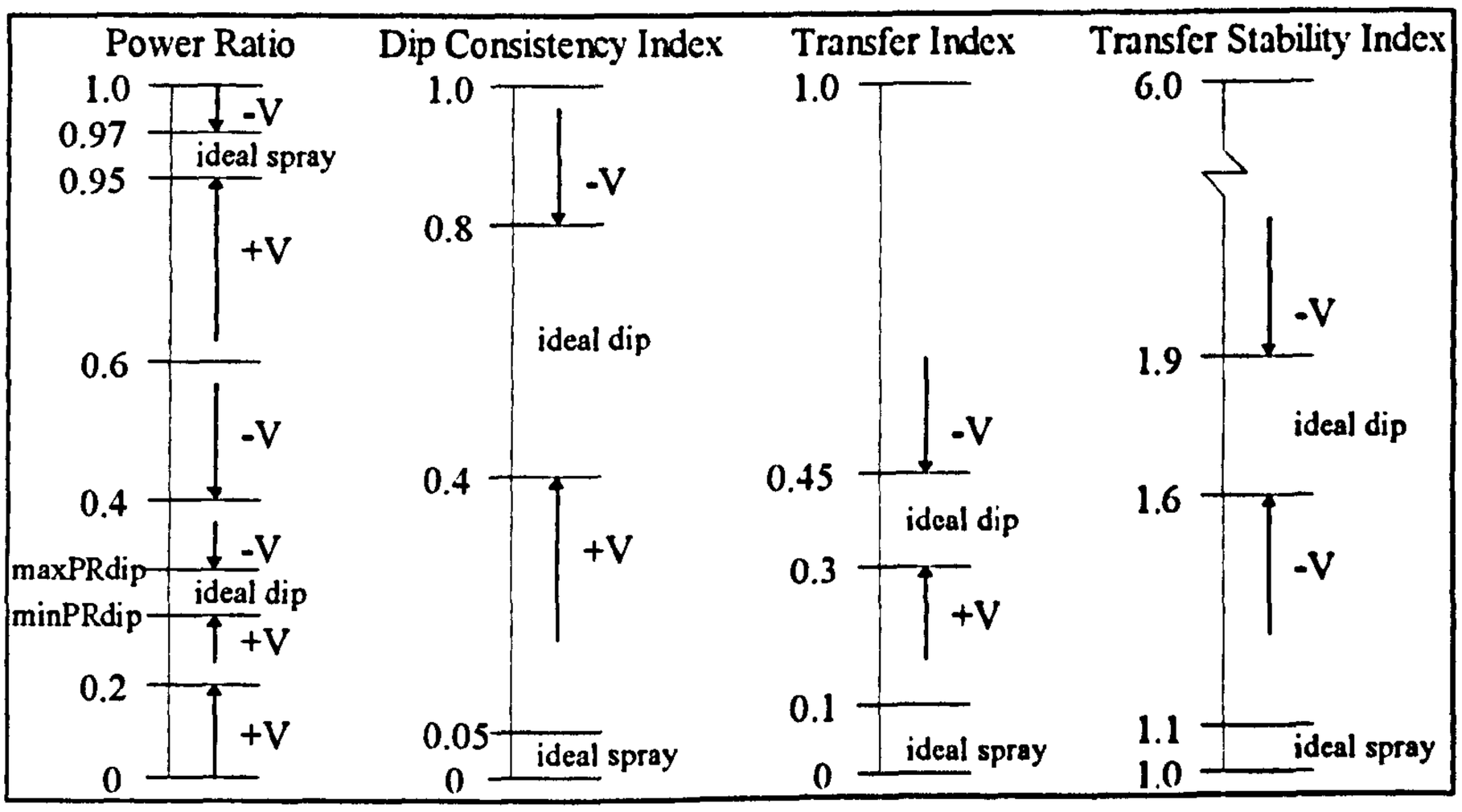

Figure 4.2 - Process control shown schematically

5. Experimental Equipment, Materials and Procedure

This chapter gives a description of the equipment and materials used in the experimental trials. The calibration curves and the experimental procedure are also presented.

5.1 Welding robot

A Panasonic AW7000 robot was used. It is a six axis articulated welding robot which can be interfaced with external equipment via digital inputs and outputs. Although analog outputs are also supplied for interfacing with a welding power source, these were not used due to the fact that they could not be freely adjusted on-line. They can only be pre-programmed.

The main draw back with the use of this robot in this work is that it was not equipped with a communications port for off-line programming. Positioning errors could, however, be simulated by intentionally on-line programming a known wrong path.

5.2 Welding power source

A Migatronic BDH-550 welding power source was utilised. This is a 100 kHz inverter-based microprocessor controlled power source with 80 volts nominal open-circuit voltage and current range from 5 A to 550 A. It works as a constant voltage power source in conventional GMAW mode and uses integral control to maintain the set up parameters constant throughout a welding operation.

The power source operates in two modes, namely manual and synergic. In manual mode both the welding voltage and the wire feed speed are directly set by the operator. In synergic mode, a welding current value is specified and the power source selects the appropriate wire feed speed and voltage according to a pre-programmed synergic curve. The power source was used in manual mode for this work.

The BDH-550 can be driven externally by using a module called Robot Interface supplied by the power source manufacturer, Migatronic. The Robot Interface is controlled by a single microprocessor (SIEMENS 80C515A) which includes, in the same chip, a 10-bit analogue-to-digital (A/D) converter, random access memory (RAM), digital inputs and outputs (I/O), serial communications and watchdog. The analogue inputs can be connected to analogue outputs from a welding robot or from a computer, allowing on-line external control of welding parameters (voltage and wire feed speed, in manual mode conventional GMAW). It interfaces with the power source control unit via a RS-232 serial communications port.

It is also possible to directly communicate with the power source control unit via RS-232 serial communications. However this is only possible if a special control program, stored in erasable programmable read only memory (EPROM) modules, is used in the power source. This program, although available, was still in the development phase. The program in its present form does not have a function for setting wire-feed-speed. This limitation led the present author to opt for the Robot Interface alternative.

5.3 Monitoring system

The monitoring system consisted of a VME/STE bus industrial computer equipped with an ARCOM VME/STE VSCIM 486 DX2 50 MHz main board, 4 megabytes of random access memory (RAM), 100 megabyte fixed disk, two 12-bit 2-channel simultaneous sampling analogue-to-digital (A/D) converter boards (ARCOM SAD-2X250) and an 8-bit 2-channel digital-to-analogue (D/A) converter board (ARCOM SADA-8). Both A/D and D/A converter boards are STE bus based. The STE bus uses 8 bits to transfer data from the peripheral boards to the main board. Each SAD2X250 board has 64 kilobytes of memory, which allows data aquisition to be carried out in blocks, independently from the main board microprocessor. A signal conditioning board was used to adjust the sensor signals to the voltage range required by the A/D converter boards (-10V to +10V). The voltage and current signals were filtered with a 1.0 kHz cut-off frequency eighth-order analogue Butterworth filter, before being digitised.

During initial welding trials, a monitoring software (CranMon), developed at Cranfield University, was used. This software has limited memory, which prevents it from acquiring welding data for long duration welds. Also, no facilities are provided for implementing the control algorithms. In order to overcome these problems a dedicated monitoring and control software, written in C programming language, was specially designed and developed by the author. It consists of two main parts, namely *monitoring* and *control*. The monitoring part was developed to make use of the windowing technique developed by Chawla [ref. **161**], which permits the analysis of the welding data in independent blocks. An attempt was made to keep the interval between windows to a minimum. This interval depends on the speed of data transfer from the acquisition boards' memory space to the program data memory and also on the time required for processing the window of data that was collected before. Due to the on-board memory available in the SAD2X250 data acquisition boards, it was possible to use some parallelism: while the main processor was calculating the statistics and performing other tasks, a new window was already being collected. Established numerical and statistical methods were implemented for extracting the statistics of each signal. The welding models developed by Ogunbiyi [ref. **51**] were built-in to provide the information about mode of metal transfer and stability characteristics of the process.

In the control part, functions were implemented to provide communication capabilities with the table controller and the power source controller. The control commands could be sent to the power source (via analogue outputs) and to the part-positioner (via RS232 serial communications) whenever required, according to the control rules developed. Further details of the software can be found in the Appendix E.

5.4 Welding voltage and current sensors

Voltage sensor

The voltage was sensed by directly connecting sensing leads (maximum continuous voltage 100 V) to the back of the welding torch and to the workpiece

mounting fixture. The voltage signal was divided by 10 and filtered in the conditioning board before being converted to the digital form.

Current sensor

The welding current was measured by using a Hall effect probe (RS Catalogue No. 256-174) with specification as follows:

Rating	500 A
Calibration accuracy at 23 °C	± 1% of range
Zero offset (23 °C)	± 0.1% of range
Zero offset (0-60 °C)	± 1% of range
dI/dt (transient) following	> 200 A/μs
Output:	0 - 10 V dc

This signal was also filtered before being converted to digital form.

5.5 Touch sensor

In order to provide touch sensing capabilities to the robot/table system, a touch sensor was devised. It was based on the fact that when the wire touches the workpiece, the resistance between the voltage sensor leads drops to zero. Measurements of resistance across the terminals of the power source, whether it is on or off, indicate that there is a constant resistance of 330 ohms in its internal circuit. This resistance appears in parallel with the one between the electrode and the workpiece. A simple electronic circuit was built to detect the drop in resultant resistance caused by the touch of the wire on the workpiece. This was accomplished by a resistive Wheatstone bridge whose output was amplified and connected to a photo-isolated relay, which would close or open another inductive relay, resulting in an optically isolated digital output. The sensor circuit could be connected to (or disconnected from) the power source terminals by closing (opening) a switch (digital input) which was linked to a digital output from the robot. In the event of accidentally leaving the touch sensor connected to the power source when attempting to strike an arc, a protection circuit, based on TransZorbs™ and common fuses, was implemented. This was tested successfully. The touch sensor circuit diagram is shown in Figure 5.1.

The output of the sensor was connected to a digital input of the table controller in order to provide it with information on when it should stop the table during a search routine.

A list of the electronic components used in the circuit can be found in the Appendix F.

5.6 Sliding table and controller

Since the robot used did not allow the user to modify its path during program run-time a moving table was used to correct the position of the workpiece relative to

the torch end. Only one degree of freedom was implemented, allowing correction of contact tip-to-workpiece distance (stand-off), when the flat welding position was used. The moving table was not a complete solution to the problem, since deviations in the path, apart from stand-off, could not be controlled. Three degrees-of-freedom would provide a good level of controllability but it would require a seam-tracker, which was not available.

The implemented sliding table consisted of a moving horizontal platform, which could be moved vertically by means of spinning a ball nut screw (see Figure 5.2). This movement was provided by a stepper motor (RS Catalogue No. 440-442), which was driven by a 2A unipolar drive (RS Catalogue No. 332-082) and controlled by a TRIO Motion Co-ordinator 2 controller. A linear resistive sensor was used to measure the position of the table relative to an adjustable "zero" position, which was set by subtracting the output of the resistive sensor from an adjustable voltage signal (0 volts to 10 volts). The result of this subtraction was used as a measurement of the table position.

The TRIO Motion Co-ordinator 2 controller[1] is a multitasking multiaxes controller which can be programmed by a dedicated BASIC language. The controller has sixteen 24V digital inputs, of which 8 can also be used as outputs. It can be connected to a personal computer via RS-232 serial communications and can control up to 12 axes. The controller used had 4 stepper motor daughter boards installed, of which only one was used.

Specification of moving table components:

Ball nut screw:

- Diameter: 14 mm
- Pitch: 5 mm/revolution
- Length: 300 mm

Stepper Motor:

- Number of steps: 200 steps
- Maximum torque: 34 Ncm (300 to 500 Hz) (see Figure 5.4)
- Maximum pull-in speed: 1000 Hz
- Rotor Moment of Inertia: 115 gr/cm^2

The stepper motor drive used could only generate full steps.

Stepper motor + ball nut screw + moving table:

- Resolution: 0.025 mm/step
- Load capacity: 7.0 kg
- Travel range: 140 mm
- Maximum speed: 20 mm/s
- Maximum acceleration rate at 20 mm/s: 494 mm/s^2

[1] Trio Motion Technology Ltd, UK

Linear resistive transducer:

- Manufacturer: Novotechnik
- Type: TLH-225
- Resistance: 5kΩ ± 20%
- Linearity: ± 0.07 %
- Voltage range 0-10 V
- Length: 234.5 mm

Measuring system:

- A/D converter board resolution: 4.9 mV
- Measuring resolution: 0.115 mm

In order to connect the digital inputs and outputs (I/Os) of the table controller to the robot's, an interface box was built. The robot I/Os were designed such that on-off switches could be connected to them. Since the table controller was designed to work with 24 volt I/Os, a series of relays were mounted in a circuit board to provide the interfacing between the robot I/Os and the table controller I/Os. The touch sensor developed was also installed in this box. The circuits and external connections of the interface box are described in Appendix G.

Figure 5.3 shows the full system in its final implementation.

5.7 Calibration

A careful calibration of the acquisition boards was performed by adjusting the gain potentiometers of each channel to output 000h (hexadecimal) and FFFh for -10V and +10V volts input.

In the conditioning board, the voltage channel was calibrated to output signals from 0V to 10V, corresponding to inputs of 0V to 100V. The current channel was calibrated to provide unitary gain.

The D/A board was calibrated to output voltages from 0 to 5V. This was amplified to provide 0 to 10V output, as required by the Robot Interface analogue inputs.

The calibration for the output of the current probe was assumed to be correct, according to the manufacturers data.

5.7.1 Moving table calibration

A calibration curve was obtained for the moving table by measuring its actual movement and comparing it with the required one (see Figure 5.6). A Mitutoyo dial gauge was used in the measurement trials.

5.7.2 Acquisition system calibration factors

The following calibration factors were used:

Voltage: 100

Current:	500
Position:	234.5

5.7.3 Wire feed speed calibration

The calibration of the BDH550 wire feeder was checked off-line by measuring the weigth of welding wire delivered during 10 seconds for different set-up wire feed speeds and comparing with the weight of 1 metre of the same welding wire. Figure 5.5 shows the calibration curve obtained.

5.7.4 Robot Interface calibration

The robot interface was supplied with two analog inputs which were used to set the desired level of welding voltage and wire-feed-speed. A 0-10 V signal in the welding voltage input channel would correspond to 0-50 V output between the power source terminals and a 0-10V signal in the wire-feed-speed input channel would map from 1 m/min to 24 m/min in the wire feed unit. The reference values for voltage and wire-feed-speed were issued in the control computer. Two conversions were necessary: one from digital to analogue values, which was performed by an 8-bit D/A converter in the control computer and another from analogue to digital values, which was carried out by a 10-bit A/D converter in the robot interface. Due to the difference in the resolution of each converter and also to some calibration error in the robot interface, which was not possible to correct, calibration curves were obtained by setting specific values in the control computer and reading the actual set values in the power source display (see Figure 5.7 and Figure 5.8). These curves were programmed in the control software along with the BDH 550 wire feeder calibration curve (see Figure 5.5).

5.8 Experimental materials

The experimental materials consisted of:

Welding wire

- Nominal diameter: 1.0 mm
- Type: BOHLER EMK 8A
- Specification: BS 2901 pt.1 GR. A18
- Wire material: Mild Steel
- Typical composition:

C	0.08 %
Si	0.8 %
Mn	1.4 %

Shielding gas

- Type: BOC Argonshield 5
- Typical composition: 93% Ar , 5% CO_2 , 2% O_2
- Flow rate: 15 l/min

Workpiece

- Material: Mild Steel
- Plate thickness: 12 mm for bead on plate welds
  3.2 mm for fillet welds
- Joint type: Tee fillet (with no gap)
- Welding position: Flat
- Test plate dimension: Flange: 76 by 250 mm
  Web: 50.8 by 250 mm

5.9 Experimental procedure

The experimental procedure consisted of:

1. Verification of the validity of the Ogunbiyi's models in the power source;
2. Collection of data for adjusting the models to the power source (bead-on-plate and fillet welds);
3. Generation of new welding procedures based on the adjusted models and validation by welding in fillet joints and checking the weld conformity with the required quality;
4. Collection of data for modelling stand-off using bead-on-plate welding trials, varying stand-off, wire feed speed and welding voltage;
5. Validation of stand-off model;
6. Implemention and tuning of voltage controller;
7. Implemention and tuning of stand-off controller;
8. Integration of both controllers together;
9. Testing the resulting control system;
10. Analysing the results.

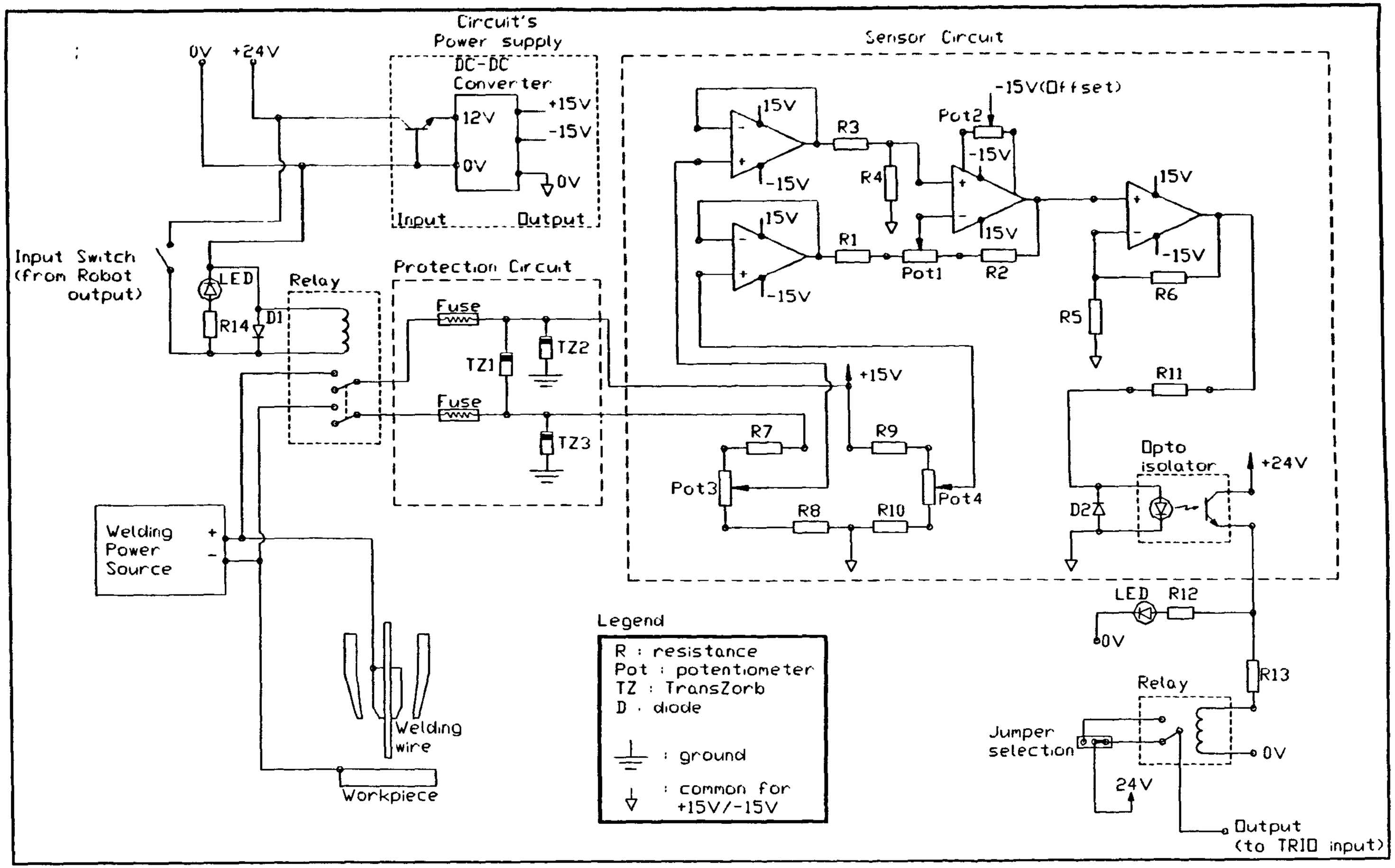

Figure 5.1 - Touch sensor schematic circuit

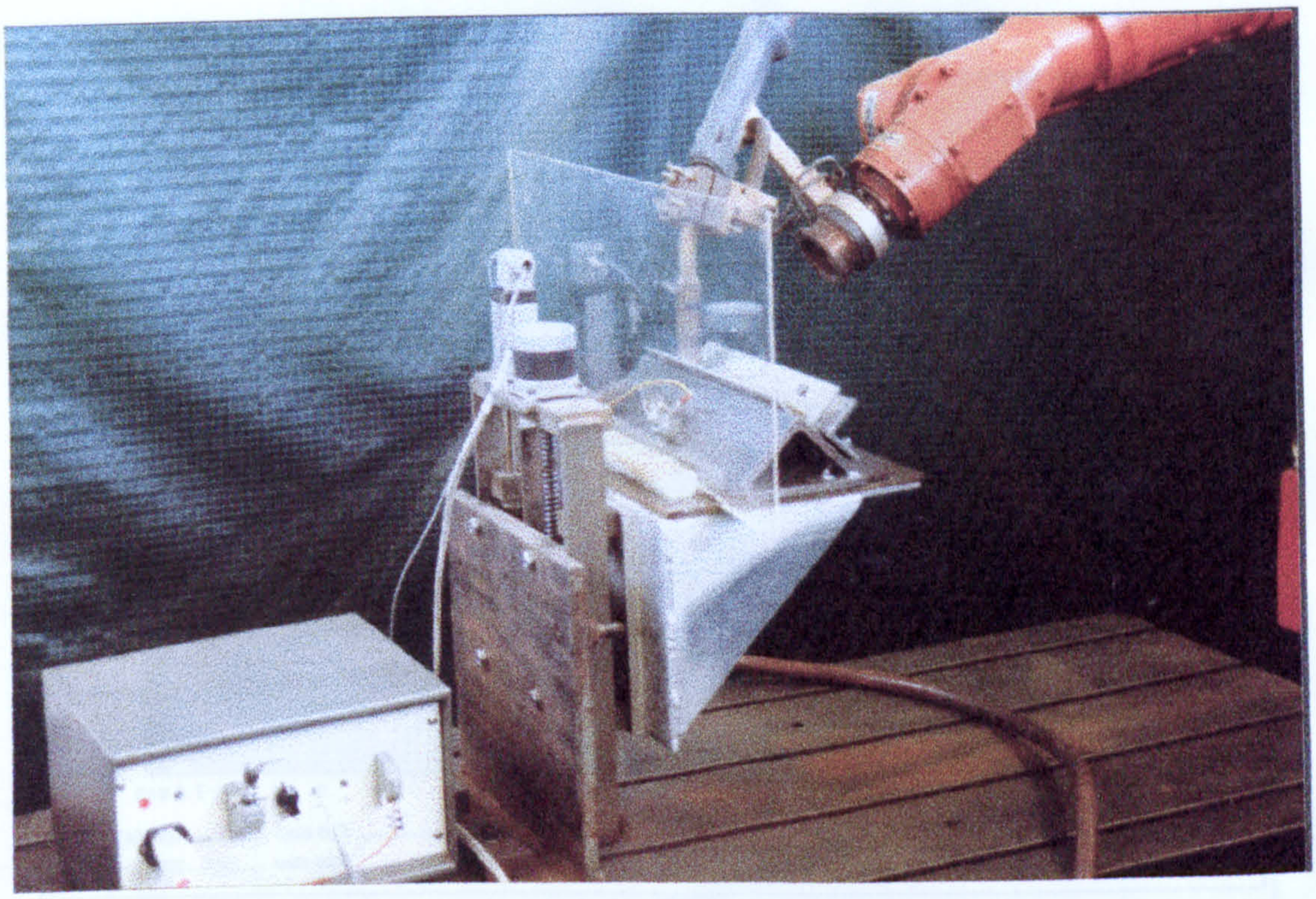

Figure 5.2 - Implemented 1 degree-of-freedom moving table

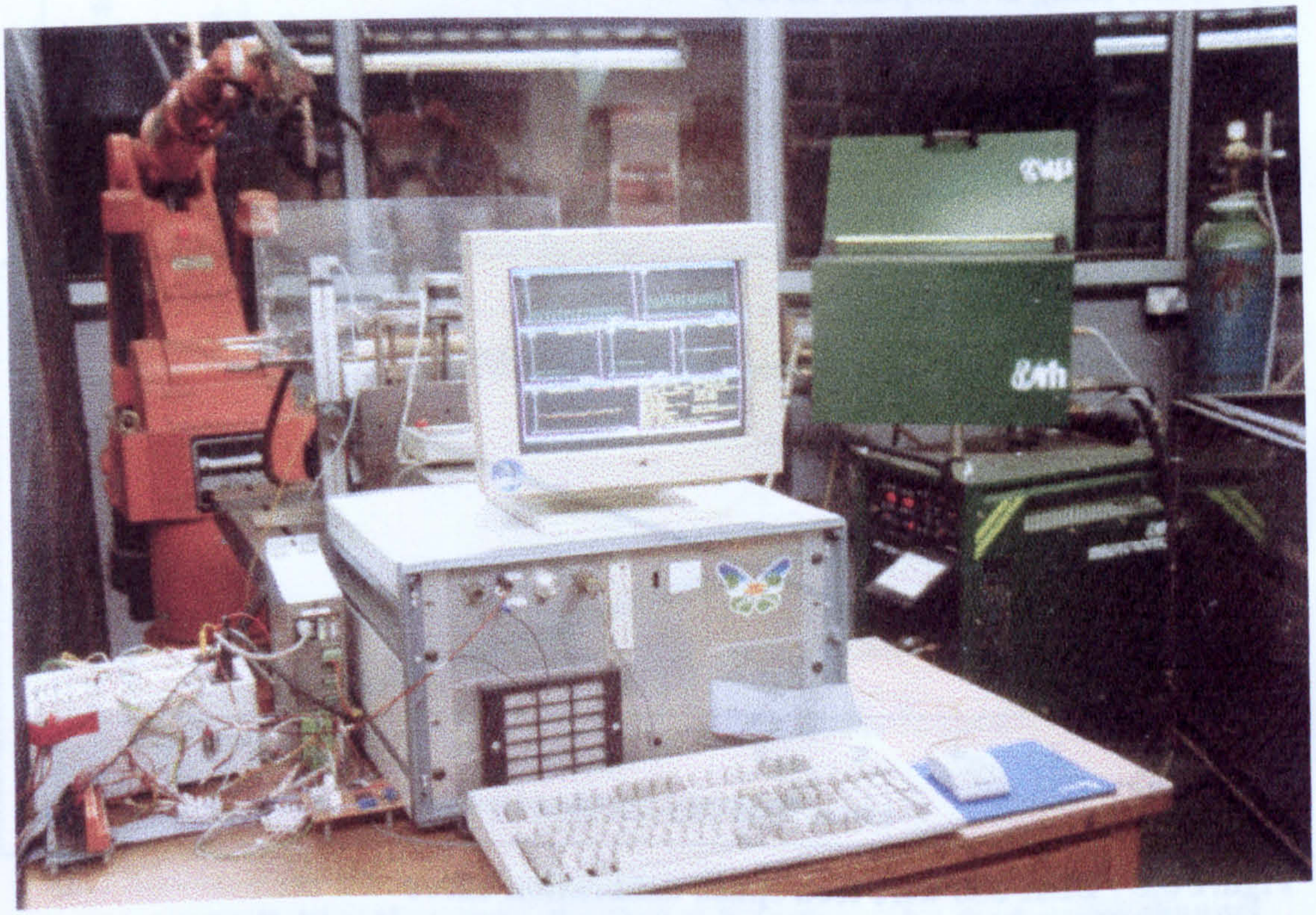

Figure 5.3 - Full system

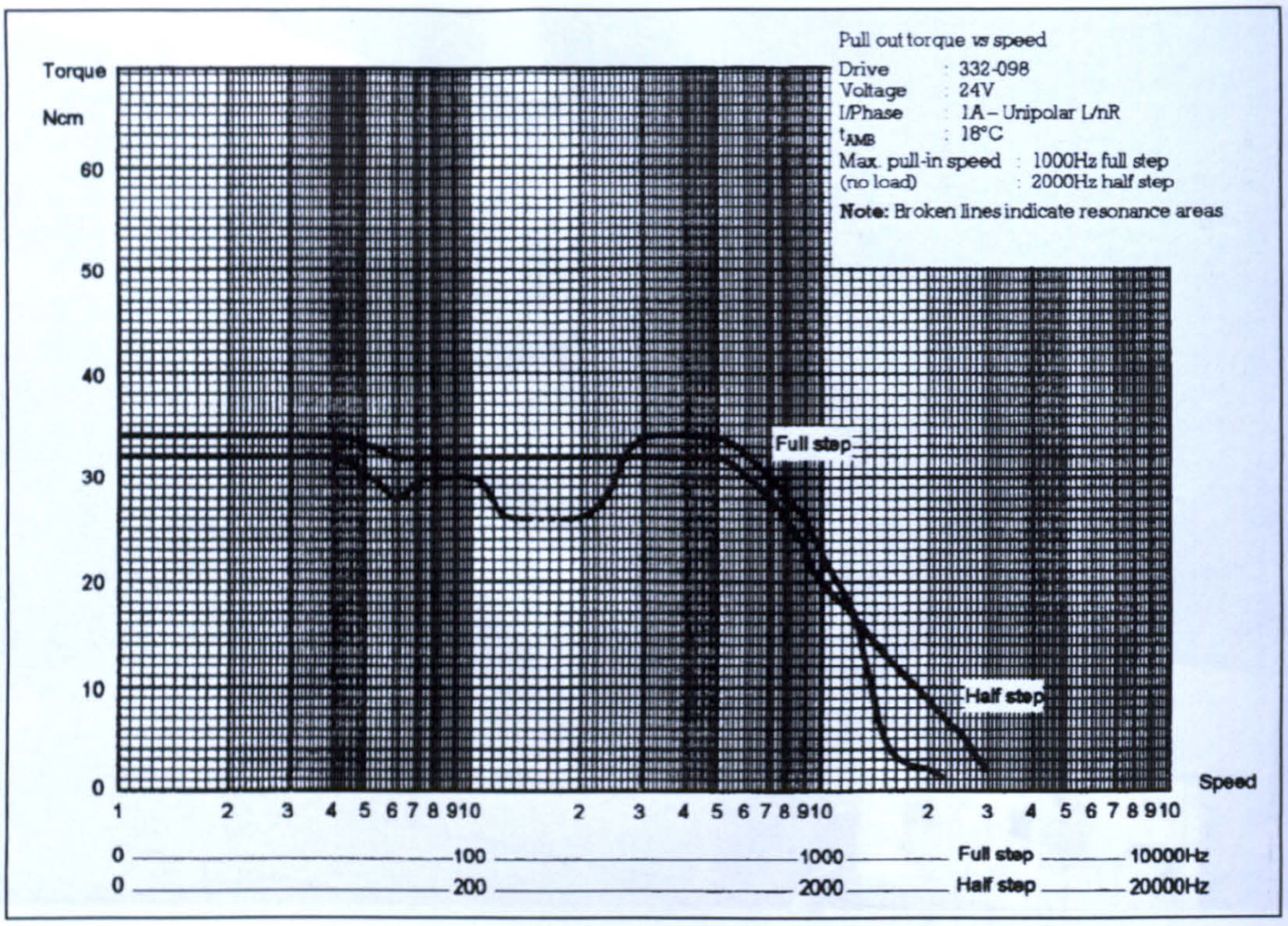

Figure 5.4 - Torque "versus" speed curves for stepper motor used (size 23, 5V, 1A, using 2A unipolar drive)

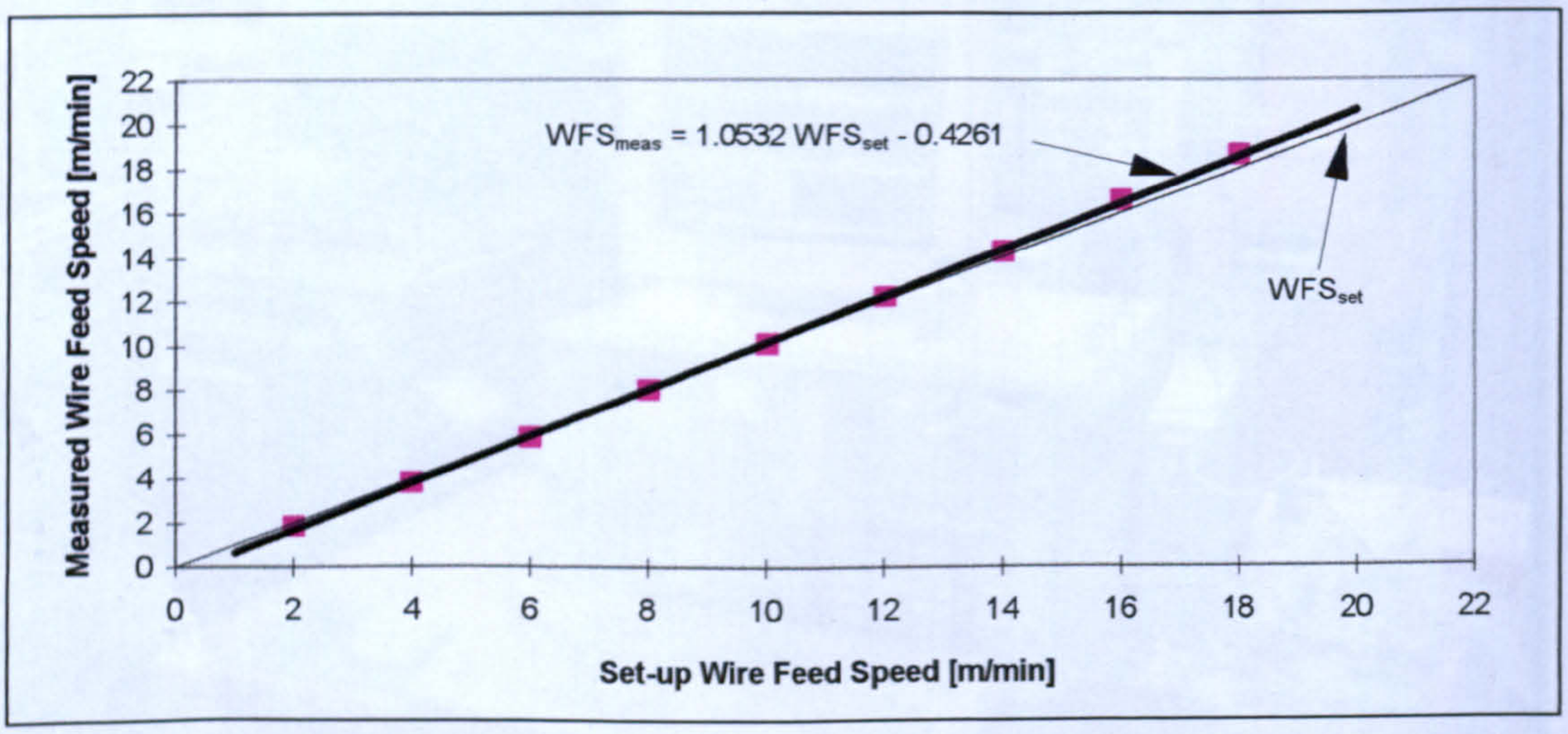

Figure 5.5 - BDH 550 wire feed speed calibration curve

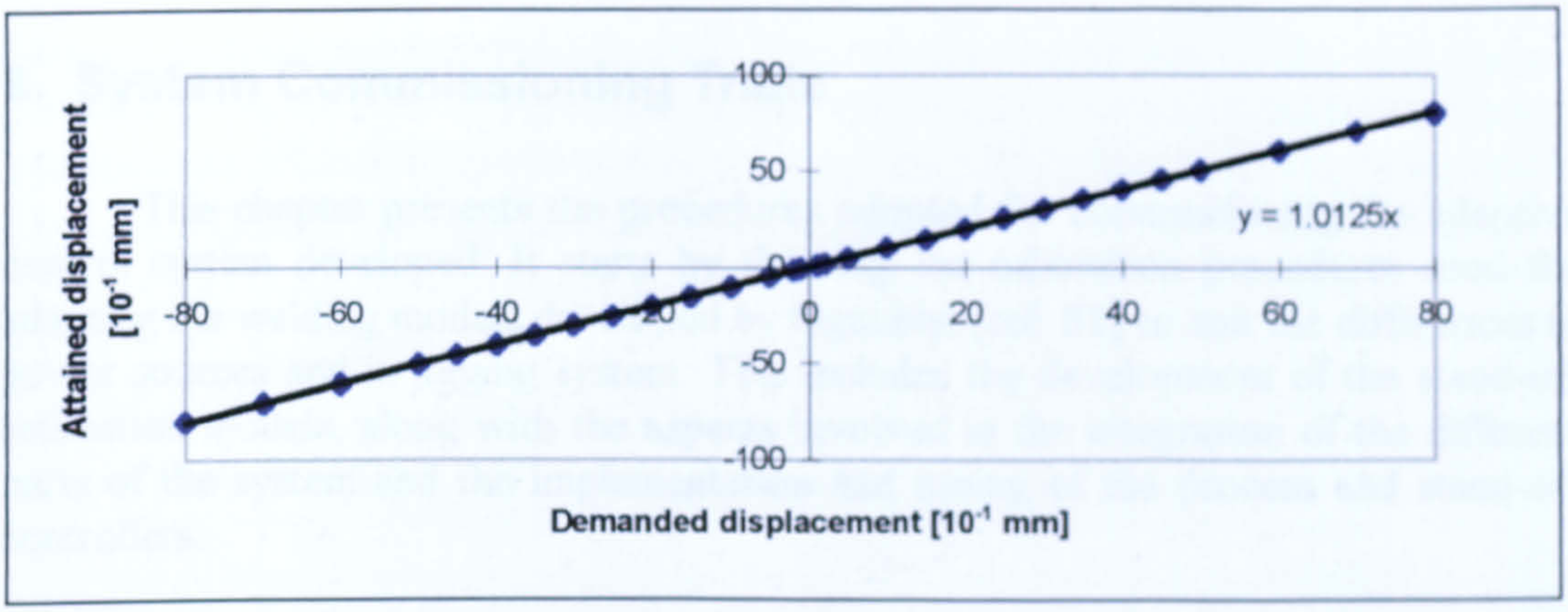

Figure 5.6 - Calibration curve for table displacement

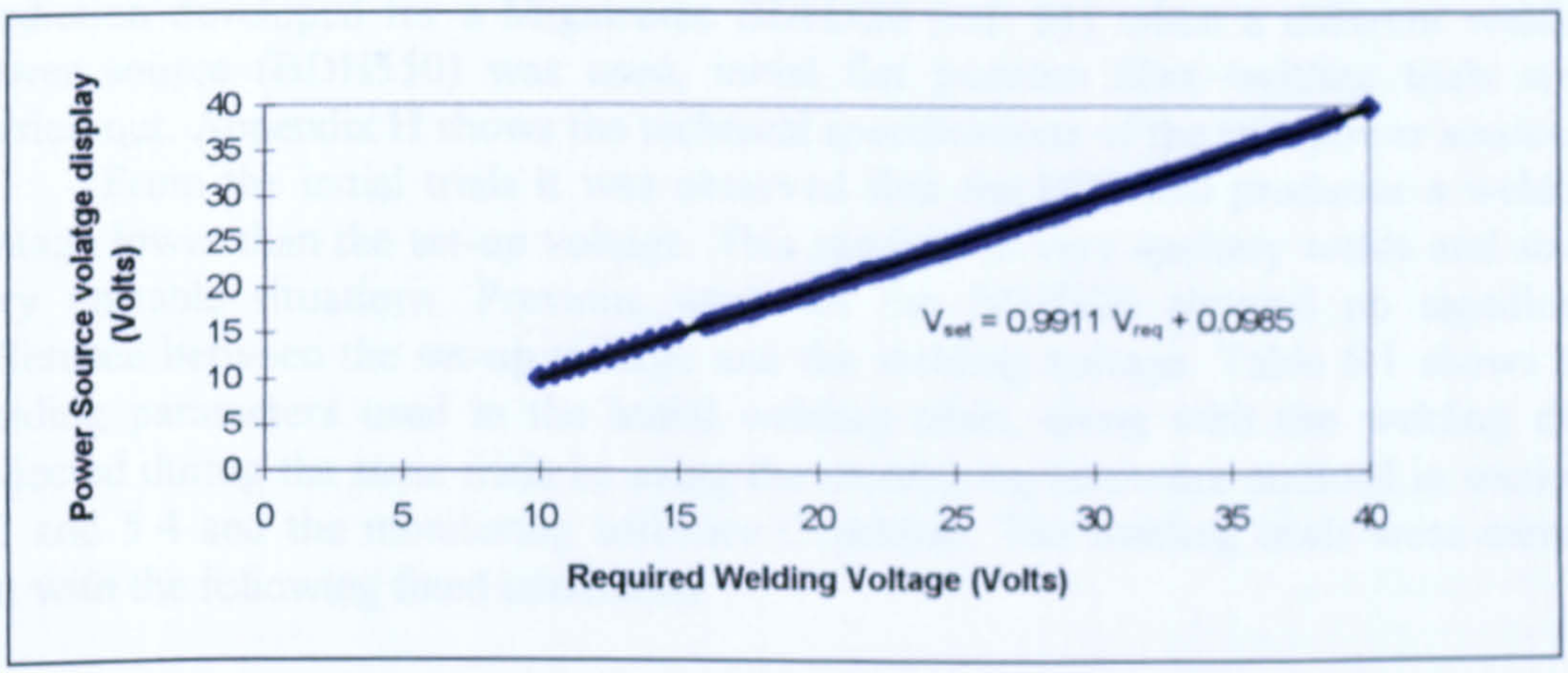

Figure 5.7 - Calibration curve for Robot Interface voltage input channel

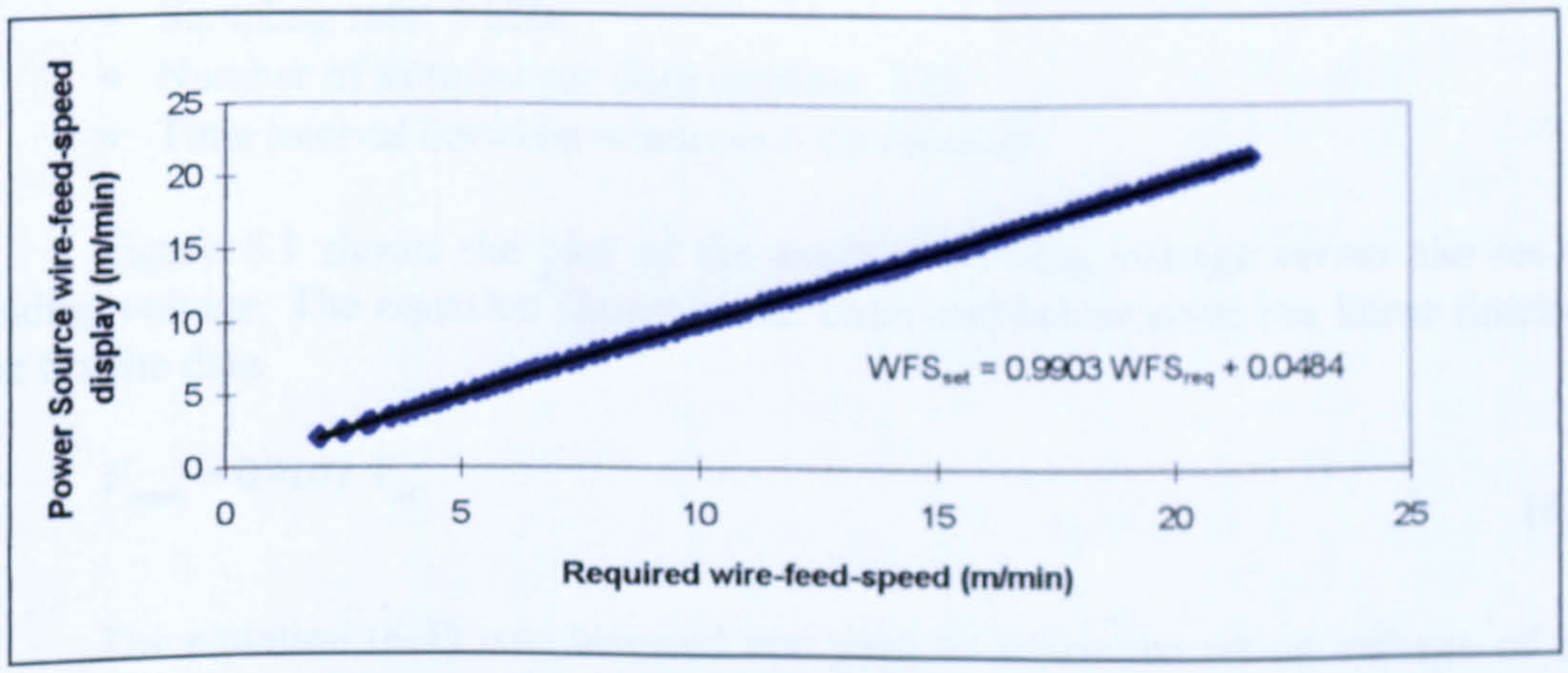

Figure 5.8 - Calibration curve for Robot Interface wire-feed-speed channel

6. System Commissioning Trials

This chapter presents the procedures adopted for commissioning the adaptive control system developed. It starts by showing the calibration procedures used for adapting the welding models developed by Ogunbiyi [ref. **51**] to suit the differences in power sources and in jigging system. This includes the development of the stand-off estimation models, along with the aspects involved in the integration of the different parts of the system and the implementation and tuning of the process and stand-off controllers.

6.1 Calibration of the welding models

In order to verify the validity of the previously established welding parameter prediction developed for a Migatronic BDH320 [ref. **51**] when a different welding power source (BDH550) was used, initial flat position fillet welding trials were carried out. Appendix H shows the technical specifications of the two power sources.

From the initial trials it was observed that the BDH550 produces a welding voltage lower than the set-up voltage. This resulted in very spattery welds and some very unstable situations. Previous work on the BDH320 showed no significant difference between the set-up voltage and the welding voltage. Table 6.1 shows the welding parameters used in the initial welding trials, along with the welding data collected during the same trials by using the monitoring hardware outlined in sections 5.3 and 5.4 and the monitoring software CranMon. The welding trials were carried out with the following fixed conditions:

- Plate thickness: 3.2 mm
- Length of weld: 232 mm
- Welding speed: 0.5 m/min
- Sampling rate: 5 kHz
- Number of samples per data window: 512
- Time interval between windows 0.25 seconds

Figure 6.1 shows the plot of the average welding voltage *versus* the set-up welding voltage. The equation shown in the chart and below gives the linear function that fits the data.

$$V_{mean} = 0.9107 \cdot V_{set} \tag{6.1}$$

The equation (6.1) was inverted and used to adjust the set-up voltage of the previous welding parameters (see Table 6.1) to the levels that supposedly would produce the required mean welding voltage. A new set of flat position fillet welding trials was carried out to observe the process behaviour with the adjusted set-up voltage. Table 6.2 shows the welding parameters used and the welding data collected.

Table 6.1 - Welding trials carried out with previously established welding parameters [ref. 51]

	Input parameters			Measured Response					
Run	WFS	SO	V_{set}	V_{mean}	I_{mean}	TSI	TI	DCI	PR
MC1	4	12	16.3	14.79	122.38	1.82	0.5	0.75	0.19
MC2	6	12	17.6	15.61	166.02	2.15	0.55	0.69	0.22
MC3	8	12	19.2	17.1	199.94	1.94	0.56	0.61	0.29
MC4	10	12	20.7	18.39	219.18	2.14	0.49	0.58	0.31
MC5	12	12	22.3	19.73	255.05	1.8	0.39	0.55	0.36
MC6	14	12	23.9	21.33	265.38	1.89	0.47	0.5	0.37
MC7	4	15	17.5	16.37	119.81	1.8	0.35	0.74	0.2
MC8	6	15	18.2	16.61	160.25	1.76	0.44	0.69	0.24
MC9	8	15	20.3	18.12	204.16	1.77	0.47	0.63	0.29
MC10	10	15	21.8	19.46	232.26	1.92	0.44	0.59	0.33
MC11	12	15	23.3	20.87	260.82	1.79	0.39	0.54	0.37
MC14	4	20	19.6	18.52	111.54	2.36	0.29	0.58	0.33
MC15	6	20	21	19.5	152.49	1.98	0.31	0.64	0.29
MC16	8	20	27.4	25.55	191.62	1.39	0.22	0.05	0.9
MC17	10	20	28.4	26.34	216.15	1.22	0.14	0.04	0.94
MC18	12	20	29.3	26.95	240.92	1.21	0.13	0.05	0.92
MC19	14	20	30.2	27.68	263.39	1.23	0.11	0.06	0.91

WFS: wire feed speed [m/min]
SO: stand-off [mm]
V_{set}: set-up welding voltage [volts]
V_{mean}: measured run average of welding voltage [volts]
I_{mean}: measured run average of welding current [Amps]
TSI, TI, DCI, PR: measured run average of monitoring indices

A considerable improvement has been observed with the adjusted set-up voltage. However, some of the conditions in dip transfer were still very spattery. A comparison between the levels of average and maximum welding current produced by the BDH320 [ref. 51] and the BDH550, for the same welding parameters (V_{req}, WFS, SO and S_w), reveals that the BDH550 delivers higher levels of average current (see Figure 6.2) and maximum current in the dip mode of metal transfer (see Figure 6.3). Since the level of spatter in the dip transfer mode is directly related to the maximum current reached during the short circuit (see section 2.1.5.2), the observed spatter levels could be explained by the higher current levels produced by the BDH550. In Figure 6.2, **Imean_320** stands for the mean welding current produced by the BDH-320, **Imean_550** stands for the mean welding current produced by the BDH-550 and **Ipred** stands for the mean welding current predicted using the equation 3.1. In Figure 6.3, **Imax_320** and **Imax_550** stand for the maximum welding currents produced by the BDH-320 and BDH-550, respectively.

Table 6.2 - Welding trials carried out with the adjusted set-up welding voltage

	Input Parameters				Measured Response					
Run	WFS	SO	V_{req}	V_{set}	V_{mean}	I_{mean}	TSI	TI	DCI	PR
MC21	4	12	16.3	18	16.84	122.9	1.94	0.35	0.75	0.19
MC22	6	12	17.6	19.4	17.7	172.6	1.68	0.37	0.7	0.24
MC23	8	12	19.2	21.1	19	215.7	1.71	0.36	0.65	0.28
MC24	10	12	20.7	22.8	20.42	246.3	1.67	0.31	0.61	0.34
MC25	12	12	22.3	24.5	21.77	270.7	1.72	0.31	0.54	0.38
MC27	4	15	17.5	19.3	18.15	121.26	2.2	0.34	0.68	0.25
MC28	6	15	18.2	20.1	18.49	164.93	1.79	0.35	0.69	0.24
MC29	8	15	20.3	22.3	20.31	203.34	1.71	0.34	0.61	0.32
MC30	10	15	21.8	23.9	21.63	231.31	1.77	0.27	0.54	0.39
MC31	12	15	23.3	25.6	23.06	258.39	1.63	0.24	0.49	0.45
MC34	4	20	19.6	21.6	20.52	113.75	2.91	0.25	0.25	0.63
MC35	6	20	21	23.1	21.56	155.28	2.31	0.26	0.5	0.41
MC36	8	20	27.4	29.9	27.98	199.13	1.05	0.05	0.01	0.97
MC37	10	20	28.4	31	28.71	236.43	1.04	0.04	0.01	0.98
MC38	12	20	29.3	32	29.46	261.14	1.04	0.05	0.01	0.98

V_{req} : voltage predicted from the welding parameter generator [volts]
V_{set} : corrected set-up voltage required for the BDH550 to produce V_{req} [volts]

Note that the actual welding current produced by the BDH320 is generally lower than the corresponding predicted value, while the currents produced by the BDH550 are very close to the same predicted values (see Figure 6.2). Since the generation of welding parameters using the algorithm shown in section 3.3.2.1 is based on the prediction of current and voltage levels which are expected to give a stable process when the BDH320 is used, it is clear that new models would be necessary to correctly map the adequate voltage and current combinations in the case of the BDH550. This led the present author to develop new models to describe the performance characteristics of the BDH550. Appendix I shows the bead-on-plate welding trials data used to develop the BDH550 models. The model structures developed by Ogunbiyi [ref. 51] (see section 3.3.2.1) fitted the available data well and were adopted. The new model coefficients are shown in Table 6.3.

Considering that differences in the welding parameters would affect the predicted bead geometry, a calibration of the bead geometry models proposed by Ogunbiyi [ref. 51] was necessary. Such calibration was carried out by measuring the geometry of the weld beads produced with the welding parameters shown in Table 6.1 and Table 6.2, and by correlating the measured values with the geometry predicted by the models shown in equations 3.6 and 3.7. Only the weld beads produced from stable processes were considered for calibration purposes. The measurement of the bead geometry was performed by cutting a bead specimen from the middle of each welded joint, polishing one of the transversal cuts, etching with a Nital[1] 2% solution and tracing the joint profile from an enlarged projected image.

[1] 2% Nitric Acid + 95% Methanol + 3% pure water, in volume.

Table 6.3 - Coefficients of Ogunbiyi's models obtained for BDH-550

		Regression Coefficients				
Variable	**Eq.No**	**α**	**β**	**δ**	**SE**	**R^2**
I_{mean}	(3.1)	53.6415	24.65153	-0.41327	9.933	0.9830
TSI	(3.2)	3.4557	-0.006043	-0.034601	0.2543	0.7585
I_{mean}	(3.3)	0.324805	0.693878	-	15.8588	0.996
V_{bk}/V_{mean}	(3.4)	-0.335025	0.002398	0.040318	0.1121	0.8545
V_{bk}	(3.5)	-30.78784	-0.031138	2.26504	1.0091	0.9921
PR	(3.10)	-0.92147	-2.8511E-6	0.068592	0.0433	0.9818

Obs.: The coefficients of the models shown in equations (3.6) to (3.9) were kept the same as shown in Table 3.1

SE standard error of the model

R^2 coefficient of determination of the model

Note that the coefficients used for predicting the bead geometry using equations 3.6 and 3.7 were developed for fillet welds carried out in the horizontal-vertical position (see Table 3.1). The welding trials in this work were carried out in the flat welding position. Thus, the average values of both predicted and measured geometrical features were used in order to apply a calibration model to the original prediction models. Table 6.4 shows the predicted and measured geometrical features for the chosen specimens.

Figure 6.4 shows the plot of the measured average leg length against the predicted average leg length. A linear function was chosen to fit the data (see equation (6.2)).

$$Leg_{pred}^{BDH550} = 0.8802 \cdot Leg_{pred}^{BDH320} + 0.623 \qquad \textbf{(6.2)}$$

$$R^2 = 0.9435$$

$$SE = 0.256$$

where

Leg_{pred}^{BDH320} Leg length predicted by using equation 3.6 with the coefficients from Table 3.1

Leg_{pred}^{BDH550} Predicted leg length adjusted to the BDH550 power source

R^2 Coefficient of determination of the model

SE Standard error of the model

Figure 6.5 shows the plot of the measured average weld penetration against the predicted average weld penetration calculated by using equation 3.7. Also, a linear function was chosen to fit the data. (see equation (6.3))

$$Pen_{pred}^{BDH550} = 1.974 \cdot Pen_{pred}^{BDH320} - 1.1965 \qquad (6.3)$$

$$R^2 = 0.9304$$

$$SE = 0.144$$

where

Pen_{pred}^{BDH320} weld penetration predicted by using equation 3.7 with the coefficients from Table 3.1

Pen_{pred}^{BDH550} Predicted weld penetration adjusted to the BDH550 power source

R^2 Coefficient of determination of the model

SE Standard error of the model

Table 6.4 - Predicted and actual geometry data for the fillet welding trials chosen from Table 6.1 and Table 6.2

	Predicted Geometry				Measured Geometry			
Run	Leg_s	Leg_b	Pen_s	Pen_b	Leg_1	Leg_2	Pen_1	Pen_2
MC14	5.95	6.58	1.15	1.15	6.1	5.7	2	0.9
MC15	3.21	3.43	0.63	0.59	4.6	2.8	0	0
MC16	4.03	4.36	0.81	0.79	5.1	3.9	0.2	0.2
MC17	4.74	5.17	1.11	1.11	5.6	4.5	1	0.9
MC18	5.37	6.58	1.25	1.26	6.7	4.9	1.5	1.5
MC19	5.95	6.58	1.34	1.36	7	5.8	2.3	1.5
MC21	3.21	3.43	0.58	0.54	3.6	2.7	0.4	0
MC22	4.03	3.43	0.76	0.73	4.7	3.3	0.7	0
MC23	4.74	5.17	1.02	1.01	5.7	5.2	1	0.9
MC24	5.37	5.9	1.11	1.11	5.8	6	1.1	1.2
MC25	5.95	6.58	1.22	1.22	6.3	6.1	1.3	1
MC27	6.49	7.2	1.29	1.3	6.7	6.8	1.8	1.4
MC28	3.21	3.43	0.58	0.54	3.6	3.1	0.4	0.1
MC29	4.03	4.36	0.76	0.73	4.7	3.5	0.8	0.1
MC30	4.74	5.17	0.92	0.9	5	4.5	1.1	0.7
MC31	5.37	5.9	1.04	1.03	5.9	5.3	1.4	0.9
MC34	5.95	6.58	1.15	1.15	5.8	5.5	1.7	1.1
MC35	3.21	3.43	0.61	0.58	3.7	3.7	0	0.2
MC36	4.03	4.36	0.76	0.73	4.9	3.7	0.6	0.1
MC37	4.74	5.17	0.92	0.9	5.1	5.4	0.5	0.9
MC38	5.37	5.9	1.04	1.03	5.3	5.3	1.2	0.9

Leg_s , Leg_b : predicted side and bottom leg length (horizontal welding position)
Pen_s , Pen_b : predicted side and bottom penetration (horizontal welding position)
Leg_1 , Leg_2 : measured leg lengths (flat welding position)
Pen_1 , Pen_2 : measured side penetrations (flat welding position)

Note that the calibration model shown in equation (6.3) also includes correction for the differences in weld penetration caused by the distinct cooling rate which results from different jigging systems used in the experimental trials carried out with the BDH320 and the BDH550.

The new model coefficients shown in Table 6.3 and the calibration models shown in equations (6.2) and (6.3) were used to make the necessary adjustments in the algorithm shown in section 3.3.2.1.

A new set of bead on plate welding trials was carried out with welding parameters generated by the adjusted algorithm. Good and stable conditions were obtained, although the process was somewhat spattery for low wire feed dip transfer. This behaviour was compensated for by reducing the high limit of PR for the dip mode of metal transfer in the **Step 17** of the algorithm shown in section 3.3.2.1. The value of 0.37 was found to reduce the welding voltage to levels that produced acceptable spatter levels in all the range of wire feed speeds in dip transfer.

In order to check the validity of the calibration models, a flat position fillet welding trial was carried out with parameters generated for producing a fillet weld with an average leg length of 4.5 mm and adequate level of penetration (between 10% and 60% of minimum plate thickness) in 3.2 mm thick plates, using a stand-off of 15 mm and no gap. Figure 6.6 shows the resulting bead geometry and Table 6.5 shows the comparison between predicted and measured values.

Table 6.5 - Bead geometry obtained from welding parameters generated with adjusted models

	Predicted values	Measured values	Prediction error[2]
I_{mean} [amps]	228.9	222.0	-3.01 %
V_{mean} [volts]	21.0	20.86	-0.67 %
Leg_{av} [mm]	4.51	4.7	4.2 %
Pen_{av} [% T_{min}]	25.6%	20.3%	-20.7 %

The large error in the penetration model was still acceptable since the actual penetration was within the requirement range. The imprecision of the penetration model has also been highlighted by Ogunbiyi [ref. **51**].

---

[2] Prediction error = $\left(\frac{Value_{measured} - Value_{predicted}}{Value_{predicted}} \right) \times 100\%$

6.2 Development of stand-off estimation models

As already mentioned in section 4.2.3, an initial attempt was made to use the stand-off estimation model proposed by Ogunbiyi [ref. **51**] to estimate the stand-off changes for control purposes. Again a new model was necessary to map the mean welding current produced by the BDH550 as a result of the combination of the set-up wire feed speed, the set-up voltage and the stand-off. The data shown in Appendix I were used for this purpose. The model structure shown in equation 2.21 fitted well the available data and was adopted. Equation (6.4) shows the resulting model.

$$I_{mean} = 28.595 + 27.417 \cdot WFS + 0.10391 \cdot SO \cdot V_{set} - 0.72938 \cdot SO \cdot WFS \qquad \textbf{(6.4)}$$
$$R^2 = 0.9905$$
$$SE = 7.425$$

where
R^2 is the coefficient of determination of the regression model and
SE is the standard error of the model.

In order to check the quality of the estimates produced by the model, a series of bead on plate welding trials were carried out with the stand-off starting at 15 mm and changing linearly as shown in Figure 6.7. Two levels of final stand-off (SO_f) were tested: 20 mm and 10 mm. In order to pinpoint the exact moment when the robot started and finished the slope path, a robot output was connected to one of the analogue input channels of the monitoring system as shown in Figure 6.8. The welding parameters used in the trials were generated by the welding parameter generator (see section 3.3.2.1) and are shown in Table 6.6, together with the measured value of the proportionality constant ϕ_{meas} required in equation 2.22, and the calculated value, ϕ_{calc} obtained from equation 2.24 with the coefficients shown in equation (6.4). This is repeated explicitly in equation (6.5) for easier reference.

$$\phi_{calc} = \frac{1}{0.10391 \cdot V_{set} - 0.72938 \cdot WFS} \qquad \textbf{(6.5)}$$

$$\phi_{meas} = \frac{\Delta SO_N}{\sum_{i=1}^{N} (I_i - I_{i-1})} \qquad \textbf{(6.6)}$$

where
I_i mean welding current measured at monitoring cycle i
$i = 0$ monitoring cycle immediately before the start of the stand-off slope
$i = N$ monitoring cycle at the end of the stand-off slope
$\Delta SO_N = SO_f - 15.0$

Table 6.6 - Welding parameters used in the stand-off slope trials and measured proportionality constants

Run	WFS	S_W	V_{set}	V_{req}	SO_f	ϕ_{meas}	ϕ_{calc}
s15_2001	5.0	0.6	21.3	19.4	20	-0.3243	-0.6975
s15_2002	6.0	0.7	21.5	19.6	20	-0.3590	-0.4668
s15_2003	7.0	0.8	21.8	19.9	20	-0.3696	-0.3521
s15_2004	8.0	0.9	22.1	20.2	20	-0.3276	-0.2826
s15_2005	9.0	0.5	22.5	20.5	20	-0.3030	-0.2366
s15_2006	9.5	0.5	22.7	20.7	20	-0.2857	-0.2188
s15_2007	11.0	0.6	33.1	30.5	20	-0.1519	-0.2182
s15_2008	12.5	0.7	33.8	31.1	20	-0.1474	-0.1784
s15_2009	13.5	0.7	34.3	31.5	20	-0.1443	-0.1592
s15_2010	14.5	0.7	34.8	32.0	20	-0.1296	-0.1437
s15_1001	5.0	0.6	21.3	19.4	10	-0.3158	-0.6975
s15_1002	6.0	0.7	21.5	19.6	10	-0.2414	-0.4671
s15_1003	7.0	0.8	21.8	19.9	10	-0.2179	-0.3521
s15_1004	8.0	0.9	22.1	20.2	10	-0.2184	-0.2826
s15_1005	9.0	0.5	22.5	20.5	10	-0.2174	-0.2366
s15_1006	9.5	0.5	22.7	20.7	10	-0.2174	-0.2188
s15_1007	11.0	0.6	33.1	30.5	10	-0.1481	-0.2182
s15_1008	12.5	0.7	33.8	31.1	10	-0.1061	-0.1784
s15_1009	13.5	0.7	34.3	31.5	10	-0.0986	-0.1592
s15_1010	14.5	0.7	34.8	32.0	10	-0.1022	-0.1437

WFS : wire feed speed [m/min] S_W : travel speed [m/min]
V_{set} : set-up welding voltage [V] V_{req} : required mean voltage [V]
SO_f : stand-off at end of slope path [mm]
ϕ_{meas} : measured constant by applying equation (6.6) to the welding data collected for these trials (see Appendix J)

Figure 6.9 shows a plot of ϕ_{meas} and ϕ_{calc} *versus* the wire feed speed. The plotted values of ϕ_{meas} correspond to the average of the values measured for positive and negative stand-off slopes (SO_f = 20 mm and SO_f = 10 mm, respectively), with the same wire feed speed. Note the difference between ϕ_{calc} and ϕ_{meas}, which grows with decreasing wire feed speed. For most of the wire feed speeds, ϕ_{calc} is smaller than ϕ_{meas} (bigger absolute value). This results in over prediction of the stand-off, might cause over correction in the table controller, hence leading to instability in the control loop. In addition, the amount by which the absolute values of ϕ_{calc} are bigger than their counterparts is not constant, thus introducing a further prediction error.

Another difficulty in applying the model of equation 2.22 is the determination of when to start estimating the stand-off, that is, which level of current should be considered as corresponding to a stable process after first striking the welding arc. This is a very difficult task since the welding current signal is generally corrupted by random noise.

The problems outlined above led the author to search for a more robust way of estimating the stand-off using primarily the welding voltage and current transient

data. Measurements of resistance between the contact tip and the workpiece showed that in dip mode of metal transfer the resistance calculated during the short circuiting phase has a strong correlation with the stand-off. This was also observed by Philpott [ref. 21], who used the term *dip resistance* to designate such resistance. Based on this observation, a method was devised to calculate the dip resistance using the windowing technique developed by Chawla [ref. 161] together with the standard statistical features extracted from each window of data (see section 2.6.3).

In the dip mode of metal transfer, a short circuiting phase is characterised by the extinction of the welding arc which occurs when the electrode wire touches the weld pool and transfers the molten droplet to the pool. During this time, the wire forms a continuous bridge between the contact-tip and the workpiece. The short circuiting phase can be detected by analysing the welding voltage transient waveform and identifying the periods when the voltage falls steeply to a value close to zero (see Figure 6.10). In this work, in order to make sure that the measured resistance would correspond to a real short circuit, only the voltage samples with magnitude equal to or smaller than the background voltage were considered for calculation purposes. The dip resistance for a window of data was obtained as the average of all the resistances calculated for voltage samples complying with $V \leq V_{bk}$. Equations (6.7) and (6.8) show the method explicitly.

$$DipR_i = \frac{V_k}{I_k} \quad , \quad \left\{ \forall k \in [1,2,\cdots,N_W] \quad ; \quad V_k \leq V_{bk} \right\} \quad , \quad i = 1,2,\cdots,N_{Dip} \tag{6.7}$$

where

V_k is a voltage sample acquired at the discrete time kT in a window of data;
I_k is a current sample acquired at the discrete time kT in a window of data;
T is the sampling period;
N_W is the number of samples contained in a window of data;
V_{bk} is the background voltage as extracted from the window using equation 2.29.
$DipR_i$ is the calculated dip resistance;
N_{Dip} is the total number of voltage samples in a window complying with $V \leq V_{bk}$;

$$DipR_{mean} = \frac{\sum_{i=1}^{N_{Dip}} DipR_i}{N_{Dip}} \tag{6.8}$$

where

$DipR_i$ are the resistances calculated using equation (6.7);
$DipR_{mean}$ is the average of the dip resistances calculated in a window of data.

Considering that the number of welding voltage samples complying with $V \leq V_{bk}$ for each short circuit depends on the sampling frequency, some tests were carried out to check if the *DipR*, as calculated with equation (6.8), is influenced by the sampling frequency. Sampling frequencies from 2 kHz to 12.5 kHz were tested with

constant set-up welding parameters and four levels of stand-off for each sampling frequency. The effect of the sampling frequency on the dip resistance measurement was analysed by comparing the measured values obtained for similar stand-off in each sampling frequency and by comparing the dispersion of the dip resistance points within the window of data. This latter was measured by calculating the standard deviation of the $DipR_i$ relative to their mean value, as shown in equation (6.9).

$$DipR_{SD} = \sqrt{\frac{\sum_{i=1}^{N_{Dip}} \left(DipR_i - DipR_{mean}\right)^2}{N_{Dip} - 1}} \qquad (6.9)$$

where $DipR_{SD}$ is the standard deviation of the measured dip resistances within a window of data.

Equations (6.8) and (6.9) show the method of calculating the figures for each window of data. To characterise a weld run carried out with constant welding parameters, the average of the $DipR_{mean}$ and $DipR_{SD}$ over the entire run is used. The average is calculated over the windows that present a reasonable stability level. The windows which contain data from the welding start and end periods are rejected. Table 6.7 shows the welding parameters and the dip resistance data collected for these trials. No significant variation was observed to occur, neither in the dip resistance values nor in their dispersion for the range of sampling frequencies tested. Hence, the sampling frequency does not affect the dip resistance calculation in the frequency range of 2.0 kHz to 12.5 kHz. Figure 6.11 shows typical transient waveforms of the welding voltage (a) and the welding current (b) for the dip mode of metal transfer with constant welding parameters[3]. Figure 6.11c shows the trace of the calculated resistance, V/I, and the dip resistance, *DipR*, as calculated using equation (6.8).

Although the method for calculating dip resistance has been devised for use in dip transfer, the analysis of the resistance calculated from welding data for spray mode of metal transfer revealed that the *dip resistance*, as calculated using equations (6.7) and (6.8), also have a good correlation with the stand-off in this mode of metal transfer. Hence, the *dip resistance* was also considered for stand-off estimation purposes in the spray transfer mode. Figure 6.12 shows the typical transient waveforms of the welding voltage (a) and the welding current (b) for the spray mode of metal transfer with constant welding parameters[4]. Figure 6.12c shows the trace of the calculated resistance, V/I, and the *DipR*, obtained from equation (6.8). Note that the *DipR* has a value very close to the mean resistance in this case.

---

[3] The time waveforms shown in Figure 6.11 were acquired in a window of 512 data points at 2 kHz sampling frequency. The setup welding parameters were: V_{set} = 21.2 V (BDH550), WFS = 5.5 m/min, S_W = 0.5 m/min, SO = 20 mm.

[4] Data acquisition characteristics as described in the previous footnote. The setup welding parameters were: V_{set} = 31.6 V (BDH550), WFS = 10.5 m/min, S_W = 0.5 m/min, SO = 20 mm

Table 6.7 - Dip resistance dispersion with different sampling frequencies

Run	SO	Freq.	N_W	V_{mean}	I_{mean}	$DipR_{mean}$	$DipR_{SD}$
Dipr1	12	4032	512	19.61	163.5	24.7	4.3
Dipr2	14	4032	512	19.71	157.2	26.6	4.4
Dipr3	16	4032	512	19.71	153.6	28.6	4.6
Dipr4	18	4032	512	19.80	148.2	30.6	4.4
Dipr5	12	8065	1024	19.60	164.6	25.1	4.2
Dipr6	14	8065	1024	19.71	159.1	26.8	4.2
Dipr7	16	8065	1024	19.71	154.2	28.9	4.3
Dipr8	18	8065	1024	19.77	149.2	30.8	4.6
Dipr9	12	12500	2048	19.66	162.0	25.0	4.0
Dipr10	14	12500	2048	19.73	158.1	27.1	4.4
Dipr11	16	12500	2048	19.75	151.9	28.9	4.5
Dipr12	18	12500	2048	19.76	148.4	31.0	4.7
Dipr13	12	2000	512	19.62	166.2	24.4	4.5
Dipr14	14	2000	512	19.69	159.3	27.3	4.5
Dipr15	16	2000	512	19.69	154.8	28.4	4.0
Dipr16	18	2000	512	19.78	148.6	30.6	4.2
Dipr17	12	4032	1024	19.61	167.8	25.0	5.3
Dipr18	14	4032	1024	19.61	159.4	27.1	4.4
Dipr19	16	4032	1024	19.71	154.5	28.8	4.3
Dipr20	18	4032	1024	19.76	148.0	31.0	4.4

SO: stand-off [mm], Freq.: sampling frequency [Hz]
$DipR_{mean}$:dip resistance (run average) [mΩ], N_W:number of samples in a window
$DipR_{SD}$: standard deviation of dip resistance (run average) [mΩ]
WFS = 6.0 m/min, V_{set} = 21.5 V, S_W = 0.5 m/min, Weld length = 200 mm

In order to develop models to estimate the stand-off based on the measured values of *dip resistance*, a good understanding of the variables involved in the measurement of such resistance is necessary. Figure 6.13 shows a schematic diagram of the welding voltage and current measurement pick-up points. Figure 6.14 shows the equivalent electrical circuit, outlining the various resistance components in a lumped form. It is assumed that the level of current drained by the voltage measurement system (signal conditioning and analog to digital converter) is negligible. Hence, it is assumed that there is no resistive voltage drop in the voltage sensor leads. The measured resistance will therefore include only the series combination of the resistance components due to the torch cable, the contact tip, the wire stickout, the welding arc, the weld pool and the solid workpiece and fixturing.

The torch cable, the weld pool and the solid workpiece/fixturing contributions can be considered as constants which depend on the materials involved and on the temperature in the steady state. The contact tip contribution depends on the wire surface condition, the contact-tip wear and the contact-tip temperature. The wire stickout contribution depends on the wire material, the cross sectional area, the

stickout length[5] and the temperature distribution along this length. The welding arc contribution depends on the type of plasma gas, the welding current, the arc length and the types of material of the electrodes (see section 2.1.3). Note that the stickout length will vary as a result of a change in the stand-off and also due to random variation in the point of electrical contact in the contact-tip and to weld pool oscillations. The contact tip can be viewed as a source of noise in the voltage/resistance measurement.

Theoretical calculations of the distribution of temperature along the stickout length show that the temperature distribution varies with wire material (electrical resistivity, thermal conductivity and thermal capacity), welding current and wire feed speed [ref. **195**]. The temperature of the wire at the point of electrical contact in the contact tip is generally assumed to be equal to the contact-tip temperature [ref. **131**]. Hence, assuming this to be true, a change in the temperature distribution along the stickout is expected to occur as a result of a change in the contact-tip temperature. Consequently, the electrical resistance is also expected to change. Considering that the torch cooling system has a limit in the amount of heat it can remove from the contact-tip per unit of time, the steady state temperature of the contact-tip will vary depending on the set-up welding parameters.

From these considerations, an empirical model with terms accounting for the effect of isolated variables and two-variable interaction was proposed to map the behaviour of the measured dip resistance as a function of the welding parameters, V_{set}, *WFS* and *SO*. These were chosen since they are the influential variables most likely to be changed during welding. Equation (6.10) shows the proposed structure.

$$\begin{aligned} DipR = {} & \beta_0 + \beta_1 \cdot WFS + \beta_2 \cdot V_{set} + \alpha_0 \cdot SO + \alpha_1 \cdot SO \cdot V_{set} + \\ & + \alpha_2 \cdot SO \cdot WFS + \beta_3 \cdot WFS \cdot V_{set} \end{aligned} \tag{6.10}$$

where α_i , i=0 to 2, and β_j , j=0 to 3, are the regression constants.

The stand-off estimation can be obtained from equation (6.10) by organising the terms in its left side and isolating *SO* , as shown in equations (6.11) and (6.12).

$$\begin{aligned} DipR = {} & (\alpha_0 + \alpha_1 \cdot V_{set} + \alpha_2 WFS) \cdot SO + \\ & + (\beta_0 + \beta_1 \cdot WFS + \beta_2 \cdot V_{set} + \beta_3 \cdot WFS \cdot V_{set}) \end{aligned} \tag{6.11}$$

$$SO_{est} = \frac{DipR}{(\alpha_0 + \alpha_1 \cdot V_{set} + \alpha_2 WFS)} - \frac{(\beta_0 + \beta_1 \cdot WFS + \beta_2 \cdot V_{set} + \beta_3 \cdot WFS \cdot V_{set})}{(\alpha_0 + \alpha_1 \cdot V_{set} + \alpha_2 WFS)} \tag{6.12}$$

The model shown in equation (6.12) was used in this work to estimate the stand-off for control purposes. The coefficients of the model were obtained from applying multiple regression analysis to the welding data collect for bead-on-plate welding trials. The welding parameters used were generated by the off-line welding

---

[5] The stickout length in this context is the length between the electrical contact point in the contact-tip and the end of the electrode wire.

parameter generator and five levels of voltage[6] were tested for each combination of stand-off and wire feed speed, such that the influence of the welding voltage could be detected. The welding parameters and the welding data collected are shown in Appendix K. Due to the differences in the resistance components present in the dip and the spray modes of metal transfer, two multiple regression models (one for each mode of metal transfer) were developed based on the model of equation (6.11). The coefficients obtained are shown in Table 6.8, together with the standard error (SE) and the coefficient of determination of the fitted models (R^2).

Table 6.8 - Coefficients for dip resistance based stand-off estimation models

	Model for dip mode metal transfer	Model for spray mode metal transfer
α_0	0.00165	0.021468
α_1	-0.000027	-0.000568
α_2	-	-
β_0	0.010645	-
β_1	-0.001485	-0.029601
β_2	-	0.004404
β_3	0.000078	0.0007
SE	0.000371	0.002110
R^2	0.9900	0.9997

Obs: The coefficients marked with an hyphen ("-") did not present a good significance level and were considered null.

Note that the stand-off estimation models developed present the general form shown in equation (4.8), that is, a linear model whose coefficients are functions of the welding parameters. This is very similar to the dip resistance model developed by Philpott [ref. 131] with the difference that this latter has a constant slope and the intercept is considered null (see equation 2.18).

In order to validate the dip resistance based estimation models, bead-on-plate welding trials were carried out with the stand-off varying linearly in different slopes. Table 6.9 shows the welding parameters used and the start and end stand-off values. Figure 6.15 to Figure 6.28 show some of the validation results and compare the actual stand-off with the dip resistance based estimation and the estimation obtained by using equation (2.22) with the coefficients shown in equation (6.4). Note that in most situations in the dip mode of metal transfer, the stand-off predicted by the dip resistance based model is more precise and presents a smaller range of oscillation than the prediction based on the welding current cumulative differences. It should also be noted that in the spray mode of metal transfer, the dip resistance based prediction oscillates in a pattern very similar to the prediction based on the welding current cumulative differences. This can be expected since in this case the measured resistance includes the component due to the welding arc, which decisively influences the welding current. Hence, it produces a less robust stand-off estimation than in the case

[6] The voltage suggested by the welding parameters generator, V_{set}, two levels below this value, V_{set}-0.5 and V_{set}-1.0 , and two levels above, V_{set}+0.5 and V_{set}+1.0.

of the dip mode of metal transfer. One advantage, though, is that the dip resistance based estimation model produces an absolute stand-off estimation, whereas the model proposed by Ogunbiyi produces an estimation relative to the initial welding current.

Table 6.9 - Welding parameters used in the validation trials for the dip resistance based stand-off estimation models

Run	WFS [m/min]	V_{set} [volts]	SO_{start} [mm]	SO_{end} [mm]	Metal transfer
val1	4.5	19.1	12	20	dip
val2	5.5	20.7	20	12	dip
val3	6.5	21.0	12	20	dip
val4	6.5	21.6	20	12	dip
val5	8.5	22.2	12	20	dip
val6	8.0	22.2	20	12	dip
val7	10.0	32.8	12	20	spray
val8	10.5	32.6	20	12	spray
val11	10.0	22.4	12	20	dip
val12	10.0	22.5	20	12	dip
val13	5.5	20.0	12	15	dip
val14	5.5	20.3	15	12	dip
val15	8.5	22.2	12	15	dip
val16	8.5	22.2	15	12	dip
val17	10.0	22.4	12	15	dip
val18	4.5	19.4	15	18	dip
val19	6.5	21.5	18	15	dip
val20	8.5	22.2	15	18	dip
val21	10.5	32.7	18	15	spray
val22	12.5	33.1	15	18	spray
val23	14.5	33.3	18	15	spray
val24	4.5	19.4	15	20	dip
val25	6.5	21.6	20	15	dip
val26	8.5	22.2	15	20	dip
val27	10.5	32.6	20	15	spray
val28	12.5	33.1	20	15	spray
val29	14.5	33.7	15	20	spray

SO_{start} : stand-off at start of the slope
SO_{end} : stand-off at the end of the slope
Weld length: 200 mm
Welding speed (S_W): 0.5 m/min

The dip resistance based stand-off estimation model developed above was validated for bead-on-plate welding trials carried out in the flat position. During initial flat position fillet welding trials, it was observed that the model produced a stand-off estimation with a value smaller than the actual stand-off. Considering that in fillet joints the weld pool is constricted, it can be expected that a certain bead build up will occur below the welding arc, thus effectively reducing the distance between the

contact tip and the weld pool and consequently, the measured resistance. It was also observed that this under estimation would depend on the deposition rate, that is, on the ratio between the wire feed speed and the welding speed, WFS/S_W. For a fixed wire feed speed, the smaller the travel speed is the smaller the estimation will result, or in other words, a larger bead build-up will occur.

Figure 6.29 shows the comparison between the stand-off estimations obtained for fillet welding trials carried out with the same setup welding voltage (20.3 V) , wire feed speed (5.5 m/min) and stand-off (15 mm), and with two different levels of travel speed: (a) 0.4 m/min and (b) 0.8 m/min. Both estimations were filtered with a third order moving average filter. Note that the estimation obtained for the welding trial carried out with 0.4 m/min travel speed is generally lower than the one obtained for 0.8 m/min travel speed. It should be noted that the difference between the actual stand-off and the estimated values for both welding trials is almost constant.

Considering that, in normal welding conditions (constant gap or no gap at all), the wire feed speed and the travel speed should be kept constant during the welding process, it is acceptable to assume that the bead build-up below the welding arc would also have a constant average size. Hence, the observed estimation error should also have a constant average value and it would, therefore, behave as an off-set in the stand-off estimation. Since in the implemented system the initial stand-off is always known, such off-set can be estimated at the beginning of the weld and added to the subsequent dip resistance based stand-off estimates. This strategy was successfully implemented and the results are presented in Chapter 7.

6.3 System integration

The integration of the system involved determining and combining the communication capabilities of each sub-system such that a master and slave control scheme could be defined. Three different ways of communicating were available in the sub-systems used: (a) digital inputs and outputs, (b) analogue inputs and outputs and (c) RS232 serial communications ports.

Digital inputs and outputs were freely available in the robot controller and in the table controller. Analogue inputs and outputs were available in the robot interface installed in the welding power source and also in the monitoring personal computer (PC). RS232 serial communication ports were available in the monitoring PC and in the table controller. Having determined the communication capabilities of each sub-system and the specific requirements of each type of communication channel, all the sub-systems were interconnected in such a way that the monitoring PC could have a supervisory function. Figure 6.30 shows the interconnections in a diagrammatic form. Table 6.10 shows the interconnections between the digital inputs and outputs and Table 6.11 shows the connections in the analogue inputs and outputs.

The communication between the robot controller and the monitoring PC was made via the table controller through digital inputs and outputs. The interconnection between the robot and the table digital inputs and outputs was provided by a specially built interface box (see Appendix G), whose primary function was to convert the two-terminal "switch-type" robot inputs and outputs to 24 V inputs and outputs, as required by the table controller. Such a box was also used to house the touch sensor,

which would become active by setting a dedicated robot output directly connected to it. The digital output of the touch-sensor was connected to a digital input in the table controller to indicate when it should stop during a welding joint search routine. In the implemented system only five robot outputs and three robot inputs were found to be necessary. However, a larger number of digital channels could be used in a more complex system. The five robot outputs could indicate up to 32 different situations, which could be assigned in a look-up table.

Table 6.10 - Digital connections between the control subsystems

Robot	Interface Box		BDH 550	Touch Sensor
Output 1	24V Output	Input 0		
Output 2	24V Output	Input 1		
Output 3	24V Output	Input 2		
Output 4	24V Output	Input 3		
Output 5	24V Output	Input 4		
Output 6	24V Output		Robot Interface Trigger	
Output 7	See Figure 6.8			
Output 8	Switch Output			Input Switch
Input 1	24V Input	Output 8		
Input 2	24V Input	Output 9		
Input 3	24V Input	Output 10		
Input 4	Not used			
Input 5	Not used			
Input 6	Not used			
Input 7	Not used			
Input 8	Not used			
		Output 15	Wire Inching	
		Input 5	Arc Detect Output	
		Input 6	Main Error Output	
		Input 7		24V Output

Wire Inching : Robot interface input used to provide wire feeding when not welding
Arc detect: Robot interface output used to indicate if the welding arc is on
Main Error: Robot interface output used to indicate a hardware failure in the power source

The three robot inputs were mainly used for returning authorization codes to the robot controller as a response to the authorization requests issued by the same controller via setting pre-determined combinations of robot outputs. The robot program was generated off-line in such a way that the robot controller would issue an authorization request and would wait for an acknowledgment code whenever a programmed action should start. This would allow the master controller to supervise the robot movements and the table controller to synchronize the table movements with the robot. The authorization requests were coded in different combinations of digital outputs and were programmed to be issued mainly during the pre-weld

movements, in which the robot and the table should move to achieve the required relative position at the weld start point. The sequence of signals and their purpose were already described in section 4.1.3.1.

Table 6.11 - Analogue signal connections in the control system

Robot	Monitoring & Control PC	Signal Conditioning		Robot Interface (BDH 550)	Moving Table
	A/D Channel 1	0 - 10V	0 - 100V	Voltage sensor	
	A/D Channel 2	0 - 10V	0 - 10V	Current Sensor	
	A/D Channel 3	0 - 10V	0 - 10V		Position sensor
	+5V				
Output 7	A/D Channel 4				
	D/A Channel 1	0 - 5V	0 - 10V	Analogue Input 1 (Setup voltage)	
	D/A Channel 2	0 - 5V	0 - 10V	Analogue Input 2 (Wire feed speed)	

A/D : Analogue to Digital Converter D/A : Digital to Analogue Converter

The digital codes issued by the robot controller could also be accessed by the monitoring PC. This was made possible by running a special program in parallel with the table control program, such that the state of the table controller inputs could be checked repeatedly and an externally accessible variable could be continuously updated. Each input was considered as corresponding to a bit in a binary number, whose equivalent integer value was assigned to a global variable, which could be accessed by the monitoring PC at any time via the serial link. The robot interface error indication outputs were also connected to the table controller and relayed to the monitoring PC in the same manner. By accessing the state of the table controller inputs, the monitoring PC would have information on which stage the robot program was at and on the error state of the welding power source.

In order to provide a means to manually stop the whole system in the event of an uncontrollable situation, one dedicated robot output was used to trigger the welding power source and another was connected directly to the table controller to indicate if the robot was executing a welding movement. By pressing the robot built-in emergency-stop button, all its outputs are reset, thus switching off the welding arc and signaling the table controller to stop any movement.

Also, two digital outputs from the robot interface were connected to the table controller to indicate a failure in the welding arc ignition or some hardware error in the welding power source. In the event of one or both errors, the table controller should stop any workpiece movement, send an error signal to the robot and move the workpiece back in the direction of the approach vector, such that the robot could continue moving until the end of the programmed weld without colliding with the workpiece. At the end of the weld movement, the robot program would be aborted as a result of the error signal issued by the table controller.

In section 4.2.5 it has been mentioned that two methods of communicating with the welding power source could have been used: (a) via direct RS232 serial communication and (b) by using a so called "Robot Interface" specially tailored to be used with robots. The use of each alternative would imply in a different transport delay, that is a time delay between the issuing of a command by the monitoring computer and the actual implementation of this command by the welding power source. In order to have an estimate of these time delays, voltage step input tests were carried out and the corresponding welding data were acquired, such that the time between the issuing of a command and the power source response could fit in one window of data. This would ensure accuracy in the time measurement. Figure 6.31 to Figure 6.34 show the results of the tests. It should be noted that for direct serial communication, an approximate delay of 50 milliseconds is observed before the power source responds to a voltage command, while a delay of approximately 200 milliseconds is observed in the case of the robot interface. This difference is expected, since the robot interface case includes, further to the digital-to-analogue and analogue-to-digital conversions, the delay of transferring data from the robot interface to the power source main controller via serial communications. Also, in the case of using the direct serial link, only the voltage command was issued, whereas in the case of the robot interface, a continuous power source error check is also carried out, which might increase the response time. Considering that the current implementation of the serial communications protocol did not have any function for setting wire feed speed, the robot interface option was chosen for implementing the proposed process controller.

6.4 Control system tuning

In order to tune the welding process controller shown in chapter 4, a series of welding trials were carried out and adjustments in the control algorithms were made until a satisfactory performance was achieved at all the levels of wire feed speeds studied. The sequence of adjustments and modifications in the algorithm were described in chapter 4.

The tuning of the stand-off controller has also been described on chapter 4. It basically consisted of choosing the threshold values for the minimum and maximum stand-off adjustments that would be allowed in each control cycle, based mainly on previous process experience. Tests were also made to check which speed and acceleration would be acceptable for moving the workpiece in one control cycle. A speed of 8 mm/s and an acceleration of 400 mm/s^2 were found to produce good performance without deteriorating the welding process stability.

6.4.1 Filtering of process estimates

Despite the improvement in accuracy provided by the dip resistance based estimation model, if compared to the model based on the cumulative differences in welding current the stand-off estimates obtained were still corrupted by random noise (see Figure 6.15 to Figure 6.28). As already mentioned in chapter 4, a third order moving average filter was used to filter the stand-off estimates. This filter was implemented in such a way that it was reset after every stand-off control cycle and a

new control cycle would occur only after three new non-filtered stand-off estimates were obtained. This strategy was adopted in order to eliminate from the estimation the effect of the stand-off estimates obtained before each control cycle, hence preventing the control system from responding to an error that has already been acted upon. In control terms, it could be called a "forgetting" property of the filter, without which an oscillatory behaviour would result, as observed in the tuning trials.

6.4.2 Dependency of Power Ratio reference range with wire feed speed

According to the final form of the welding process controller described in section 4.2.1, the best performance for the dip mode of metal transfer was found to occur when the allowed range of variation of the power ratio was considered as a function of the wire feed speed. Figure 6.35 shows that this is in agreement with the actual behaviour of the power ratio when different wire feed speeds are used.

Figure 6.36 shows the variation of the other monitoring indices with the wire feed speed for stable dip mode of metal transfer. Note that TSI is the most affected index, while TI and DCI remain fairly constant. Considering that TSI is used only for a minor voltage trimming rule, the allowed range of variation was kept constant, despite the observed dependency on the wire feed speed.

No pronounced trends in the monitoring indices were observed when varying the wire feed speed in stable spray mode of metal transfer.

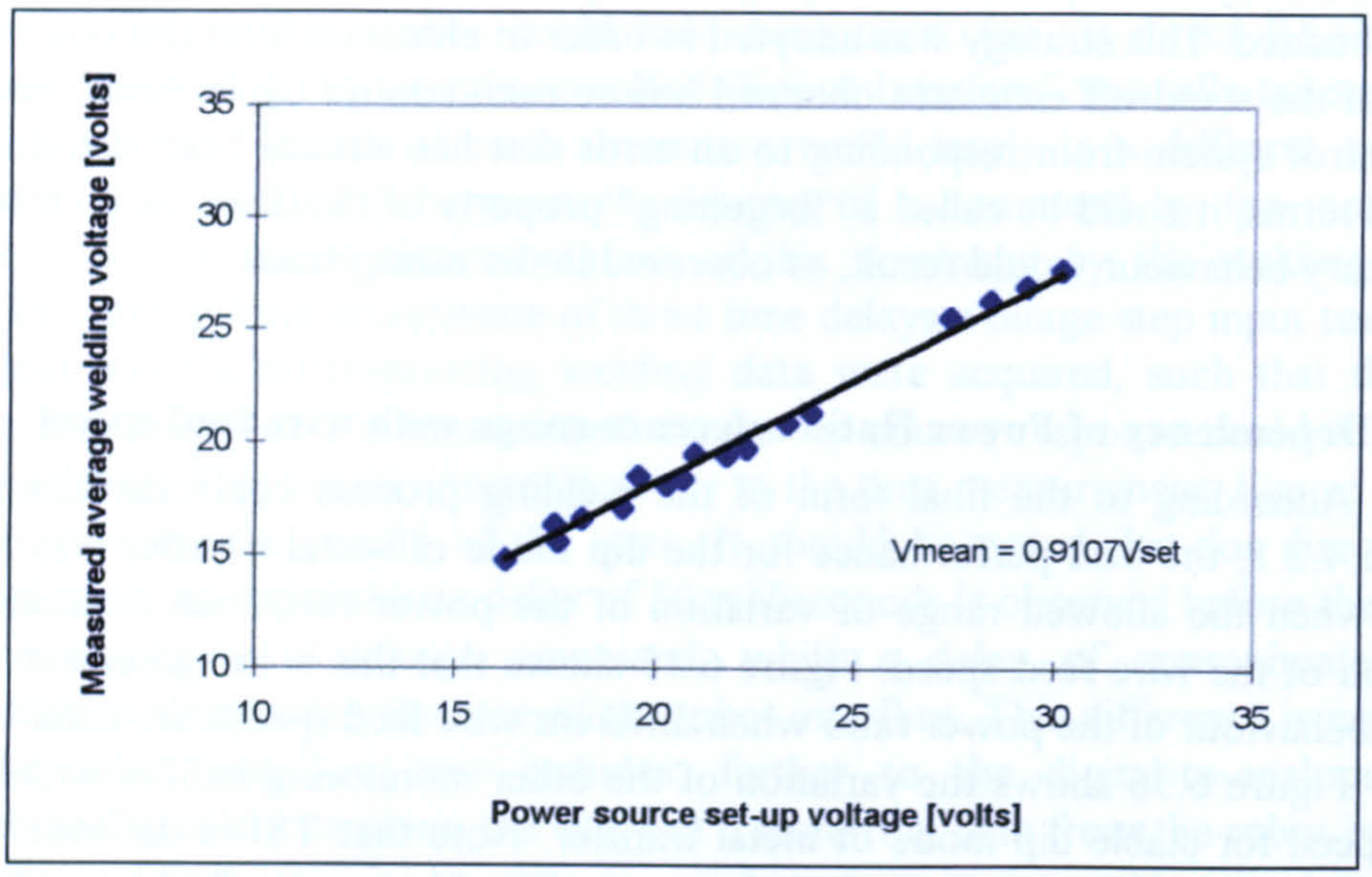

Figure 6.1 - Mean Voltage "versus" Set-up Voltage chart for the BDH 550 welding power source

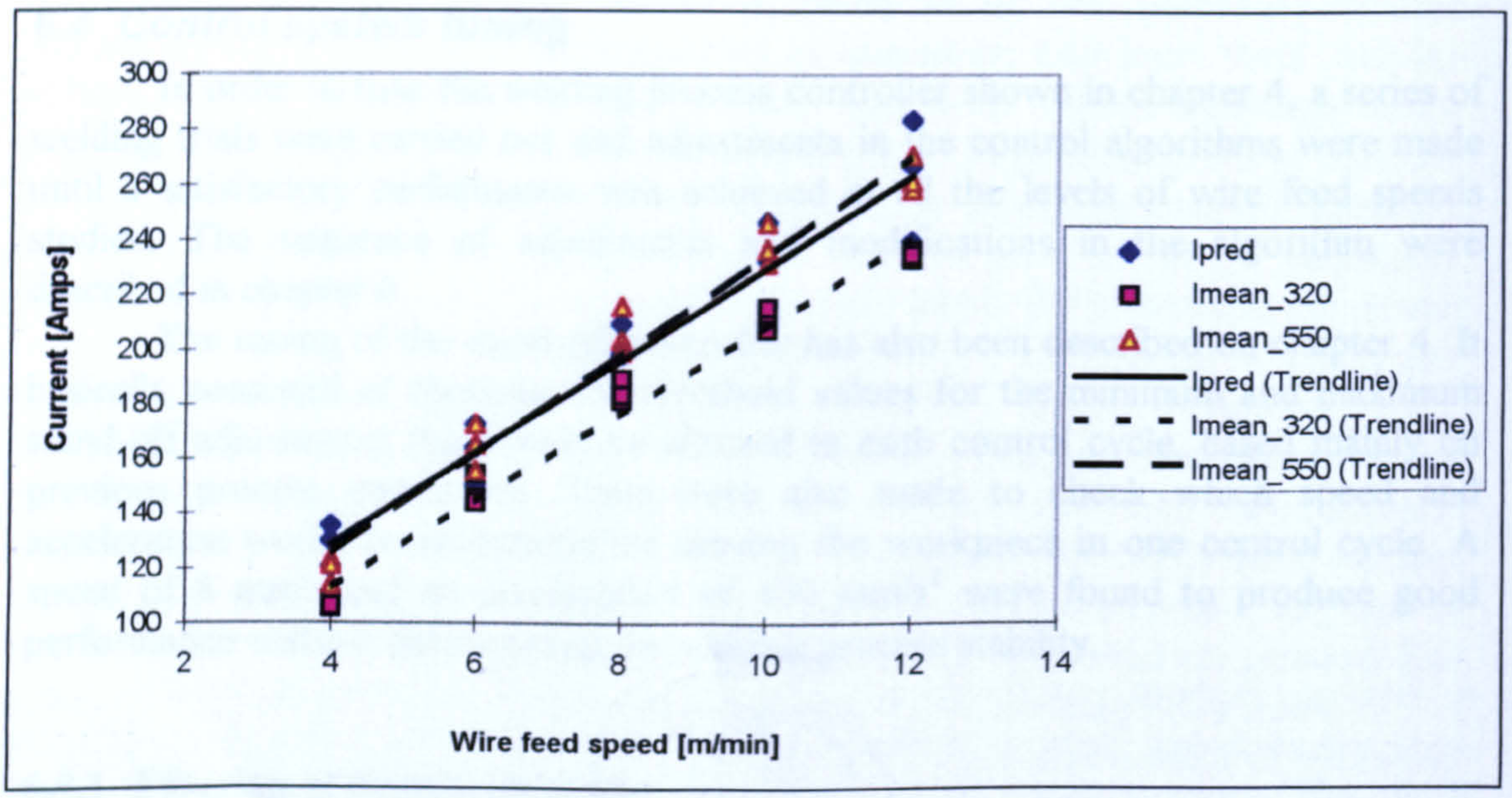

Figure 6.2 - Comparison between predicted welding current and actual welding current delivered by BDH320 and BDH550 welding power sources

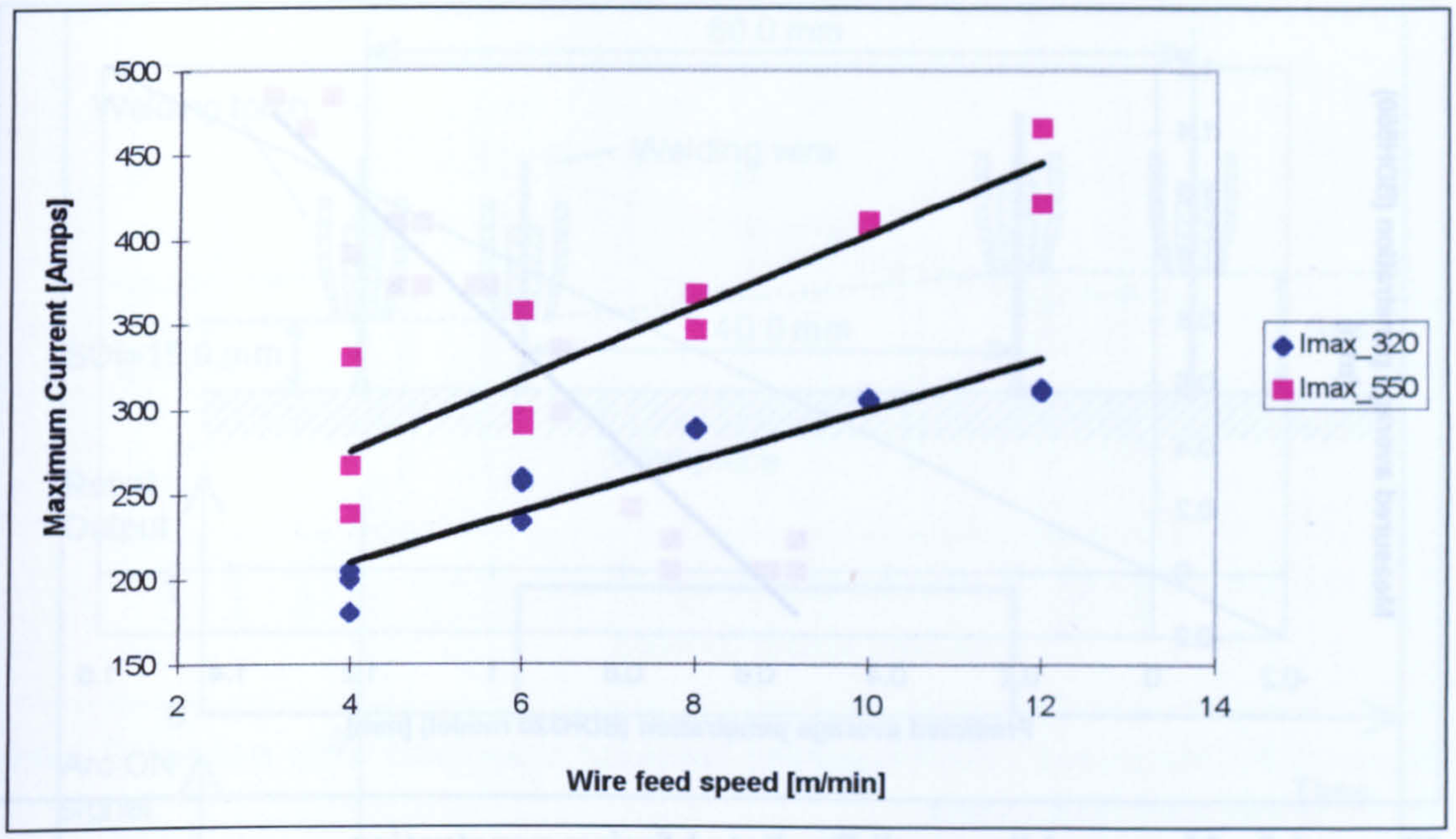

Figure 6.3 - Comparison between maximum welding currents in dip mode of metal transfer delivered by BDH320 and BDH550 welding power sources

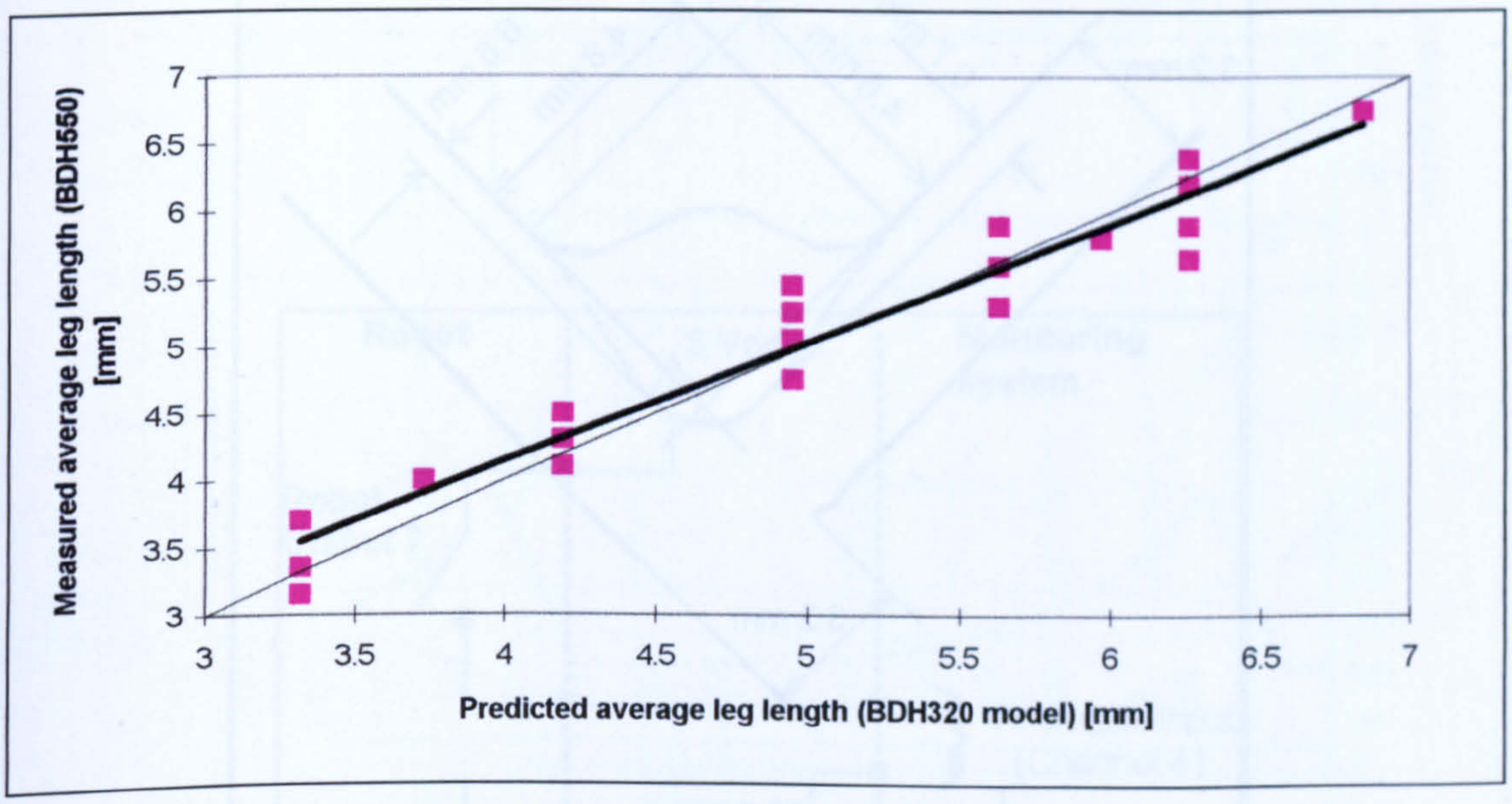

Figure 6.4 - Measured "versus" Predicted leg length

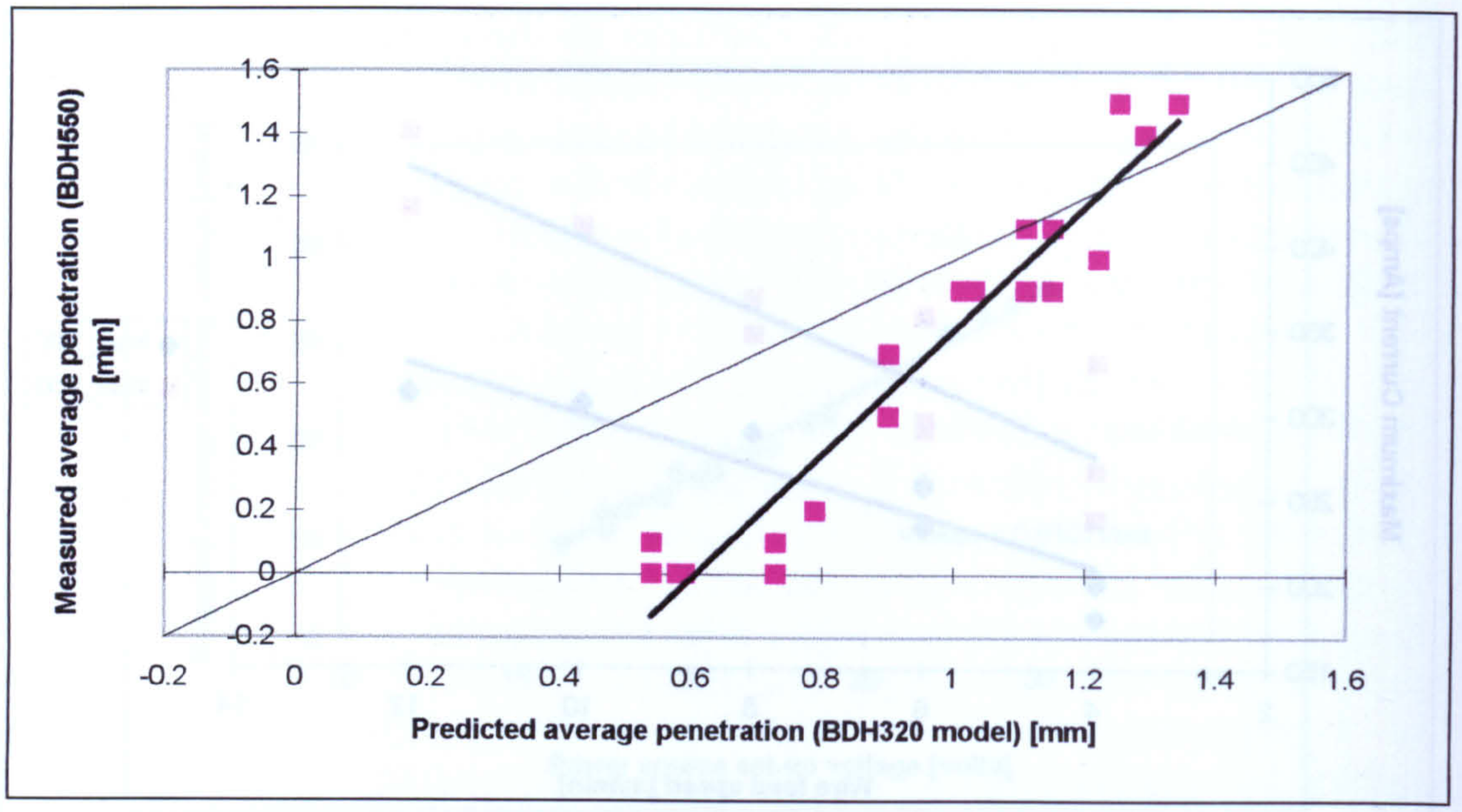

Figure 6.5 - Measured "versus" Predicted fusion penetration

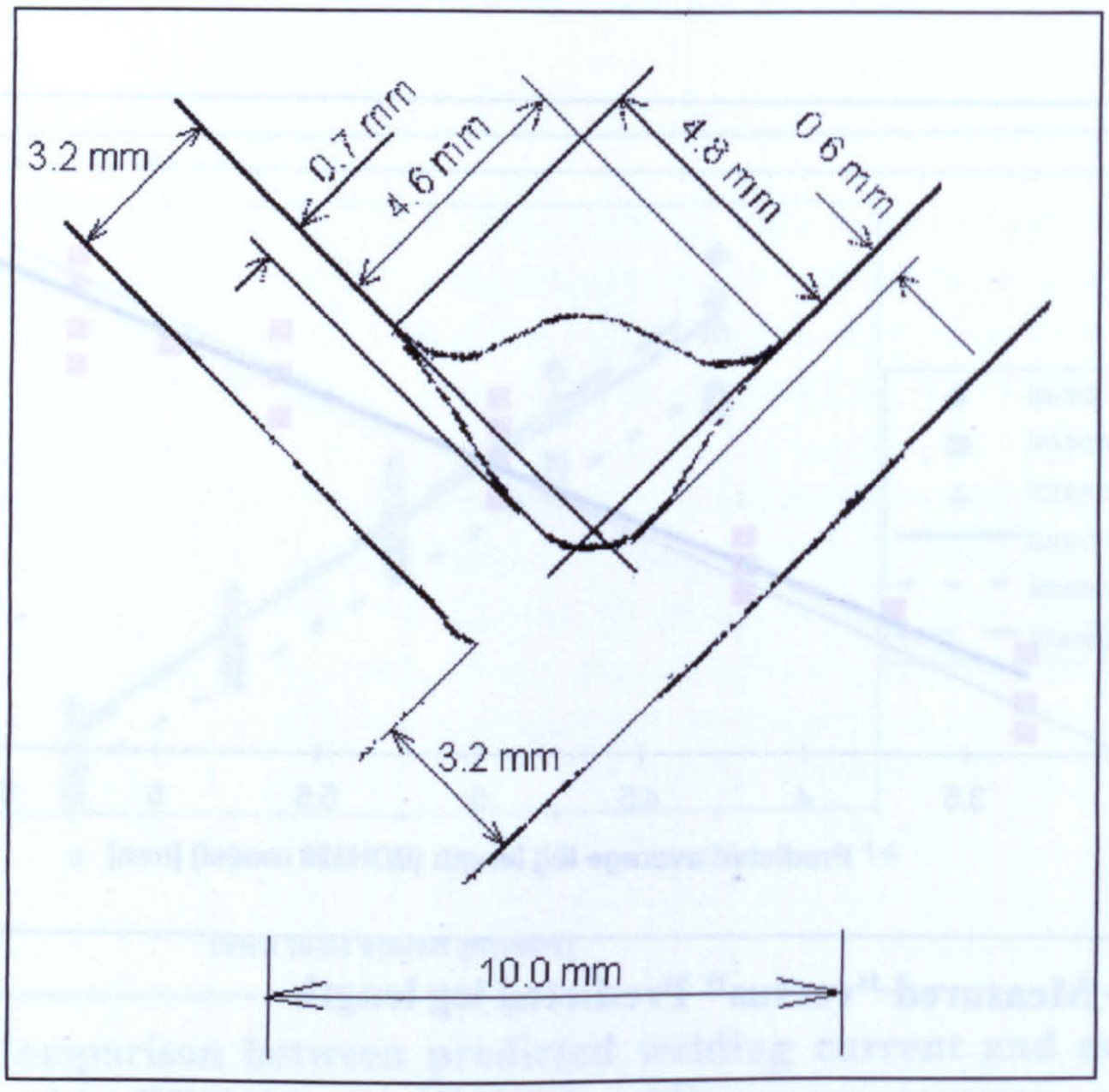

Figure 6.6 - Validation of the calibrated welding models

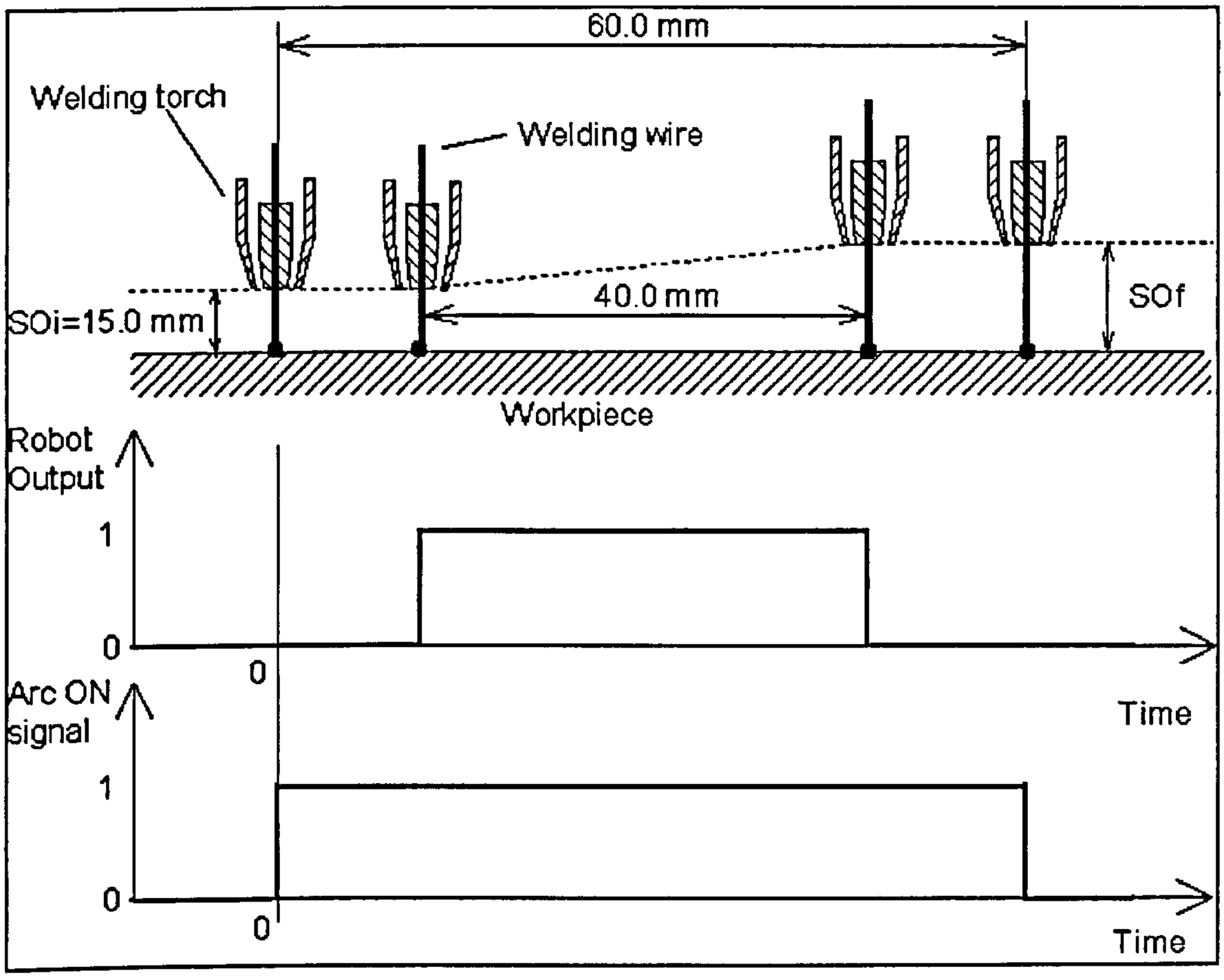

Figure 6.7 - Scheme used to test Ogunbiyi's stand-off estimation method

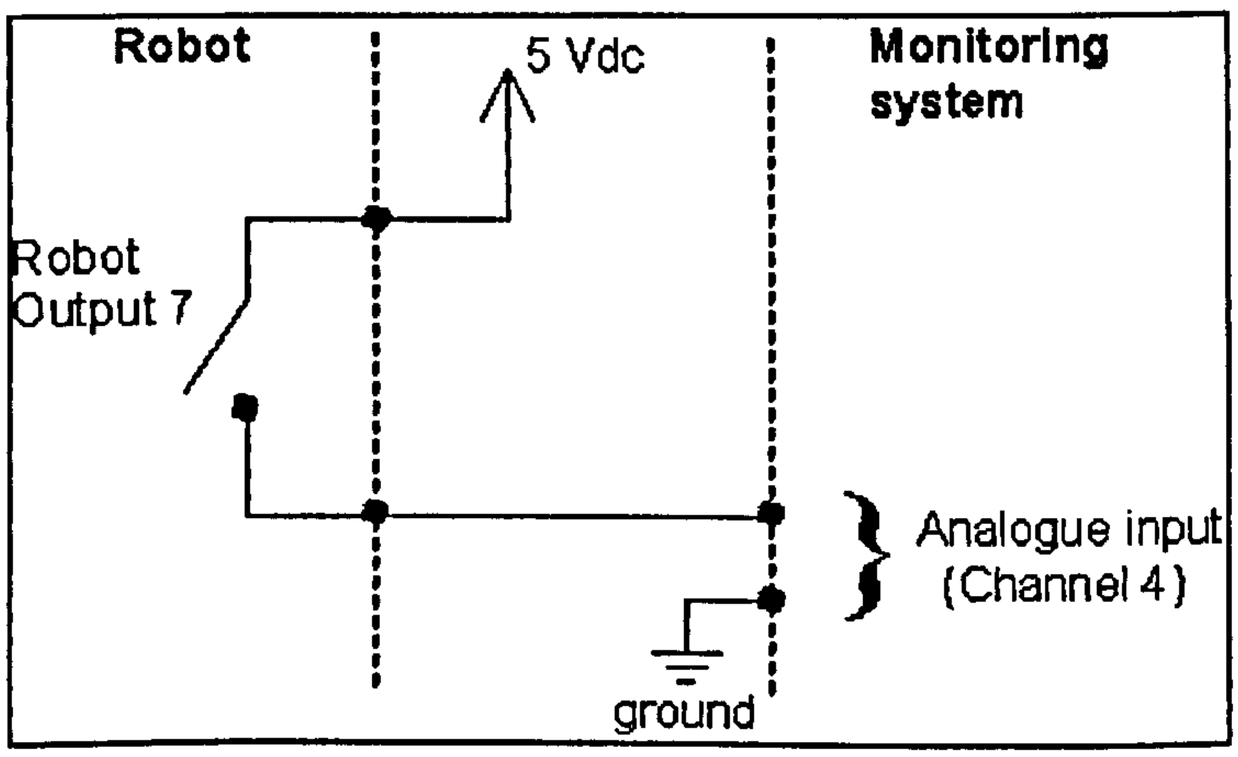

Figure 6.8 - Robot output connection to allow the monitoring system to pinpoint the start and end of the torch slope path

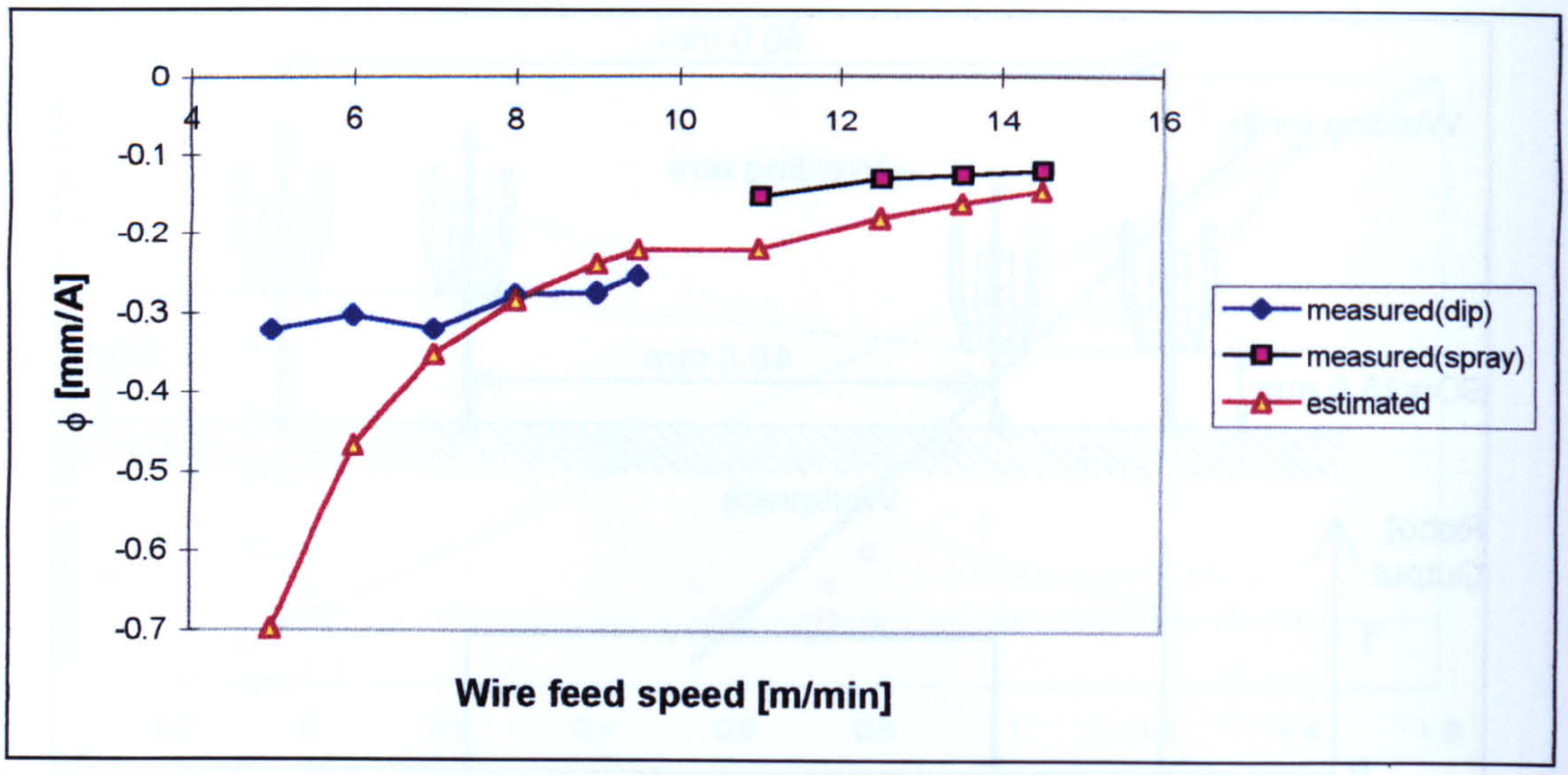

Figure 6.9 - Measured proportionality constant compared with estimated value for different wire feed speeds

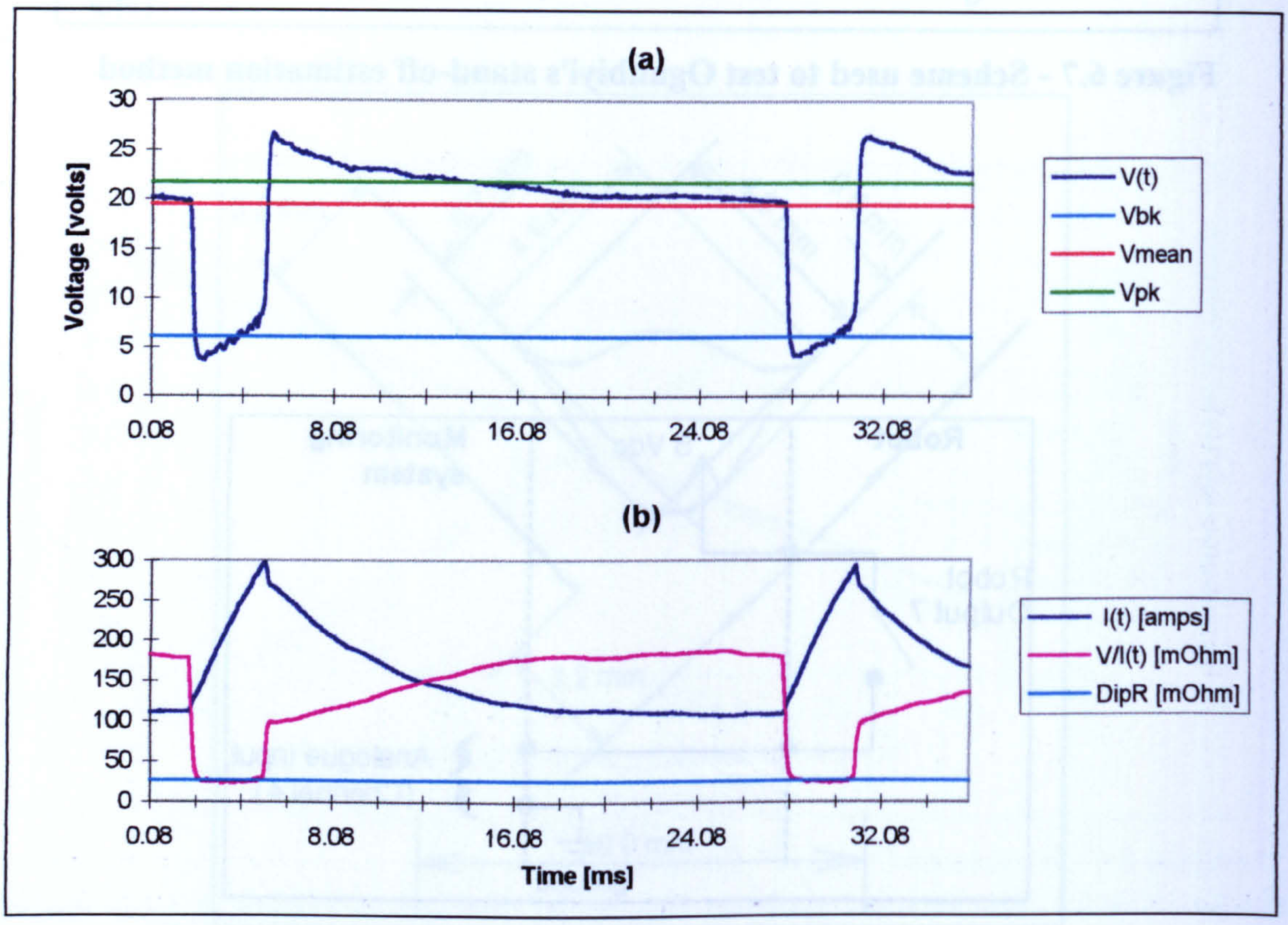

Figure 6.10 - Variation of voltage, current and contact tip-to-workpiece resistance for two successive short circuits: (a)voltage, (b)current and resistance.

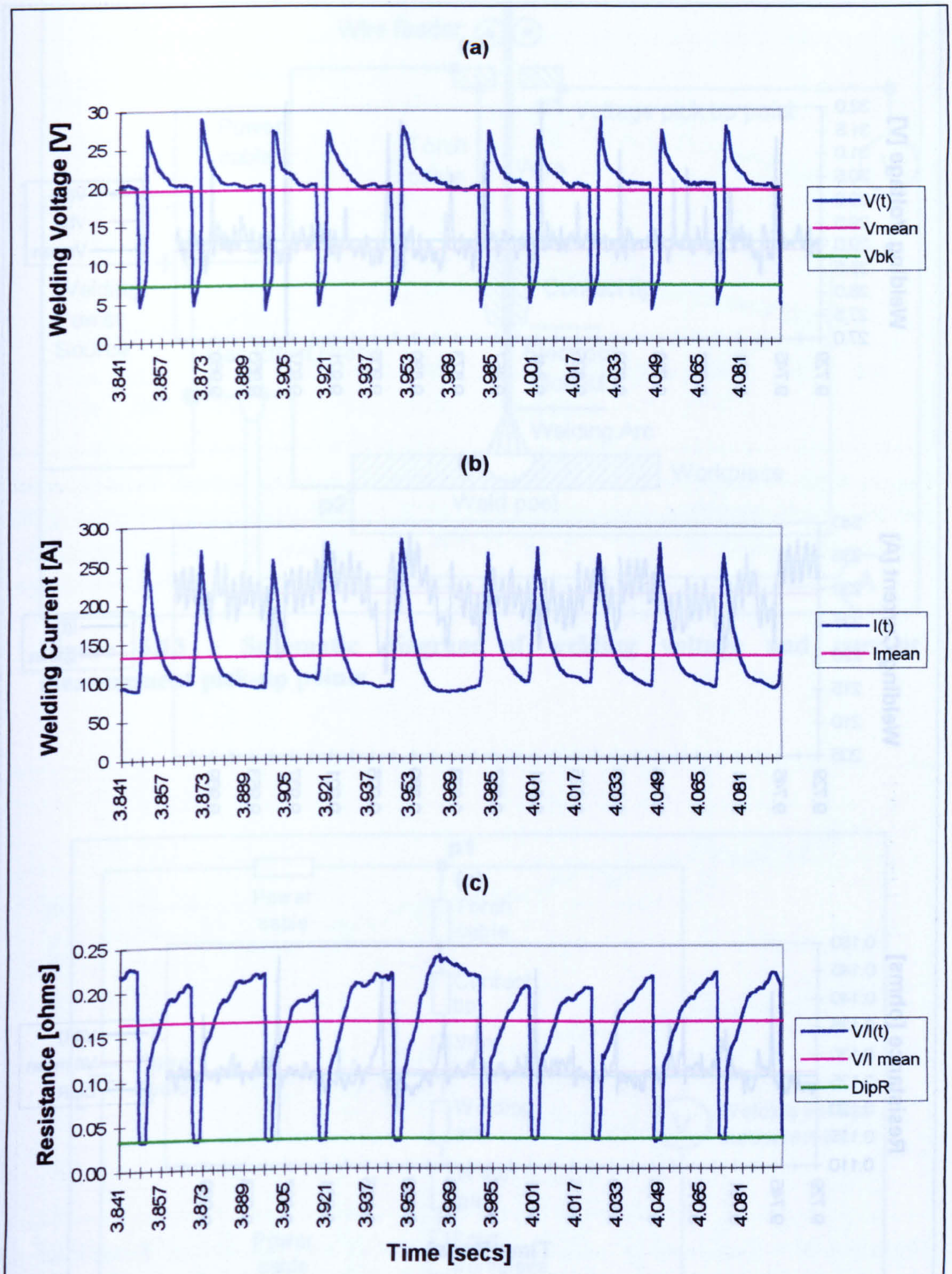

Figure 6.11 - Characteristic waveforms for dip mode of metal transfer as acquired in one window of data: (a) Voltage, (b) Current, (c) Resistance.

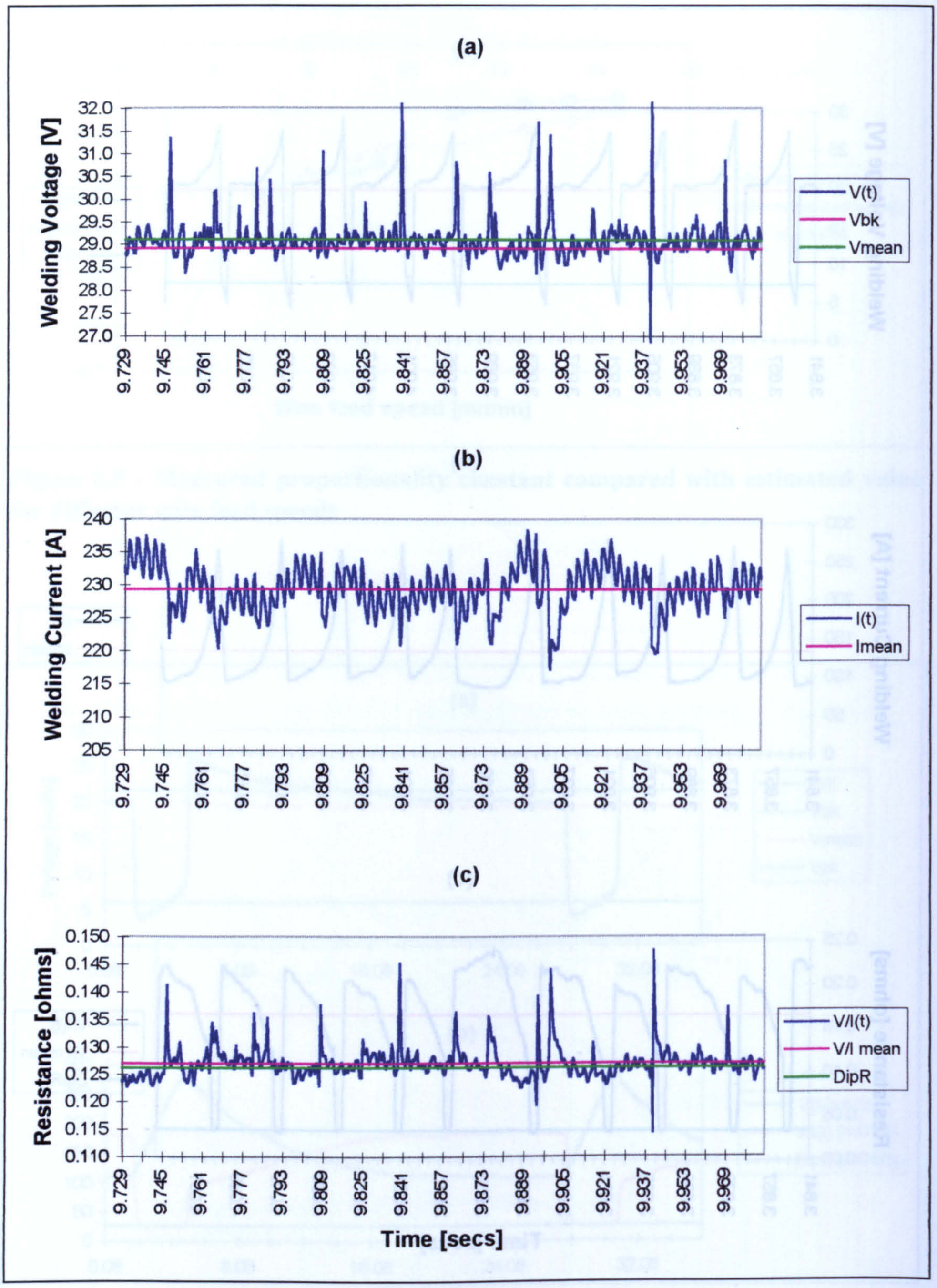

Figure 6.12 - Characteristic waveforms for spray mode of metal transfer as acquired in one window of data: (a) Voltage, (b) Current, (c) Resistance.

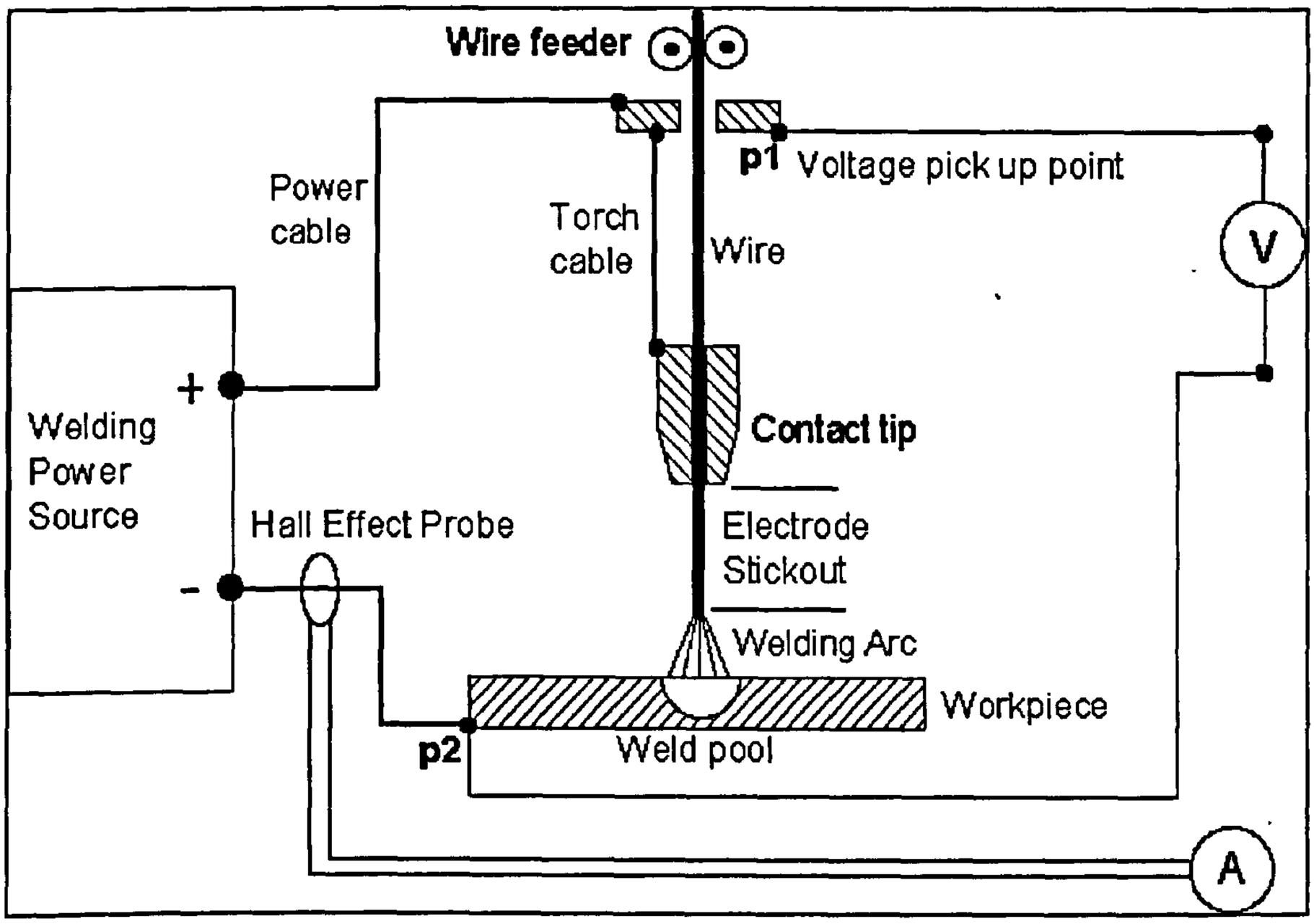

Figure 6.13 - Schematic diagram of welding voltage and current measurement pick-up points

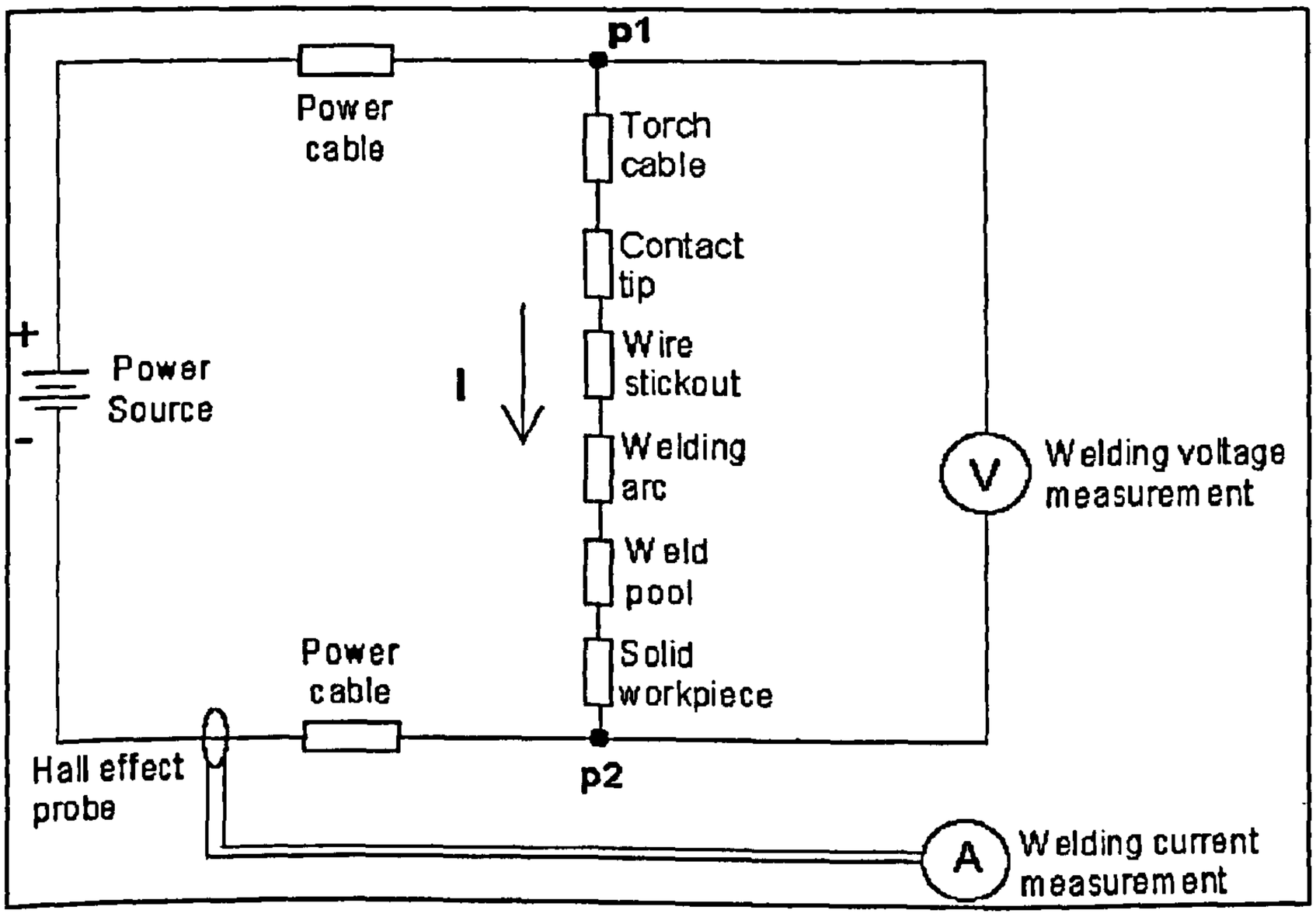

Figure 6.14 - Gas metal arc welding equivalent resistive circuit.

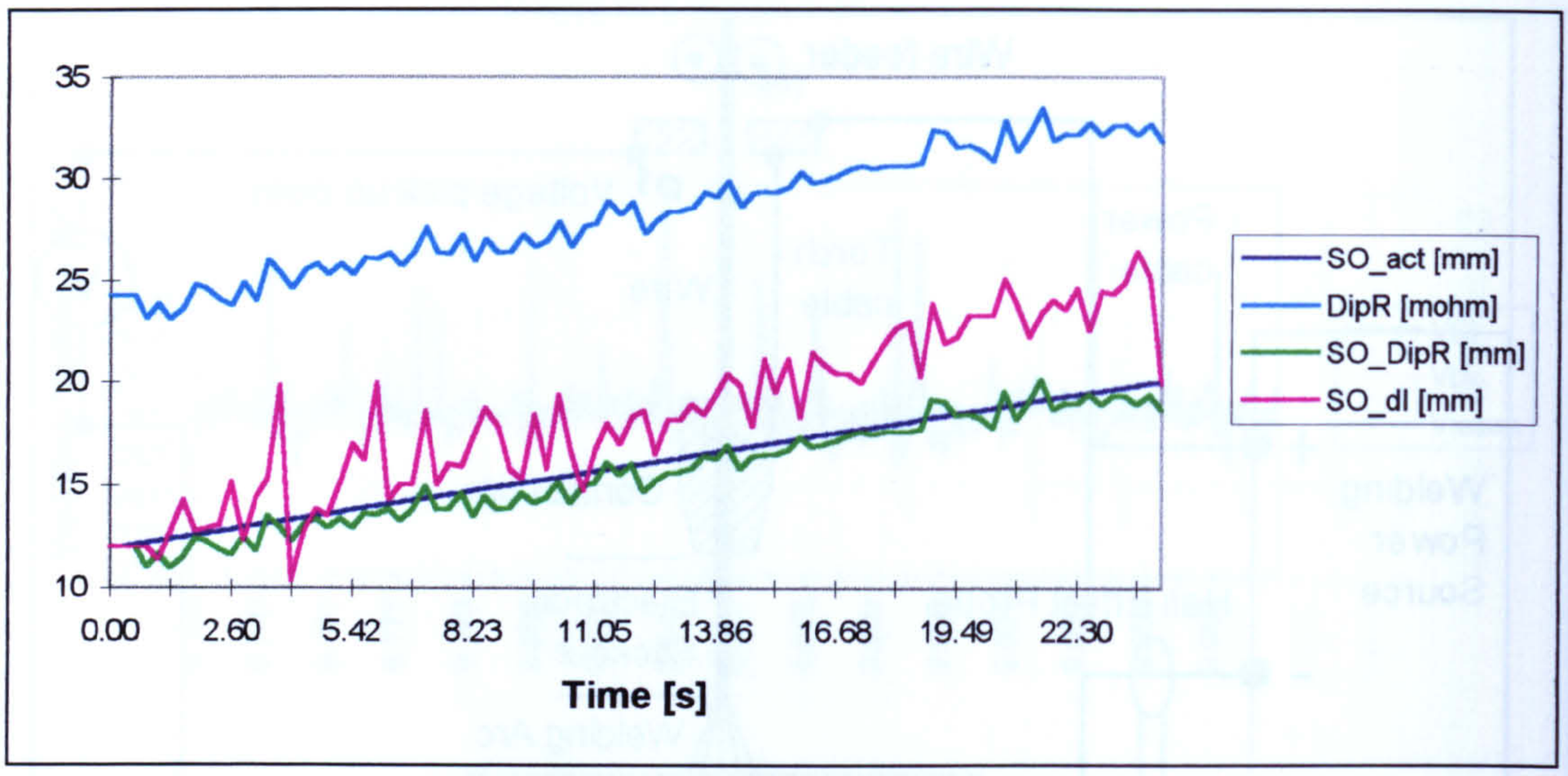

Figure 6.15 - Comparison between the predicted[7] and the actual[8] behaviour of the stand-off. (WFS=4.5 m/min, V_{set} =18.3V, S_W =0.5 m/min, 4kHz at 1024 samples/window)

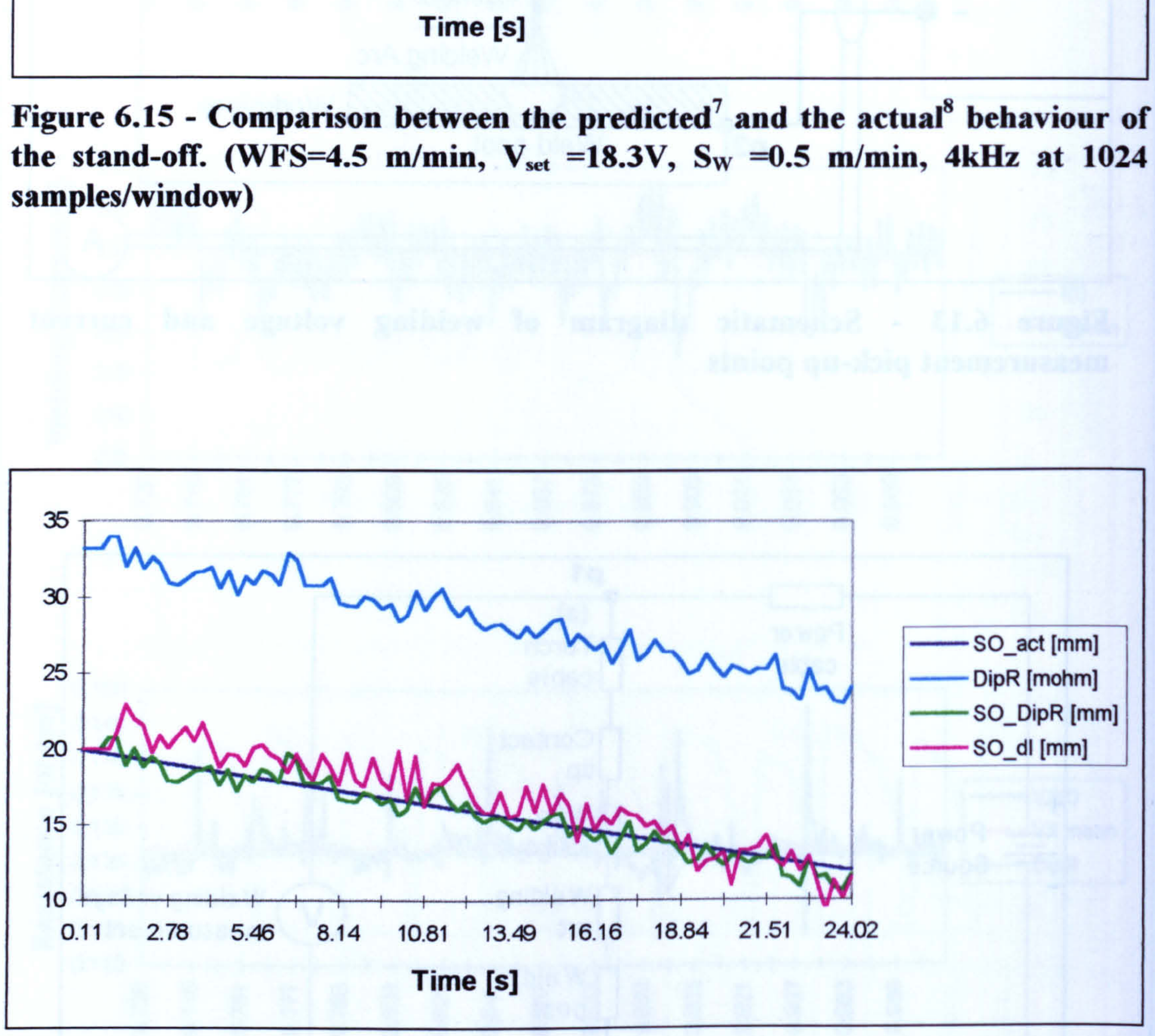

Figure 6.16 - Comparison between the predicted and the actual behaviour of the stand-off. (WFS=5.5 m/min, V_{set} =20.7V, S_W =0.5 m/min, 2kHz at 512 samples/window)

---

[7] SO_DipR = estimation from dip resistance based model;
SO_dI = estimation from Ogunbiyi's model.

[8] SO_act = actual stand-off value.

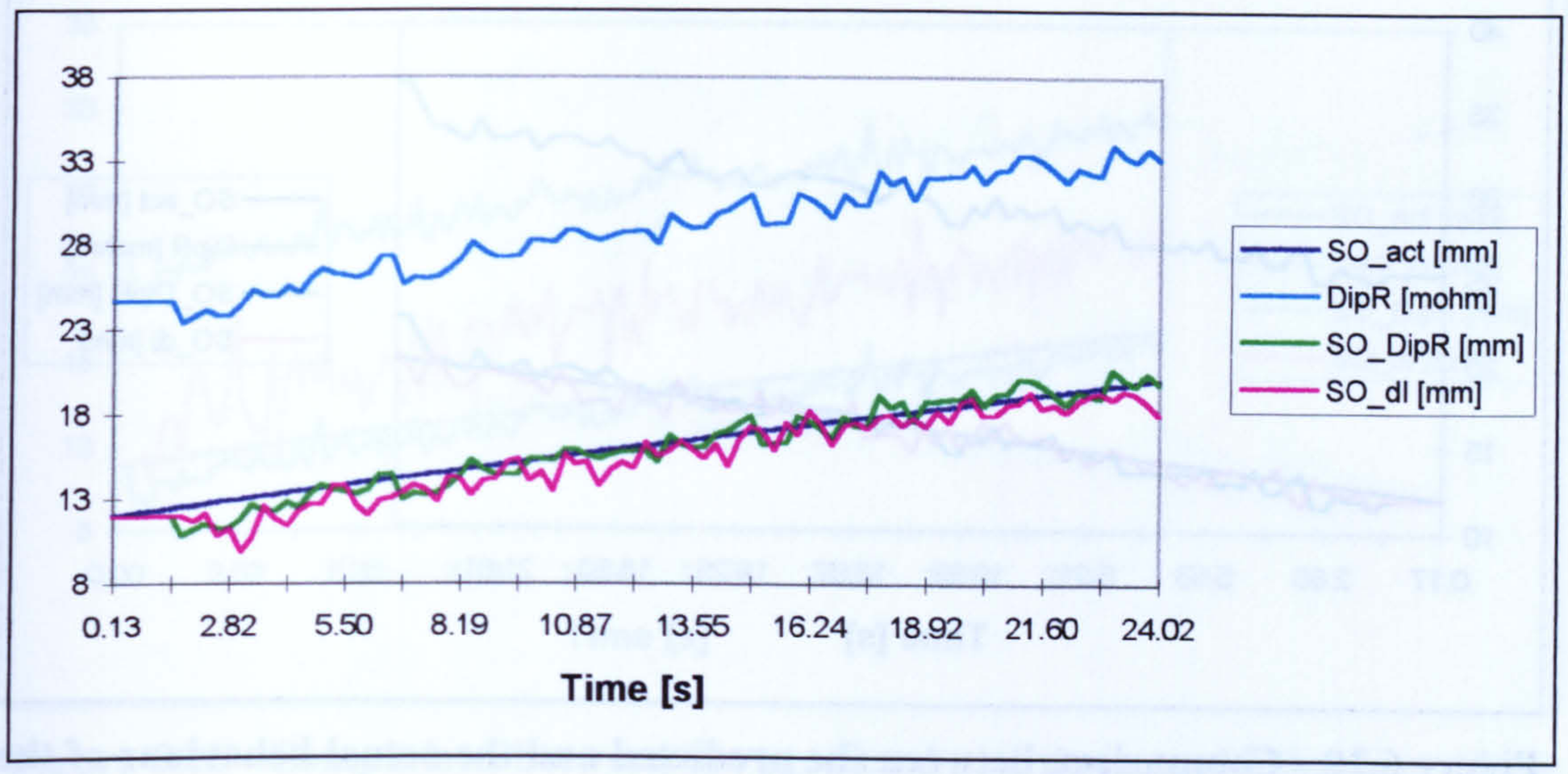

Figure 6.17 - Comparison between the predicted and the actual behaviour of the stand-off. (WFS=6.5 m/min, V_{set} =21.0 V, S_W =0.5 m/min, 2kHz at 512 samples/window)

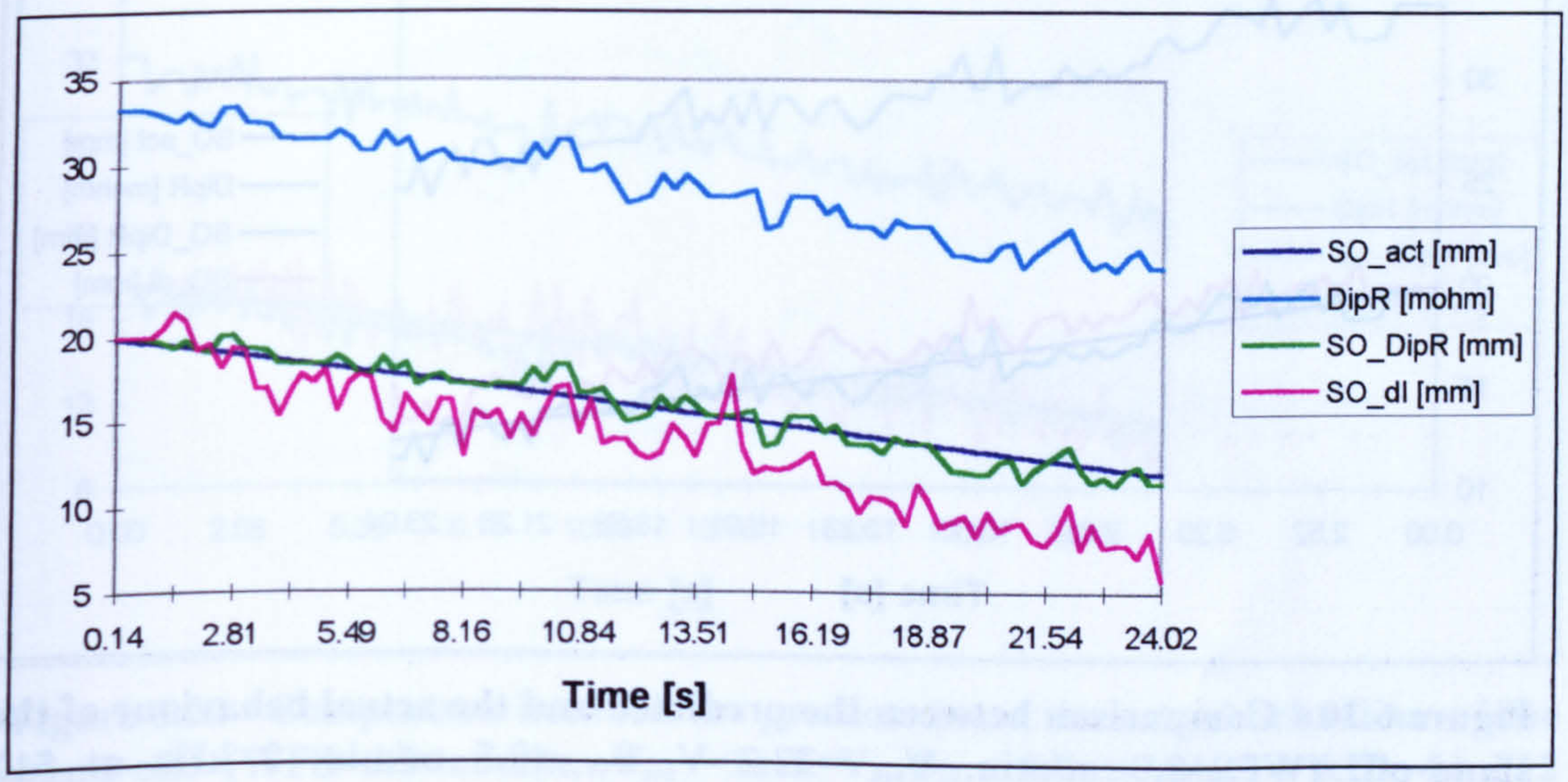

Figure 6.18 - Comparison between the predicted and the actual behaviour of the stand-off. (WFS=6.5 m/min, V_{set} =21.6 V, S_W =0.5 m/min, 2kHz at 512 samples/window)

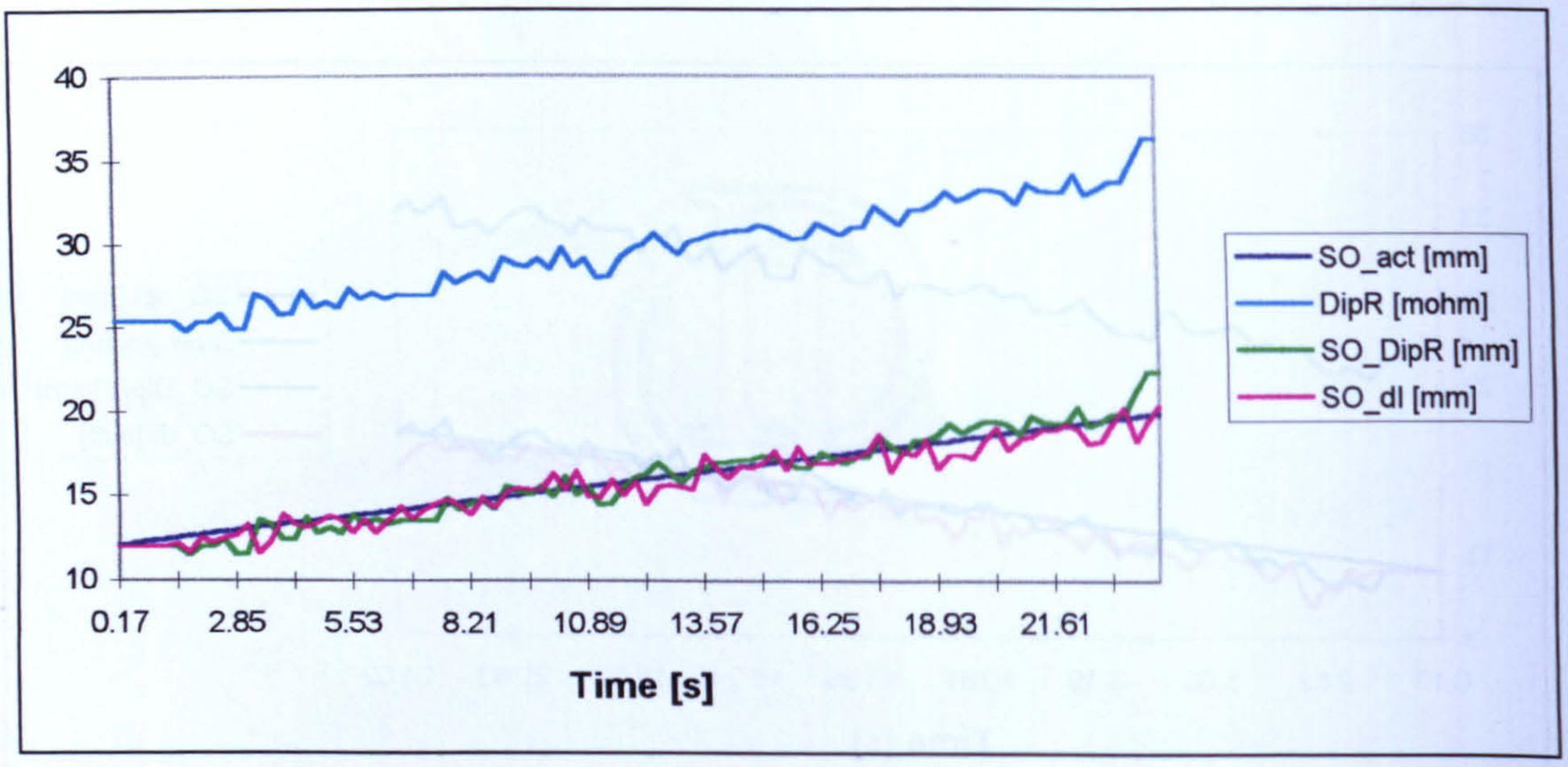

Figure 6.19 - Comparison between the predicted and the actual behaviour of the stand-off. (WFS=8.5 m/min, V_{set} =22.2 V, S_W =0.5 m/min, 2 kHz at 512 samples/window)

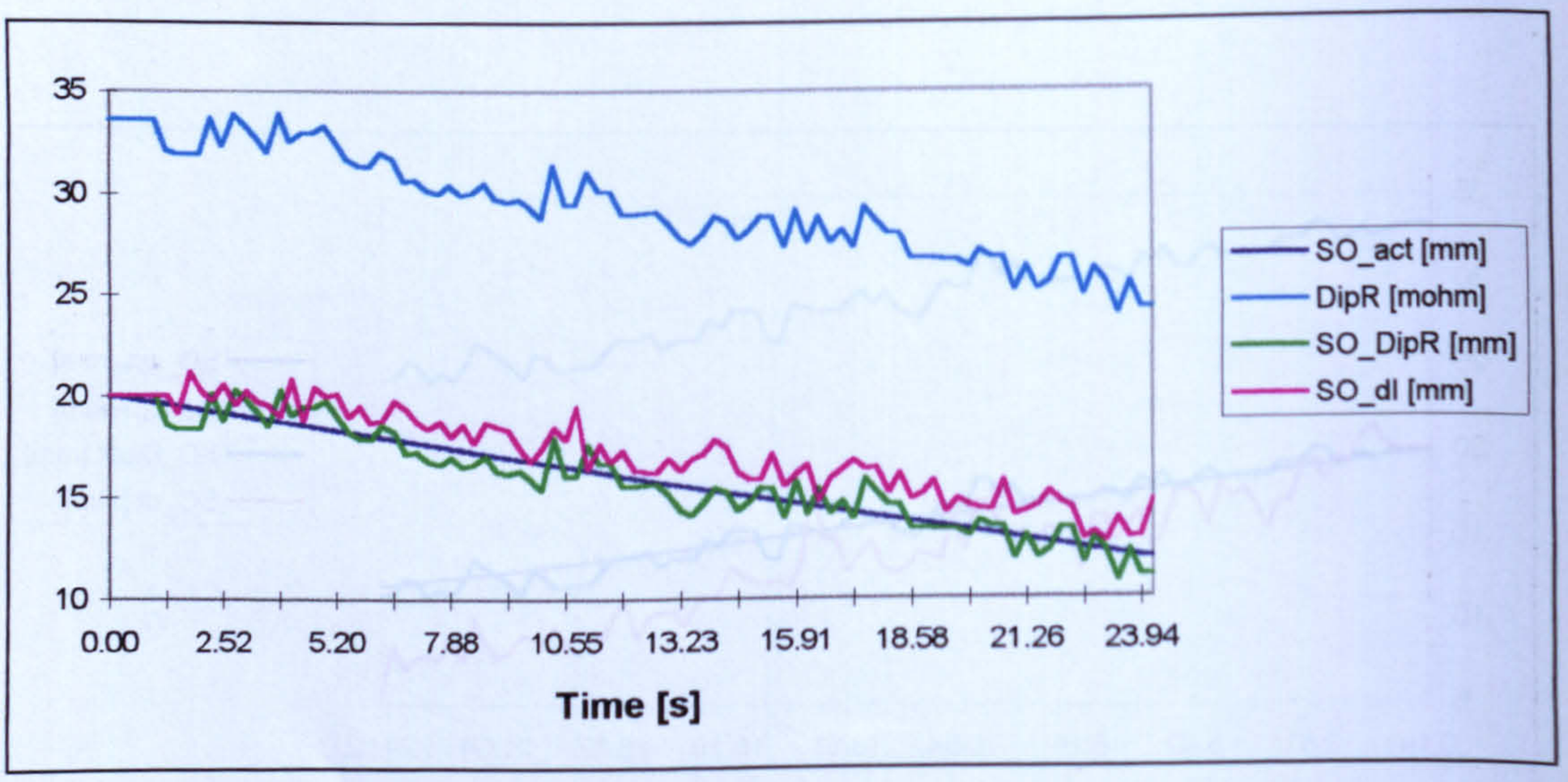

Figure 6.20 - Comparison between the predicted and the actual behaviour of the stand-off. (WFS=8.0 m/min, V_{set} =22.2 V, S_W =0.5 m/min, 2 kHz at 512 samples/window)

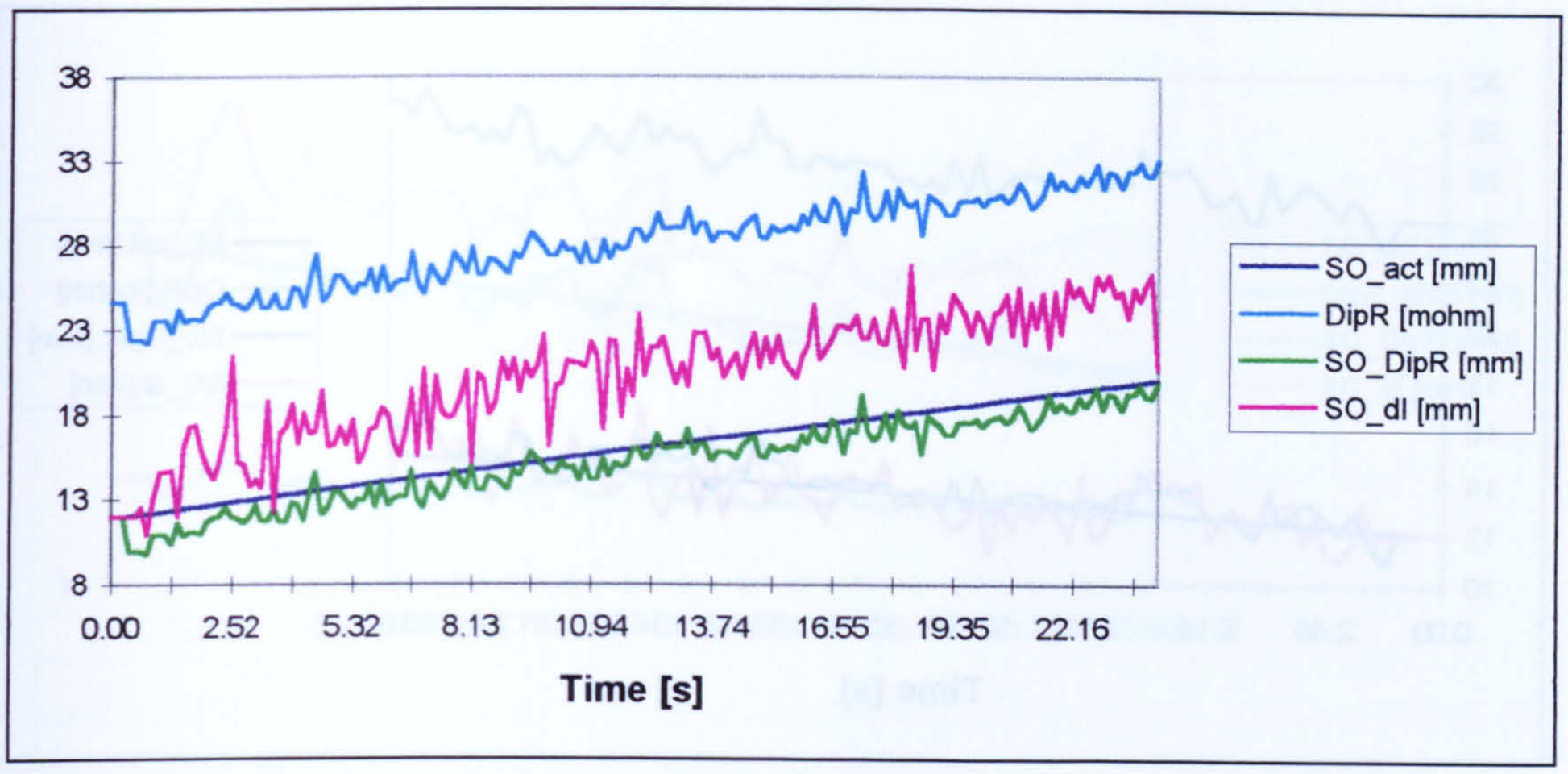

Figure 6.21 - Comparison between the predicted and the actual behaviour of the stand-off. (WFS=6.5 m/min, V_{set} =21.0 V, S_W =0.5 m/min, 4 kHz at 512 samples/window)

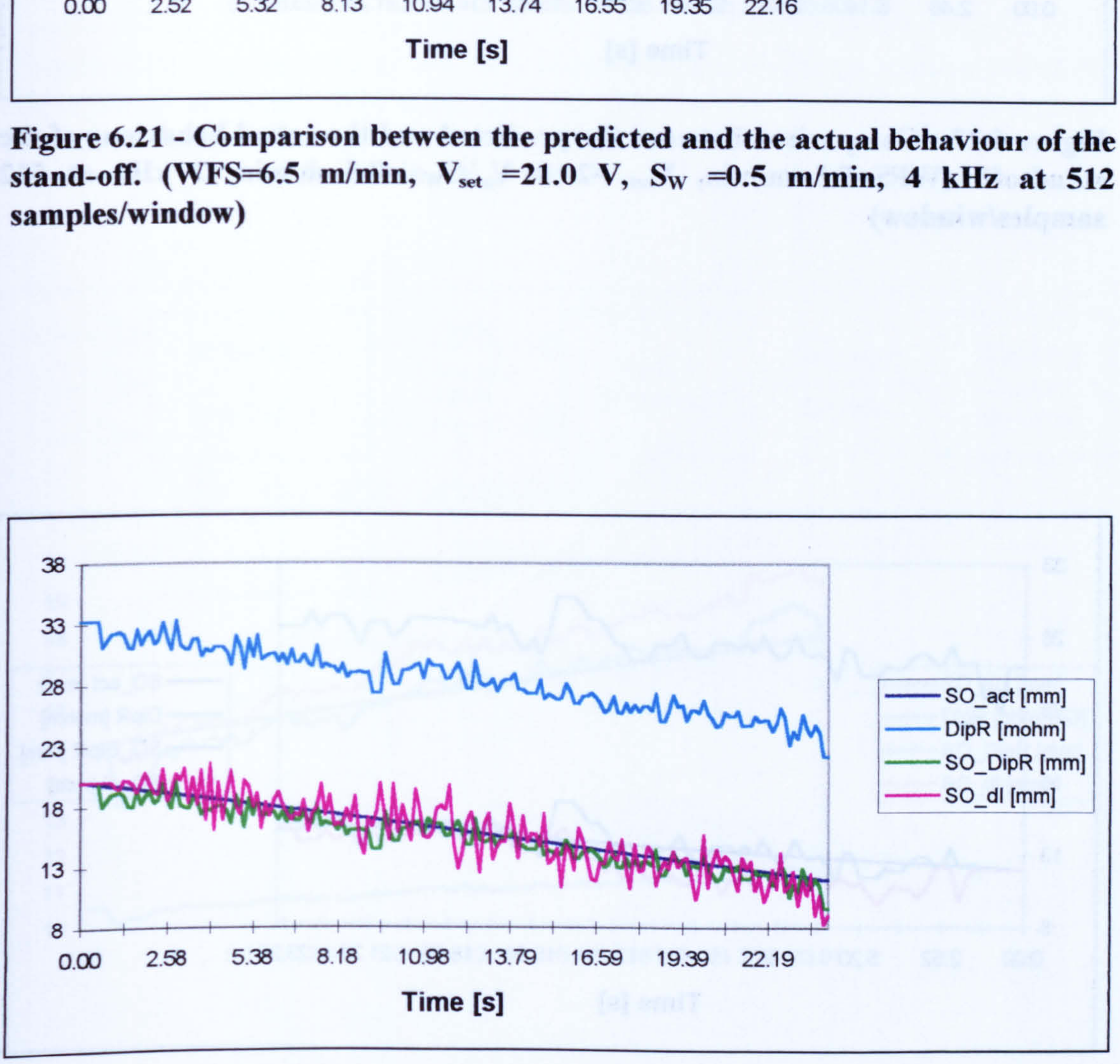

Figure 6.22 - Comparison between the predicted and the actual behaviour of the stand-off. (WFS=6.5 m/min, V_{set} =21.5 V, S_W =0.5 m/min, 4 kHz at 512 samples/window)

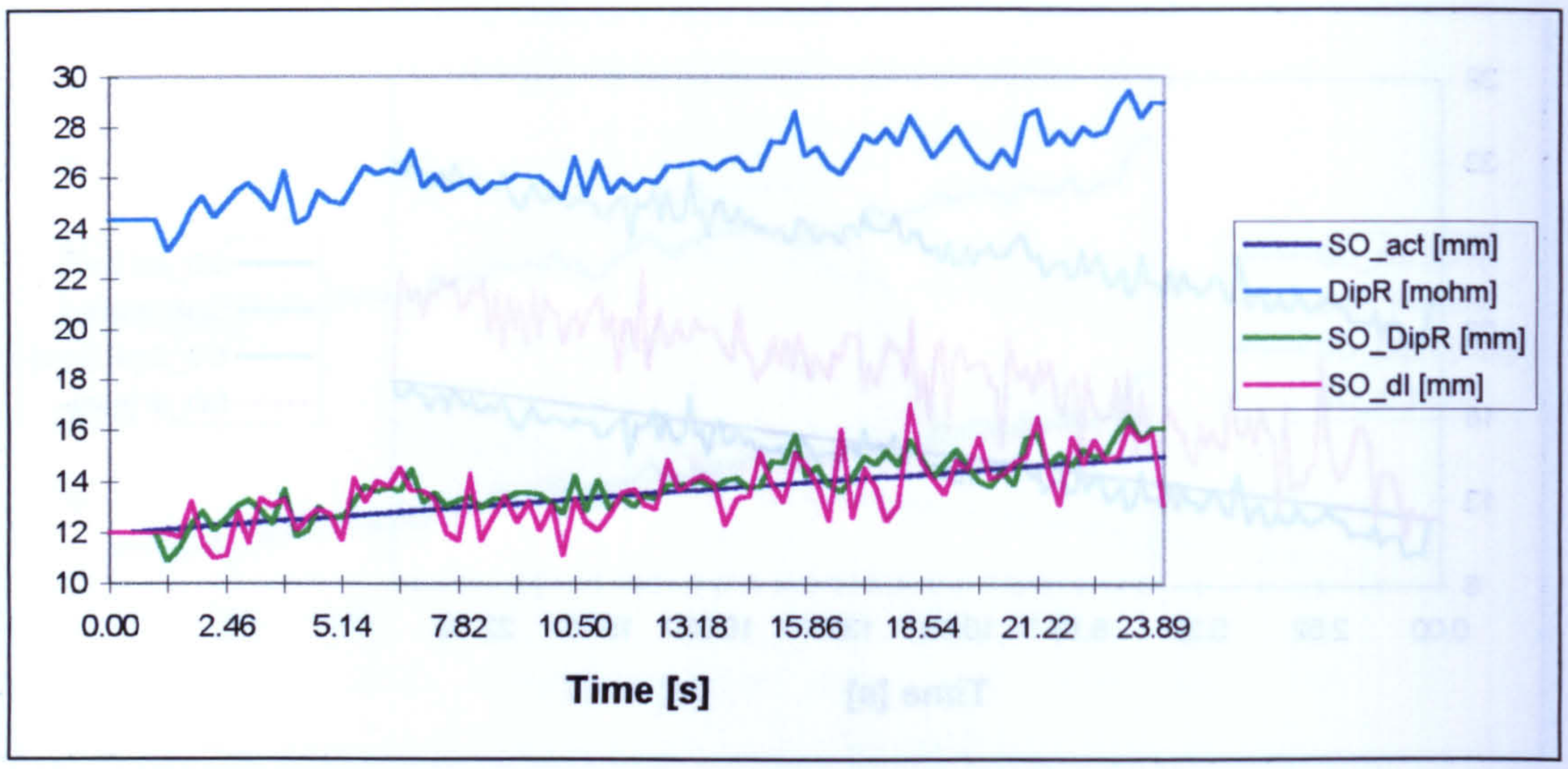

Figure 6.23 - Comparison between the predicted and the actual behaviour of the stand-off. (WFS=5.5 m/min, V_{set} =20.0 V, S_W =0.5 m/min, 2 kHz at 512 samples/window)

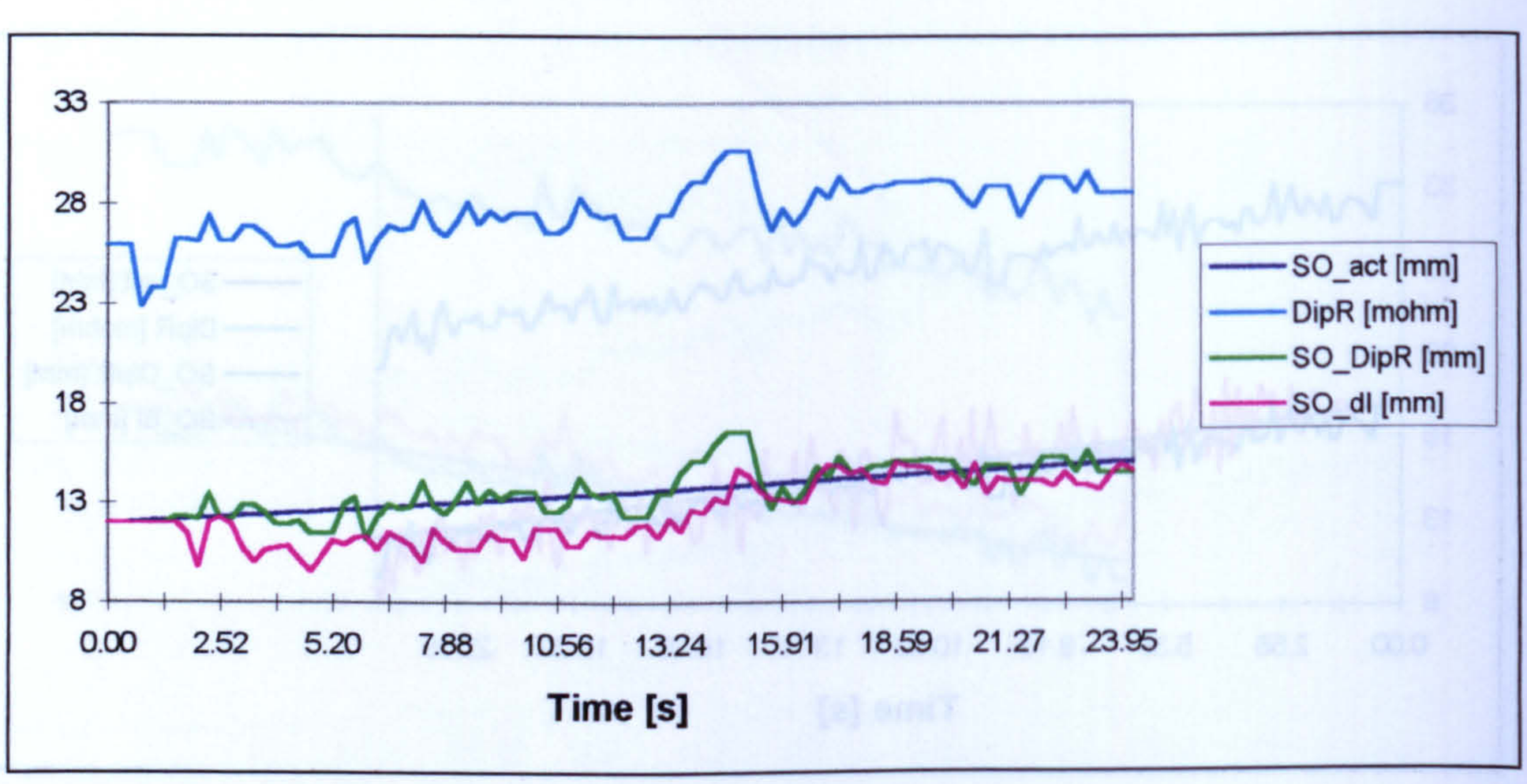

Figure 6.24 - Comparison between the predicted and the actual behaviour of the stand-off. (WFS=10.0 m/min, V_{set} =22.4 V, S_W =0.5 m/min, 2 kHz at 512 samples/window)

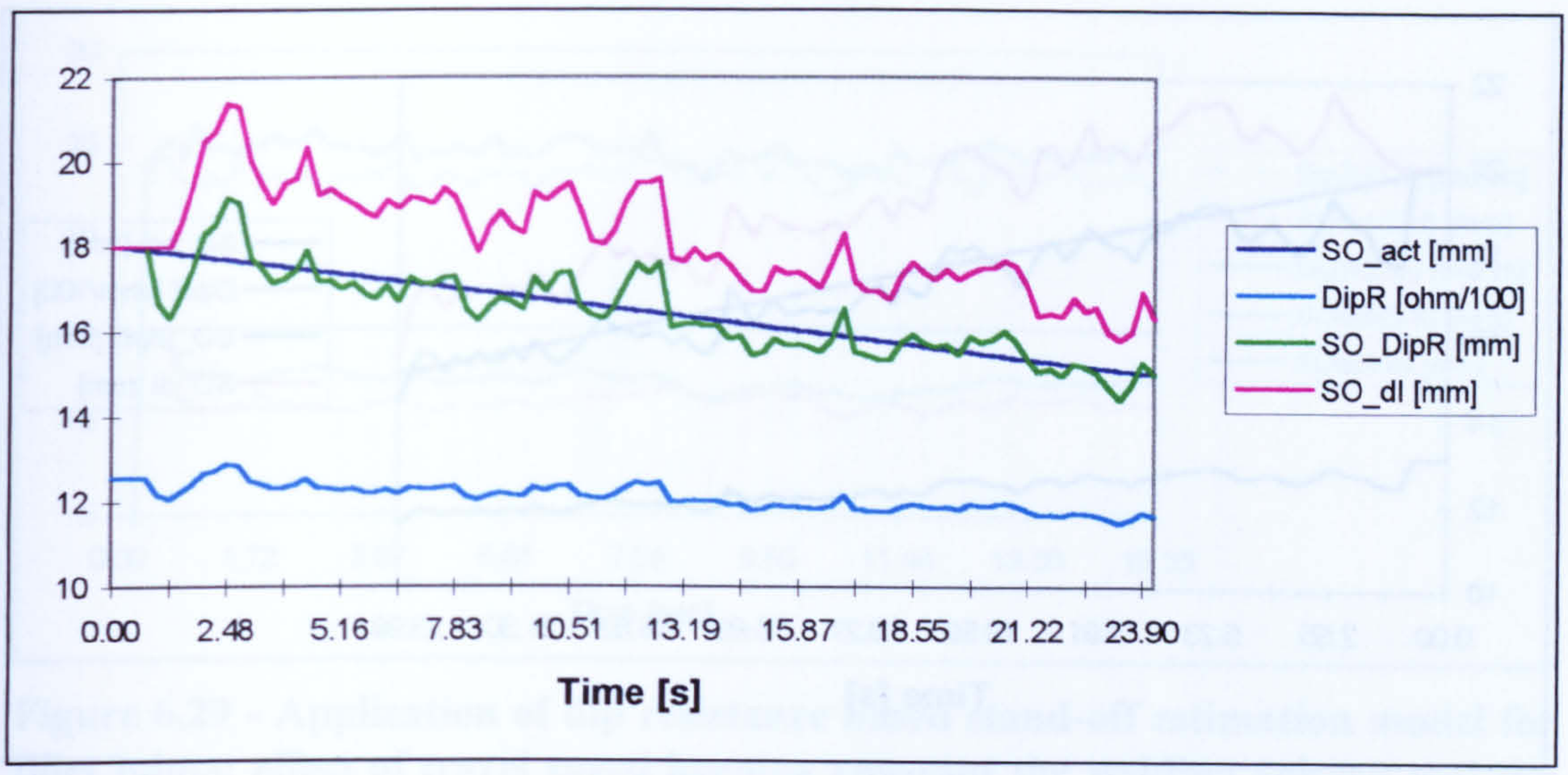

Figure 6.25 - Comparison between the predicted and the actual behaviour of the stand-off. (WFS=10.5 m/min, V_{set} =32.7V, S_W =0.5 m/min, 2 kHz at 512 samples/window)

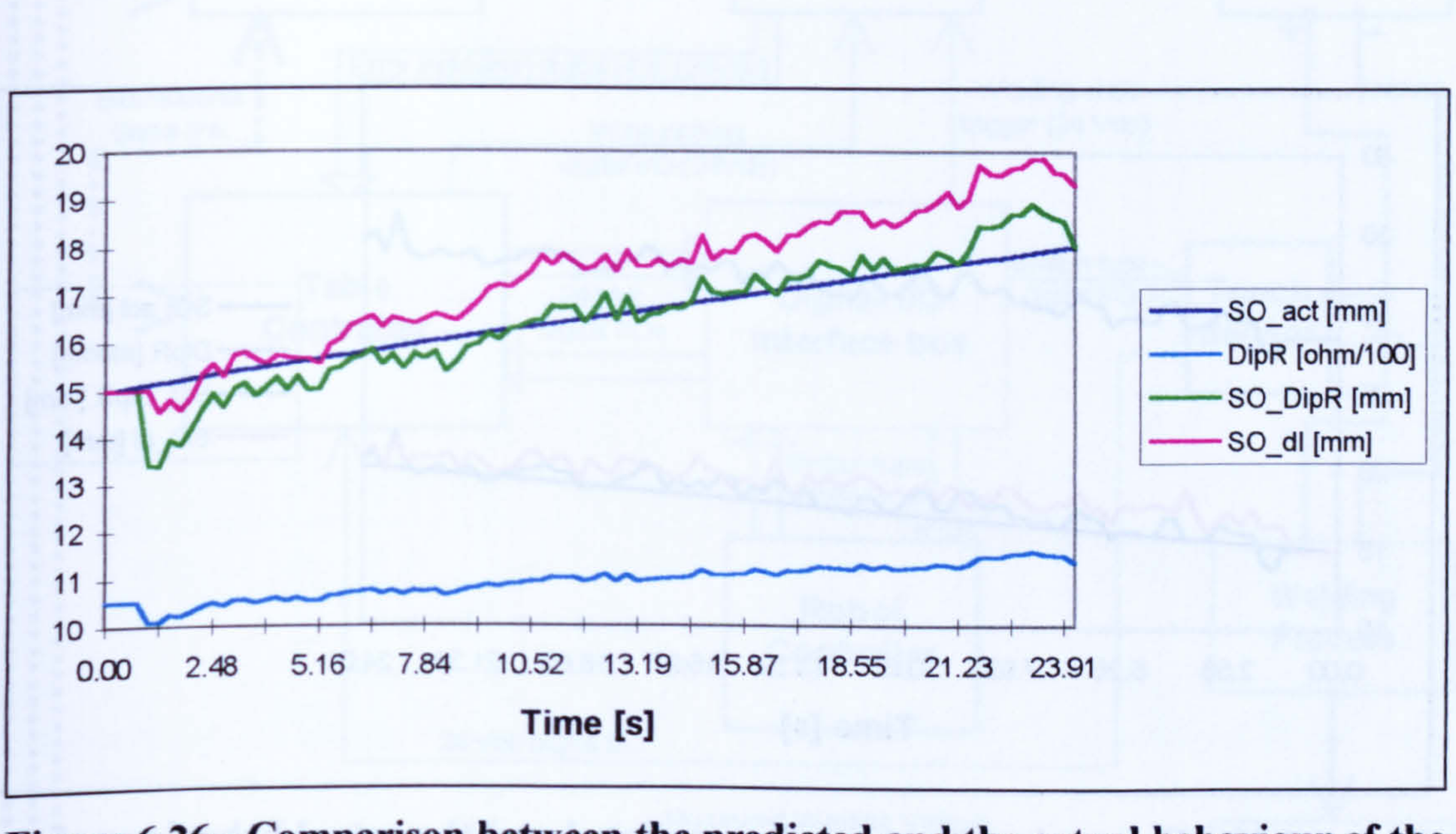

Figure 6.26 - Comparison between the predicted and the actual behaviour of the stand-off. (WFS=12.5 m/min, V_{set} =33.1V, S_W =0.5 m/min, 2 kHz at 512 samples/window)

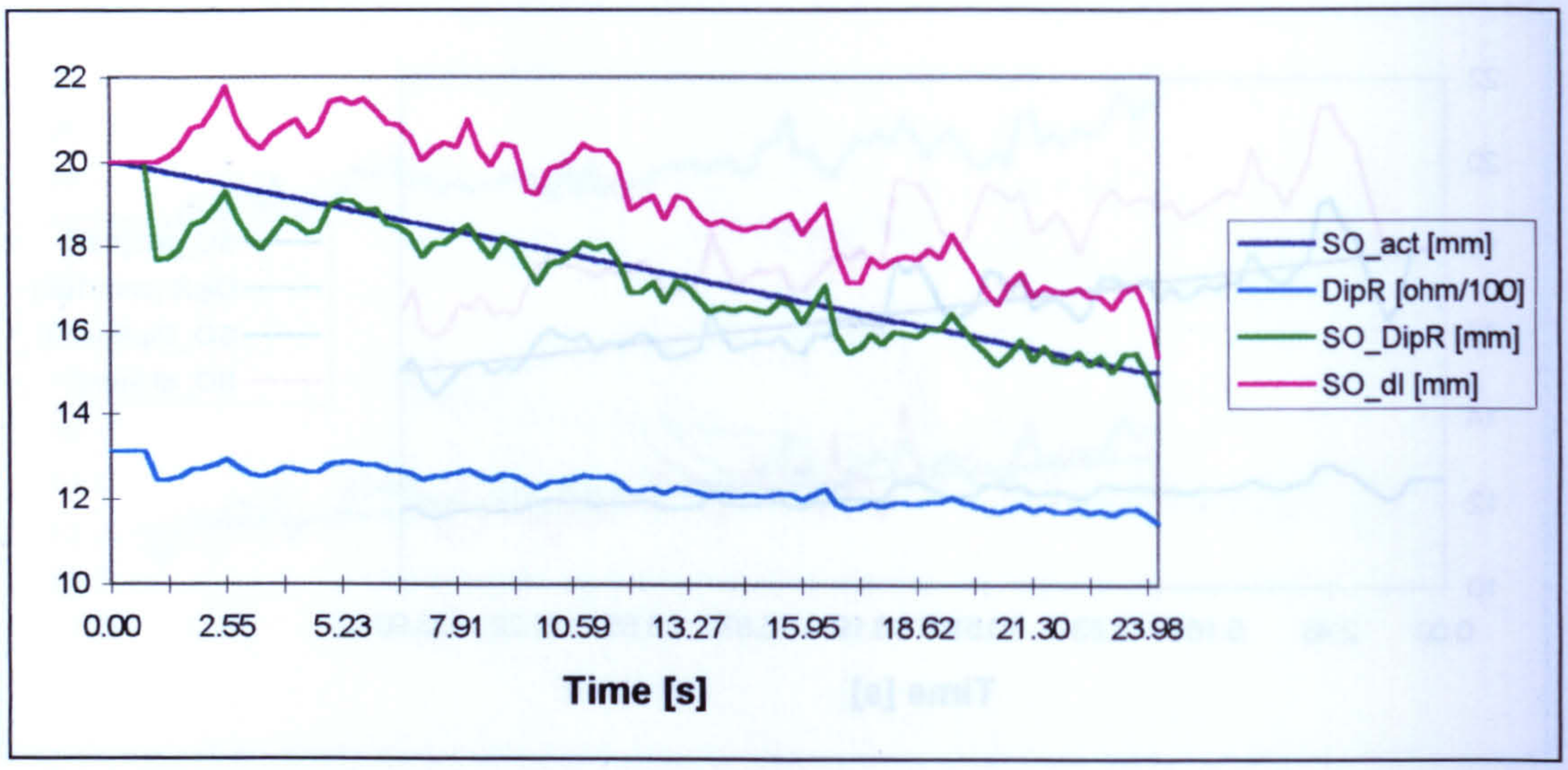

Figure 6.27 - Comparison between the predicted and the actual behaviour of the stand-off. (WFS=10.5 m/min, V_{set} =32.6V, S_W =0.5 m/min, 2 kHz at 512 samples/window)

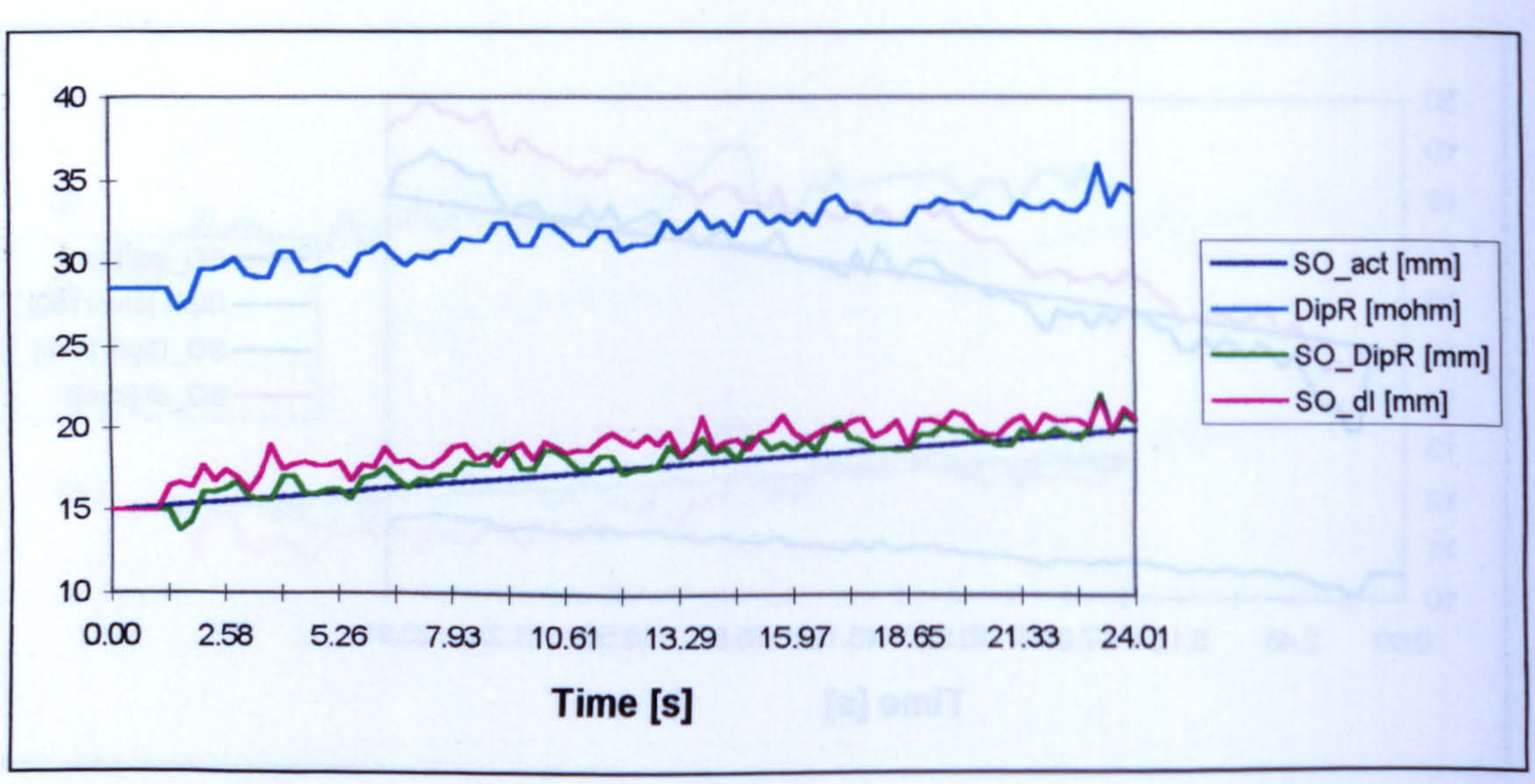

Figure 6.28 - Comparison between the predicted and the actual behaviour of the stand-off. (WFS=8.5 m/min, V_{set} = 22.2V, S_W = 0.5 m/min, 2 kHz at 512 samples/window)

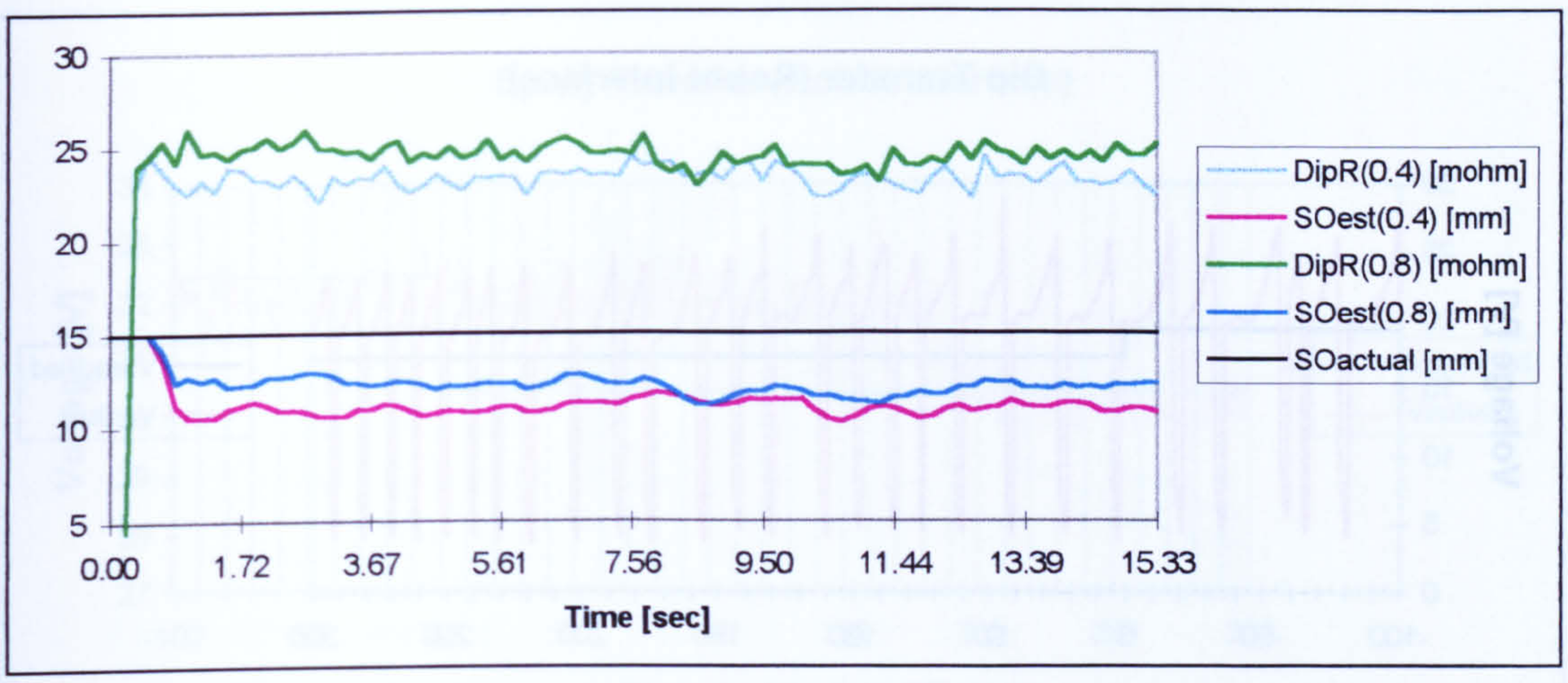

Figure 6.29 - Application of dip resistance based stand-off estimation model for fillet joints: effect of travel speed keeping constant the welding voltage and the wire feed speed (WFS=5.5 m/min, V_{set}=20.3V, Travel speeds: 0.4 and 0.8 m/min)

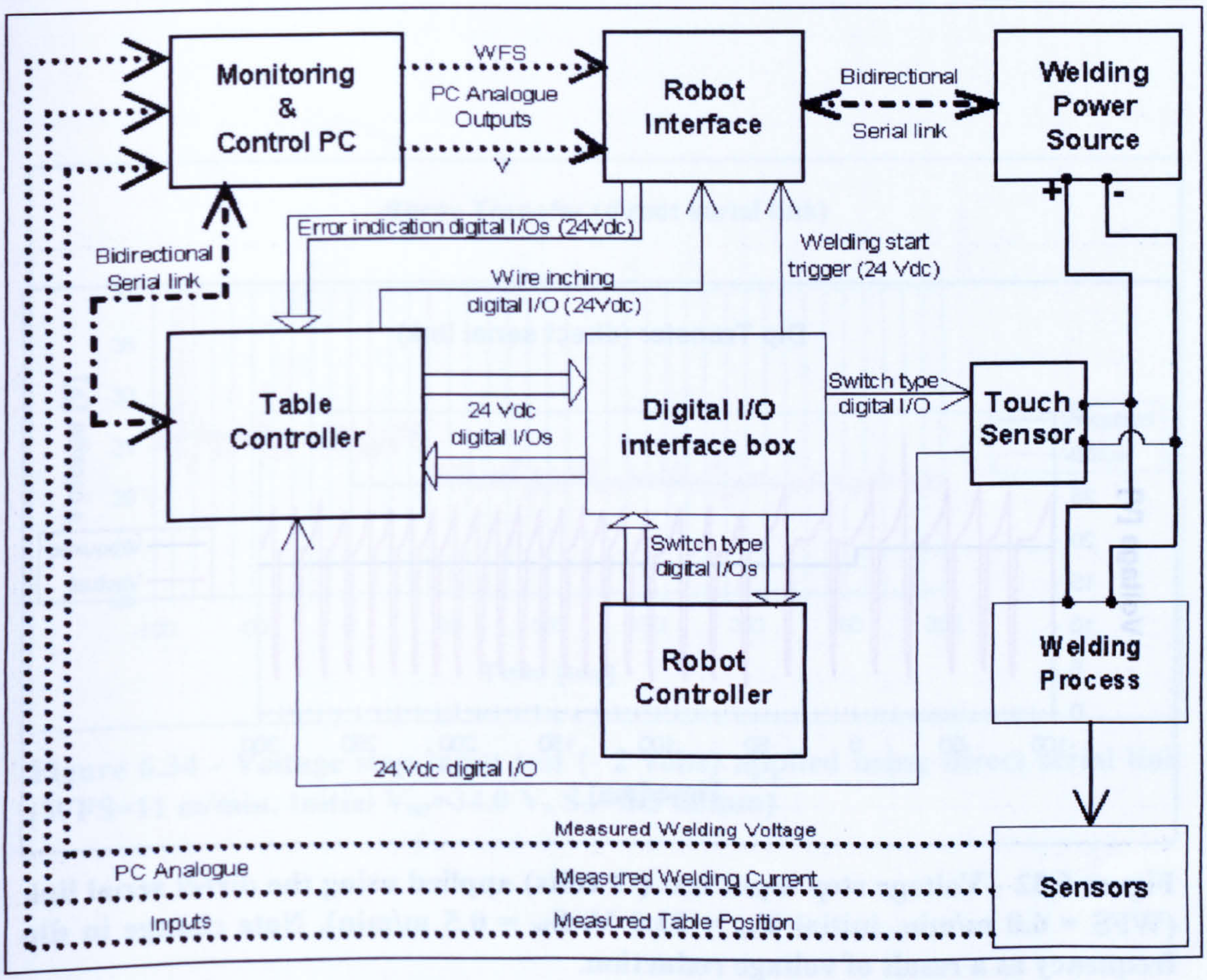

Figure 6.30 - Diagram of the interconnections between the subsystems

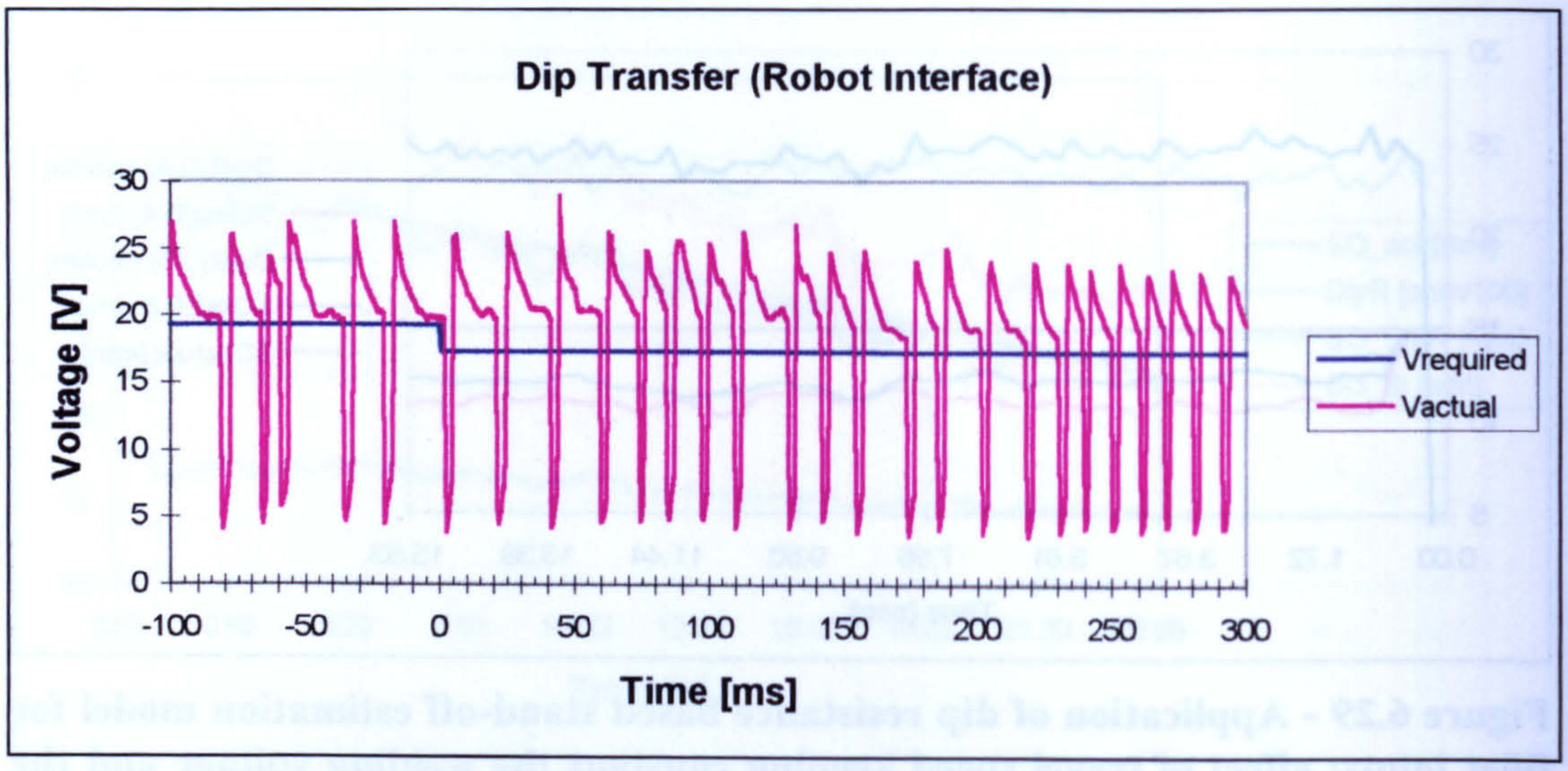

Figure 6.31 - Voltage step input test (-2 volts) applied using the Robot Interface (WFS = 6.0 m/min, initial V_{set} = 23.0 V, S_W = 0.5 m/min). Note change in dip frequency as a result of voltage reduction.

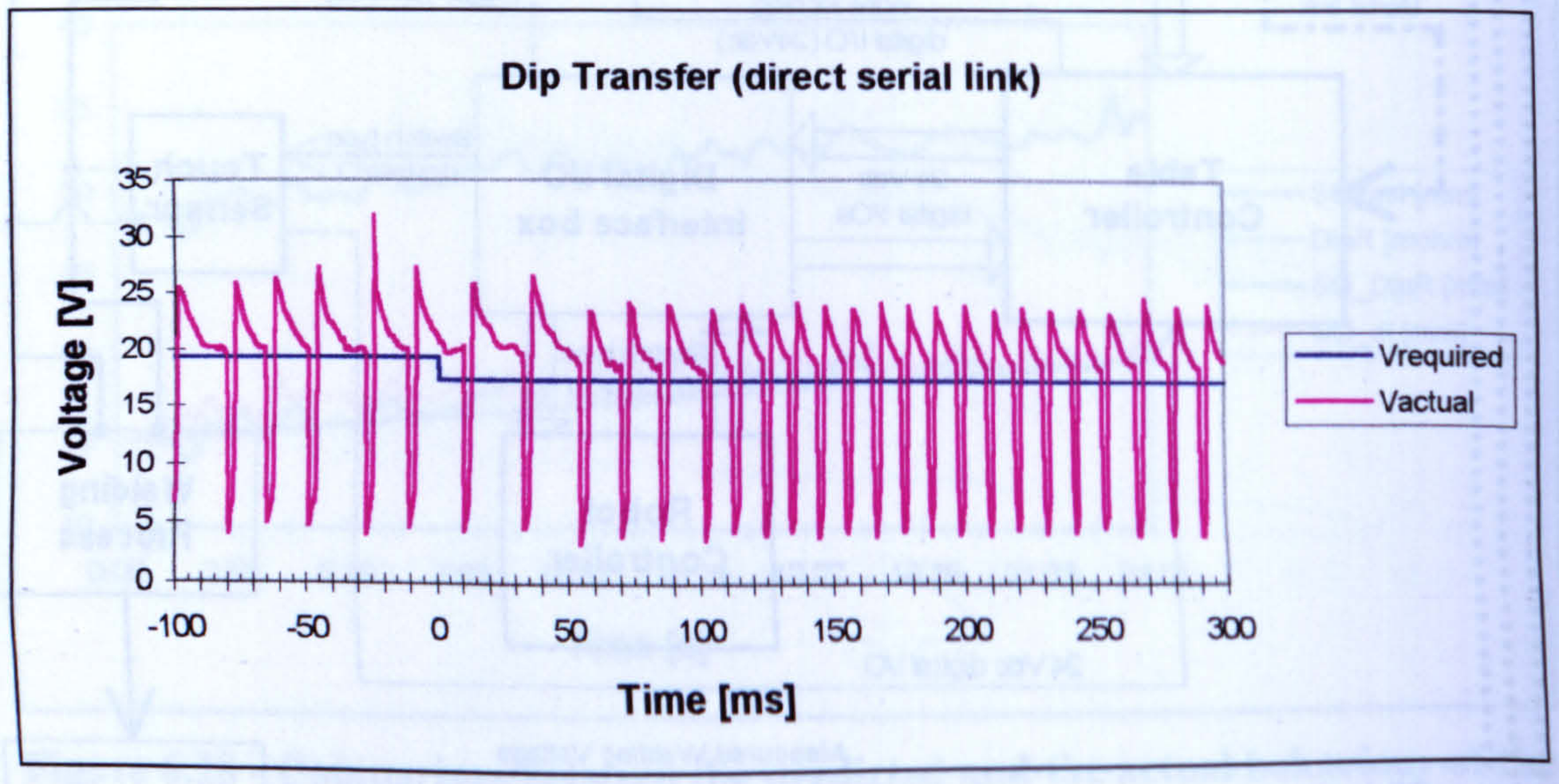

Figure 6.32 - Voltage step input test (-2 volts) applied using the direct serial link (WFS = 6.0 m/min, initial V_{set} = 23.0 V, S_W = 0.5 m/min). Note change in dip frequency as a result of voltage reduction.

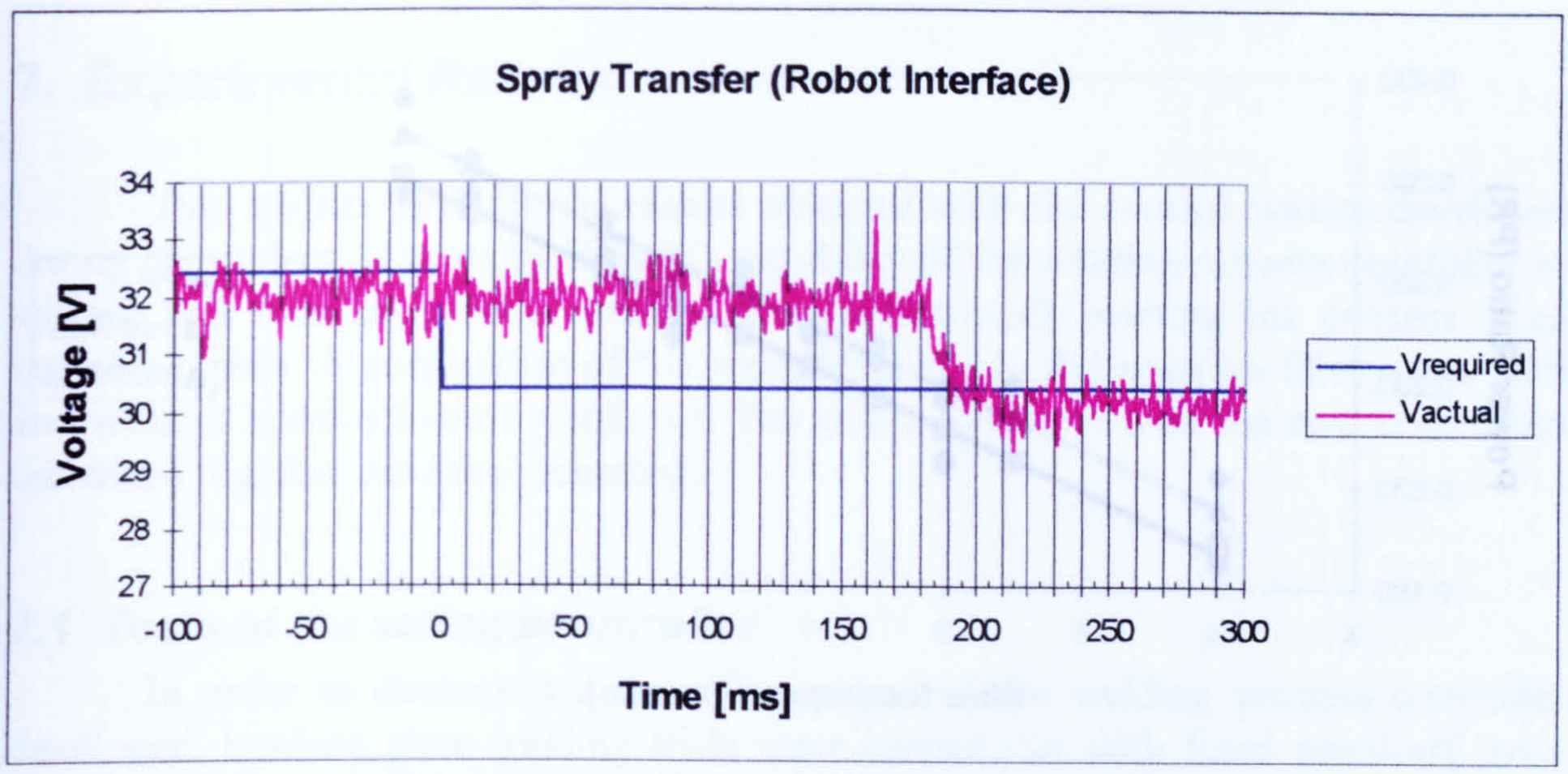

Figure 6.33 - Voltage step input test (-2 volts) applied using Robot Interface (WFS = 10.5 m/min, initial V_{set} = 33.5 V, S_W = 0.5 m/min)

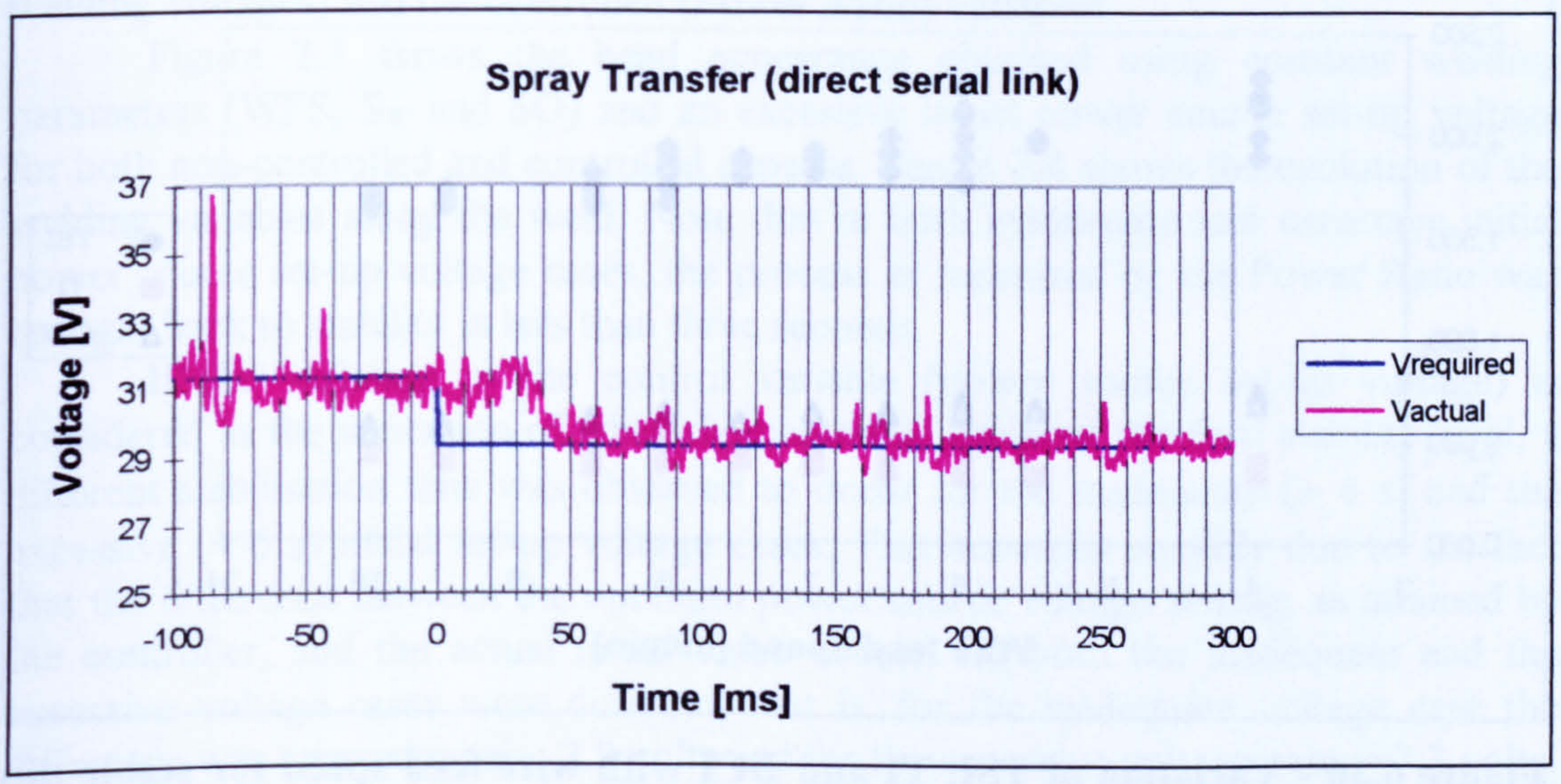

Figure 6.34 - Voltage step input test (- 2 volts) applied using direct serial link (WFS=11 m/min, Initial V_{set}=34.0 V, S_W=0.5 m/min)

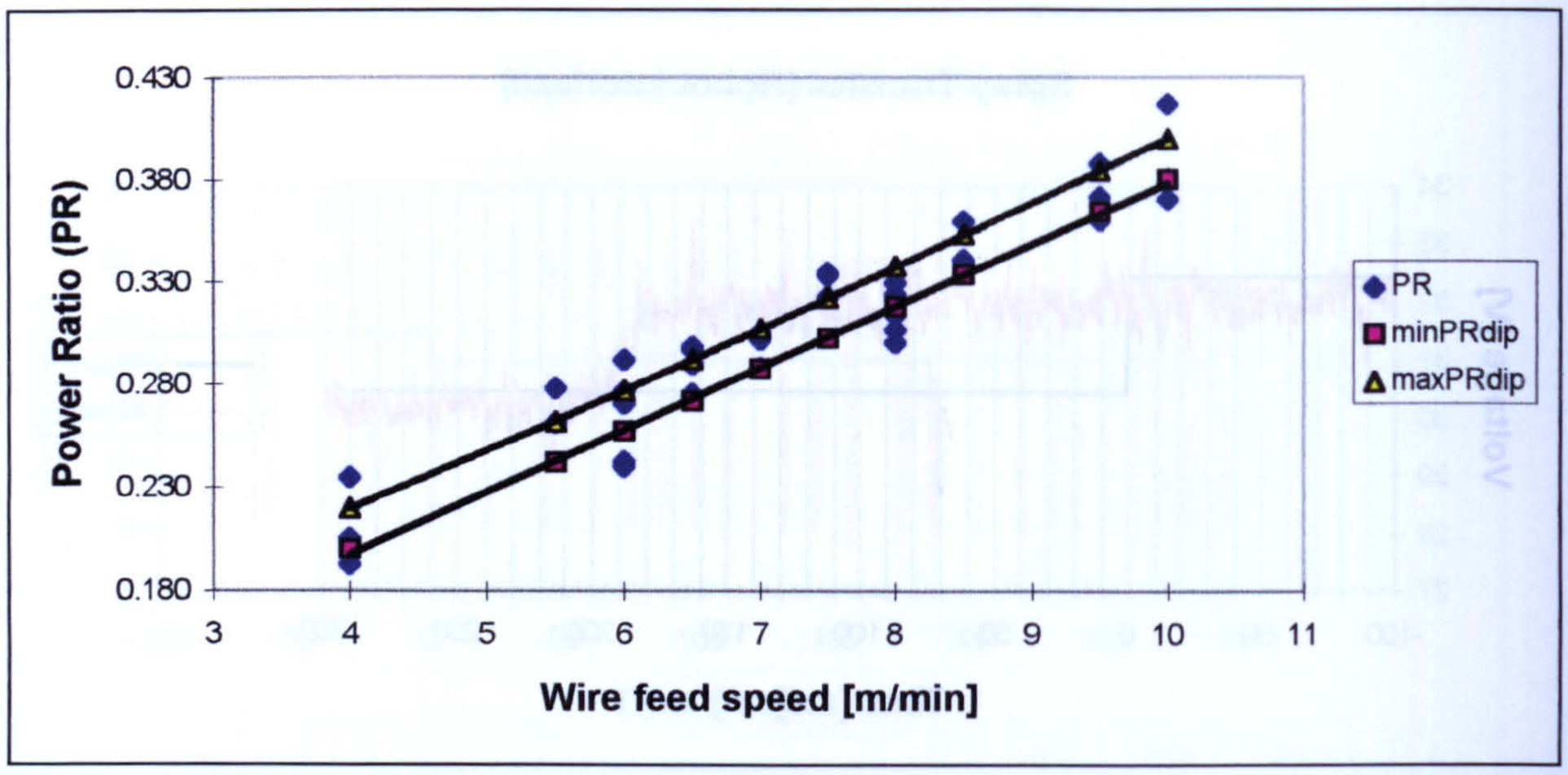

Figure 6.35 - Variation of power ratio with wire feed speed for stable dip mode of metal transfer and comparison with the allowed variation range (minPRdip ≤ PR ≤ maxPRdip)

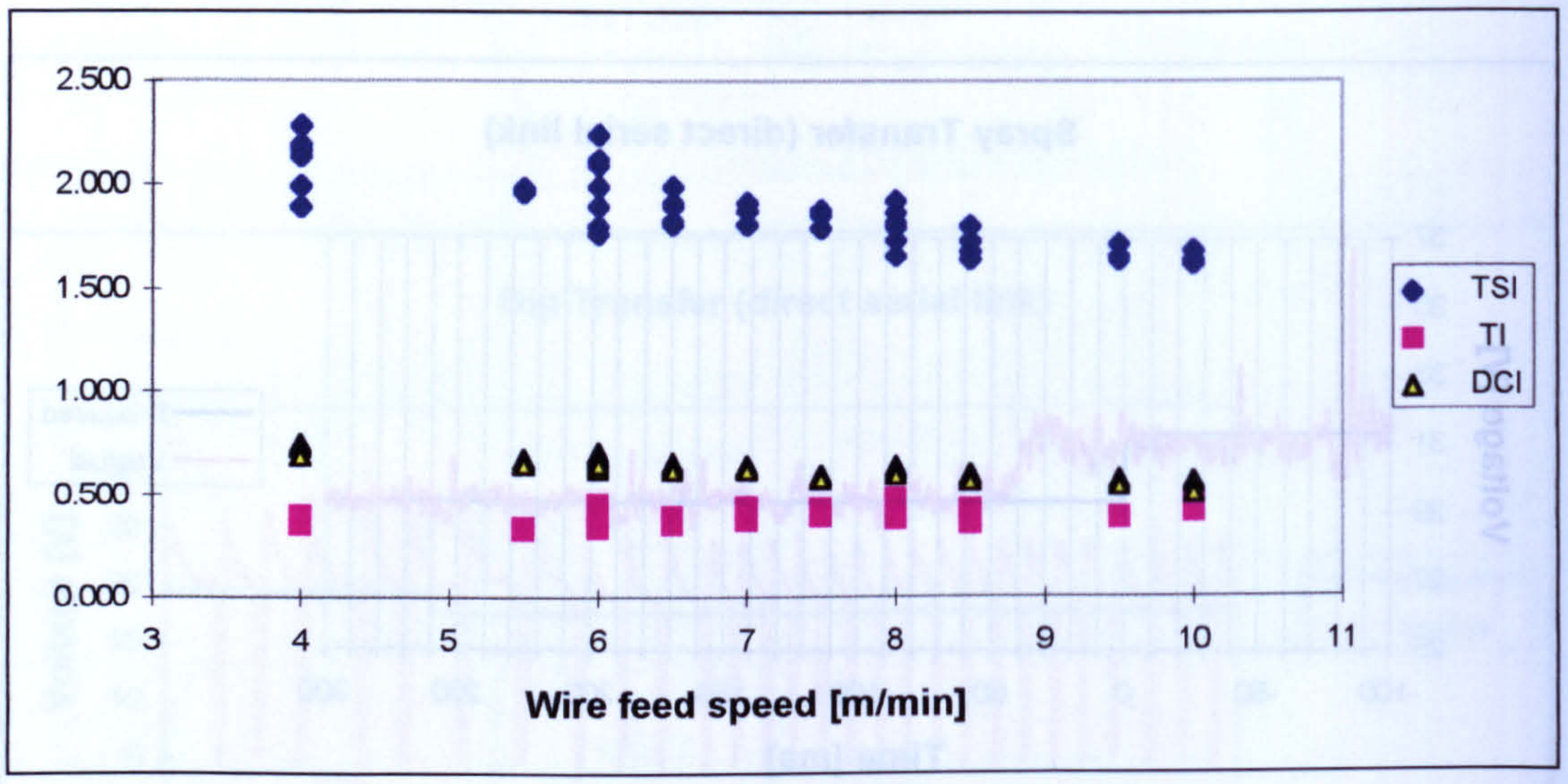

Figure 6.36 - Variation of TSI, TI and DCI with wire feed speed for stable dip mode of metal transfer

7. Experimental Results

This chapter presents the results obtained with the control system developed during the project. It starts by showing the ability of the welding process controller to achieve and maintain process stability when intentionally starting the process in an unstable region. A comparison of the welds obtained in flat position fillet joints with and without stand-off control follows. The results obtained with the two controllers combined together are then presented.

7.1 Tests of the voltage controller

In order to demonstrate the effectiveness of the welding process controller developed, bead-on plate welding trials were carried out with fixed stand-off, wire feed speed and welding speed. The initial power source set-up voltages were purposely chosen such that unstable situations would occur. These tests concentrated on the dip mode of metal transfer since this is more sensitive to variations of voltage around the optimum value.

Figure 7.1 shows the bead appearance obtained using constant welding parameters (WFS, S_w and SO) and inadequate initial power source set-up voltage for both the non-controlled and controlled process. Figure 7.2 shows the corresponding welding data and the evolution of both the control (power source set-up and mean welding voltages) and the controlled (Power Ratio) variables.

Figure 7.3 shows the bead appearance obtained using constant welding parameters (WFS, S_w and SO) and an excessive initial power source set-up voltage for both non-controlled and controlled process. Figure 7.4 shows the evolution of the welding variables along the weld. Note that in both inadequate and excessive initial power source set-up voltage cases, the process as measured by the Power Ratio was brought back to stability in less than three seconds.

If the variation in the control variable (power source set-up voltage) is considered as the indication of when the controller achieved the final stability level, a different stabilisation time was observed to occur for the inadequate ($\approx$ 4 s) and the excessive ($\approx$ 6 s) initial set-up voltage cases. This occurred possibly due to the fact that the difference between the optimum power source voltage setting, as attained by the controller, and the actual initial value chosen for both the inadequate and the excessive voltage cases were different, that is, for the inadequate voltage case the difference was approximately -2.8 volts and for the excessive voltage case, +7.3 volts. Also, the instability in the latter case is characterised mainly by the level of spatter generation, the mean voltage level being fairly stable. On the other hand, the instability in the case of inadequate voltage is characterised by the wire stubbing in the weld pool, causing large variations in the mean voltage level and therefore in the main controlled variable, PR. However, despite this difference the resulting controlled weld beads were still satisfactory (see Figure 7.1 and Figure 7.3).

7.2 Tests with varying stand-off and no control applied

These tests were carried out on fillet joints with the pre-weld joint search to ensure precise initial stand-off[1]. Since only one degree of freedom was implemented in the moving table and the robot used did not have facilities for off-line programming, a mismatch between an off-line generated program and the actual joint position was simulated by on-line programming the robot to move the welding torch along a sloping path which would start at the programmed stand-off and finish with a stand-off 8 mm bigger than the starting one. Care was taken to provide alignment between the electrode wire and the joint line. The welding parameters used were generated by the welding parameter generator for 3.2 mm mild steel plates set in a fillet joint in the flat position without a gap, using the initial stand-off as a reference value. Table 7.1 shows the parameters along with the required and the expected leg lengths. All the fillet welds were 200 mm in length.

Table 7.1 - Welding parameters used in the non-controlled flat position fillet joint welding trials

Run	WFS [m/min]	V_{set} [V]	S_W [m/min]	SO_{start} [mm]	SO_{end} [mm]	Leg_{req} [mm]	Leg_{pred} [mm]	Pen_{pred} [%]
M2	8.0	22.1	0.6	12	20	4.0	4.46	30.3
M3	10.0	22.4	0.4	12	20	6.0	6.41	39.5
M4	11.0	32.9	0.8	15	23	4.0	4.54	39.4
M5	13.0	33.2	0.7	15	23	5.0	5.40	53.1
M6	15.0	33.4	0.8	15	23	5.0	5.43	58.0

SO_{start}: initial stand-off SO_{end}: final stand-off after 200 mm weld length
Leg_{req}: leg length required in the welding parameter generator
Leg_{pred}: expected average leg length predicted by the welding parameter generator
Pen_{pred}: expected average penetration predicted by the welding parameter generator

Figures 7.5 to 7.14 show the bead appearances, the bead profiles and the welding data obtained from the welds produced with the welding parameters shown in Table 7.1. Figures 7.6, 7.8, 7.10, 7.12 and 7.14 show the quality of the on-line stand-off estimation when applying the dip-resistance-based estimation model to the fillet joint case. It should be noted that in these cases, the estimation model included the off-set calculation at the start of the welding and the estimates produced were filtered using a third order moving average filter.

Weld defects in the form of porosity (see Figure 7.9) and undercut (see Figures 7.9, 7.11 and 7.13) were observed in the spray transfer welding trials. These were possibly caused by a combination of excessive welding voltage and travel speed. Also, a pronounced finger-like penetration profile was observed in these spray transfer trials.

Although changing along the weld, the levels of average penetration obtained from these welding trials were still above the minimum required level (10% of the minimum plate thickness), despite the severe variation imposed on the stand-off (see Table 7.2).

---

[1] the set-up parameters, WFS, V_{set} and S_W were kept constant during the whole weld.

Table 7.2 - Bead geometry along the welds produced in the non-controlled flat position fillet welding trials

Run	Measured feature [mm]	Position along the weld [mm]					Geometry feature	
		30	65	100	135	170	Min. Required	Expected
M2	Leg_{sv}	4.90	4.79	4.46	4.72	4.47	4.00	4.46
	Pen_{sv}	0.78	0.69	0.63	0.54	0.46	0.32	0.60
	Max. Undercut	0.0	0.0	0.0	0.0	0.0	0.0	0.0
M3	Leg_{sv}	6.13	6.25	5.98	5.80	5.73	6.00	6.41
	Pen_{sv}	0.99	0.87	0.85	0.78	0.81	0.32	1.26
	Max. Undercut	0.0	0.0	0.0	0.0	0.0	0.0	0.0
M4	Leg_{sv}	4.39	4.05	4.31	4.68	4.06	4.00	4.54
	Pen_{sv}	1.09	1.19	1.17	1.06	1.10	0.32	1.26
	Max. Undercut	0.28	0.55	0.37	0.37	0.48	0.0	0.0
M5	Leg_{sv}	4.61	4.68	5.03	4.74	4.97	5.00	5.40
	Pen_{sv}	2.04	1.86	1.74	1.57	1.47	0.32	1.70
	Max. Undercut	0.30	0.32	0.21	0.30	0.30	0.0	0.0
M6	Leg_{sv}	5.08	5.21	5.14	4.93	5.03	5.00	5.43
	Pen_{sv}	1.78	1.70	1.67	1.57	1.59	0.32	1.86
	Max. Undercut	0.21	0.11	0.18	0.32	0.32	0.0	0.0

7.3 Tests with only stand-off control

Some tests using only stand-off control were carried out with the same welding parameters as shown in Table 7.1. The welding trials were referenced as "Sn" (n=2, ...,6) and the resulting bead appearances and bead profiles are shown in Figures 7.15, 7.17, 7.19 and 7.21. Figures 7.16, 7.18, 7.20 and 7.22 show the variation of the mean welding voltage and current as well as the stand-off along the welds. The stand-off was maintained within -1.0 mm and 2.5 mm from the required stand-off for all the welds. The resulting weld beads did not present any significant differences in appearance from the non-controlled trials. However a more consistent penetration depth was obtained along the weld beads. Table 7.3 shows the geometry features measured along the welds produced in the stand-off controlled welding trials.

The same defects observed in the non-controlled spray transfer welding trials were observed to occur in the stand-off controlled ones. One difference observed, however, was that the defects occurred with the same intensity through-out the weld beads, while in the non-controlled trials a reduction in the level of defects was observed towards the end of the welds. This difference was possibly caused by the fact that the stand-off was kept almost constant in the controlled trials whereas in the case of the non-controlled trials the increase in stand-off reduced the damaging effect of the excessive set-up welding voltage. Also, the finger-like penetration profile was observed to occur.

Table 7.3 - Bead geometry along the welds produced in the stand-off controlled flat position fillet welding trials

Run	Measured feature [mm]	Position along the weld [mm]					Geometry feature	
		30	65	100	135	170	Min. Required	Expected
S2	Leg_{av}	4.82	4.76	4.51	4.70	5.01	4.00	4.46
	Pen_{av}	0.68	0.75	0.78	0.63	0.73	0.32	0.60
	Max. Undercut	0.0	0.0	0.0	0.0	0.0	0.0	0.0
S3	Leg_{av}	5.73	5.72	5.69	5.89	5.75	6.00	6.41
	Pen_{av}	1.06	0.97	0.87	0.88	1.04	0.32	1.26
	Max. Undercut	0.0	0.0	0.0	0.0	0.0	0.0	0.0
S4	Leg_{av}	3.77	2.85	3.84	4.38	4.36	4.00	4.54
	Pen_{av}	1.11	0.98	0.90	1.08	1.06	0.32	1.26
	Max. Undercut	0.49	0.55	0.42	0.36	0.28	0.0	0.0
S5	Leg_{av}	4.67	4.81	4.87	4.79	5.35	5.00	5.40
	Pen_{av}	1.77	1.72	1.71	1.79	1.67	0.32	1.70
	Max. Undercut	0.68	0.45	0.40	0.35	0.30	0.0	0.0
S6	Leg_{av}	4.70	4.79	4.99	5.30	5.03	5.00	5.43
	Pen_{av}	2.05	2.01	1.95	1.87	2.04	0.32	1.86
	Max. Undercut	0.25	0.21	0.21	0.23	0.15	0.0	0.0

7.4 Tests with both stand-off and voltage control

Some welding trials were carried out in order to test the performance of both stand-off and voltage controllers acting together. The welding parameters used are shown in Table 7.4 and were generated for producing the same weld geometry as the ones shown in Table 7.1 with the difference that a stand-off of 15 mm was considered for calculation purposes in all the cases. The weld runs were referenced as "SVn" (n=2, ...,6), in this case.

Table 7.4 - Welding parameters used in the voltage and stand-off controlled flat position fillet welding trials

Run	WFS [m/min]	V_{set} [V]	S_W [m/min]	SO_{start} [mm]	SO_{end} [mm]	Leg_{req} [mm]	Leg_{pred} [mm]	Pen_{pred} [mm]
SV2	8.0	22.2	0.6	15	23	4.0	4.46	17.9
SV3	10.0	22.4	0.4	15	23	6.0	6.41	37.9
SV4	11.0	32.9	0.8	15	23	4.0	4.54	39.4
SV5	13.0	33.2	0.7	15	23	5.0	5.40	53.1
SV6	15.0	33.4	0.8	15	23	5.0	5.43	58.0

SO_{start}: initial stand-off SO_{end}: final stand-off after 200 mm weld length
Leg_{req}: leg length required in the welding parameter generator
Leg_{pred}: expected average leg length predicted by the welding parameter generator
Pen_{pred}: expected average penetration predicted by the welding parameter generator

Figures 7.23, 7.25, 7.27, 7.29 and 7.31 show the bead appearances and the bead profiles obtained from the controlled trials. Figures 7.24, 7.26, 7.28, 7.30 and 7.32 show the variation in the welding voltage and current as well as in the stand-off

during the controlled welding trials. More consistent bead appearances were observed to be produced from the dip transfer trials (see Figures 7.23 and 7.25). Reduced levels of spatter were also observed to occur. In the spray transfer trials, a considerable reduction in the levels of defects was obtained. The porosity was eliminated completely and the undercut largely reduced (see Figures 7.27, 7.29, 7.31). Also, consistent penetration levels were obtained through-out the welds. The stand-off was controlled to ±2.5 mm in all welding trials. Table 7.5 shows the bead geometry measured from the weld beads produced in the voltage and stand-off controlled trials.

Table 7.5 - Bead geometry along the welds produced in the voltage and stand-off controlled flat position fillet welding trials

Run	Measured feature [mm]	Position along the weld [mm]					Geometry feature	
		30	65	100	135	170	Min. Required	Expected
SV2	Leg_{sv}	4.85	4.56	4.58	4.78	4.59	4.00	4.46
	Pen_{sv}	0.58	0.63	0.53	0.56	0.55	0.32	0.57
	Max. Undercut	0.0	0.0	0.0	0.0	0.0	0.0	0.0
SV3	Leg_{sv}	5.95	5.87	5.91	6.03	5.83	6.00	6.41
	Pen_{sv}	1.00	1.14	1.07	0.93	1.01	0.32	1.21
	Max. Undercut	0.0	0.0	0.0	0.0	0.0	0.0	0.0
SV4	Leg_{sv}	4.08	4.11	3.98	4.07	4.19	4.00	4.54
	Pen_{sv}	1.32	1.25	1.40	1.27	1.33	0.32	1.26
	Max. Undercut	0.37	0.25	0.37	0.32	0.30	0.0	0.0
SV5	Leg_{sv}	5.73	5.39	5.55	5.63	5.53	5.00	5.40
	Pen_{sv}	1.70	1.90	1.92	1.85	2.08	0.32	1.70
	Max. Undercut	0.0	0.0	0.0	0.0	0.0	0.0	0.0
SV6	Leg_{sv}	4.82	4.73	4.99	5.21	5.12	5.00	5.43
	Pen_{sv}	2.22	2.31	2.12	2.20	2.14	0.32	1.86
	Max. Undercut	0.0	0.0	0.0	0.0	0.0	0.0	0.0

Note the improvement on the penetration profile obtained in the spray transfer trials. The finger-like penetration was greatly reduced and in some cases even eliminated.

Some bead misalignment was observed to occur in some welds, even though the robot was carefully programmed on-line to ensure good alignment. This was believed to occur due to some joint movement allowed in the welding jig (see Figure 5.1) during the joint fit-up. Also, the cast of the wire together with differences in the heat sink characteristics provided in both sides of the joint were believed to affect the symmetry of the bead profiles relative to the joint bisection plane. These observations confirm the already mentioned necessity of a means to ensuring the alignment of the wire relative to the joint line, which could be provided by a proper seam tracking facility.

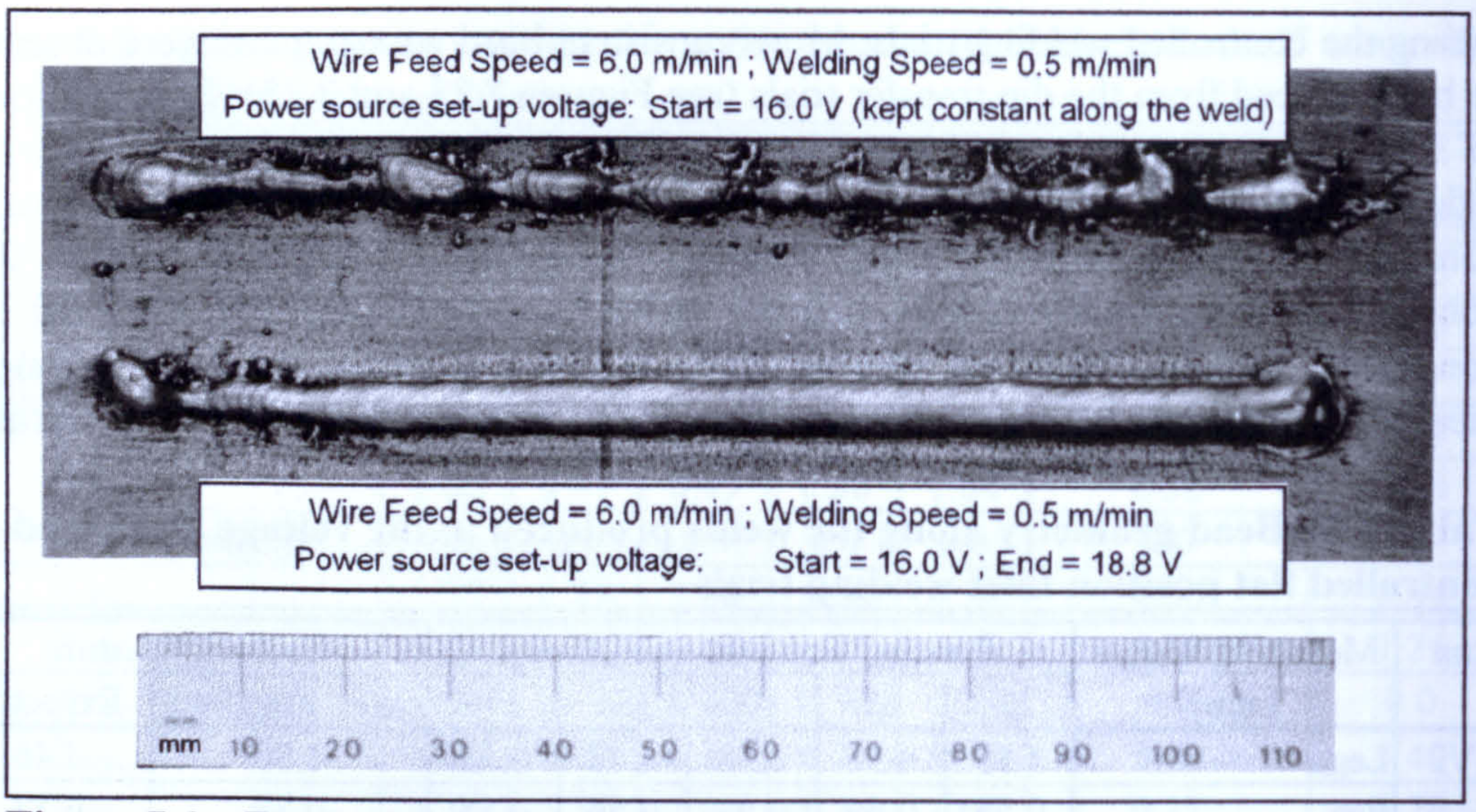

Figure 7.1 - Bead appearance for controlled and uncontrolled trials carried out using inadequate set-up voltage for the dip mode of metal transfer.

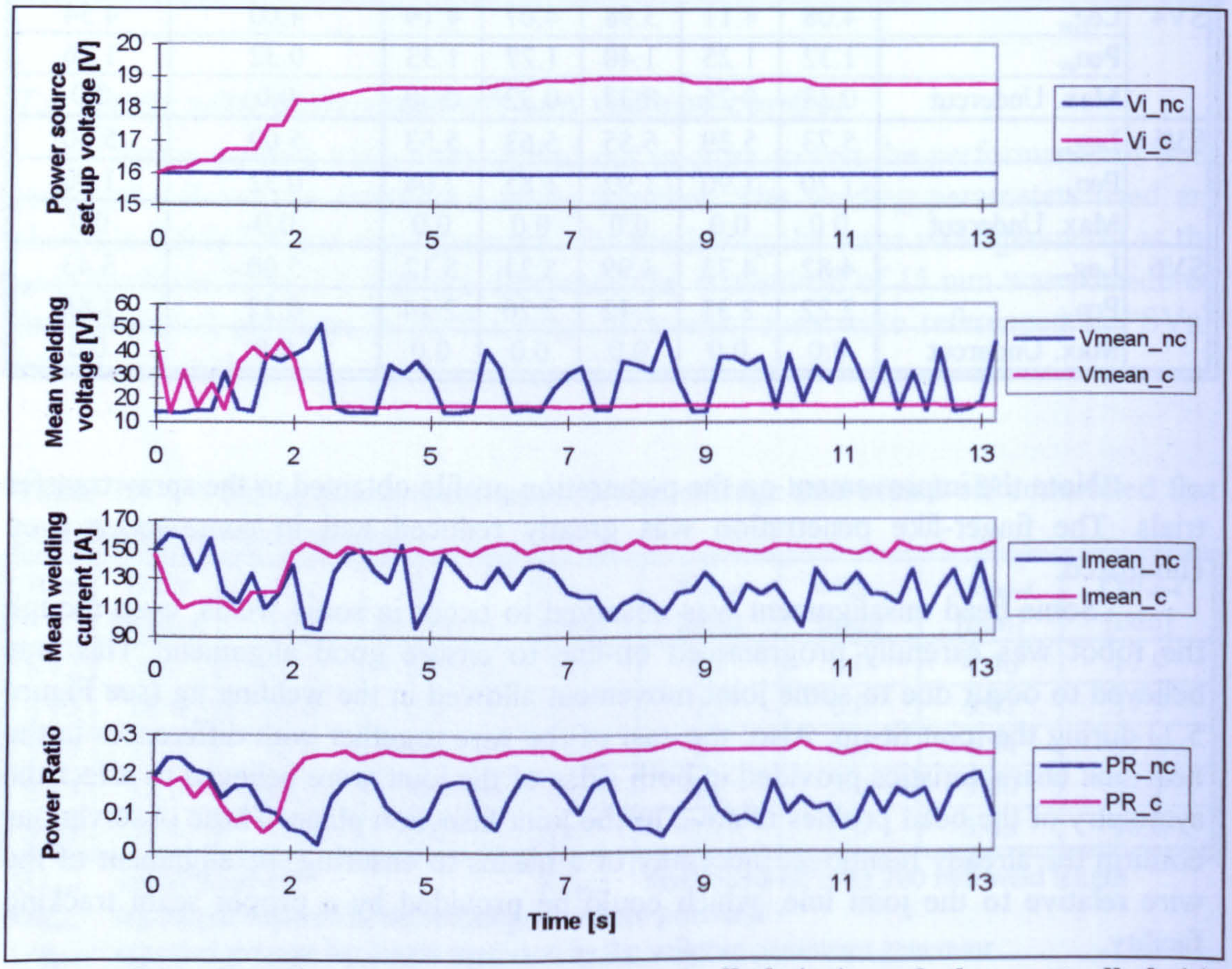

Figure 7.2 - Welding data of the non-controlled (nc) and the controlled (c) welding trials shown in Figure 7.1

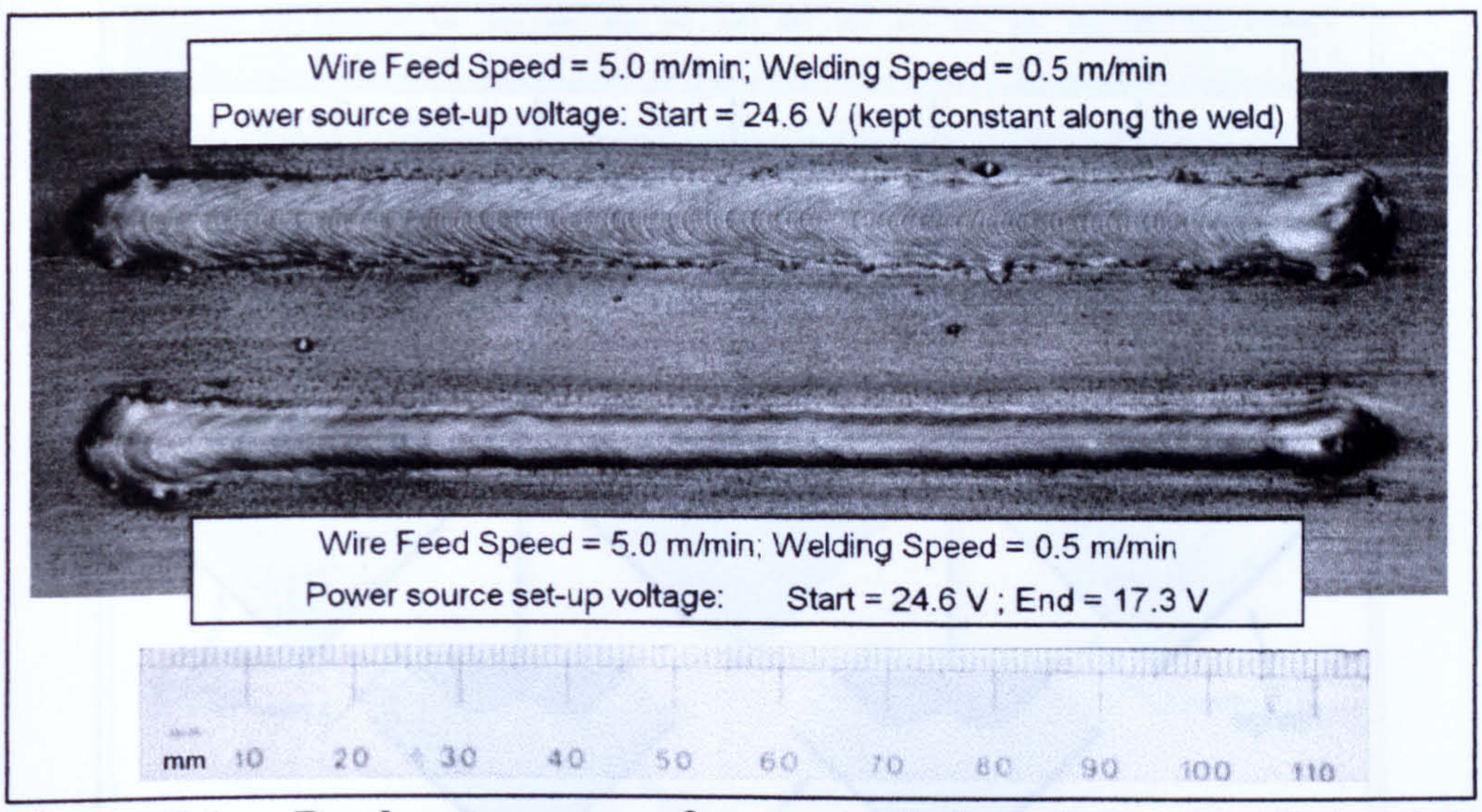

Figure 7.3 - Bead appearance for controlled and uncontrolled trials carried out using excessive set-up voltage for the dip mode of metal transfer.

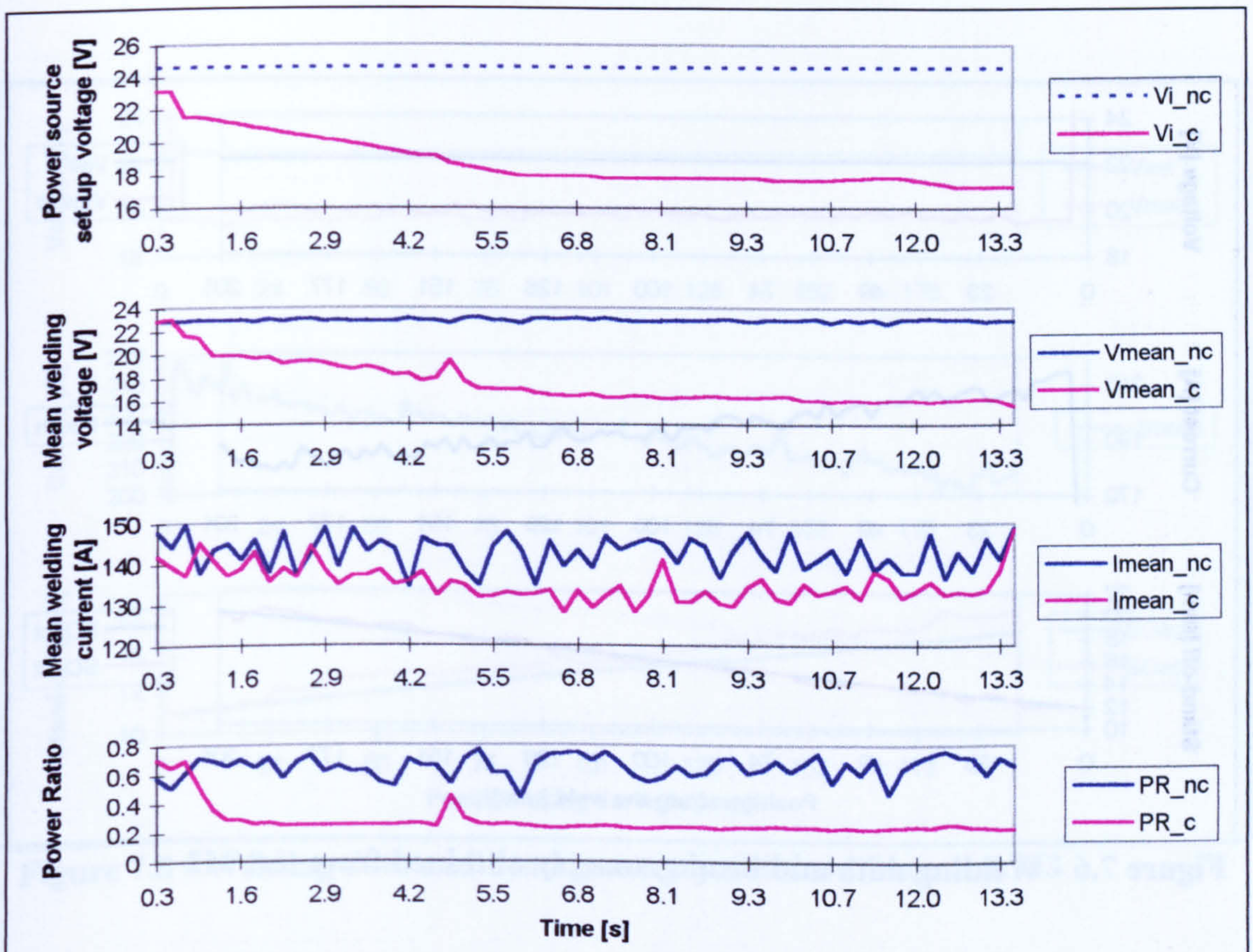

Figure 7.4 - Welding data of the non-controlled (nc) and the controlled (c) welding trials shown in Figure 7.3.

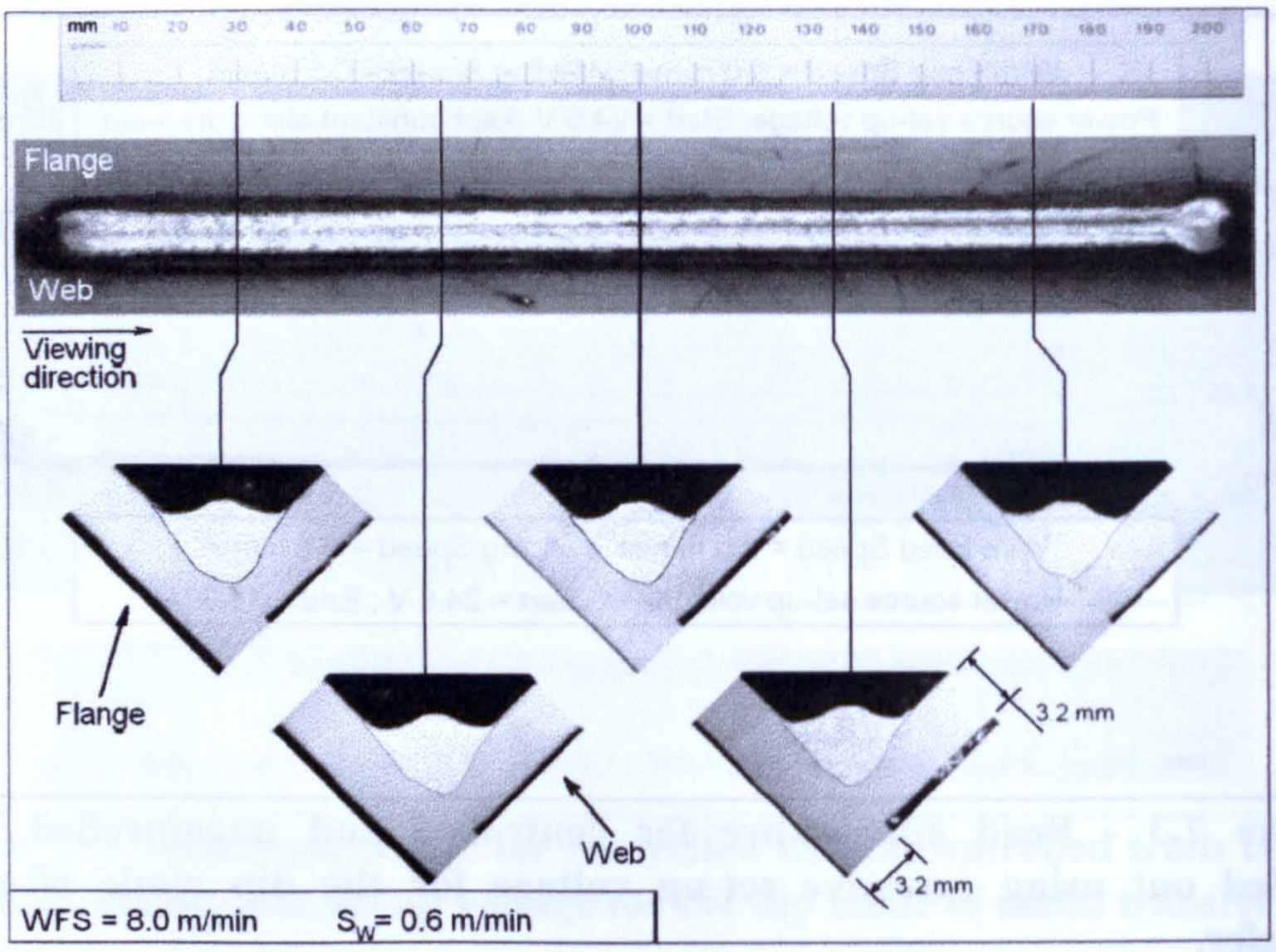

Figure 7.5 - Bead appearance and bead profiles along the weld for non-controlled fillet welding trial "M2".

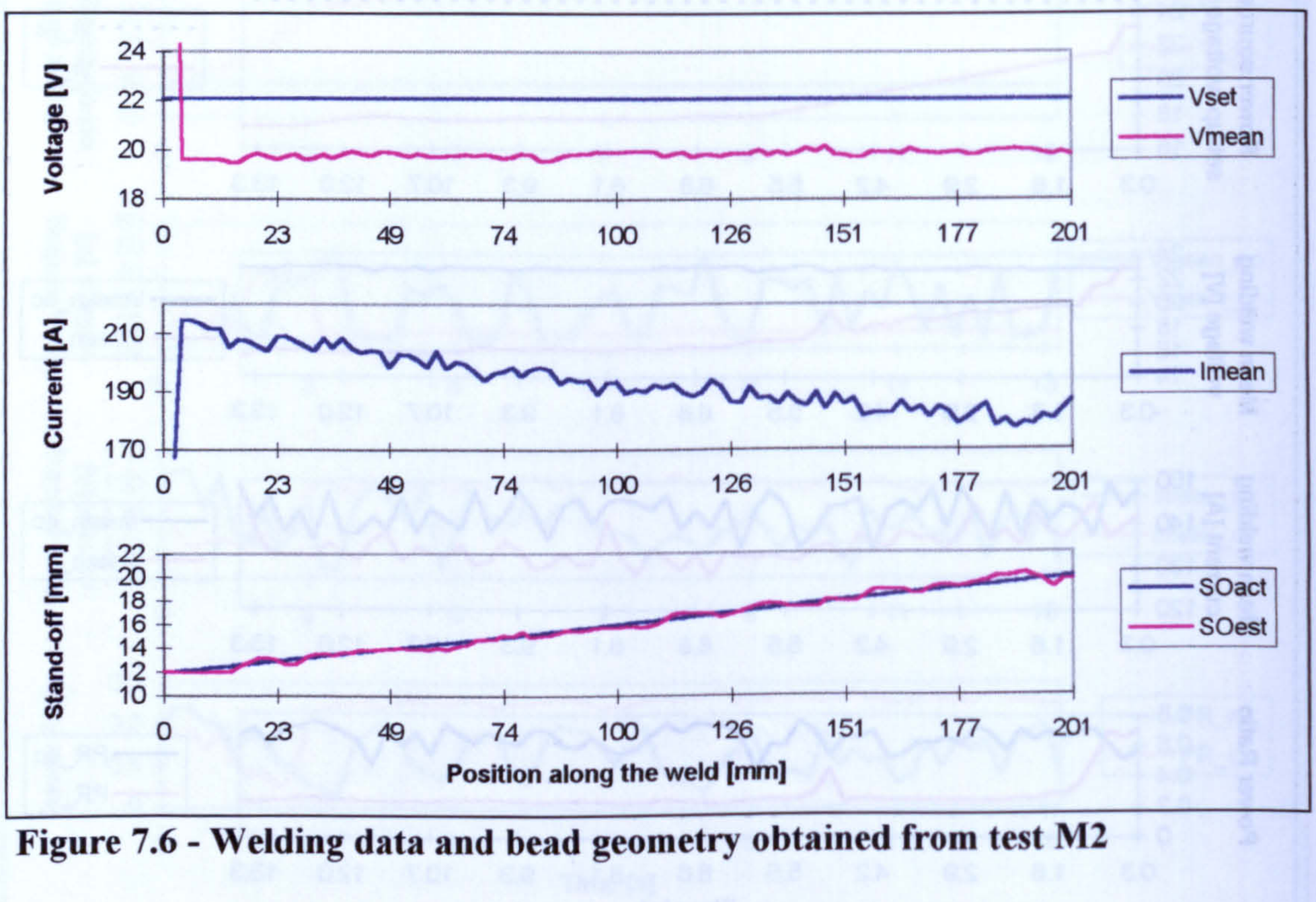

Figure 7.6 - Welding data and bead geometry obtained from test M2

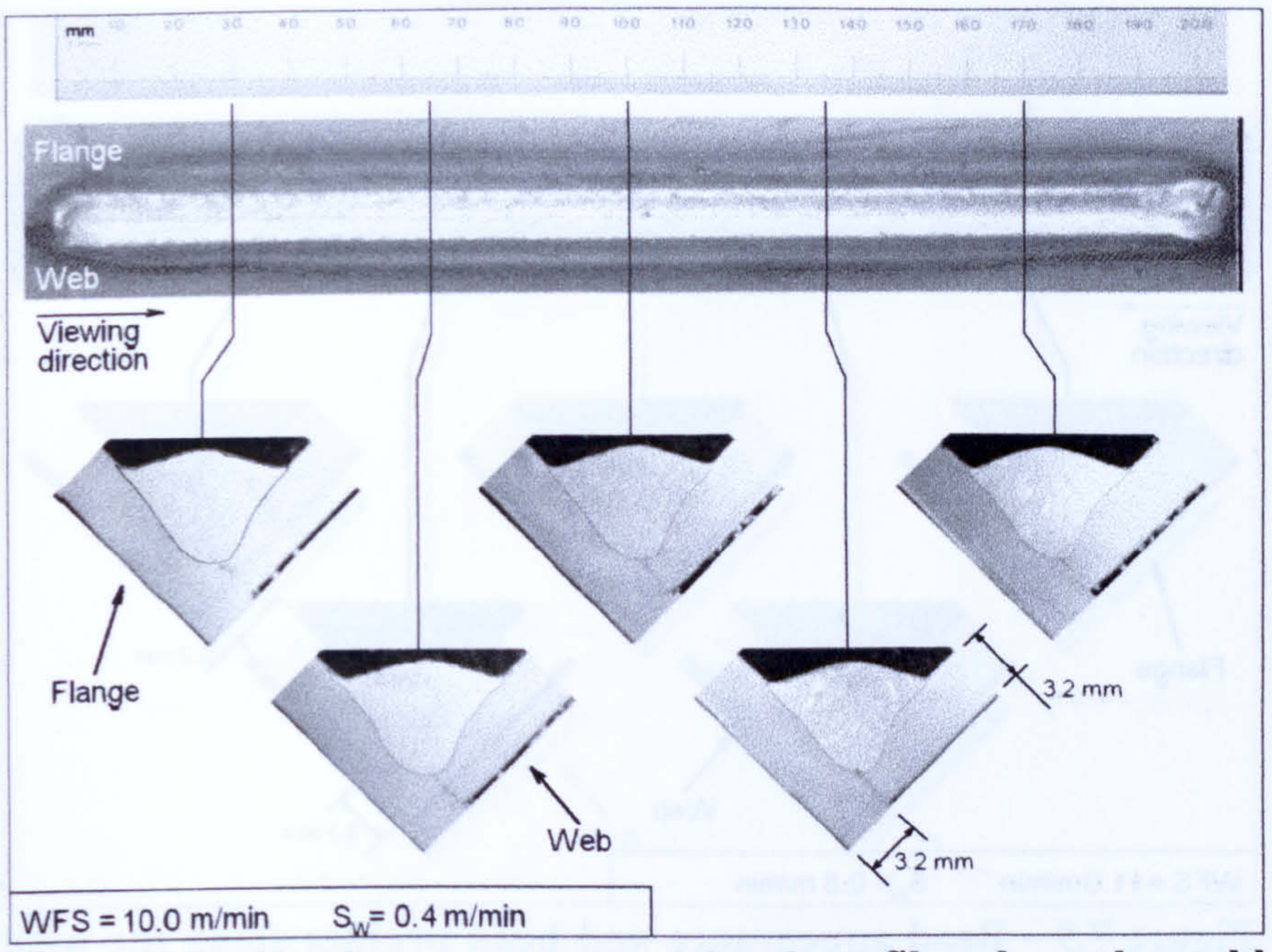

Figure 7.7 - Bead appearance and bead profiles along the weld for the non-controlled fillet welding trial "M3".

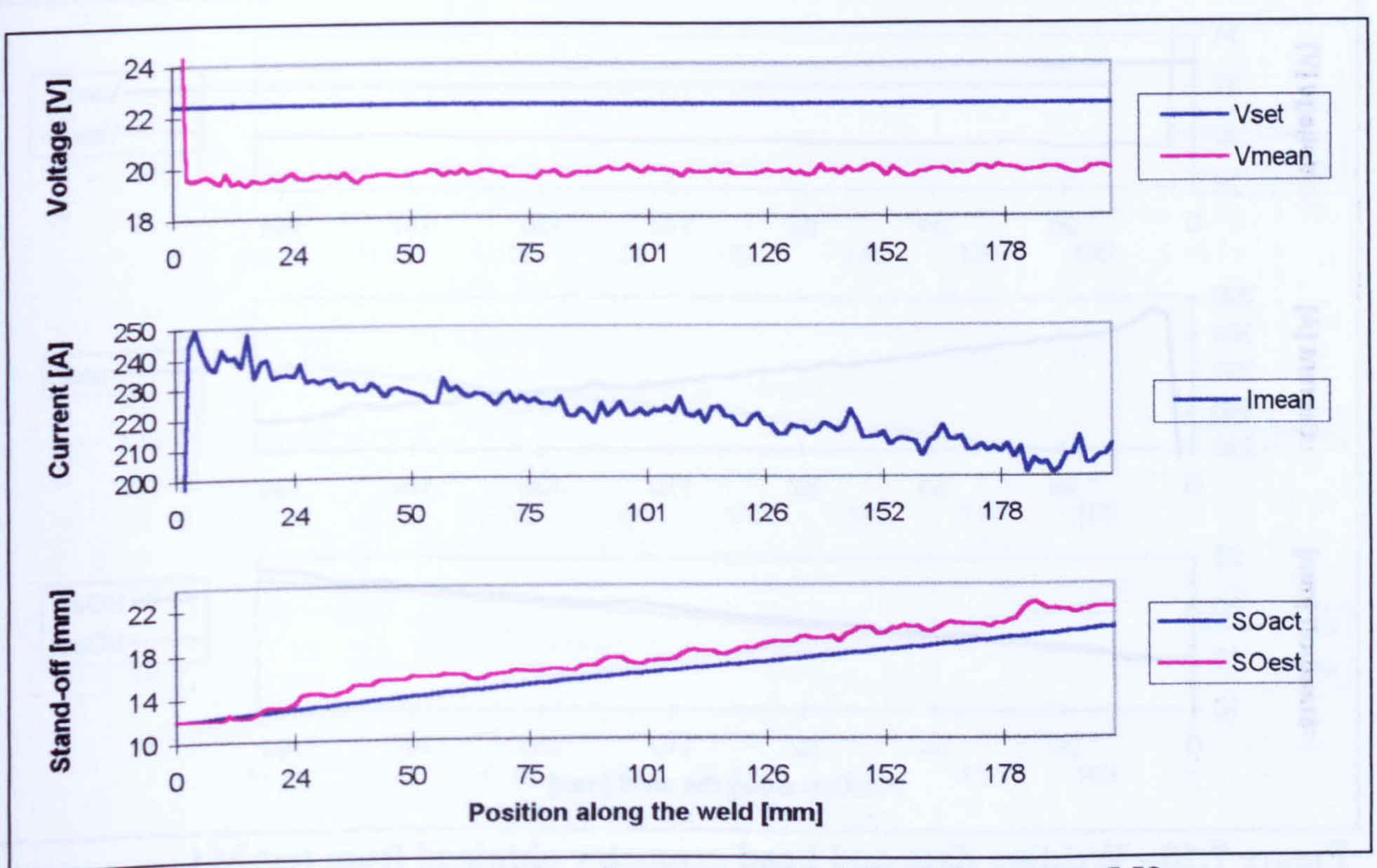

Figure 7.8 - Welding data and bead geometry obtained from test M3

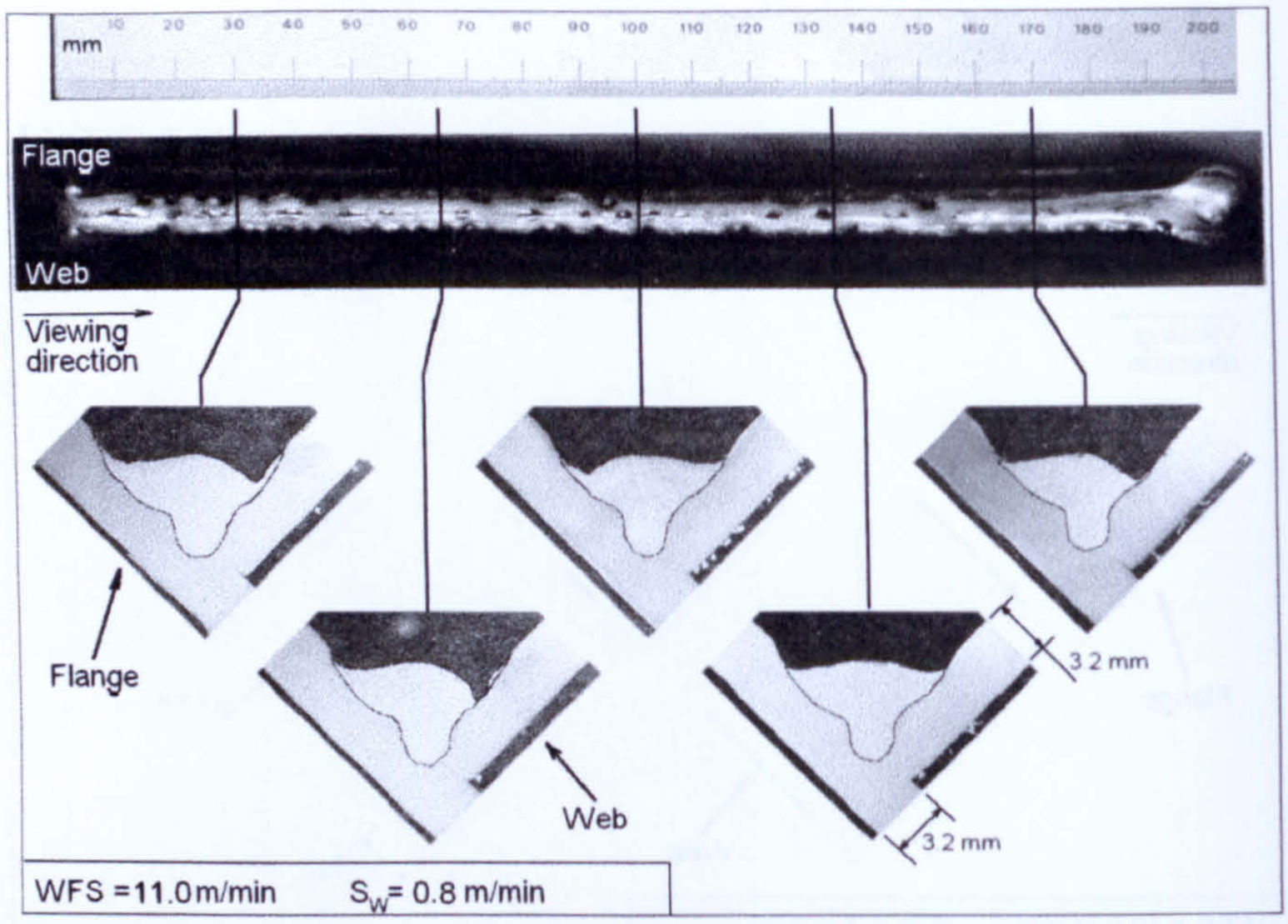

Figure 7.9 - Bead appearance and bead profiles along the weld for the non-controlled fillet welding trial "M4".

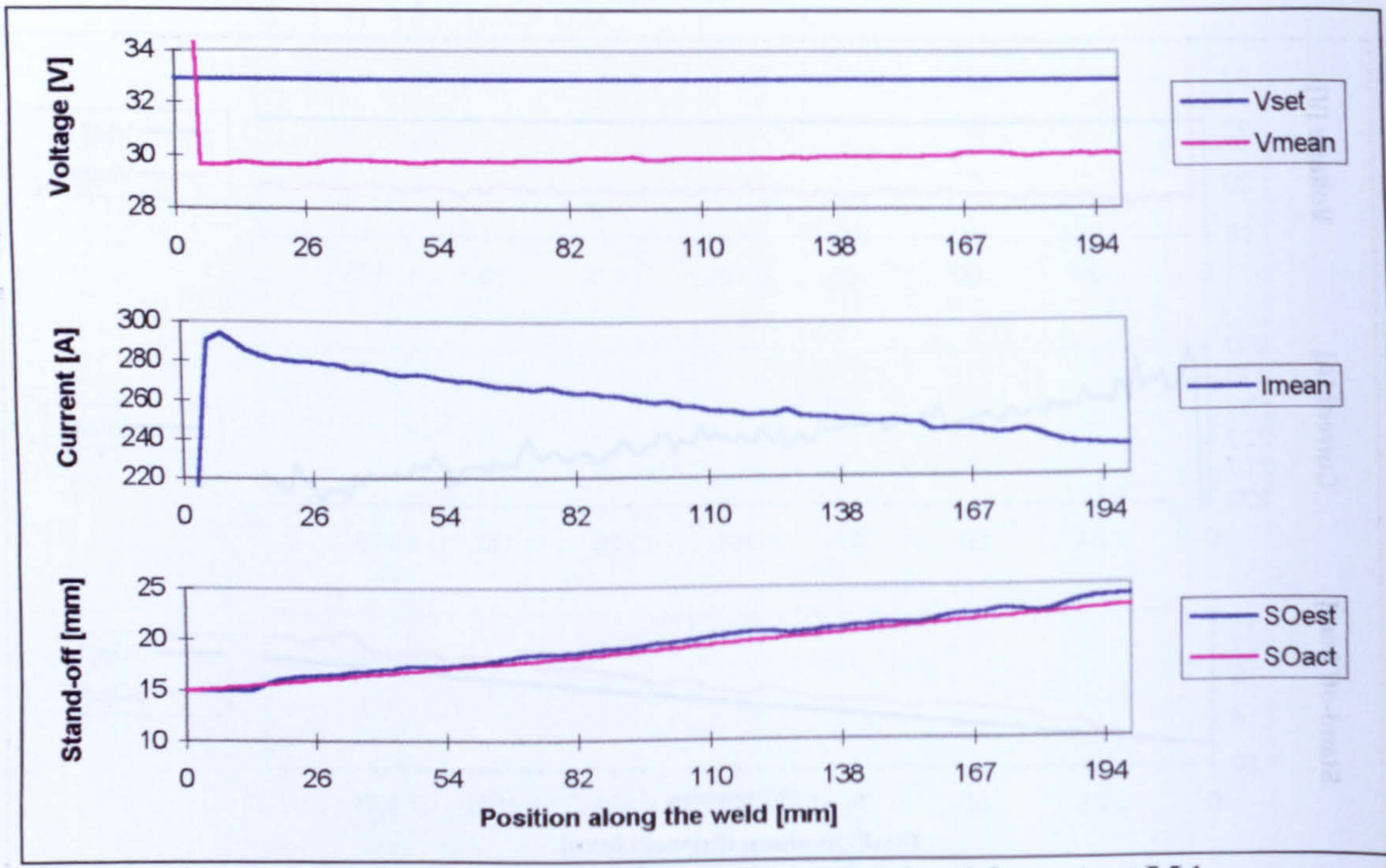

Figure 7.10 - Welding data and bead geometry obtained from test M4

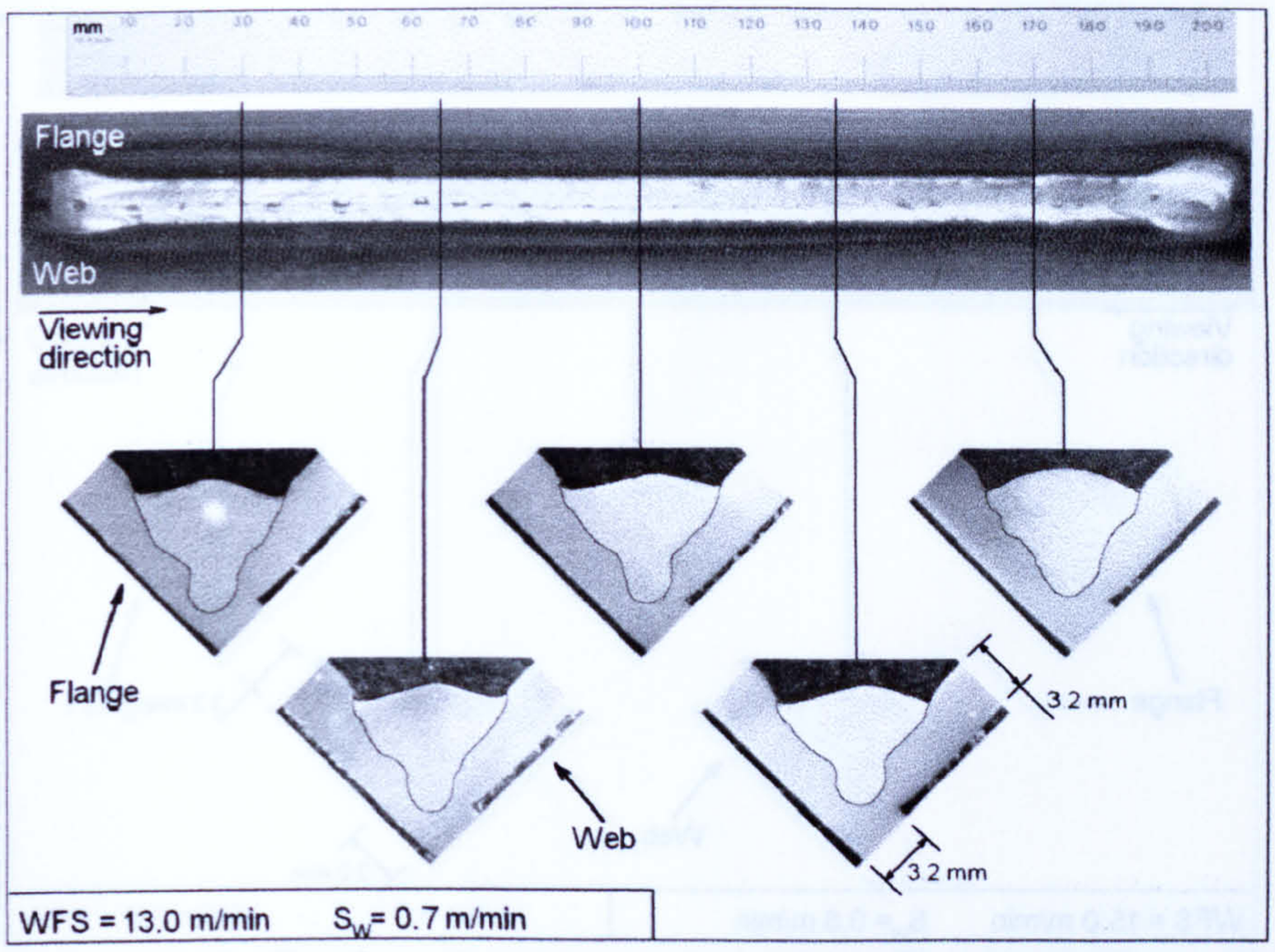

Figure 7.11 - Bead appearance and bead profiles along the weld for the non-controlled fillet welding trial "M5".

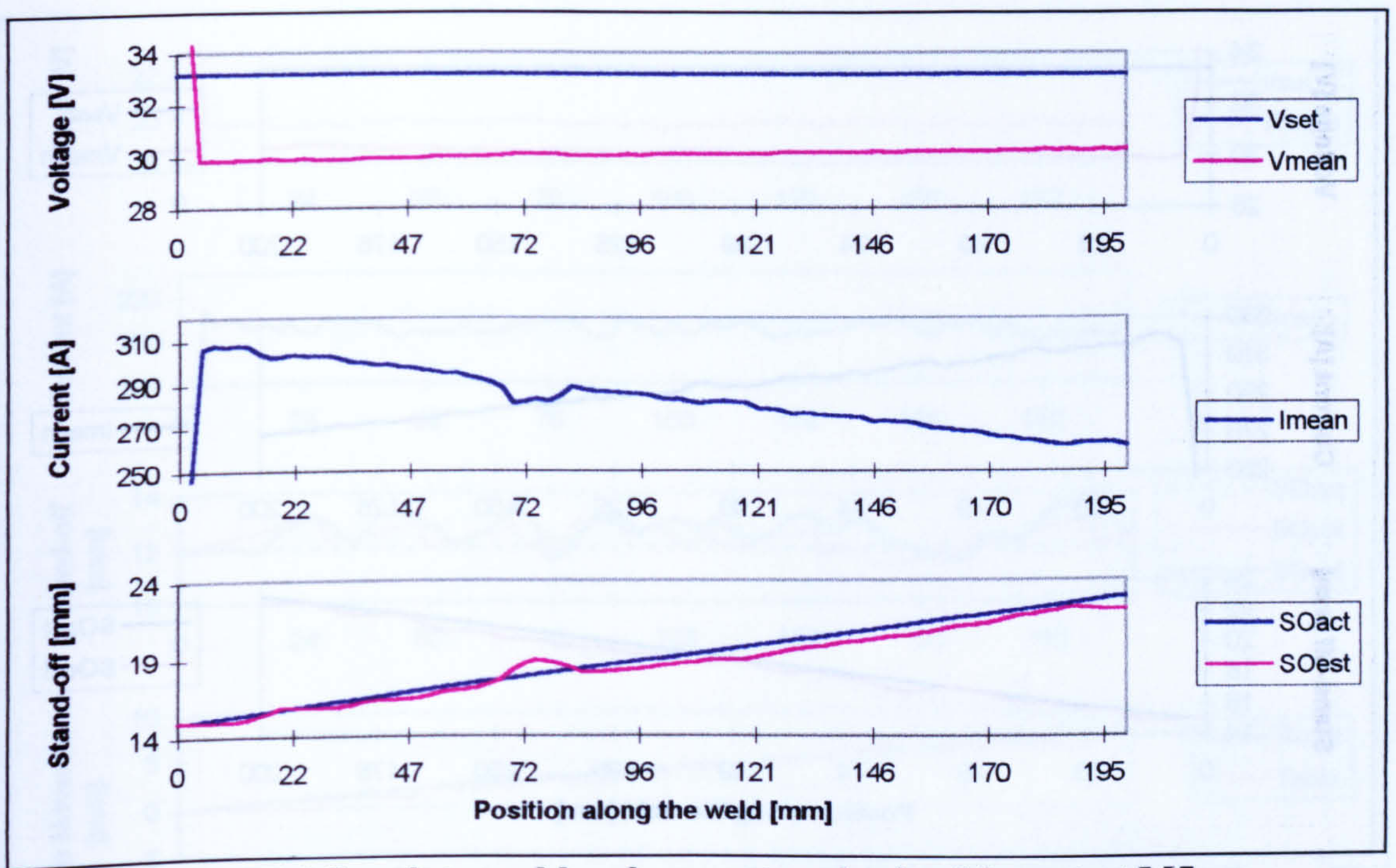

Figure 7.12 - Welding data and bead geometry obtained from test M5

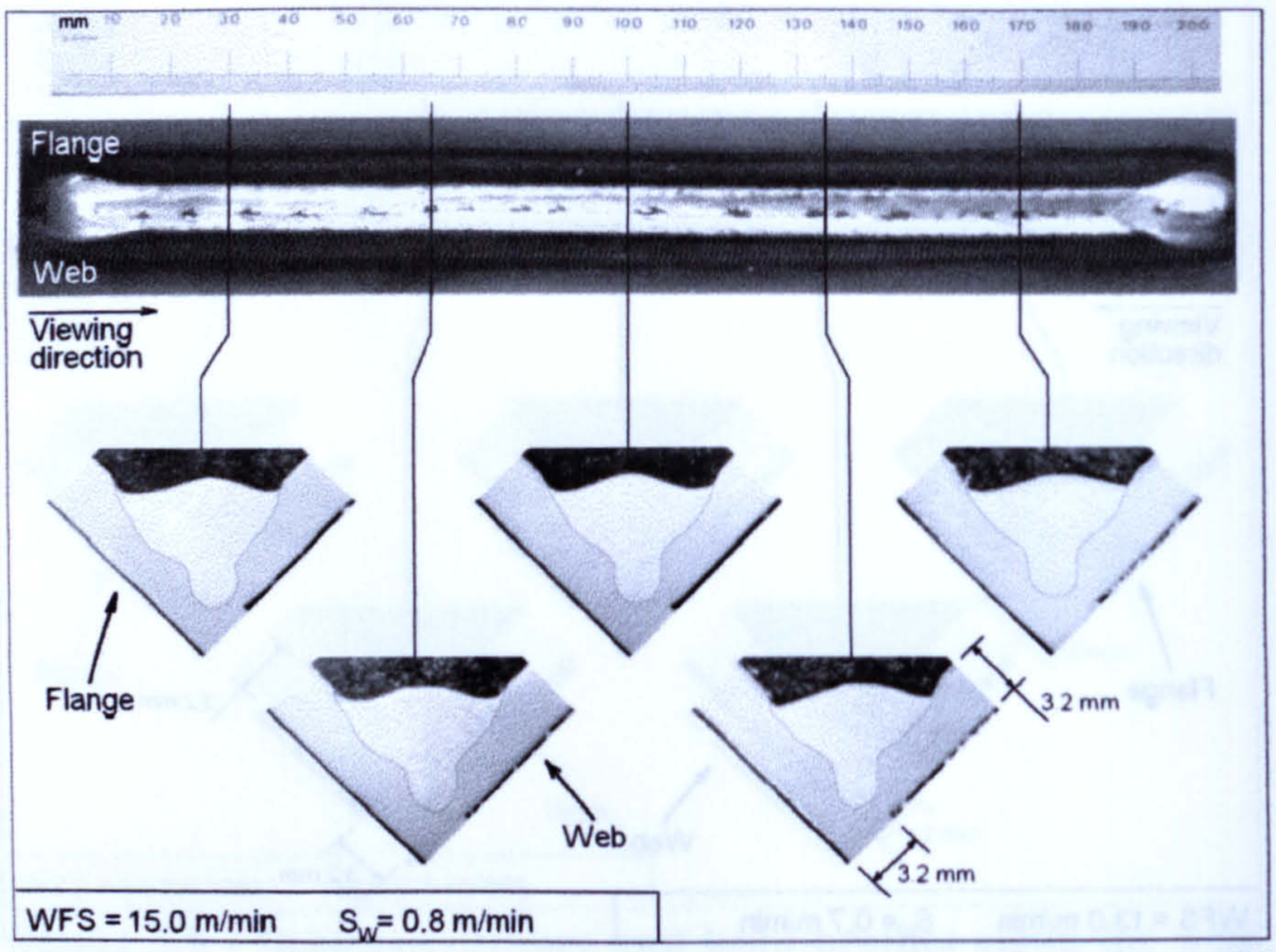

Figure 7.13 - Bead appearance and bead profiles along the weld for the non-controlled fillet welding trial "M6".

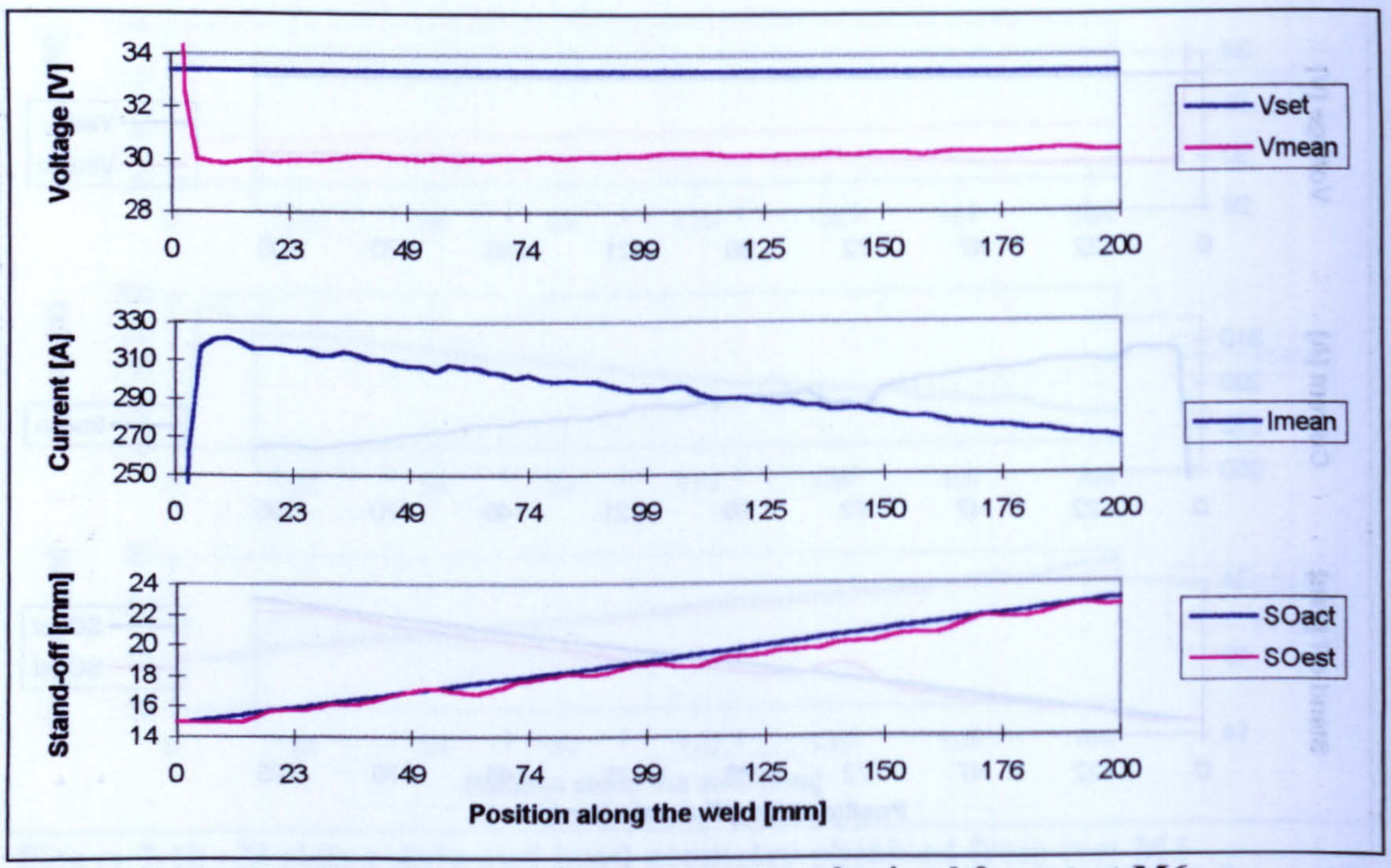

Figure 7.14 - Welding data and bead geometry obtained from test M6

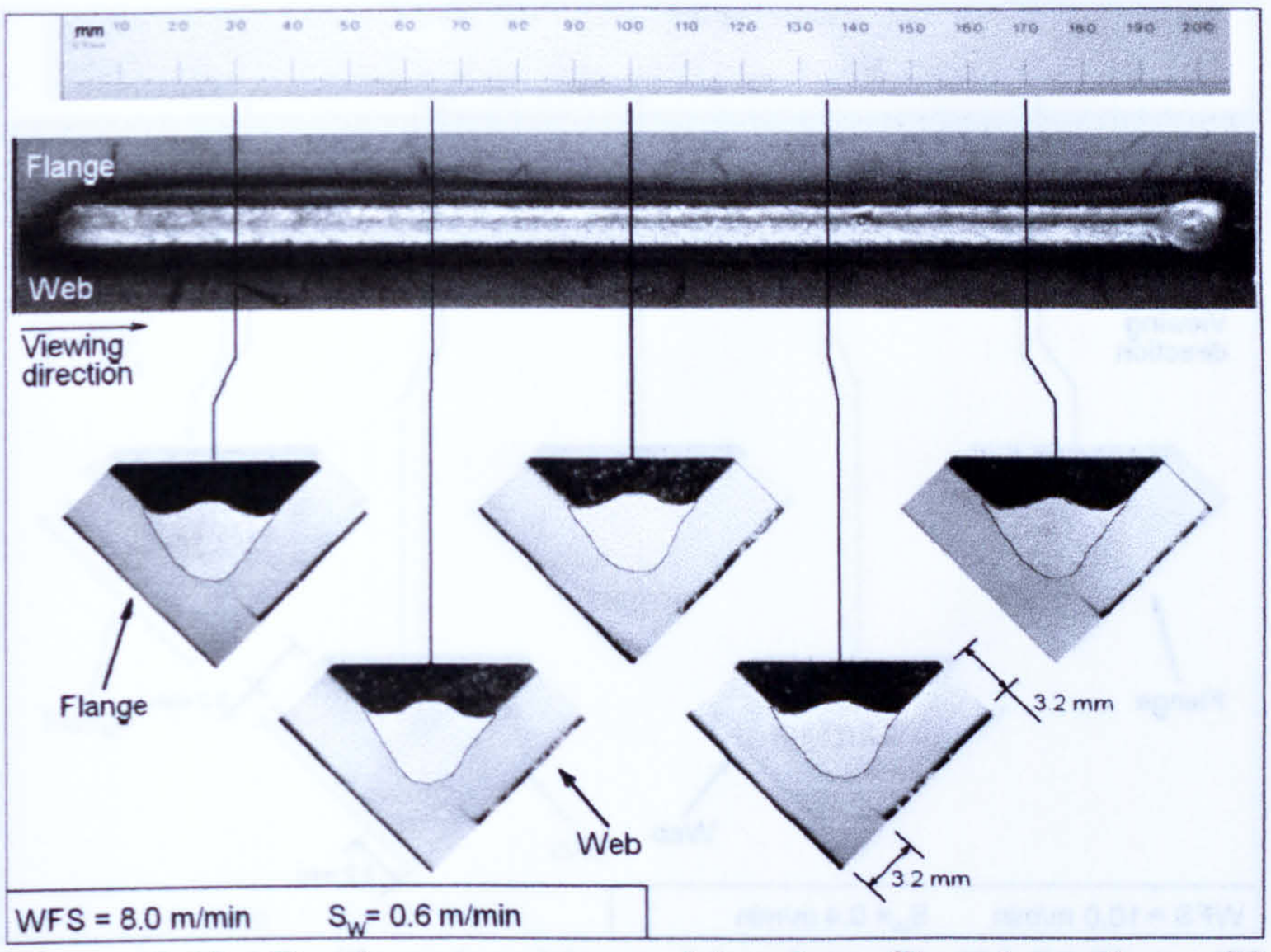

Figure 7.15 - Bead appearance and bead profiles along the weld for the stand-off controlled fillet welding trial "S2".

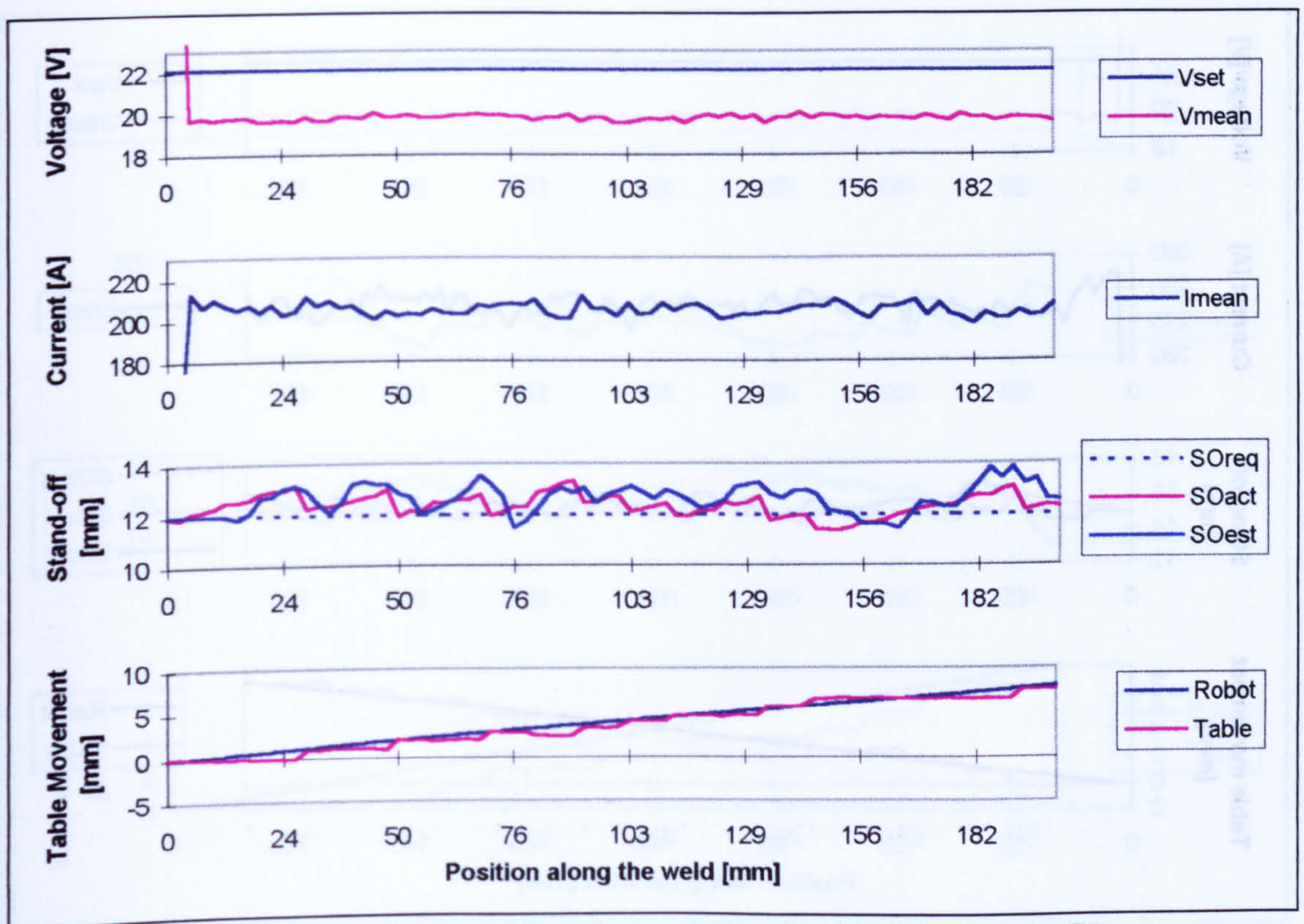

Figure 7.16 - Welding data and bead geometry obtained from test S2

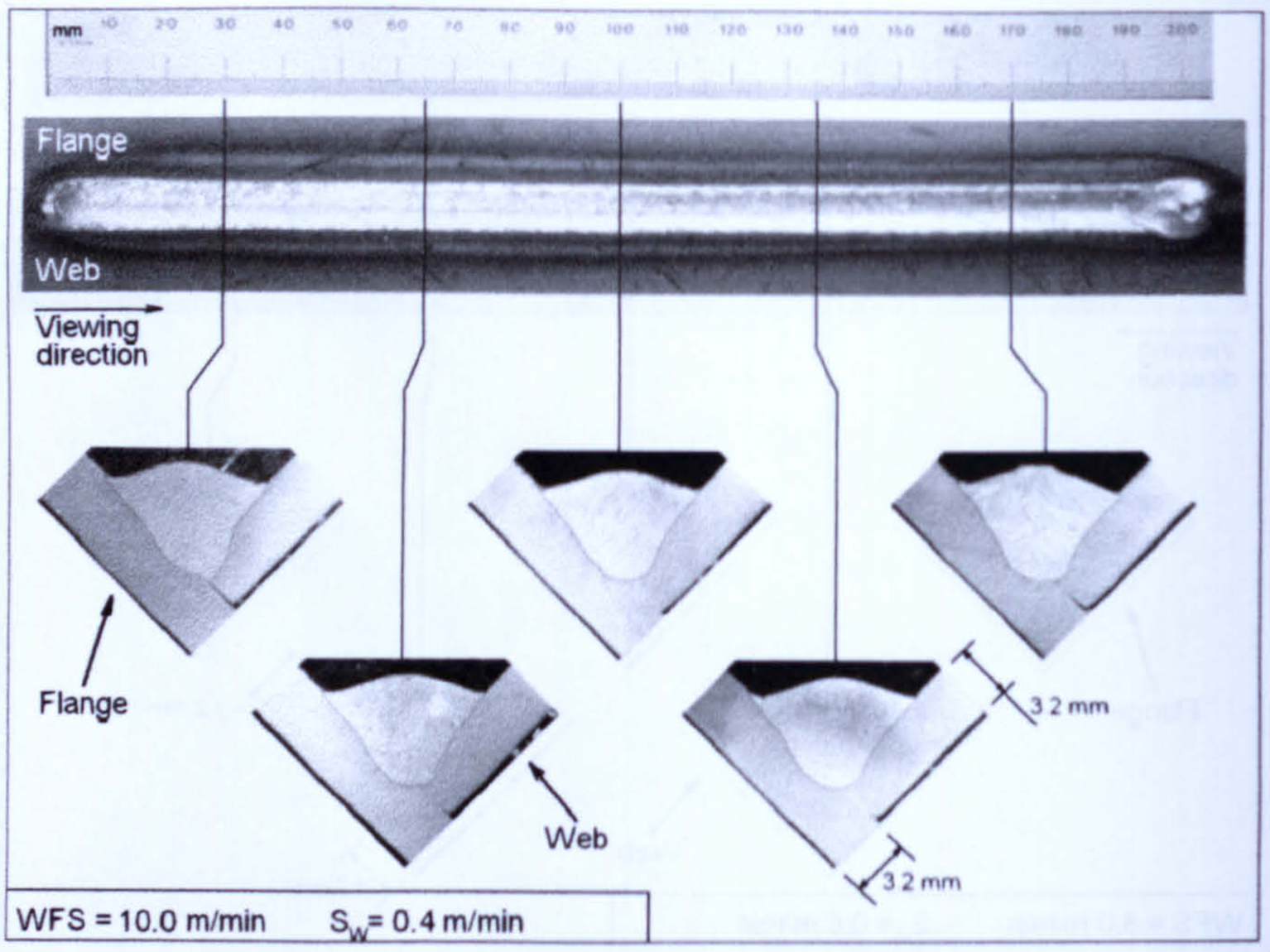

Figure 7.17 - Bead appearance and bead profiles along the weld for the stand-off controlled fillet welding trial "S3".

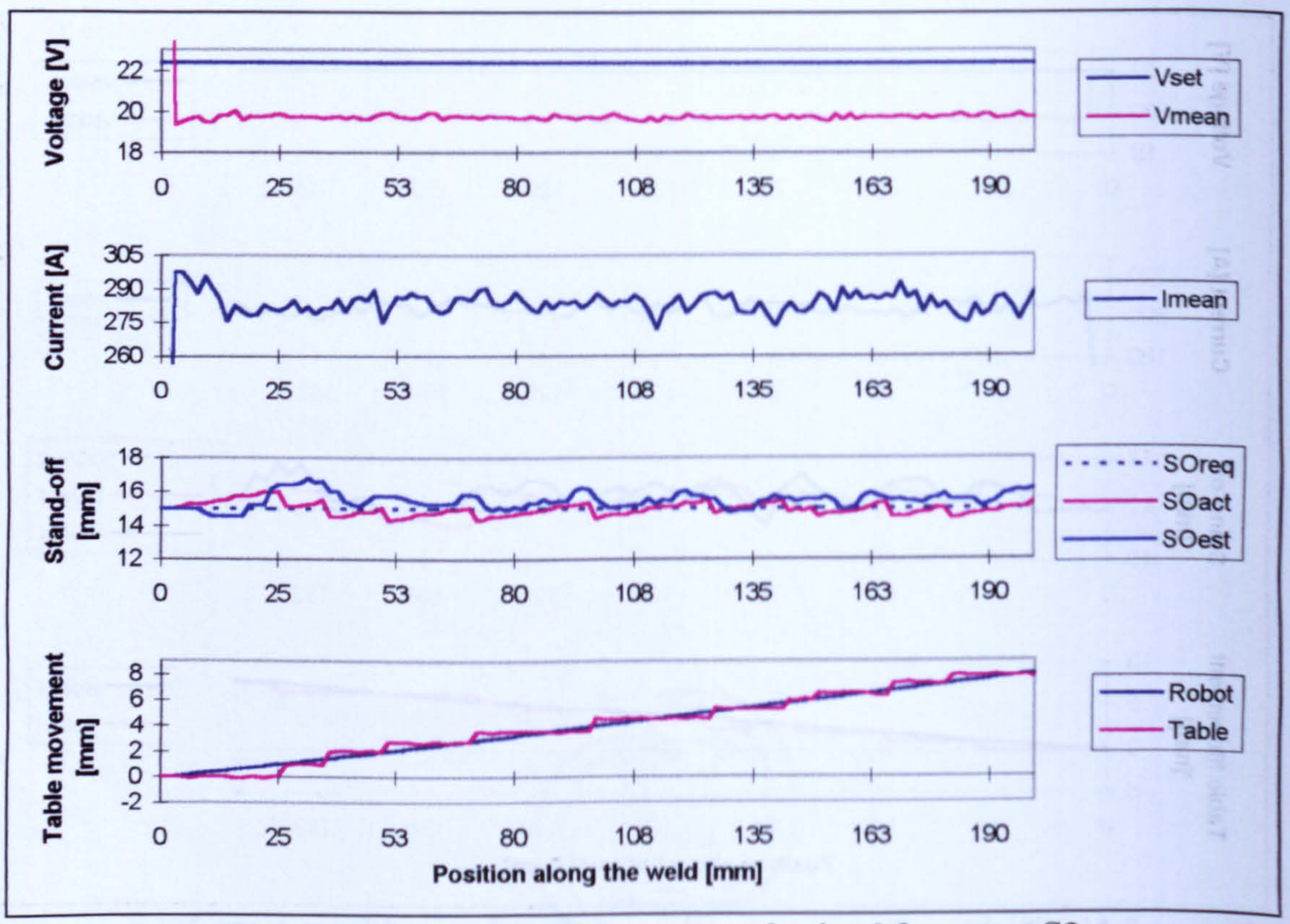

Figure 7.18 - Welding data and bead geometry obtained from test S3

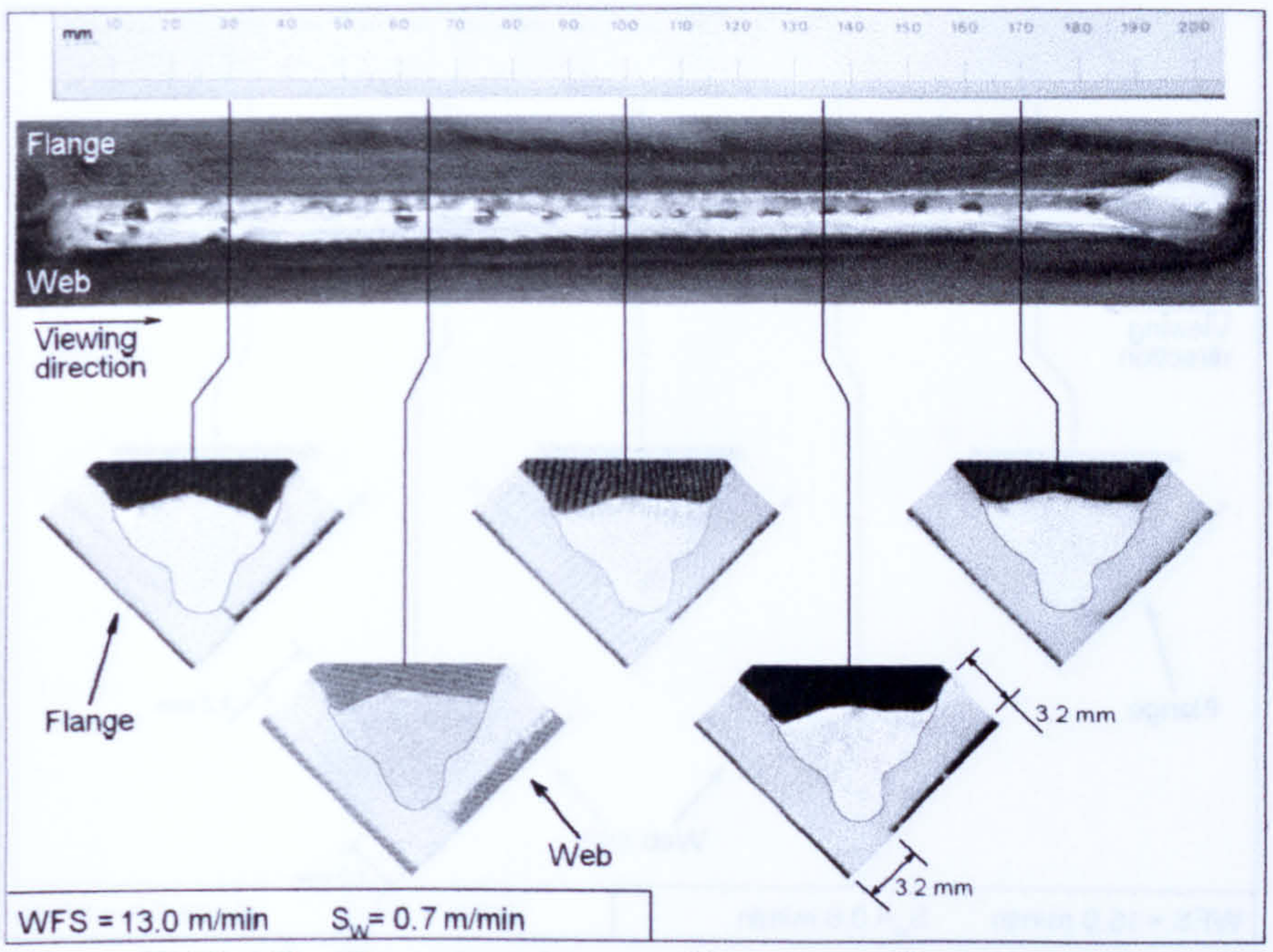

Figure 7.19 - Bead appearance and bead profiles along the weld for the stand-off controlled fillet welding trial "S5".

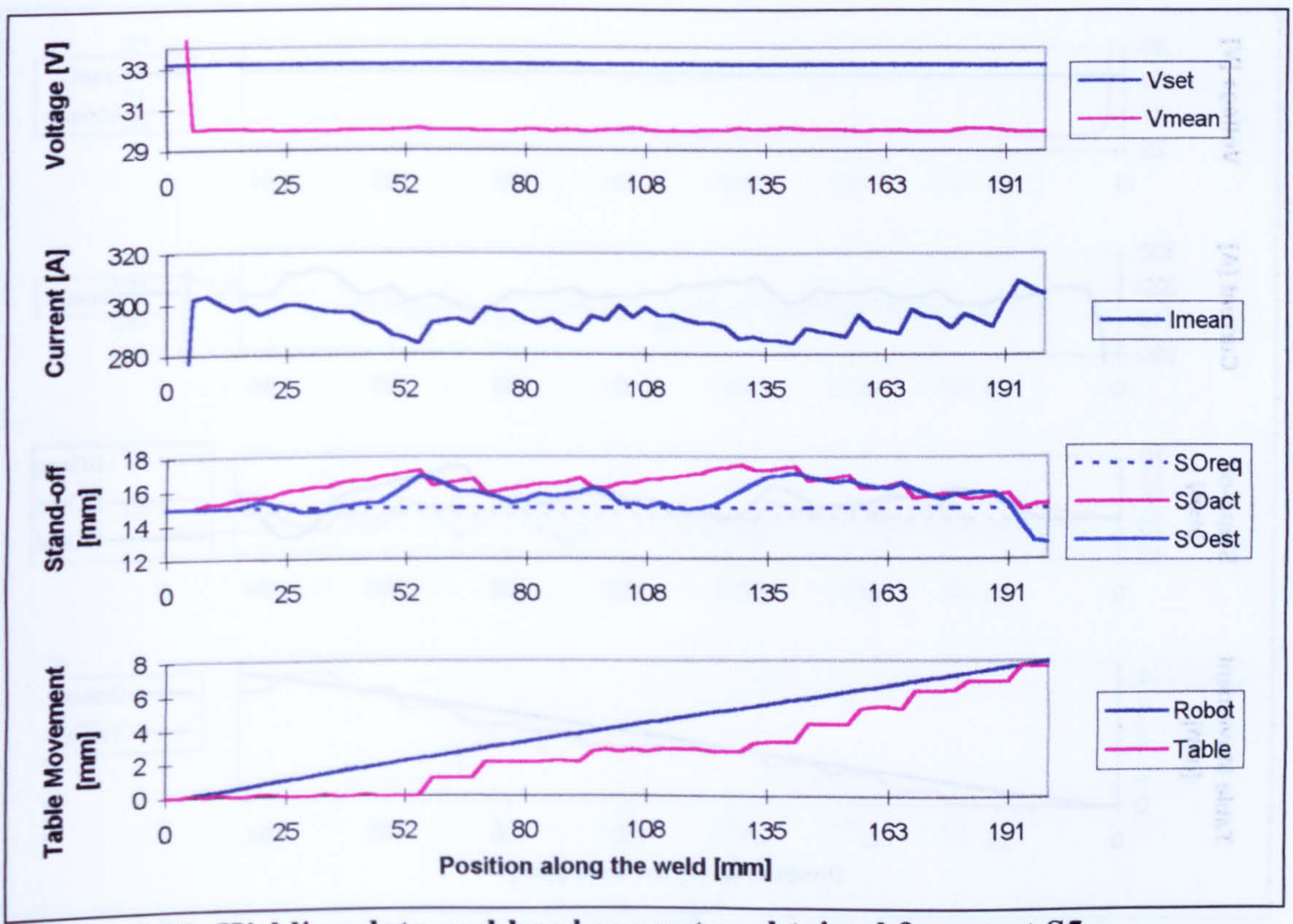

Figure 7.20 -Welding data and bead geometry obtained from test S5

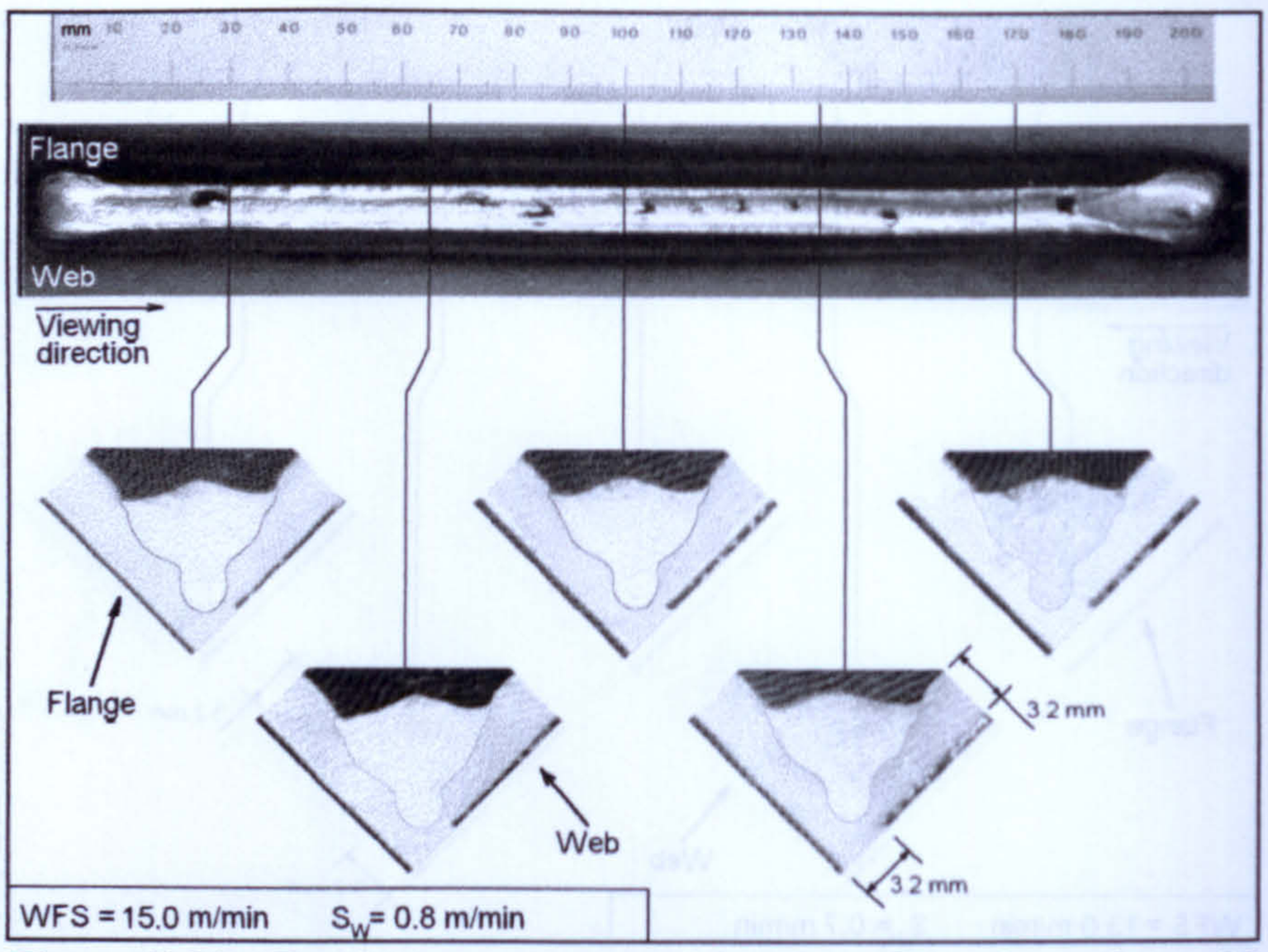

Figure 7.21 - Bead appearance and bead profiles along the weld for the stand-off controlled fillet welding trial "S6".

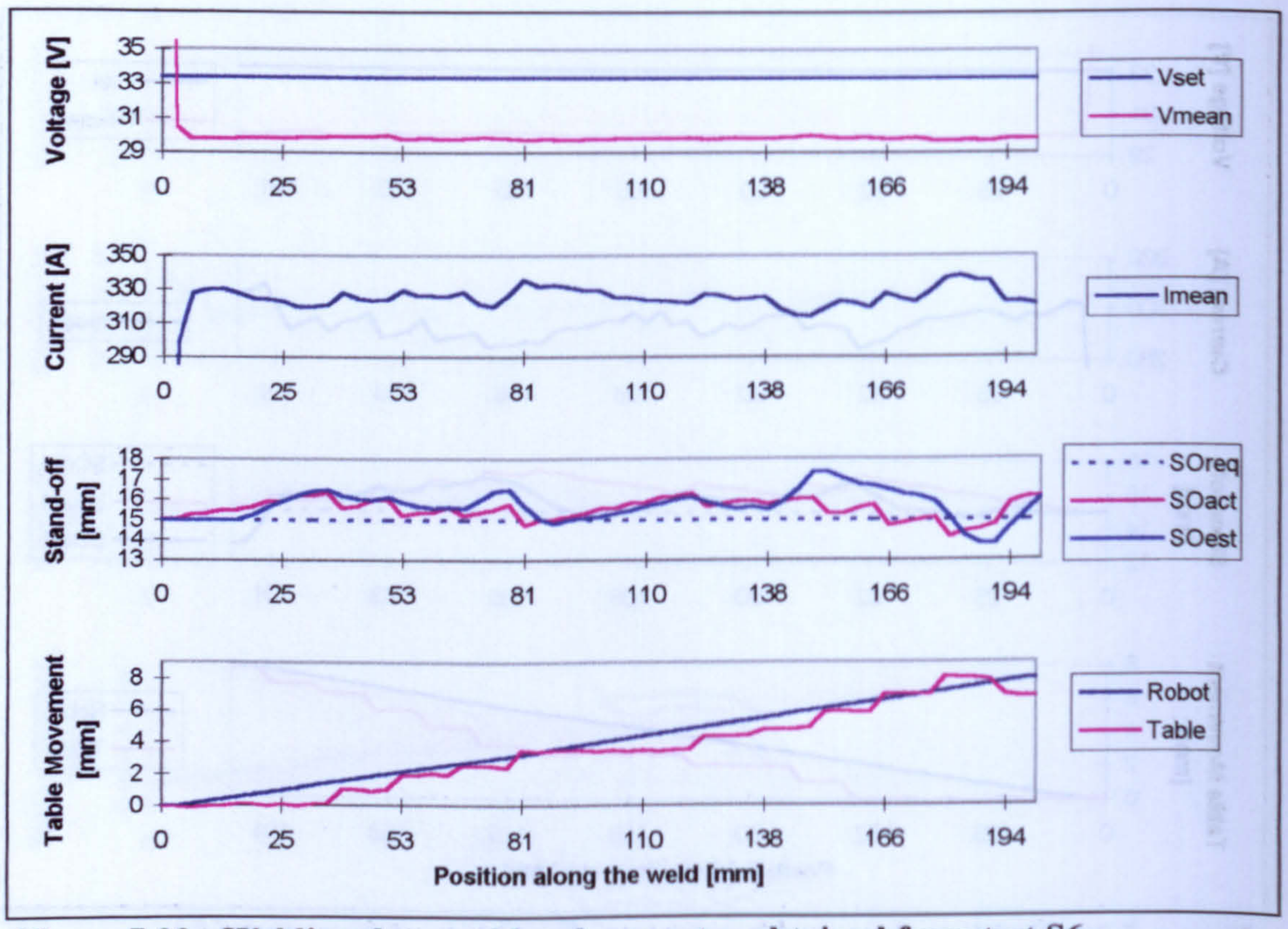

Figure 7.22 - Welding data and bead geometry obtained from test S6

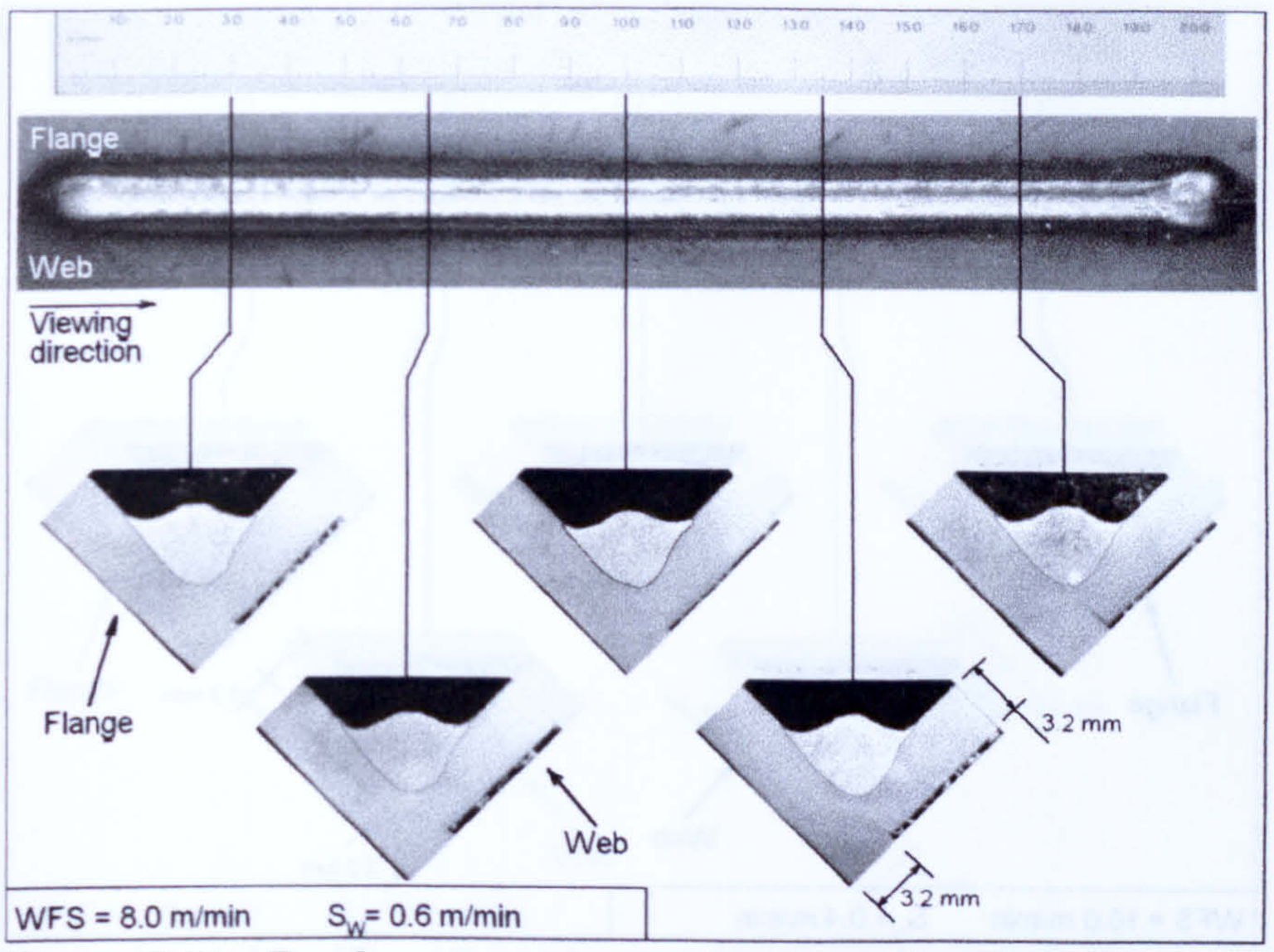

Figure 7.23 - Bead appearance and bead profiles along the weld for the voltage and stand-off controlled welding trial "SV2".

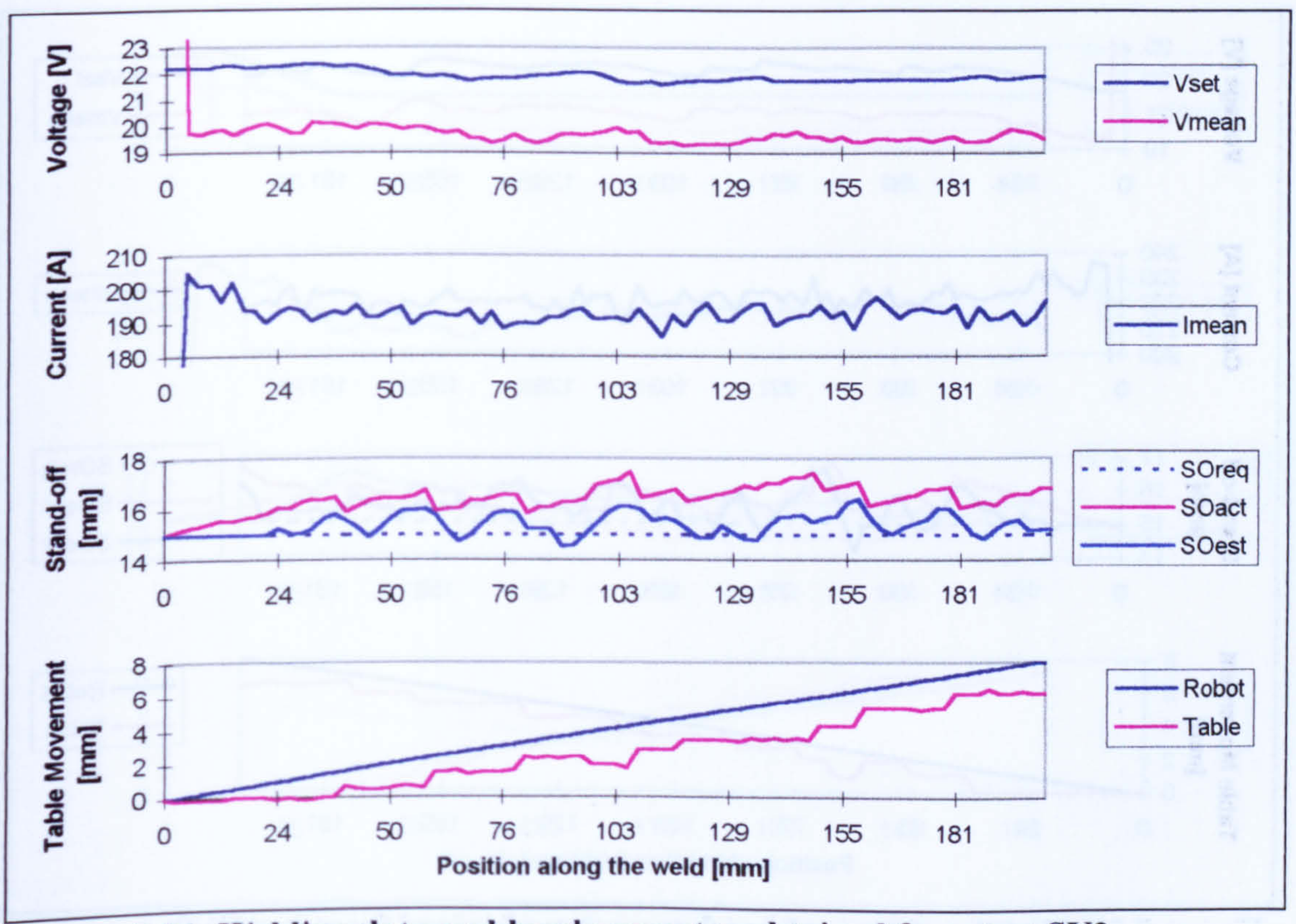

Figure 7.24 -Welding data and bead geometry obtained from test SV2

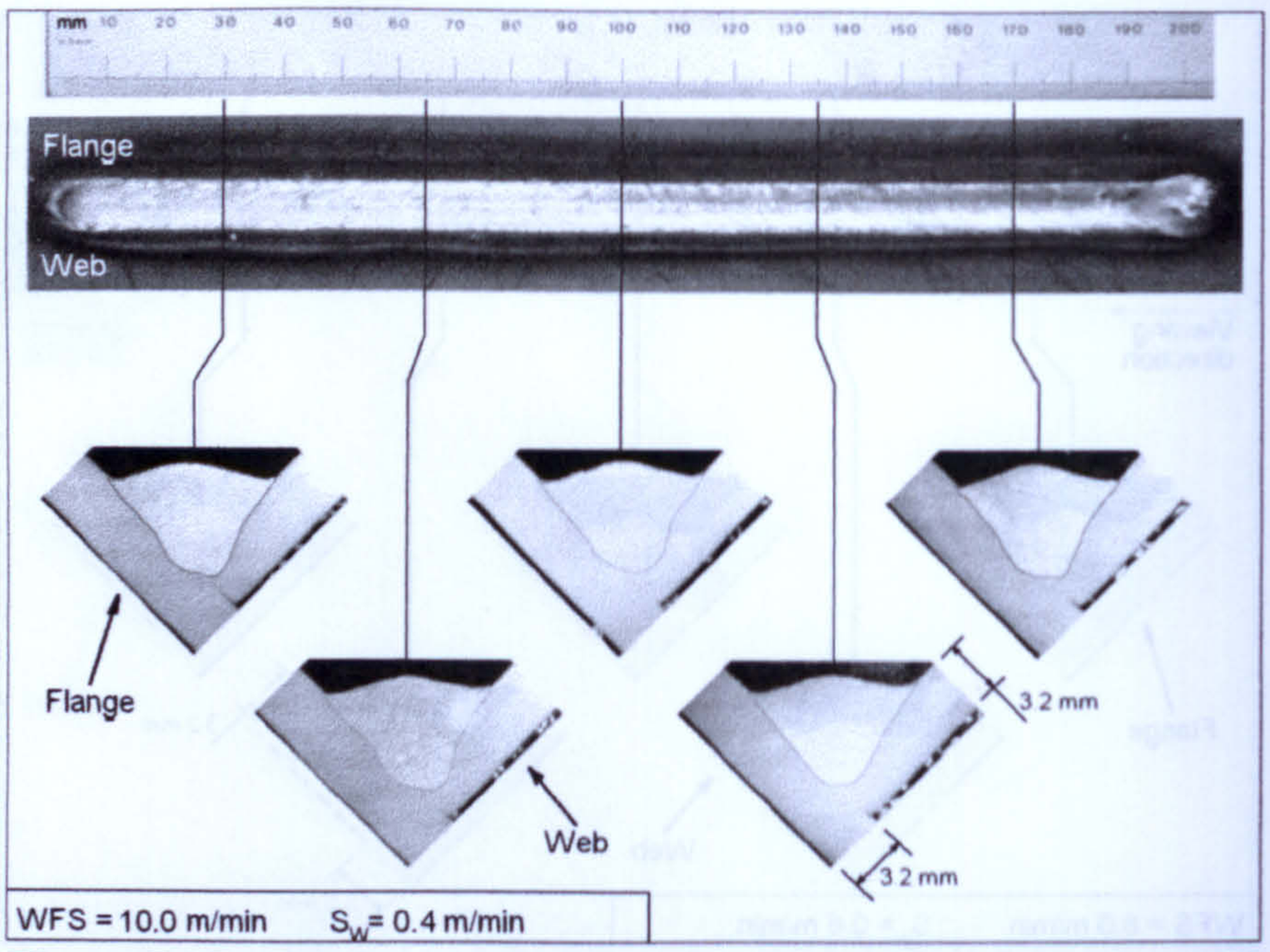

Figure 7.25 - Bead appearance and bead profiles along the weld for the voltage and stand-off controlled welding trial "SV3"

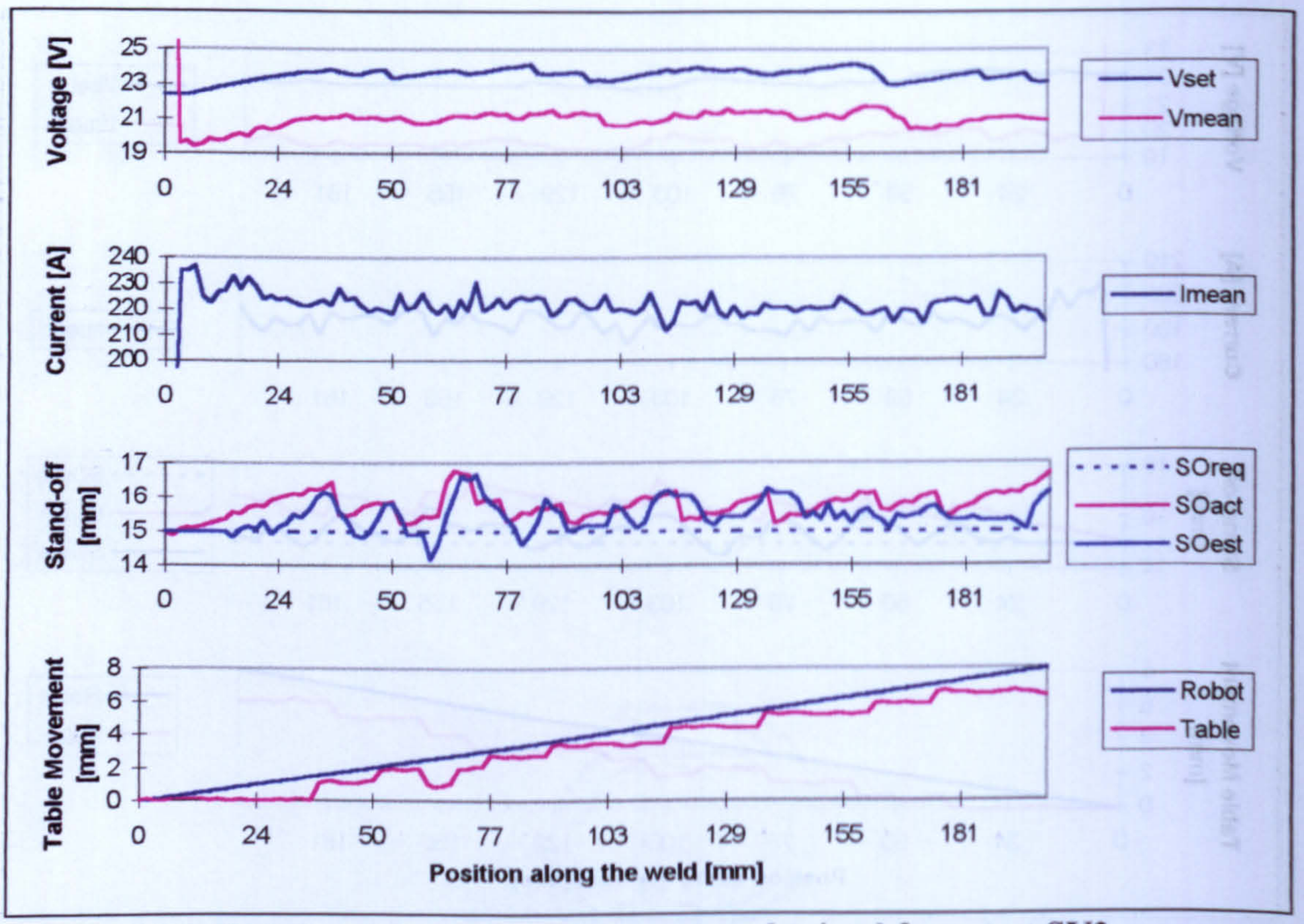

Figure 7.26 -Welding data and bead geometry obtained from test SV3

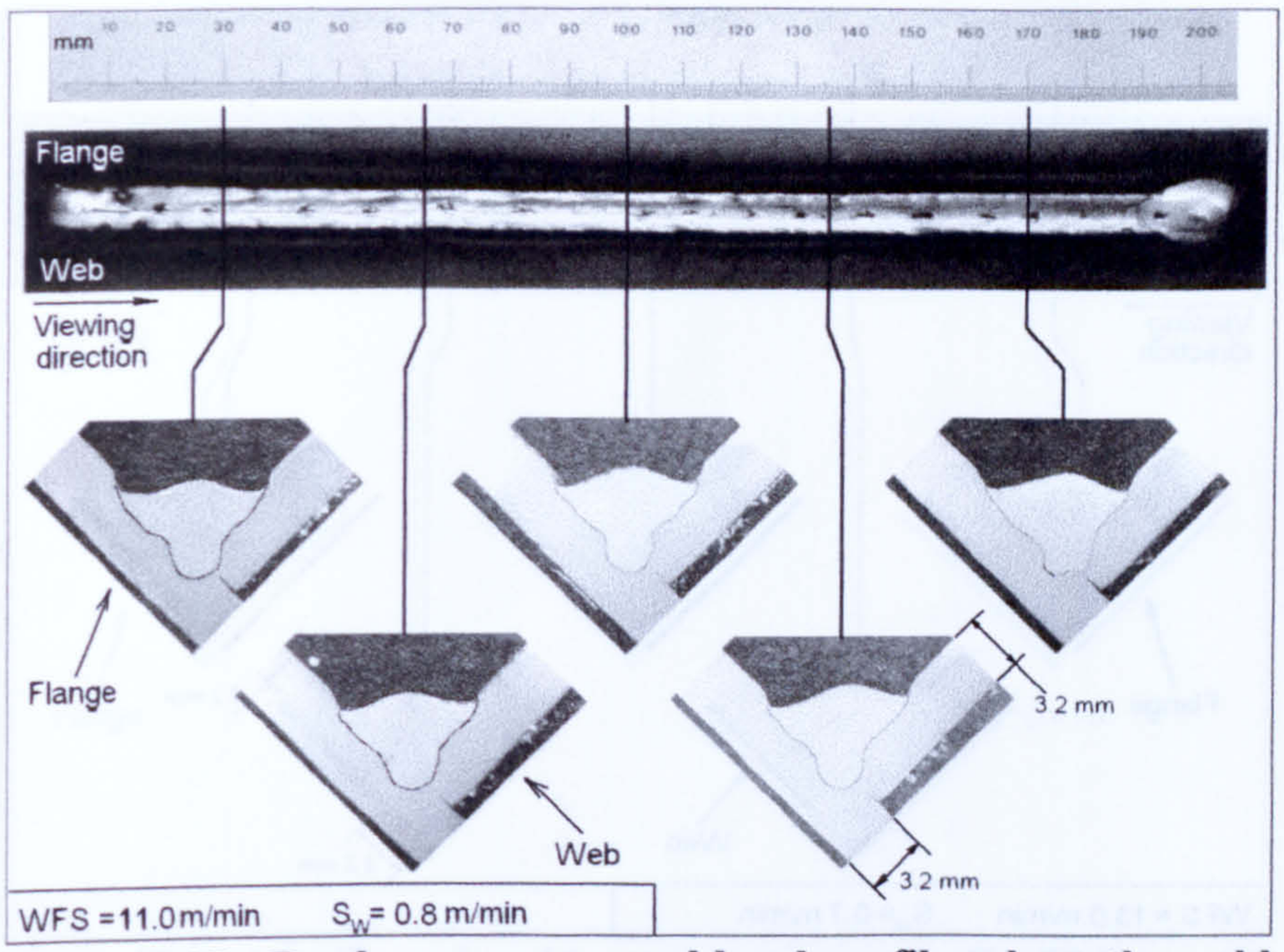

Figure 7.27 - Bead appearance and bead profiles along the weld for the voltage and stand-off controlled welding trial SV4.

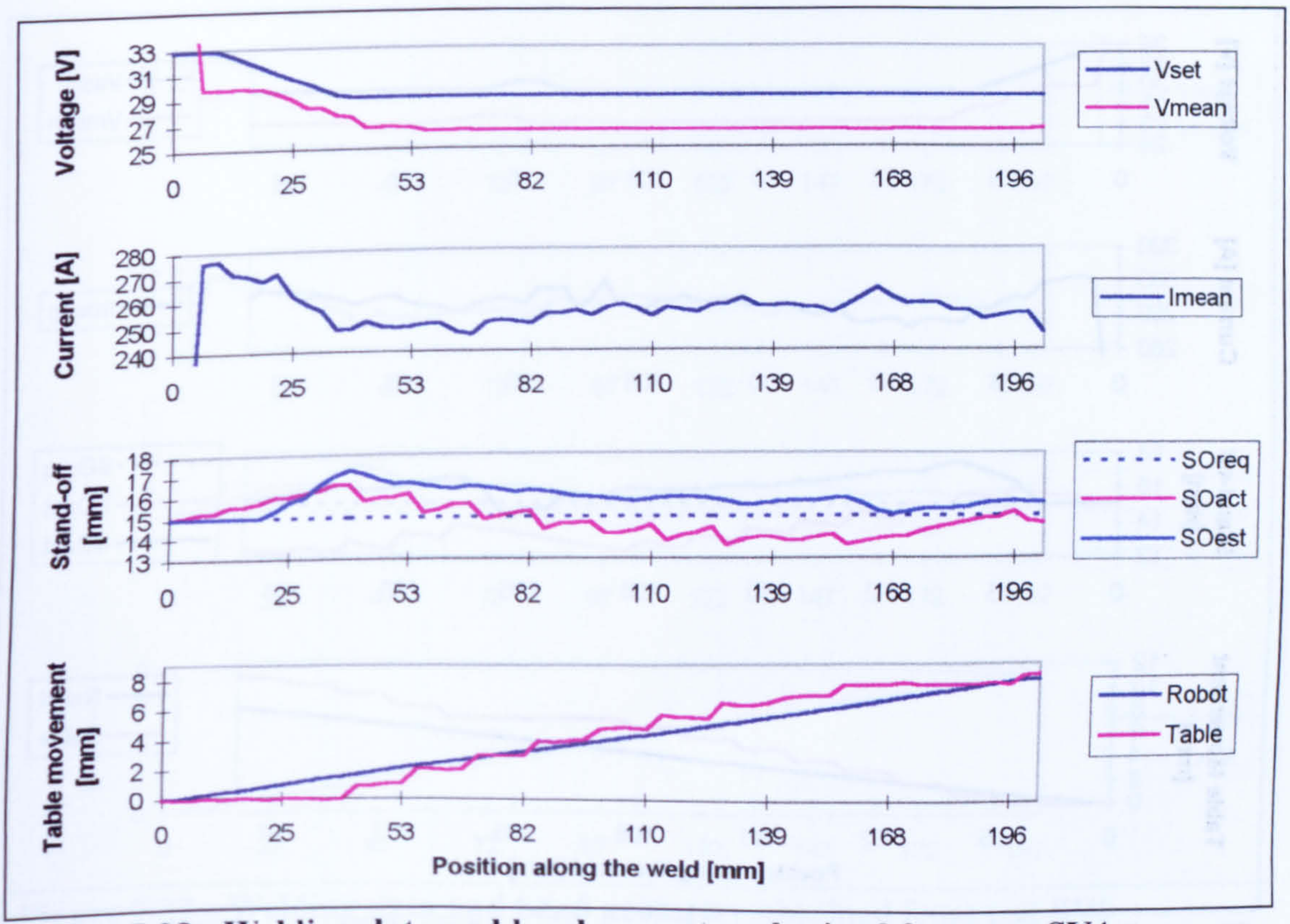

Figure 7.28 - Welding data and bead geometry obtained from test SV4

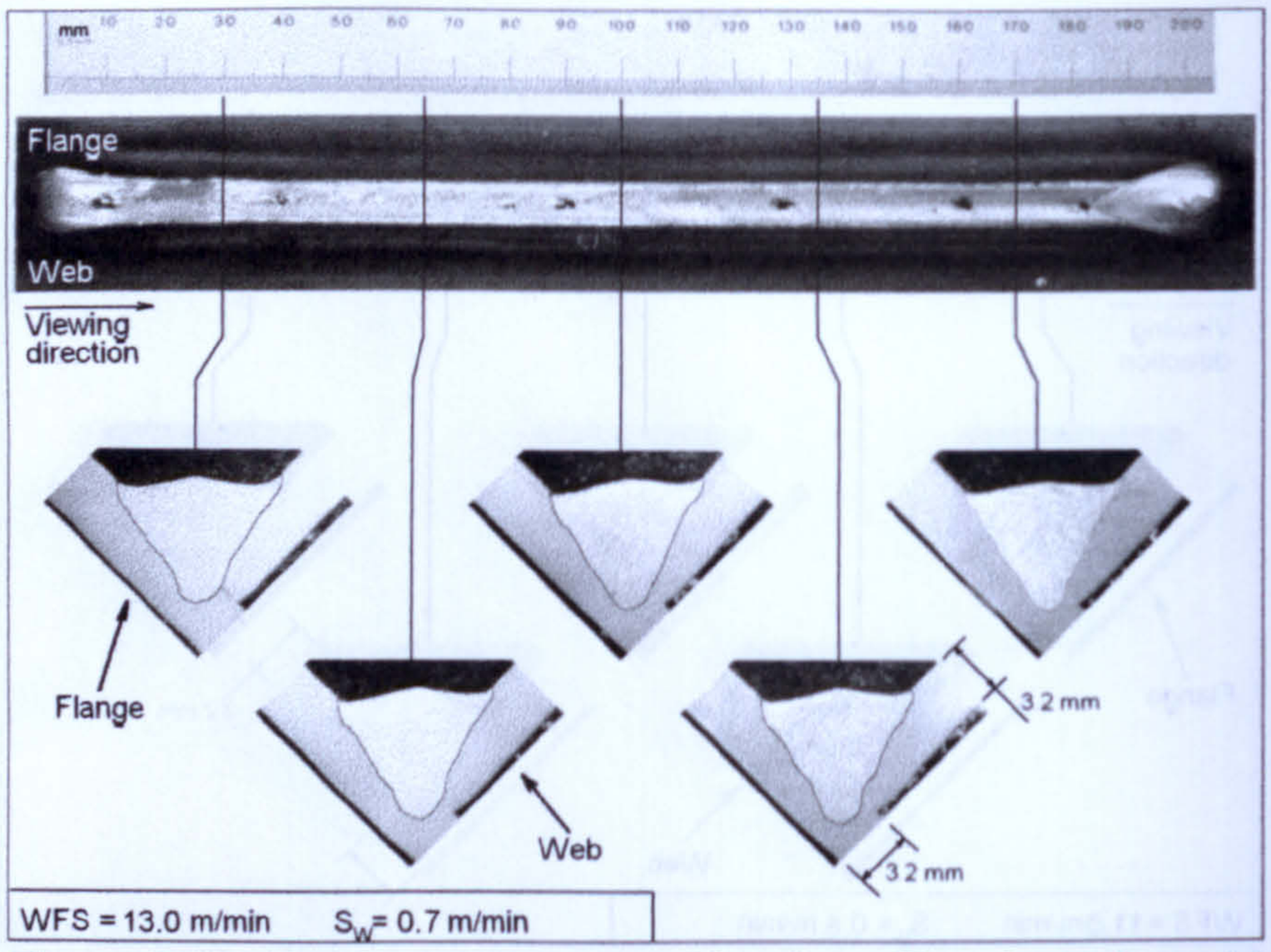

Figure 7.29 - Bead appearance and bead profiles along the weld for the voltage and stand-off controlled welding trial "SV5".

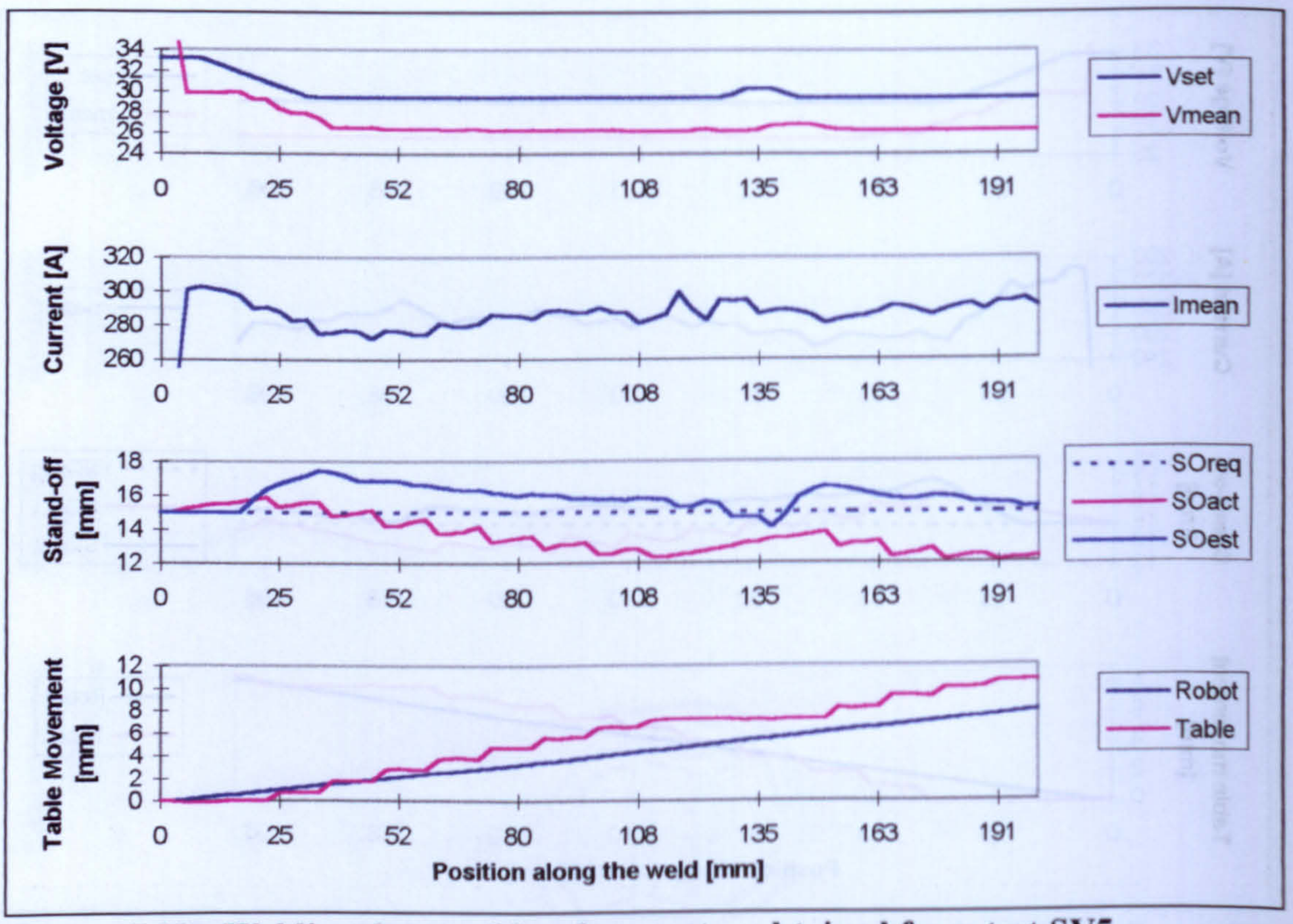

Figure 7.30 - Welding data and bead geometry obtained from test SV5

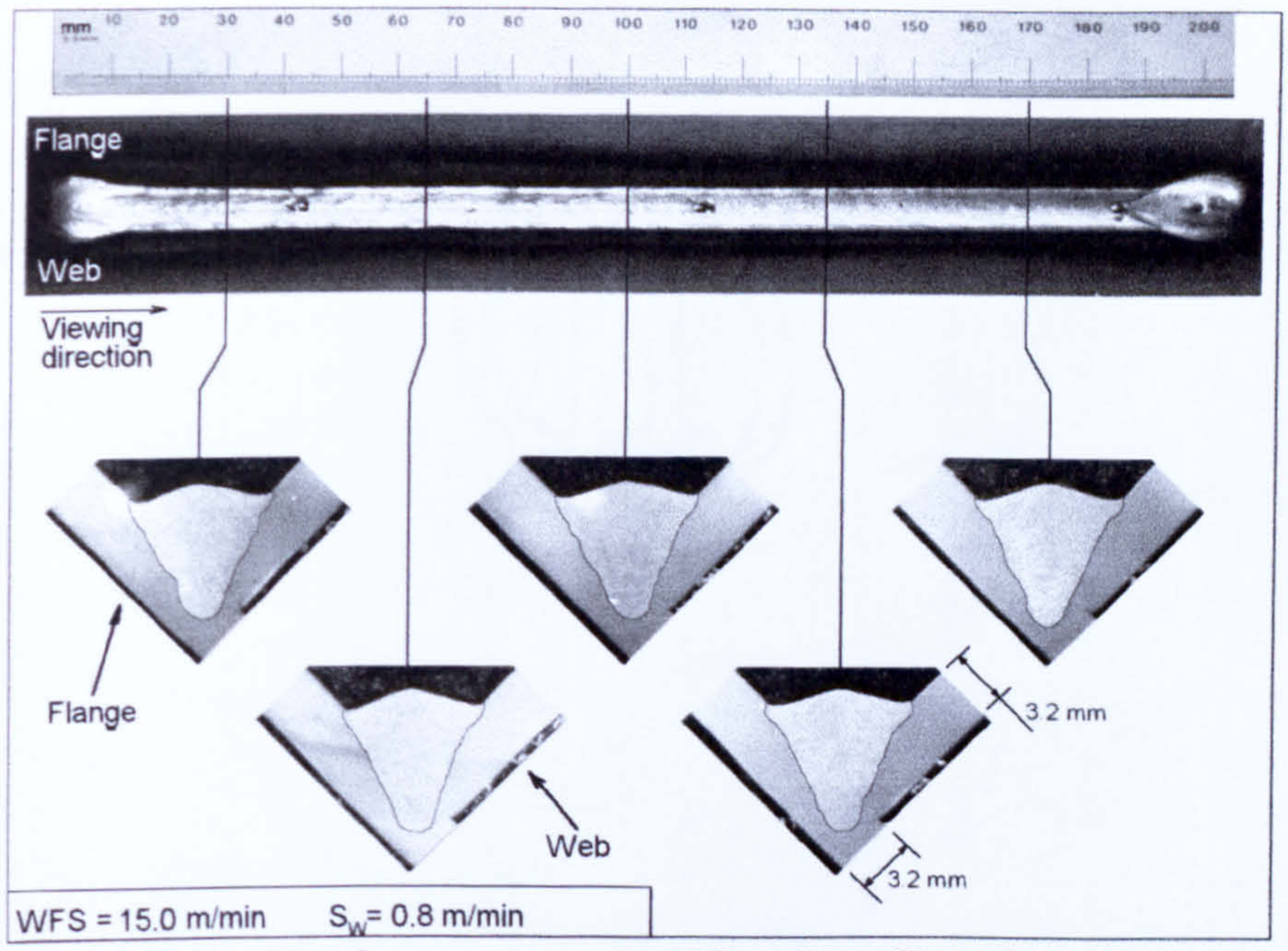

Figure 7.31 - Bead appearance and bead profiles along the weld for the voltage and stand-off controlled welding trial "SV6".

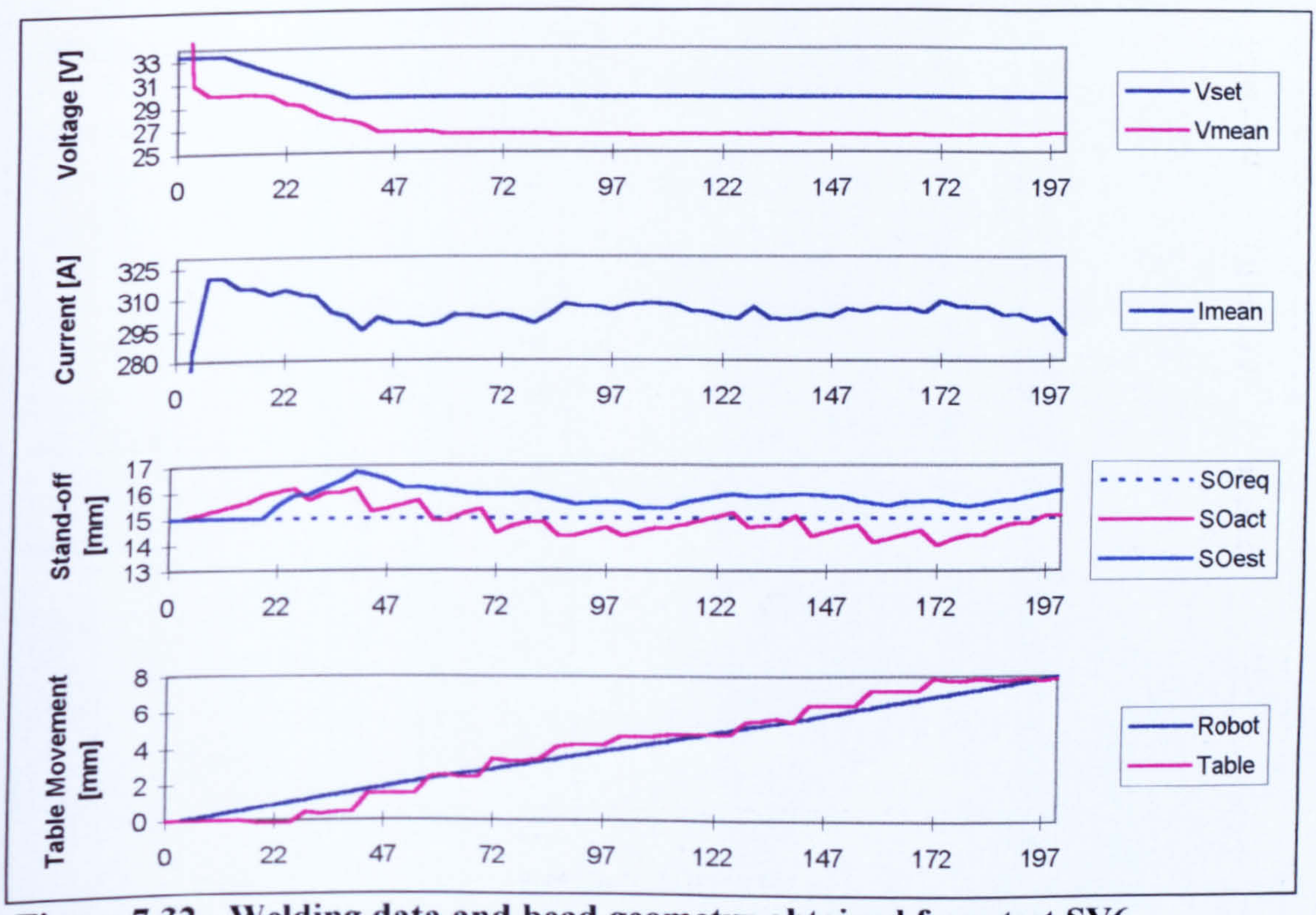

Figure 7.32 - Welding data and bead geometry obtained from test SV6

8. Discussion

8.1 Introduction

The aim of this work was to develop an integration concept between robot off-line programming, welded component design, welding procedure generation, process monitoring and adaptive control to ensure weld quality in robotic gas metal arc welding of thin sheet steel. Based on this concept, a self-adjusting system capable of adapting the off-line generated robot program to changes in the welding cell environment as well as performing position and process monitoring and control was implemented.

Robot off-line programming has received increased attention due to its obvious potential in increasing robot productivity by not stopping the production for robot programming. However, this technique has not been widely adopted by the industry due to positional and process related errors (see Chapter 3) which makes the off-line generated program inaccurate and, therefore, requires further calibration before satisfactory welds can be produced.

Generally, most of the errors that occur are due to changes in the robot environment but sometimes improper selection of power source set-up welding parameters and/or differences between the welding wire or shielding gas batches may cause an inadequate weld quality to be produced. This could, however, be compensated for by on-line fine tuning of the welding parameters.

Although several off-line programming systems are reported in the literature, very few are specifically designed for welding. Most of the available systems do not incorporate any welding knowledge or expertise; generally the task of setting the welding procedure is left to the user. Only one published work [ref. **85**] was found that reports a fully automated system that was able to generate the robot program from the part geometrical data contained in CAD drawings and select the welding procedure which satisfies the appropriate welding code from a previously stored procedure database. This system was designed, however, for a very specific task, which was welding bridge panels normally consisting of heavy gauge fillet joints. No process monitoring and control was reported to be used apart from a spin-arc system used for seam tracking.

The analysis of the current state-of-the-art of off-line programming for arc welding applications clearly showed the need for an integrated system that allows off-line programming to be used without the need for calibration and incorporating a means of monitoring and controlling the quality of the weld.

Based on this analysis, the following objectives were defined in order to produce the integrated system:

- to identify the sources of error and propose corrective measures;
- to incorporate welding models into a CAD system, that is integrating the weld design and the welding procedure generation;
- to generate positional data for off-line programming based on the CAD model of the part and on the geometry of the welding cell;

- to design and build the hardware necessary for on-line monitoring and control;
- to develop a sensor for pre-weld position adjustment;
- to develop monitoring algorithms for metal transfer, process stability and stand-off;
- to develop a robot independent part positioning system giving precise stand-off control.

8.2 Robot off-line programming

8.2.1 Analysis of sources of error

The analysis of the possible sources of error and corresponding corrective actions have shown that their detrimental effect could be reduced or eliminated (see Chapter 3). For a better understanding of the nature of each possible source of error, the errors identified were classified into three main groups, namely: (a) Robot errors, (b) Programming errors and (c) Component errors.

The robot error group included those errors caused mainly by the positioning hardware, including the robot itself and the positioning table, when present. The programming errors included mainly the inaccuracy in the geometrical models used to represent the robot and its environment in the computer "virtual world". They also included the errors caused by using an inadequate inverse kinematics algorithm to calculate the robot joint angles. Although very different in nature, these two error groups presented the similarity of having a means to reduce or even eliminate their detrimental effect. The robot errors could be greatly reduced by using robot calibration techniques [ref. **94**]. The programming errors could also be reduced by correcting the robot model using the parameters obtained from the calibration procedures and the robot environment model using the positional data which could be obtained utilising the calibrated robot as a measuring tool [ref. **88, 92**].

The component error group included the errors due to part, joint fit-up and fixturing tolerances and also due to wire cast, contact-tip wear, thermal distortion and part positioning. Despite not being all originated at the components themselves, these errors often affect the relative positioning between the tip of the welding wire and the joint line and also the geometry of the joint in the form of gap and misalignment. Their detrimental effect have the similarity of being variable and not always possible to predict. Therefore, some form of process and relative position monitoring and control is needed in order to minimise or eliminate their detrimental effect on weld quality.

Since robot calibration techniques are relatively well established, existing methodology [refs. **94**], such as the one implemented using the RoboTrak system [ref. **97**], could be used to correct for the robot and the programming errors. Hence, this present work has concentrated only on compensating for the errors originated in the component error group.

8.2.2 Integration between geometrical design and weld design

In order to illustrate how the geometrical data available in the component CAD drawings could be used to generate positional data for off-line programming and how welding models could be used to generate welding procedures, a special program, written in AutoLisp programming language, was developed to be utilised as an AutoCAD application. The program was designed for linear fillet joints and consists of two main modules: (a) welding parameters generator and (b) robot programming module. Both modules and the algorithms used in the modules are fully described in sections 3.3.2.1 and 3.3.2.2.

The welding parameters generator uses an adaptation of the algorithm developed by Ogunbiyi [ref. **51**] to predict welding parameters which are expected to produce the required weld quality. It outputs a list containing all the possible combinations of welding parameters which are expected to produce the required quality, giving the user the option of selecting the preferred combination based on criteria such as possible risk of defects (e.g. undercut) or productivity requirements (e.g. minimum welding speed).

The algorithm in this work was implemented in a flexible way that allows the use of different coefficients for the welding models. Each set of coefficients is stored in a specific file, in a special format (see Appendix B). Before the user starts defining a weld, he must choose the set of coefficients (defined by the combination of shielding gas, wire type, jigging system and power source), which correspond to the actual welding cell. Ideally, this means that new model coefficients should be obtained for each different combination, implying more welding trials. This could be viewed as a restriction to the implementation of the method.

However, the process controller developed in this work incorporates an automatic voltage tuning algorithm designed to optimise the welding voltage (see sections 4.2 and 7.1), which means that fewer welding trials would be needed to develop new welding procedures, even if different power sources, welding wires and shielding gas types were used [refs. **35, 199**]. Also, based on conclusions from previous work by Luijendijk and Hermans [ref. **29**], which state that for Argon rich gases with 5% to 20% CO_2 there are no significant changes in the short circuiting frequency and deposition rate, it could be assumed that no further welding trials would be necessary to define new coefficients for gases in this range (Ar +5% to 20% CO_2), if all the other variables are kept constant.

8.2.3 Extraction of positional data for off-line programming

The advantage of integrating the off-line programming into the CAD system is that it makes it possible to directly extract the joint geometry data[1] and transform it into a suitable robot path. The software developed in this work used the solid modelling techniques provided by the AutoCAD Modelling Extension (AME) to define the weld joint. The joint line was obtained by extracting the geometrical data from the intersection line between two adjacent semi-planes which formed a fillet joint.

---

[1] Joint position and orientation, joint length and start and end points.

Although only linear joints were implemented in this work, it should be noted that non-linear joints could also be included for off-line programming by sub-dividing the non-linear curves obtained from the intersection between two adjacent surfaces into small linear segments and treating these as a series of successive linear joints. This could increase the application scope of the program to deal with, for example, fillet welds in pipe sections. It should also be noted that the currently available robots are limited to linear and circular interpolation. That is, they can only perform ruled paths either passing through specified points in the form of a line between two teach-points or an arc passing through a third teach-point located between the teach-points which define the start and end of the arc. Hence, a non-linear non-circular robot path can only be defined as a series of successive linear paths with the torch orientation changing linearly between the teach-points.

The benefit of integrating the welding procedure generation and the geometrical data extraction for off-line programming into the CAD software is that the resulting welding data[2] and the weld positional data[3] can be stored in the same CAD drawing file in the form of data associated with the line segment which defined the weld joint. Therefore, if a different welding cell and robot is used, the only modification needed for generating the new robot teach-points would be the definition of the CAD-to-Robot transformation matrix. It should be noted that the definition of this transformation matrix depends on a set of points which are located using the robot.

The orientation of the torch relative to the joint line was set by default as being perpendicular to the joint line at the point being defined (start or end point) and contained in the joint bisection plane. For example, for a 90 deg included angle flat position fillet joint, the default orientation would be parallel to the gravitational vector. This orientation could be changed by the user if required.

Also, an offset for the position of the weld start and end points along the joint line was introduced to ensure that there would always be base material to receive the weld metal. No transversal tolerance was allowed, however this could be easily implemented. This could be necessary for welding steels with different heat sink characteristics in each side of the joint.

The rules used to generate the orientation necessary for the welding torch to achieve different joint approach and withdrawing directions were devised from prior on-line programming experience of a welding robot with a specific torch configuration. Therefore, for a different robot/welding torch combination, a modification in the angles of the planes defining the different orientation regions would be necessary (see section 3.3.2.2).

The teach-points defining the welding torch approach and withdrawing paths relative to the joint were generated based on the assumption that the component, once fixed in the jigging system, would not be moved until the completion of the welding operation. This implies that the component clearance box (see section 3.3.2.2) would also be fixed and, therefore, the approach and withdrawing points and vectors. However, different rules could be defined in situations where the component

---

[2] Required welding quality and chosen welding procedure

[3] Relative to the CAD coordinates frame.

orientation can be modified to improve the welding process, but this was not implemented in this work.

Although the implemented software was also designed to generate the robot program in ARLA language, this capability was only introduced to give the user the logical sequence of events necessary for the accomplishment of the positioning and external communication tasks. The actual implementation of the off-line generated programs was not carried out due to the fact that the available welding robot did not have any off-line programming facilities. However, it is well established that this can be performed if suitable robot hardware and communications programs are available [refs. **196, 197**]. The programs generated were tested by simulation in software using Workspace[4] versions 3.2 and 3.3. This was carried out manually "step-by-step", taking the robot through the teach-points according to the order required in the generated program. This proved the programs viable and the assumed torch orientations adequate.

The logic sequence of inputs and outputs was successfully tested using an on-line programmed robot and the sequence presented the expected performance. It should be noted that the input/output sequence was the only means of communication between the robot and the external equipment.

8.3 Process modelling

8.3.1 Models used in the welding parameters generator

The main objective of the modelling work in this project was to obtain models to predict the bead geometry, the risk of defects (undercut, burn-through, lack of fusion), the stability characteristics of the process and the levels of welding current and voltage suitable for producing a stable process.

The modelling work by Ogunbiyi [ref. **51**] was used as the starting point for the development of the welding parameter generator. This was initially based on models developed for the Migatronic BDH320 welding power source, using BOC Argonshield 5 shielding gas and 1 mm mild steel wire (A18-8). However, in this work, a different power source (Migatronic BDH550) was used. The specifications for both power sources are shown in Appendix H.

The welding parameters obtained using the BDH320 models, which have been proven to produce stable process [ref. **51**], did not produce stable welding conditions with the BDH550. Analysis of the welding data acquired using the data acquisition system (see Chapter 5) showed that BDH550 delivers a welding voltage that is approximately 91% of the required power source set-up voltage (see Figure 6.1). According to Ogunbiyi, the BDH320 produces a welding voltage which was not significantly different from the power source set-up voltage. The power source (BDH550) also delivers a higher current level for the same set-up wire feed speed and stand-off compared to BDH320 (see Figures 6.2 to 6.3). This resulted in bad ignition, spatter generation, unstable arc and poor bead appearance, mainly due to inadequate voltage setting. To overcome these, the models were adapted (see section 6.1) and a voltage controller was developed (see section 4.2). It should be noted that the models

---

[4] Robot Simulations Ltd., UK.

for predicting possibility of bad arc ignition and possibility of undercut were applied directly, without modification.

In adapting the models, new welding trials were carried out using the BDH550. The range of welding parameters used in the trials was selected to cover the whole range of conditions normally used for gas metal arc welding thin sheet steel. The voltage levels were chosen to produce a stable process in all the trials. Models were then developed to map the behaviour of the BDH550, based on the set-up welding parameters and on the statistical features (see equations 2.25 to 2.32) extracted from each welding trial. The welding data was analysed using the multiple regression analysis tools provided by Statgraphics[5] and the model structures proposed by Ogunbiyi [ref. **51**] were adopted. In order to reduce the number of experimental trials, the welding speed was fixed at 500 mm/min.

Simple linear regression models were used to calibrate the leg length and weld penetration prediction models developed by Ogunbiyi [ref. **51**] so that they could fit the corresponding measurements obtained in this work. This model calibration was necessary[6] to compensate or account for differences in the heat sink provided by the jigging system, the welding position and the welding power source. It should be noted that Ogunbiyi's models were developed for horizontal-vertical fillet joints whereas in this work the flat position was used. Due to the different welding positions and in order to reduce the masking effect caused by bead misalignment, the calibration functions were obtained considering the average values of the geometrical features of interest (i.e. average leg length and average penetration).

The BDH550 models and the bead geometry calibration models (see section 6.1) were successfully used in the welding parameter generator. Although calibrated, the penetration model was still imprecise, a fact which was also observed by Ogunbiyi [ref. **51**]. However, considering that the quality criteria for penetration are quite flexible [refs. **107, 190**] and that penetration is normally assessed as either adequate or inadequate, the output of the model was found to be acceptable.

The models developed were used to predict bead geometry and welding parameters in both dip and spray metal transfer modes. Although the bead and the penetration profile in both modes are essentially different, a single model was used to map welds from both modes of metal transfer. This was due to the fact that it is difficult to establish a limit above which a determined mode of metal transfer should predominate and, in addition, it is sometimes beneficial to use mixed mode transfer.

8.3.2 Stand-off estimation models

The stand-off estimation model proposed by Ogunbiyi [ref. **51**] (see equations 2.21 to 2.24) was initially implemented. Taking into consideration the differences in power sources, a new welding current model was built for the BDH550 using the model structure utilised by Ogunbiyi [ref. **51**]. This model was a function of the power source set-up voltage, the stand-off and the wire feed speed (see equation 6.4). However, during the stand-off model (see equation 2.22) validation trials (see

---

[5] PC software for statistical analysis

[6] A similar approach has been previously used by Doherty and Plummer [ref. **198**] to calibrate a welding rig.

Appendix J), it was observed that the proportionality constant ϕ used in equation 2.22 and calculated using equation 6.5 differs from the measured value (see Figure 6.9). The value of the difference observed was found to be dependent on the wire feed speed and the mode of metal transfer.

This observed inaccuracy in the estimation of ϕ was possibly caused by the fact that the model does not fully describe the non-linearities present in the process. Also, the model (see equation 2.21) is not a theoretical model but an empirical one and the model inversion carried out could be a possible source of error.

While adequate for indicating changes in stand-off, Ogunbiyi's model does not provide the accuracy and robustness necessary for control purposes, especially when using low wire feed speed dip transfer (see Figure 6.9).

Previous work by Philpott [ref. **131**] has shown that the dip-resistance can be used for stand-off monitoring. Based on this, a method for monitoring the dip resistance was developed and the dip resistance measurements were correlated to stand-off variation. A stand-off estimation model based on the dip resistance was developed and used in conjunction with the windowing technique developed by Chawla [ref. **161**] (see section 2.6.3).

The dip resistance based stand-off estimation model was found to be less sensitive to process instabilities in dip transfer because it uses the resistance measured during the short circuiting phase only. Hence, voltage and current spikes do not affect the prediction as was the case in the Ogunbiyi's model (see Figures 6.15 to 6.24).

It should be noted that the model proposed by Ogunbiyi used an integral approach[7] to reduce the effect of random variation commonly observed in the welding current. However, the use of the integral approach makes the model very sensitive to the stability of the process at the start of the welding. Also, Ogunbiyi's model only outputs estimated changes in the stand-off while the dip resistance based model produces an absolute stand-off estimation.

The dip resistance model was also extended to the spray transfer mode, the only difference being that, in this mode, the measured resistance also included a component due to the welding arc (see section 6.2 and Figures 6.13, 6.14 and 6.25 to 6.27).

The stand-off models for dip and spray transfer were validated successfully for bead-on-plate welding trials. However, when transferred to fillet joints in the flat position, it was observed that the models would produce a prediction smaller than the actual stand-off by a constant average value. This was hypothesised to be caused by the weld pool build-up under the welding arc which occurs due to the restricted flow of the molten metal resulting from the geometry of the fillet joint. This was confirmed by changing the deposition rate and comparing the resulting estimation errors (see Figure 6.29). In order to compensate for the weld pool constriction effect found in fillet joints, the offset in the stand-off prediction (illustrated in Figure 6.29) was estimated at the start of the weld and its value was added to the subsequent estimations (see section 6.2). It should be noted, however, that this approach can only be applied if the initial stand-off is known, as was the case in this work. Good results were obtained for the fillet weld trials (see Figures 7.6 to 7.14).

---

[7] Characterised by the use of a cumulative summation of the differences between successive welding current values.

8.4 Process monitoring and control

It is well established that through-the-arc sensing can be used for prediction, monitoring and control of arc welding (see section 2.6). In this work, through-the-arc sensing was used for assessing process stability and metal transfer, and for estimating stand-off. The aspects involved in the stand-off estimation have been discussed in section 8.3.2. The process stability and the mode of metal transfer were assessed using the monitoring indices developed by Ogunbiyi [ref. **51**]. These indices were found to be useful in assessing the stability state of the process by flagging up phenomena such as bad arc ignition, excessive spatter and excessive fuming and for providing an objective way of characterising the mode of metal transfer (see section 4.2.1). They also give an indication of whether an inappropriate voltage for the set wire feed speed is being used and whether an increase or decrease in the voltage level is necessary to bring the process to an acceptable stability level (see Figure 4.2). Therefore, they were used to develop the voltage controller (see section 4.2.1).

The monitoring of process stability was very important, since a reliable stand-off estimation would depend on the process stability. The stand-off estimation models (welding current cumulative differences and dip-resistance based models) were implemented in such a way that they would only update the estimated values if a pre-determined level of stability, estimated by using the *Confidence of Bad Ignition* model (see section 4.2.3), was assured.

Two different controllers were integrated together in this work, one addresses the positioning of the welding torch relative to the workpiece and the other addresses the attainment and maintenance of the process stability.

8.4.1 Position controller

The control of relative position (stand-off) between the welding torch and the workpiece was performed using an independent workpiece positioning table. This approach was adopted after extensive consideration of the options available for implementing relative position control between the welding torch and the workpiece during the robot program run-time (see sections 4.1.1 and 4.1.2).

The position control was performed by pre-weld searching the joint starting point and in-process adjusting of the joint position so that it would follow the programmed robot movement. The position controller was implemented making the assumption that any programming errors had been corrected prior to welding and that the robot and the welding cell had been properly calibrated. Although not critical, the assumption that the robot had been calibrated was important to ensure that the joint positioning errors would be due mainly to the component errors. It should be noted that component errors are relatively small and normally restricted by the manufacturing tolerances (see section 3.1.1.3). Also, the position controller is constrained by the fact that the moving table has a limited range of movement, implying that it can only compensate for errors within this range.

Only one degree of freedom was implemented in the position controller in order to demonstrate that the positioning errors between the weld joint and the programmed weld path can be minimised or corrected by adjusting the joint position.

It should be noted, however, that this is not a complete solution to the problem, since further degrees of freedom would be needed to provide seam tracking, if a proper sensor was available.

In this work, a touch sensor was developed to provide pre-weld joint search capabilities to the system. The touch of the welding wire on the workpiece was detected by measuring the parallel combination of the power source internal resistance and the wire-to-workpiece resistance. The parallel combination would have either the value of the power source internal resistance or zero, when the welding wire touched the workpiece. This parallel combination was connected in series with a fixed resistor and the resulting combination was made an arm of a Wheatstone bridge circuit (see Section 5.5 and Figure 5.1). This would become unbalanced in the event of a touch between the welding wire and the workpiece, thus generating a detection signal. Although this design was effective in the laboratory controlled trials, it cannot be used in a non-controlled environment without modification to the circuit, since the low voltage used (7.5 V dc) might not be enough to overcome the insulating effect caused by grease, oxidation and/or dirt normally present in the industrial environment.

The position control was based on the stand-off estimation provided by the dip resistance based models. Depending on the mode of metal transfer (dip or spray), a suitable model was chosen by the control software (see Section 6.2). A third order moving average filter was used to reduce the noise present in the estimation. Also, a "forgetting" property was introduced in this filter in order to prevent the controller from responding to signals that have been dealt with before. This was accomplished by resetting the filter every time a filtered stand-off estimate was sent to the table controller and only sending a new filtered value after obtaining three new non-filtered estimates (see section 4.2.4). Threshold values were introduced in the position controller so that it would only respond to errors greater than 0.5 mm and the maximum correction per cycle was limited to 1 mm. This resulted in good performance without oscillation (see Figures 7.15 to 7.32). However, the performance was found to be affected by the travel speed. This was due to the limit imposed on the maximum correction per cycle, which restricted the table movement to a maximum average speed of 1.3 mm/s. This speed was dependent on the time taken to acquire each "window of data" and on the speed of the processing hardware. A faster speed could have been obtained if a higher sampling frequency (in spray transfer) was used and if a faster hardware was available.

The use of an independent controller for the moving table in this work can be viewed as an added complication to a welding cell. However, considering the fact that on-line robot position adjustment is only possible when allowed by the robot manufacturers and usually only with their own specific sensing hardware, this perceived added complexity then becomes very important by giving added flexibility to the system.

8.4.2 Welding process control

The welding process control strategy in this work was implemented in two stages, namely: (a) the off-line optimisation of the welding parameters and (b) the on-line tuning of the welding voltage and control of stand-off. The off-line optimisation was used to predict the welding parameters which would produce a weld that would

satisfy the required quality criteria (see section 3.3.2.1). The on-line voltage tuning was used to ensure that an adequate voltage level would be attained and maintained throughout the welding process (see Section 4.2). Good results were obtained with the voltage controller (see Section 7.1).

The voltage controller presented in Section 4.2 is a combination of fuzzy control and rule based incremental control. The use of this incremental control architecture ensured that the controller would always achieve a stable state. The time taken to reach the stable state is, however, dependent on how far the process is from stability and also on the voltage increment size used in each control cycle and on the control cycle duration. This includes the monitoring/processing time and the power source response delay.

Although not implemented in this work, control of deposition rate by adjusting wire feed speed and/or travel speed could be introduced if sensor(s) for measuring gap and bead geometry were available [ref. **183**]. In cases when the robot does not allow on-line speed correction, the wire feed speed could be used to adjust the deposition rate. However, a change in wire feed speed could lead the process to an unstable condition. A synergic control scheme could be used for adjusting the welding voltage to a level close to the new stability region and the automatic voltage tuning algorithm could be used to fine tune the voltage, thus restoring the process stability.

Tests were performed in flat position fillet joints with no control, only stand-off control (i.e. without voltage control) and both controls (stand-off and voltage) acting together. All tests started using the off-line optimised welding parameters. From the non controlled trials it can be seen that the process is very robust to changes in stand-off. For example, changing the stand-off from 12 mm to 20 mm in dip transfer and from 15 mm to 23 mm in spray transfer resulted in a small reduction in the average penetration: from 0.78 mm to 0.46 mm in dip transfer and from 2.04 mm to 1.47 mm in spray transfer (see Table 7.2). The minimum penetration values obtained would still satisfy the minimum quality requirement for penetration.

The welding parameters generated for fillet welds using spray transfer resulted in porosity, undercut and pronounced finger-like penetration profile (see Figures 7.9 to 7.13 and 7.19 to 7.21) due to excessive voltage. Analysis shows that the prediction of these welding parameters is due to the fact that the threshold of the undercut model was too high (see Section 3.3.2.1), thus allowing these inadequate conditions. If the threshold value of Pr(*und*) was reduced to 0.16, these conditions would have not been predicted. The results show that for the plate thickness used (3.2mm) Pr(*und*)= 0.293, 0.162 and 0.196 (runs M4, M5 and M6 in Table 7.1) correspond to an average maximum[8] undercut depth of 0.41, 0.36 and 0.20 mm respectively. The use of these spray conditions, however, allowed the capabilities of the control system to be demonstrated.

The results show that the control of stand-off and voltage reduces the depth of undercut (see Table 7.5), eliminates porosity (see Figure 7.27) and produces a more consistent weld. A surprising result in this work was the marked influence of the voltage control on the finger like penetration profile observed in spray mode (see Figures 7.29 and 7.31). The penetration profile changed from a pronounced finger like

[8] Average of the maximum undercut depth of sections cut along the weld length

profile to a more uniform profile. Also, a greater depth of penetration[9] in the workpiece was observed in all the stand-off and voltage controlled spray transfer trials, despite lower welding voltages and currents being applied. The change in the bead profile and the increase in fusion depth were possibly caused by a change in the fluid flow and heat transfer mechanisms inside the weld pool. Such a change was probably due to a more efficient transfer of power from the arc and the molten droplets which resulted from the reduced arc length and the more constricted arc [refs. **6, 32, 202**]. It should be noted, however, that a detailed study of penetration mechanism was beyond the scope of this work.

8.5 The significance of this work

The proposed strategy of moving the workpiece in order to adapt to positioning errors between the weld joint and the programmed robot welding path provides a flexible way of compensating for positioning errors independently of the type of robot being used. This gives rise to the possibility of development of adaptive jigging systems.

The main benefit of the automatic voltage tuning method developed in this work is that it could reduce for the power source manufacturers the time and effort used in developing synergic welding curves for different gases and wires, by automatically setting up the welding voltage. It is noted that most power sources already have voltage trim facility, the effective use of which requires (and depends on) skilled welder(s). The results of this research work show that the voltage control method developed could be used to replace the trim facility, thus ensuring that an unskilled welder could still produce good quality welds.

The integration of welding procedure generation into a CAD software makes it possible to use the component geometrical data and the welding information for optimising component design and productivity. For example, by using simulation it would be possible to determine the welding procedures and the sequence of welds in a component that would result in the highest production rate.

---

[9] Measured axially to the arc from the joint line (intersection between joint adjacent surfaces) towards the base plate.

9. Conclusions and Recommendations for Further Work

9.1 Conclusions

The following conclusions can be drawn from this research work.

1. Using only through-the-arc sensing, an integrated stand-off and voltage controller has been implemented for gas metal arc welding of thin sheet steel.

2. A novel rule based metal transfer and welding voltage control technique has been developed and successfully implemented in a robotic gas metal arc welding cell.

3. A novel through-the-arc dip resistance monitoring technique for stand-off estimation has been devised for use in dip and spray modes of metal transfer.

4. A position control strategy was implemented to demonstrate the feasibility of using a robot independent part positioner for adjusting the weld joint location, without changing the programmed robot path.

5. An architecture for integrating component design, off-line programming, welding procedure generation and adaptive control has been proposed.

6. Robot and cell calibration are important issues when using off-line programming.

7. The possible sources of error in off-line programmed robotic welding were identified and corrective measures proposed.

8. Component geometrical data available in CAD drawings can be used to generate the co-ordinates of the points defining a robot path for welding.

9. A simple wire touch sensor has been developed for use in a laboratory controlled environment for pre-weld joint location.

9.2 Recommendations for further work

This project has demonstrated the possibility of developing a flexible off-line programming and control system for robotic gas metal arc welding of thin sheet. The following further work is suggested.

9.2.1 Development of welding models to deal with other types of joints

In order to make the welding procedure generator more flexible and expand its application scope, welding models describing the relationship between the input variables (set-up welding parameters) and the geometrical characteristics of other

types of joints and multi-pass welds should be developed and integrated in the off-line programming system.

9.2.2 Integration of simulation tools into the CAD software and support for non-linear joints.

Using the standard AutoCAD programming facilities, robot simulation tools could be developed and integrated into the software, thus providing visualization of the welding cell without the need for a different simulation sofware.

Also, the introduction of programming techniques for non-linear joints would give a more general applicability to the software.

9.2.3 Development/integration of robust sensors for seam tracking and gap detection, and implementation of further axes in the joint positioner.

In order to make the system applicable to the real industrial environment, further controllable axes should be integrated into the moving table. The control of all the integrated axes would depend on the information provided by the stand-off estimation model together with the measurements of lateral deviation and gap size provided by suitable sensors. The integration of currently available sensors or the development of new sensors give a wide scope for research of measurement and control strategies. The sensor arrangement proposed in Appendix D would be a good starting point.

9.2.4 Experimental and theoretical study of the influence of welding voltage on the weld pool formation in fillet joints.

In view of the penetration profile obtained in the controlled spray transfer trials (see Figures 7.29 and 7.31) a more specific theoretical and experimental study of the influence of the welding voltage on the heat transfer and fluid flow mechanisms inside the weld pool would provide a better understanding of the physical aspects involved on the weld bead formation.

References

[1] LLOYD, B. Robot Facts 1994 : Annual report of UK investment in robot automation in manufacturing industry. BRA report, 1995.

[2] O'BRIEN, R.L. (ed.) Welding Handbook. 8th ed. Miami: American Welding Society, 1991, vol. 2, 109-154.

[3] NORRISH, J. Advanced Welding Processes. Bristol: Institute of Physics, 1992.

[4] BLOT, R. **A guide to shielding gases for gas metal arc welding**. *Welding Quarterly*, September, 1988, 12-15.

[5] NORRISH, J. AND RICHARDSON, I **Metal transfer mechanisms**. *Welding and Metal Fabrication*, 56(1), Jan/Feb. 1988, 17-22.

[6] LANCASTER, J. F. (ed.) The physics of welding. Oxford: Pergamon Press, 1984, Chapter 7.

[7] USHIO, M. et al. **Effects of shielding gas composition on metal transfer phenomena in high current GMA welding**. *Transactions of Japan Welding Research Institute*, 20(1), 1993, 7-12.

[8] COOKSEY, C. J. and MILNER, D. R. **Metal transfer in gas shielded arc welding**. IN: "Physics of the Welding Arc", Institute of Welding Symposium, 29 Oct. to 2 Nov., 1962, 123-132.

[9] MA, J. and APPS, R.L. **Analysing metal transfer during MIG welding**. *Welding and Metal Fabrication*, 51(3), April 1983, 119-128.

[10] MA, J. and APPS, R.L. **New MIG process results from metal transfer mode control**. *Welding and Metal Fabrication*, 51(4), May 1983, 168-175.

[11] SICARD, P. and LEVINE, M.D. **An approach to an expert robot welding system**. *IEEE Transactions on Systems, Man and Cybernetics*, 18(2), March/April 1988, 204-222.

[12] DYURGEROV, N.G. **Causes of periodic short-circuiting of the arc gap during welding with a short arc**. *Welding Production*, 21(9), 1974, 1-4.

[13] HAMØY, E. **Wire melting rate, droplet temperature, and effective anode melting potential**. IN: Arc physics and weld pool behaviour : an international conference, 8-10 May 1979, London. Cambridge: Welding Institute, 1980, Vol. 1, 49-57.

[14] NEMCHINSKY, V.A. **The effect of the type of plasma gas on current constriction at the molten tip or an arc electrode.** *Journal of Physics D: Applied Physics*, 29(5), 1996, 1202-1208.

[15] RHEE, S. and KANNATEY-ASIBU, JR. **Observation of metal transfer during gas metal arc welding**. *Welding Journal*, 71(10), October 1992, 381s-386s.

[16] PATON, B.E., MANDEL'BERG, S.L. , SIDORENKO, B.G. **Certain special features of the formation of welds made at high speeds.** *Automatic Welding*, 24(8), 1971, 1-6.

[17] LEBEDEV, V.K. **Stability of the metal pool when thin metal is welded.** *Automatic Welding*, 28(6), 1975, 57-58.

[18] STOLBOV, V.I. and MASAKOV, V.V. **The formation of burn-through in the fusion welding of thin sheets.** *Welding Production*, 24(10), 1977, 26-28.

[19] PATON, B.E. and ZARUBA, I. I. **Peculiarities of arc discharge when welding with a short circuiting arc gap.** IN: "Physics of the Welding Arc", Institute of Welding Symposium, 29 Oct. to 2 Nov. 1962, London, 102-107.

[20] LAHNSTEINER, R. et al. *State of the art and definitions of the notions arc-stability, spattering and arc-striking characteristics.* IIW Document XII-1364-94.

[21] PHILPOTT, M.L. *Direct arc sensing for robotic MIG welding.* Cranfield Institute of Technology, PhD thesis, 1986.

[22] MODENESI, P.J. and NIXON, J.H. **Arc instability phenomena in GMA welding**. *Welding Journal*, 73(9), September 1994, 219s-224s.

[23] ZARUBA, I. I. **Condition for stability of processes in which welds are made with short-circuiting**. *Automatic Welding*, 24(2), 1971, 1-4.

[24] ZARUBA, I. I. et al. **The effects of current supply source dynamic properties on CO_2 welding using 2 mm diameter electrode wire.** *Automatic Welding*, 14(8), 1961, 28-37.

[25] ZARUBA, I. I. **Electrical explosions as the cause of metal spatter.** *Automatic Welding*, 23(3), 1970, 12-17.

[26] ZARUBA, I. I. **Factors governing metal spatter during welding with short-circuiting**. *Automatic Welding*, 27(8), 1974, 68.

[27] HUTT, G.A. , LUCAS, W. *Arc disturbances in consumable electrode welding - a review of the literature*. The Welding Institute, Research Report 173/1982.

[28] RODWELL, M.H. *A preliminary investigation into arc disturbances and poor weld appearance in the spray transfer MIG welding of stainless steel*. The Welding Institute, Research Report 273/1985.

[29] LUIJENDIJK, T. and HERMANS, M.J.M. **Short circuiting GMA welding with Ar-CO_2 gas mixtures**. *Welding Review International*, 15(3), August 1996, 91,94-95.

[30] OUDEN, G. den , XIAO, Y.H. , HERMANS, M.J.M. **The role of weld pool oscillation in arc welding**. *International Journal for the Joining of Materials*, 5(4), 1993, 123-129.

[31] HERMANS, M.J.M. , SIPKES, M.P. , OUDEN, G. den **Characteristic features of the short circuiting arc welding process**. *Welding Review International*, 12(2), 1993, 80-86.

[32] KIM, J. -W. and NA, S. -J. **A study on the effect of contact tube-to-workpiece distance on weld pool shape in gas metal arc welding**. *Welding Journal*, 74(5), May 1995, 141s-152s.

[33] LIU, S. , SIEWERT, T.A. **Metal transfer in gas metal arc welding: droplet rate**. *Welding Journal*, 68(2), 1989, 52s-58s.

[34] GUPTA, S.R. and GUPTA, P.C. **Effect of some variables on spatter loss**. *Welding and Metal Fabrication*, 52(9), November/December 1984, 361-362, 364.

[35] OGUNBIYI, T.E.B. and NORRISH, J. **GMAW metal transfer and arc stability assessment using monitoring indices**. IN: TWI Conference on Computer Technology in Welding, 9-12 June 1996, Lanaken, Belgium, Paper 11.

[36] NEEDHAM, J.C. **Control in short-circuit MIG arc welding**. IN: TWI International Conference on Advanced Welding Systems, 19-21 Nov. 1985, London, 331-339.

[37] MITA, T. , SAKABE, A. , YOKOO, T. **The estimation of arc stability on CO_2 gas shielded arc welding**. IN: TWI International Conference on Advanced Welding Systems, 19-21 Nov. 1985, London, 261-271.

[38] DILTHEY, U. , REICHELL, T. , SCHELLER, W. **Statistical process parameter surveillance in GMA welding**. *International Journal for the Joining of Materials*, 8(3), 1996, 120-126.

[39] SHINODA, T. , NISHIKAWA, H. **Monitoring and signal processing of short circuiting metal transfer of metal active gas welding process**. IN: JOM-7 International Conference on the Joining of Materials, 31 May - 2 June, 1995, Helsingør, Denmark, 558-565.

[40] SHINODA, T. , NISHIKAWA, H. , SHIMIZU, T. **The development of data processing and assessment of arc stability as affected by the titanium content of GMAW wires during metal transfer**. IN: TWI Conference on Computer Technology in Welding, 9-12 June, 1996, Lanaken, Belgium, Paper 57.

[41] DYURGEROV, N. **Bridge rupture between electrode and molten pool.** *Welding Production*, 19(3), 1972, 5-8.

[42] LEBEDEV, V. et al. *On technological (welding) properties of power sources for arc welding*. IIW Doc. USSR Academy of Sciences, USSR National Welding Committee, 1979.

[43] LIPEI, J. et al. **The effect of the dynamic behaviour of welding rectifiers on spatter**. *Welding International*, 2(3), 1988, 263-268.

[44] LEBEDEV, V. , SIDOREIKO, M. **The technological features of rectifiers for manual arc welding**. *Automatic Welding*, 16(7), 1963, 64-68.

[45] JENNINGS, C. **Dynamic characteristics of DC welding machines**. *Welding Journal*, 30(2), February 1951, 117-138.

[46] LEBEDEV, A. **Optimisation of parameters of the welding circuit in mechanised CO_2 welding**. *Paton Welding Journal*, 1(1), 1989, 36-39.

[47] VOROUIN, R. , GOLOSHCAPOV, S. **Evaluating the thin wire gas shielded arc welding process**. *Welding Production*, 16(9), 1969, 51-55.

[48] POPKOV, A. et al. **Reducing the spatter of liquid metal in CO_2 welding by means of optimisation of the welding parameters**. *Welding Production*, 24(3), 1977, 26-27.

[49] NEEDHAM, J. **Evolution of power sources in arc welding - transition from passive to active role**. *TWI Research Bulletin*, 28(4), April 1987, 113-118.

[50] GUPTA, S. et al. *Application of statistical analysis for process stability evaluation in GMA welding*. IIW Doc. 212.710-88, 1988.

[51] OGUNBIYI, T.E.B. *Process monitoring and adaptive quality control for robotic gas metal arc welding*. Cranfield University, PhD thesis, 1995.

[52] BRITISH STANDARD INSTITUTION: **Quality vocabulary**. BS4778 Part 1, 1987.

[53] OGUNBIYI, T.E.B. and NORRISH, J. **Procedure modelling for GMA robotic welding of thin sheet**. IN: JOM 5 - International Conference on the Joining of Materials, 1993, Helsingør, Denmark, (annex to conference proceedings).

[54] NORRISH, J. and OGUNBIYI, T.E.B. **An adaptive quality control concept for robotic GMA welding**. IN: TWI Conference on Computer Technology in Welding, 15-16 June, 1994, Paris, France, Paper 45.

[55] MOON, H-S. , NA, S-J. **A neuro-fuzzy approach to select welding conditions for welding quality improvement in horizontal fillet welding**. *Journal of Manufacturing Systems*, 15(6), 1996, 392-403.

[56] APPS, R.L. and NORRISH, J. *A flexible process control system for robotic MAG welding of sheet steel*. BRITE-EURAM CT91-0415, Synthesis Report for Publication, Project BE-4006-90, 1995.

[57] McMASTER, R.S. **Overview of robotic manufacture world-wide**. IN: WESTON, J. (ed.) Exploiting robots in arc welded fabrication. Cambridge: The Welding Institute, 1989, 11-15.

[58] SALTER, G.R. and WESTON, J. **Principles and terminology of robotic arc welding**. IN: WESTON, J. (ed.) Exploiting robots in arc welded fabrication. Cambridge: The Welding Institute, 1989, 16-21.

[59] YAMAMOTO, H. et al. **Improved current control makes inverters the power sources of choice**. *Welding Journal*, 76(2), 1997, 47-49.

[60] YAMAMOTO, H. et al. **Inverters advance welding automation**. *Welding Design and Fabrication*, March 1993, 29-32.

[61] MITA, T. **Reducing spatter in CO_2 gas-shielded arc welding - wave form control**. *Welding International*, 3(3), 1989, 227-232.

[62] PINCHUK, I.S. **Stabilisation of transfer and methods of reducing the spattering of metal in CO_2 welding with a short arc**. *Welding Production*, 27(6), 1980, 12-14.

[63] DZIUBINSKI, J. and SLANIA, J. **An assessment of the welding properties which are characteristic of the power source used in robotic arc welding**. *Welding International*, 9(8), 1995, 601-606.

[64] KING, F-J. and HIRSCH, P. **Seam tracking systems with the arc as sensor**. IN: Proceedings of the Fourth International Conference on Advances in Welding Processes, 9-11 May 1978, Harrogate, England, The Welding Institute, Paper 37, 193-202.

[65] KANNATEY-ASIBU, E. Jr. **Analysis of the GMAW process for microprocessor control of arc length**. *Transactions of the ASME - Journal of Engineering for Industry*, 109(2), May 1987, 172-176.

[66] STORR, A., SCHUMACHER, H. **Programming methods for industrial robots**. IN: Storr, A., McWaters, J.F. (eds.), "Off-line programming of industrial robots", Proceedings of IFIP WG 5.3/IFAC Working Conference on Off-line Programming of Industrial Robots, 2-3 June 1986, Stuttgart, FRG, 1-4.

[67] KUSIAK, A. **Programming, off-line languages**. IN: Dorf, R.C. , Nof, S.Y. (eds.), International encyclopaedia of robotics: applications and automation. New York : Wiley, 1988. Vol. 2, 1235-1250.

[68] OWEN, T. Robots out of wonderland: how to use robots in the age of CIM. Cranfield, UK: Cranfield Press, 1987.

[69] GREEN, M.A. *A study of robotic programming methodologies, with particular reference to, and comparison between off-line programming systems.* Cranfield Institute of Technology, M.Sc. Thesis, 1986.

[70] SMITH, J.S., EGBELU, P.J. **Off-line robot programming using natural language interface**. IN: "ROBOTS 14 Conference", Conference Proceedings Society of Manufacturing Engineers, 12-15 November 1990, Detroit, MI, USA, 10.37-10.48

[71] BOLMSJÖ, G. and NIKOLERIS, G. **Task planning for welding applications**. IN: IEEE International Conference on Systems, Man and Cybernetics: Systems Engineering in the Service of Humans, 17 Oct. 1993, Le Touquet, France, 515-519.

[72] GRUVER, W.A. , SOROKA, B.I. **Programming, high level languages**. IN: Dorf, R.C. , Nof, S.Y. (Eds.), International encyclopaedia of robotics: applications and automation. New York : Wiley, 1988. Vol. 2, 1203-1235.

[73] BONNEY, M.C. , MARSHALL, R.J. , GREEN, J.L. **Off-line programming using the GRASP robot simulation system**. IN: Storr, A., McWaters, J.F. (eds.), "Off-line programming of industrial robots", Proceedings of IFIP WG 5.3/IFAC Working Conference on Off-line Programming of Industrial Robots, 2-3 June 1986, Stuttgart, FRG, 171-179.

[74] KORTUS, M. , WARD, T. , WU, M.H. **An alternative approach to off-line programming**. *Industrial Robot*, 20(4), 1993, 17-20.

[75] OWENS, J. **Simultaneous Design**. *Industrial Robot*, 20(4), 1993, 9-11.

[76] COOK, G.E. , FERNANDEZ, K.R. , LEVICK, P.C. **Robot simulation**. IN: WESTON, J. (ed.) Exploiting robots in arc welded fabrication. Cambridge: The Welding Institute, 1989, 132-135.

[77] RENFORS, J. and AALTO, H. **Feature based programming of an arc welding robot: from design to shop floor**. IN: TWI Conference on Computer Technology in Welding, 9-12 June 1996, Lanaken, Belgium, Paper 16.

[78] LOUREIRO, R.L. and LEONG, H. **Off-line programming of robots with large workplaces**. IN: Proceedings of International Conference on Mechatronics & Robotics, 13-15 April 1994, Aachen, Germany, 243-255.

[79] SCHIFFERS, C. and DREWS, P. *Tools for integrating sensors in robot welding cells*. International Institute of Welding, IIW Doc. XII-1406-95, 1995.

[80] CHAN, K.C. , LIN, G.C.I. , WANG, T.C. **CAD based off-line robot programming**. IN: Proceedings of the International Conference on Computer Integrated Manufacturing, ICCIM 91, 1991, Singapore, 381-384.

[81] LEE, D.M.A. and ELMARAGHY, W.H. **ROBOSIM: a CAD-based off-line programming and analysis system for robotic manipulators**. *Computer-Aided Engineering Journal*, 7(5), October 1990, 141-148.

[82] KODAIRA, N. et al. **An off-line programming system for spot welding robots**. IN: Lane, J.D. (Ed.), Robotic Welding - International trends in manufacturing technology. Bedford, UK : IFS, 1987, 317-326.

[83] QUARTIER, F. and DREWS, P. *MacroWeld - Robot simulation and programming based on AutoCAD®*. IIW Document XII - 1404 - 95. International Institute of Welding, 1995, 195-206.

[84] BRÉAT, J.L. et al. **ACT WELD, a unique off-line programming software tailored for robotic welding applications**. IN: Proceedings of the TWI Conference on Computer Technology in Welding, 15-16 June 1994, Paris, France, Paper 33.

[85] SUGITANI, Y. , KANJO, Y. , MURAYAMA, M. **CAD/CAM welding robot system in steel bridge panel fabrication**. *Quarterly Journal of Japan Welding Society*, 13(1), 1995, 28-38.

[86] CARGNELLI, M. and ROGOWSKI, A. **A CAD-based program generator for a welding application**. IN: KOPACEV, P. (ed.) Cost Effective Use of Computer Aided Technologies and Integration Methods in Small and Medium Sized Companies. Pergamon Press: Oxford, 1993, 49-51.

[87] CARVALHO, G.C. , McMASTER, R.S. , BLACKMAN, S. **A strategy for off-line programming and adaptive control of a robotic welding cell**. *Science and Technology of Welding and Joining*, 1(1), 1996, 11-15.

[88] NORRISH, J. and GRAY, D. **Computer simulation and off-line programming in integrated welding systems**. *Welding & Metal Fabrication*, 60(3), April 1992, 119-120,122.

[89] PEARSON, D. **Realism when approaching robotic arc welding applications**. IN: WESTON, J. (ed.) Exploiting robots in arc welded fabrication. Cambridge: The Welding Institute, 1989, 22-27.

[90] STARK, G. , BENZ, E. and HÜTTENHOFER, M. **Calibration experiences in industry**. IN: BERNHARDT, R. and ALBRIGHT, S.L. (eds.) Robot Calibration. London: Chapman & Hall, 1993, 283-295.

[91] EVERETT, L.J. **Research topics in robot calibration**. IN: BERNHARDT, R. and ALBRIGHT, S.L. (eds.) Robot Calibration. London: Chapman & Hall, 1993, 19-36.

[92] McMASTER, R.S. and RIBEIRO, F.M. **Cell calibration and robot tracking.** IN: IEE Coloquium on Next Steps for Industrial Robotics, 17 May 1994, London, England, 3/1-3/7.

[93] BRITISH STANDARDS INSTITUTION: **Industrial robots / British Standards Institution - Part 4: Performance criteria and testing, Section 4.1: Methods for comprehensive testing**. Milton Keynes : BSI, 1991. (BS 7228 : Section 4.1: 1991) - (ISO 9283 : 1990).

[94] BERNHARDT, R. , ALBRIGHT, S.L. (ed.) Robot calibration. London: Chapman & Hall, 1993, 3-12.

[95] ZUPANCIC, J. **Calibration of an SMT robot assembly cell**. *Journal of Robotic Systems*, 11(4), 1994, 301-310.

[96] HWANG, H. and CHOI, D.Y. **CMAC toward intelligent robot: motion and calibration**. IN: Proceedings of IEEE International Workshop on Intelligent Robots and Systems (IROS 90), 3-6 Jul. 1990, Ibaraki, Japan, 517-526.

[97] OWENS, J. and PIATKOWSKI, K. **Simulation case study**. *Industrial Robot*, 22(4), 1995, 29-31.

[98] BOLMSJÖ, G. , OLSSON, M. , BRINK, K. **Programming GMA robotic welding systems using advanced graphical simulation tools**. IN: TWI Conference on Computer Technology in Welding, 9-12 June 1996, Lanaken, Belgium, Paper 28.

[99] ALLEN, J.M. **Implementation procedures for robotic arc welding**. IN: LANE, J.D. (ed.) Robotic Welding, Bedford-UK: IFS, 1987, 29-46.

[100] MIDDLE, J.E. and THORNE, R.G. **Factors affecting successful implementation of robotic arc welding systems in batch manufacturing**. IN: LANE, J.D. (ed.) Robotic Welding, Bedford-UK: IFS, 1987, 47-57.

[101] RICHARDSON, R.W. et al. **The feasibility of robotic arc welding of a low-volume sheet metal fabrication**. IN: LANE, J.D. (ed.) Robotic Welding, Bedford-UK: IFS, 1987, 59-72.

[102] LI, Y. and MIDDLE, J.E. **Fault detection system for troubleshooting problems in robotic arc welding**. *Welding & Metal Fabrication*, 60(9), November, 1992, 428-436.

[103] Anon. **Welding Robots - do they meet expectations?** *Weld & Metal Fabrication*, 61(4), May 1993, 180-185.

[104] WIDFELDT, M. , GUSTAFSSON, B. , LUNDIN, R. **The operator's computer – a way to increase productivity by off-line programming and expert system in advanced robotic welding cells**. IN: EUROJOIN 1 – 1st European Conference on Joining Technology, 5-7 November 1991, Strasbourg, France, 113-120.

[105] MIDDLE, J.E. **Component design for robot welding**. IN: WESTON, J. (ed.) Exploiting robots in arc welded fabrication. Cambridge: The Welding Institute, 1989, 155-167.

[106] STENKE, V. *Allowable wire positioning tolerances in fully mechanised MAG (GMA) welding*. International Institute of Welding, Commission XII, IIW Doc. XII-1054-88, 1988.

[107] AMERICAN WELDING SOCIETY - SOCIETY OF AUTOMOTIVE ENGINEERS STANDARD: **Specification for automotive frame weld quality - arc welding**. AWS D8.8-79, SAE HS JII96.

[108] KUK, K.A. **Determining acceptable joint mislocation in systems without adaptive control**. *Welding Journal*, 64(11), 1985, 65-66.

[109] KURKIN, N.S. and DRIKKER, V.E. **Evaluation of limiting deviations during robotised arc welding T joints**. *Welding International*, 4(7), 1990, 553-555.

[110] WADSWORTH, P. *Assessment of Weld Wire-to-joint Positional Tolerances for Robotic Arc Welding*. Edison Welding Institute, Abstract of Report MR8703 (http://www.ewi.org:2001/cgi-bin/cgicookie?dq3re.0.5jn0v9.0.1), 1987.

[111] NISSLEY, L. **Understanding positioning errors in robotic arc welding system**. *Welding Journal*, 62(11), 1983, 30-37.

[112] YAMADA, T. and TANAKA, O. **Fluctuation of the wire feed rate in gas metal arc welding**. *Welding Journal*, 66(9), 1987, 35-42.

[113] QUINN, T.P. et al. **Contact tube wear detection in gas metal arc welding**. *Welding Journal*, 74(4), 1995, 115s-121s.

[114] NOMURA, H. et al. (Eds.) Welding guide II – Sensors and control systems in arc welding – The state of the art in Japan. Technical Commission on Welding Processes, Japan Welding Society, 1991.

[115] USHIO, M. and MAO, W. **Sensors for arc welding: advantages and limitations**. *Transactions of Japan Welding Research Institute*, 23(2), 1994, 135-141.

[116] HANRIGHT, J. **Robotic arc welding under adaptive control - a survey of current technology**. *Welding Journal*, 65(11), 1986, 19-24.

[117] SMITH, P.A. **An example of FMS robot arc welding**. IN: Weston, J. (Ed.) Exploiting Robots in Arc Welded Fabrication. Cambridge: The Welding Institute, 1989, 124-131.

[118] TAKEUCHI, N. **Some kinds of wire ground sensors**. IN: Nomura, H. et al. (Eds.) Welding guide II – Sensors and control systems in arc welding – The state of the art in Japan. Technical Commission on Welding Processes, Japan Welding Society, 1991, II-125 to II-128.

[119] NAKAJIMA, J. et al. **Touch sensor and arc sensor for arc welding robots**. IN: Nomura, H. et al. (Eds.) Welding guide II – Sensors and control systems in arc welding – The state of the art in Japan. Technical Commission on Welding Processes, Japan Welding Society, 1991, II-74 to II-79.

[120] FUKUOKA, H. **Application of touch sensor to arc welding robot**. IN: Nomura, H. et al. (Eds.) Welding guide II – Sensors and control systems in arc welding – The state of the art in Japan. Technical Commission on Welding Processes, Japan Welding Society, 1991, II-129 to II-133.

[121] BOILLOT, J.P. et al. **Why the new generation of laser vision systems will create a revolution in robotic arc welding**. IN: Proceedings of the International Conference on Mechatronics & Robotics, 13-15 April 1994, Aachen, Germany, 293-303.

[122] CHEUNG, W. et al. **Model based tracking using a real-time laser rangefinder**. IN: "Conference on Vision, Sensors, and Control for Automated Manufacturing Systems", Proceedings of the Society of Photo-optical Instrumentation Engineers (SPIE) , 09 September 1990, Boston, MA, USA, Vol. 2063, 178-189.

[123] JONES, S.B. **Trends in robotic arc welding**. IN: Weston, J. (Ed.) Exploiting Robots in Arc Welded Fabrication. Cambridge: The Welding Institute, 1989, 171-180.

[124] ARSICAULT, M. and LALLEMAND, J.P. **Joint tracking with a self-teaching system**. *Welding Journal*, 69(12), 1990, 41-45.

[125] HOWARTH, M.P. and GUYOTE, M.F. **Eddy current and ultrasonic sensors for robot arc welding**. *Sensor Review*, 3(2), April 1983, 90-93.

[126] NUNES, U. and ALMEIDA, A.T. **Use of ultrasonic sensors towards robotic surface following**. IN: IEEE International Workshop on Intelligent Motion Control, 20-22 August 1990, Istanbul, Turkey, vol. 1, 341-346.

[127] GOLDBERG, F. **Inductive seam-tracking improves mechanised and robotic welding**. IN: "Automation and robotization in welding and allied processes" , Proceedings of the IIW International Conference on Automation and Robotization in Welding and Allied Processes, 2-3 September 1985, Strasbourg, France, 393-400.

[128] COOK, G.E. et al. **Electric arc sensing for robot positioning control**. IN: Lane, J.D. (Ed.), Robotic Welding - International trends in manufacturing technology. Bedford, UK : IFS, 1987, 181-216.

[129] FUJIMURA, H et al. **Robot welding with arc sensing**. IN: Nomura, H. et al. (Eds.) Welding guide II – Sensors and control systems in arc welding – The state of the art in Japan. Technical Commission on Welding Processes, Japan Welding Society, 1991, II-91 to II-96.

[130] USHIO, M. , LIU, W. , MAO, W. **An experimental investigation of dynamic behaviour of arc sensor in GMA welding in short-circuit transfer mode.** *Transactions of Japan Welding Research Institute*, 24(1), 1995.

[131] PHILPOTT, M.L. **Robot MIG weld seam tracking by "dip-resistance monitoring".** IN: Washington State University 20th Conference of the North American Manufacturing Research Institution of the Society of Manufacturing Engineers (NAMRC 20), 20-22 May 1992, Pullman, WA, 355-360.

[132] LESNEVICH, A. **Control of melting rate and metal transfer is gas shielded metal arc welding.** *Welding Journal*, 37(8), 1958, 343-353.

[133] KIM, J.W. and NA, S.J. **A study on prediction of welding current in gas metal arc welding - Part 2: experimental modelling of relationship between welding current and tip-to-workpiece distance and its application to weld seam tracking system.** *Proceedings of Intitution of Mechanical Engineers Part B:Journal of Engineering Manufacture*, 205(B1), 1991, 64-69.

[134] NOMURA, H. et al. **Development and application of arc sensor control with high speed rotating arc process.** IN: Nomura, H. et al. (Eds.) Welding guide II – Sensors and control systems in arc welding – The state of the art in Japan. Technical Commission on Welding Processes, Japan Welding Society, 1991, II-103 to II-108.

[135] PARROT, R. **Panasonic spins the arc.** *Industrial Robot*, 21(3), 1994, 15-17.

[136] SUGITANI, Y. et al. **Intelligent robot controls penetration and bead height.** *Welding Journal*, 69(12), 1990, 31-38.

[137] ARAYA, T., SAIKAWA, S. **Keynote address - Recent activities on sensing and adaptive control of arc welding.** IN: "International Trends in Welding Science and Technology" Proceedings of the 3rd International Conference on Trends in Welding Research, 1-5 June 1992, Gatlinburg, Tennessee, USA, 833-842.

[138] OOMEN, G.L. , VERBEEK, W.J.P.A. **A real-time optical profile sensor for robot arc welding.** IN: Lane, J.D. (Ed.), Robotic Welding - International trends in manufacturing technology. Bedford, UK : IFS, 1987, 117-128.

[139] BJÖRKELUND, M. **A true seam-tracker for arc welding.** IN: Lane, J.D. (Ed.), Robotic Welding - International trends in manufacturing technology. Bedford, UK : IFS, 1987, 167-177.

[140] SICARD, P., LEVINE, M.D. **Joint recognition and tracking for robotic arc welding**. *IEEE Transactions on Systems, Man, and Cybernetics*, 19(4), July/August 1989, 714-728.

[141] BAMBA, T. **An arc-welding robot with a compact visual sensor**. IN: Nomura, H. et al. (Eds.) Welding guide II – Sensors and control systems in arc welding – The state of the art in Japan. Technical Commission on Welding Processes, Japan Welding Society, 1991, II-23 to II-27.

[142] BACK, B., FRAZEN, A. **See, weld**. *Manufacturing Engineer*, 71(4), April/May, 1992, 19, 22-23.

[143] DREWS, P., STARKE, G. **Development approaches for advanced adaptive control in automated arc welding**. IN: Proceedings of the IIW International Conference on Automation and Robotization in Welding and Allied Processes, 2-3 September 1985, Strasbourg, France, 115-124.

[144] DAVEY, P.G. et al. **Laser sensors for arc welding robots**. IN: Lane, J.D. (Ed.), Robotic Welding - International trends in manufacturing technology. Bedford, UK : IFS, 1987, 105-115.

[145] NIEPOLD, R., BRÜMMER, F. **Pass - a visual sensor for seam tracking and on-line process parameter control in arc welding applications**. IN: Lane, J.D. (Ed.), Robotic Welding - International trends in manufacturing technology. Bedford, UK : IFS, 1987, 129-140.

[146] NAKATA, S., JIE, H. **Construction of a visual sensing system for in-process control of arc welding and its application in automatic weld line tracking - study on visual sensing systems for in-process control of arc welding (4th report)**. *Welding International*, 4(11), 1990, 845-850.

[147] SAMEDA, Y. **Fuzzy seam-tracking controller**. IN: Proceedings of the IEEE International Conference on Industrial Electronics, Control, Instrumentation, and Automation (IECON 92), 09-13 November 1992, San Diego, CA, USA, 966-970.

[148] RICHARDSON, R.W. et al. **Coaxial arc weld pool viewing for process monitoring and control**. *Welding Journal*, 63(3), 1984, 43-50.

[149] SUGA, Y. et al. **Recognition of the weld line by a visual sensing system and weld line tracking in automatic welding of thin aluminum plates.** *Welding International*, 7(4), 1993, 273-279.

[150] GROOM, K.N. et al. **Automatic single V-groove welding utilising infrared images for error detection and correction**. *Welding Journal*, 69(12), 1990, 441s to 445s.

[151] DAVIS, A. R. *On-line gap detection techniques for adaptive control of GMAW*. Cranfield University. M.Sc. Thesis, 1993.

[152] YAMANE, S. et al. **Sensing and fuzzy logic control of weld pools in pulsed MIG welding**. *Welding International*, 7(5), 1993, 378-383.

[153] INOUE, K. YI, N. **Application of neural network to visual inspection of weld beads**. *Welding International*, 7(11), 1993, 857-862.

[154] LUCAS, W. **Computers in arc welding - the next industrial revolution. Part 3: Instrumentation and process analysis**. *Metal Construction*, 17(7), 1985, 431-436.

[155] VANDOREN, A.H. Data acquisition systems. Reston, VA, USA: Reston Publishing Company, 1982.

[156] REHFELDT, D. et al. **Microcomputer-based instrumentation for analysing and monitoring arc welding processes**. 3th TWI International Conference on Computer Technology in Welding, 4-7 June 1990, Brighton, UK, 36-45.

[157] STEIN, J. and DOMNFELD, D. **A classification and design methodology for manufacturing process sensor systems.** IN: ISCIE Japan-USA Symposium on Flexible Automation - A Pacific Rim Conference, 1990, Kyoto, Japan, 675-679.

[158] SCHELLHASE, M. *Investigation into arc welding process monitoring by statistical signal analysis*. IIW Doc. 212-497-81, 1981.

[159] DOEBELIN, E.O. Measurement systems: application and design, 4th Edition. New York: McGraw-Hill, 1990.

[160] LOVE, P. and SIMAAN, M. **Automatic recognition of primitive changes in manufacturing process signals.** *Pattern Recognition*, 21(4), 1988, 333-342.

[161] CHAWLA, K.S. *Objective on-line assessment of the performance of flux cored wires by real time computer based monitoring*. Cranfield Institute of Technology, PhD Thesis, 1993.

[162] SIEWERT, T.A. et al. **Through-the-arc sensing for monitoring arc welding**. IN: "International Trends in Welding Science and Technology", Proceedings of the 3rd International Conference on Trends in Welding Research, 1-5 June 1992, Gatlinburg, Tennessee, USA, 1037-1040.

[163] HOUPIS, C.H. and LAMONT, G.B. Digital control systems: theory, hardware, software. New York: McGraw-Hill, 1985, 87-88.

[164] RICHARDS, R.J. An introduction to dynamics and control. Cambridge: Longman Scientific & Technical, 1979.

[165] CORNISH, H.L. et al. Computerised process control: A management decision. New York : Hobbs, Dorman, 1968.

[166] KASATKIN, O.G. **Experimental design system for solving the problems of welding operational parameters optimization.** IN: "Weld quality The role of computers", Proceedings of the IIW International Conference on Improved Control with Special Reference to Computer Technology, 4-5 July 1988, Vienna, Austria, 169-173.

[167] MONTGOMERY, D.C. Design and analysis of experiments. 2nd Edition. New York: John Wiley & Sons, 1983.

[168] HUNTER, J.J. , BRYCE, G.W. and DOHERTY, J. **On line control of the arc welding process**. IN: TWI International Conference on Developments in Mechanised Automated and Robotic Welding, 18-20 November 1980, London, paper 37.

[169] ALFARO, S.C.A. *Mathematical modelling of narrow gap submerged arc welding*. Cranfield Institute of Technology, PhD Thesis, 1989.

[170] HARRIS, P. and SMITH, B.L. **Factorial techniques for weld quality prediction**. *Metal Construction*, 15(11), 1983, 661-666.

[171] LAMBERT, J. and GILSTON, P. **Hot-wire GTAW for nuclear repairs**. *Welding Journal*, 69(9), 1990, 45-52.

[172] JOHNSON, D.E. **Harnessing the power of multiple regression**. *Chemical Engineering*, 96(11), November 1989, 176-188.

[173] WALPOLE, R.E. and MYERS, R.H. Probability and statistics for engineers, 4th Edition. New York: Mcmillan, 1989.

[174] ÅSTRÖM, K. J. , WITTENMARK, B. Adaptive control. Reading: Addison-Wesley, 1989.

[175] COOK, G.E. , ANDERSEN, K. , BARRET, R.J. **Keynote address - feedback and adaptive control in welding**. IN: "Recent Trends in Welding Science and Technology" Proceedings of 2nd International Conference on Trends in Welding Research, 14-18 May 1989, Gatlinburg, Tennessee, USA, 891-903.

[176] DOUMANIDIS, C.C. **Multiplexed and distributed control of automated welding**. *IEEE Control Systems*, 14(4), 1994, 13-24.

[177] COOK, G.E. **Feedback and adaptive control of process variables in arc welding.** IN: TWI International Conference on Developments in Mechanised Automated and Robotic Welding, 18-20 November 1980, London, Paper 32.

[178] HUISSON, J.P. et al. **Design of an integrated robotic welding system**. IN: "International Trends in Welding Science and Technology", Proceedings of the 3rd International Conference on Trends in Welding Research, 1-5 June 1992, Gatlinburg, Tennessee, USA, 915-919.

[179] HUISSON, J.P. et al. **Multi-variable control of robotic gas metal arc welding**. *Journal of Materials Processing Technology*, 43(1), 1994, 1-12.

[180] AGAPAKIS, J.E. et al. **Joint tracking and adaptive robotic welding using vision sensing of the weld joint geometry**. *Welding Journal*, 65(11),1986, 33-41.

[181] NISHAR, D.V. et al. **Adaptive control of temperature in arc welding**. *IEEE Control Systems*, 14(4), 1994, 4-12.

[182] SONG, J.-B. , HARDT, D.E. **Dynamic modelling and adaptive control of the gas metal arc welding process**. *Transactions of the ASME - Journal of Dynamic Systems, Measurement, and Control*, 116(3), September 1994, 405-413.

[183] SUGITANI, Y. , MAO, W. , USHIO, M. *Adaptive control of weld bead shape utilizing arc sensor in one side GMAW process with backing plate*. International Institute of Welding Document, IIW Doc. XII-1360-94, 1994.

[184] OHSHIMA, K. et al. *Knowledge based information processing for the penetration control in the robotic welding by fuzzy inference*. IIW Document XII-1375-94, 1994.

[185] USHIO, M. (ed.) *The state-of-the-art and the subjects of arc welding automation in various industries in Japan*. Technical Commission on Welding Processes, JWS, IIW Doc. XII-1359-94, 1994.

[186] USHIO, M. (ed.) *Automation technology of arc welding*. Technical Commission on Welding Processes, JWS, IIW Doc. XII-1471-96, 1996.

[187] NAUCK, D. , KLAWONN, F. , KRUSE, R. **Fuzzy sets, fuzzy controllers, and neural networks.** *Scientific Journal of the Humboldt-University of Berlin*, Series Medicine 41(4), 1992, 99-120.

[188] SHAW, H.F. , LUCAS, W. **The potencial of neural networks in welding**. IN: TWI Conference on Computer Technology in Welding, 15-16 June 1994, Paris, France, Paper 52.

[189] BROWN, M. , HARRIS, C. Neurofuzzy adaptive modelling and control. New York: Prentice Hall, 1994.

[190] *Product/Weld requirements: performance requirements.* Brite Euram Project BE-4006-90. Technical Report Sub-Task 1.2, Ref. No. 1.2.2.92, February, 1992

[191] CONNOR, L.P. (ed.) Welding Handbook. 8th ed. Miami: American Welding Society, 1987, Vol. 1, Chapter 14.

[192] McKERROW, P.J. Introduction to robotics. Sydney, AU : Addison-Wesley, 1991, 154.

[193] CRAIG, J.J. Introduction to robotics - mechanics and control. Reading, Massachusetts : Addison-Wesley, 1986.

[194] LUZEAUX, D. **Process control and machine learning rule-based incremental control**. *IEEE Transactions on Automatic Control*, 39(6), 1994, 1166-1171.

[195] AMSON, J.C. **Electrode voltage in the consumable-electrode arc system.** *Journal of Physics D: Applied Physics*, 5(1), 1972, 89-96.

[196] RIBEIRO, A.F.M. , NORRISH, J. and McMASTER, R.S. **Practical case of rapid prototyping using gas metal arc welding.** IN: TWI Conference on Computer Technology in Welding, 15-16 June 1994, Paris, France, Paper 55.

[197] RIBEIRO, A.F.M. and NORRISH, J. **Metal based rapid prototyping for more complex shapes.** IN: TWI Conference on Computer Technology in Welding, 9-12 June 1996, Lanaken, Belgium, Paper 60.

[198] DOHERTY, J. and PLUMMER, R. **Calibrating a computer-regulated welding rig - a technical note**. *The Welding Institute Research Bulletin*, 22(2), February 1981, 49-50.

[199] CARVALHO, G.C. , OGUNBIYI, T.E.B. and McMASTER, R. **A method for automatic voltage tuning of conventional GMAW.** IN: AWS 7th International Conference on Computer Technology in Welding, 8-11 July 1997, San Francisco, CA, USA, (Proceedings not yet published).

[200] MITA, T. et al. **Automatic setting of arc voltage using fuzzy logic**. *Welding Review International*, 15(4), November 1996, 130-132.

[201] WON, Y.J. and CHO, H.S. **A fuzzy rule-based method for seeking stable arc condition under short-circuiting mode of GMA welding process**. *Proceedings of the Institution of Mechanical Engineers Part I - Journal of Systems and Control Engineering*, 206(I2), 1992, 117-125.

[202] JÖNSSON, P.G. et al. **Power characteristics in GMAW: experimental and numerical investigation**. *Welding Journal*, 74(3), March 1995, 93s-102s.

[203] TSAO, K.C. and WU, C.S. **Fluid flow and heat transfer in GMA weld pools**. *Welding Journal*, 67(3), March 1988, 70s-75s.

Further Reading

[1] AutoCAD Release 12 - Customization Manual, Autodesk Inc., USA, 1992.

[2] AutoCAD Release 12 - AutoLISP Programmer's Reference, Autodesk Inc., USA, 1992.

[3] AutoCAD Release 12 - AME 2.1 AutoLISP and API Manual, Autodesk Inc. USA, 1992.

Appendices

[1] Data structure used in AutoLISP

Appendix A

This appendix shows the geometrical and welding data obtained using the off-line programming module developed for AutoCAD (see Chapter 3). These data are stored in the CAD drawing as *extended entity data* associated with the edge curve that represents the weld joint. The data are presented in Table A.1 in a *list*[1] format, as they are stored in the AutoCAD database and as they should appear when extracted from their respective edge using dedicated AutoLISP functions. Parentheses are the standard form of delimiting each list. It should be noted that a *list* can contain other *lists*. The data shown in Table A.1 was written in a way that makes it easier to visualise the different *lists* contained in it. Each list is defined by a header and the corresponding value. The header is separated from the value by a point and the list is delimited by parentheses. The header defines the type of data stored (e.g. integer, real, vector, string, list delimiter, list type) and the value is the data stored in that particular position in the major list. For more details, readers are referred to the AutoCAD R12 AutoLISP programming manual.

Before presenting the list, some global and local variables defined in the programs and some standard AutoLISP functions are defined below:

XDATA: abreviation of extended entity data.

CRANWELD: registered AutoLISP application name. This name must be used in order to retrieve the welding extended entity data.

"WSETUP": header for the sublist containing the welding setup.

GASWIRE: global variable containing the list which defines the file of coefficients for the welding models. The list format is shown below:
([filename] [default stand-off] [wire diameter] [file description]).

car: standard AutoLISP function used to extract the first element of a list. For example, ***(car GASWIRE)*** returns the string [filename].

cadr: standard AutoLISP function used to extract the second element of a list. For example, ***(cadr GASWIRE)*** returns real number [default stand-off].

caddr: standard AutoLISP function used to extract the third element of a list. For example, ***(caddr GASWIRE)*** returns the real number [wire diameter].

nth: AutoLISP function used to extract the nth component of the list, the first element being 0 (zero). For example ***(nth 3 GASWIRE)*** returns the string [file description], which is the fourth element in the list.

"WGEOM": header for the sublist containing the joint geometry.

---

[1] Data structure used in AutoLISP to store data.

wnum:	local variable which defines the number (integer) of the weld being stored.
jtype:	local variable which defines the string corresponding to the joint type: "FILLET" or "LAP" or "BUTT".
leg or pen:	local variable (real number) defining the main required dimension: leg length in the case of fillet and lap joints or penetration in the case of butt joints.
A0:	global variable (real number) storing the accepted oversize in the main required dimension (leg length or penetration).
SO:	global variable (real number) defining the required stand-off.
pthick:	local variable (real number) containing the minimum plate thickness
gap:	local variable (real number) containing the user estimated gap size
pos:	binary variable (16 bit integer) defining if the weld is positional (1) or non-positional (0)
wpos:	string defining the welding position: "flat", "horizontal", "vertical" and "overhead"
"OFFLINE":	header for the sublist containing the off-line programming data
strtpt:	list containing the co-ordinates of the starting point of the line defining the weld, in CAD world co-ordinates: (xstrt ystrt ztsrt)
appr_strt:	list containing the unit vector which defines the torch approach direction at the starting point, in CAD world co-ordinates.
tang_strt:	list containing the unit vector which defines the direction tangent to the joint line at the starting point, in CAD world co-ordinates.
endpt:	list containing the co-ordinates of the end point of the line defining the weld, in CAD world co-ordinates: (xend yend zend)
appr_end:	list containing the unit vector which defines the torch approach direction at the end point, in CAD world co-ordinates.
tang_end:	list containing the unit vector which defines the direction tangent to the joint line at the end point, in CAD world co-ordinates.
edgeid:	real number containing the AutoCAD Modelling Extension (AME) identification for the edge defining the weld in the CAD drawing.
shandl:	variable containing the handle for the edge parent solid model.
ctype:	local variable containing the integer number which defines the edge curve type: line (0), ellipse (1), hyperbola (2) or parabola (3).
wlength:	weld length.
offset1:	distance between the edge starting point and the weld starting point, measured along the edge towards its mid-point.

offset2:	distance between the edge end point and the weld end point, measured along the edge towards its mid-point
"WPARAMS":	header for the sublist containing the selected welding parameters
S:	predicted welding speed
V:	predicted power source set-up voltage
WFS:	predicted wire feed speed
leg_pred:	predicted leg length
[transfer mode]:	predicted transfer mode according to expected power ratio: "UNSTABLE", "DIP", "GLOBULAR" or "SPRAY"

Table A.1 - Welding extended entity data list

List item	Description
(-3 ("CRANWELD"	flag indicating that XDATA follows start welding extended entity data using "CRANWELD" as the registered application name
(1002 . "{") (1000 . "WSETUP") (1000 . (car GASWIRE)) (1000 . (caddr GASWIRE)) (1002 . "}")	start sublist WSETUP header for the sublist containing the welding setup filename containing the models' coefficients description of shielding gas and wire end sublist WSETUP
(1002 . "{") (1000 . "WGEOM") (1070 . wnum) (1000 . jtype) (1040 . leg/pen) (1040 . A0) (1040 . SO) (1040 . pthick) (1040 . gap) (1070 . pos) (1000 . wpos) (1002 . "}")	start sublist "WGEOM" header for the sublist containing weld geometry 16 bit integer containig the weld number string ("FILLET" or "LAP" or "BUTT") real - leg length (pen=penetration for butt joints) real - tolerance for the leg length or penetration real - stand-off real - minimum plate thickness real - gap size 16 bit integer - positional(1) or non-positional(0) string - welding position "flat", "horizontal", "vertical", "overhead" close sublist "WGEOM"

Table A.1 - continuation

List item	Description
(1002 . "{")	start sublist OFFLINE
(1000 . "OFFLINE")	header for the sublist containing offline programming information
(1011 . strtpt)	3d world space position - weld start point
(1002 . "{")	start list containing weld start orientation vectors
(1013 . appr_strt)	3d World space welding-torch approach vector
(1013 . tang_strt)	3d World space welding-torch tangent vector
(1002 . "}")	end weld start orientation vectors list
(1011 . endpt)	3d world space position - weld end point
(1002 . "{")	start list containing weld end orientation vectors
(1013 . appr_end)	3d World space welding-torch approach vector
(1013 . tang_end)	3d World space welding-torch tangent vector
(1002 . "}")	end list containing weld end orientation vectors
(1040 . edgeid)	real containing the AME id for the edge
(1005 . shandl)	AME handle for the parent solid
(1070 . ctype)	integer containing the edge curve type
(1040 . wlength)	real containing the weld length
(1040 . offset1)	real containing the weld start point offset from the edge start
(1040 . offset2)	real containing the weld end point offset from the edge end
(1002 . "}")	close sublist "OFFLINE"
(1002 . "{")	start "WPARAMS" sublist
(1000 . "WPARAMS")	header for the welding parameter sublist
(1040 . S)	real - welding speed
(1040 . V)	real - welding voltage
(1040 . WFS)	real - wire feed speed
(1040 . Leg)	real - calculated leg length
(1000 . "Transfer mode")	string - metal transfer mode
(1002 . "}")	end "WPARAMS" sublist
(1000 . "END WXDATA")	
)	closing welding extended entity data list
)	closing extended entity data list

Appendix B

This appendix shows the format in which the file containing the coefficients of the welding models must be written so that it can be correctly read by the off-line programming module. The file defined for power source used in this work (Migatronic BDH550) is shown below. The sintax used is explained in the header of the file, between the asterisk (*) lines. The file name extension defines the type of joint which the file corresponds to. The valid extension names are: "fil" for fillet joints, "lap" for lap joints and "but" for butt joints. The name of the file shown below was chosen to be "AR5MS10A.FIL", "AR5" standing for Argonshield 5 shielding gas, "MS10" standing for mild steel 1.0mm welding wire and "A" indicating that a power source other than the BDH320 was used.

File start:

```
;Coefficients for models obtained from "cal" data series
;*****************************************************************
;
;                    Welding models
; Coefficients obtained for 1mm mild steel wire and BOC Argonshield 5
; shielding gas in fillet joints.
;
; -Each line corresponds to a model, containing the respective
; coeficients.
; -Each number must be separated by a space, a comma or a tab.
; -Each line must finish with a #.
; -A line begining with a semi-colon is considered a comment.
; -A line begining with a colon indicates a label. An equal sign (=)
; indicates the end of the label and the begining of the label value.
; The valid labels are:
;   Material: indicates the welded material.
;   GasType: indicates the shielding gas.
;   WireDiameter: indicates the wire diameter in mm.
;   WPS: indicates the Welding Power Supply used to obtain the coeffitients
; -Observation:
;  !!! It is mandatory that the four labels are defined !!!
;*****************************************************************
;
;
: Material = Mild Steel
: GasType = BOC Argon-Shield 5 (Ar 5%CO2 2%O2)
: WireDiameter = 1.0
: WPS = BDH550
;
;
; Coefficients of the regression models
;
; Leg length model coefficients
; Side leg (a1_1  b1_1)
1   0.561068#
; Bottom leg (a1_2 b1_2)
1   0.592637#
; Off-line mean current model coefficients (a2 b2 c2 d2) (bead on plate)
```

; Imean = a2 + b2*WFS + c2*SO + d2*SO*WFS, SE=9.933 R2=0.9830
53.64149 24.65153 0.0 -0.413273#
; TSI coefficients (a3 b3 c3 d3)
; TSI = a3 + b3*Imean + c2*SO + d2*SO*Imean, SE= 0.254314 R2=0.7585
3.455699 -0.006043 -0.034601 0.0#
; On-line mean current model coefficients (a4 b4)
; Imean = a4*Imax + b4*Imin, SE=15.8588 R2=0.9960
0.324805 0.693878#
; Vbk/Vmean model coefficients (a5 b5 c5 d5)
; = a5 + b5*Imin + c5*SO + d5*SO*Imin, SE=0.112111 R2=0.8545
-0.335025 0.002398 0.040318 0.0#
; Vbk estimation model coefficients (a6 b6 c6)
; a6 + b6*Imean + c6*Vmean; SE=1.00907 R2=0.9921
-30.787835 -0.031138 2.265039#
; Imax estimation model coefficients (a7 b7 c7 d7)
; Imax = a7 + b7*Imean + c7*Vmean + d7*Imean*Vmean, SE=36.000 R2=0.9881
0.0 3.364032 0.0 -0.072541#
; Penetration models
; Side penetration model coefficients (a8, b8)
0.01782 -0.449818#
; Side penetration model coefficients (a9, b9)
0.019058 -0.639698#
; Undercut possibility measure model coefficients (a10 b10 c10)
-0.0982 0.0044 0.0265#
; Possibility measure for stable wire melting and ignition model
; (a11 b11)
13.519345 0.97619#
; PR model coefficients (a12 b12 c12 d12)
; a12 + b12*Vmean + c12*Imean^2 + d12*Vmean*Imean, SE=0.0433, r2=0.9818
-0.92147 0.068592 -0.0000028511 0.0#
; Pr_spray model coefficients (a13 b13 c13 d13 e13)
; Pr_spray = 1- Pr_dip ; e13=SE
; Pr_spray = a13 + b13*TSI + c13*DCI + d13*TI SE=0.09532 r2=0.9650
1.379678 -0.294549 -0.807387 -0.763514 0.09532#
; Correction of average penetration model coefficients (a14 b14)
-1.15857 2.114041#
; Correction of set up voltage model coefficients (a15 b15 c15 d15)
; case e15=0 then (Vmean = a15 + b15*Vset + c15*WFS + d15*Vset*WFS) linear fit
; case e15=1 then (Vmean = a15*exp(b15*Vset)) exponential fit
; case e15=2 then (Vmean = a15*Vset^b15) logarithmic fit
; linear fit SE=0.354 R2=0.99604
0.0 0.917431 0.0 0.0 0#
; Correction of average leg length model coefficients (a16 b16)
0.623039 0.880194#

Appendix C

This appendix shows the user interface of the off-line programming module developed for AutoCAD r12 using the AutoLISP programming language. The dialogue boxes were defined using the Dialogue Control Language[1] .

The user interface was designed to guide the user through all the steps necessary to define a weld. To use the off-line programming module the user must create the solid model of the component in its final welded form. When the model is ready, the off-line programming module must be loaded. This is carried out by activating the AutoCAD pull down menu, selecting "Welding" and choosing "Load Welding Module..." (see Figure C.1). Once the off-line programming module is loaded a weld can be defined. If no weld has been previously defined, the program will show the dialogue box shown in Figure C.2, which is used to define the model coefficients' file which corresponds to the welding cell set-up. If the user wants to see and/or modify a file shown in the list, he has to select it and "press" the button "View File..." (see Figure C.2). If a new file is to be added to the list, the user must select "Add new file...". If no change is necessary, the user just has to select the suitable file description in the list and "press" the "OK" button (see Figure C.2).

After selecting the coefficients file, the welding procedure generator main dialogue box will appear (see Figure C.3). This dialogue box guides the user interactively through all the steps necessary to fully define a weld. These steps start by defining the identification number for the weld followed by the selection of the edge that represents the joint. The start and end points of the weld are then defined by choosing the start and end points of the edge, respectively, and the offsets by which the weld start and end points will be displaced from the corresponding edge points along the joint line (see Figure C.4). After having the weld positioning aspects defined, the weld geometrical requirements are input (see Figure C.5 and Figure C.6). If it is known from previous production experience that a gap is expected to be present, its estimated value can be input by selecting "Yes" in the Gap definition window (see Figure C.5). The last parameter requested is the stand-off; this is defaulted to 15 mm but the user can change this to any value within the allowable range (12 mm to 15 mm). Having defined all the necessary parameters, the welding parameters generator lists a series of possible welding parameters, from which the user has to select one set (see Figure C.7). The selected set is stored together with other data as extended entity data associated with the edge representing the joint line (see Appendix A).

After defining all the welds of the component, the robot program and the file containing the robot teach points can be generated. This is carried out by selecting the "Welding" pull down menu, "Output" and "Teach Robot". If no program has been generated before during the same off-line programming session, a dialogue box used to define the transformation matrix between the CAD co-ordinates system and the Robot world co-ordinates system is launched (see Figure C.8). In this dialogue box, other data such as maximum and normal robot speed for non-welding movements and

---

[1] For more details please refer to the AutoCAD r12 Customisation Manual

TCP[2] number are also defined. The off-line programming module then generates the robot program in ARLA language, the teach points file and the welding parameters file.

Software requirements and list of files

The following requirements are necessary to run the off-line programming software developed:

- AutoCAD release 12 or above and AutoCAD Modelling Extension (AME);
- Some environment variables must be set before running AutoCAD. These could be included in the batch file used by AutoCAD 12 DOS386 to define its own environment variables. The necessary variables are listed below as they should appear in the DOS batch file:

```
SET WELDING=X:\ACAD\WELDING
SET API=X:\ACAD\API
SET OFFLINE=X:\ACAD\WELDING\OFFLINE
```

  The environment variable *WELDING* stores the path in which the program files are stored, in the example *X:\ACAD\WELDING*. The enviroment variable *API* defines the path where the AutoCAD API files are stored. The *OFFLINE* environment variable defines the path where the generated robot programs should be stored

- The welding pop down menu must be defined in the *ACAD.MNU*. This can be done by backing up the original file and adding the following lines after the last POPn (n=0,1,...,9 or more) menu description. The example shows that the menu is the tenth to appear on the screen, from the left to the right side (see Figure C.1).

  Example:

```
***POP10
[Welding]
[Load Welding Module...]^C^C^C(load (strcat (getenv "WELDING") "/loadwm"))
[~Unload Welding Module...]^C^C^C(setq wmodule nil) (xunload "AME") (princ)
[--]
[~Define Weld...]^C^C^C(wmodule)
[~View Weld...]^C^C^C(viewweld nil nil)
[--]
[~Delete Weld...]^C^C^C(delete_weld nil)
[--]
[~->Setup]
[Welding]^C^C^C(load (strcat (getenv "WELDING") "/loadwset"))
[<-Robot]^C^C^C(load (strcat (getenv "WELDING") "/robset"))
[--]
[~->Output]
[Teach Robot]^C^C^C(load (strcat (getenv "WELDING") "/teach"))
[<-Parameters]^C^C^C(load (strcat (getenv "WELDING") "/opwpar"))
```

---

[2] Tool Centre Point. It is used to define the position of the origin and the orientation of the co-ordinates frame attached to the welding torch.

Once modified, the new ACAD.MNU must be compiled. This is automatically done if the old ACAD.MNX (compiled version of ACAD.MNU) file is deleted.

- The following files are necessary to run the program:
  - ♦ LOADWM.LSP: This file is used to load the program.
  - ♦ LOADWSET.LSP: This file contains the routine called by selecting "Setup" and "Welding" in the pull down menu (see Figure C.1). This routine loads the SGASWIRE.LSP file to display the window shown in Figure C.2.
  - ♦ SGASWIRE.LSP: This file contains the routine used to show the coefficients file selection window (see Figure C.2) and to set the "GASWIRE" global variable (see Appendix A).
  - ♦ READCOEF.LSP: This file contains the function used to read the coefficients from the corresponding file, selected through the window shown in Figure C.2.
  - ♦ MODELCFT.DCL: This file contains the definition of the fields which compose the window shown in Figure C.2.
  - ♦ WMODINT.LSP: This file contains the routines that produce the user interface of the welding parameters generator.
  - ♦ WMODINT.DCL: This file contains the definition of the windows that are shown in the user interface of the welding parameters generator.
  - ♦ WMODELS.LSP: This file contains the welding models and the optimisation routine used.
  - ♦ FILLET.SLD, BUTT.SLD, LAP.SLD: These files contain the slides of the three different types of joint, with the variables that are requested by the program shown explicitly on the drawings. The corresponding drawing files (fillet.dwg, butt.dwg and lap.dwg) are not needed but are also available.
  - ♦ WELDPROC.LSP: This file contains the routine used to output the list of possible welding parameters generated by the program for a specific weld.
  - ♦ TEACH.LSP: This file is used by the pull down menu selection "Output" + "Teach Robot" (see Figure C.1) to load the off-line programming routines, stored in the file OFFLINE.LSP.
  - ♦ OFFLINE.LSP: This file contains the routines used to generate the robot program and the teach points file.
  - ♦ ROBSET.LSP: This file contains the routine used to show the Robot Set-up window (see Figure C.8).
  - ♦ ROBSET.DCL: This file contains the description of the fields which compose the window shown in Figure C.8.
  - ♦ AR5MST10.FIL: Coefficients file for fillet joints obtained by Ogunbiyi [ref. 51] for the Migatronic BDH320 welding power source.
  - ♦ AR5MS10A.FIL: Coefficients file for fillet joints obtained in this work for the Migatronic BDH550 welding power source.
  - ♦ ROBOTYPE.DAT: This file contains a list of the robots implemented in the off-line programming software (in this work, only the ABB IRB2000 was implemented).

- ROBSET.DAT: This file is created by the program to store the co-ordinates of the points used to define the CAD-to-Robot Transformation Matrix. Its is not critical, since a new file is created if it is not available.
- GAS_WIRE.DAT: This file is created by the program to store the description of the registered coefficients file. It is not critical, since a new file will be created if it is not found.

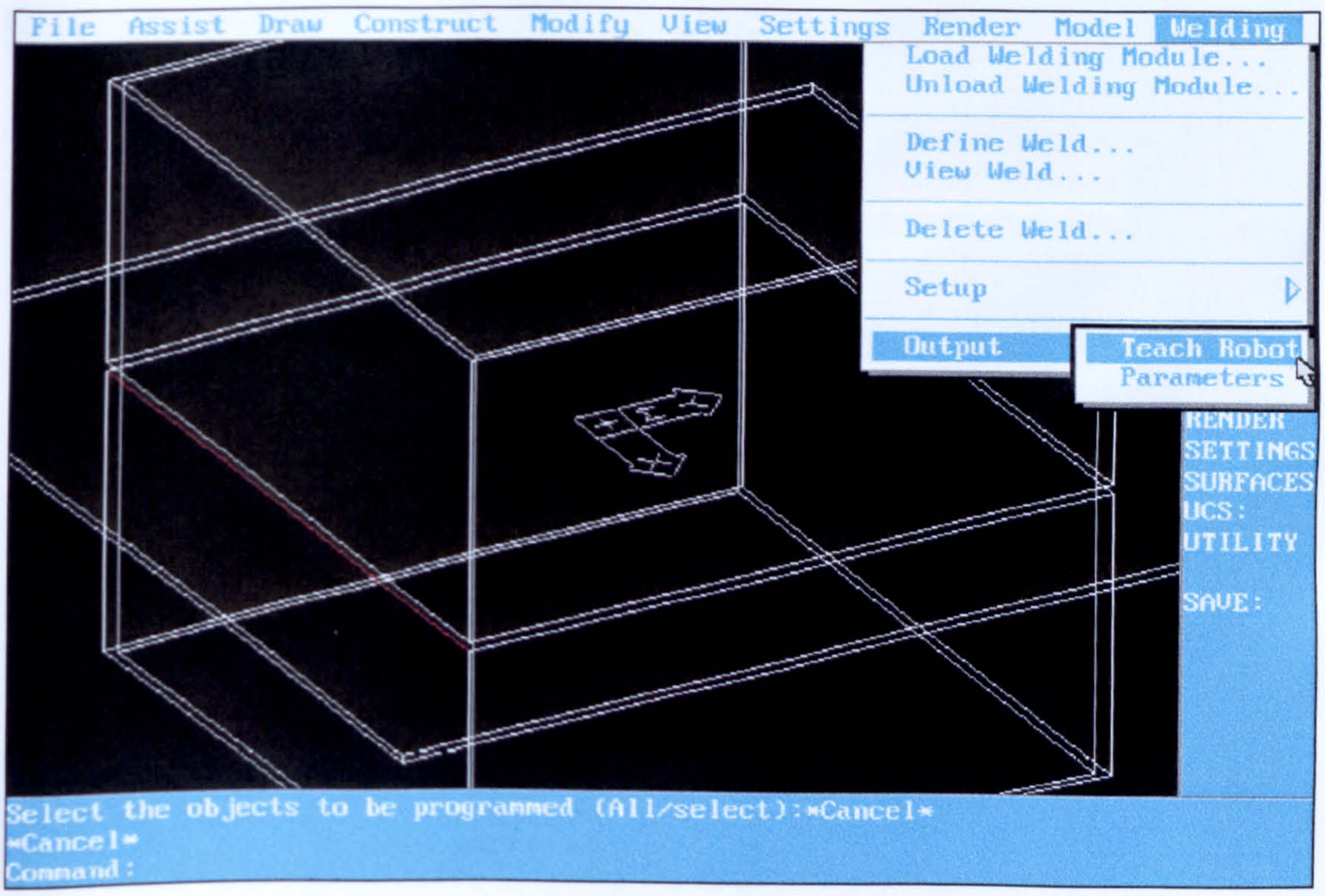

Figure C.1 - Off-line programming module pull down menu

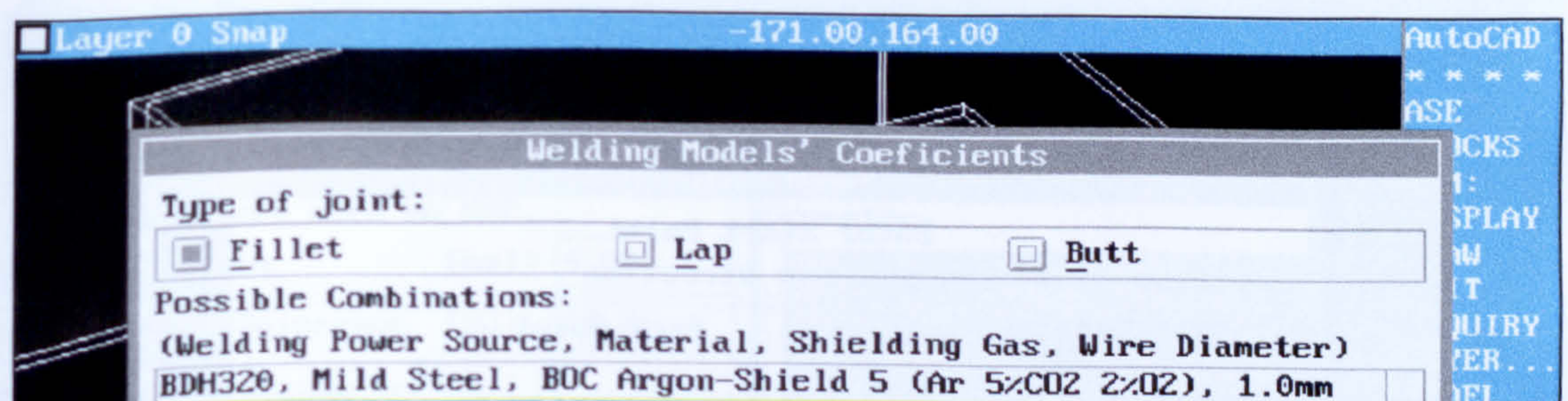

Figure C.2 - Dialogue box used to define the file containing the coefficients of the welding models

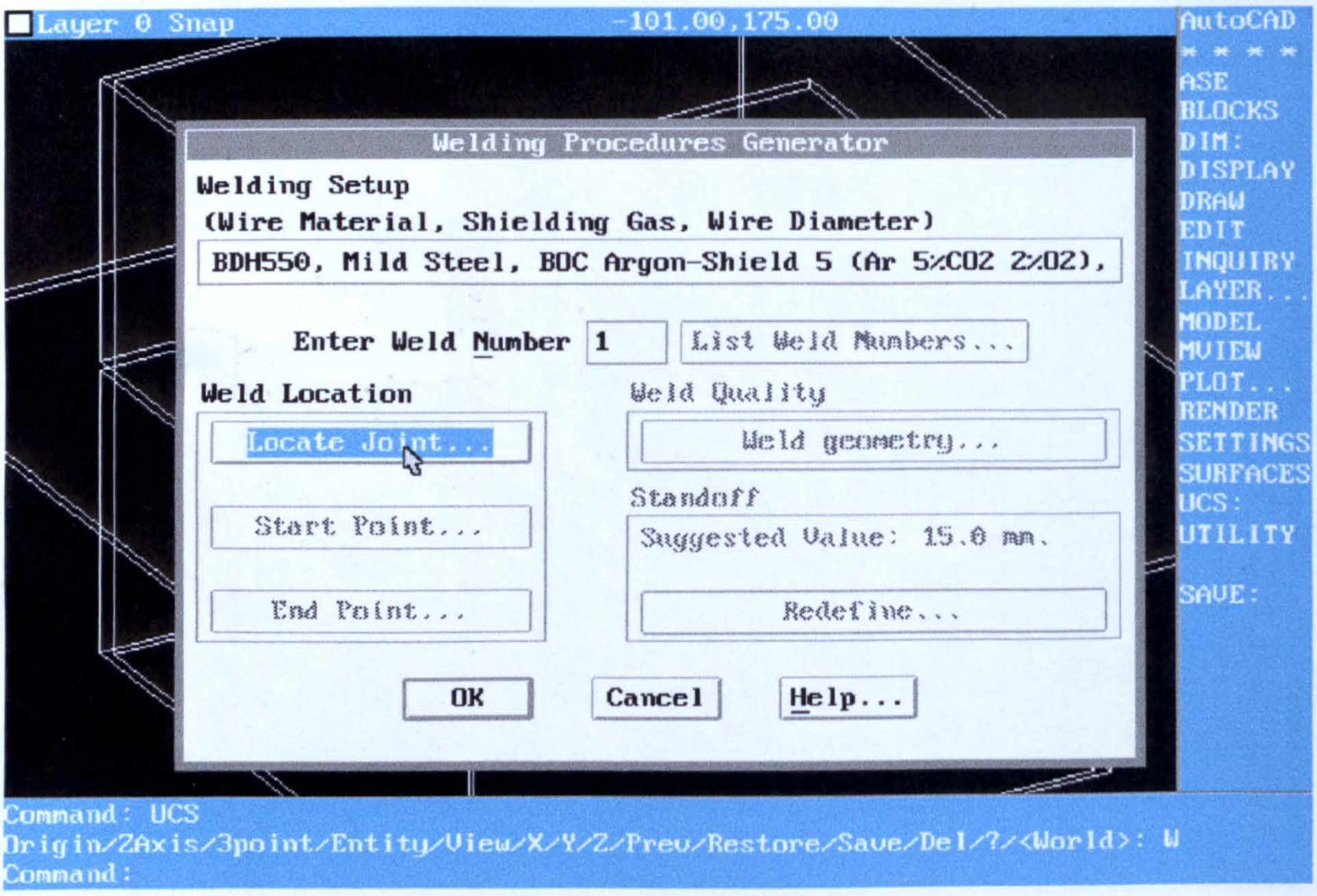

Figure C.3 - Main dialogue box of the welding procedure generator

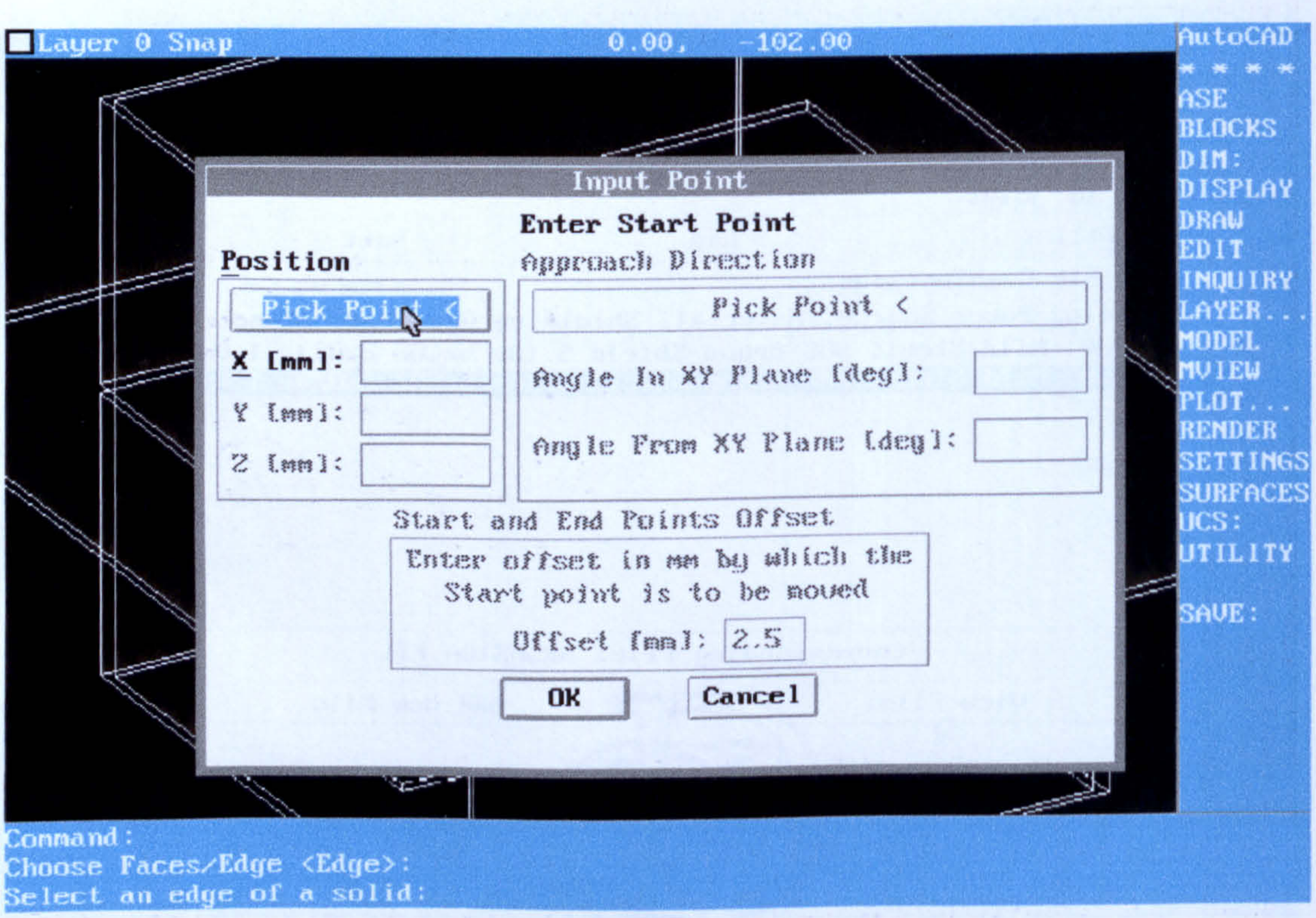

Figure C.4 - Dialogue box for defining the starting point of the weld

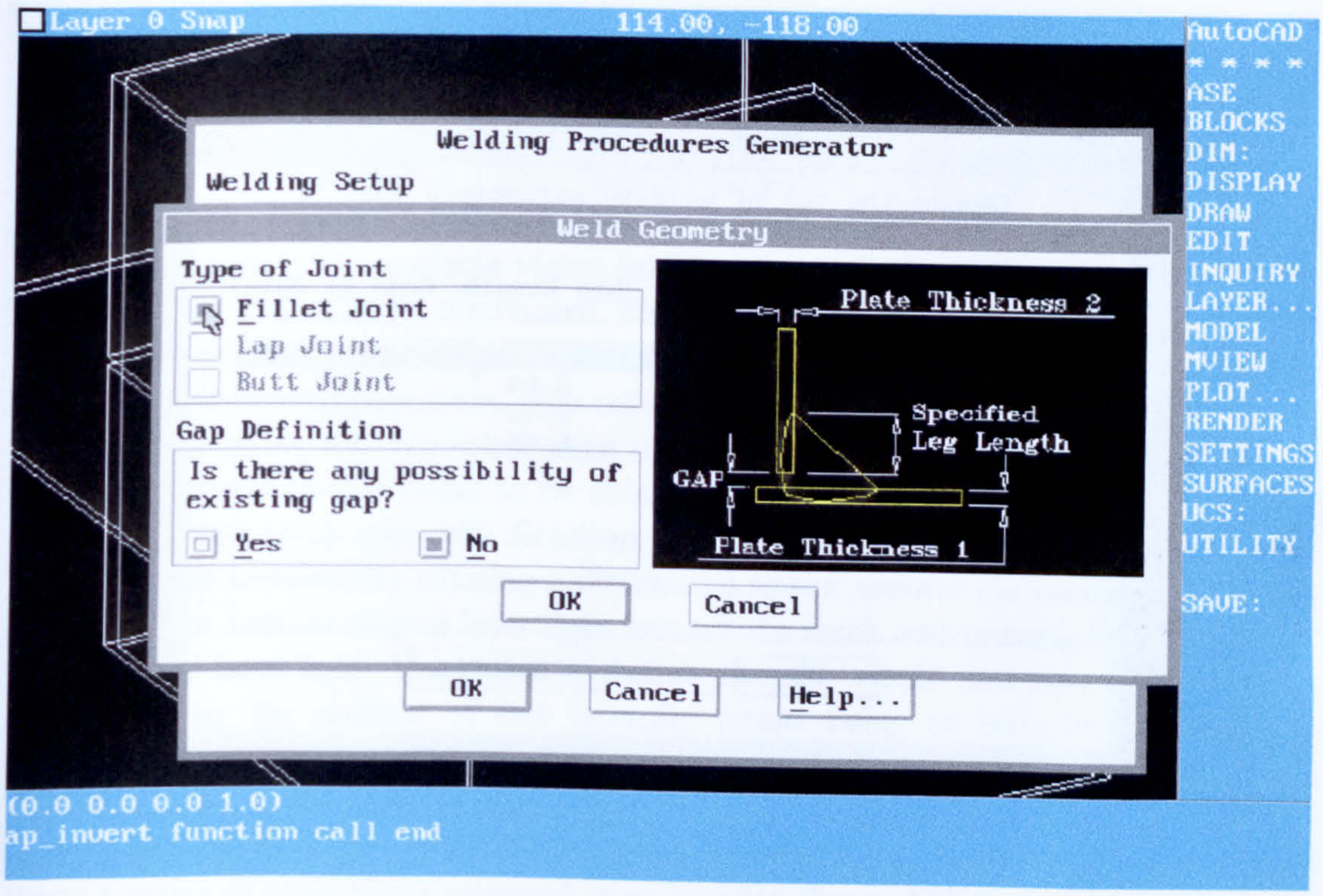

Figure C.5 - Dialogue box for defining the required weld geometry

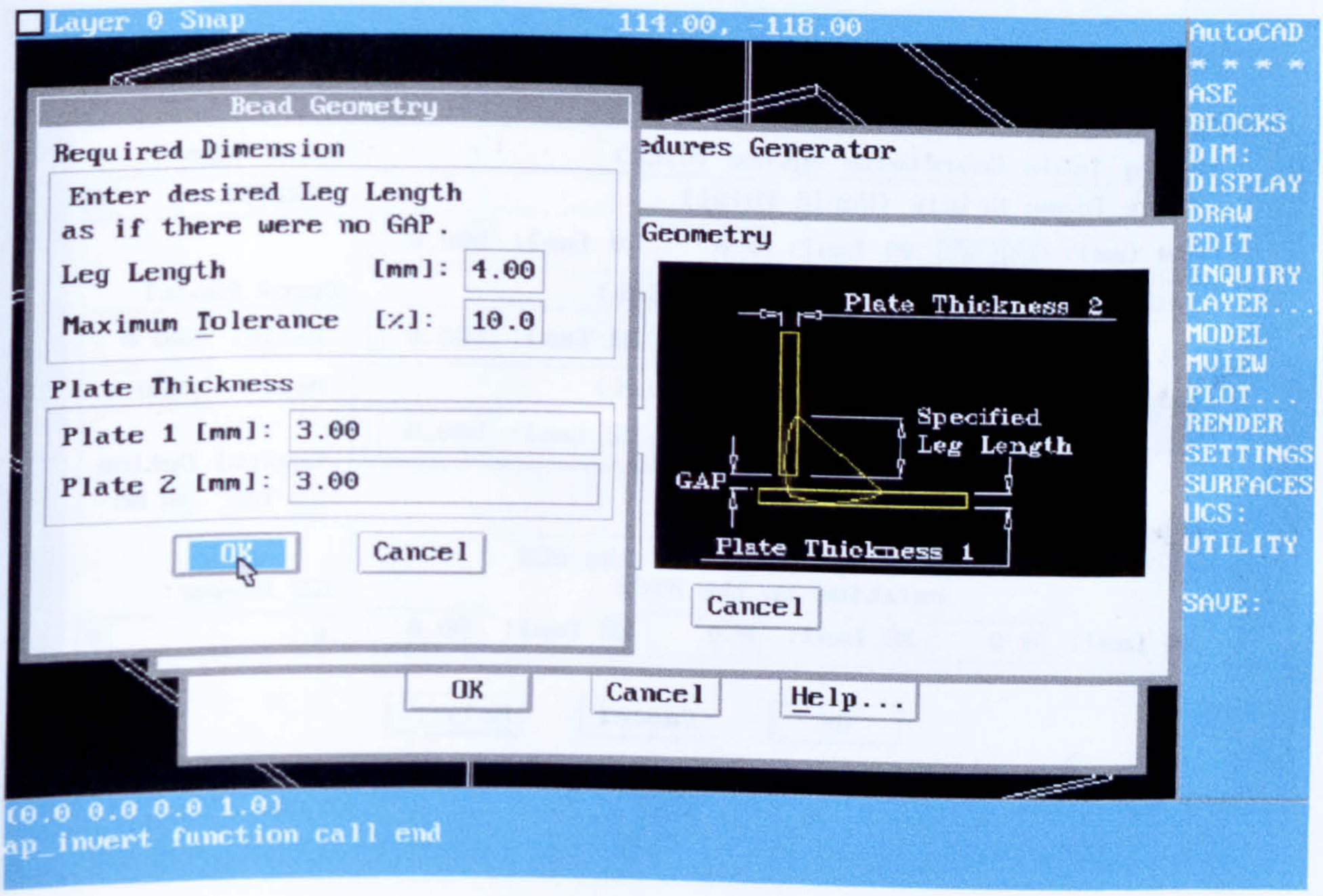

Figure C.6 - Data input dialogue for defining the bead geometry in fillet joints

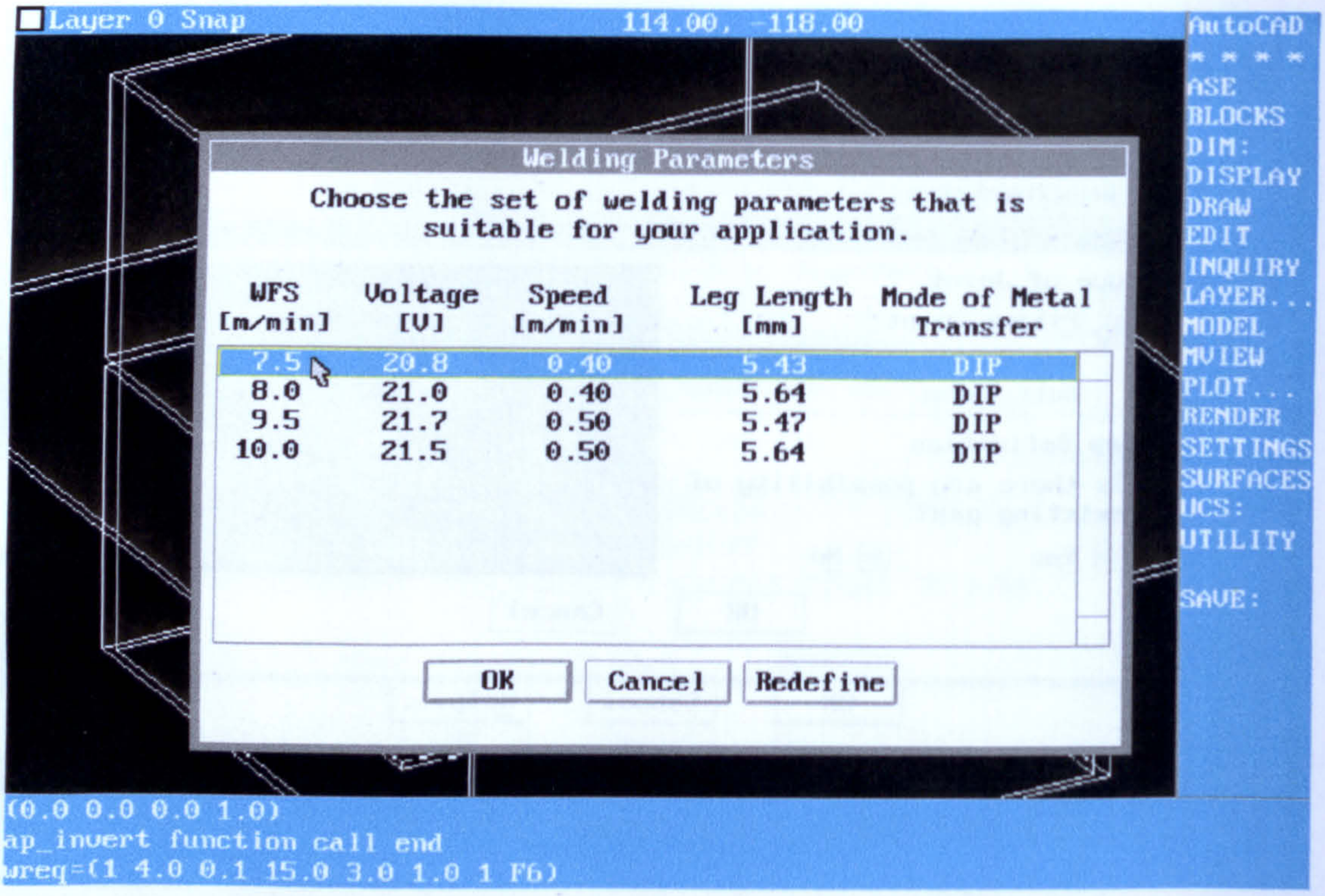

Figure C.7 - Welding parameters output dialogue

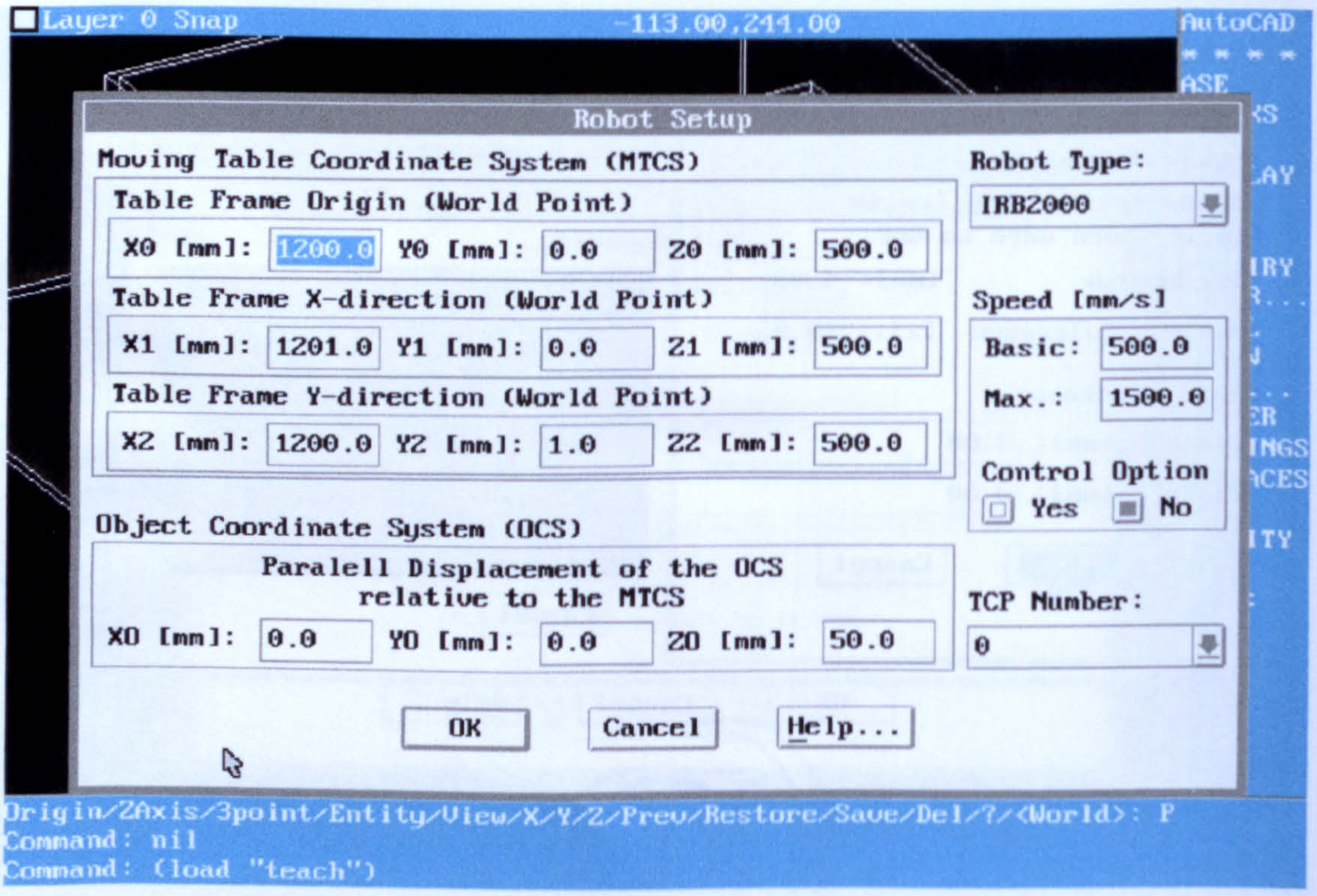

Figure C.8 - Input dialogue for defining the transformation matrix between the CAD co-ordinates system and the Robot world co-ordinates system

Appendix D

This Appendix shows a fibre optic based sensor concept for gap detection and seam tracking. Figure D.1 shows the proposed concept. This was devised after analysing the currently available vision based seam trackers. These were observed to have the similarity of being directional, that is, they are only effective if the projected laser light precedes the welding torch during seam tracking. This restricts the welding torch to determined orientations, thus reducing the flexibility of the robot.

Considering that the robot must change the orientation of the torch (rotation around the torch axis) in order to be able to reach certain positions in its workspace with a constant torch approach direction, a non-directional sensor would be needed. This could be obtained by rotating a directional sensor around the torch as needed or projecting an annular shaped laser light around the torch and sensing the intensity of the reflected laser light. The points with low intensity would correspond to the joint line or a gap, the number of low intensity points being an indication of the gap dimension. The exact position of these points in the circle could be known by using a coherent fibre bundle in the sensing ring.

Some tests were carried out to check the viability of projecting a ring of laser using a series of optic fibres arranged in an annular shape. Although promising results were obtained, the development of this sensor was considered to be out of the scope of the thesis.

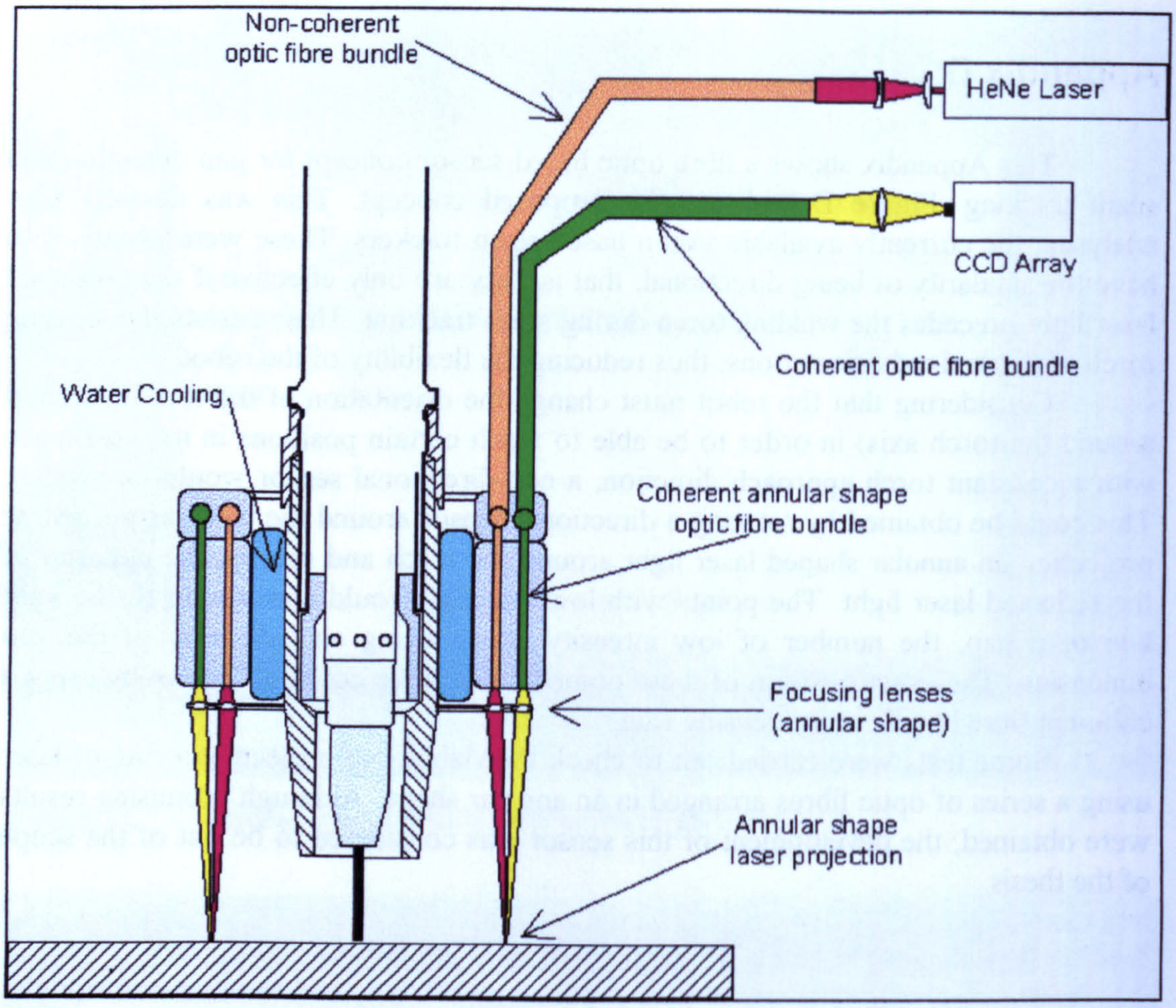

Figure D.1 - Fibre optic based sensor for seam tracking and gap detection

Appendix E

This Appendix describes the monitoring and control software developed in this work. The software was specifically designed to be used in a STE/VME industrial computer using two ARCOM SAD2X250 STE bus based analogue-to-digital data acquisition boards and an ARCOM SADA-8 digital-to-analogue converter board. The memory addresses of the former boards were set at E0000h[1] (board 1, channels 1 and 2) and E8000h (board 2, channels 3 and 4). If necessary, these addresses can be changed to suit the availability of memory space of the computer by using the set-up menu of the program. The digital-to-analogue converter board had its port addresses fixed at 4e8h (voltage channel) and 4e9h (wire feed speed channel). Figure E.1 shows the graphical interface of the monitoring and control software in the replay mode, showing a recorded dip transfer controlled welding trial.

In this mode, a previously recorded weld run can be viewed and analysed window by window. The top two windows display the transient welding voltage (top left) and current (top right). The centre windows display the window average values for the welding voltage (left), the welding current (centre) and the absolute position of the moving table (right) for the whole weld run. The bottom left window shows the stand-off estimates as calculated using the dip resistance estimation model and Ogunbiyi's estimation model. The bottom right window shows information about the run, the monitoring indices, the set-up welding parameters, the dip resistance (see equation 6.8) and its standard deviation (see equation 6.9) and the confidence of bad ignition (see equation 4.11).

The same display format is used during data acquisition and control, the only difference being on the available functions, accessible through special keys assigned by the program. Also, the transient waveforms are not displayed during monitoring and control.

In order to view the graphical interface, the user must go through a series of text based menu driven screens through which calibration factors can be set and general set-up functions are available. Also, the software can display values acquired in the four channels in the hexadecimal form, thus allowing a calibration of the acquisition boards to be performed.

It should be noted, however, that the control functions can only work if the system is correctly set-up. For the table control to be performed, the computer must be linked to the table controller via the serial port 2 and a specific program must be loaded into the table controller memory. The voltage control can only be performed if the power source is linked to the computer via the analogue channels (voltage and wire feed speed).

The following files are needed in order to run the software:

- WCTRL.EXE: main program file;
- WCONTROL.DAT: file containing default set up values;
- EGAVGA.BGI: file containing the VGA functions used for the graphics screen

[1] Hexadecimal number

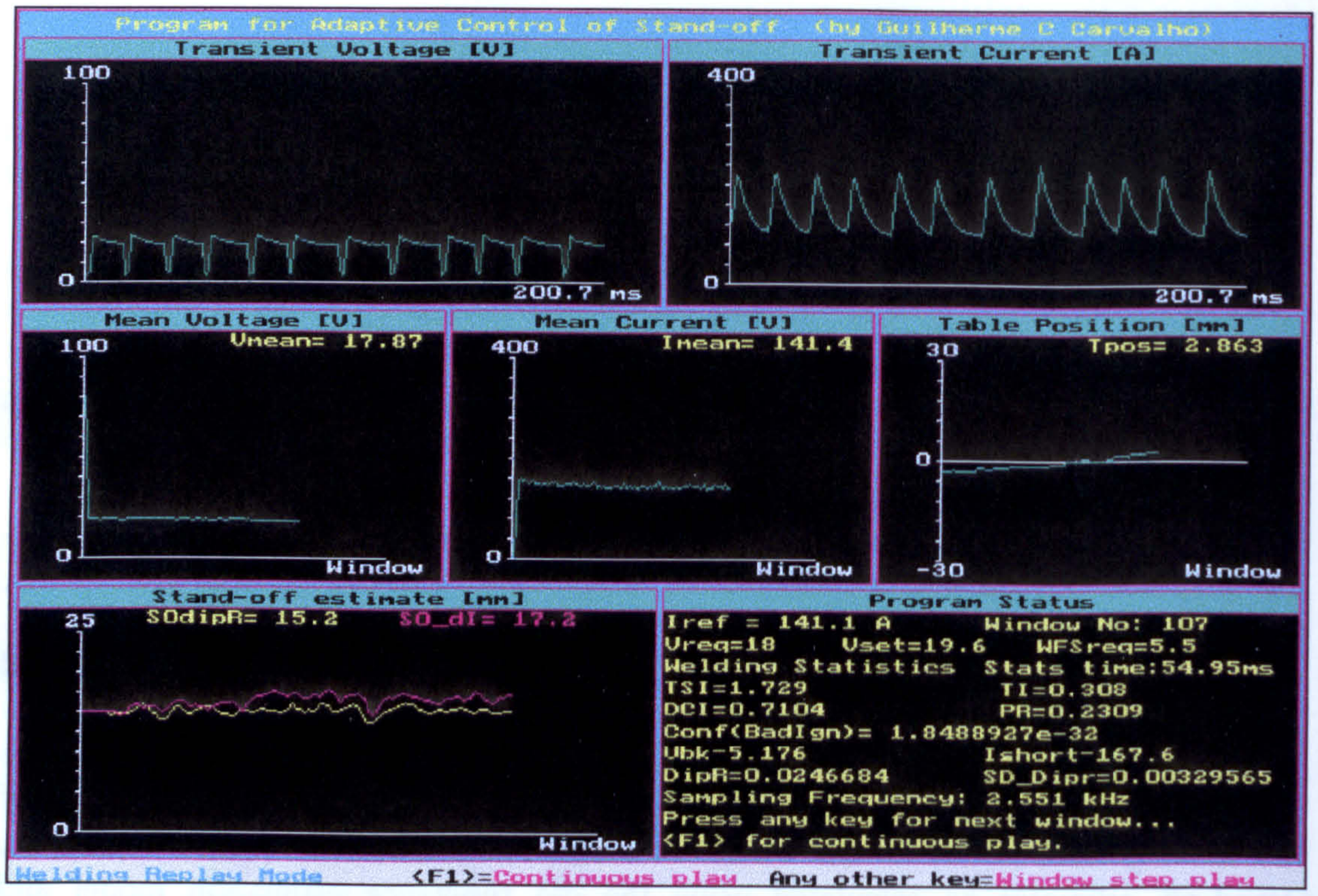

Figure E.1 - Main graphical screen of the monitoring and control software developed, in the replay mode.

Appendix F

This Appendix gives the list of the electronic components used to build the touch sensor circuit shown in Figure 5.1.

List of electronic components:

- 4 operational amplifiers: μA741CP
- 14 Resistors (0.25mW):

R1	9.1 kΩ	R8	1.2 kΩ
R2	9.1 kΩ	R9	1.2 kΩ
R3	10 kΩ	R10	1.2 kΩ
R4	10 kΩ	R11	270 Ω
R5	1 kΩ	R12	2.4 kΩ
R6	27 kΩ	R13	3.6 kΩ
R7	1 kΩ	R14	2.4 kΩ

- 4 Potentiometers (0.5 mW):

Pot1	2 kΩ	Pot3	2 kΩ
Pot2	10 kΩ	Pot4	1 kΩ

- 1 DC-DC Converter: NMH1215D
- 2 Voltage Regulator: MC78L12ACP mounted in parallel.
- 1 Opto Isolator: SFH 610-2
- 1 Output relay: single pole relay 5V (3.7 V - 10 V), 1 kΩ
- 1 Power source connection relay: High isolation double pole relay 24 V (16.8 - 60 V), 2057 Ω
- 3 TransZorbs: SA15A, type unidirectional 500W
- 2 Fuses: 250mA
- 3 Diodes
- 2 LEDs

Appendix G

This Appendix shows the external connections of the interface box built in this work and gives information about its internal electronic circuits. Figure G.1 shows the external view of the Interface Box. This box was primarily built to transform available robot inputs and outputs (I/Os) from switch-type to 24 Vdc I/Os, so that they could be connected to the table controller and the power source robot interface. It was designed to allow up to 8 robot inputs and up to 8 outputs to be used as 24 Vdc I/Os. The transformation between the robot I/Os and the 24V I/Os was provided by using an internally built 24 Vdc (800 mA) power supply and contact relays. The circuits for the outputs and the inputs are shown in Figure G.2 and Figure G.3, respectively. Table G.1 gives the connections made in the Interface Box internal relay board and Table G.2 gives the connections made in the 37-way D-connector. The touch sensor was also mounted inside the interface box and its circuit is shown in Figure 5.1.

Table G.1 - Relay board connector pin layout

PIN	Terminal			
Input Relay	A**	B**	C**	D**
1	1	com***	2	3
2	5	com	6	7
3	10	com	8	9
4	13	com	11	12
5	15	com	14	16
6	22	com	20	21
7	23	com	24	25
8	28	com	26	27
9*	31	com	29	30

* This relay was mounted but was not used. ** See Figure G.4

*** Pins 4 and 32 were connected to the common of the 24V power supply, which was also powering the table controller.
Pins 17, 18 and 19 were not connected.

Table G.2 - Interface box external 37-way D-connector pin layout

Connector pin	Robot I/O	Connector pin	Robot I/O
1	output 1	9	output 5
2	output 1	10	output 5
3	output 2	11	output 6
4	output 2	12	output 6
5	output 3	13	output 7
6	output 3	14	output 7
7	output 4	15	output 8
8	output 4	16	output 8
17	input 1	22	input 5
18	input 2	23	input 6
19	input 3	24	input 7
20	input 4	25	input 8
21	robot common*	26	robot common

Obs.: Pins 27 to 37 were not connected.

* See Figure G.3

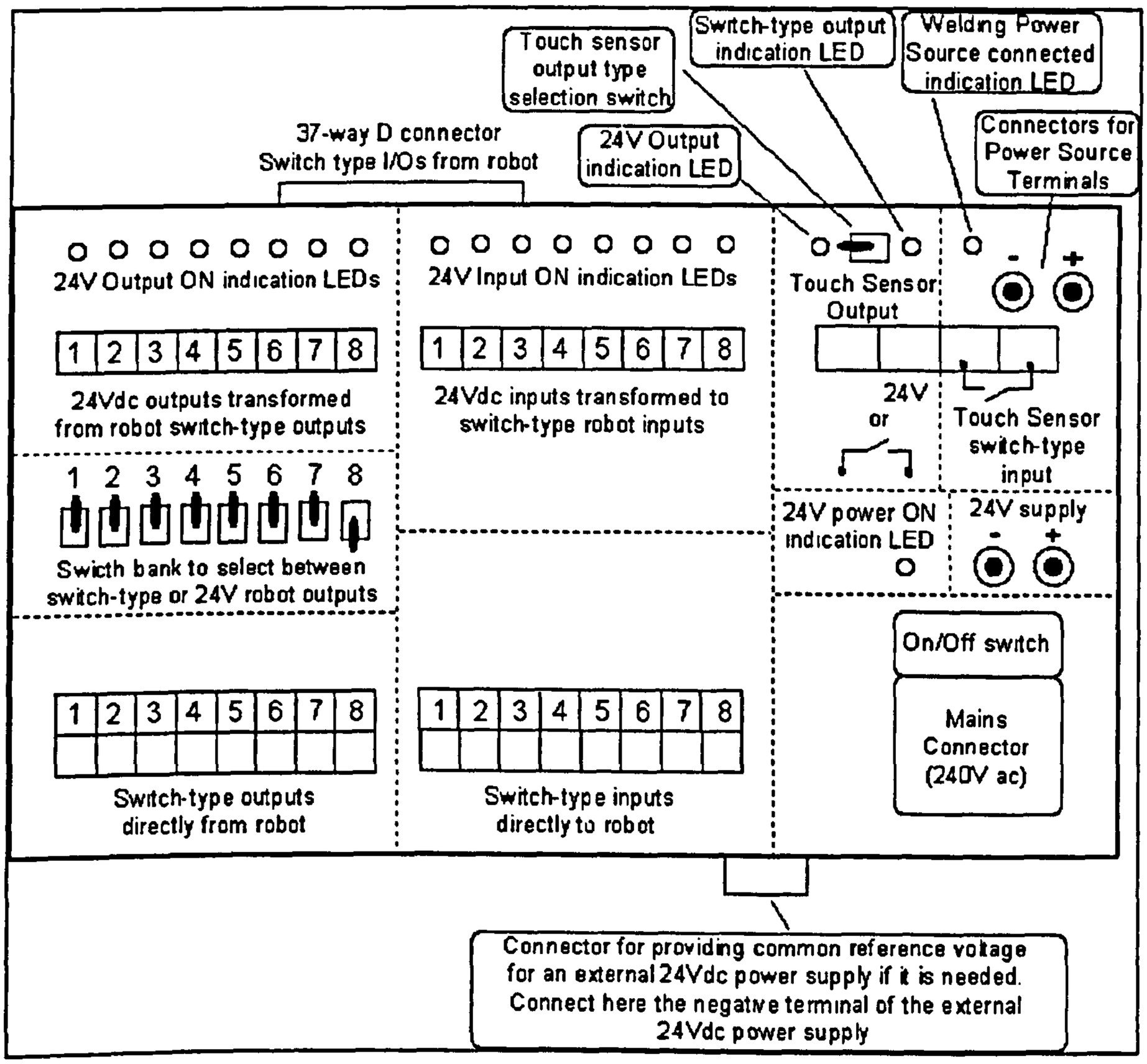

Figure G.1 - External connections of the Interface Box

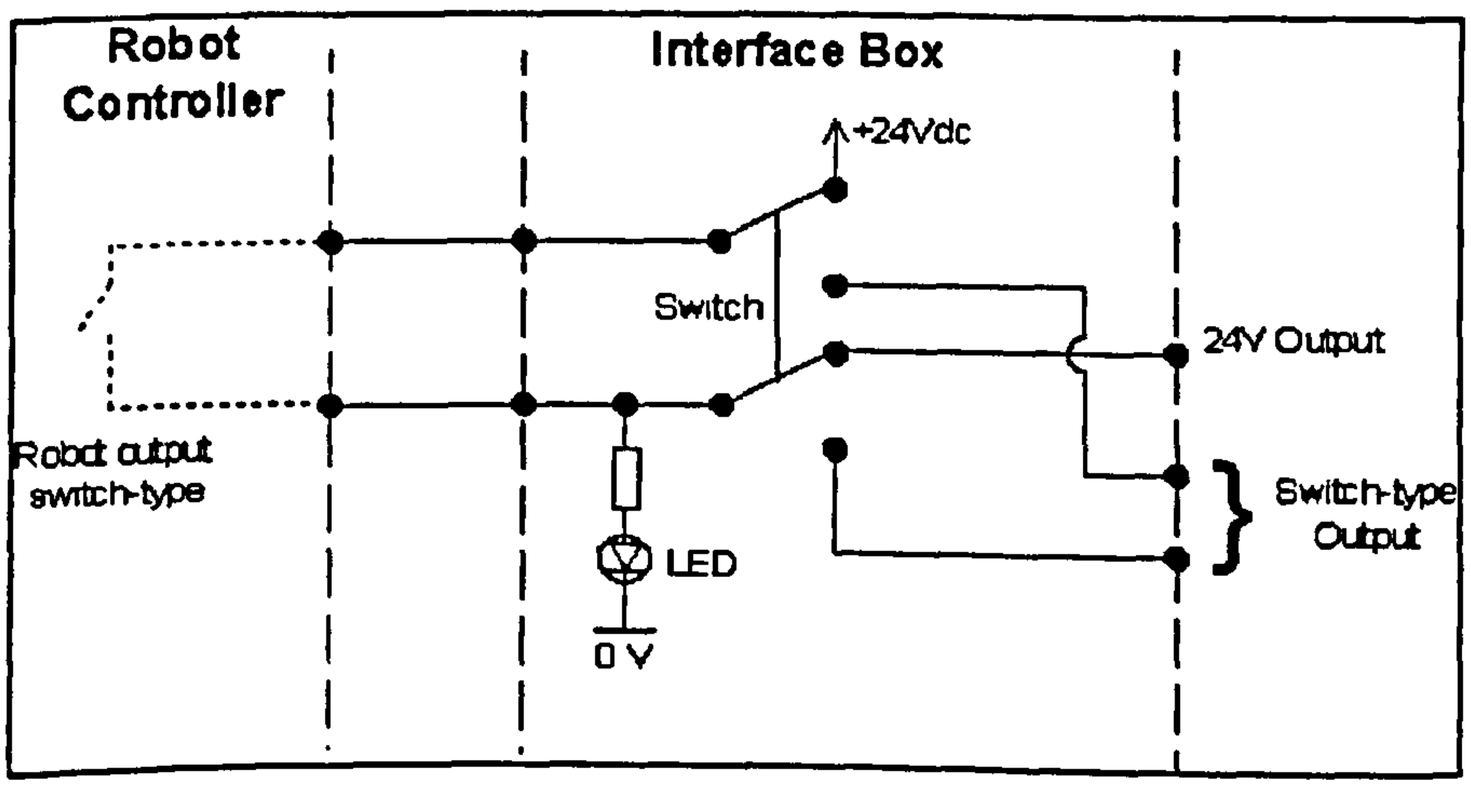

Figure G.2 - Switch-type to 24 V output transformation circuit

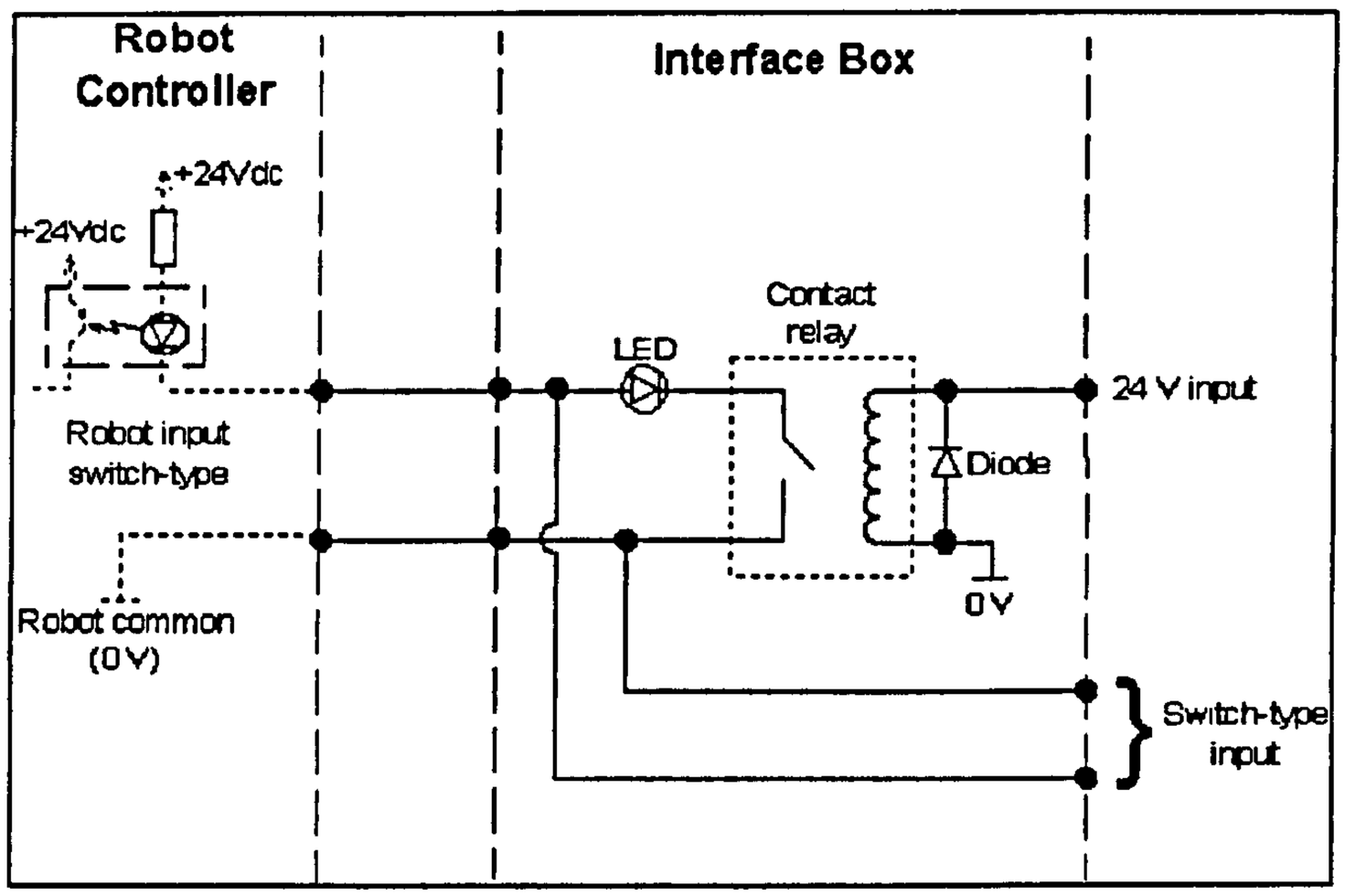

Figure G.3 - 24 V to switch-type input transformation circuit

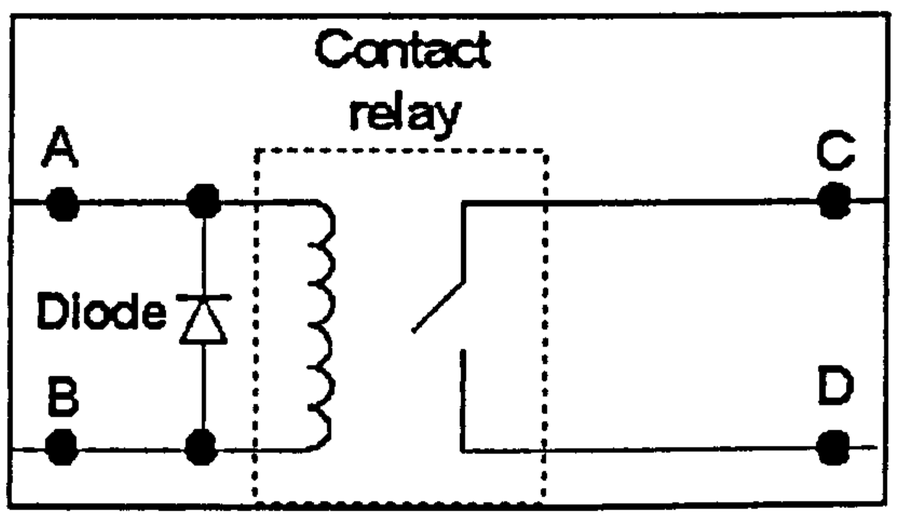

Figure G.4 - Relay terminals as mounted in the relay board

Appendix H

Table H.1 Technical specifications of Migatronic BDH320 and BDH550 welding power sources

Power source	BDH 320	BDH 550
Mains voltage - standard version - version with change-over switch	3x400 V ±10% 3x230 V ±10% 3x400/440/500 V ±10%	3x400 V ±10% 3x230 V ±10% 3x400/440/500 V ±10%
Fuse	According to typeplate on the machine	According to the typeplate on the machine
Consumption max.	12.1 kVA	30 kVA
Efficiency	0.85	0.85
No-load effect	100 W	100 W
Permitted load: - 40% duty cycle - 60% duty cycle - 100% duty cycle	 320 A 260 A / 30.8 V	 550 A / 42 V 400 A / 36 V 500 A / 40 V
Open circuit voltage MMA. MIG/MAG, TIG	80 V	80 V
Current range	5 - 320 A	5 - 550 A
Internal wire feed unit (Compact /Combi)	as KT14	not available
Water module: - Cooling effect - Cooling capacity	 850 W 7 l	 1600 W 4 l
Application class	S	S
Protection class	IP 21	IP 21
Norm	EN60974 EN50199	EN60974 EN50199
Dimensions without wire feed unit	67x46x80 cm	67x46x80 cm
Weight incl. water module	110 kg	135 kg
Wire feed unit, type	**KT12/KT14**	**KT22/KT24**
Operating supply voltage	24 V ac	24 V ac
Effect, 1-2 pcs.	105 W	105 W
Wire dimension	0.8 - 3.2 mm	0.8 - 3.2 mm
Wire reel capacity	5 - 15 kg	5 - 15 - 30 kg
Wire speed	1 - 24 m/min.	1 - 24 m/min.
Dimensions	70x40x21 cm	61x22.5x28 cm
Weight	22 kg	14.6 kg

Data from: **BDH 320/550 Instruction Manual.** Migatronic, Fjerritslev, Denmark, 4/12/1995

Appendix I

Table I.1 Welding data used to develop models to map the BDH-550 performance characteristics

Run	Transfer mode	SO [mm]	WFS	V_{set} [V]	V_{mean} [V]	I_{mean} [A]	I_{min} [A]	I_{max} [A]	V_{bk} [V]	I_{bk} [A]
cal1	dip	12	4	18.80	17.58	126.9	80.1	247.12	4.65	98.94
cal2	dip	12	6	20.50	18.82	173.4	111.2	317.54	6.18	136.83
cal3	dip	12	8	22.20	20.08	211.1	102.2	368.93	8.25	173.45
cal4	dip	12	10	24.00	21.78	232.7	104.1	417.85	11.84	193.8
cal5rr	spray	12	12	34.50	31.51	306.1	295.0	316.7	31.28	302.83
cal6rr	spray	12	14	35.70	32.41	335.9	325.4	346.42	32.2	332.45
cal7	spray	12	16	37.00	33.40	364.8	352.5	375.93	33.17	361.07
cal8	dip	15	4	20.10	18.92	120.4	80.9	267.82	6.06	94.8
cal9	dip	15	6	21.60	20.00	165.7	105.7	342.66	7.84	129.87
cal10	dip	15	8	23.30	21.36	199.3	99.9	382.42	10.37	164.56
cal11	dip/globy	15	10	25.10	22.95	225.6	102.6	402.18	14.53	191.55
cal12	spray	15	12	33.80	31.01	286.6	274.9	296.04	30.8	283.49
cal13	spray	15	14	35.00	31.90	318.9	306.2	330.18	31.65	315.44
cal14	spray	15	16	36.30	32.93	342.4	330.7	353.97	32.69	338.75
cal15	dip	15	6	19.00	17.43	161.0	86.9	298.92	6.25	125.77
cal16	dip	20	4	22.40	21.23	112.7	79.8	319.34	15.42	92.53
cal17	glob/spray	20	6	29.60	27.86	164.7	129.2	237.86	27.36	153.17
cal18	glob/spray	20	8	30.70	28.76	193.9	151.3	279.88	28.14	179.85
cal19	spray	20	10	31.70	29.45	230.9	215.2	240.01	29.26	228.11
cal20	spray	20	12	32.80	30.29	257.1	225.5	267.28	30.03	252.98
cal21	spray	20	14	33.90	31.17	276.2	260.8	289.01	30.85	272.55
cal22	spray	20	16	34.50	31.54	301.8	287.1	313.15	31.26	298.09

WFS = wire feed speed [m/min]

Table I.1 - continuation

Run	V_{pk} [V]	I_{pk} [A]	Vt_{pk} [ms]	Vt_{bk} [ms]	It_{pk} [ms]	It_{bk} [ms]	TSI	TI	DCI	PR
cal1	19.69	172.73	17.02	2.8	7.55	12.23	1.95	0.37	0.74	0.21
cal2	21.47	224.89	12.72	2.74	7.65	10.77	1.83	0.36	0.67	0.26
cal3	22.87	260.43	7.74	1.83	7.44	10.07	1.75	0.52	0.59	0.34
cal4	24.29	284.06	6.74	1.77	7.9	11.34	1.8	0.55	0.46	0.45
cal5rr	31.76	308.47	1.25	1.29	1.77	1.76	1.03	0.04	0.01	0.98
cal6rr	32.67	338.55	1.19	1.38	1.71	1.73	1.03	0.03	0.01	0.98
cal7	33.68	367.59	1.22	1.42	1.72	1.73	1.03	0.03	0.01	0.98
cal8	20.46	173.9	23.68	2.8	9.73	20.57	2.23	0.33	0.68	0.25
cal9	22.2	226.4	13.76	2.54	8.57	14.87	2.07	0.36	0.61	0.31
cal10	23.61	260.03	9.83	2.05	8.43	15.04	1.92	0.5	0.51	0.4
cal11	25.26	278.79	6.92	1.93	7.8	12.8	1.78	0.55	0.37	0.54
cal12	31.26	289.68	1.23	1.39	1.84	1.81	1.03	0.04	0.01	0.98
cal13	32.2	321.78	1.2	1.49	1.84	1.82	1.04	0.04	0.01	0.98
cal14	33.21	345.19	1.21	1.4	1.74	1.78	1.03	0.03	0.01	0.98
cal15	21.11	203.07	7.78	2.6	5.42	6.4	1.86	0.46	0.64	0.28
cal16	22.26	182.85	11.29	1.98	14.2	53.53	2.84	0.29	0.27	0.6
cal17	28.28	178.85	3.05	2.56	19	24.66	1.44	0.21	0.02	0.91
cal18	29.24	208.01	3.27	2.66	12.48	12.91	1.44	0.22	0.02	0.91
cal19	29.68	233.53	1.35	1.56	2.46	2.25	1.04	0.07	0.01	0.98
cal20	30.67	260.03	1.17	1.85	2.32	2.05	1.04	0.12	0.01	0.98
cal21	31.74	279.65	1.14	1.93	2.27	2.12	1.05	0.06	0.01	0.98
cal22	31.91	305.28	1.26	1.64	1.99	1.9	1.04	0.05	0.01	0.98

Appendix J

This appendix shows the welding data collected from the stand-off slope trials carried out with the welding parameters shown in Table 6.6 to measure the proportionality constant, ϕ, which is used in the stand-off estimation model shown in equations 2.22 and 2.23.

The constant value is obtained by dividing the slope of the linear function[1] that fits the points ΔSO_k by the slope of the linear function that best fits the cumulative differences in welding current, $\Sigma(I_{mean,\,k} - I_{mean,(k-1)})$ (see equation 6.6). Note that the intercept of the latter will not be taken into account due to the fact that it corresponds to an offset which is probably caused by random noise present in the measurement of the initial value of welding current, $I_{mean,\,0}$.

The following tables and graphs show the welding data collected from the trials and the fitted lines from which the value of ϕ was calculated. The ϕ values obtained in this Appendix are shown in the Table 6.6 and are compared with the corresponding ϕ values estimated using equation 6.5. The results are plotted in Figure 6.9.

Table J.1 - Welding data collected from stand-off slope trial "s15_2001"

Time [ms]	*SO* [mm]	I_{mean} [A]	ΔSO [mm]	$\Sigma[I_{mean,\,k}-I_{mean,(k-1)}]$ [A]
0	15	148.6	0	0
512	15.63506	144.9	0.635059	-3.7
1024	16.27012	143.2	1.270118	-5.4
1536	16.90518	142.3	1.905178	-6.3
2048	17.54024	139.9	2.540237	-8.7
2560	18.1753	138.2	3.175296	-10.4
3072	18.81036	136.4	3.810355	-12.2
3584	19.44541	134.5	4.445414	-14.1
4096	20.08047	132.3	5.080474	-16.3

WFS = 5 m/min
Vset = 21.3 V

S_W = 0.6 m/min
Vreq = 19.4 V

[1] y(x) = ax+b, a = slope, b = intercept

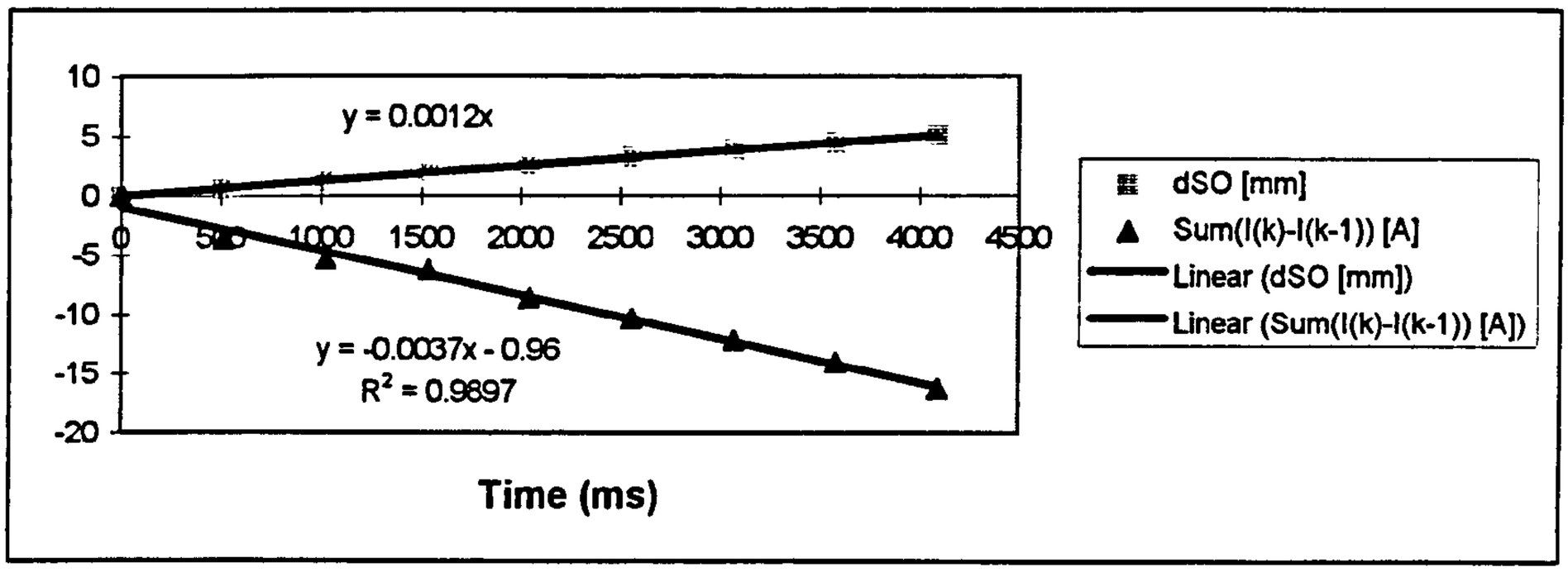

Figure J.1 - Plot of stand-off variation and cumulative changes in welding current for welding trial "s15_2001"

Table J.2 - Welding data collected from stand-off slope trial "15_2002"

time [ms]	SO [mm]	I_{mean} [A]	ΔSO [mm]	$\Sigma[I_{mean,\,k} - I_{mean,(k-1)}]$ [A]
0	15	162.8	0	0
512	15.74	161.7	0.74	-1.1
1024	16.48	156.7	1.48	-6.1
1536	17.22	156.6	2.22	-6.2
2048	17.96	155.7	2.96	-7.1
2560	18.70	150.4	3.70	-12.4
3072	19.44	150.7	4.45	-12.1
3584	20.19	149.5	5.19	-13.3

WFS = 6 m/min **S_W = 0.7 m/min**
Vset = 21.5 V **Vreq = 19.6 V**

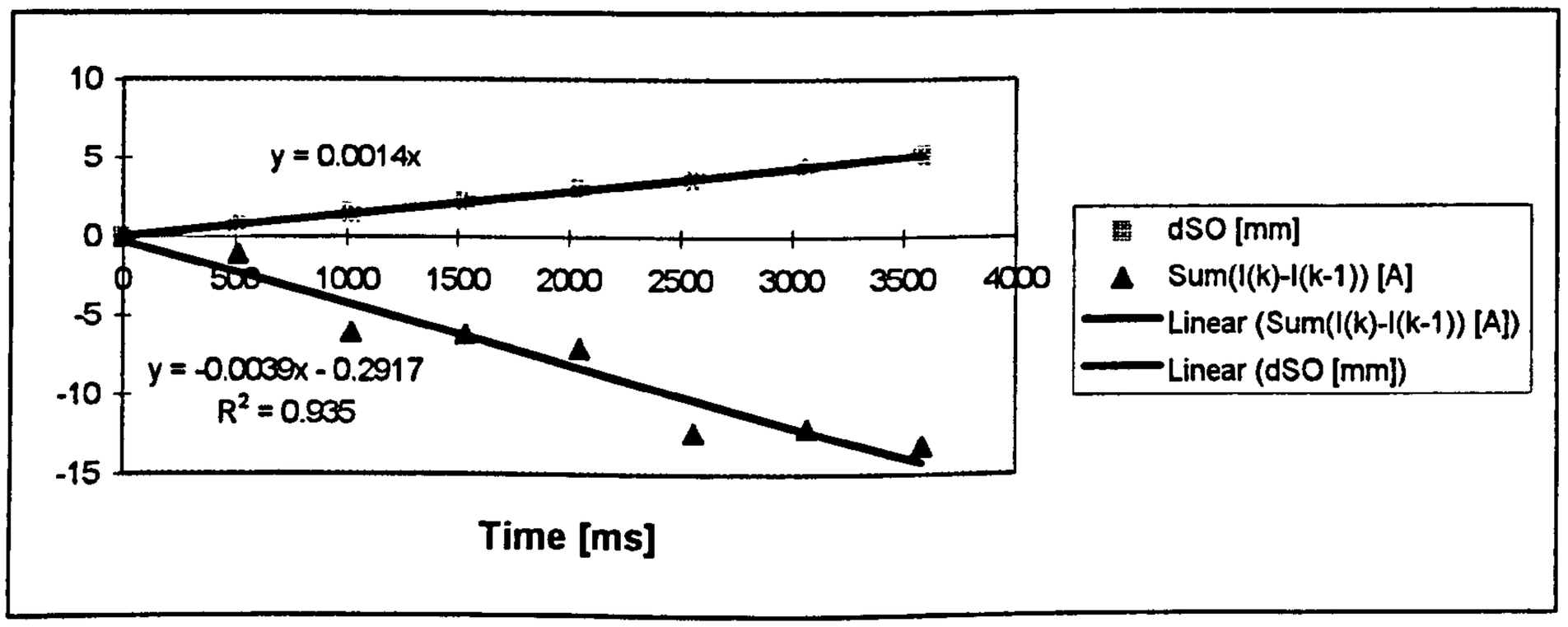

Figure J.2 - Plot of stand-off variation and cumulative changes in welding current for welding trial "s15_2002"

Table J.3 - Welding data collected from stand-off slope trial "s15_2003"

Time [ms]	*SO* [mm]	I_{mean} [A]	ΔSO [mm]	$\Sigma[I_{mean,\,k} - I_{mean,(k-1)}]$ [A]
0	15	179.2	0	0
512	15.85	174.6	0.85	-4.6
1024	16.69	172.2	1.69	-7.0
1536	17.54	171.4	2.54	-7.8
2048	18.39	167.6	3.39	-11.6
2560	19.23	165.6	4.23	-13.6
3072	20.08	164.6	5.08	-14.6

WFS = 7 m/min S_W = 0.8 m/min
Vset = 21.8 V Vreq = 19.9 V

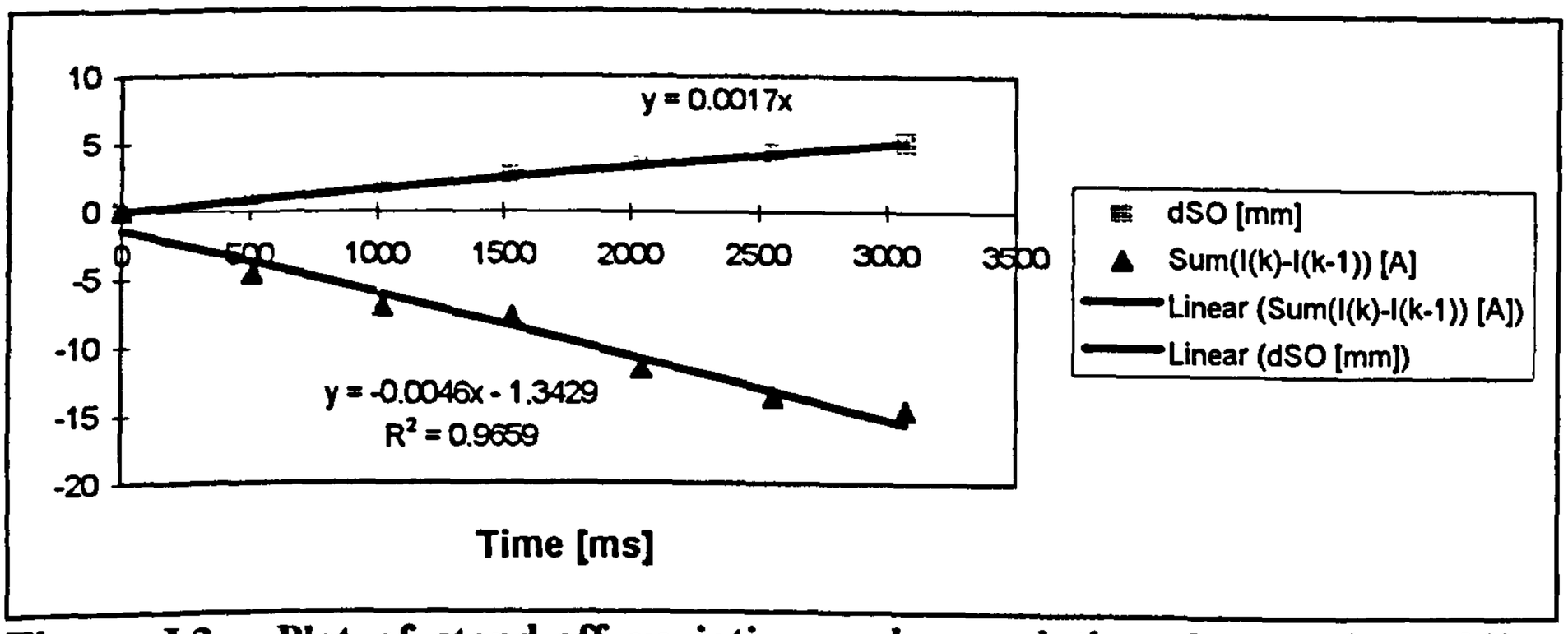

Figure J.3 - Plot of stand-off variation and cumulative changes in welding current for welding trial "s15_2003"

Table J.4 - Welding data collected from stand-off slope trial "s15_2004"

Time [ms]	*SO* [mm]	I_{mean} [A]	ΔSO [mm]	$\Sigma[I_{mean,\,k} - I_{mean,(k-1)}]$ [A]
0	15	196.7	0	0
512	15.95	192.1	0.95	-4.6
1024	16.91	188.0	1.91	-8.8
1536	17.86	186.3	2.86	-10.4
2048	18.81	184.2	3.81	-12.5
2560	19.76	178.4	4.76	-18.3

WFS = 8 m/min S_W = 0.9 m/min
Vset = 22.1 V Vreq = 20.2 V

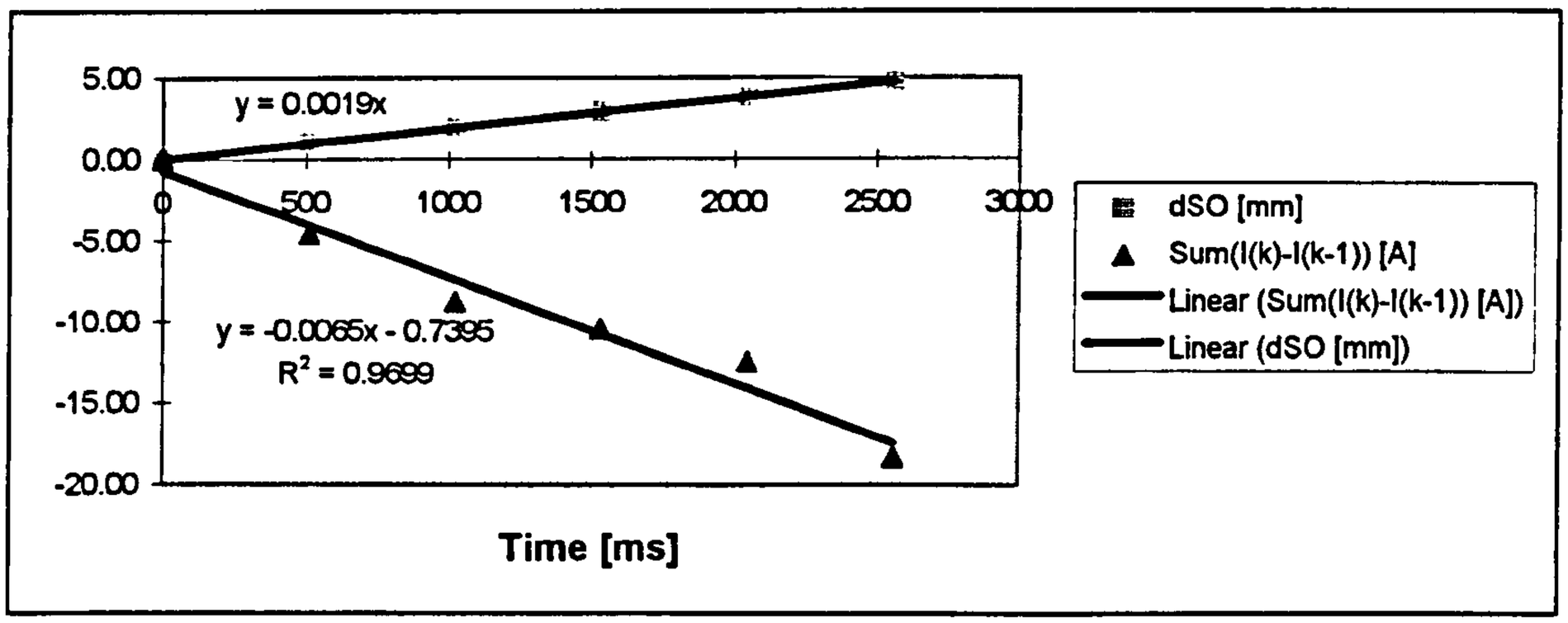

Figure J.4 - Plot of stand-off variation and cumulative changes in welding current for welding trial "s15_2004"

Table J.5 - Welding data collected from stand-off slope trial "s15_2005"

Time [ms]	*SO* [mm]	$I_{mean,k}$ [A]	ΔSO [mm]	$\Sigma[I_{mean,k} - I_{mean,k-1}]$ [A]
0	15	210.4	0	0
512	15.53	207.5	0.53	-2.9
1024	16.06	202.6	1.06	-7.8
1536	16.59	202.8	1.56	-7.6
2048	17.12	200.4	2.12	-10.0
2560	17.65	196.3	2.65	-14.2
3072	18.18	194.4	3.18	-16.0
3584	18.70	197.2	3.70	-13.2
4096	19.23	194.6	4.23	-15.8
4608	19.76	195.9	4.76	-14.5

WFS = 9 m/min **S_W = 0.5 m/min**
Vset = 22.5 V **Vreq = 20.5 V**

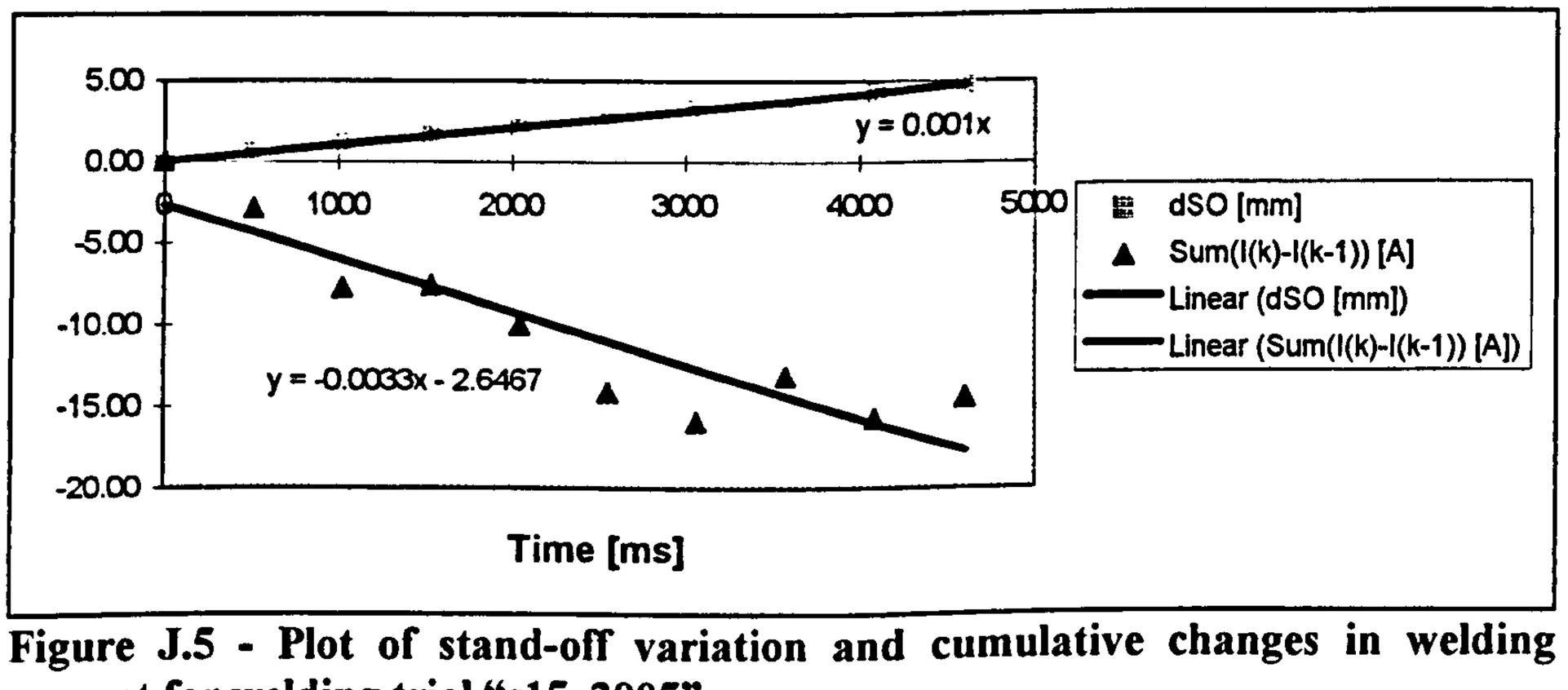

Figure J.5 - Plot of stand-off variation and cumulative changes in welding current for welding trial "s15_2005"

Table J.6 - Welding data collected from stand-off slope trial "s15_2006"

Time [ms]	*SO* [mm]	$I_{mean,k}$ [A]	ΔSO [mm]	$\Sigma[I_{mean,\,k} - I_{mean,(k-1)}]$ [A]
0	15	217.2	0	0
512	15.53	212.0	0.53	-5.2
1024	16.06	213.5	1.06	-3.7
1536	16.59	211.9	1.59	-5.4
2048	17.12	209.3	2.12	-8.0
2560	17.65	207.6	2.65	-9.6
3072	18.18	205.4	3.18	-11.8
3584	18.70	204.2	3.70	-13.0
4096	19.23	200.1	4.23	-17.1
4608	19.76	200.9	4.76	-16.3

WFS = 9.5 m/min **S_W = 0.5 m/min**
Vset = 22.7 V **Vreq = 20.7 V**

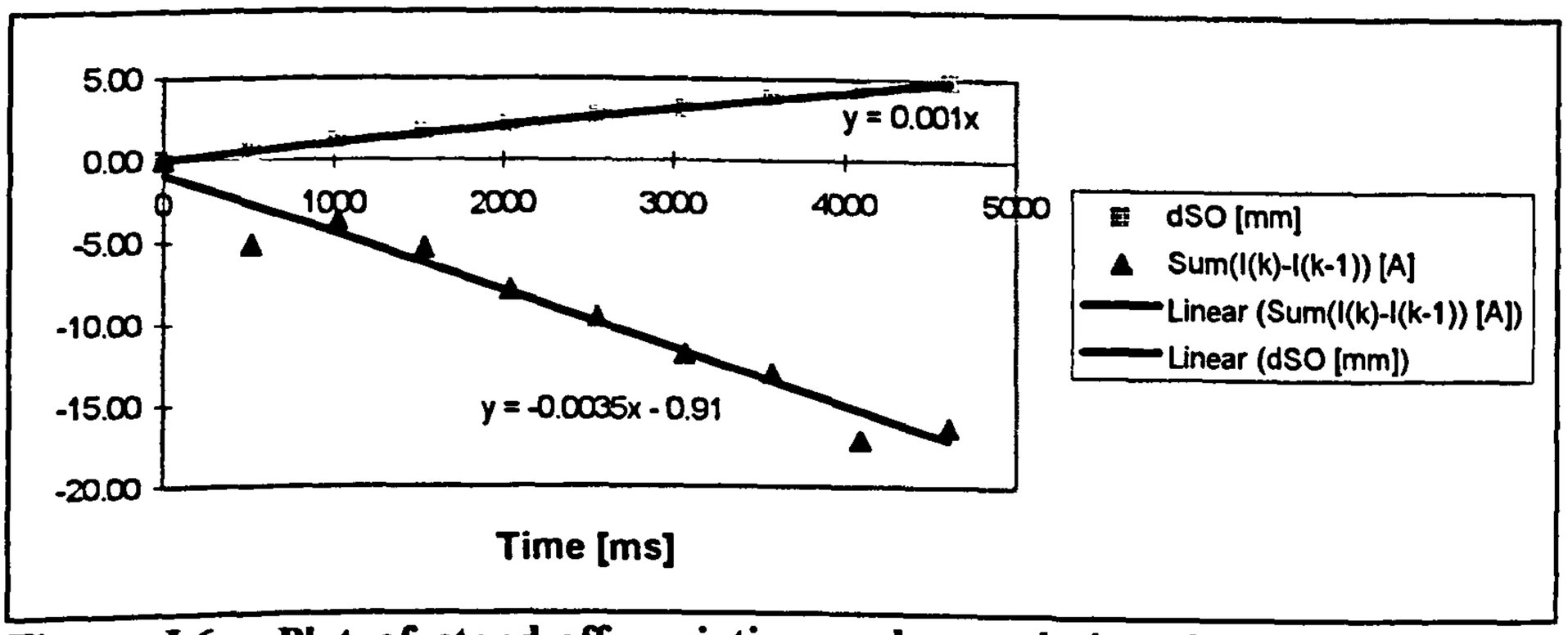

Figure J.6 - Plot of stand-off variation and cumulative changes in welding current for welding trial "s15_2006"

Table J.7 - Welding data collected from stand-off slope trial "s15_2007"

Time [ms]	*SO* [mm]	$I_{mean,\,k}$ [A]	ΔSO [mm]	$\Sigma[I_{mean,\,k} - I_{mean,(k-1)}]$ [A]
0	15	279.1	0	0
512	15.64	269.9	0.64	-9.2
1024	16.27	266.3	1.27	-12.8
1536	16.91	262.0	1.91	-17.1
2048	17.54	257.4	2.54	-21.7
2560	18.18	254.1	3.18	-25.0
3072	18.81	253.2	3.81	-25.9
3584	19.45	247.3	4.45	-31.8
4096	20.08	243.9	5.08	-35.2

WFS = 11 m/min S_w = 0.6 m/min
Vset = 33.1 V Vreq = 30.5 V

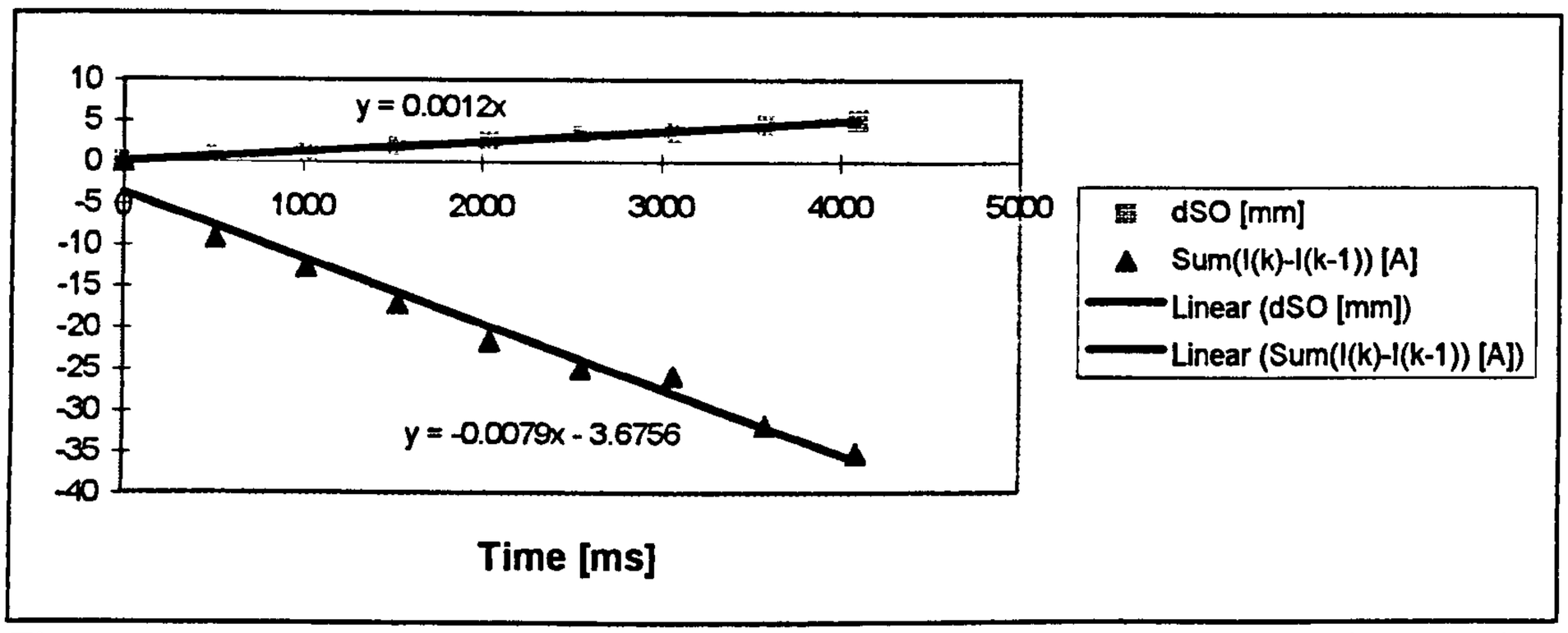

Figure J.7 - Plot of stand-off variation and cumulative changes in welding current for welding trial "s15_2007"

Table J.8 - Welding data collected from stand-off slope trial "s15_2008"

Time [ms]	*SO* [mm]	$I_{mean,\,k}$ [A]	ΔSO [mm]	$\Sigma[I_{mean,\,k} - I_{mean,(k-1)}]$ [A]
0	15	299.4	0	0
512	15.74	289.9	0.74	-9.5
1024	16.48	284.8	1.48	-14.6
1536	17.22	283.4	2.22	-16.0
2048	17.96	275.2	2.96	-24.2
2560	18.70	269.6	3.70	-29.8
3072	19.45	267.1	4.45	-32.3
3584	20.19	265.0	5.19	-34.4

WFS = 12.5 m/min S_w = 0.7 m/min
Vset = 33.8 V Vreq = 31.1 V

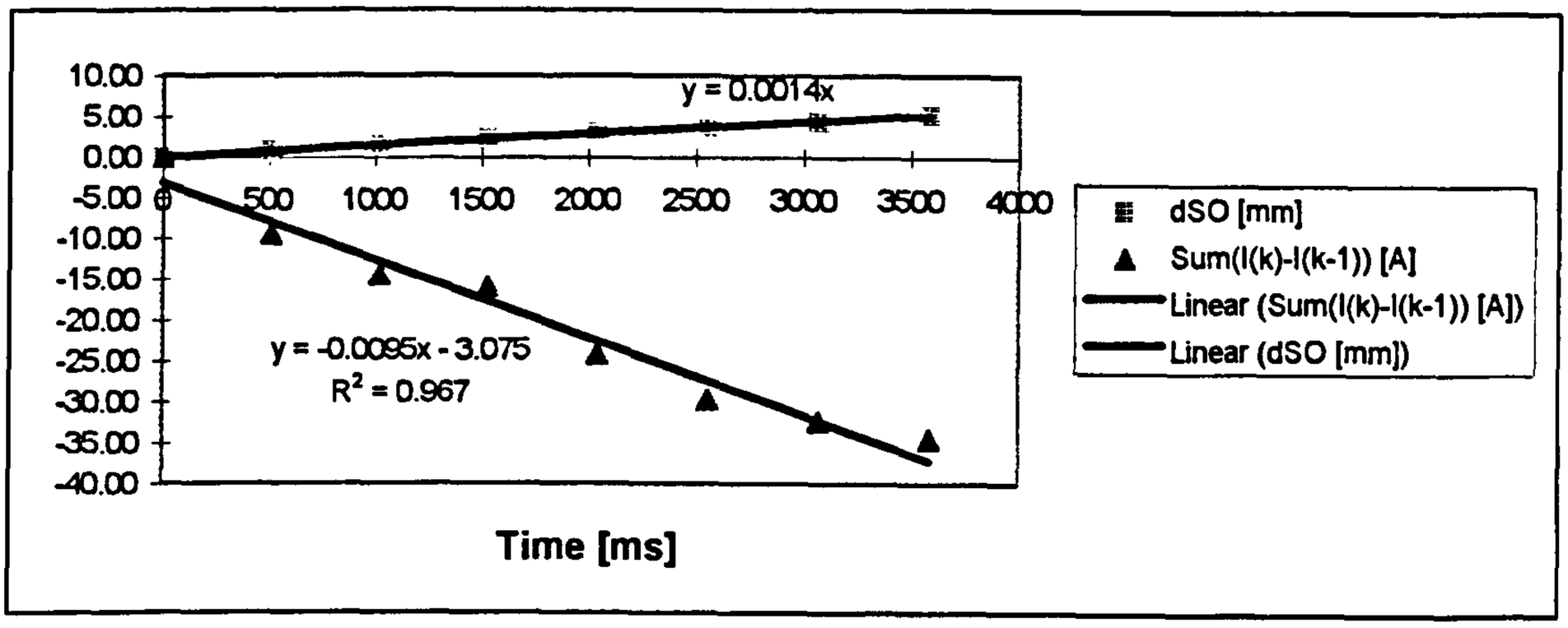

Figure J.8 - Plot of stand-off variation and cumulative changes in welding current for welding trial "s15_2008"

Table J.9 - Welding data collected from stand-off slope trial "s15_2009"

Time [ms]	*SO* [mm]	$I_{mean,\,k}$ [A]	ΔSO [mm]	$\Sigma[I_{mean,\,k} - I_{mean,(k-1)}]$ [A]
0	15	311.1	0	0
512	15.74	302.8	0.74	-8.3
1024	16.48	298.4	1.48	-12.7
1536	17.22	293.6	2.22	-17.5
2048	17.96	288.7	2.96	-22.4
2560	18.70	284.7	3.70	-26.4
3072	19.45	279.9	4.45	-31.2

WFS = 13.5 m/min
Vset = 34.3 V

S_W = 0.7 m/min
Vreq = 31.5 V

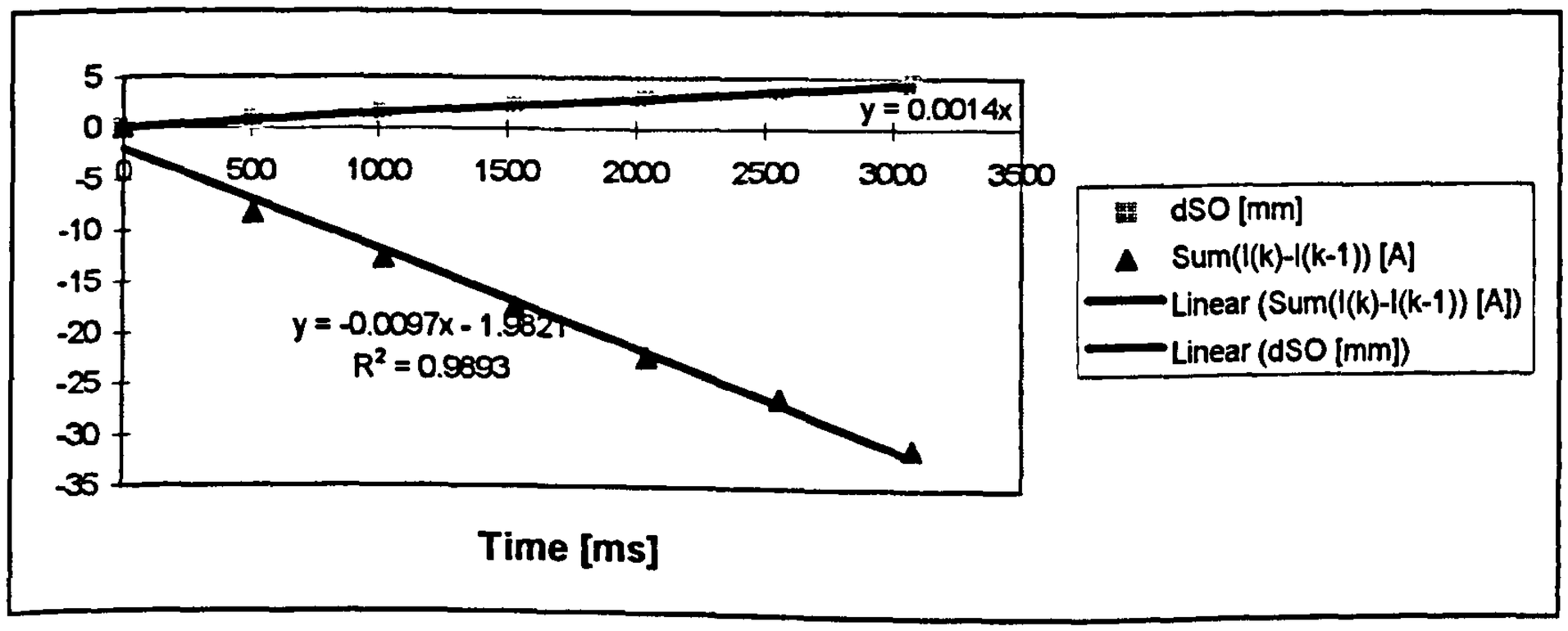

Figure J.9 - Plot of stand-off variation and cumulative changes in welding current for welding trial "s15_2009"

Table J.10 - Welding data collected from stand-off slope trial "s15_2010"

Time [ms]	*SO* [mm]	$I_{mean,\,k}$ [A]	ΔSO [mm]	$\Sigma[I_{mean,\,k} - I_{mean,(k-1)}]$ [A]
0	15.00	328.1	0.00	0.0
512	15.74	319.0	0.74	-9.1
1024	16.48	312.1	1.48	-16.0
1536	17.22	307.6	2.22	-20.5
2048	17.96	302.4	2.96	-25.7
2560	18.70	296.9	3.70	-31.2
3072	19.45	294.4	4.45	-33.7

WFS = 14.5 m/min
Vset = 34.8 V

S_W = 0.7 m/min
Vreq = 32.0 V

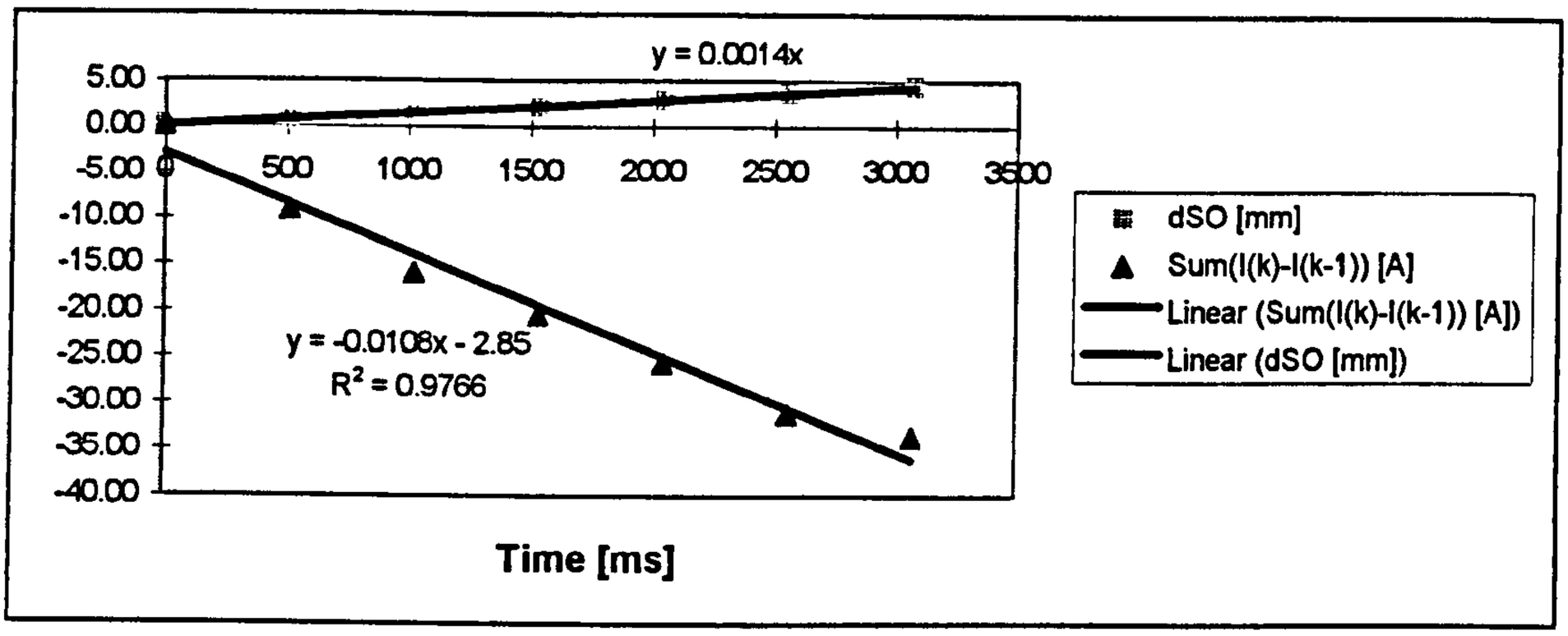

Figure J.10 - Plot of stand-off variation and cumulative changes in welding current for welding trial "s15_2010"

Table J.11 - Welding data collected from stand-off slope trial "s15_1001"

Time [ms]	*SO* [mm]	$I_{mean,\,k}$ [A]	ΔSO [mm]	$\Sigma[I_{mean,\,k} - I_{mean,(k-1)}]$ [A]
0	15.00	147.3	0.00	0.0
512	14.36	149.3	-0.64	2.0
1024	13.73	150.2	-1.27	2.9
1536	13.09	153.7	-1.91	6.4
2048	12.46	154.8	-2.54	7.5
2560	11.82	157.8	-3.18	10.6
3072	11.19	160.0	-3.81	12.7
3584	10.55	159.5	-4.45	12.2

WFS = 5.0 m/min
Vset = 21.3 V

S_W = 0.6 m/min
Vreq = 19.4 V

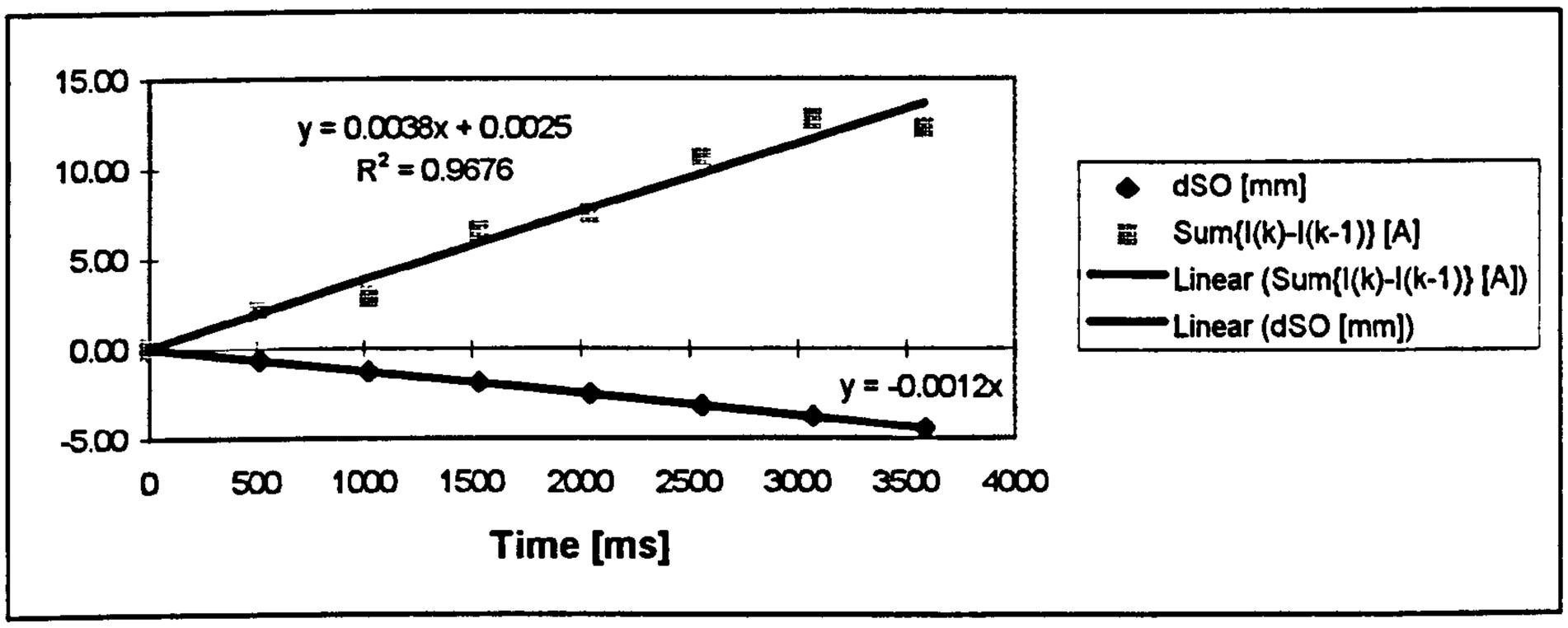

Figure J.11 - Plot of stand-off variation and cumulative changes in welding current for welding trial "s15_1001"

Table J.12 - Welding data collected from stand-off slope trial "s15_1002"

Time [ms]	*SO* [mm]	$I_{mean,\,k}$ [A]	ΔSO [mm]	$\Sigma[I_{mean,\,k} - I_{mean,(k-1)}]$ [A]
0	15.00	163.5	0.00	0.0
512	14.26	164.9	-0.74	1.4
1024	13.52	169.4	-1.48	5.9
1536	12.78	173.4	-2.22	10.0
2048	12.04	176.6	-2.96	13.2
2560	11.30	177.1	-3.70	13.6
3072	10.56	180.6	-4.45	17.1

WFS = 6.0 m/min S_w = 0.7 m/min
Vset = 21.5 V Vreq = 19.6 V

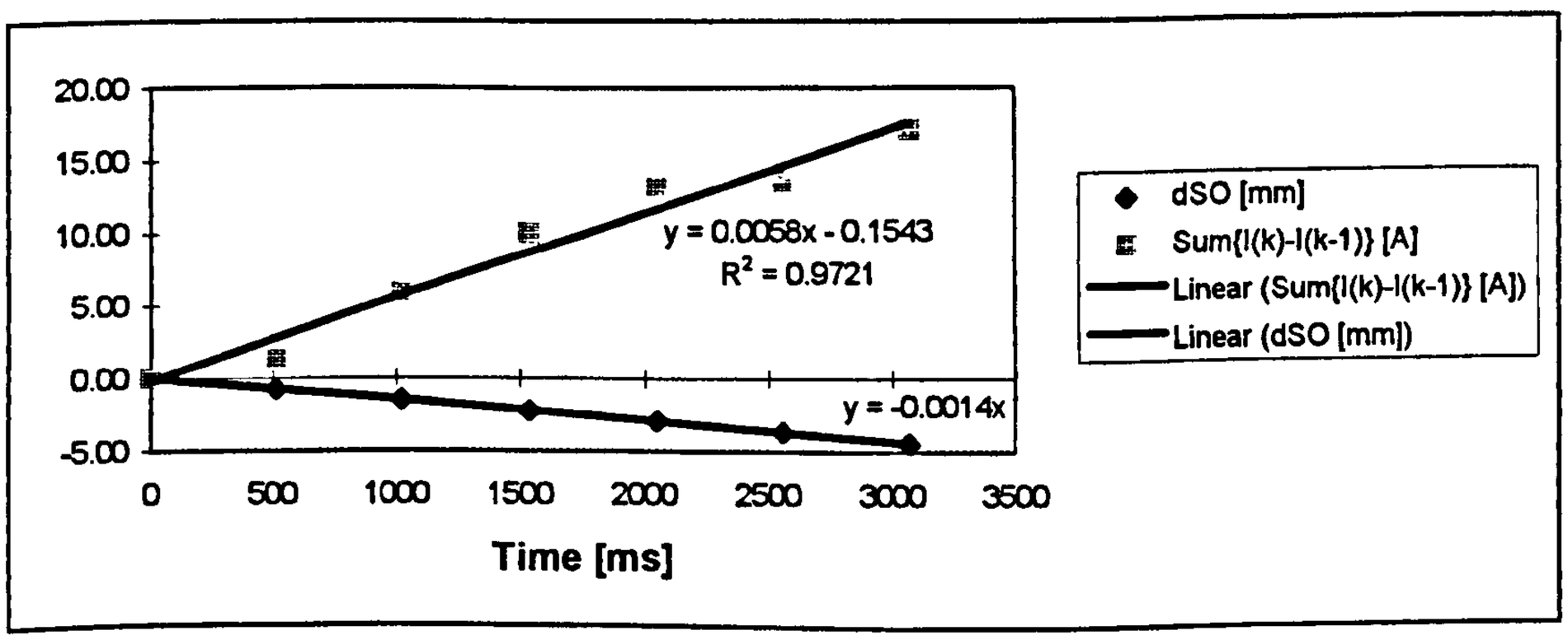

Figure J.12 - Plot of stand-off variation and cumulative changes in welding current for welding trial "s15_1002"

Table J.13 - Welding data collected from stand-off slope trial "s15_1003"

Time [ms]	*SO* [mm]	$I_{mean,\,k}$ [A]	ΔSO [mm]	$\Sigma[I_{mean,\,k} - I_{mean,(k-1)}]$ [A]
0	15.00	184.0	0.00	0.0
512	14.15	184.9	-0.85	0.8
1024	13.31	188.2	-1.69	4.1
1536	12.46	193.1	-2.54	9.1
2048	11.61	197.1	-3.39	13.1
2560	10.77	200.3	-4.23	16.3
3072	9.92	204.6	-5.08	20.6

WFS = 7.0 m/min
Vset = 21.8 V

S_W = 0.8 m/min
Vreq = 19.9 V

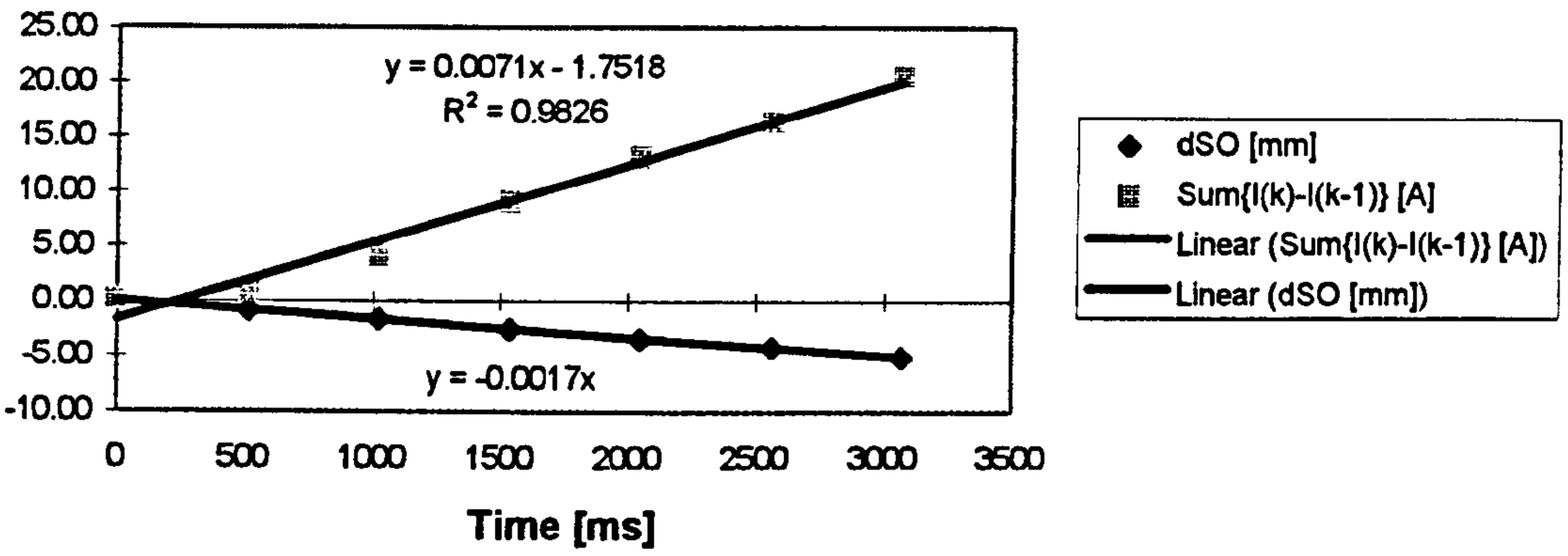

Figure J.13 - Plot of stand-off variation and cumulative changes in welding current for welding trial "s15_1003"

Table J.14 - Welding data collected from stand-off slope trial "s15_1004"

Time [ms]	*SO* [mm]	$I_{mean,\,k}$ [A]	ΔSO [mm]	$\Sigma[I_{mean,\,k} - I_{mean,(k-1)}]$ [A]
0	15.00	199.5	0.00	0.0
256	14.52	202.5	-0.48	3.0
512	14.05	201.9	-0.95	2.4
768	13.57	208.7	-1.43	9.2
1024	13.09	200.0	-1.91	0.5
1280	12.62	211.6	-2.38	12.1
1536	12.14	213.3	-2.86	13.8
1792	11.67	216.9	-3.33	17.4
2048	11.19	217.5	-3.81	18.0
2304	10.71	218.2	-4.29	18.7
2560	10.24	220.6	-4.76	21.1

WFS = 8.0 m/min
Vset = 22.1 V

S_W = 0.9 m/min
Vreq = 20.2 V

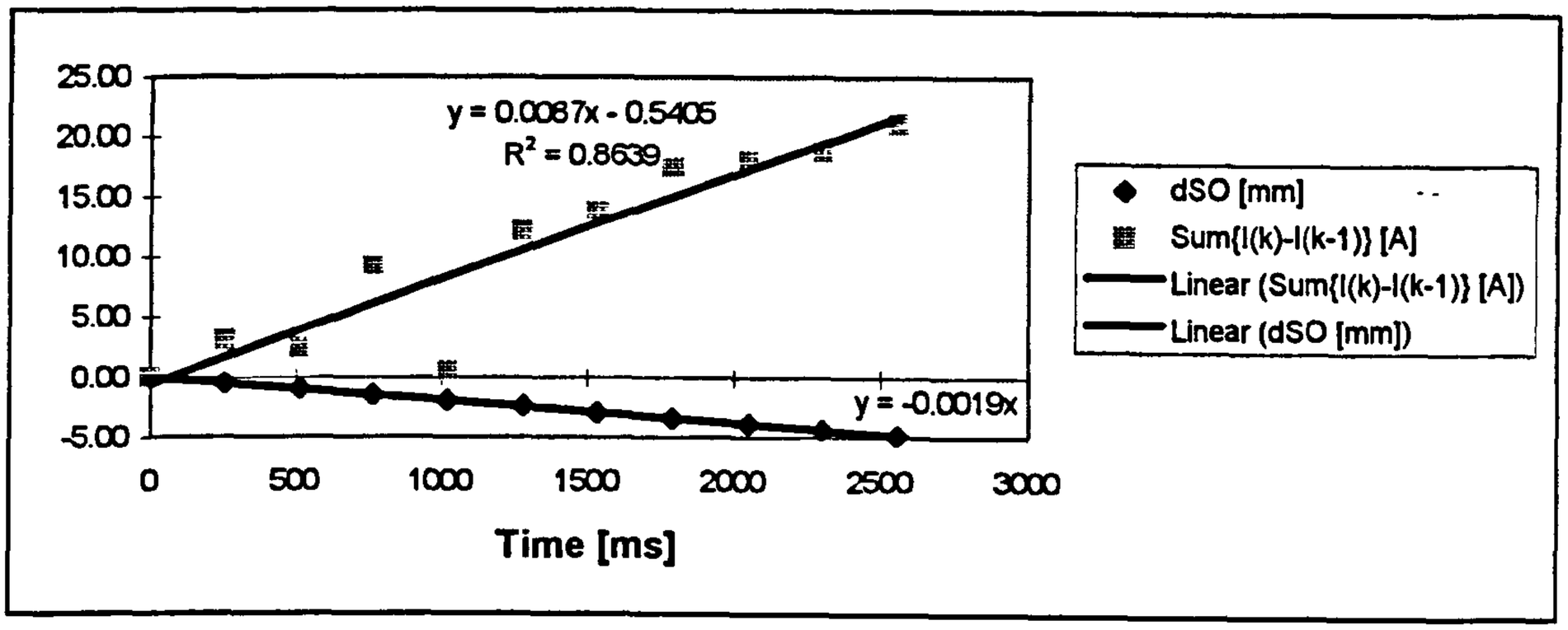

Figure J.14 - Plot of stand-off variation and cumulative changes in welding current for welding trial "s15_1004"

Table J.15 - Welding data collected from stand-off slope trial "s15_1005"

Time [ms]	*SO* [mm]	$I_{mean,\,k}$ [A]	ΔSO [mm]	$\Sigma[I_{mean,\,k} - I_{mean,(k-1)}]$ [A]
0	15.00	211.5	0.00	0.0
512	14.47	212.5	-0.53	0.9
1024	13.94	212.1	-1.06	0.6
1536	13.41	215.9	-1.59	4.4
2048	12.88	218.0	-2.12	6.4
2560	12.35	225.6	-2.65	14.0
3072	11.82	221.9	-3.18	10.4
3584	11.30	228.3	-3.70	16.8
4096	10.77	228.4	-4.23	16.8
4608	10.24	230.8	-4.76	19.3

WFS = 9.0 m/min
Vset = 22.5 V

S_W = 0.5 m/min
Vreq = 20.5 V

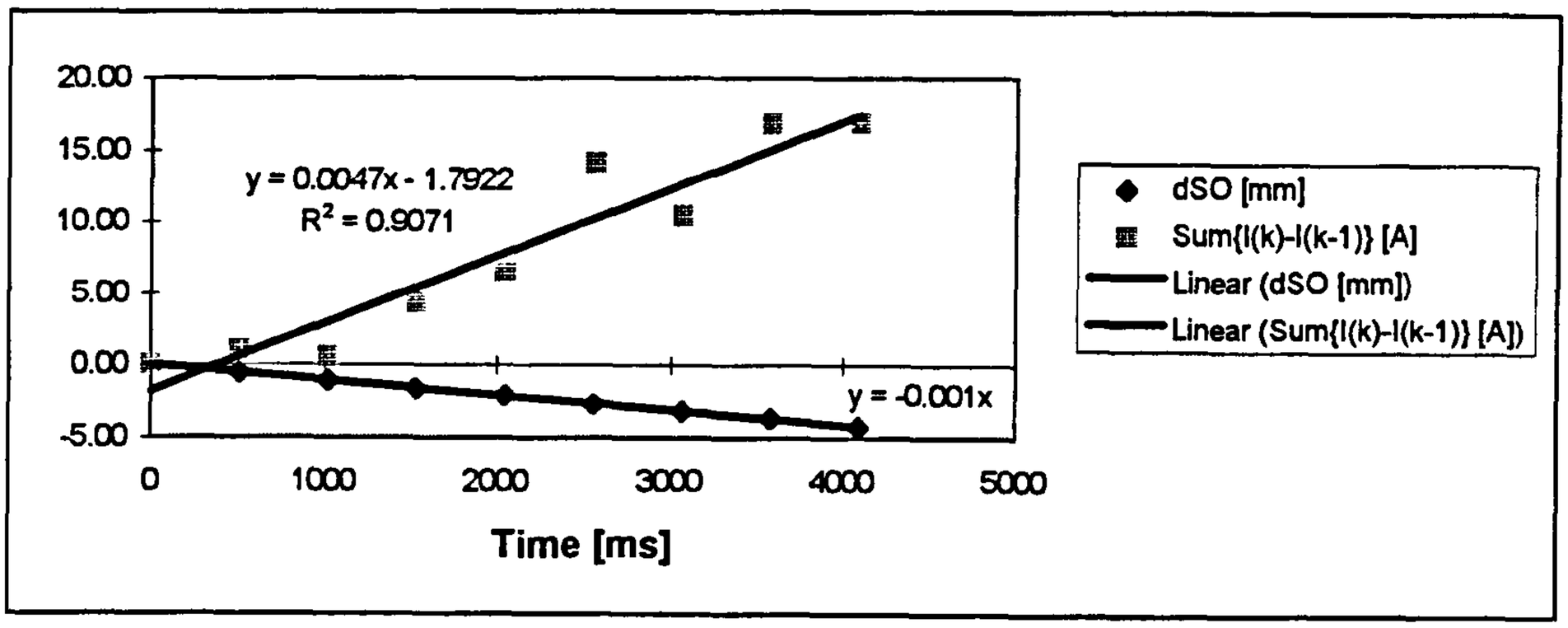

Figure J.15 - Plot of stand-off variation and cumulative changes in welding current for welding trial "s15_1005"

Table J.16 - Welding data collected from stand-off slope trial "s15_1006"

Time [ms]	*SO* [mm]	$I_{mean,\,k}$ [A]	ΔSO [mm]	$\Sigma[I_{mean,\,k} - I_{mean,(k-1)}]$ [A]
0	15.00	216.2	0.00	0.0
512	14.47	218.7	-0.53	2.6
1024	13.94	220.3	-1.06	4.1
1536	13.41	222.8	-1.59	6.6
2048	12.88	224.0	-2.12	7.9
2560	12.35	227.3	-2.65	11.1
3072	11.82	231.7	-3.18	15.5
3584	11.30	233.7	-3.70	17.6
4096	10.77	233.6	-4.23	17.5
4608	10.24	237.7	-4.76	21.5
5120	9.71	239.3	-5.29	23.1

WFS = 9.5 m/min
Vset = 22.7 V

S_W = 0.5 m/min
Vreq = 20.7 V

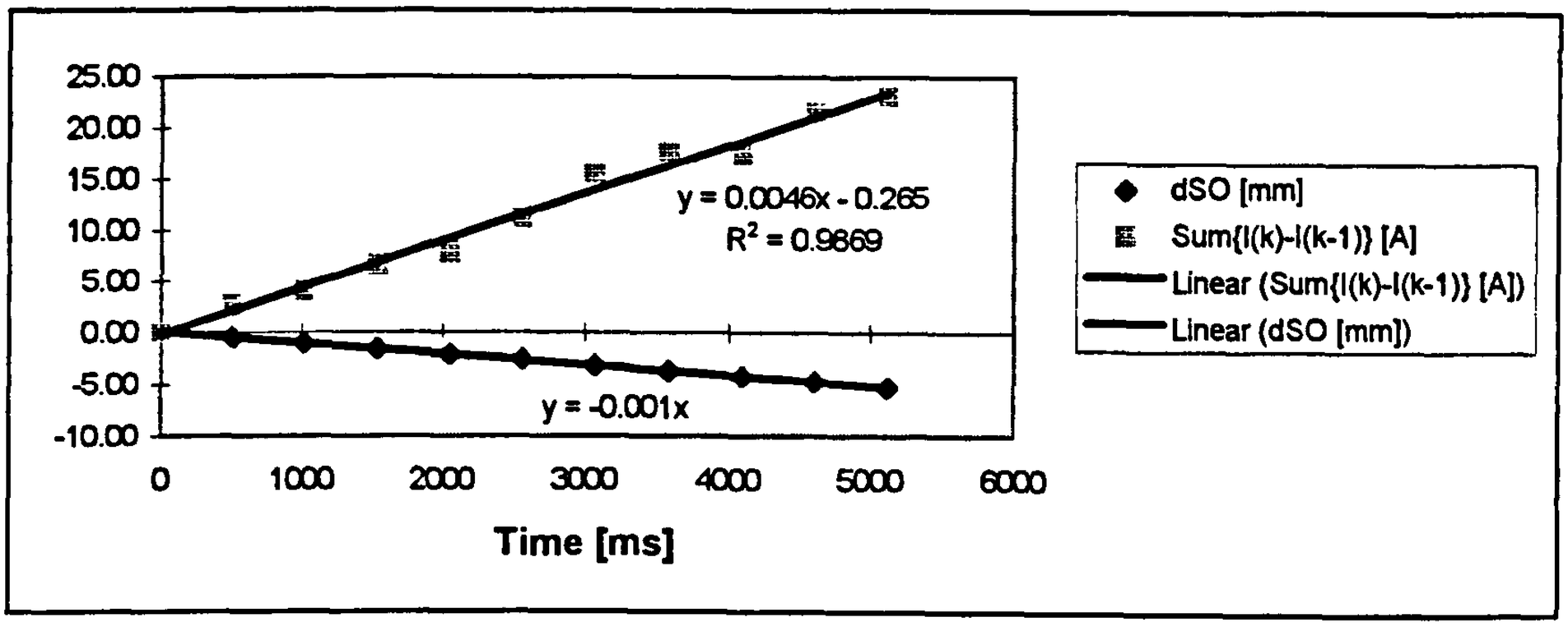

Figure J.16 - Plot of stand-off variation and cumulative changes in welding current for welding trial "s15_1006"

Table J.17 - Welding data collected from stand-off slope trial "s15_1007"

Time [ms]	*SO* [mm]	$I_{mean,\,k}$ [A]	ΔSO [mm]	$\Sigma[I_{mean,\,k} - I_{mean,(k-1)}]$ [A]
0	15.00	275.3	0.00	0.0
512	14.36	276.3	-0.64	1.0
1024	13.73	280.9	-1.27	5.5
1536	13.09	284.4	-1.91	9.0
2048	12.46	289.1	-2.54	13.8
2560	11.82	293.8	-3.18	18.5
3072	11.19	294.3	-3.81	19.0
3584	10.55	305.8	-4.45	30.5
4096	9.92	312.4	-5.08	37.1

WFS = 11.0 m/min
Vset = 33.1 V

S_W = 0.6 m/min
Vreq = 30.5 V

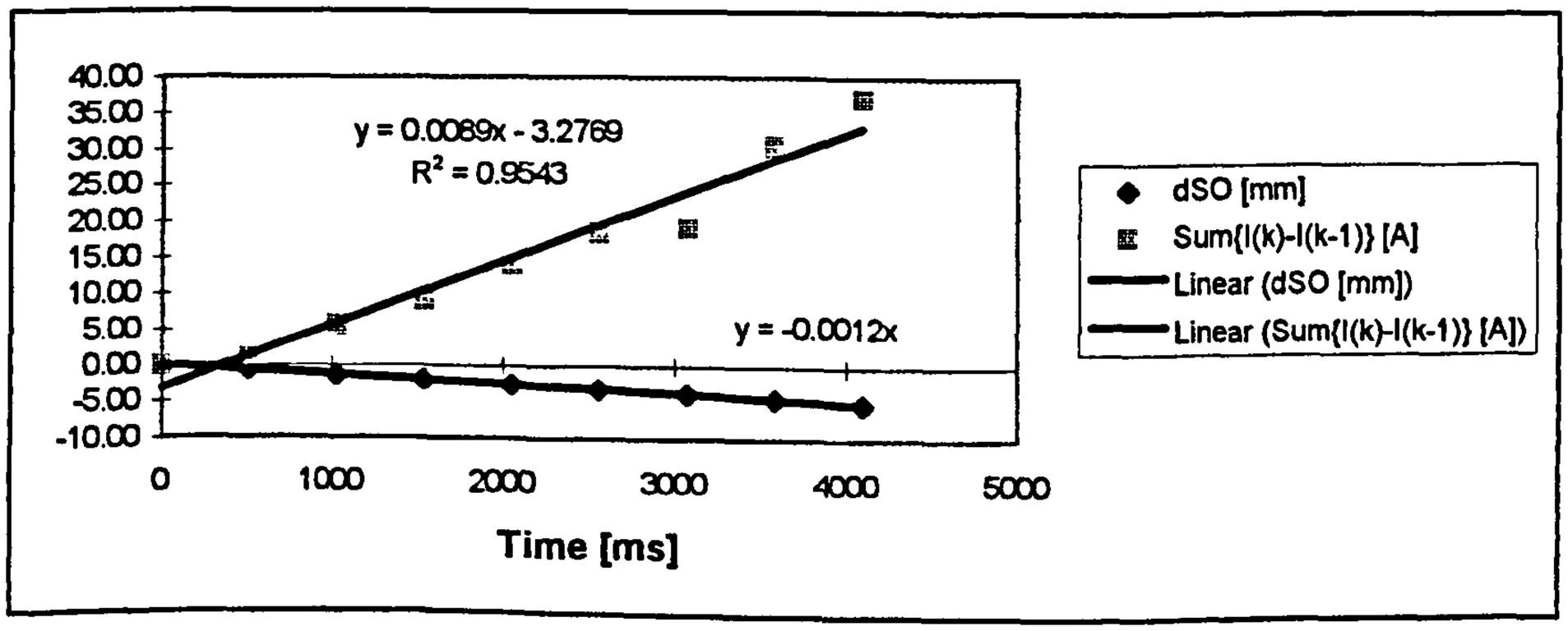

Figure J.17 - Plot of stand-off variation and cumulative changes in welding current for welding trial "s15_1007"

Table J.18 - Welding data collected from stand-off slope trial "s15_1008"

Time [ms]	*SO* [mm]	$I_{mean,\,k}$ [A]	ΔSO [mm]	$\Sigma[I_{mean,\,k} - I_{mean,(k-1)}]$ [A]
0	15.00	295.6	0.00	0.0
512	14.26	301.5	-0.74	5.99
1024	13.52	306.9	-1.48	11.32
1536	12.78	313.5	-2.22	17.90
2048	12.04	321.2	-2.96	25.63
2560	11.30	329.7	-3.70	34.16
3072	10.55	335.1	-4.45	39.55

WFS = 12.5 m/min S_W = 0.7 m/min
Vset = 33.8 V Vreq = 31.1 V

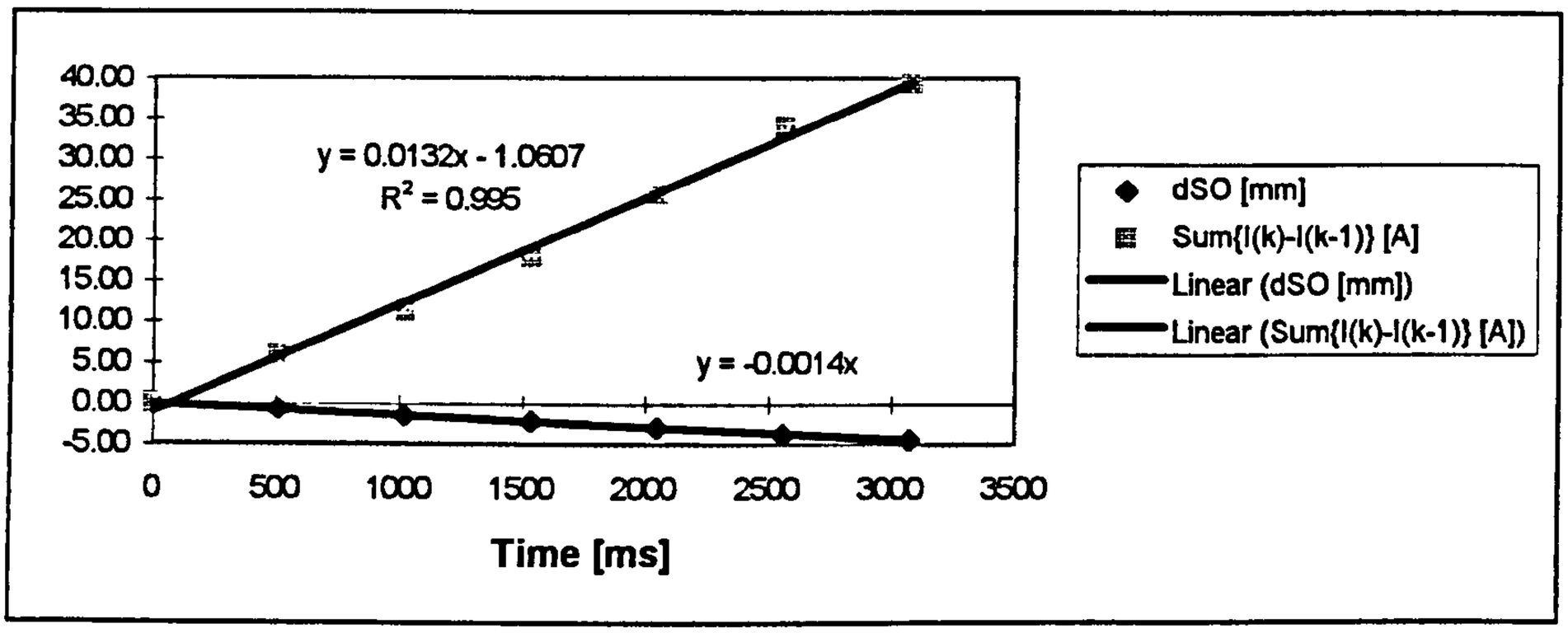

Figure J.18 - Plot of stand-off variation and cumulative changes in welding current for welding trial "s15_1008"

Table J.19 - Welding data collected from stand-off slope trial "s15_1009"

Time [ms]	*SO* [mm]	$I_{mean,\,k}$ [A]	ΔSO [mm]	$\Sigma[I_{mean,\,k} - I_{mean,(k-1)}]$ [A]
0	15.00	309.8	0.00	0.0
512	14.26	313.7	-0.74	3.9
1024	13.52	321.3	-1.48	11.5
1536	12.78	326.5	-2.22	16.7
2048	12.04	334.2	-2.96	24.4
2560	11.30	342.1	-3.70	32.2
3072	10.55	351.6	-4.45	41.8
3584	9.81	356.0	-5.19	46.2

WFS = 13.5 m/min S_W = 0.7 m/min
Vset = 34.3 V Vreq = 31.5 V

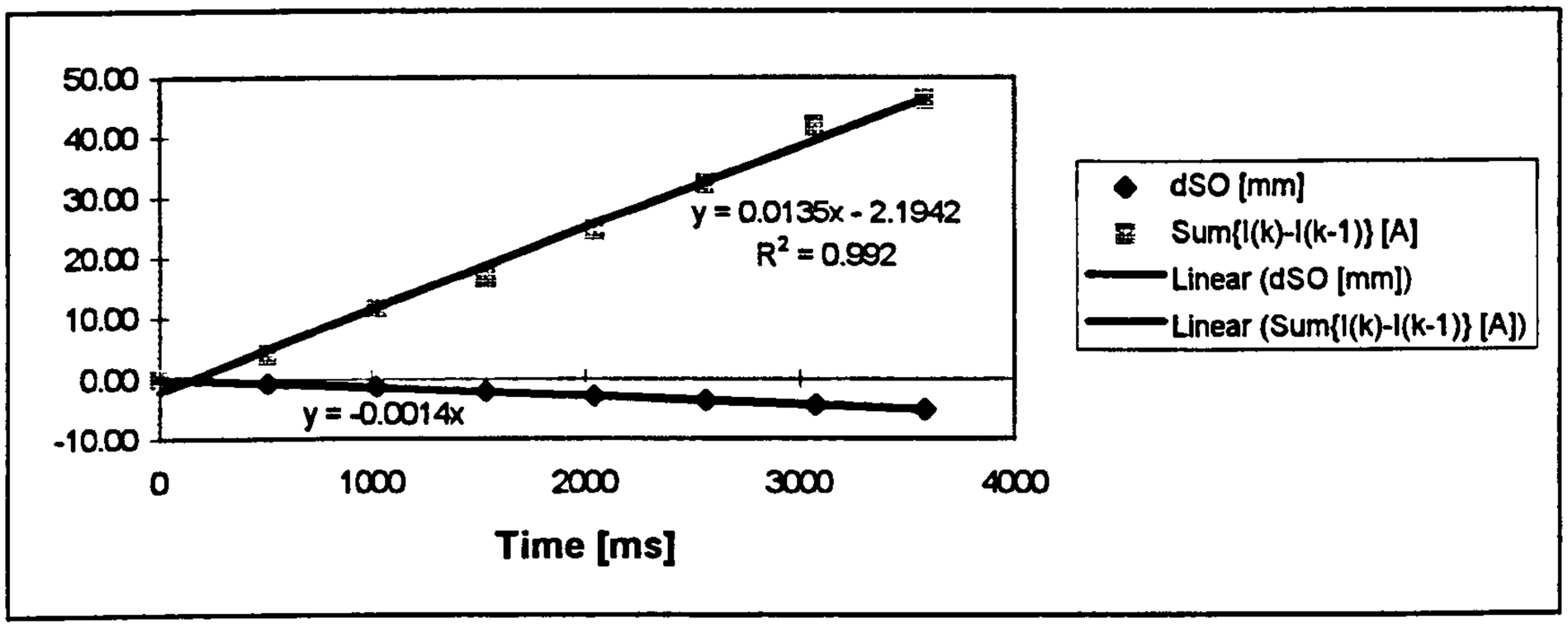

Figure J.19 - Plot of stand-off variation and cumulative changes in welding current for welding trial "s15_1009"

Table J.20 - Welding data collected from stand-off slope trial "s15_1010"

Time [ms]	*SO* [mm]	$I_{mean,\,k}$ [A]	ΔSO [mm]	$\Sigma[I_{mean,\,k} - I_{mean,(k-1)}]$ [A]
0	15.00	323.0	0.00	0.0
512	14.26	328.5	-0.74	5.5
1024	13.52	334.7	-1.48	11.7
1536	12.78	342.0	-2.22	19.0
2048	12.04	350.0	-2.96	27.0
2560	11.30	356.3	-3.70	33.3
3072	10.55	363.0	-4.45	40.0

WFS = 14.5 m/min S_W = 0.7 m/min
Vset = 34.8 V Vreq = 32.0 V

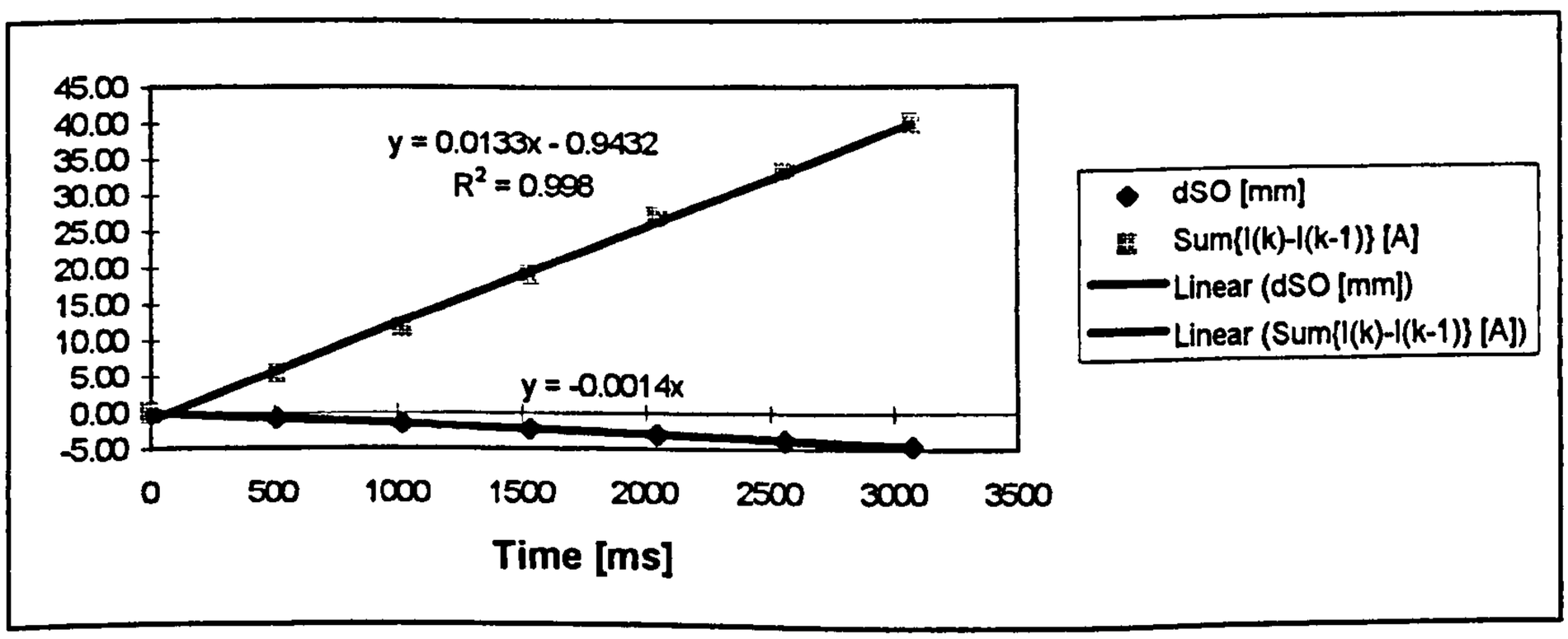

Figure J.20 - Plot of stand-off variation and cumulative changes in welding current for welding trial "s15_1010"

Appendix K

This appendix shows the data collected from bead on plate welding trials used for developing the dip resistance based stand-off estimation models.

Table K.1 - Welding data used to develop the dip resistance models - Welding Voltage features

	Set-up parameters			Welding voltage extracted features						
Run	WFS	SO	V_{set}	V_{mean}	V_{bk}	V_{pk}	V_{max}	V_{min}	Vt_{bk}	Vt_{pk}
1	4	12	18.0	16.74	4.25	18.71	28.37	2.25	2.73	16.44
2	4	12	18.5	17.14	4.48	19.36	29.80	2.42	2.69	14.51
3	4	12	19.0	17.62	4.76	19.57	30.16	2.52	3.01	18.55
4	4	12	19.5	18.11	5.07	19.86	29.99	2.61	2.99	20.67
5	4	12	20.0	18.58	5.58	20.22	31.33	2.71	2.95	21.97
6	6	12	20.6	18.84	5.67	21.15	31.96	3.23	2.96	15.94
7	6	12	21.1	19.31	6.06	21.50	32.54	3.35	3.18	18.18
8	6	12	21.6	19.83	7.08	21.78	33.07	3.40	2.74	16.94
9	6	12	22.1	20.35	8.59	22.07	33.63	3.61	2.23	14.34
10	6	12	22.6	20.79	9.10	22.39	34.02	3.59	2.10	14.71
91	7	12	20.9	18.87	6.81	21.86	31.75	3.72	2.41	9.52
92	7	12	21.4	19.41	7.30	22.17	33.08	3.81	2.28	9.66
93	7	12	21.9	19.87	7.53	22.35	32.92	4.06	2.20	10.64
94	7	12	22.4	20.40	8.57	22.84	35.03	4.13	2.42	11.21
95	7	12	22.9	20.84	9.02	22.92	33.92	4.23	2.39	13.10
11	8	12	21.3	19.15	7.43	22.21	32.28	3.77	1.93	7.22
12	8	12	21.8	19.65	7.93	22.41	33.04	4.00	1.93	7.98
13	8	12	22.3	20.30	8.94	22.96	36.01	4.17	2.05	8.49
14	8	12	22.8	20.65	9.42	23.07	36.37	4.03	1.83	8.33
15	8	12	23.3	21.06	10.15	23.27	33.86	4.25	1.71	8.23
16	10	12	22.3	19.79	8.65	23.20	32.08	4.37	1.55	4.97
17	10	12	22.8	20.38	9.04	23.61	32.77	4.71	1.57	5.40
18	10	12	23.3	20.85	10.31	23.56	32.96	4.54	1.39	5.30
19	10	12	23.8	21.38	11.38	23.81	33.66	4.69	1.25	5.08
20	10	12	24.3	21.85	13.70	23.97	34.11	4.98	1.30	4.84

Table K.1 - continuation

	Set-up parameters			Welding voltage extracted features						
Run	WFS	SO	V_{set}	V_{mean}	V_{bk}	V_{pk}	V_{max}	V_{min}	Vt_{bk}	Vt_{pk}
21	5.5	15	20.3	18.65	6.08	20.82	29.41	3.63	2.82	15.48
22	5.5	15	20.8	19.13	6.44	21.22	32.00	3.73	3.06	17.46
23	5.5	15	21.3	19.56	6.76	21.62	32.75	3.79	3.28	19.14
24	5.5	15	21.8	20.12	8.20	21.91	32.54	3.82	3.13	19.65
25	5.5	15	22.3	20.61	9.97	22.19	32.96	4.05	2.95	18.59
26	6.5	15	20.6	18.70	6.45	21.35	29.00	3.85	2.63	11.65
27	6.5	15	21.1	19.19	7.02	21.73	30.25	3.98	2.68	12.44
28	6.5	15	21.6	19.72	7.37	22.00	31.11	4.06	2.56	13.19
29	6.5	15	22.1	20.18	8.05	22.37	32.78	4.27	2.46	13.09
30	6.5	15	22.6	20.71	8.81	22.64	32.86	4.35	2.48	14.60
31	8.5	15	21.2	18.97	7.64	22.56	29.36	4.37	2.09	6.49
32	8.5	15	21.7	19.52	8.04	22.77	30.35	4.55	2.01	6.94
33	8.5	15	22.2	19.98	8.26	22.98	30.94	4.73	2.00	7.58
34	8.5	15	22.7	20.51	8.90	23.17	32.35	4.74	1.99	8.44
35	8.5	15	23.2	20.99	9.45	23.38	32.91	4.87	1.97	9.26
36	9.5	15	21.6	19.25	8.12	23.11	30.09	4.73	2.00	5.69
37	9.5	15	22.1	19.72	8.43	23.22	30.51	4.77	1.86	5.95
38	9.5	15	22.6	20.26	8.96	23.46	31.11	4.90	1.83	6.36
39	9.5	15	23.1	20.80	9.54	23.66	31.88	4.98	1.75	6.73
40	9.5	15	23.6	21.29	10.49	23.90	32.42	5.16	1.76	7.08
41	10.5	15	31.5	28.84	28.62	29.09	32.39	27.53	1.62	1.43
42	10.5	15	32.0	29.32	29.09	29.56	32.16	28.28	1.57	1.45
43	10.5	15	32.5	29.80	29.58	30.03	32.05	28.91	1.54	1.44
44	10.5	15	33.0	30.26	30.01	30.51	31.92	29.22	1.52	1.57
45	10.5	15	33.5	30.72	30.45	31.00	32.51	29.64	1.59	1.60
46	11.5	15	31.9	29.05	28.84	29.32	32.78	27.80	1.76	1.35
47	11.5	15	32.4	29.52	29.32	29.77	32.28	28.55	1.61	1.32
48	11.5	15	32.9	30.00	29.80	30.22	32.03	29.13	1.46	1.32
49	11.5	15	33.4	30.48	30.26	30.71	32.55	29.62	1.49	1.40
50	11.5	15	33.9	30.94	30.72	31.17	32.70	29.98	1.44	1.42

Table K.1 - continuation

	Set-up parameters			Welding voltage extracted features						
Run	WFS	SO	V_{set}	V_{mean}	V_{bk}	V_{pk}	V_{max}	V_{min}	Vt_{bk}	Vt_{pk}
51	13.5	15	32.9	29.80	29.57	30.11	32.72	28.28	1.68	1.28
52	13.5	15	33.4	30.28	30.06	30.54	32.85	29.29	1.54	1.35
53	13.5	15	33.9	30.74	30.54	30.98	33.05	29.86	1.51	1.35
54	13.5	15	34.4	31.36	30.92	31.79	33.42	29.87	2.85	2.88
55	13.5	15	34.9	31.81	31.32	32.27	33.95	29.87	2.85	3.00
56	5.5	20	20.2	18.66	6.57	20.96	30.36	4.01	2.87	14.50
57	5.5	20	20.7	19.11	6.68	21.29	32.37	3.98	3.16	17.06
58	5.5	20	21.2	19.64	7.44	21.65	32.60	4.10	3.36	19.15
59	5.5	20	21.7	20.12	7.91	21.92	32.71	4.23	3.30	20.95
60	5.5	20	22.2	20.72	10.04	22.59	34.64	4.24	3.25	17.90
61	6.5	20	20.5	18.75	7.00	21.52	29.50	4.26	2.70	11.21
62	6.5	20	21.0	19.28	7.26	21.78	29.53	4.50	2.90	13.25
63	6.5	20	21.5	19.78	7.62	22.09	31.30	4.50	2.98	15.00
64	6.5	20	22.0	20.30	8.56	22.72	34.85	4.60	3.06	14.52
65	6.5	20	22.5	20.77	10.40	22.83	36.25	4.71	2.79	13.41
66	7.5	20	20.8	18.96	7.75	22.20	31.02	4.46	2.58	8.71
67	7.5	20	21.3	19.43	8.26	22.40	31.91	4.57	2.62	9.58
68	7.5	20	21.8	19.92	8.39	22.62	31.38	4.86	2.64	10.86
69	7.5	20	22.3	20.41	8.85	22.93	32.68	5.03	2.50	11.07
70	7.5	20	22.8	20.93	9.40	23.19	33.90	5.24	2.49	12.28
71	8.5	20	30.8	28.68	28.33	28.95	30.87	27.75	2.77	3.40
72	8.5	20	31.3	29.15	28.80	29.44	31.19	28.21	2.89	3.55
73	8.5	20	31.8	29.65	29.30	29.96	32.11	28.65	2.95	3.36
74	8.5	20	32.3	30.12	29.76	30.41	32.13	29.11	2.83	3.33
75	8.5	20	32.8	30.59	30.26	30.88	32.64	29.63	2.67	3.07
76	10.5	20	31.6	29.16	28.94	29.47	36.59	27.28	1.83	1.32
77	10.5	20	32.1	29.64	29.44	29.86	34.73	28.67	1.63	1.38
78	10.5	20	32.6	30.10	29.89	30.31	32.36	29.31	1.52	1.44
79	10.5	20	33.1	30.59	30.39	30.79	32.31	29.84	1.56	1.47
80	10.5	20	33.6	31.04	30.80	31.27	32.86	30.19	1.57	1.60

Table K.1 - continuation

	Set-up parameters			Welding voltage extracted features						
Run	WFS	SO	V_{set}	V_{mean}	V_{bk}	V_{pk}	V_{max}	V_{min}	Vt_{bk}	Vt_{pk}
81	12.5	20	32.2	29.52	29.19	30.22	38.85	25.43	2.48	1.20
82	12.5	20	32.7	30.00	29.74	30.44	36.91	28.09	2.11	1.23
83	12.5	20	33.2	30.44	30.23	30.73	34.45	28.59	1.74	1.32
84	12.5	20	33.7	30.93	30.73	31.15	33.74	29.85	1.60	1.33
85	12.5	20	34.2	31.37	31.18	31.59	33.53	30.53	1.52	1.37
86	14.5	20	33.1	30.18	29.85	30.69	35.28	26.29	1.92	1.22
87	14.5	20	33.6	30.64	30.38	31.00	34.42	28.24	1.79	1.29
88	14.5	20	34.1	31.10	30.86	31.40	34.03	29.12	1.63	1.35
89	14.5	20	34.6	31.57	31.34	31.85	34.15	30.13	1.68	1.42
90	14.5	20	35.1	32.02	31.80	32.28	34.49	31.07	1.55	1.36
96	4	10	18.0	16.59	4.20	18.97	28.15	2.16	2.50	12.52
97	4	10	19.0	17.56	4.47	19.47	29.30	2.36	3.01	19.20
98	4	10	20.0	18.54	4.91	20.15	31.94	2.48	2.88	22.22
99	6	10	19.0	17.10	5.18	20.54	28.89	2.70	2.22	7.56
100	6	10	20.0	18.08	5.42	20.94	29.17	2.95	2.37	10.18
101	6	10	21.0	19.13	5.80	21.42	32.42	3.00	3.01	16.77
102	8	10	20.0	17.66	6.37	21.80	30.86	3.21	2.07	5.58
103	8	10	21.0	18.67	6.78	22.09	31.36	3.48	1.79	6.12
104	8	10	22.0	19.67	7.75	22.47	32.69	3.58	1.53	6.44
105	4	18	19.5	18.19	5.81	19.81	31.70	3.04	2.88	20.40
106	4	18	18.5	17.22	5.31	19.21	29.52	2.88	2.75	15.37
107	4	18	20.5	19.19	7.11	20.66	33.34	3.21	2.45	18.90
108	6	18	20.5	18.79	6.35	21.24	28.78	3.87	2.79	13.64
134	6	18	21.5	19.80	7.41	21.89	33.37	4.18	3.05	16.13
109	6	18	22.5	20.78	10.05	22.51	34.40	4.31	2.09	12.44
110	8	18	20.8	18.85	7.30	22.04	30.44	4.21	2.35	8.28
111	8	18	21.8	19.83	8.01	22.54	33.43	4.47	2.28	9.67
112	8	18	22.8	20.84	9.89	23.12	34.86	4.82	2.15	10.10
113	10	18	29.4	27.06	26.65	27.78	39.15	20.12	1.38	0.80
114	10	18	30.4	28.07	27.88	28.29	33.90	26.46	0.95	0.80
115	10	18	31.4	28.92	28.73	29.15	32.66	27.74	0.90	0.72

Table K.2 - Welding data used to develop the dip resistance models - Welding Current features

	Set-up parameters			Welding current extracted features						
Run	WFS	SO	V_{set}	I_{mean}	I_{bk}	I_{pk}	I_{max}	I_{min}	It_{bk}	It_{pk}
1	4	12	18.0	107.3	80.8	153.0	232.5	65.8	12.42	7.24
2	4	12	18.5	118.9	91.5	162.7	236.7	72.9	10.89	6.92
3	4	12	19.0	119.8	90.3	172.0	262.3	72.9	14.31	8.26
4	4	12	19.5	120.5	91.7	176.2	276.7	76.9	16.88	8.99
5	4	12	20.0	120.9	92.9	178.8	284.0	77.8	19.29	9.72
6	6	12	20.6	154.4	121.0	208.1	312.6	98.7	12.48	7.89
7	6	12	21.1	154.3	119.2	215.2	327.6	98.1	14.93	8.83
8	6	12	21.6	155.1	120.3	221.0	347.5	93.7	17.68	9.66
9	6	12	22.1	152.9	120.0	223.2	354.8	93.8	21.81	10.63
10	6	12	22.6	156.4	124.4	230.3	368.4	101.1	24.60	11.23
91	7	12	20.9	179.8	142.5	228.1	325.2	107.1	8.57	6.57
92	7	12	21.4	180.2	143.1	231.1	338.5	101.1	9.34	6.87
93	7	12	21.9	182.8	146.7	236.5	350.5	115.1	11.12	7.61
94	7	12	22.4	183.1	148.0	240.6	363.8	106.5	12.72	8.01
95	7	12	22.9	183.2	149.1	245.6	375.6	109.2	14.97	8.43
11	8	12	21.3	190.6	153.5	237.1	346.7	102.5	7.03	5.59
12	8	12	21.8	190.9	153.5	242.1	356.2	99.7	8.70	6.48
13	8	12	22.3	187.4	150.2	244.3	371.2	98.6	10.74	7.23
14	8	12	22.8	195.6	160.6	251.7	379.0	104.2	11.46	7.30
15	8	12	23.3	201.6	167.9	258.9	382.2	107.9	12.87	7.55
16	10	12	22.3	227.6	193.4	267.9	373.5	126.8	5.30	4.49
17	10	12	22.8	221.3	190.3	260.7	358.1	130.2	5.60	4.47
18	10	12	23.3	227.2	192.0	272.9	383.2	118.2	7.42	5.81
19	10	12	23.8	225.7	193.2	271.9	385.3	122.0	9.06	6.43
20	10	12	24.3	230.5	200.3	278.0	391.9	137.1	11.32	7.15

Table K.2 - continuation

	Set up parameters			Welding current extracted features						
Run	WFS	SO	V_{set}	I_{mean}	I_{bk}	I_{pk}	I_{max}	I_{min}	It_{bk}	It_{pk}
21	5.5	15	20.3	146.4	117.4	194.7	287.9	98.1	12.02	7.43
22	5.5	15	20.8	147.3	117.1	200.5	299.5	94.7	13.89	8.01
23	5.5	15	21.3	148.7	116.8	209.1	322.1	98.2	15.93	8.72
24	5.5	15	21.8	148.1	116.8	211.8	331.3	93.4	19.28	9.74
25	5.5	15	22.3	148.4	118.6	216.8	343.2	96.2	24.16	11.22
26	6.5	15	20.6	163.5	130.7	209.3	295.8	103.5	9.13	6.57
27	6.5	15	21.1	165.0	130.8	214.0	313.1	100.2	10.20	7.16
28	6.5	15	21.6	165.6	131.2	219.2	329.9	106.9	12.24	8.05
29	6.5	15	22.1	167.5	133.9	224.2	337.6	108.0	13.13	7.90
30	6.5	15	22.6	168.1	135.7	229.9	357.1	112.3	16.48	8.89
31	8.5	15	21.2	198.5	164.2	237.2	325.4	121.3	5.29	4.67
32	8.5	15	21.7	197.6	162.6	238.0	332.3	113.5	5.95	5.11
33	8.5	15	22.2	198.2	163.4	241.4	342.7	127.7	6.91	5.61
34	8.5	15	22.7	198.2	164.0	245.3	357.5	122.8	8.89	6.53
35	8.5	15	23.2	198.0	164.8	251.1	368.0	126.7	11.13	7.09
36	9.5	15	21.6	211.9	179.8	248.8	338.9	129.0	4.79	4.19
37	9.5	15	22.1	212.6	179.8	251.0	347.5	129.9	5.40	4.64
38	9.5	15	22.6	211.1	177.2	251.7	350.4	128.2	6.25	5.23
39	9.5	15	23.1	210.8	178.3	254.4	361.9	130.5	7.54	5.65
40	9.5	15	23.6	209.8	177.1	258.2	370.8	134.3	9.38	6.37
41	10.5	15	31.5	248.7	245.4	251.8	259.0	229.8	2.22	2.45
42	10.5	15	32.0	250.6	247.6	253.6	261.2	235.1	2.07	2.15
43	10.5	15	32.5	250.9	248.0	253.8	260.9	238.8	2.08	2.07
44	10.5	15	33.0	253.6	250.4	256.8	264.8	242.1	2.28	2.22
45	10.5	15	33.5	257.5	254.0	261.0	269.9	244.6	2.35	2.35
46	11.5	15	31.9	267.9	264.6	270.9	278.3	252.7	2.20	2.34
47	11.5	15	32.4	268.7	265.8	271.7	278.8	256.6	1.99	2.02
48	11.5	15	32.9	270.2	267.4	273.1	280.1	259.1	1.99	1.95
49	11.5	15	33.4	272.2	269.2	275.3	282.7	260.9	1.96	1.93
50	11.5	15	33.9	274.3	271.2	277.4	284.8	262.6	1.90	1.89

Table K.2 - Continuation

	Set-up parameters			Welding current extracted features						
Run	WFS	SO	V_{set}	I_{mean}	I_{bk}	I_{pk}	I_{max}	I_{min}	It_{bk}	It_{pk}
51	13.5	15	32.9	291.8	288.3	295.3	302.5	278.5	1.86	1.88
52	13.5	15	33.4	294.0	290.4	297.6	305.9	280.6	1.88	1.83
53	13.5	15	33.9	296.0	292.5	299.6	307.4	284.0	1.80	1.78
54	13.5	15	34.4	282.6	277.7	287.6	299.2	266.6	2.72	2.67
55	13.5	15	34.9	287.3	281.8	293.0	306.5	268.6	2.91	2.81
56	5.5	20	20.2	127.4	100.5	173.7	253.1	83.7	11.08	6.58
57	5.5	20	20.7	132.5	103.6	184.9	272.8	87.0	13.19	7.51
58	5.5	20	21.2	132.6	102.4	192.2	292.0	82.7	15.86	8.34
59	5.5	20	21.7	134.2	104.2	199.2	312.0	86.8	19.20	9.33
60	5.5	20	22.2	134.3	106.0	202.4	319.0	86.9	23.25	10.09
61	6.5	20	20.5	149.8	119.3	194.3	273.7	95.2	8.83	6.16
62	6.5	20	21.0	148.2	117.5	196.4	284.4	95.1	10.60	6.90
63	6.5	20	21.5	150.8	119.1	203.0	300.7	96.8	12.09	7.42
64	6.5	20	22.0	152.5	119.4	209.8	318.4	93.5	13.85	8.12
65	6.5	20	22.5	151.6	119.8	213.8	334.1	76.7	16.41	8.75
66	7.5	20	20.8	163.0	128.4	207.7	292.2	92.5	7.27	5.71
67	7.5	20	21.3	164.9	129.9	212.7	305.8	95.8	8.43	6.21
68	7.5	20	21.8	165.3	130.8	215.4	310.8	100.6	9.74	6.85
69	7.5	20	22.3	168.5	133.6	221.2	329.0	104.4	10.76	7.28
70	7.5	20	22.8	167.9	133.6	226.0	344.6	109.1	13.09	7.90
71	8.5	20	30.8	193.6	190.8	196.2	201.4	181.5	2.56	2.91
72	8.5	20	31.3	195.7	192.9	198.2	203.8	184.5	2.55	2.80
73	8.5	20	31.8	196.0	192.9	198.6	204.7	182.6	2.57	2.94
74	8.5	20	32.3	199.5	196.4	202.2	208.3	186.6	2.56	2.83
75	8.5	20	32.8	201.2	198.1	204.0	209.9	187.7	2.39	2.71
76	10.5	20	31.6	228.0	224.3	230.7	236.9	201.7	2.14	2.79
77	10.5	20	32.1	228.8	225.9	231.3	237.2	210.2	2.01	2.21
78	10.5	20	32.6	232.0	229.3	234.7	241.0	220.9	2.11	2.15
79	10.5	20	33.1	233.0	230.4	235.7	241.8	222.3	2.07	2.09
80	10.5	20	33.6	235.0	232.0	237.9	245.0	223.0	2.21	2.24

Table K.2 - Continuation

	Set-up parameters			Welding current extracted features						
Run	WFS	SO	V_{set}	I_{mean}	I_{bk}	I_{pk}	I_{max}	I_{min}	It_{bk}	It_{pk}
81	12.5	20	32.2	250.6	245.4	254.4	263.9	213.3	2.38	3.18
82	12.5	20	32.7	252.7	248.7	256.1	263.6	229.4	2.25	2.66
83	12.5	20	33.2	255.3	252.2	258.3	265.1	239.9	2.00	2.14
84	12.5	20	33.7	257.9	255.0	260.8	267.0	245.4	1.94	1.98
85	12.5	20	34.2	261.1	258.3	263.9	270.4	250.0	1.85	1.86
86	14.5	20	33.1	274.5	270.6	278.1	288.1	254.6	2.32	2.57
87	14.5	20	33.6	277.2	273.8	280.5	287.9	262.5	2.18	2.28
88	14.5	20	34.1	279.4	276.1	282.5	289.9	266.5	1.95	1.99
89	14.5	20	34.6	281.4	278.1	284.6	292.0	269.0	1.97	1.99
90	14.5	20	35.1	286.1	282.7	289.5	296.6	274.4	1.77	1.75
96	4	10	18.0	119.7	93.5	159.4	226.7	72.3	9.23	6.13
97	4	10	19.0	122.3	93.1	175.3	265.0	77.1	14.82	8.48
98	4	10	20.0	124.7	96.6	180.6	284.7	81.0	19.04	10.04
99	6	10	19.0	168.3	134.4	209.0	297.2	91.9	6.15	5.07
100	6	10	20.0	170.4	136.4	216.1	307.2	106.3	8.36	6.31
101	6	10	21.0	161.1	124.9	220.7	332.1	97.3	13.92	8.66
102	8	10	20.0	211.3	174.0	253.7	355.8	110.9	5.09	4.51
103	8	10	21.0	210.5	174.4	252.3	349.2	120.4	5.69	4.91
104	8	10	22.0	209.4	174.8	255.3	363.1	116.8	7.62	5.77
105	4	18	19.5	108.7	84.0	162.3	254.6	71.8	17.66	8.83
106	4	18	18.5	106.4	80.8	152.2	227.1	67.2	12.32	6.98
107	4	18	20.5	108.4	83.2	166.7	274.7	70.4	21.89	9.98
108	6	18	20.5	144.7	115.9	190.0	275.2	95.7	10.29	6.63
134	6	18	21.5	148.2	116.0	206.8	310.3	97.5	14.30	8.32
109	6	18	22.5	147.6	117.0	214.5	341.3	87.4	20.44	9.87
110	8	18	20.8	168.5	133.2	213.5	302.4	101.2	6.96	5.48
111	8	18	21.8	171.0	135.5	221.1	329.3	106.1	8.80	6.28
112	8	18	22.8	172.3	137.8	231.3	358.2	92.7	12.70	7.60
113	10	18	29.4	216.8	209.0	221.1	240.0	158.5	2.65	4.71
114	10	18	30.4	214.9	212.0	217.7	225.0	195.9	2.37	2.47
115	10	18	31.4	229.0	226.4	231.4	237.2	215.1	1.84	2.00

Table K.3 - Welding data used to develop the dip resistance models - Monitoring Indices and Dip Resistance

	Set-up Parameters			Monitoring indices and dip resistance					
Run	WFS	SO	V_{set}	TSI	TI	DCI	PR	$DipR_{mean}$	$DipR_{SD}$
1	4	12	18.0	2.166	0.387	0.746	0.190	24.45	4.58
2	4	12	18.5	1.991	0.387	0.739	0.201	24.43	4.32
3	4	12	19.0	2.191	0.391	0.730	0.204	24.40	4.33
4	4	12	19.5	2.296	0.361	0.720	0.213	24.30	4.31
5	4	12	20.0	2.349	0.356	0.700	0.231	24.34	4.87
6	6	12	20.6	2.026	0.361	0.699	0.236	24.37	3.70
7	6	12	21.1	2.123	0.364	0.686	0.242	24.54	3.91
8	6	12	21.6	2.241	0.395	0.643	0.276	24.52	4.45
9	6	12	22.1	2.322	0.386	0.578	0.332	25.14	5.80
10	6	12	22.6	2.357	0.353	0.562	0.352	24.06	5.53
91	7	12	20.9	1.809	0.404	0.640	0.288	25.89	4.59
92	7	12	21.4	1.878	0.440	0.624	0.302	25.69	4.07
93	7	12	21.9	1.919	0.372	0.622	0.305	25.60	4.12
94	7	12	22.4	1.987	0.418	0.582	0.341	25.98	6.15
95	7	12	22.9	2.051	0.405	0.568	0.352	25.74	5.14
11	8	12	21.3	1.820	0.462	0.612	0.314	25.21	4.01
12	8	12	21.8	1.866	0.478	0.597	0.324	25.17	4.35
13	8	12	22.3	1.982	0.475	0.561	0.351	26.63	6.37
14	8	12	22.8	1.939	0.466	0.545	0.374	25.95	6.07
15	8	12	23.3	1.895	0.466	0.518	0.401	25.19	6.17
16	10	12	22.3	1.642	0.443	0.563	0.371	25.88	4.06
17	10	12	22.8	1.619	0.413	0.556	0.380	27.91	3.96
18	10	12	23.3	1.687	0.479	0.505	0.417	26.30	5.23
19	10	12	23.8	1.707	0.462	0.468	0.456	27.30	6.43
20	10	12	24.3	1.701	0.406	0.374	0.544	27.10	8.63

Table K.3 - Continuation

	Set-up parameters			Monitoring indices and dip resistance					
Run	WFS	SO	V_{set}	TSI	TI	DCI	PR	$DipR_{mean}$	$DipR_{SD}$
21	5.5	15	20.3	1.966	0.330	0.674	0.262	28.26	4.02
22	5.5	15	20.8	2.034	0.356	0.664	0.268	28.28	4.09
23	5.5	15	21.3	2.166	0.340	0.655	0.272	-	-
24	5.5	15	21.8	2.238	0.369	0.594	0.322	28.01	5.32
25	5.5	15	22.3	2.313	0.352	0.516	0.388	27.67	5.10
26	6.5	15	20.6	1.809	0.368	0.656	0.275	27.54	3.81
27	6.5	15	21.1	1.898	0.394	0.634	0.290	27.81	4.13
28	6.5	15	21.6	1.992	0.354	0.627	0.297	27.93	4.33
29	6.5	15	22.1	2.017	0.354	0.602	0.318	28.17	4.51
30	6.5	15	22.6	2.124	0.333	0.575	0.342	28.18	5.03
31	8.5	15	21.2	1.640	0.389	0.597	0.334	28.46	3.39
32	8.5	15	21.7	1.682	0.425	0.588	0.338	28.66	3.61
33	8.5	15	22.2	1.729	0.356	0.586	0.341	28.73	3.67
34	8.5	15	22.7	1.804	0.381	0.566	0.359	28.54	4.51
35	8.5	15	23.2	1.859	0.361	0.550	0.375	28.41	4.66
36	9.5	15	21.6	1.600	0.391	0.578	0.358	29.00	3.38
37	9.5	15	22.1	1.635	0.389	0.573	0.360	28.70	3.81
38	9.5	15	22.6	1.659	0.394	0.558	0.372	29.15	3.91
39	9.5	15	23.1	1.716	0.381	0.542	0.388	29.14	4.59
40	9.5	15	23.6	1.768	0.360	0.507	0.416	29.47	5.21
41	10.5	15	31.5	1.041	0.076	0.010	0.979	114.96	1.99
42	10.5	15	32.0	1.042	0.063	0.010	0.979	115.98	1.90
43	10.5	15	32.5	1.040	0.048	0.010	0.980	117.78	1.70
44	10.5	15	33.0	1.044	0.045	0.010	0.979	117.90	1.92
45	10.5	15	33.5	1.048	0.050	0.010	0.979	117.59	2.08
46	11.5	15	31.9	1.039	0.057	0.010	0.979	107.61	1.65
47	11.5	15	32.4	1.037	0.045	0.010	0.980	109.22	1.46
48	11.5	15	32.9	1.037	0.041	0.009	0.980	110.35	1.39
49	11.5	15	33.4	1.038	0.042	0.010	0.980	111.19	1.46
50	11.5	15	33.9	1.038	0.043	0.010	0.980	111.97	1.51

Table K.3 - Continuation

	Set-up parameters			Monitoring indices and dip resistance					
Run	WFS	SO	V_{set}	TSI	TI	DCI	PR	$DipR_{mean}$	$DipR_{SD}$
51	13.5	15	32.9	1.037	0.046	0.010	0.980	0.00	0.00
52	13.5	15	33.4	1.040	0.045	0.010	0.980	102.57	1.45
53	13.5	15	33.9	1.038	0.041	0.010	0.980	103.65	1.32
54	13.5	15	34.4	1.059	0.058	0.012	0.968	108.50	2.36
55	13.5	15	34.9	1.066	0.065	0.013	0.965	107.81	2.69
56	5.5	20	20.2	1.986	0.344	0.648	0.278	35.24	5.02
57	5.5	20	20.7	2.060	0.343	0.651	0.273	33.25	4.46
58	5.5	20	21.2	2.203	0.378	0.621	0.292	33.62	4.71
59	5.5	20	21.7	2.326	0.353	0.607	0.305	33.32	5.31
60	5.5	20	22.2	2.376	0.353	0.516	0.381	32.87	6.45
61	6.5	20	20.5	1.828	0.365	0.627	0.297	33.11	4.44
62	6.5	20	21.0	1.918	0.358	0.623	0.298	33.91	4.57
63	6.5	20	21.5	1.994	0.358	0.615	0.304	33.16	4.39
64	6.5	20	22.0	2.088	0.387	0.580	0.329	33.23	5.21
65	6.5	20	22.5	2.203	0.495	0.499	0.397	33.86	6.98
66	7.5	20	20.8	1.793	0.434	0.592	0.322	33.88	4.32
67	7.5	20	21.3	1.854	0.420	0.575	0.335	33.31	4.45
68	7.5	20	21.8	1.880	0.391	0.579	0.333	33.55	4.41
69	7.5	20	22.3	1.952	0.381	0.567	0.344	33.91	4.76
70	7.5	20	22.8	2.052	0.350	0.551	0.359	34.41	5.90
71	8.5	20	30.8	1.041	0.063	0.010	0.972	145.62	2.13
72	8.5	20	31.3	1.042	0.057	0.010	0.973	146.52	1.93
73	8.5	20	31.8	1.044	0.069	0.010	0.971	148.92	2.28
74	8.5	20	32.3	1.045	0.065	0.010	0.973	148.61	2.19
75	8.5	20	32.8	1.044	0.067	0.010	0.973	150.01	2.32
76	10.5	20	31.6	1.039	0.115	0.010	0.976	127.39	2.78
77	10.5	20	32.1	1.038	0.082	0.008	0.980	128.95	2.08
78	10.5	20	32.6	1.039	0.048	0.009	0.980	128.87	1.82
79	10.5	20	33.1	1.038	0.046	0.010	0.980	130.36	1.77
80	10.5	20	33.6	1.042	0.051	0.010	0.980	130.78	2.04

Table K.3 - Continuation

	Set-up parameters			Monitoring indices and dip resistance					
Run	WFS	SO	V_{set}	TSI	TI	DCI	PR	$DipR_{mean}$	$DipR_{SD}$
81	12.5	20	32.2	1.053	0.148	0.010	0.967	116.48	3.52
82	12.5	20	32.7	1.043	0.092	0.010	0.977	117.95	2.29
83	12.5	20	33.2	1.039	0.061	0.010	0.980	118.67	1.87
84	12.5	20	33.7	1.034	0.048	0.010	0.980	119.42	1.55
85	12.5	20	34.2	1.035	0.042	0.009	0.980	119.71	1.44
86	14.5	20	33.1	1.049	0.073	0.010	0.976	108.29	2.61
87	14.5	20	33.6	1.039	0.053	0.010	0.980	109.43	1.89
88	14.5	20	34.1	1.037	0.047	0.010	0.980	110.41	1.65
89	14.5	20	34.6	1.038	0.045	0.010	0.980	111.39	1.55
90	14.5	20	35.1	1.037	0.042	0.010	0.980	111.55	1.34
96	4	10	18.0	1.893	0.396	0.748	0.197	22.22	3.98
97	4	10	19.0	2.166	0.369	0.745	0.193	22.30	4.02
98	4	10	20.0	2.282	0.350	0.735	0.205	21.79	4.17
99	6	10	19.0	1.767	0.454	0.697	0.242	22.02	3.36
100	6	10	20.0	1.803	0.376	0.701	0.240	21.75	3.21
101	6	10	21.0	2.061	0.396	0.696	0.234	21.87	3.81
102	8	10	20.0	1.684	0.475	0.640	0.297	22.29	2.96
103	8	10	21.0	1.660	0.428	0.637	0.301	22.43	3.40
104	8	10	22.0	1.734	0.443	0.607	0.329	22.61	4.35
105	4	18	19.5	2.342	0.339	0.681	0.246	30.67	5.06
106	4	18	18.5	2.135	0.369	0.692	0.235	31.20	5.17
107	4	18	20.5	2.533	0.350	0.630	0.284	31.07	6.41
108	6	18	20.5	1.901	0.339	0.662	0.271	31.23	4.48
134	6	18	21.5	2.094	0.342	0.626	0.292	30.63	4.36
109	6	18	22.5	2.312	0.408	0.517	0.384	31.33	6.52
110	8	18	20.8	1.795	0.399	0.613	0.307	31.09	4.02
111	8	18	21.8	1.926	0.380	0.596	0.319	31.14	4.50
112	8	18	22.8	2.079	0.462	0.525	0.379	31.51	5.74
113	10	18	29.4	1.107	0.270	0.014	0.949	123.63	7.84
114	10	18	30.4	1.047	0.088	0.010	0.980	129.54	2.41
115	10	18	31.4	1.036	0.061	0.010	0.980	125.61	1.70